AD NUMBER

AD822104

NEW LIMITATION CHANGE

TO

Approved for public release, distribution unlimited

FROM

Distribution authorized to U.S. Gov't. agencies and their contractors; Administrative/Operational Use; Jul 1967. Other requests shall be referred to Air Force Materials Lab., Wright-Patterson AFB, OH 45433.

AUTHORITY

USAF ltr, 2 Mar 1972

EVALUATION OF THERMAL PROTECTION MATERIALS
FOR
LIFTING AND BALLISTIC RE-ENTRY HEAT SHIELD MATERIALS

Shirley L. Grindle
Daphne S. Christensen
Marvin W. Searcy

Space-General
A Division of Aerojet General Corporation

TECHNICAL REPORT AFML-TR-67-222

July 1967

This document is subject to special export controls and each transmittal to foreign governments or foreign nationals may be made only with prior approval of the Materials Applications Division(MAA), Air Force Materials Laboratory, Wright-Patterson Air Force Base, Ohio 45433.

Air Force Materials Laboratory
Directorate of Laboratories
Air Force Systems Command
Wright-Patterson Air Force Base, Ohio

EVALUATION OF THERMAL PROTECTION MATERIALS

FOR

LIFTING AND BALLISTIC RE-ENTRY HEAT SHIELD MATERIALS

Shirley L. Grindle
Daphne S. Christensen
Marvin W. Searcy

See form 1423

Space-General, A Division of Aerojet-General Corporation

FOREWORD

This report covers work performed during the period from June 1966 to July 1967 under Contract AF33(615)-5235. This contract was initiated under Project No. 7381 "Materials Applications" and Task No. 738102, "Materials and Process Evaluation." The work was administered under the direction of the Applications Division, Air Force Materials Laboratory, Wright-Patterson Air Force Base, Ohio; Capt. D. R. James and Lt. E. H. Beardslee were Project Monitors for this work.

The Space-General program managers were Shirley L. Grindle and Daphne S. Christensen. The authors wish to thank the following individuals who made major contributions to this program: Miss Hazel V. Porter, Mr. Marvin W. Searcy, and Dr. R. F. Brodsky.

The writers also wish to express thanks to numerous companies who supplied material samples and furnished information relative to the technical importance and content of this report.

The entire contents of this report including materials data presentation are unclassified.

This technical report has been reviewed and is approved.

ALBERT OLEVITCH, Chief
Materials Engineering Branch
Materials Applications Division
Air Force Materials Laboratory

ABSTRACT

This report presents test data obtained in a hyperthermal plasma arc environment on newly-developed materials and materials concepts applicable to re-entry heat shield design including both ballistic and lifting re-entry vehicles.

The experimental work concentrated on evaluation of candidate materials in the following six categories:

- Low-Density Ablators
- High-Density Ablators
- Special Class Low-Density Ablators for Lockheed ENCAP Program
- Coated Refractories (Sylvania Electric Products Coatings)
- Graphitic Materials and Carbon Composites
- Char Layer Formation on Phenolic-Carbon

Calibration of the plasma arc re-entry environment obtained in the Electro-Thermal Facility at Space-General, A Division of Aerojet-General Corporation, ~~is presented in detail.~~

Materials test data obtained in the various test programs include the effects of model shape, material density, commercial versus high purity grades of graphite and carbon cloth materials, high pressure, and high enthalpy. Performance data of the low-density and high-density ablators evaluated under this contract are compared with previously-tested ablators of each category.

In addition to the materials evaluation portion of this study, a secondary objective of this project was directed toward the development of a graphical method for correlating test data. Various correlation procedures are investigated and a method using the transfer parameter of $\dot{q}\sqrt{p}$ is described and used for presenting test data obtained from the materials evaluated under this contract. Correlation of data and projections from accumulated data has thus far been successful for the various materials attempted.

TABLE OF CONTENTS

Page

TABLE OF CONTENTS
(Continued)

LIST OF ILLUSTRATIONS AND TABLES

TABLES

ILLUSTRATIONS

LIST OF ILLUSTRATIONS AND TABLES
(Continued)

ILLUSTRATIONS

LIST OF ILLUSTRATIONS AND TABLES
(Continued)

ILLUSTRATIONS

LIST OF ILLUSTRATIONS AND TABLES
(Continued)

ILLUSTRATIONS

LIST OF ILLUSTRATIONS AND TABLES
(Continued)

ILLUSTRATIONS

LIST OF ILLUSTRATIONS AND TABLES
(Continued)

ILLUSTRATIONS

LIST OF ILLUSTRATIONS AND TABLES
(Continued)

ILLUSTRATIONS

LIST OF ILLUSTRATIONS AND TABLES
(Continued)

ILLUSTRATIONS

LIST OF SYMBOLS

B	Mass addition parameter
C_H	Stanton Number
C_{H_o}	Stanton Number without mass addition
H	Enthalpy, Btu/lb
L_v	Heat of sublimation, Btu/lb
L_T	Material heat capacity up to sublimation temperature, Btu/lb
$\dot{m}$	Mass loss rate, grams/second
M	Mach Number
p	Pressure, atmospheres
p_o	Model stagnation pressure behind bow shock, atmospheres
p_T	Nozzle stagnation pressure, atmospheres
$\dot{q}$	Average heat flux, Btu/ft^2-sec
$\dot{q}\sqrt{P}$	Transfer parameter, Btu/ft^2-sec x atm.$^{.5}$
R	Radius, feet
$\dot{s}$	Recession rate, inches/second
u	Velocity, feet/second
x	Distance from leading edge, inches
ρ	Density, lb/ft^3
ψ	Transfer parameter, non-dimensional

Subscripts

s	Stagnation conditions behind bow shock wave
T	Upstream stagnation conditions
∞	Free-stream conditions

INTRODUCTION

The primary objectives of this project were to initiate test programs using newly-developed materials concepts and to extend the range and accuracy of certain previous test programs investigating special problem areas associated with a number of different types of heat shield materials. Each experimental program represented an individual effort with specialized measuring techniques and selected test conditions depending on the development need and application. A secondary objective of this project was directed toward developing graphical methods for correlating test data. The specific objectives and accomplishments of each of these efforts are described in the Summary.

This report is organized giving separate chapters to each of six materials categories: 1) Low-Density Ablators, 2) High-Density Ablators, 3) Special Class Low-Density Ablators, 4) Coated Refractory Metals, 5) Carbon Composites and Graphitic Materials, and 6) Char Layer Formation. Each chapter is subdivided into sections describing 1) objectives of the test, 2) particular materials investigated, 3) calibration of the test environment and special instrumentation, and 4) a summary of the test results. The exploratory work on studying data correlation methods is presented as a separate chapter utilizing in part test results from the earlier chapters in addition to test data gathered from other sources.

1.0 SUMMARY

The experimental work concentrated on producing accurate and reliable test data for the following six materials classifications:

A. Low-Density Ablators
B. High-Density Ablators
C. Special Class Low-Density Ablators
D. Coated Refractory Metals
E. Carbon Composites and Graphitic Materials
F. Char Layer Formation

A summary chart showing the variety of models and test conditions is presented in Table 1.

The majority of the work concentrated on the study of low and high-density ablators and graphitic and carbon composite materials, Items A, B and E above. A total of 112 models were tested in these materials categories as compared with a total of 43 models in the other materials classes, Items C, D and F, above. The individual objectives of each of the test programs numerated above were as follows:

A. The four primary objectives associated with the Low-Density Ablator Program were: 1) to extend the range of heating loads applied to the models above those tested in previous work, 2) to compare relative performance of newly-developed materials provided by Douglas Aircraft Company, Boeing Aircraft Company, and the Armstrong Cork Company, 3) to determine the relative merits of flat-face versus 'iso-q' shaped test models, and 4) to evaluate the influence of systematic changes in density level.

B. The major objectives of the High-Density Ablator Program were similar to those of A above with the exception that only hemispherical shapes were considered, with the materials suppliers in this case being Union Carbide Corporation and Dow Corning Corporation.

C. The objective of the Special Class Low-Density Program was to provide specific performance information, primarily resistance to erosion and char spallation, for a number of candidate materials considered for the Lockheed ENCAP program.

D. The main objective of the Coated Refractory Metals Program was to determine the failure (melting) temperature of selected Sylvania coatings under conditions of low pressure.

E. The three major objectives of the Carbon Composites and Graphitic Materials Program were 1) to compare commercial versus high-purity grades of carbon and graphite, 2) to compare corresponding materials (carbon and graphite) from various vendors, and 3) to compare the influence of high pressure (4 atmospheres) versus low pressure (0.06 atmospheres) test environments.

F. The objective of the Char Layer Program was to produce a $\frac{1}{4}$-inch to $\frac{1}{2}$-inch thick, uniform char, under transient test conditions, suitable to provide the necessary performance information to be used by Boeing Aircraft Company in performing detailed analyses of the char layer in a phenolic-carbon composite material under Contract AF 33(615)-3804.

All of the test work was carried out in the Space-General Electro-Thermal Arc Facility, which is described in the facilities brochure (Ref. 1, December 1966). All testing was done under supersonic flow conditions. Although the facility provides for nozzle test streams up to eight inches in diameter, the model sizes evaluated in the present program were in a size category which permitted exclusive use of the three-inch exit diameter nozzle. Most of the testing was accomplished using the low pressure/high enthalpy arc generator with the exception of the high pressure test work in the Carbon Composite and Graphitic Materials program, which employed the high pressure (up to 40 atmospheres possible) arc generator. Test times varied from a few seconds to one hour at either constant or transient heating conditions, depending on the need of the evaluation program.

Data Correlation Study

The amount of experimental test data available throughout the country is increasing at such a rate as to make it essential to have some general way of comparing the order of merit of tested materials. Specifically, it is necessary that some way be found which will include both enthalpy and pressure effects (i.e. altitude and velocity effects) for practical flight applications. Further, the data correlation procedure must be reasonably simple to use, based on measured quantities usually obtained in an arc tunnel.

As a preliminary step in studying this problem, various correlation procedures were investigated using arc tunnel data compiled from various sources. A method using a transfer parameter of $\dot{q}\sqrt{p}$ was found to be particularly promising. This work is reported in Section 8.0.

TABLE 1

SUMMARY OF MATERIALS EVALUATED UNDER THIS CONTRACT

Test Category	Material	Material Supplier	Density of Virgin Material-lb/ft^3	Evaluated at Test Condition: Heat Flux (Btu/ft^{2}sec)	Evaluated at Test Condition: Enthalpy (Btu/lb)	Evaluated at Test Condition: Model Stag. Press (atms)
Low-Density Ablators	Armstrong Cork No. 2755	Armstrong Cork	30	30,60,90, 120, 150	8,000 - 12,000	0.003 - 0.03
Low-Density Ablators	Carborazole	Boeing	31	30,60,90, 120,150,300	8,000 - 16,000	0.003 - 0.05
Low-Density Ablators	SMORS-25	Douglas	20 - 35	30,60,90, 120,150	8,000 - 12,000	0.003 - 0.03
High-Density Ablators	93-002	Dow Corning	88.7	40,140, 300,650	7,000 - 13,000	0.002 - 0.13
High-Density Ablators	93-069	Dow Corning	107.4	40,140, 300,650	7,000 - 13,000	0.002 - 0.13
High-Density	Boron Nitride Grade HDB Grade HDF Grade HBN Grade HBR	Union Carbide	 187.4 174.9 128.0 121.8	40,140, 300,650	7,000 - 13,000	0.002 - 0.13
Low-Density Ablators	Reinforced Silicone Resin Composites	Lockheed	20 - 45	25 and 45	10,000 - 11,000	0.013 and 0.044
Coated Refractories	R512A and R512E	Sylvania	---	30 - 75	6,000 - 10,000	0.007 - 0.01
Graphites	Various	Various	Various	156 - 1027	17,000 and 3,000	0.06 and 4.0
Carbon Composites	Various	Various	Various	156 - 1027	17,000 and 3,000	0.06 and 4.0
Char Layer Formation	Phenolic-Graphite	Boeing	90	90 - 500	8,500 - 16,000	0.02 - 0.1

PRECEDING PAGE BLANK- NOT FILMED.

2.0 LOW-DENSITY ABLATOR PROGRAM

Ablative materials possessing a density range from 20 - 35 lb/ft^3 were provided by Douglas Aircraft Company, Armstrong Cork Company, and Boeing Aircraft Company. All candidate materials were subjected to identical environmental heating conditions and performance data obtained from these tests were compared with each other and with earlier materials performance data obtained on other low-density ablators, as reported in Ref. 2 (Welsh, et al, 1966).

2.1 Objectives

An Air Force - sponsored program was completed in January 1966 by Aerospace Corporation, El Segundo, California, in which low-density ablation materials were surveyed; a final report issued under Report No. TDR-669(6240-10)-5 summarizes the test results obtained for the following materials:

General Electric ESM 1001 and ESM 1004 - elastomer type
Lockheed Lockheat 1 and 2 - inorganic laminate type
McDonnell S-6 - elastomer type
AVCO Avcoat 5026-39 - rigid composite type
Martin ESA 3560 and ESA 3560HF - elastomer type
Emerson T-500-111 - rigid composite type
Langley Purple Blend - elastomer type
Langley Phenolic Nylon - rigid composite type

The above materials were evaluated at cold-wall heating rates of 20, 60, 90, 120 and 150 Btu/ft^2-sec in a reconstituted air plasma arc. Model configuration was a 2.0-inch diameter flat-face cylinder instrumented with chromel/alumel thermocouples at specific locations in the model and at the back-face. The objective of this phase of our contract was to provide additional data on other materials in the low-density ablator category and to compare the results of this new data with that presented in Ref. 2 (Welsh, et al, 1966).

2.2 Description of Materials Tested

Three companies actively participated in the low-density ablator program by providing test materials and, in two cases, fully-instrumented test models. The supplier and type of material supplied were:

Armstrong Cork Company - Armstrong Cork No. 2755
Boeing Aircraft Company - Boeing Carborazole
Douglas Aircraft Company - Douglas SMORS-25

The model configuration used in the evaluation of the Boeing and Armstrong materials was a 2.0-inch diameter flat-face cylinder, instrumented with four chromel/alumel thermocouples at distances from the leading edge of 0.250, 0.500, 0.750 and 1.000 inches. A sketch of the model configuration and thermocouple location is presented in Figure 1.

Two model configurations were investigated for Douglas Aircraft Company using their SMORS-25 low-density ablator material. Initially, 2.0-inch diameter flat-face cylinders identical to the design presented in Figure 1, were evaluated. Due to the characteristics of the ablation profile at the higher heating rates of 60 - 150 Btu/ft^2-sec, it was decided to use 'iso-q' shaped models in an effort to minimize the tendency of the model to form a cavity in the stagnation area of the exposed frontal surface. The iso-q shape is depicted in Figure 2; note that this particular model configuration was utilized for the Douglas model tests only.

The test models supplied by Boeing Aircraft Company and Douglas Aircraft Company were instrumented in accordance with our instructions as described in Figures 1 and 2. Space-General personnel fabricated and instrumented the Armstrong Cork models using bulk material supplied by Armstrong at no charge. All thermocouples utilized on this series of model tests were of chromel/alumel, 36 gage, and were recorded on a null-balance recorder (Texas Instruments Servo-Riter II), $\frac{1}{4}$% full-scale accuracy. Where possible, exposure times were ten minutes; however, a number of the models could not withstand the heating environment for this length of time. Surface temperatures were read manually using a Leeds and Northrup manual optical brightness pyrometer. All surface temperatures plotted are apparent brightness temperatures, uncorrected for material surface emissivity. Color film coverage was obtained on most of the model tests and has been forwarded to the respective material suppliers.

2.2.1 Armstrong Cork No. 2755 Material

The Armstrong Cork No. 2755 material, with a density of 30 lb/ft^3, represents one of the most recent improvements of the Armstrong low-density ablators. Erosion rates had been obtained by Armstrong using an oxy-acetylene torch at heating rates of 93 and 750 Btu/ft^2-sec and were found to be 0.00520 and 0.01693 in/sec, respectively. Additional performance data at heating rates of 30, 60, 90, 120 and 150 Btu/ft2-sec was obtained. One model each was evaluated at the above cold-wall heat fluxes. Calibration data obtained on each model test and model test data (including weight loss and recession rates, and surface temperatures) are tabulated in Tables 2 and 3 on the following page. Model surface brightness and internal and back-face temperature-time histories are presented graphically in Figures 3 through 7. Pre- and post-exposure black and white photographs showing the external and cross-sectional views of the exposed models are included in Figures 8 through 12.

2.2.2 Boeing Carborazole Material

A low-density ablator with a density of 31 lb/ft^3 was provided by the Boeing Aircraft Company for evaluation at the five levels of heat flux ranging between 30 and 150 Btu/ft^2-sec. One model was evaluated at a cold-wall heat flux of 300 Btu/ft^2-sec using a hardened version of the Carborazole (Boeing tradename of this particular low-density ablator) material. The Carborazole models were laminated with lay-up direction perpendicular to the axis of the test stream. During exposure to the hot flow, the layers of material rapidly peeled off during the first ten seconds (it is estimated that approximately twenty to thirty layers were removed from the test model during the initial exposure period), the material then appeared to stabilize with maybe five to ten additional layers peeling off during the next thirty seconds. The latter portion of each model test appeared to be without peeling-off of the layers.

TABLE 2

CALIBRATION DATA

Armstrong Cork 2755 Model Tests

Test Condition	Model No.	Gas Enthalpy (Btu/lb)	Model Stag. Pressure (atm)	Model Cold-Wall Heat Flux (Btu/ft^2-sec)	Nozzle Stag. Pressure (atms)	Nozzle Static Pressure (atms)	Gas Flow Rate (lb/sec)
1	1-1	8,180	0.0030	33.6	0.0147	0.00028	0.000655
2	1-2	9,110	0.0071	62.2	0.0362	0.00069	0.001569
3	1-3	10,500	0.0130	91.1	0.0702	0.00128	0.002995
4	1-4	11,000	0.0200	124.4	0.1091	0.01970	0.004475
5	1-5	11,350	0.0320	158.1	0.1760	0.03145	0.007100

TABLE 3

MODEL TEST DATA

Armstrong Cork 2755 Model Tests

Test Condition	Model No.	Exposure Time (seconds)	Weight Loss (grams)	Recession (inches)	Weight Loss Rate (grams/sec)	Recession Rate (inches/sec)	Surface Temp. (°F)
1	1-1	600	19.7	Swelling	0.0328	--------	2200
2	1-2	600	23.0	0.643	0.0383	0.001072	2600
3	1-3	420	36.6	0.909	0.0871	0.002164	3000
4	1-4	360	36.9	0.770	0.1025	0.002139	3100
5	1-5	345	37.2	0.779	0.1078	0.002258	3200

TABLE 4

CALIBRATION DATA

Boeing Carborazole Model Tests

Test Condition	Model No.	Gas Enthalpy (Btu/lb)	Model Stag. Pressure (atm)	Model Cold-Wall Heat Flux (Btu/ft^2-sec)	Nozzle Stag. Pressure (atm)	Nozzle Static Pressure (atm)	Gas Flow Rate (lb/sec)
1	32019-1	8,225	0.0030	33.8	0.0144	0.00029	0.00065
1	32019-6	8,200	0.0039	34.1	0.0145	0.00028	0.00055
2	32019-2	9,155	0.0069	53.8	0.0361	0.00072	0.00155
3	32019-4	10,510	0.0133	91.2	0.0704	0.00131	0.002[illegible]
3	32019-5	10,525	0.0134	92.4	0.0706	0.00132	0.00299
4	32019-7	11,155	0.0305	122.1	0.1095	0.00192	0.00447
5	32019-3	11,485	0.0319	161.0	0.1777	0.00316	0.00710
5	32019-8	11,510	0.0320	160.9	0.1777	0.00316	0.00710
5	32019-9	11,495	0.0321	161.1	0.1777	0.00316	0.00710
Unassigned	32019-10	16,110	0.0502	304.2	0.2752	0.00474	0.01330

TABLE 5

MODEL TEST DATA

Boeing Carborazole Model Tests

Test Condition	Model No.	Exposure Time (seconds)	Weight Loss (grams)	Recession (inches)	Weight Loss Rate (gms/sec)	Recession Rate (inches/sec)	Surf. Temp. (^oF)
1	32019-1	600	19.2	0.344	0.03200	0.0005733	2400
1	32019-6	600	19.6	0.483	0.03267	0.0008050	2400
2	32019-2	180	18.6	0.488	0.1033	0.002711	3000
3	32019-4	180	21.8	0.556	0.1211	0.003089	3500
3	32019-5	180	25.0	0.510	0.1389	0.002833	3500
4	32019-7	120	24.1	0.614	0.2008	0.005117	3740
5	32019-3	90	21.4	0.519	0.2378	0.005767	3800
5	32019-8	90	23.0	0.351	0.2556	0.003900	3800
5	32019-9	90	18.1	0.391	0.2011	0.004344	3800
Unassigned	32019-10	50	18.4	0.428	0.3680	0.008560	4200

Tunnel calibration data obtained on the Boeing model tests is presented in Table 4; note that the heating rate of 300 Btu/ft^2-sec is not one of the standard test conditions for the low-density ablator tests and hence is not assigned a test condition number. Model test data consisting of the weight loss and recession rates, and the surface brightness temperatures, are tabulated in Table 5. Surface and internal and back-face temperature-time histories are graphed in Figures 13 through 22. The back-face temperature for all models tested under this portion of the contract is that thermocouple located 1.0-inch from the leading edge. Pre- and post-exposure photographs for each of the models tested are included in Figures 23 through 32; color film coverage obtained during each of the model exposures to the high-temperature plasma stream, has been forwarded to the Boeing technical monitors.

2.2.3 Douglas SMORS-25 Material

The Douglas SMORS-25 material, classified as a low-density elastomeric ablator (density range from 20 - 35 lb/ft^3), is comprised of a silicone resin with microballoon additives. Initially, eight flat-faced models were evaluated at the five heat flux values selected for low-density ablator analysis. Fairly uniform ablation profiles resulted at the lower heat flux levels of 30 and 60 Btu/ft^2-sec; however, severe concaving of the center portion of the models was experienced at the heat flux levels above 60 Btu/ft^2-sec. In view of this occurrence, additional models were fabricated by Douglas using an 'iso-q' profile, designed to provide a surface shape which would ablate more evenly. An additional six models were then tested using the iso-q models and ablation profiles were found to be more uniform than in the case of the flat-faced models. These first two series of tests (designated by a letter 'A' and 'AA' after each model number) were fabricated from the Douglas SMORS-25 material with a density of 32 lb/ft^3. Later on in the test program, a third series of tests was performed using variations of the original Douglas SMORS-25 material. Eleven models were evaluated - nine of which had a density of 20 lb/ft^3 and two of which had a density of 25 lb/ft^3. The latter two models are designated as Douglas SMORS-25A material in Table 6. All of the models evaluated under this third series of tests were of the iso-q shape and were subjected to cold-wall heat flux levels of 30, 60, 90, 120 and 150 Btu/ft^2-sec.

In order to permit a comparison between the flat-face and the iso-q shaped models, it was essential that duplicate cold-wall heat flux environments be maintained. Since the heating rate to a flat-face will be somewhat different than that to an iso-q shaped face at the same input test conditions, adjustments in the gas stagnation enthalpy were necessary to achieve identical heating rates to both model configurations. Theoretical predictions of the heat flux to an iso-q shaped body are difficult to make in view of the uncertainty of the effect of body shape. To avoid unnecessary estimates in this important criterion, a calorimeter was constructed of the same geometry as the iso-q test models - this calorimeter was used to define the cold-wall heat flux and to assure a valid basis for comparing the flat-face and iso-q model performance data.

Tables 6 and 7 present the tunnel calibration data and model test data for the complete series of Douglas model tests. Graphical presentations of the internal and surface temperature histories are included in Figures 33 through 57. To present a clearer picture of the Douglas model tests, Figures 58 and 59 have been prepared, which clearly show the performance of the various

TABLE 6

CALIBRATION DATA

Douglas SMORS Model Tests

Test Condition	Model No.	Gas Enthalpy (Btu/lb)	Model Stag. Pressure (atm)	Model Cold-Wall Heat Flux *** (Btu/ft^2-sec)	Nozzle Stag. Pressure (atm)	Nozzle Static Pressure (atm)	Gas Flow Rate (lb/sec)
1	4A	8,210	0.0031	34.1	0.0146	0.00027	0.000655
1	12A	8,185	0.0030	35.0	0.0145	0.00028	0.000655
1-A **	1B	5,110	0.0029	30.5	0.0147	0.00030	0.000655
1-A	2B	5,080	0.0029	31.5	0.0145	0.00031	0.000655
2	5A	9,185	0.0071	63.5	0.0364	0.00070	0.001569
2	6A	9,210	0.0071	64.1	0.0365	0.00071	0.001569
2-A	3B	5,855	0.0069	61.5	0.0359	0.00073	0.001569
2-A	4B	5,910	0.0069	62.0	0.0360	0.00073	0.001569
3	7A	10,455	0.0131	90.4	0.0700	0.00126	0.002995
3	8A	10,505	0.0130	91.3	0.0701	0.00127	0.002995
3-A	1	6,500	0.0130	94.7	0.0675	0.00131	0.002995
3-A	1A	6,610	0.0130	95.5	0.0676	0.00130	0.002995
3-A	5B	6,620	0.0131	95.3	0.0676	0.00129	0.002995
3-A	6B	6,590	0.0130	94.8	0.0675	0.00131	0.002995
4	10A	11,105	0.0202	121.5	0.1089	0.00198	0.004475
4-A	3AA	7,210	0.0200	117.8	0.0986	0.00202	0.004475
4-A	4AA	7,315	0.0202	118.5	0.0984	0.00202	0.004475
4-A	12B	7,180	0.0201	121.6	0.0987	0.00202	0.004475
5	11A	11,400	0.0321	158.5	0.1759	0.00315	0.007100
5-A	5AA	7,850	0.0319	161.8	0.1686	0.00322	0.007100
5-A	6AA	8,885	0.0319	163.5	0.1689	0.00322	0.007100
5-A	9B	7,910	0.0320	159.8	0.1690	0.00322	0.007100
5-A	10B	7,890	0.0321	157.0	0.1689	0.00321	0.007100
5-A	13B*	7,910	0.0321	164.5	0.1691	0.00322	0.007100
5-A	14B*	7,885	0.0322	161.7	0.1691	0.00322	0.007100

NOTE:

* Models 13B and 14B constructed of Douglas SMORS-25A material.

** Models tested at -A Test Conditions were "iso-q" shaped models.

*** All cold-wall heat flux values tabulated are those measured with geometrically-similar calorimeters.

TABLE 7

MODEL TEST DATA

Douglas SMORS Model Tests

Test Condition	Model No.	Exposure Time (seconds)	Weight Loss (grams)	Recession (inches) ***	Weight Loss Rate (grams/sec)	Recession Rate (inches/sec)	Surface Temp. (^oF)
1	4A	889.2	12.9	+0.069	0.01451	+0.0000776	2405
1	12A	753.4	11.3	+0.014	0.01450	+0.0000186	2345
1-A**	1B	600.0	6.8	-0.088	0.01134	0.0001467	2000
1-A	2B	600.0	7.3	-0.080	0.01217	0.0001334	2030
2	5A	750.0	22.1	+0.110	0.02947	+0.000147	2820
2	6A	919.2	16.5	+0.135	0.01795	+0.000147	2850
2-A	3B	600.0	13.8	-0.047	0.02300	0.00007835	2550
2-A	4B	525.0	15.5	-0.043	0.02952	0.00008190	2550
3	7A	534.0	21.4	-0.390	0.04007	0.000730	3050
3	8A	703.5	14.4	-0.266	0.02047	0.000378	3010
3-A	1	600.0	16.3	+0.137	0.02717	+0.000228	2800
3-A	1AA	600.0	17.4	+0.078	0.02900	+0.000130	2790
3-A	5B	540.0	8.2	-0.113	0.01519	0.0002093	2740
3-A	6B	540.0	8.3	-0.076	0.01537	0.0001407	2740
4	10A	429.7	20.9	-0.583	0.04864	0.001357	3500
4-A	3AA	600.0	25.2	-0.046	0.04201	0.0000767	3130
4-A	4AA	600.0	24.0	-0.090	0.04000	0.0001500	3070
4-A	12B	510.0	14.1	-0.489	0.02765	0.0009588	3120
5	11A	360.0	23.1	-0.643	0.06417	0.001786	3700
5-A	5AA	600.0	27.2	-0.334	0.04534	0.0005568	3180
5-A	6AA	600.0	28.8	-0.406	0.04801	0.0006768	3120
5-A	9B	270.0	15.7	-0.819	0.05815	0.003033	3650
5-A	10B	270.0	15.7	-0.796	0.05815	0.002948	3650
5-A	13B*	330.0	23.5	-0.602	0.07121	0.001824	3740
5-A	14B*	285.0	20.5	-0.566	0.07228	0.001986	3700

NOTE:

* Models 13B and 14B constructed of Douglas SMORS-25A material.

** Models tested at -A Test Conditions were "iso-q" shaped models.

*** (+) Designates model expanded.

density levels of the SMORS material, and the effect of model shape on the material's performance. Figure 58 is a bar graph indicating the average front surface recession rates of three variations of the Douglas SMORS-25 material - the variations being different density levels of 20, 25 and 32 lb/ft^3. Front surface brightness temperatures for the three density levels are also shown on Figure 58. Measured recession rates and surface brightness temperature both decreased with corresponding increases in material density. A significant difference was noted between the performance of the flat-faced model and the iso-q model (for the same density level of 32 lb/ft^3), with the iso-q model showing superior performance. This result was expected in view of the fact that the flat-faced models exhibited severe concave ablation profiles. The iso-q model shape is designed so as to provide a nearly uniform heat flux distribution across the front surface of the model, hence resulting in a constant-shape ablation profile during the model exposure period.

Back-face temperature-time histories for each of the various material densities and the flat-face and iso-q shaped models, are presented in Figure 59. Similar trends in temperature response with density level are present, with the lower density materials exhibiting higher thermal conductivity. Also, the iso-q model performed in a superior manner to the flat-faced model of the same material density.

Pre- and post-exposure black and white photographs of all models evaluated for Douglas Aircraft are presented in Figures 60 through 80. Color film footage of the model behavior during exposure to the high-temperature environment, has been forwarded to Douglas personnel.

2.3 Calibration of Test Conditions

The low-density ablator test program was performed in a hyperthermal plasma arc test facility (ElectroThermal Facility) located at Space-General Corporation. A low pressure/high enthalpy plasma arc generator was used in conjunction with a supersonic Mach 3 three-inch exit diameter contoured nozzle exhausted into an evacuated test chamber. Reconstituted air (79% nitrogen and 21% oxygen) was used as the test medium to simulate the re-entry atmosphere.

The test procedures used in performing the evaluation of the candidate low-density ablator materials consisted first of establishing the operating conditions of the plasma arc generator and nozzle system at which the specified re-entry stagnation enthalpy, pressure and model heating rates would be attained. The generator and nozzle components are of water-cooled copper and tungsten, with contamination rates well below 0.1% by weight. Five test conditions were selected as the standard simulated re-entry conditions; a sixth condition was also utilized for evaluating the Boeing Carborazole material. These selected test conditions are defined by:

Test Condition	Gas Stagnation Enthalpy (Btu/lb)	Model Stagnation Pressure (atm)	Model Heat Flux (Btu/ft^2-sec)
1	8,200	0.0030	30
2	9,100	0.0071	60
3	10,500	0.0131	90
4	11,000	0.0203	120
5	11,350	0.0320	150
Unassigned	16,110	0.0502	300

Routine calibration data consisting of gas stagnation enthalpy, model stagnation pressure, nozzle stagnation and static pressures, gas flow rates, power input and power losses, were obtained on each model test. Additional calibration data consisting of the model heat flux measurements was obtained using geometrically-similar calibration models instrumented with asymptotic calorimeters to ascertain the model stagnation point heat flux. Two calibration models were fabricated and instrumented for this purpose - one each of the flat-face and iso-q model configurations.

The gas stagnation enthalpy was based on the energy balance method in which the power input, power losses to the water-cooled portions of the plasma generator and nozzle system, and gas flow rates are measured and reduced to the proper form for calculating the enthalpy in terms of Btu's/lb. The power lost by radiation is neglected in this method; however, previous experimental measurements of the power lost due to radiation have indicated this amount to be less than 1% of the total power input, and hence well within the measurement accuracy of this system. This method of enthalpy calculation represents an average enthalpy at the nozzle exit plane, and does not account for 'hot cores' or cold-wall boundary layer effects. Hot cores have been eliminated in our generator-nozzle systems by proper injection of the gas constituents and optimized design of the nozzle contour (expansion section) and the mixing (plenum) chamber. Consequently, there is virtually no 'hot coring' of our plasma streams. Since the nozzle walls are cool compared to the hot gas flow, there are cold-wall boundary layer effects which tend to cause peak heating in the center of the plasma stream. Surveys with enthalpy probes (obtained on similarly-designed generator-nozzle systems) have shown this boundary layer effect to result in centerline enthalpies no more than 5% higher than the average gas stagnation enthalpy calculated by the energy balance method, at the test conditions tabulated in the table above.

Model stagnation pressure was measured with our facility water-cooled pitot probe. Radial surveys of the stagnation pressure were made at radii of 0.25, 0.50, 0.75, 1.00, 1.25 and 1.50 inches; pressure surveys obtained at each of the five heat flux levels are plotted in Figure 81. There is some indication

at the highest heat flux operating point (Test Condition No. 5 - heat flux of 150 Btu/ft^2-sec) that a weak shock diamond is present, as evidenced by the slight dips in the pressure profile at radii of $\pm$ 0.75 inches.

Model stagnation radial heat flux surveys were obtained using a two-inch diameter flat-faced model instrumented with an asymptotic calorimeter located at the stagnation point. These heat flux profiles, presented in Figure 82, were obtained at quarter-inch radial increments (as in the pressure profile surveys) for each of the five test conditions. It is apparent from the plotted surveys that a fairly uniform distribution of heat flux over the two-inch diameter flat-face surface was available in the three-inch diameter test stream. Cold-wall boundary layer effects are evident, particularly at Test Condition No. 5. Shock-wave effects at Test Condition No. 5 are not as apparent as in the corresponding pressure survey presented in Figure 81. This is to be expected since the pressure profile and an enthalpy profile (which was not obtained) complement each other and tend to equalize the heat flux parameter.

Typical environmental parameters and their measurement accuracy levels are presented in Figure 83. Pressure taps appropriately located in the nozzle exit plane and in the plenum (mixing) chamber upstream of the nozzle throat are utilized for measuring the nozzle static and stagnation pressures, respectively.

Gas flow rates are measured using calibrated ($\pm$ 1% accuracy) critical flow orifice plates in conjunction with $\frac{1}{4}$% accuracy Heise pressure gauges for the upstream pressure measurements. A mixture of 79% dry nitrogen and 21% oxygen is injected into the arc chamber where it is thoroughly mixed and heated to provide uniform concentration of the oxygen in the three-inch diameter test stream.

2.4 Comparison of Low-Density Ablator Performance

The heat flux levels chosen for the thermal test series on the low-density ablators are representative of levels which would be encountered on the major body surfaces of an ablative lifting re-entry vehicle. Heat fluxes up to 150 Btu/ft^2-sec were emphasized because of potential problems with recession during peak heating near the forward portion of the body. Air enthalpy levels ranged from 8200 Btu/lb at the lowest heat flux to 11,350 Btu/lb at the highest heat flux. Model stagnation pressures correspondingly ranged between 0.0030 and 0.0320 atmospheres. Test duration was typically 600 seconds at the two lower heat flux levels and somewhat less at higher heat fluxes.

It is recognized that these results are preliminary and do not constitute an unqualified and final characterization of the materials tested. However, the prime intent of this test program was to obtain additional data on newly-developed candidate materials and to compare this data with that obtained previously on other low-density ablators. The front surface brightness temperature and recession results and the back-face (1.0-inch depth) temperature results are considered valid and comparable in most cases. These results furnish an initial comparison of ablation performance for these materials.

An effective recession rate for the thermal tests was calculated from the length change of the specimen and test duration. The initial and final length measurements were always made at the centerline of the specimen, which usually corresponded to the point of maximum recession. Many of the low-density ablators exhibited swelling characteristics at the lower heat flux level; consequently, data for the models tested at heating rates of 60, 90, 120 and 150 Btu/ft^2-sec are used for comparison purposes.

Figure 84 is a bar graph showing the recession rates calculated for each of the above four heat flux levels. Swelling rates are represented by plus signs; all other data is for length loss during the test. In those instances where more than one model of a material was tested at identical heat flux conditions, the data was averaged (unless there was obviously something wrong with either the test conditions or the model test results).

Of the new candidate materials evaluated under this contract (Douglas SMORS-25, Armstrong Cork No. 2755, and Boeing Carborazole materials), the Douglas material exhibited superior recession characteristics. The Boeing Carborazole material ranked high in recession rate along with a number of previously-tested materials, such as the General Electric ESM 1001 and 1004, and McDonnell S-6 ablators.

The front-surface brightness temperature of each specimen was measured using a Leeds and Northrup optical brightness pyrometer. In most cases, a stabilized surface temperature was reached and maintained throughout the major portion of the exposure period. This stabilized surface temperature data was used for preparing the bar graphs presented in Figure 85. The surface temperatures presented in this report and in the bar graph in Figure 85 have not been corrected for emissivity values, but are the apparent brightness temperatures as read directly with the optical brightness pyrometer. The pyrometer view of the ablator surface was at an angle of 30^o to the model stagnation surface. A 0.500-inch thick quartz viewing port was located in the optical path between the pyrometer and the model being tested; wavelength corrections for the quartz viewing port have not been applied to the surface temperatures presented in this report.

The back-face temperature was measured using a chromel/alumel thermocouple imbedded in the ablator material at a depth of 1.0-inch from the stagnation point of the model; refer to Figures 1 and 2 for details of thermocouple installation. Although the temperature-time histories presented in Figures 86 and 87 are confusing, it is apparent that the Douglas SMORS-25 iso-q model tests (using the 32 lb/ft^3 version of the SMORS-25 material) resulted in superior performance in terms of its greater insulative characteri[illegible]ics. The Armstrong cork material behaved similarly to the other low-density ablators previously reported (Ref. 2, Welsh, et al, 1966).

The following table has been prepared to provide the reader with an overall summary of the low-density ablators previously evaluated and the three additional ablators considered under this contract.

TABLE 8

SUMMARY OF LOW-DENSITY ABLATORS EVALUATED

Material Designation	Material Supplier	Density of Virgin Material-lb/ft^3	Description of Material
ESM 1001	General Electric	30 - 35	RTV-60 silicone elastomeric resin system with 4.3% asbestos and 0.8% glass fillers.
ESM 1004	General Electric	30 - 35	RTV-560 foamed phenyl silicone base elastomeric resin system with 12% aluminum silicate fibers as filler.
Avcoat 5026-39	AVCO Corporation	30 - 35	Epoxy resin system filled with silica and glass fibers and phenolic microballoons.
MAC S-6	McDonnell Corporation	30 - 35	Foamed and filled silicone elastomeric.
Thermolag T-500	Emerson Electric	35	Inorganic salt, organic binder system.
Purple Blend	NASA/Langley	32.6	Elastomeric silicone resin with phenolic microballoons.
Phenolic Nylon	NASA/Langley	32.6	Phenolic resin and microballoons and Dupont nylon.
Cork No. 2755	Armstrong Cork Company	30.0	Cork (natural resin foam) with a phenolic resin.
Carborazole	Boeing Aircraft Company	31.0	Organic elastomeric resin system - Proprietary
SMORS-25	Douglas Aircraft Company	20 - 35	Silicone resin with microballoon additives.

STANDARD MODEL DESIGN FOR LOW DENSITY ABLATOR TESTS

2.0-Inch Diameter Flat-Face Cylinder

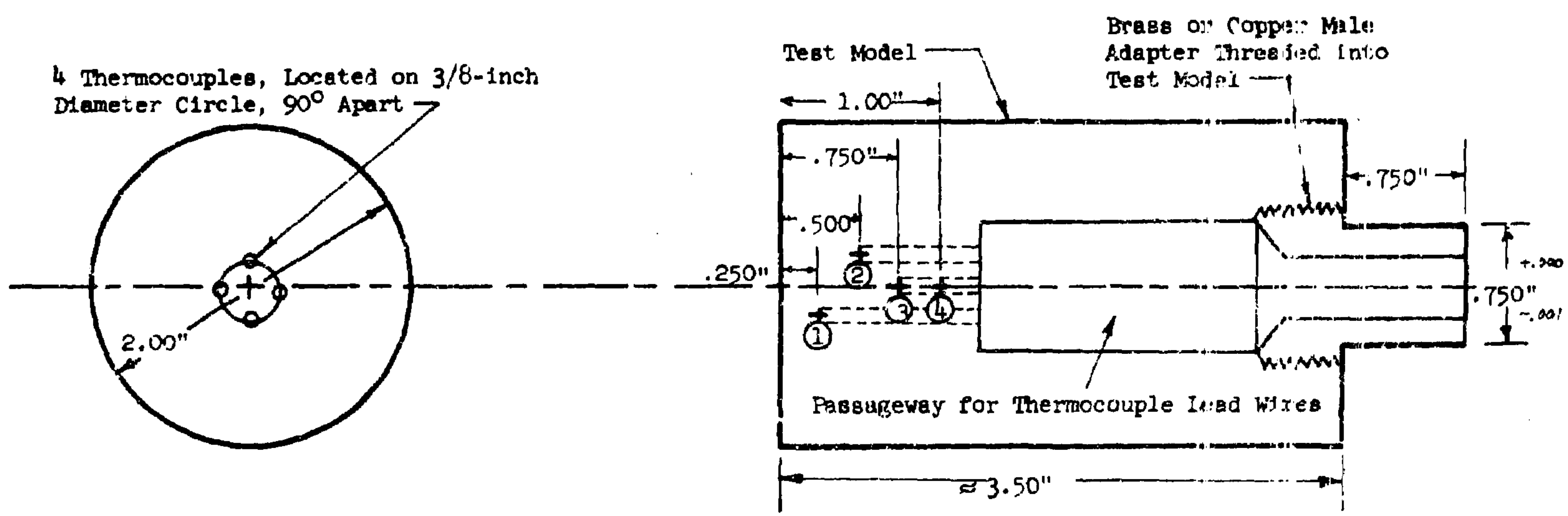

NOTE:
Thermocouples to be Constructed of 36 Gage Chromel/Alumel. Lead Wire Length of 6-7 Ft. Required.

Figure 1-- Standard Model Design for Low Density Ablator Tests

ISO-Q MODEL DESIGN FOR LOW DENSITY ABLATOR TESTS

2.0-Inch Diameter Cylinder

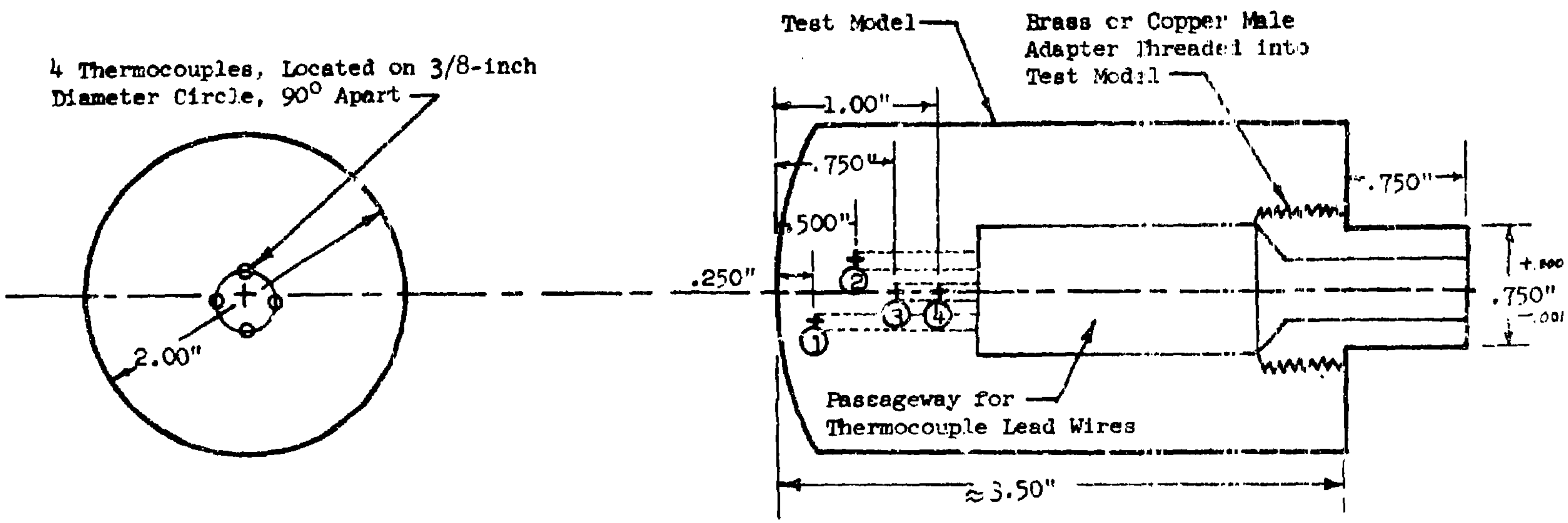

NOTE:
Thermocouples to be Constructed of 36 Gage Chromel/Alumel. Lead Wire Length of 6-7 Ft. Required.

Figure 2 -- Iso-Q Model Design for Low Density Ablator Tests

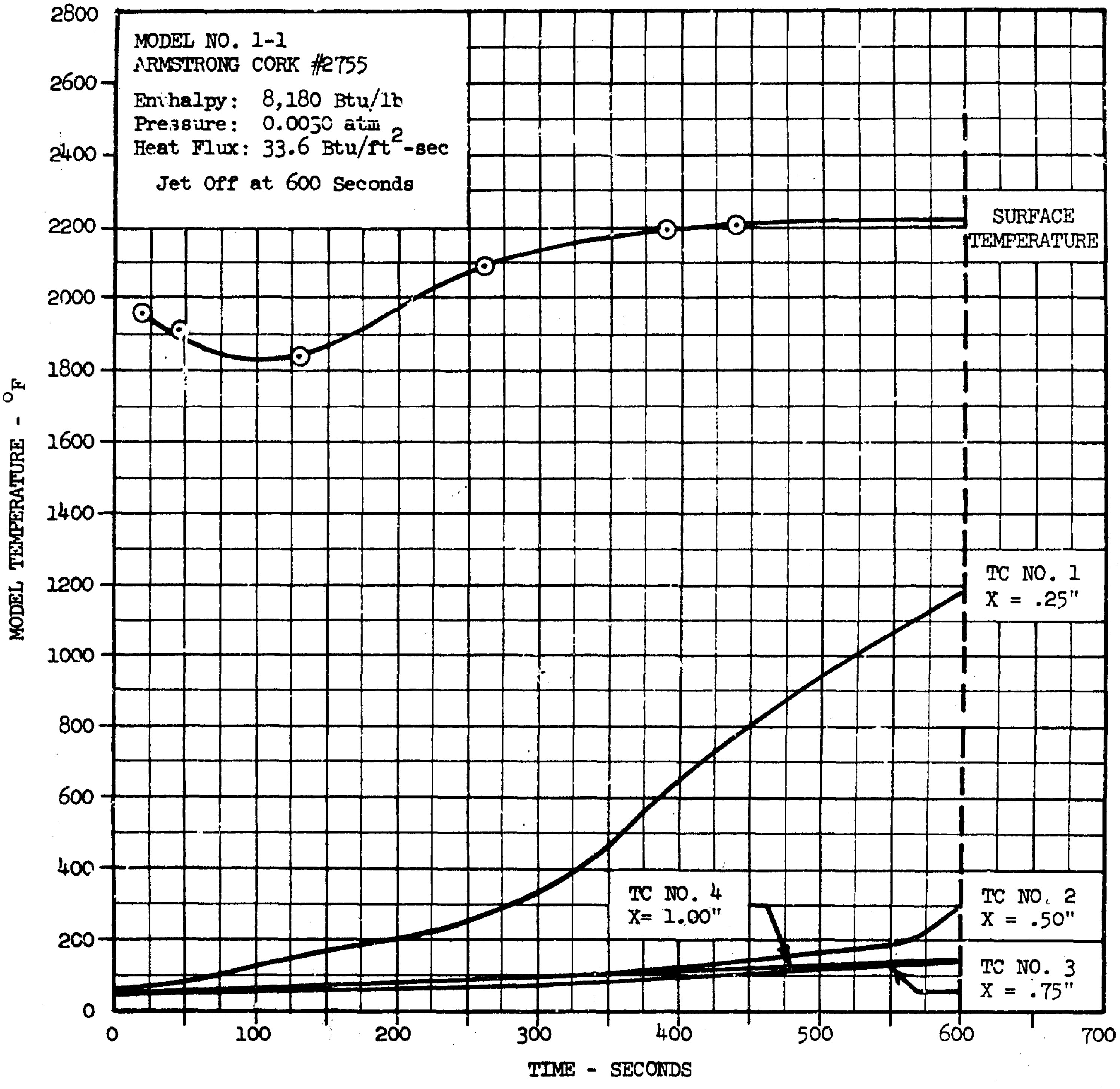

Figure 3 -- Armstrong Cork #2755 Model 1-1 Temperature History

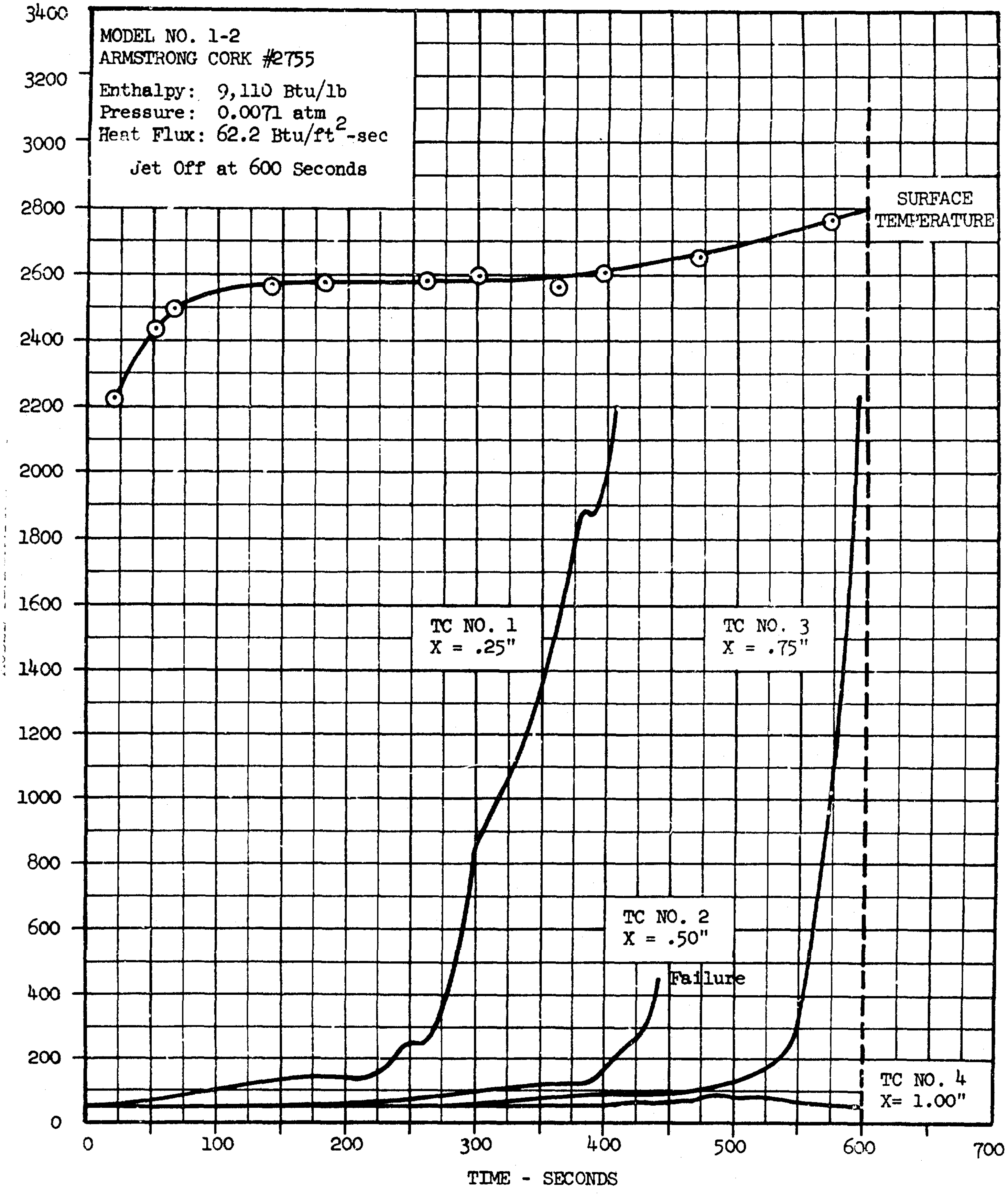

Figure 4 -- Armstrong Cork #2755 Model 1-2 Temperature History

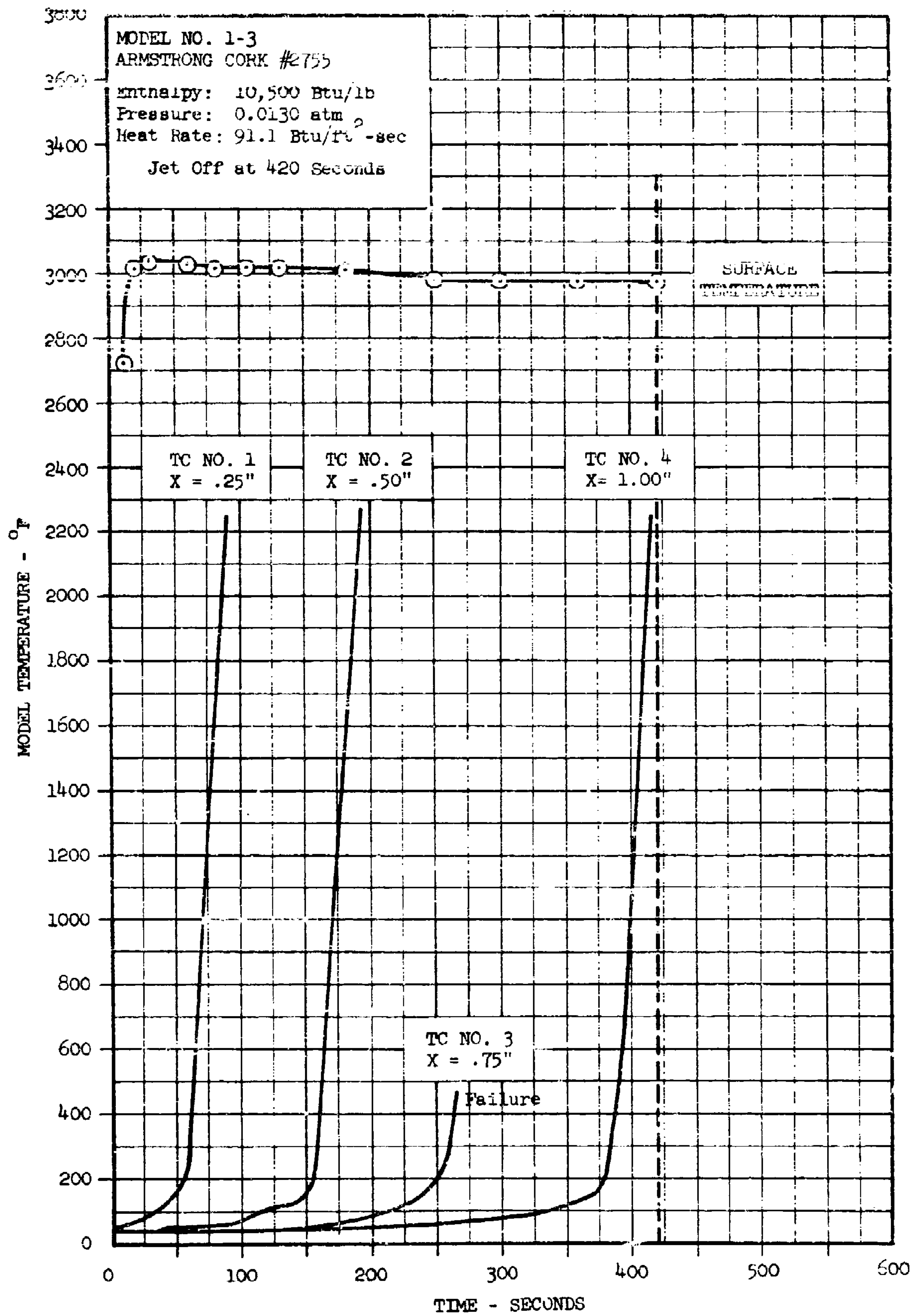

Figure 5 -- Armstrong Cork #2755 Model 1-3 T... History

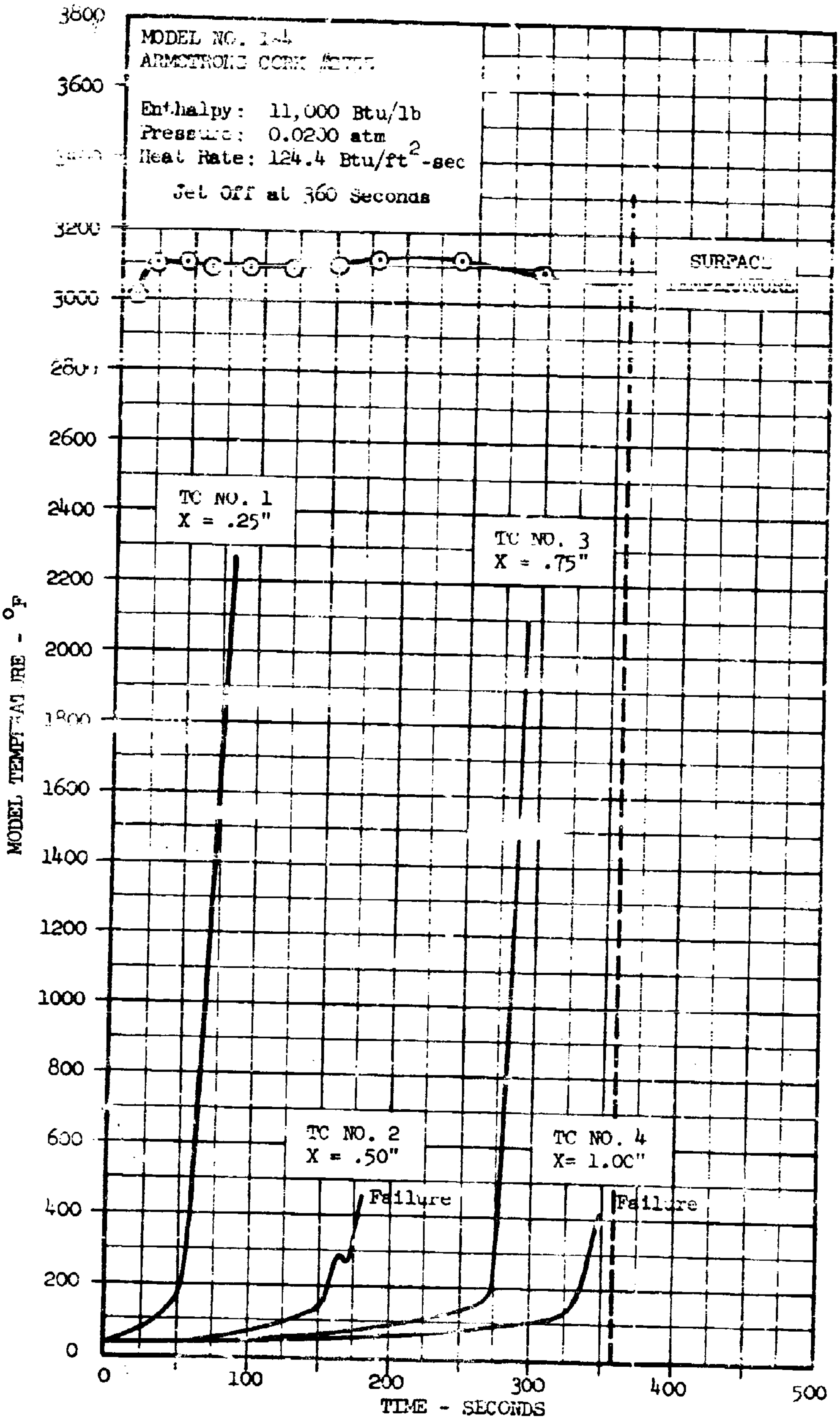

Figure 6 -- Armstrong Cork #2755 Model 1-4 Temperature History

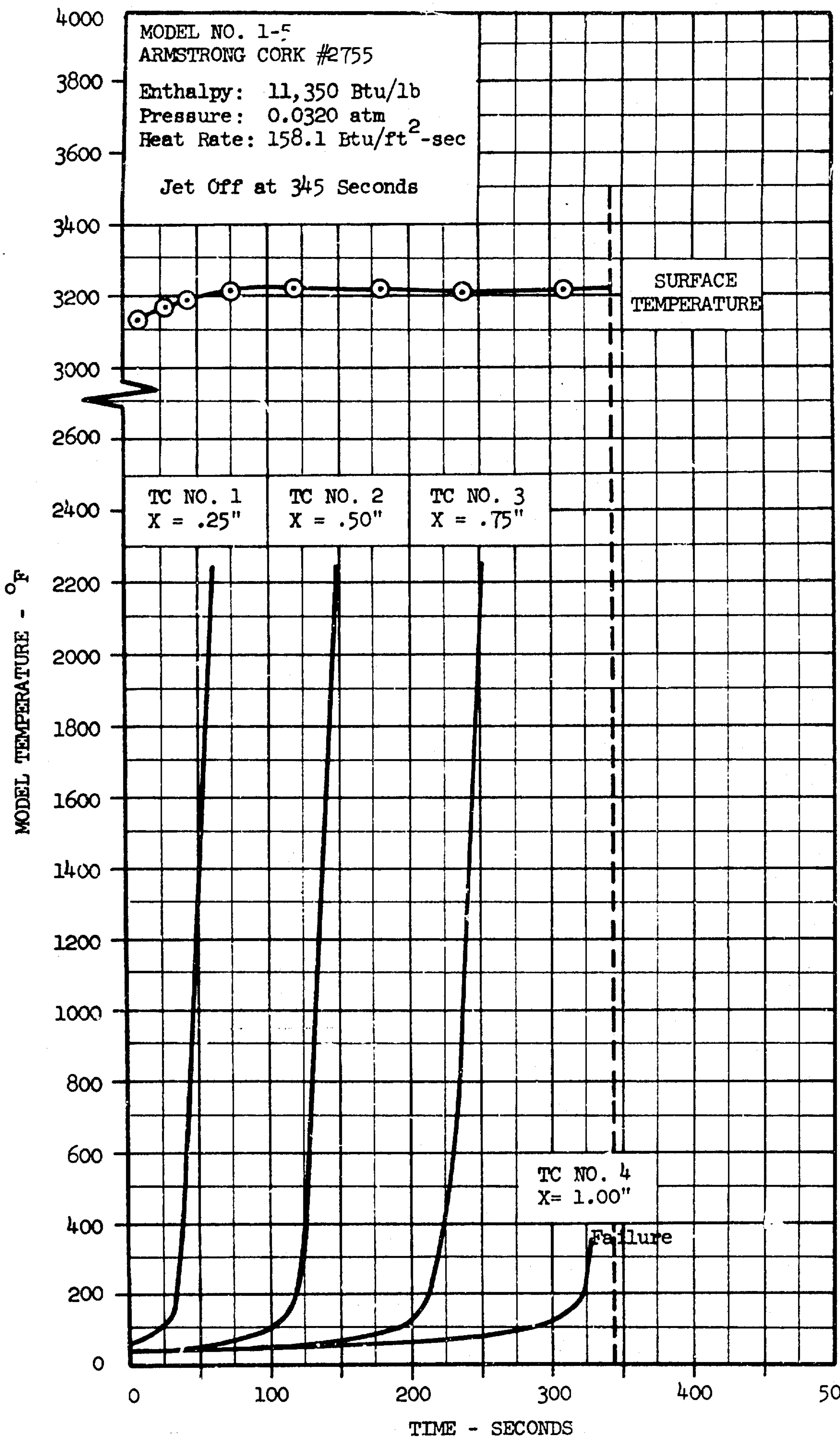

Figure 7 -- Armstrong Cork #2755 Model 1-5 Temperature History

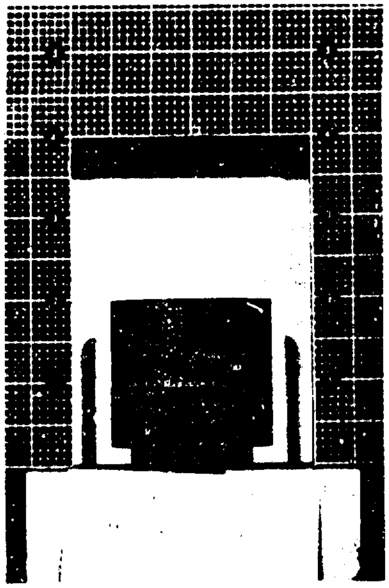

Model 1-1 - Pre-Exposure

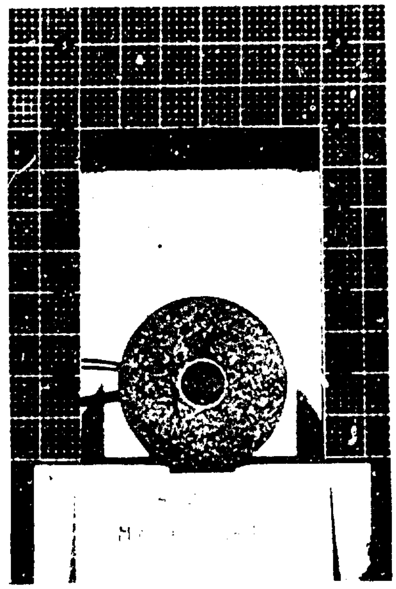

Model 1-1 - Pre-Exposure

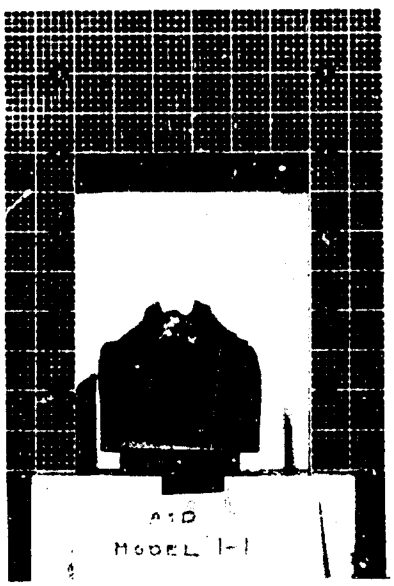

Model 1-1 - Post-Exposure

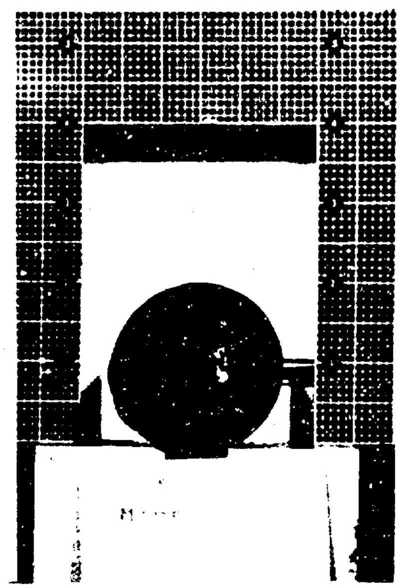

Model 1-1 - Post-Exposure

Figure 8 -- Photographs of Armstrong Cork 2755
Model 1-1

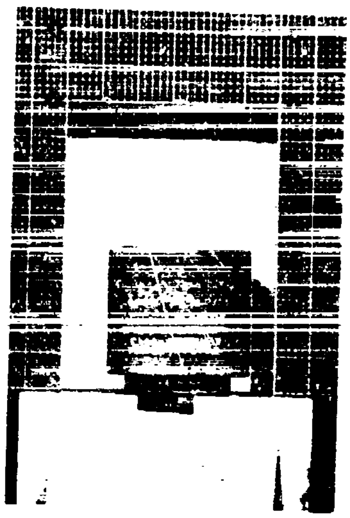

Model 1-2 - Pre-Exposure

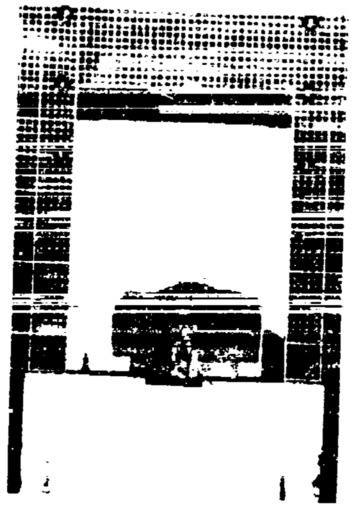

Model 1-2 - Post-Exposure

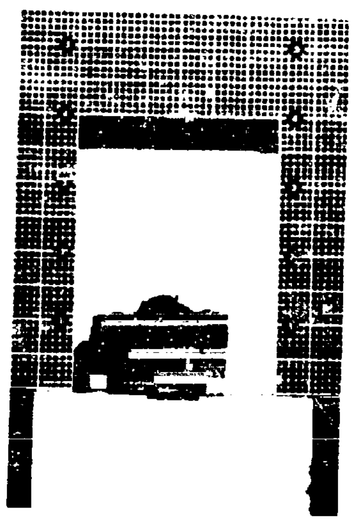

Model 1-2 - Post-Exposure

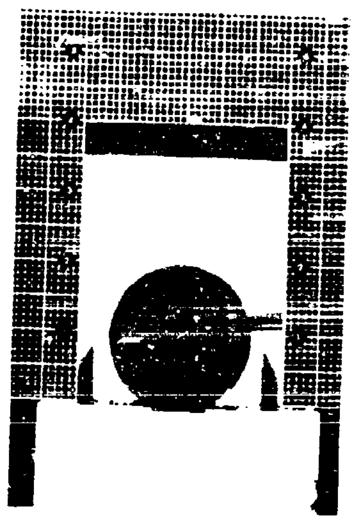

Model 1-2 - Post-Exposure

Figure 9 -- Photographs of Armstrong Cork 2755
Model 1-2

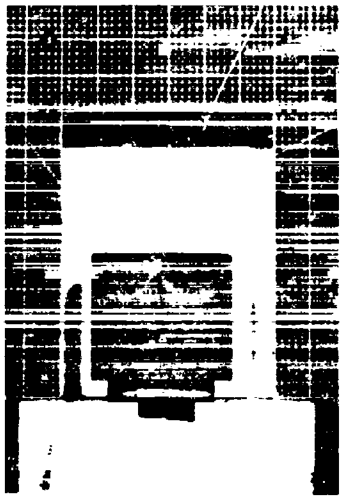

Model 1-3 - Pre-Exposure

Model 1-3 - Post-Exposure

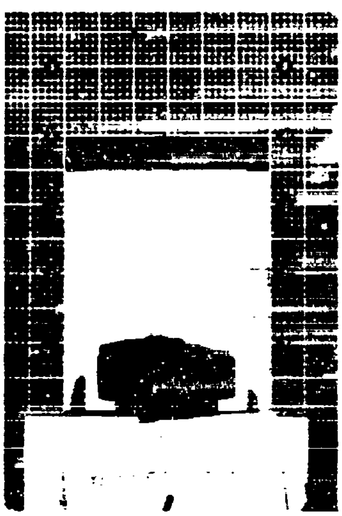

Model 1-3 - Post-Exposure

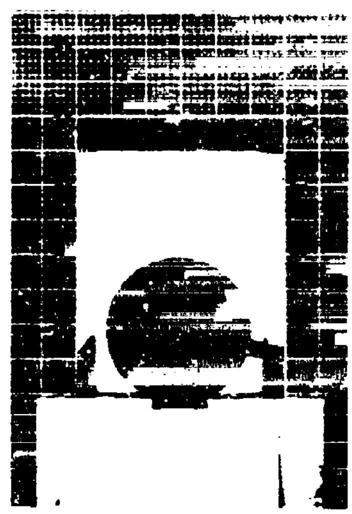

Model 1-3 - Post-Exposure

Figure 10 -- Photographs of Armstrong Cork 2755
Model 1-3

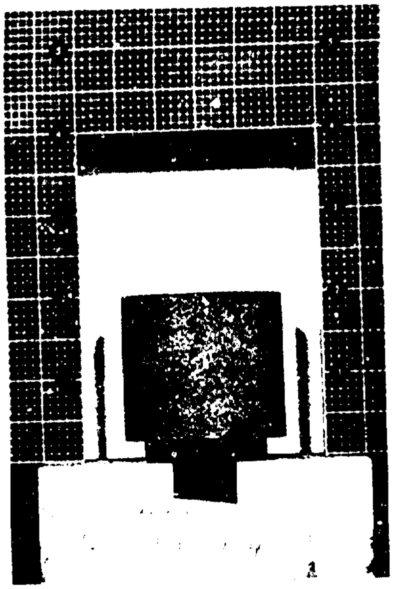

Model 1-4 - Pre-Exposure

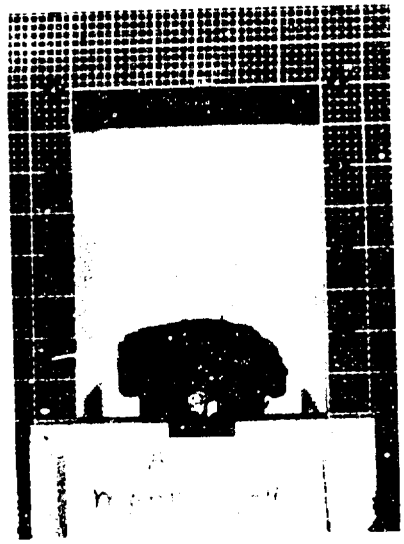

Model 1-4 - Post-Exposure

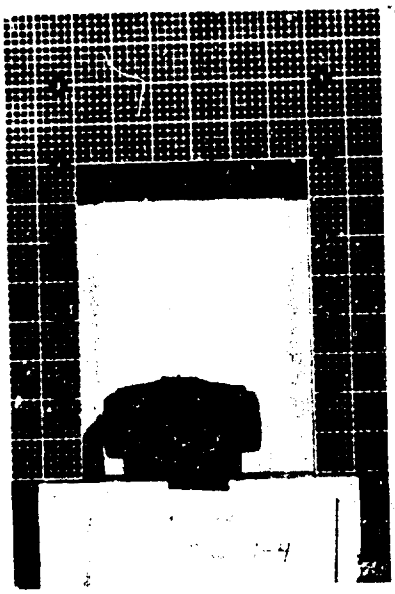

Model 1-4 - Post-Exposure

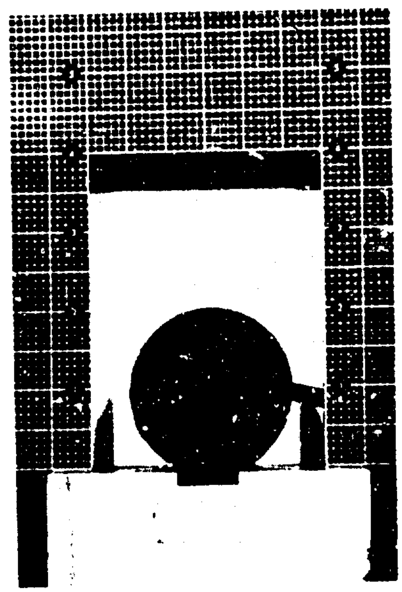

Model 1-4 - Post-Exposure

Figure 11 -- Photographs of Armstrong Cork 2755
Model 1-4

Model 1-5 - Pre-Exposure

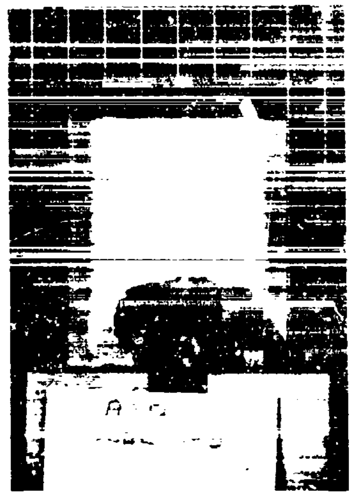

Model 1-5 - Post-Exposure

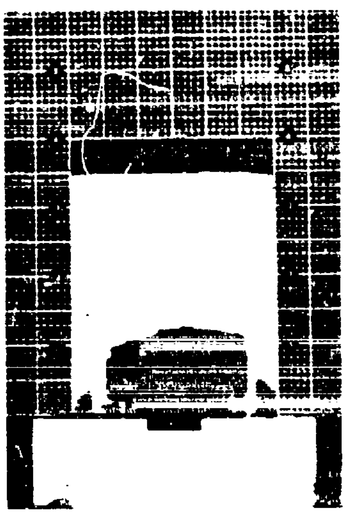

Model 1-5 - Post-Exposure

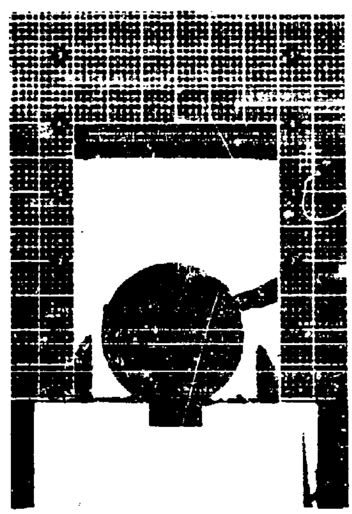

Model 1-5 - Post-Exposure

Figure 12-- Photographs of Armstrong Cork 2755
Model 1-5

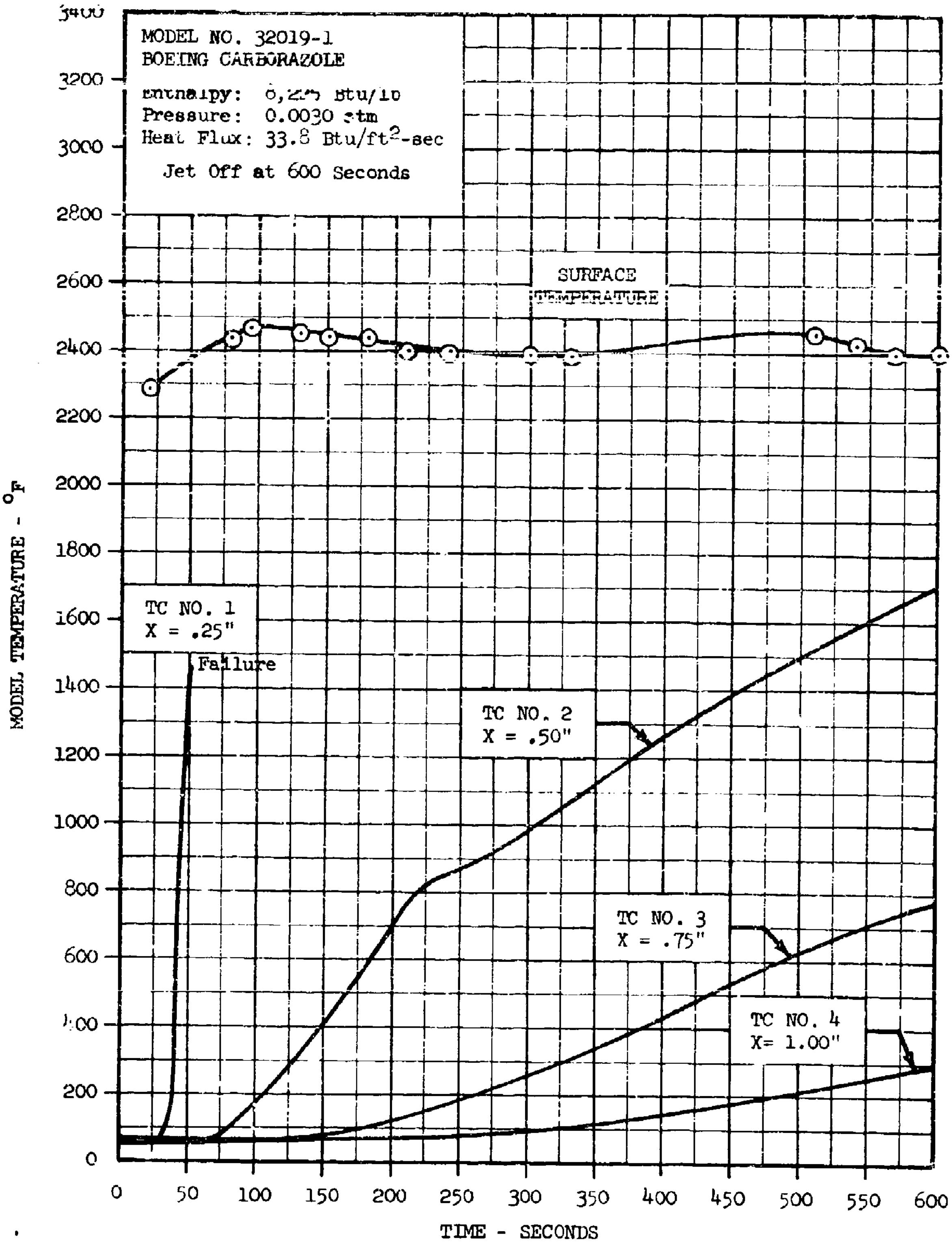

Figure 13 -- Boeing Carborazcle Model 32019-1 Temperature History

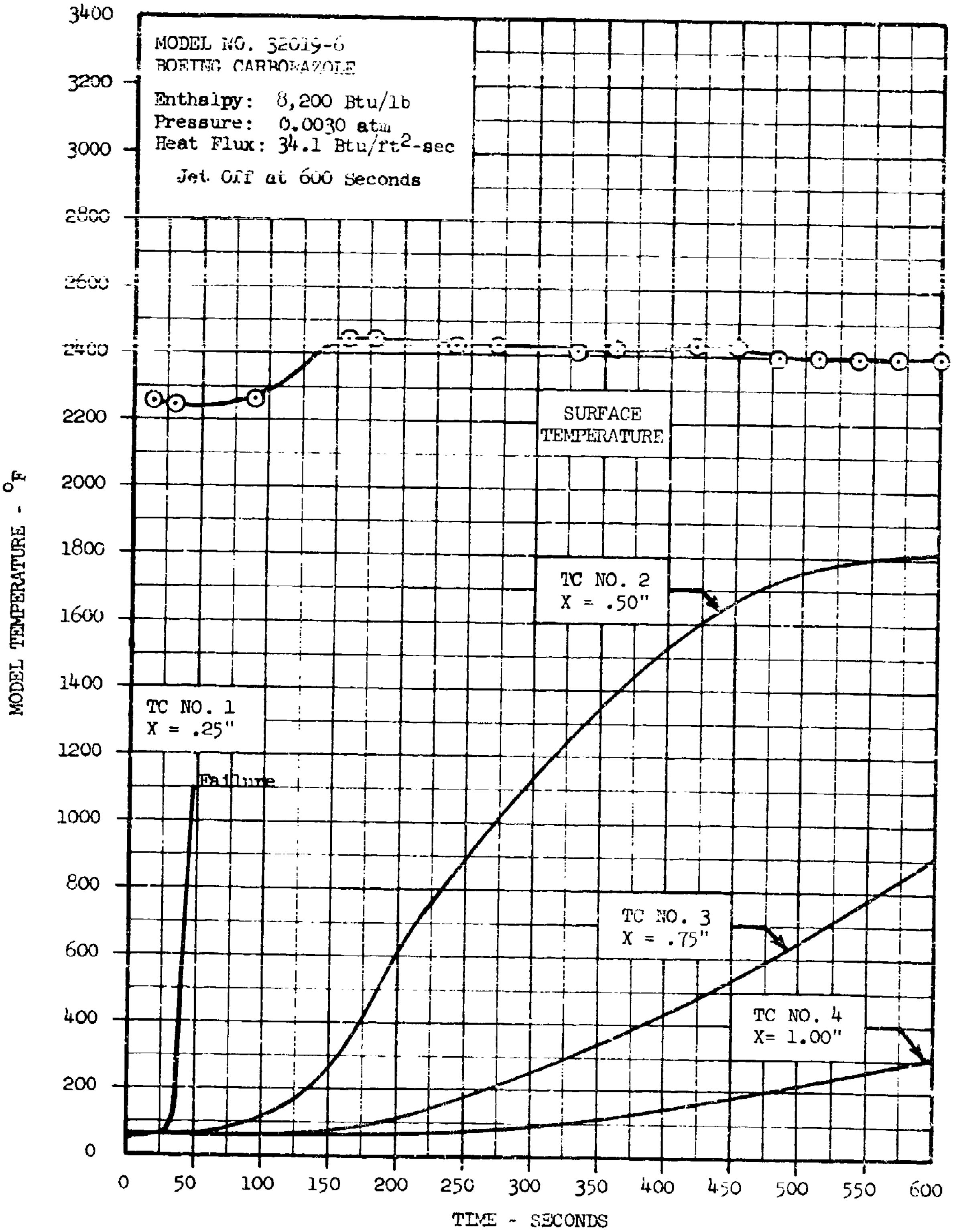

Figure 14 -- Boeing Carborazole Model 32019-6 Temperature History

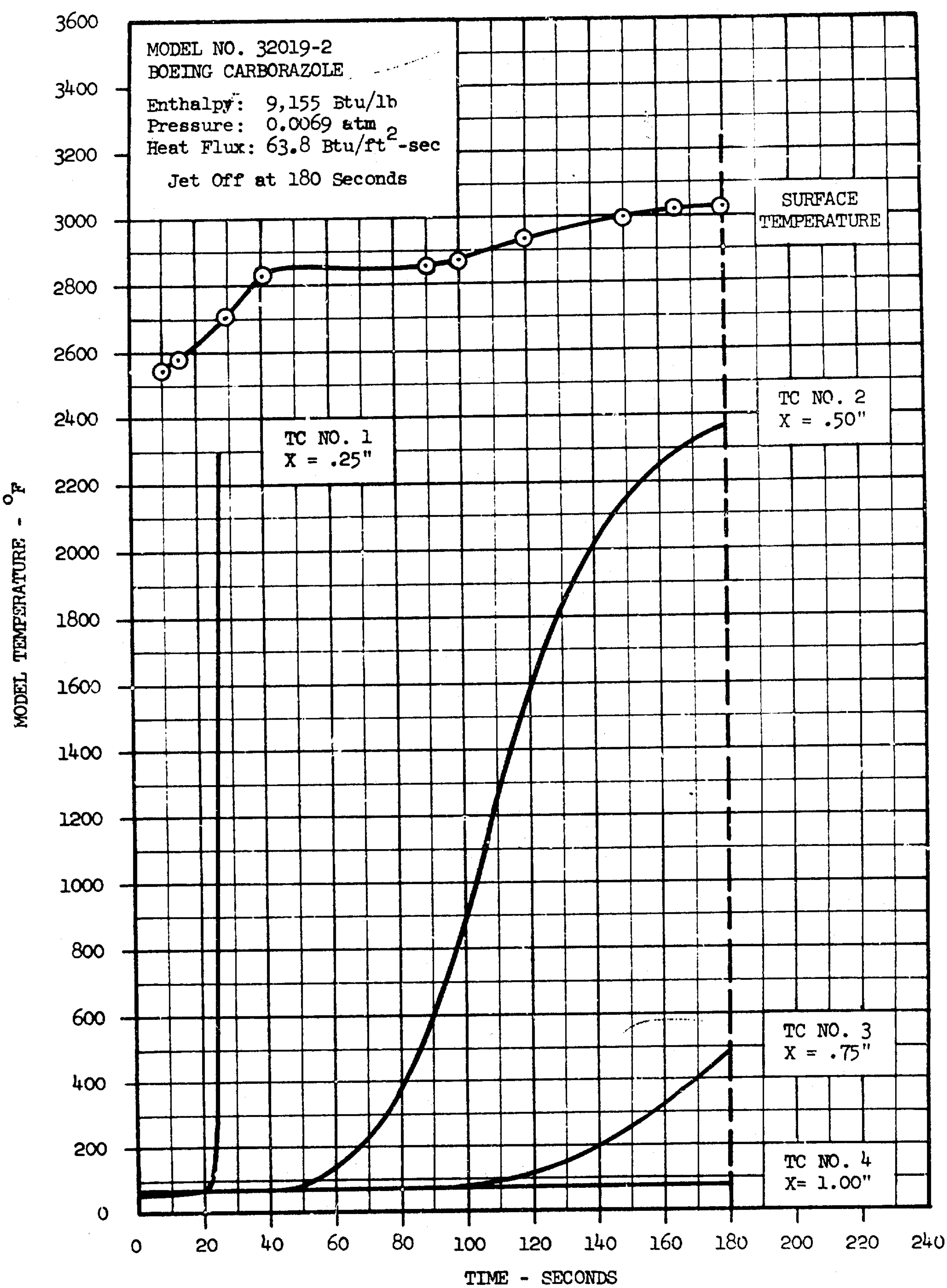

Figure 15 -- Boeing Carborazole Model 32019-2 Temperature History

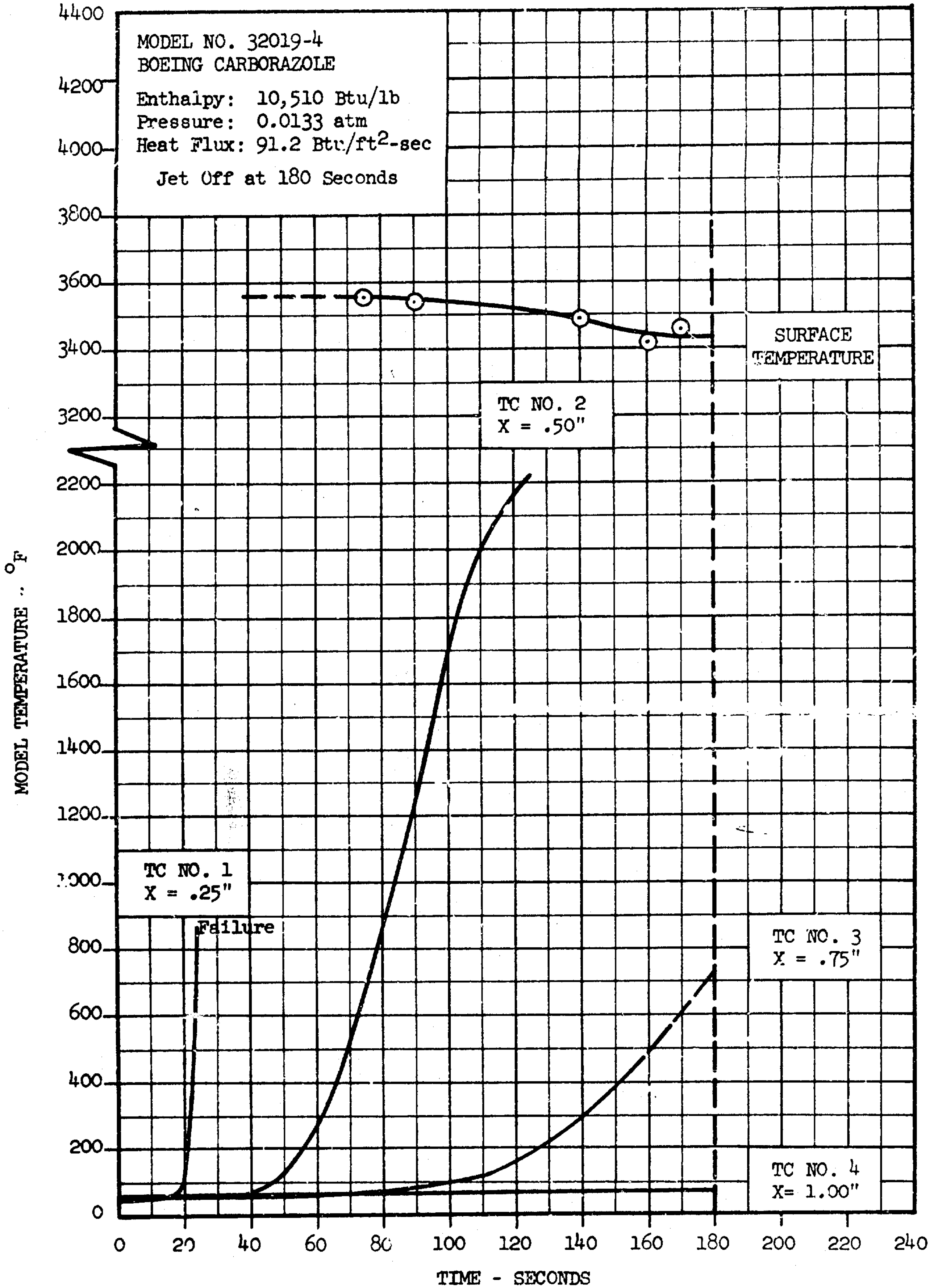

Figure 16 -- Boeing Carborazole Model 32019-4 Temperature History

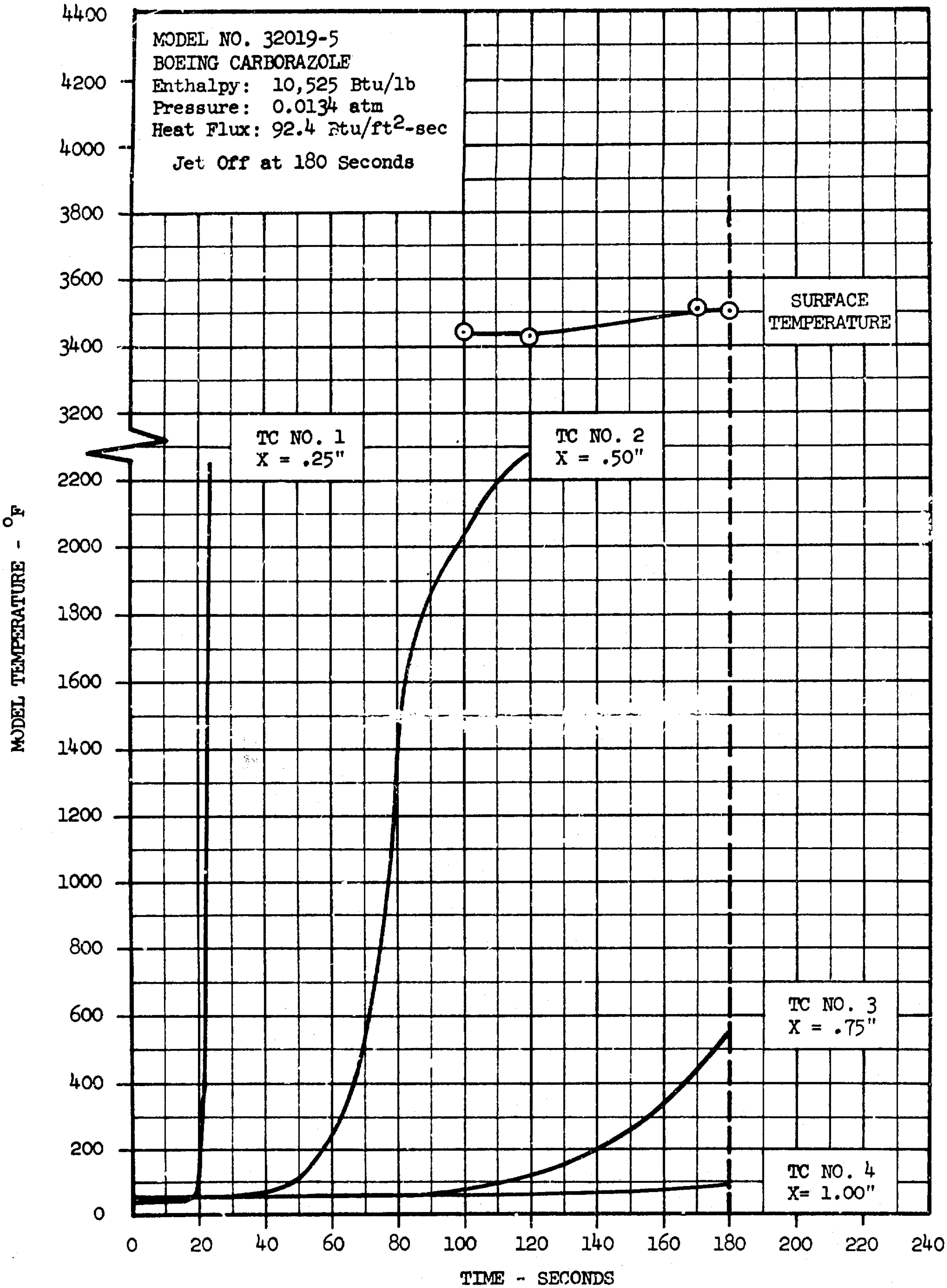

Figure 17 -- Boeing Carborazole Model 32019-5 Temperature History

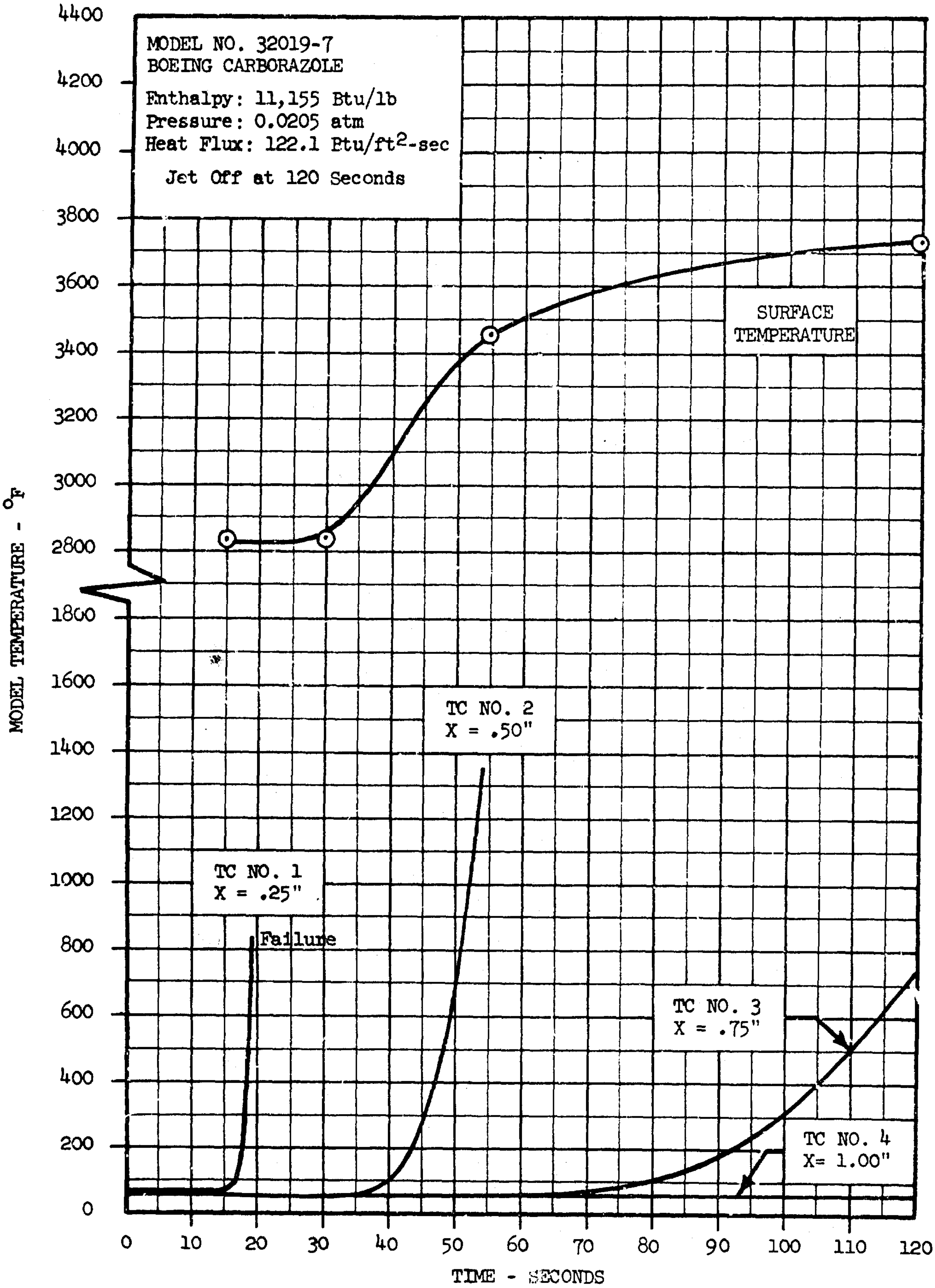

Figure 18 -- Boeing Carborazole Model 32019-7 Temperature History

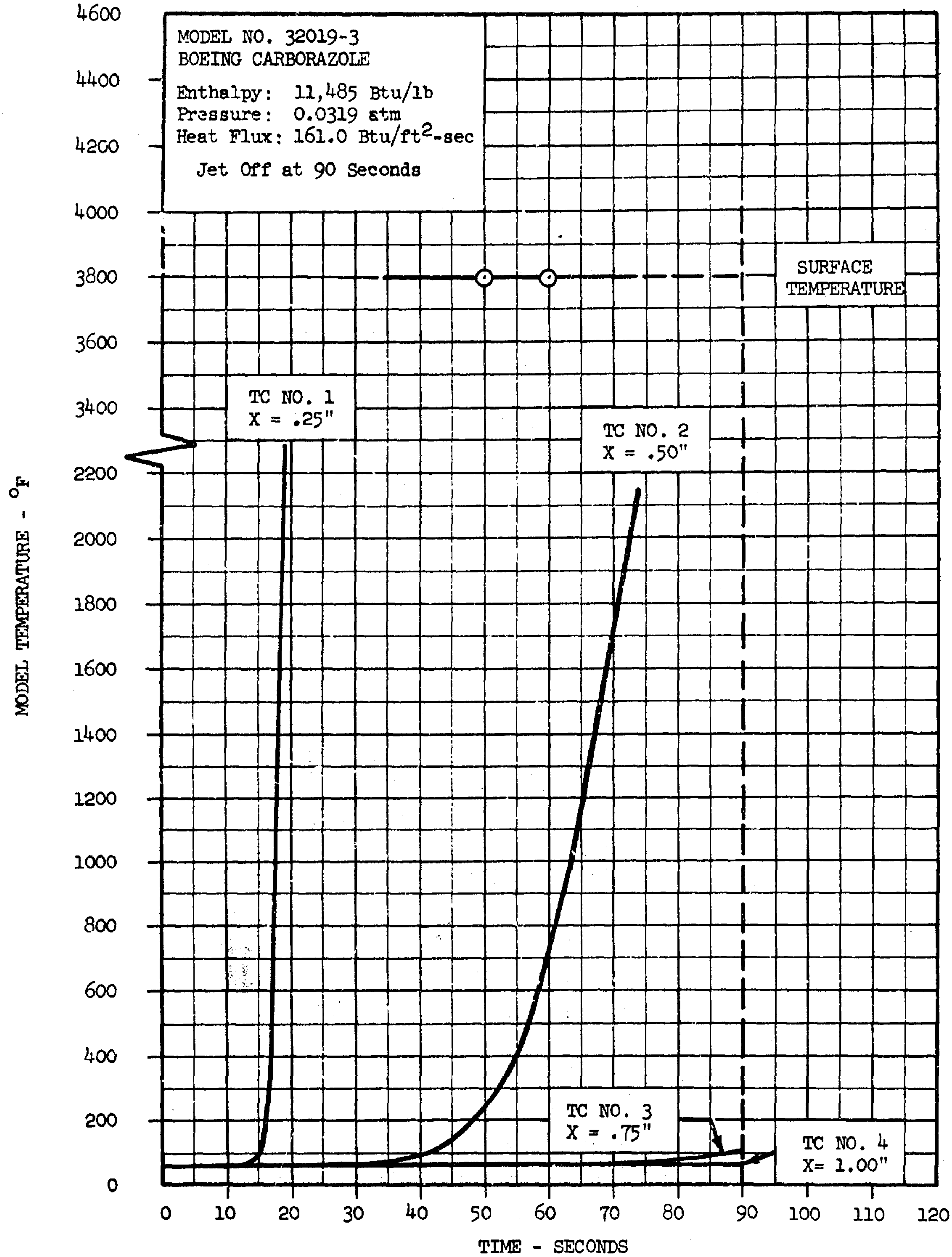

Figure 19 -- Boeing Carborazole Model 32019-3 Temperature History

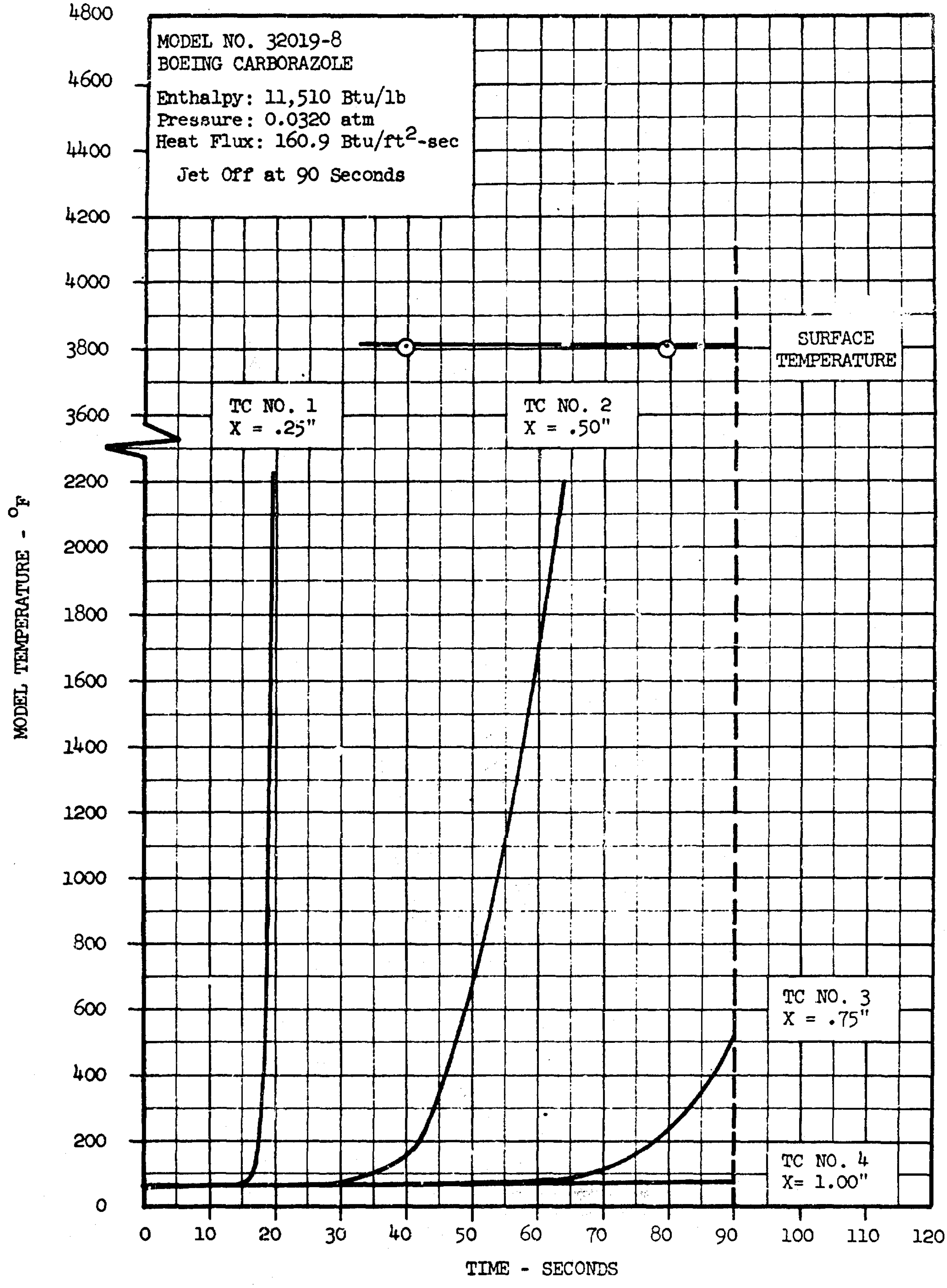

Figure 20 -- Boeing Carborazole Model 32019-8 Temperature History

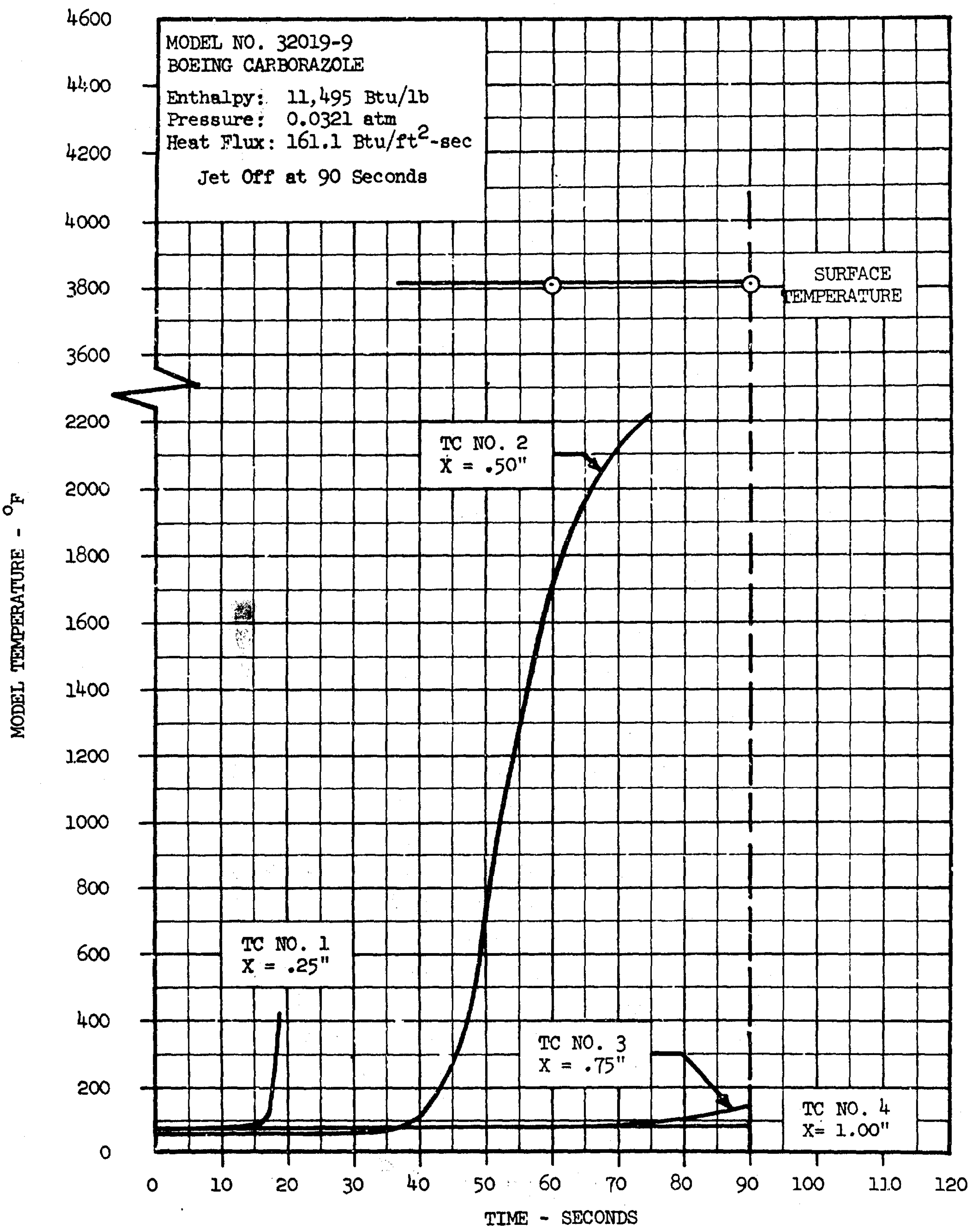

Figure 21 -- Boeing Carborazole Model 32019-9 Temperature History

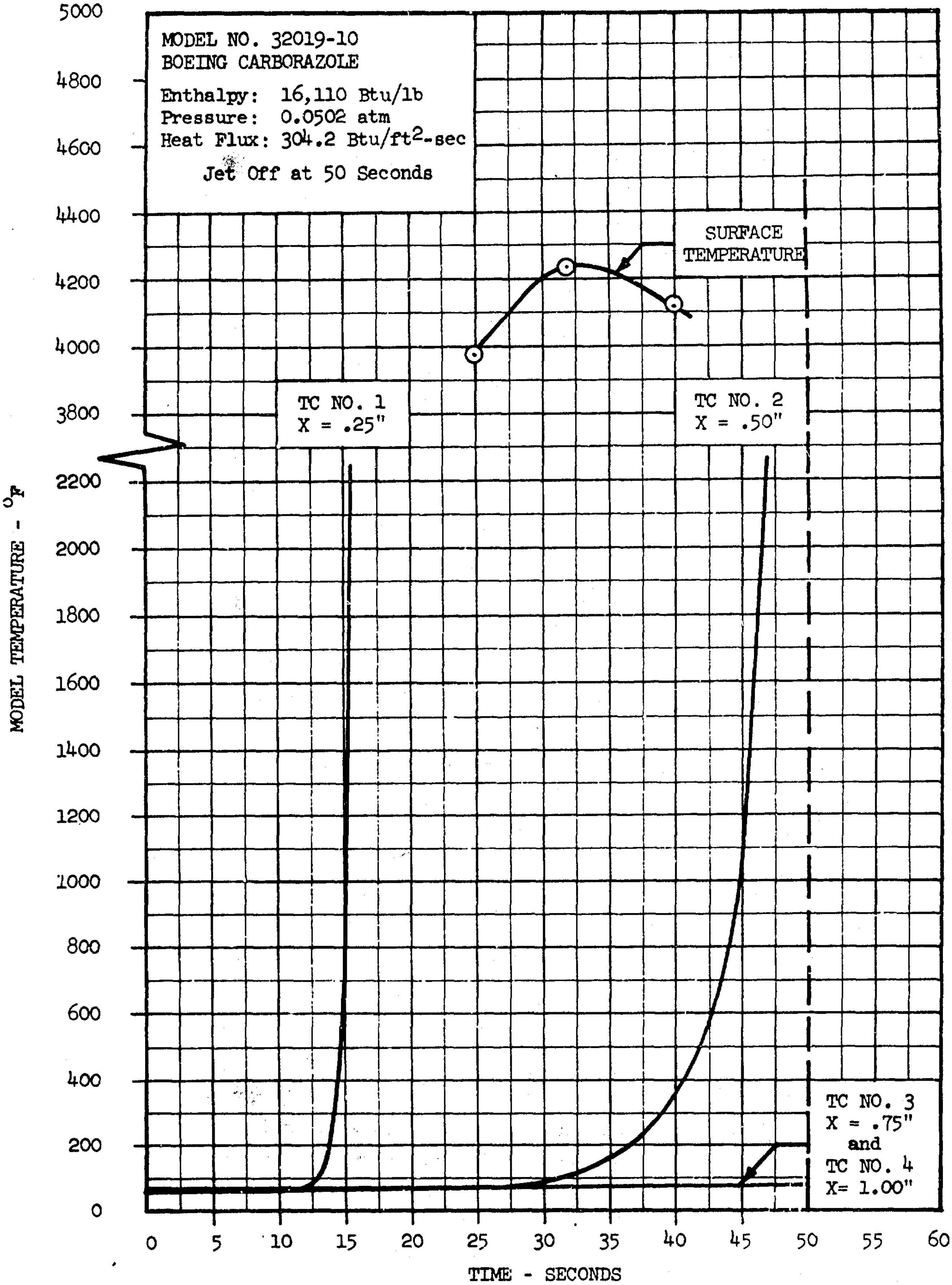

Figure 22 -- Boeing Carborazole Model 32019-10 Temperature History

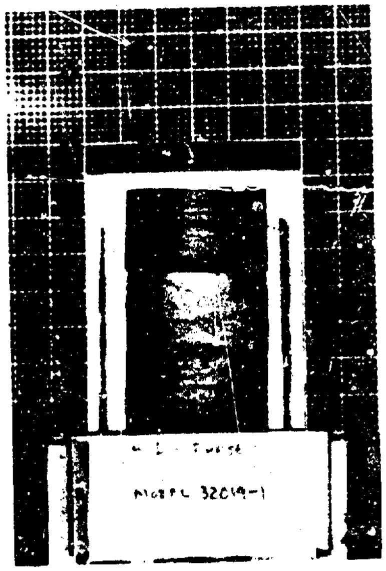

Model 32019-1 - Pre-Exposure

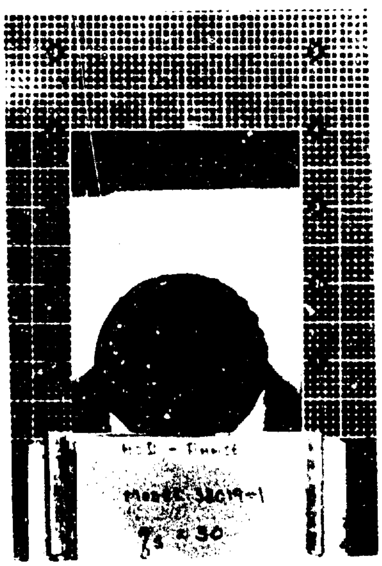

Model 32019-1 - Post-Exposure

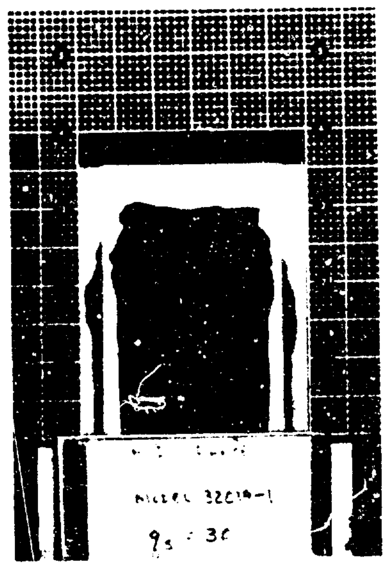

Model 32019-1 - Post-Exposure

Figure 23 -- Photographs of Boeing Carborazole Model 32019-1

Model 32019-2 - Pre-Exposure

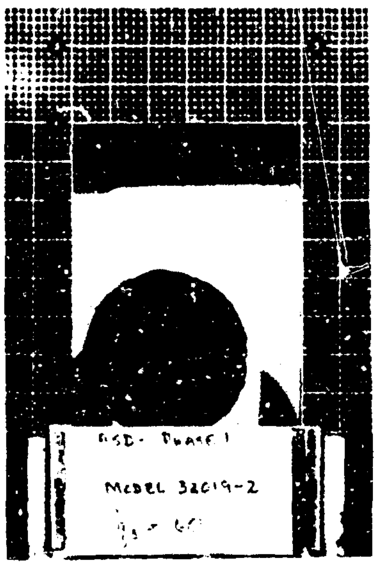

Model 32019-2 - Post-Exposure

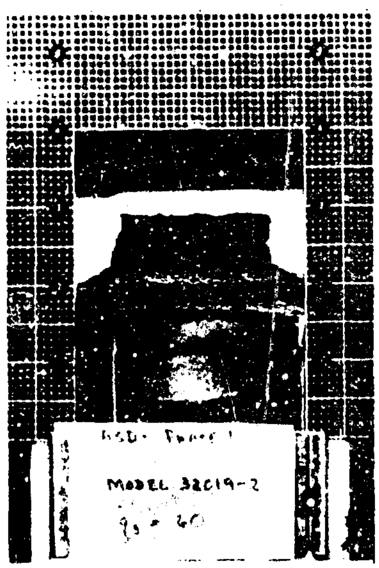

Model 32019-2 - Post-Exposure

Figure 24 -- Photographs of Boeing Carborazole Model 32019-2

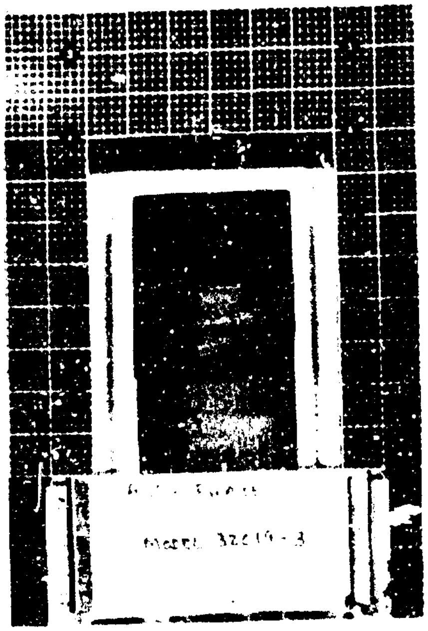

Model 32019-3 - Pre-Exposure

Model 32019-3 - Post-Exposure

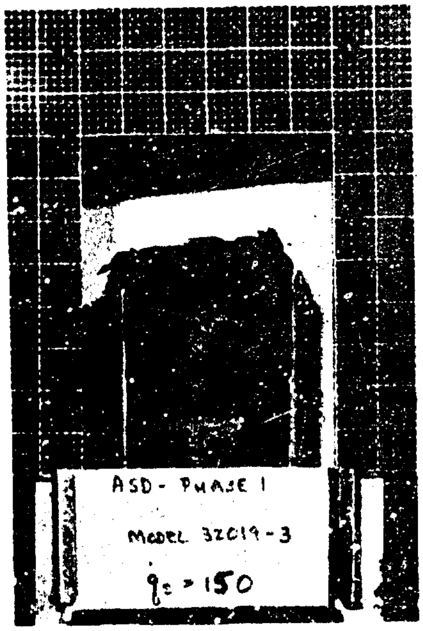

Model 32019-3 - Post-Exposure

Figure 25 -- Photographs of Boeing Carborazole
Model 32019-3

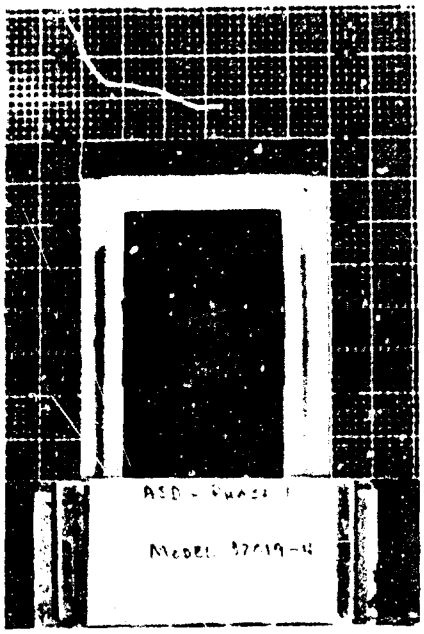

Model 32019-4 - Pre-Exposure

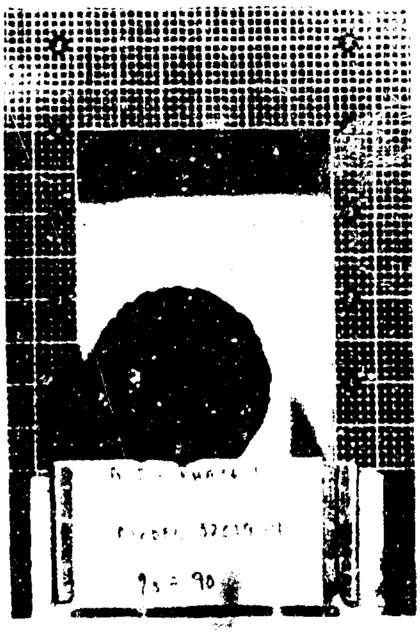

Model 32019-4 - Post-Exposure

Model 32019-4 - Post-Exposure

Figure 26 -- Photographs of Boeing Carborazole Model 32019-4

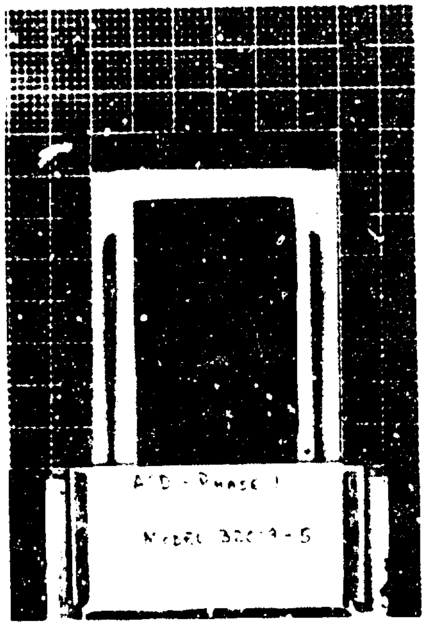

Model 32019-5 - Pre-Exposure

Model 32019-5 - Post-Exposure

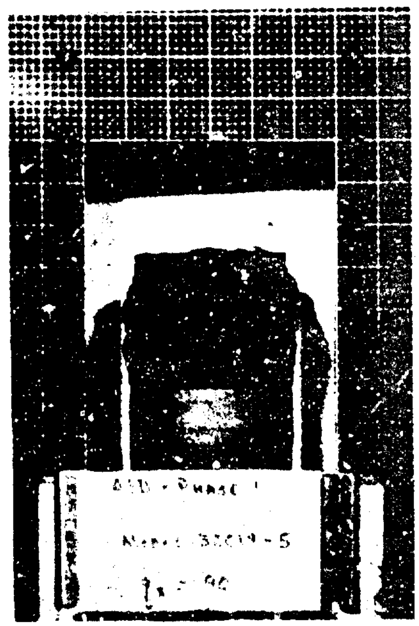

Model 32019-5 - Post-Exposure

Figure 27 -- Photographs of Boeing Carborazole
Model 32019-5

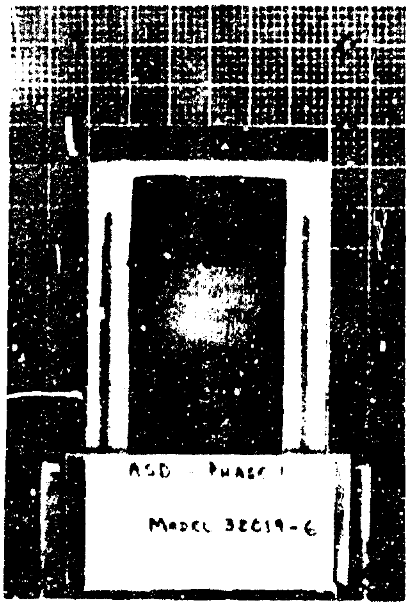

Model 32019-6 - Pre-Exposure

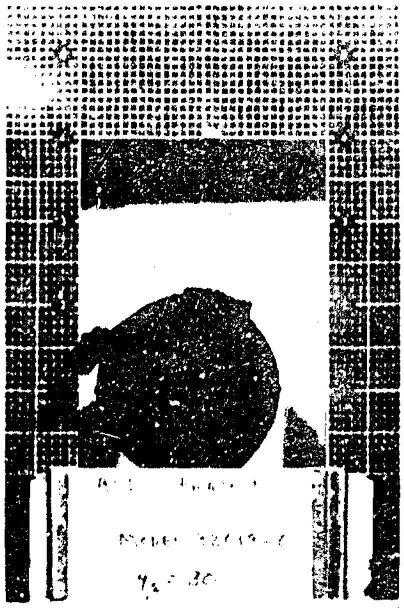

Model 32019-6 - Post-Exposure

Figure 28 -- Photographs of Boeing Carborazole
Model 32019-6

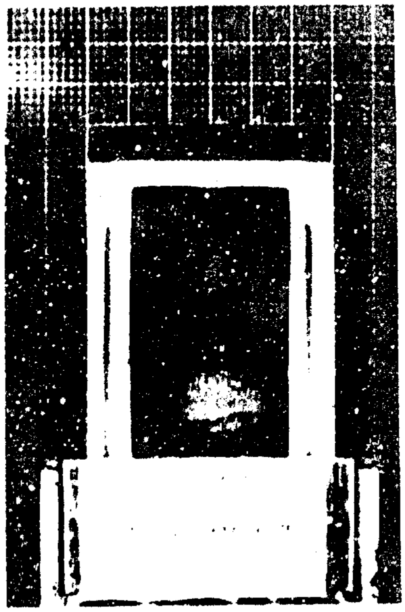

Model 32019-7 - Pre-Exposure

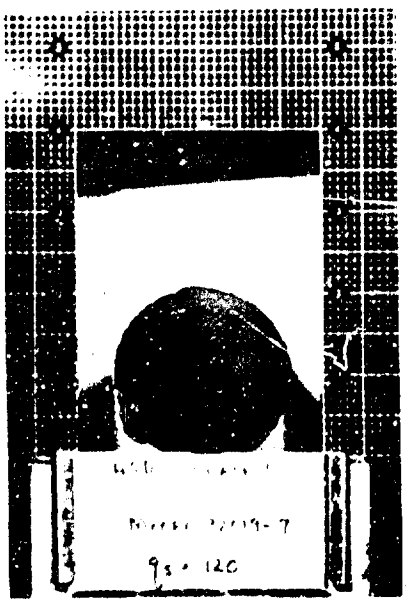

Model 32019-7 - Post-Exposure

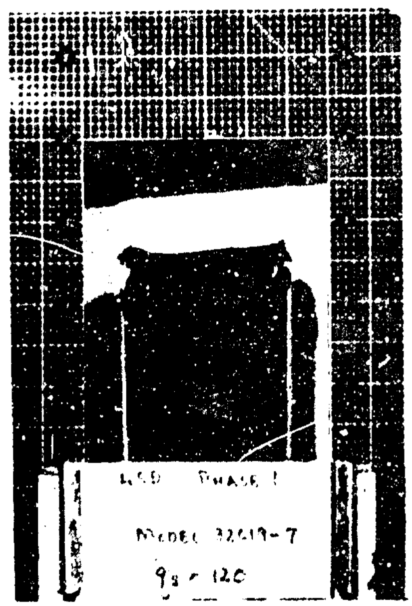

Model 32019-7 - Post-Exposure

Figure 29 -- Photographs of Boeing Carborazole
Model 32019-7

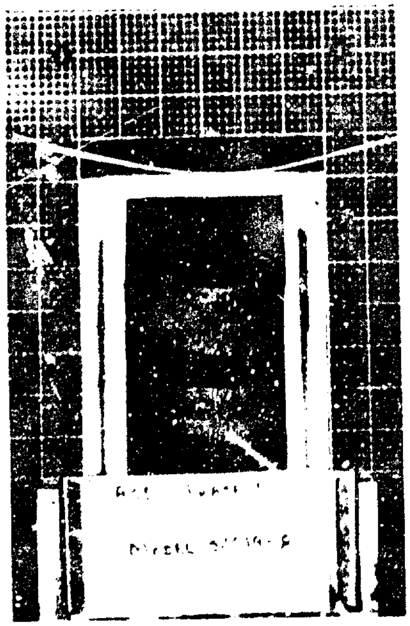

Model 32019-8 - Pre-Exposure

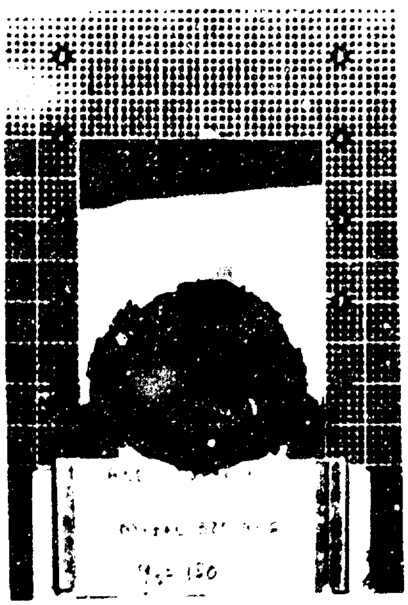

Model 32019-8 - Post-Exposure

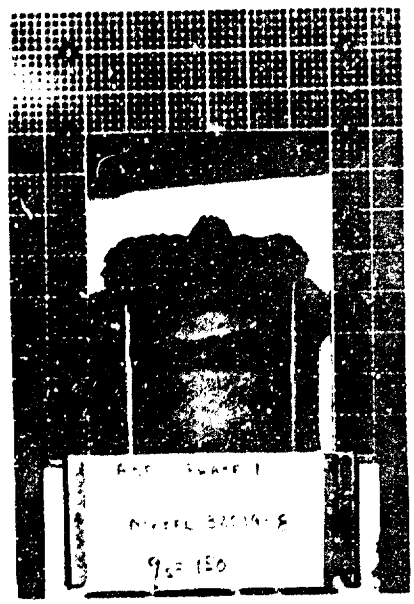

Model 32019-8 - Post-Exposure

Figure 30 -- Photographs of Boeing Carborazole
Model 32019-8

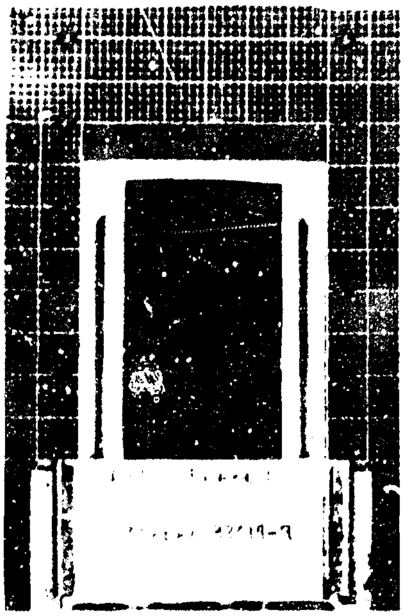

Model 32019-9 - Pre-Exposure

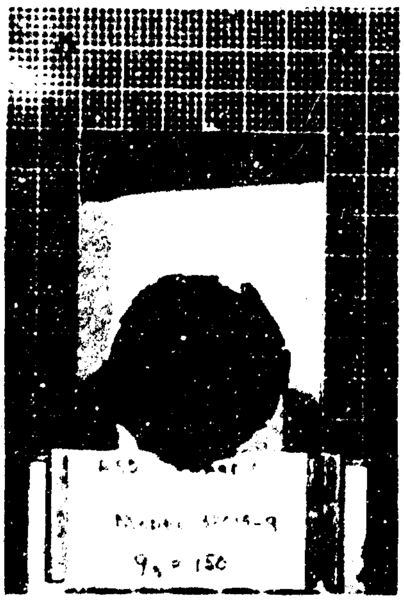

Model 32019-9 - Post-Exposure

Model 32019-9 - Post-Exposure

Figure 31 -- Photographs of Boeing Carborazole Model 32019-9

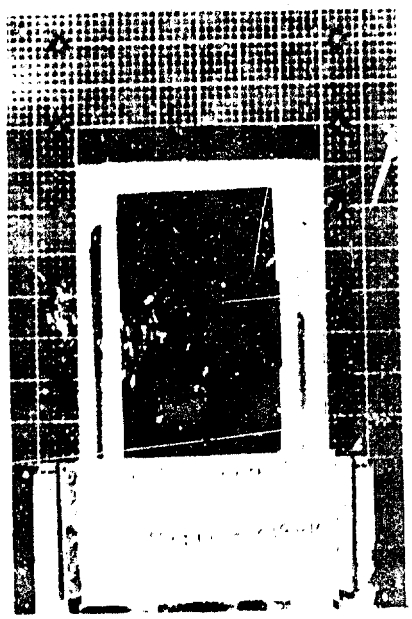

Model 32019-10 - Pre-Exposure

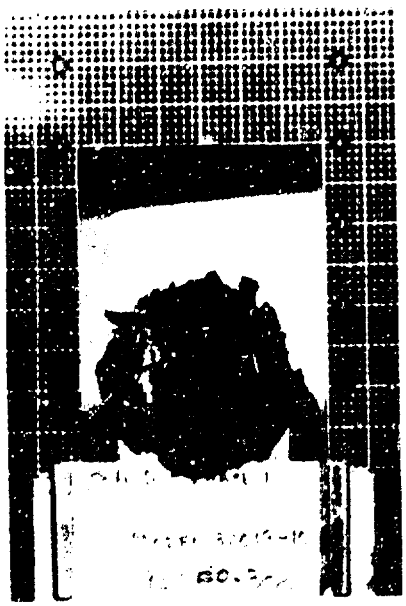

Model 32019-10 - Post-Exposure

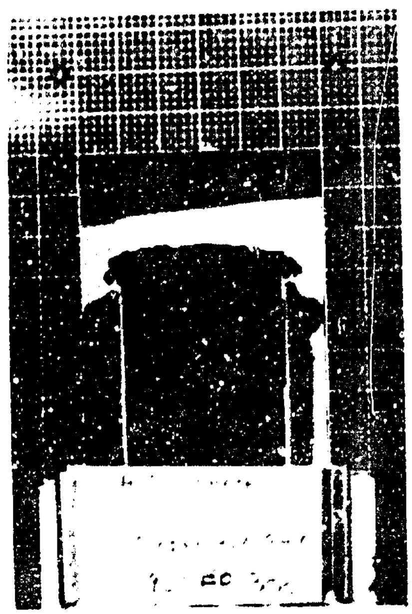

Model 32019-10 - Post-Exposure

Figure 32 -- Photographs of Boeing Carborazole Model 32019-10

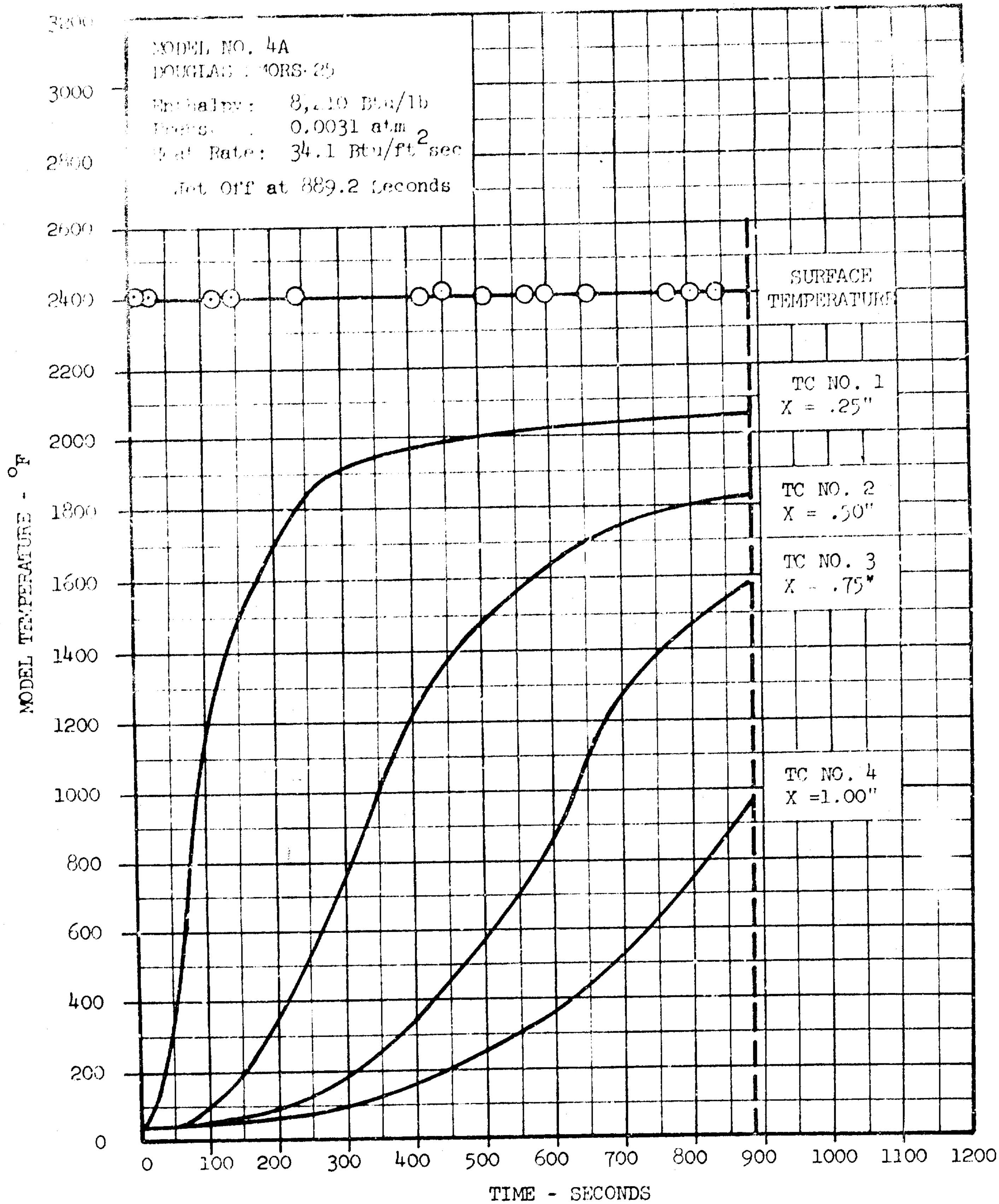

Figure 33 -- Douglas SMORS-25 Model 4A Temperature History

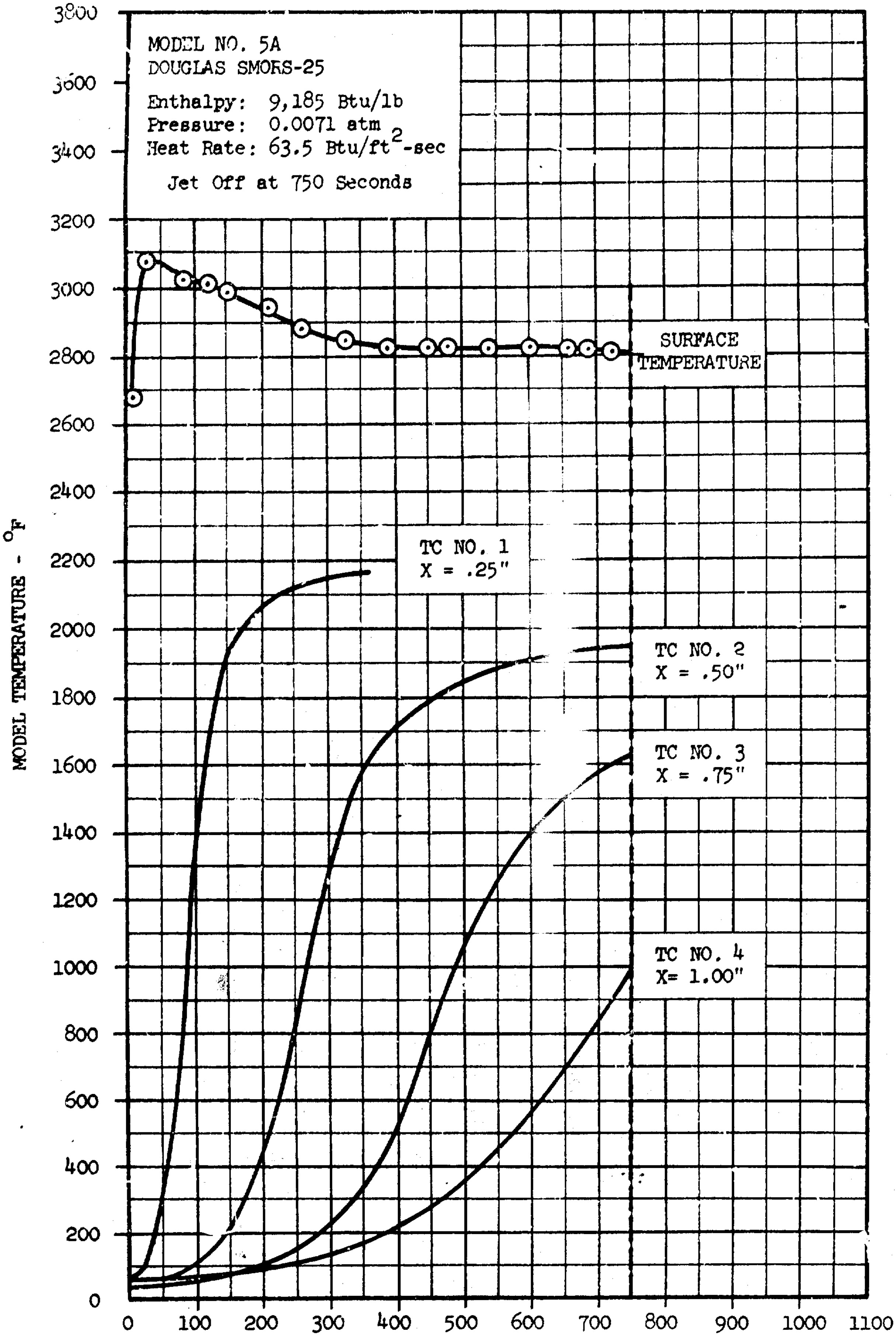

Figure 34 -- Douglas SMORS-25 Model 5A Temperature History

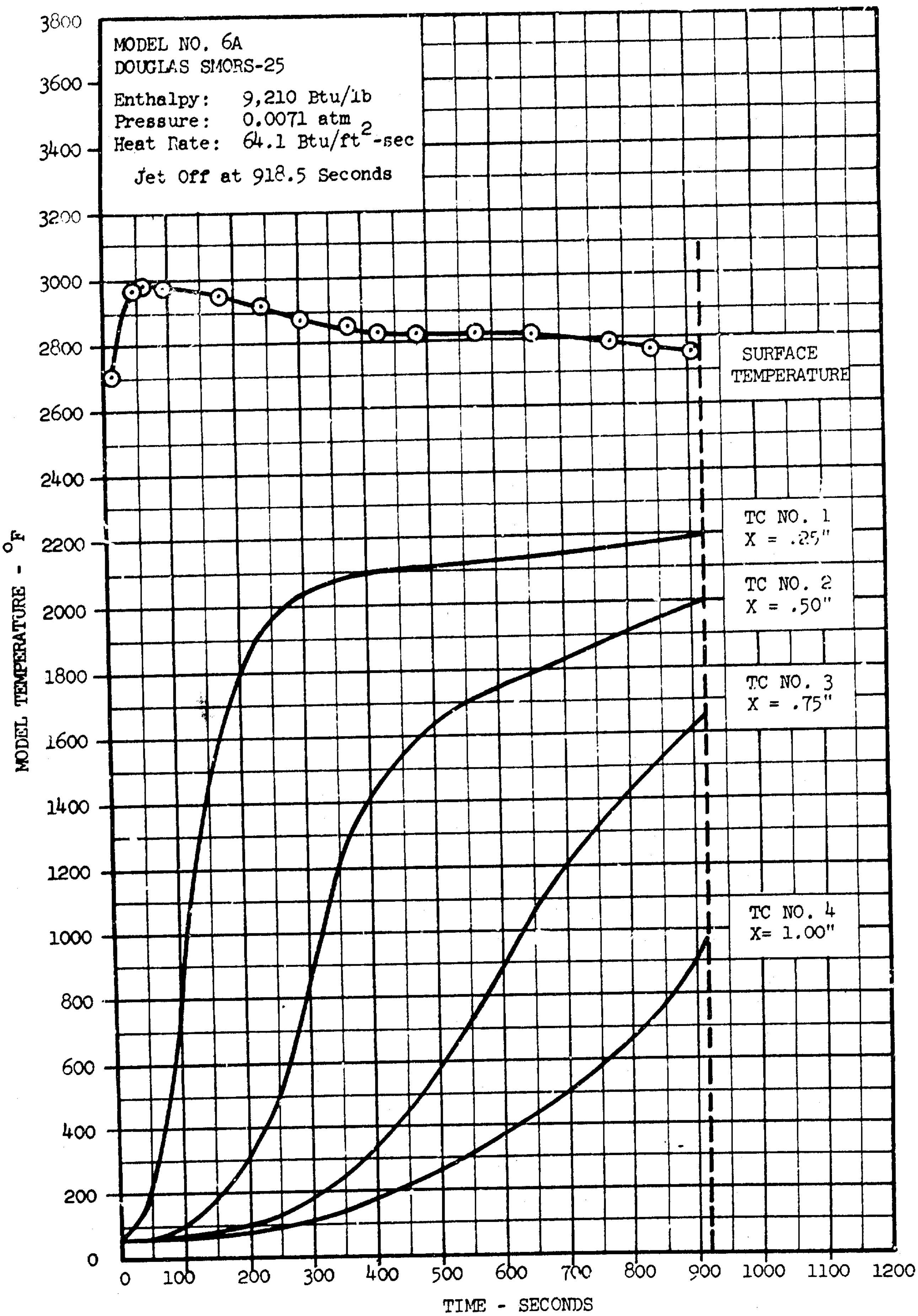

Figure 35 -- Douglas SMORS-25 Model 6A Temperature History

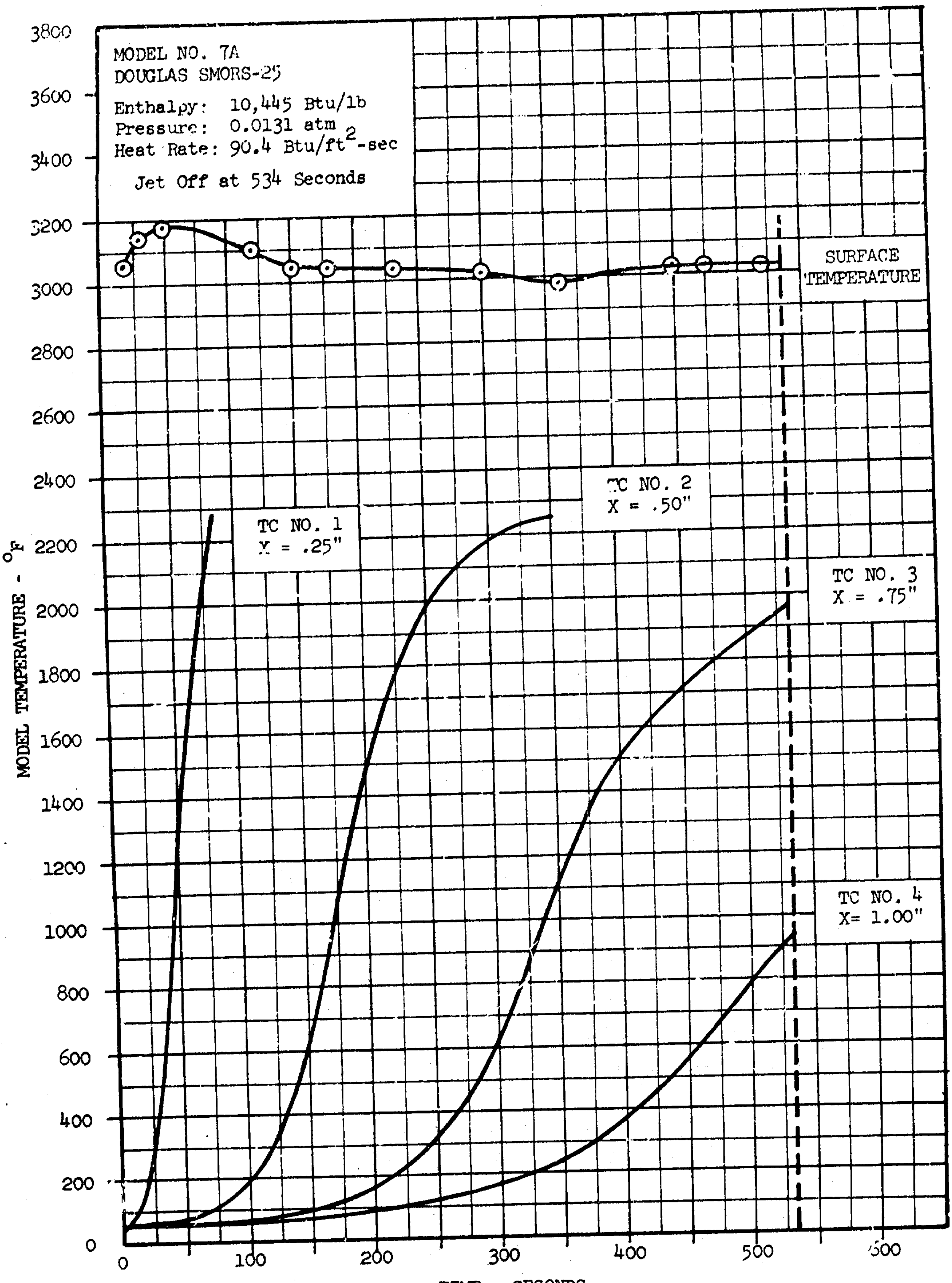

Figure 36 -- Douglas SMORS-25 Model 7A Temperature History

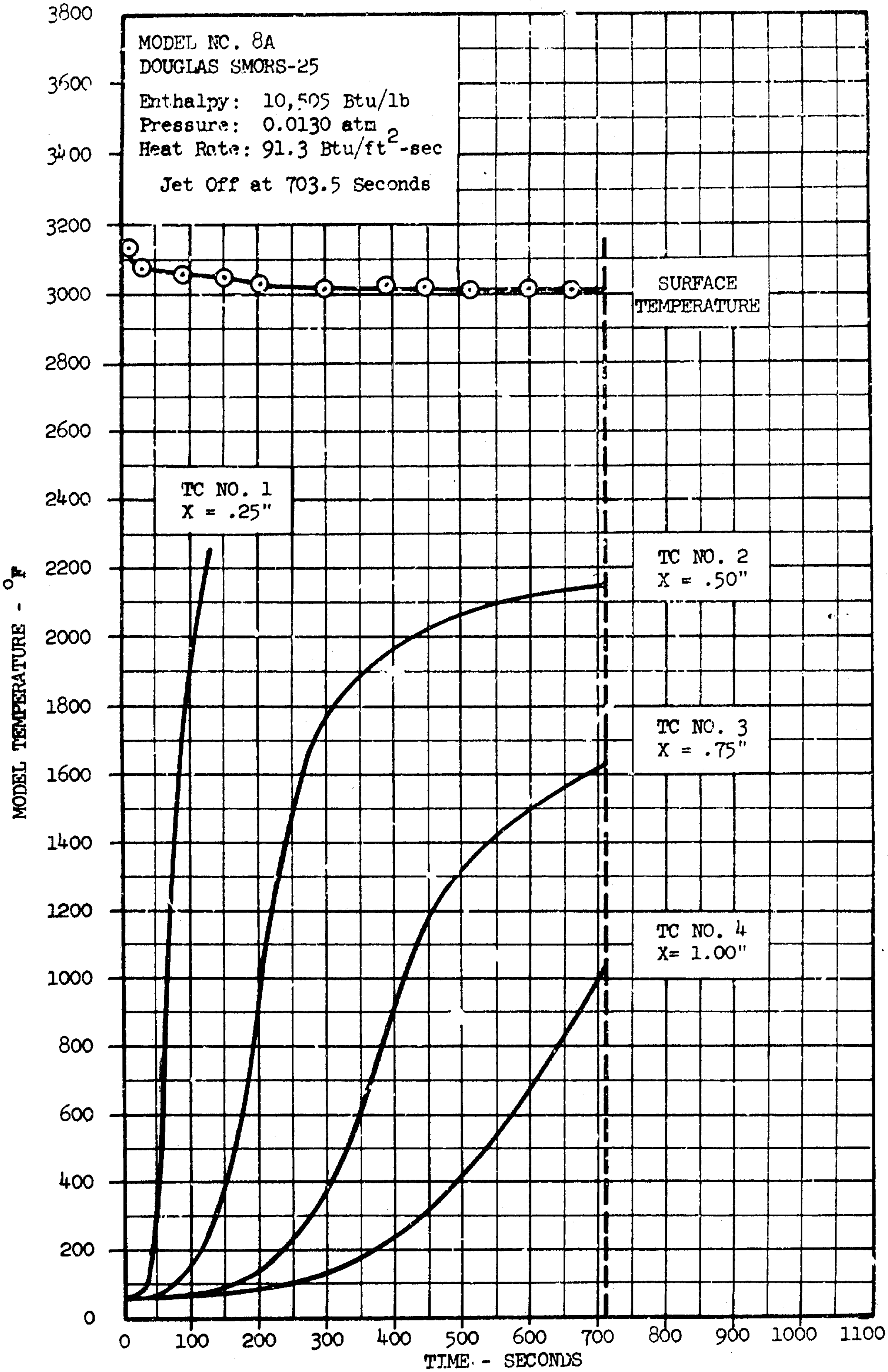

Figure 37 -- Douglas SMORS-25 Model 8A Temperature History

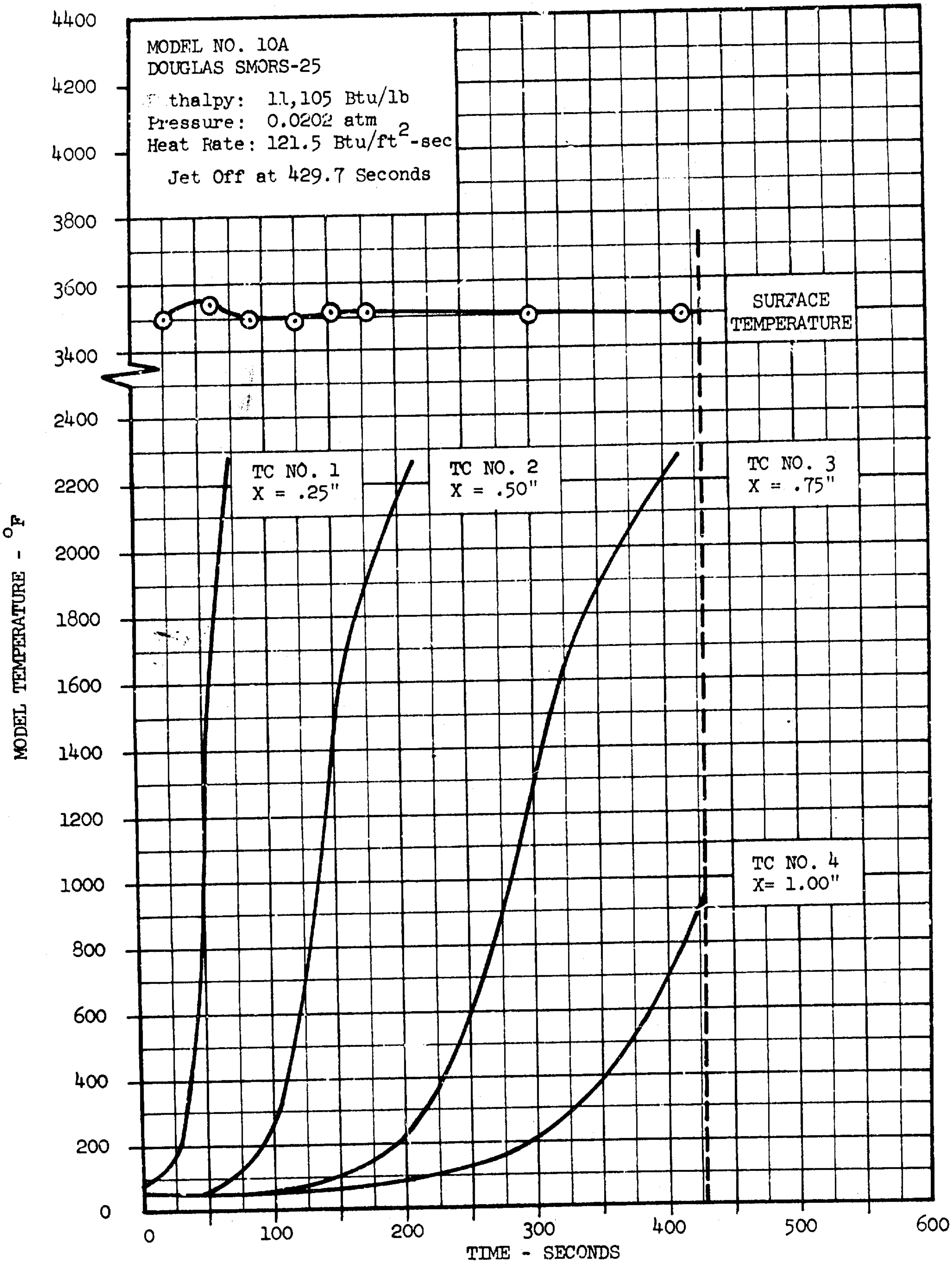

Figure 38 -- Douglas SMORS-25 Model 10A Temperature History

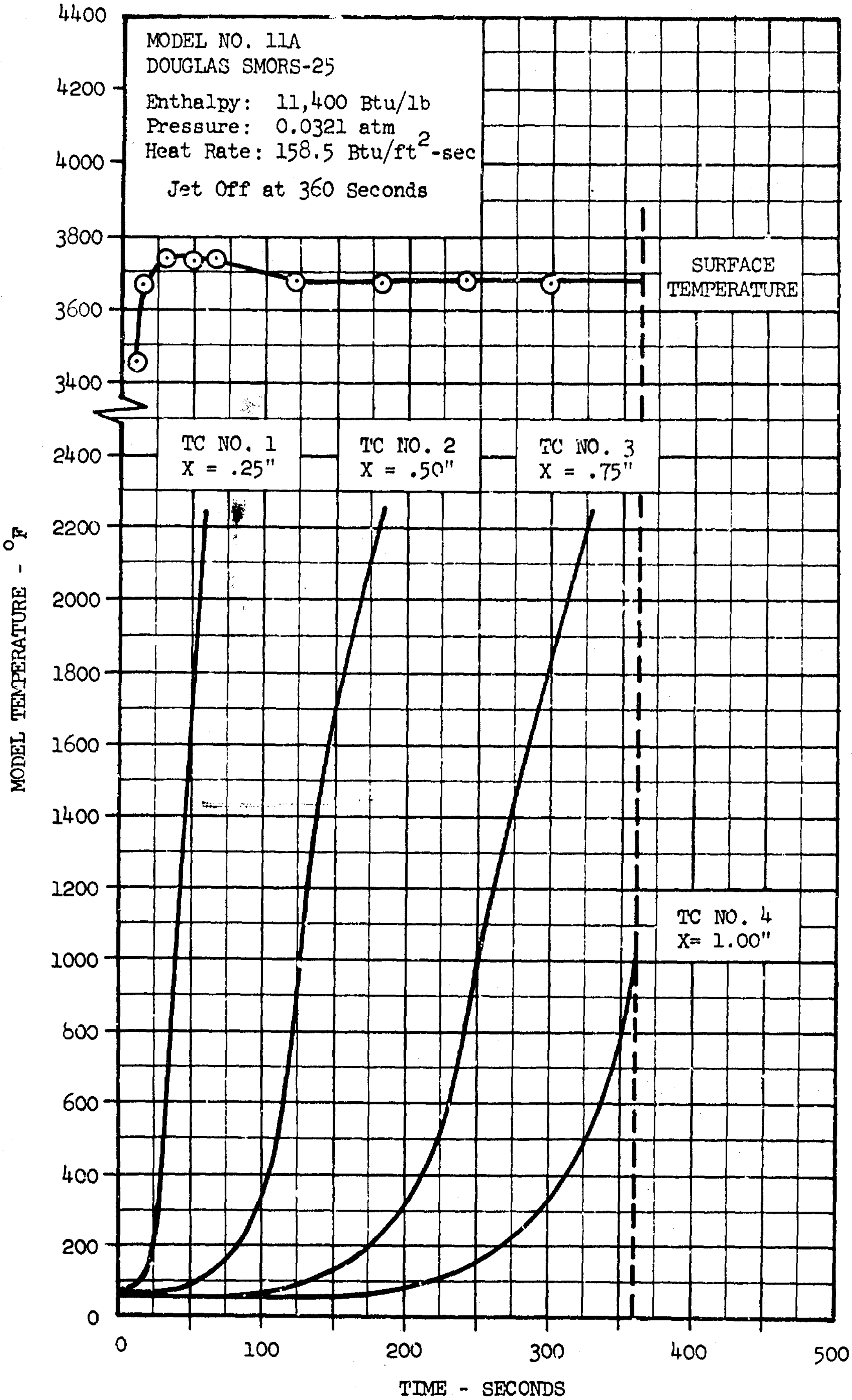

Figure 39 -- Douglas SMORS-25 Model 11A Temperature History

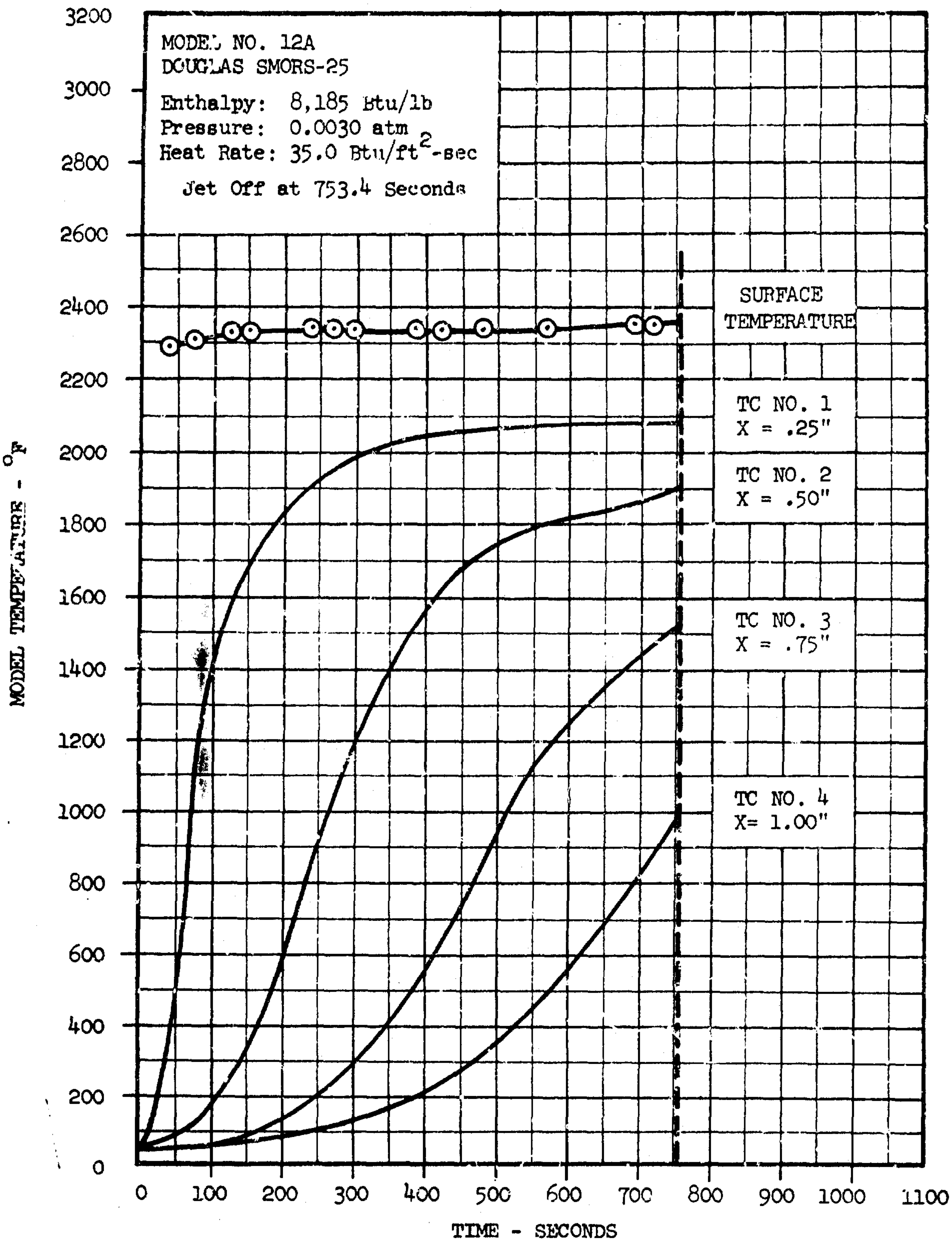

Figure 40 -- Douglas SMORS-25 Model 12A Temperature History

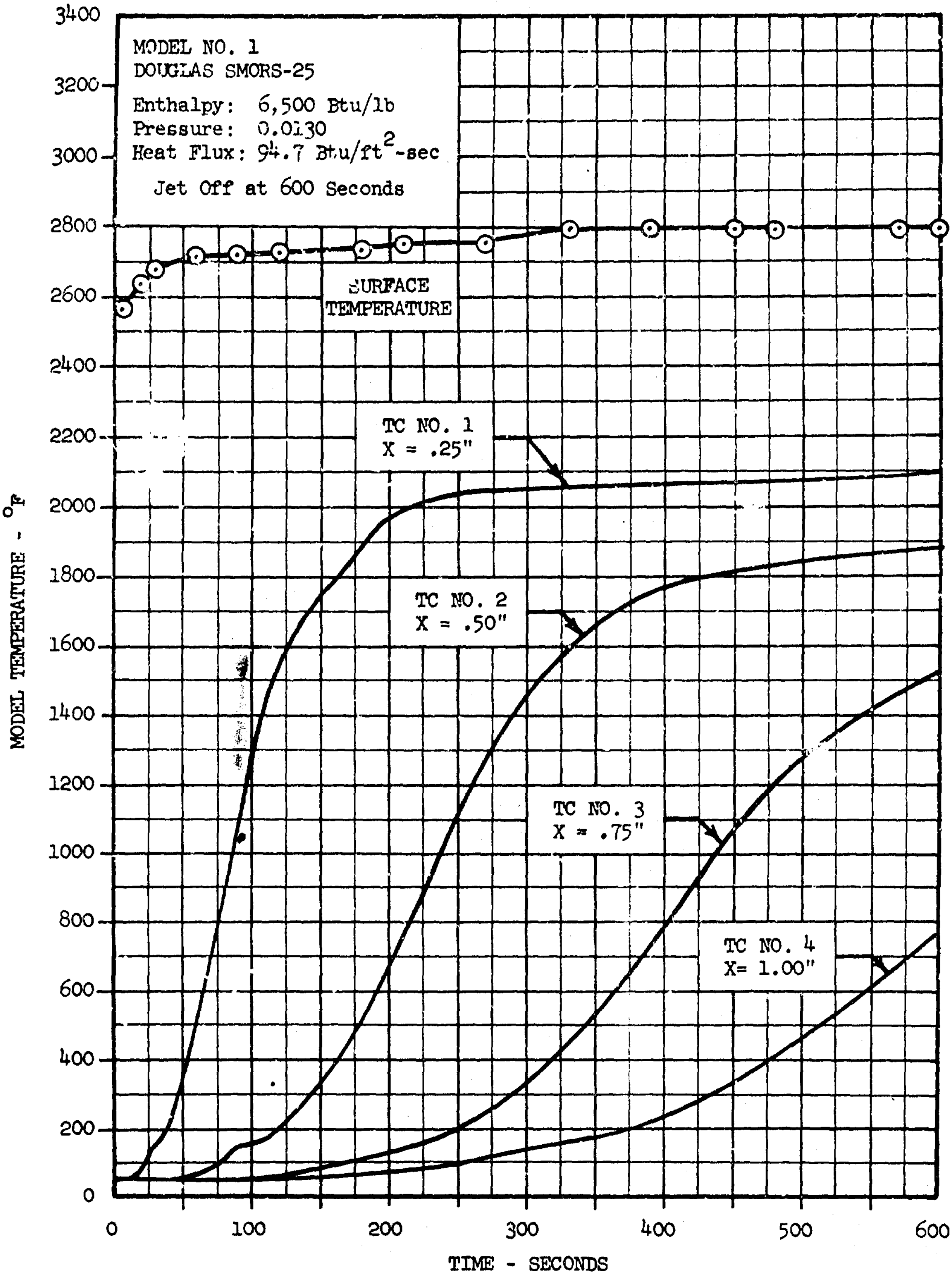

Figure 41 -- Douglas SMORS-25 Model 1 Temperature History

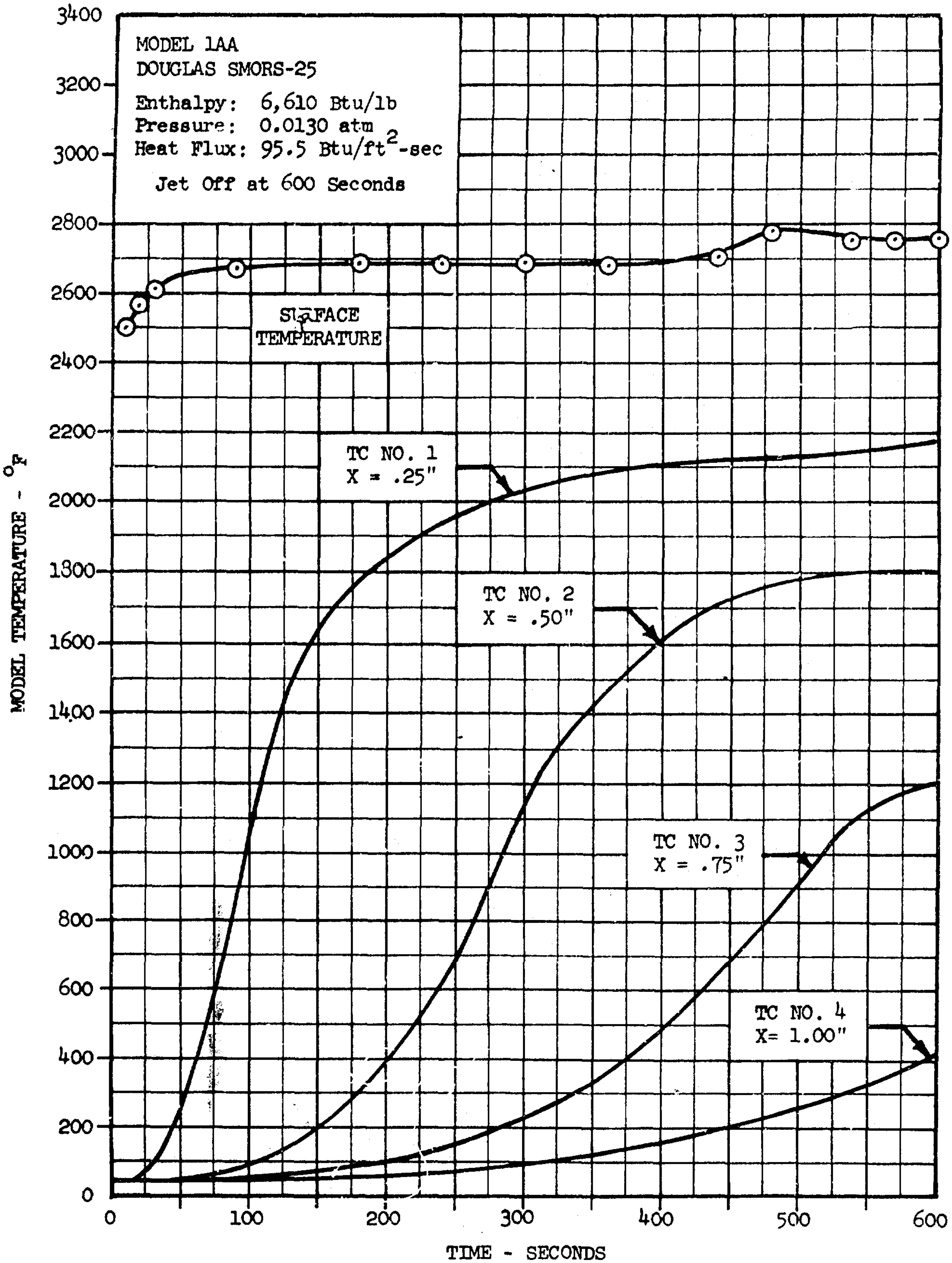

Figure 42 -- Douglas SMORS-25 Model 1AA Temperature History

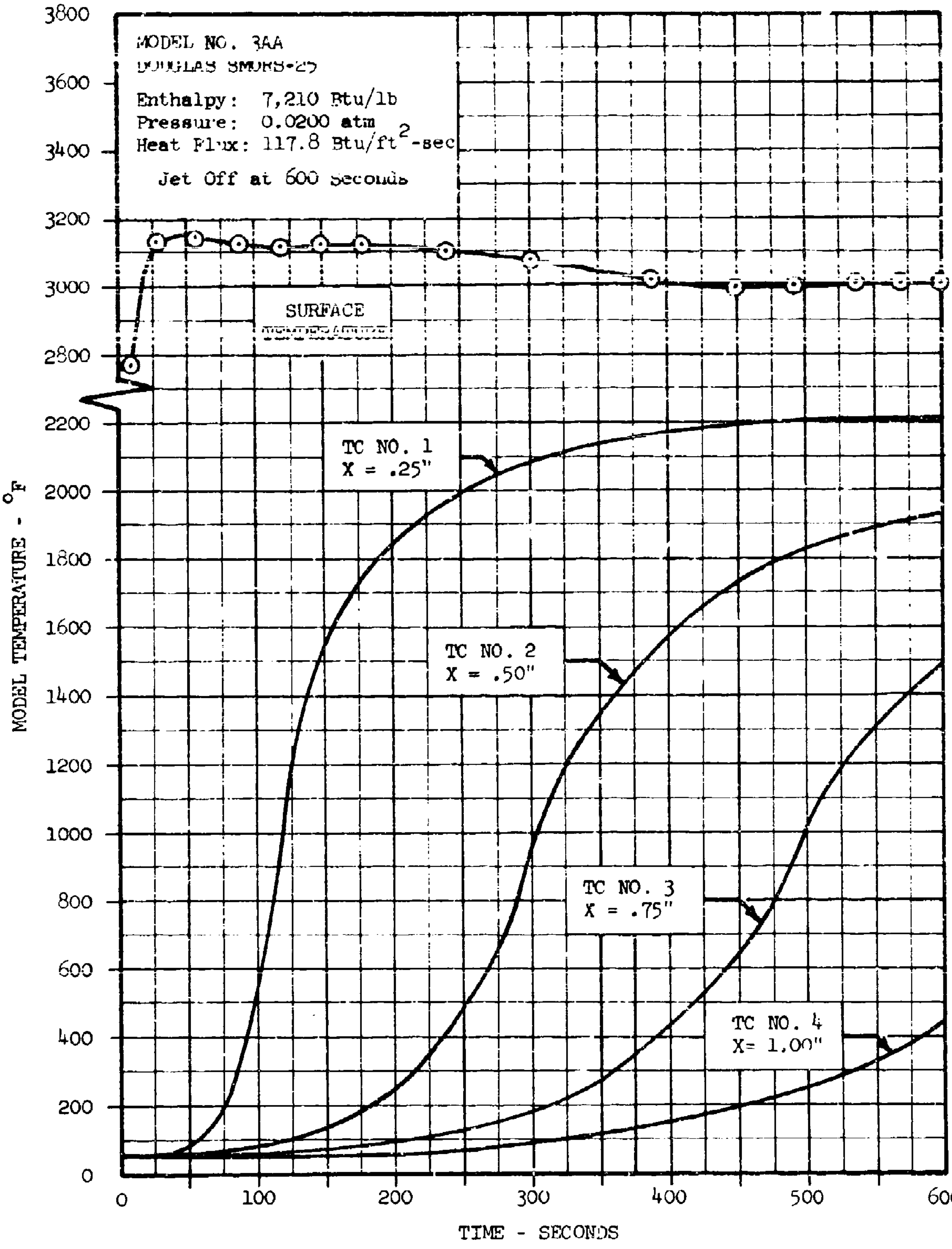

Figure 43 -- Douglas SMORS-25 Model 3AA Temperature History

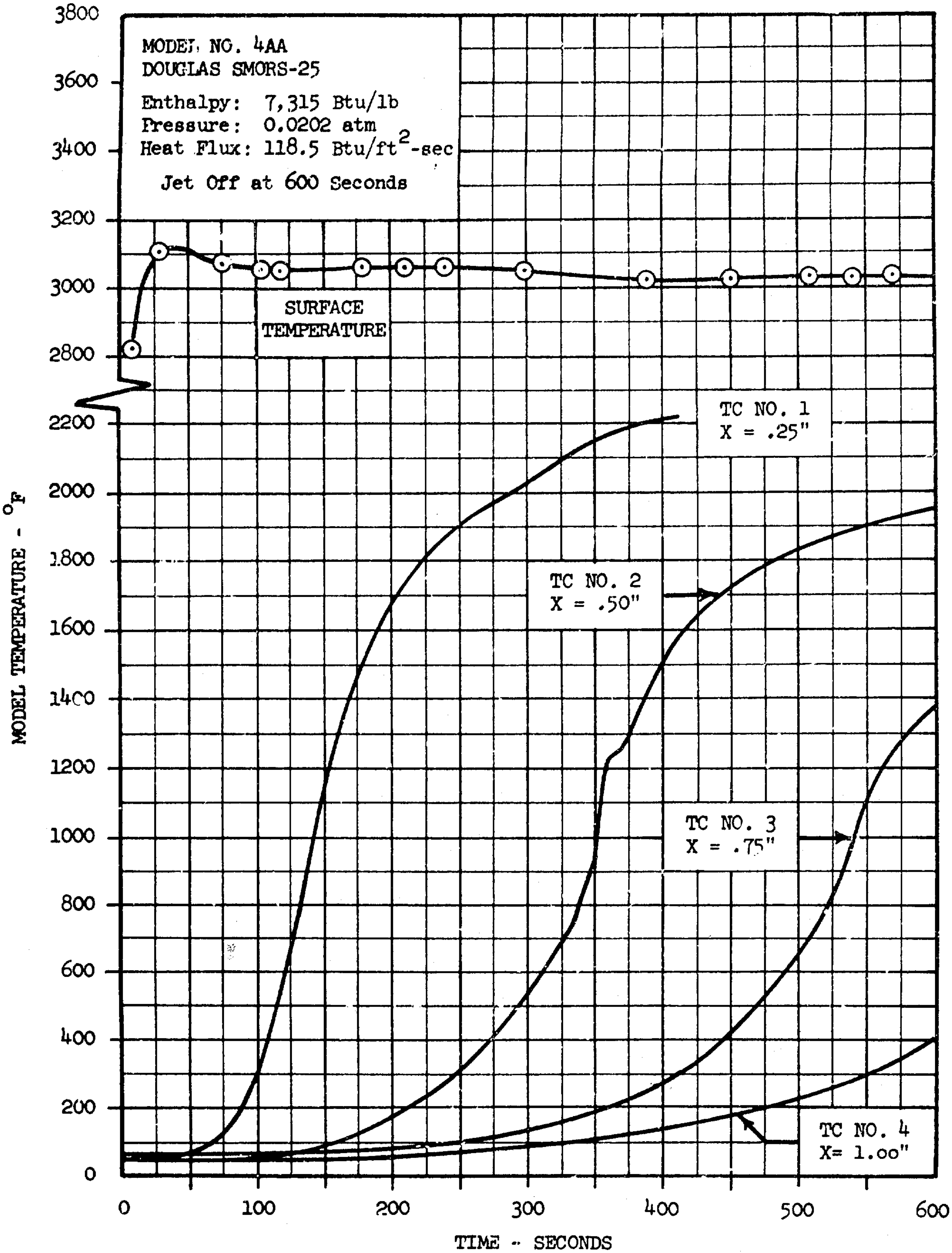

Figure 44 -- Douglas SMORS-25 Model 4AA Temperature History

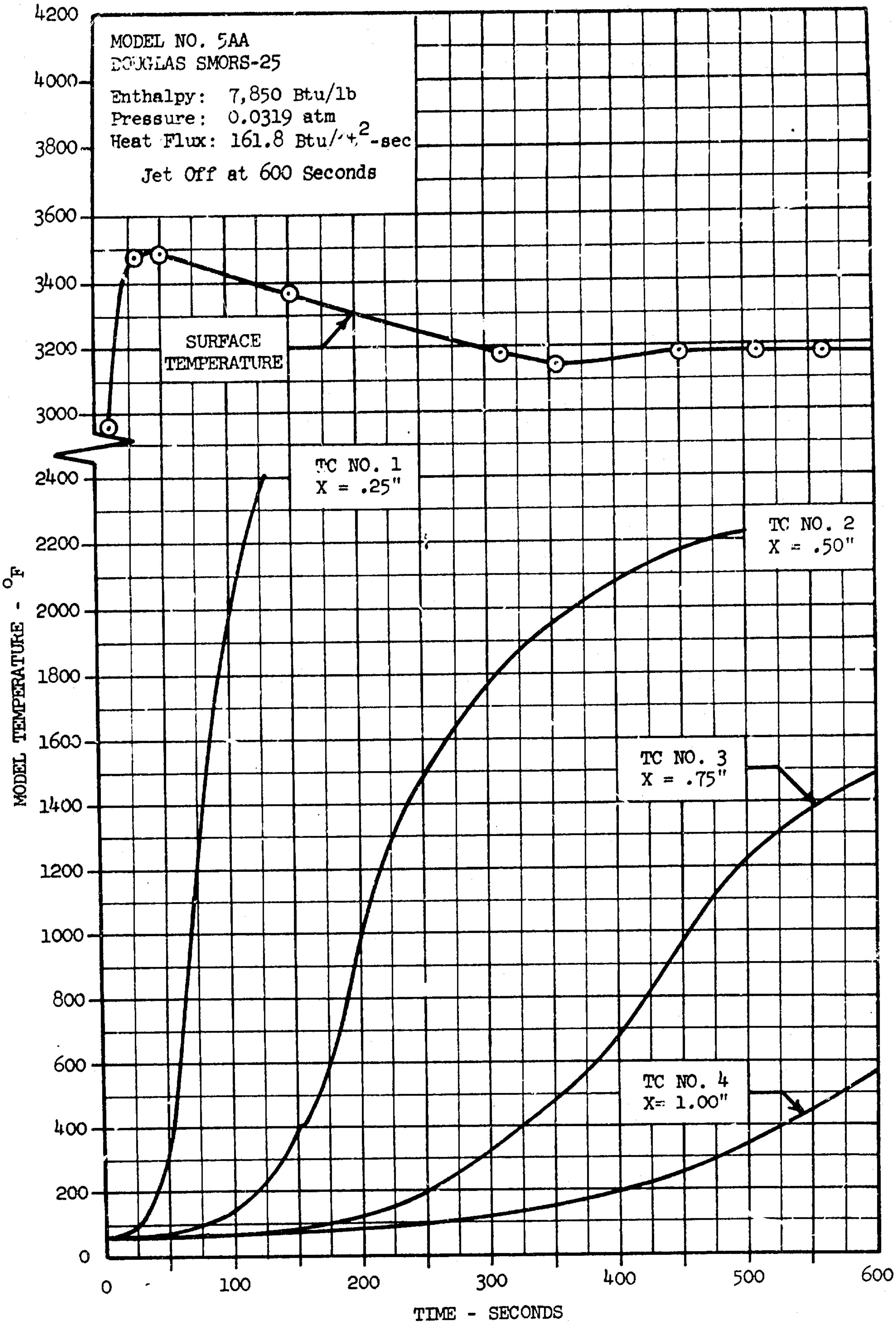

Figure 45 -- Douglas SMORS-25 Model 5AA Temperature History

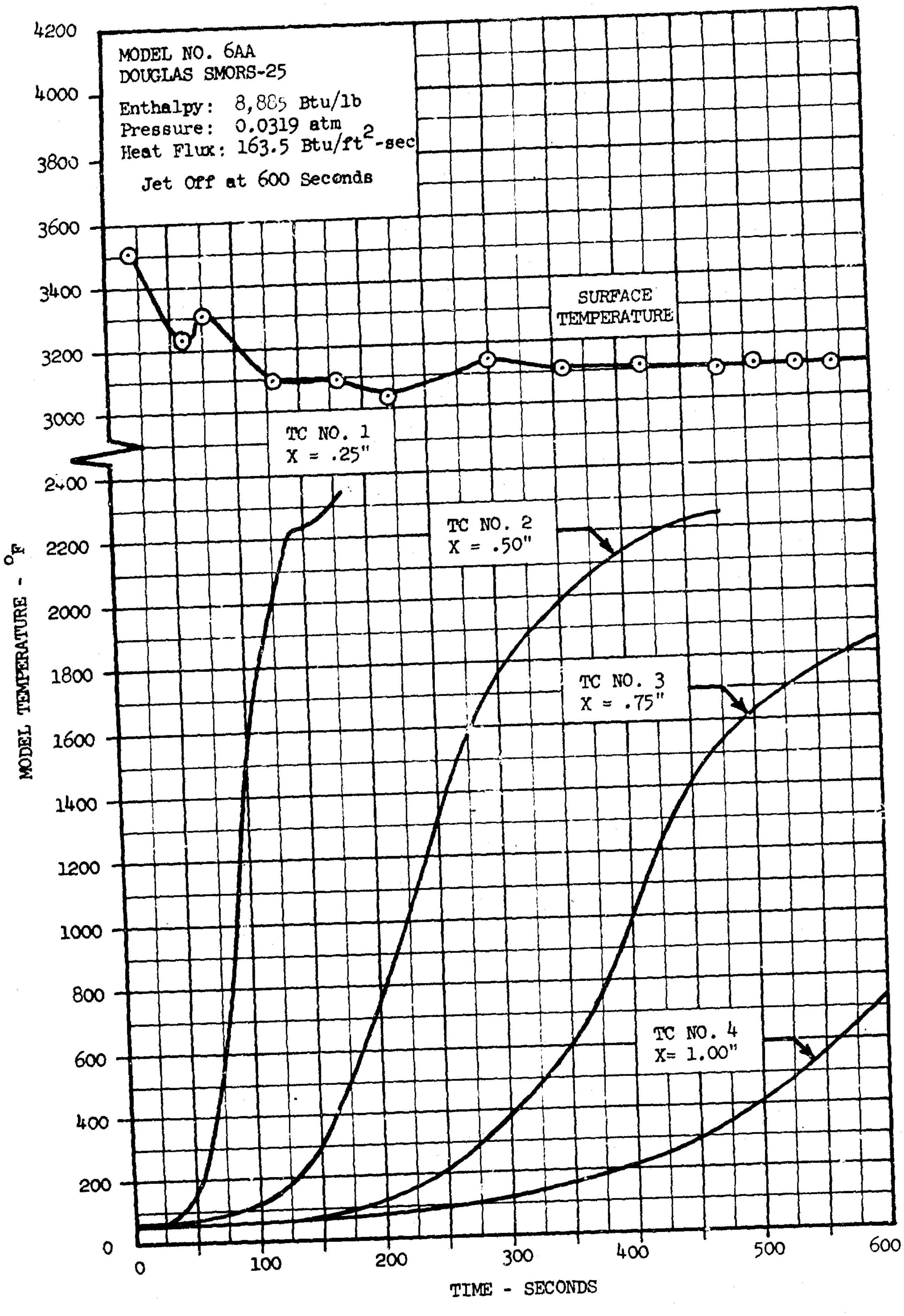

Figure 46 -- Douglas SMORS-25 Model 6AA Temperature History

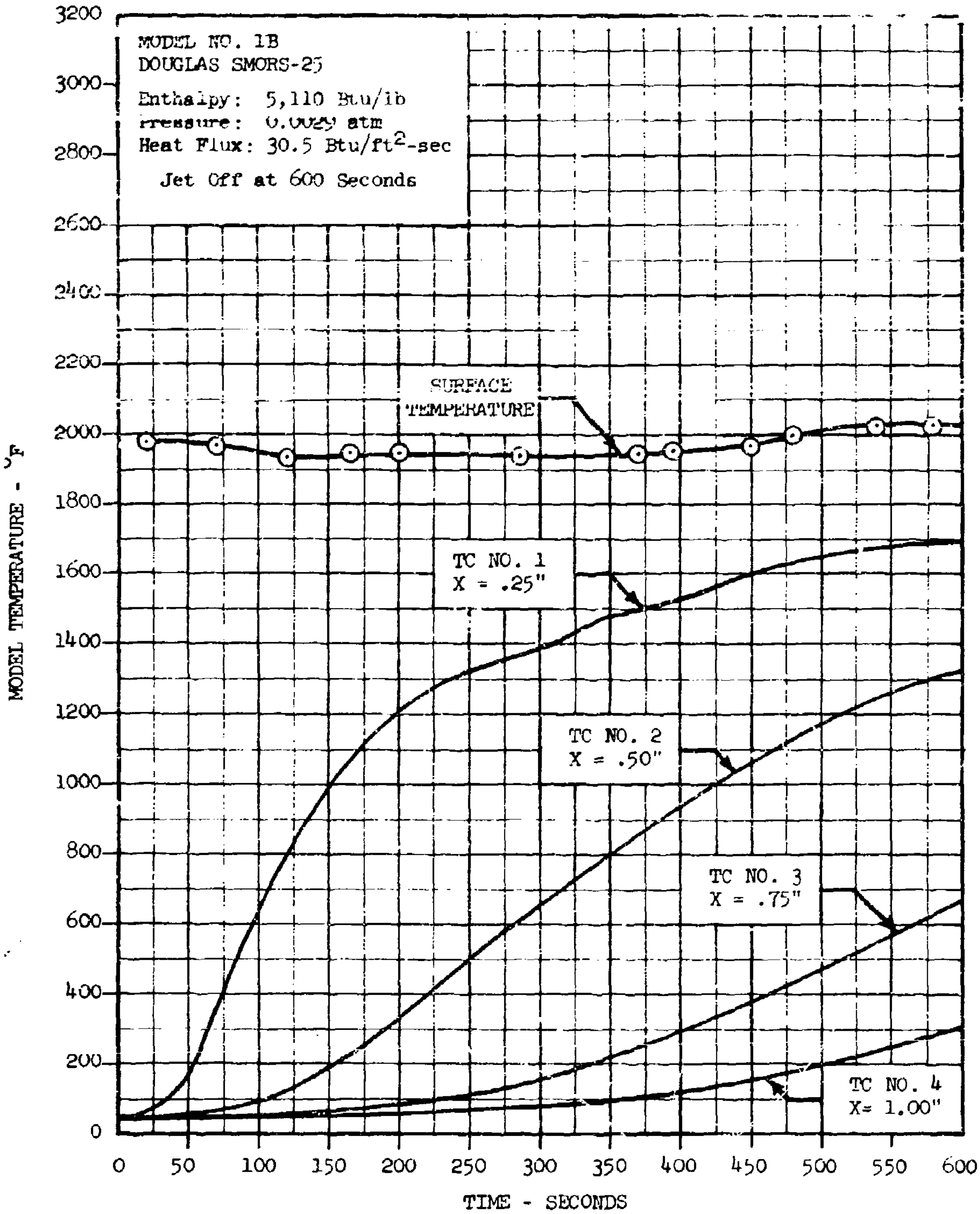

Figure 47 -- Douglas SMORS-25 Model 1B Temperature History

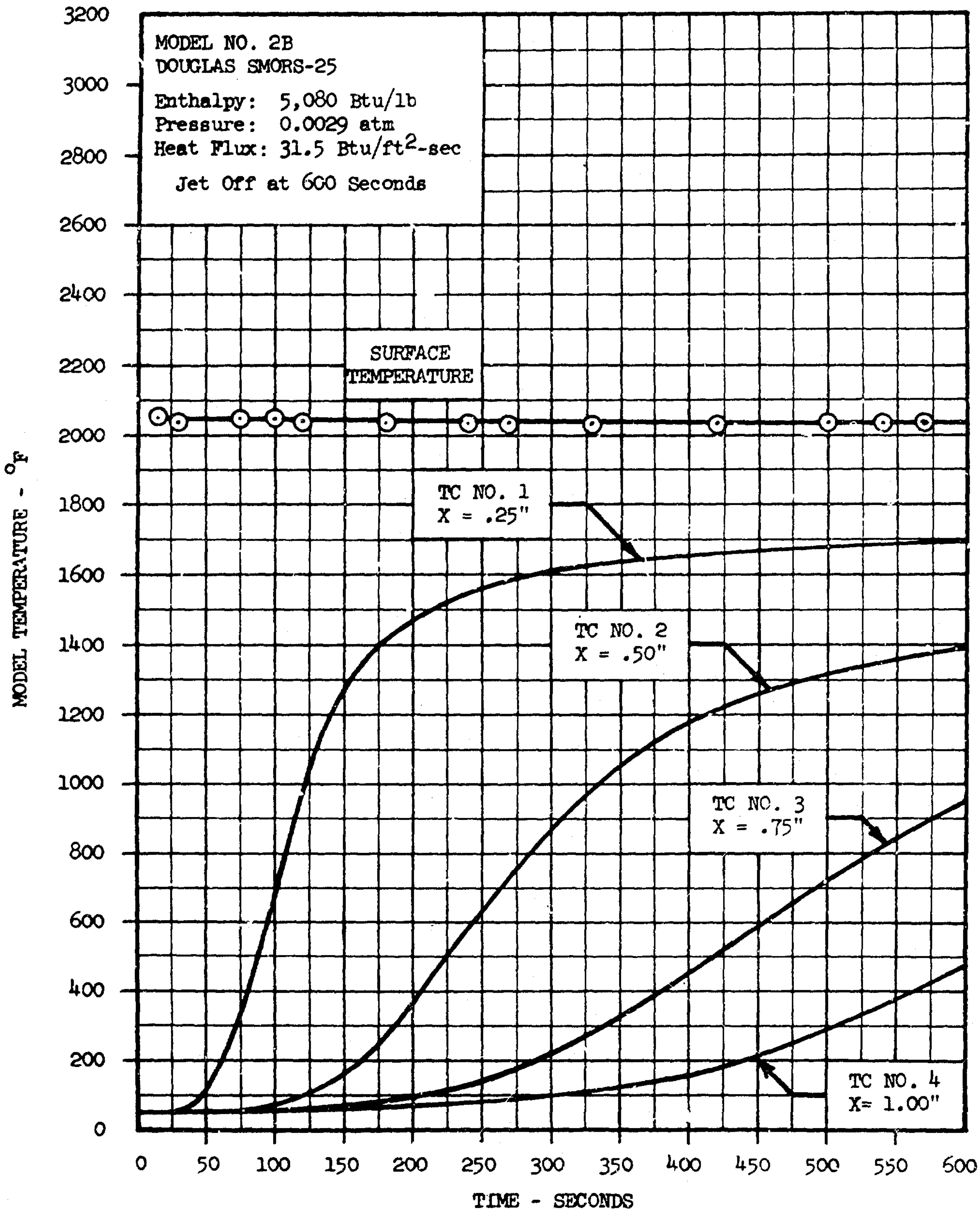

Figure 48 -- Douglas SMORS-25 Model 2B Temperature History

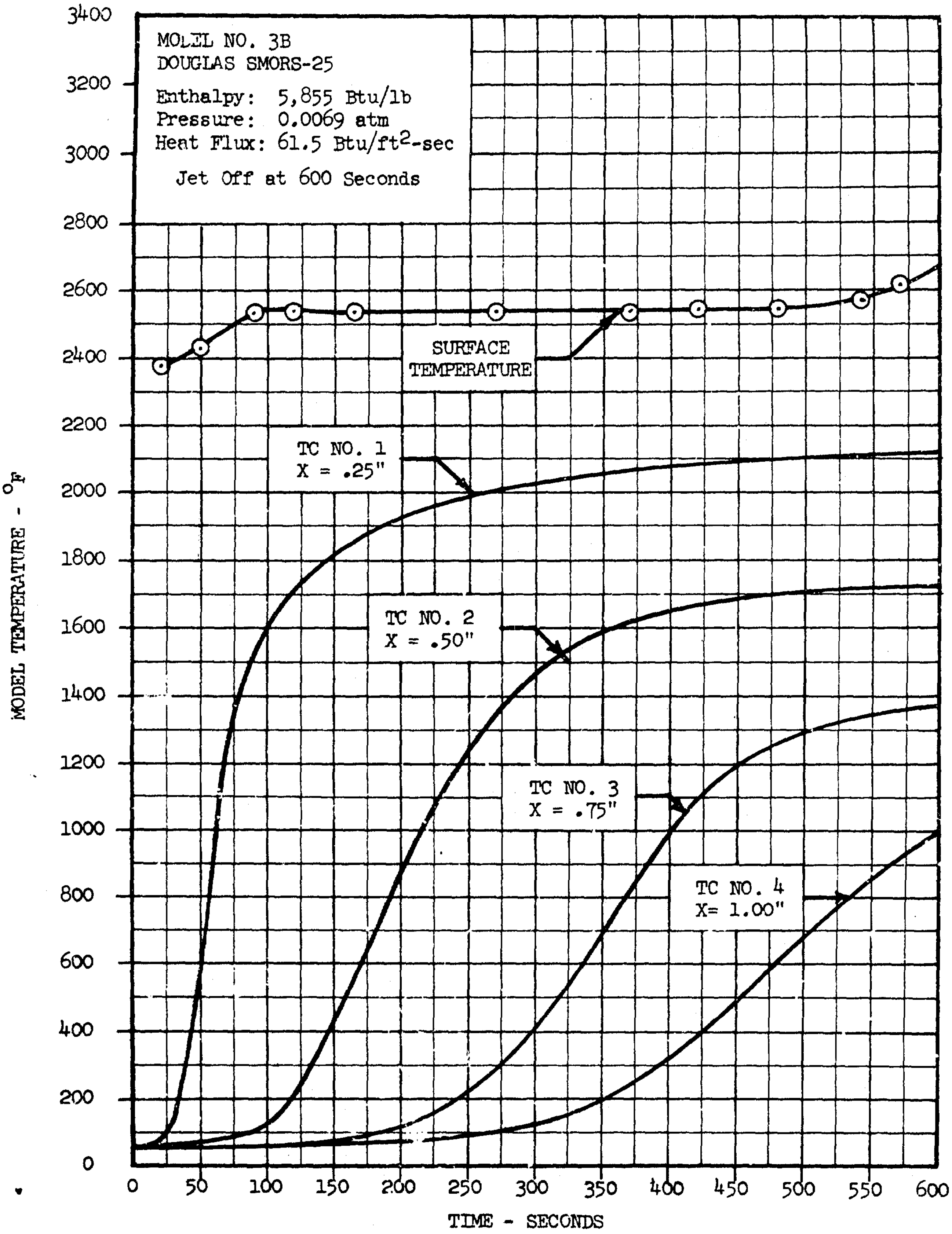

Figure 49 -- Douglas SMORS-25 Model 3B Temperature History

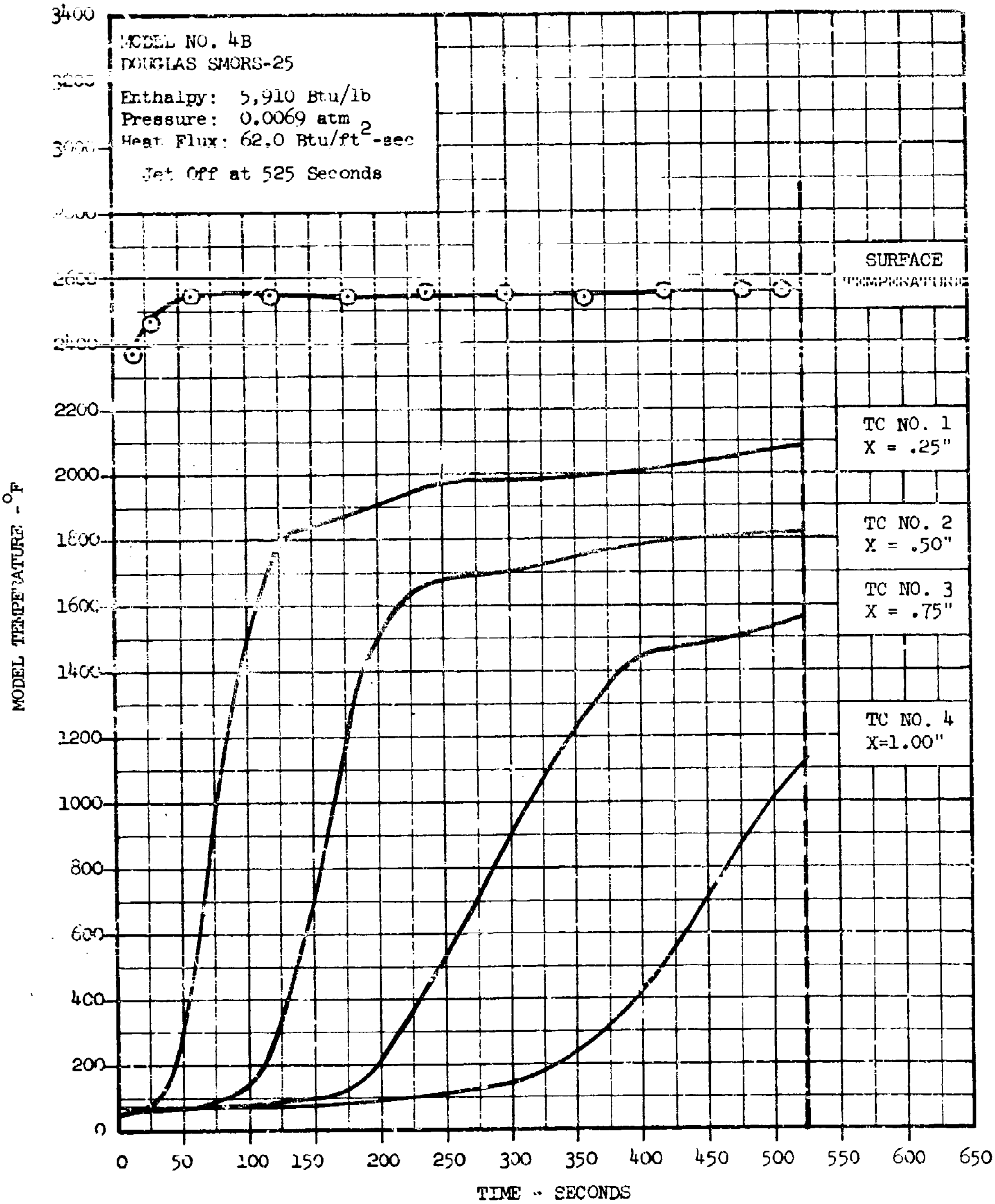

Figure 50 -- Douglas SMORS-25 Model 4B Temperature History

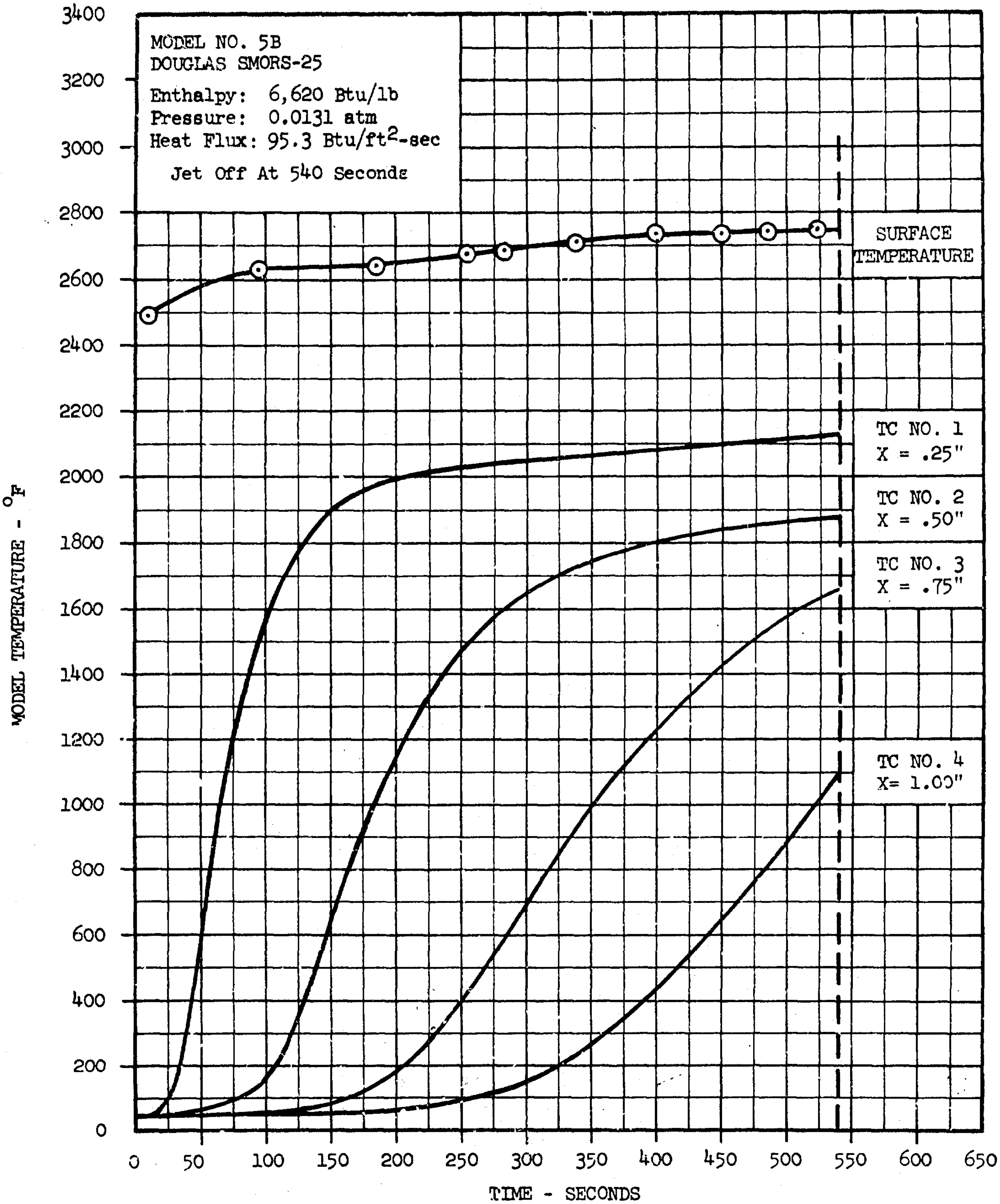

Figure 51 -- Douglas SMORS-25 Model 5B Temperature History

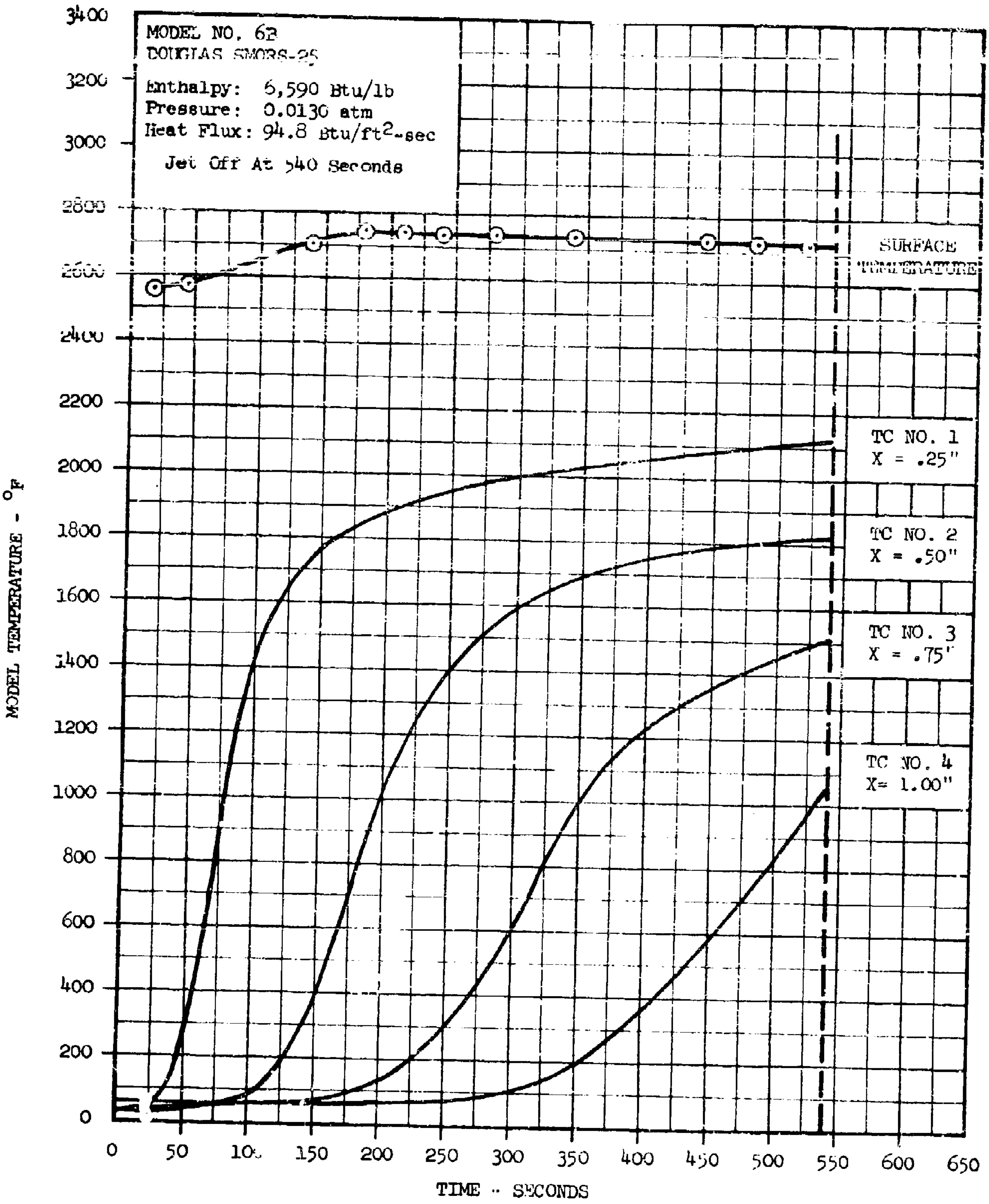

Figure 52 -- Douglas SMORS-25 Model 6B Temperature History

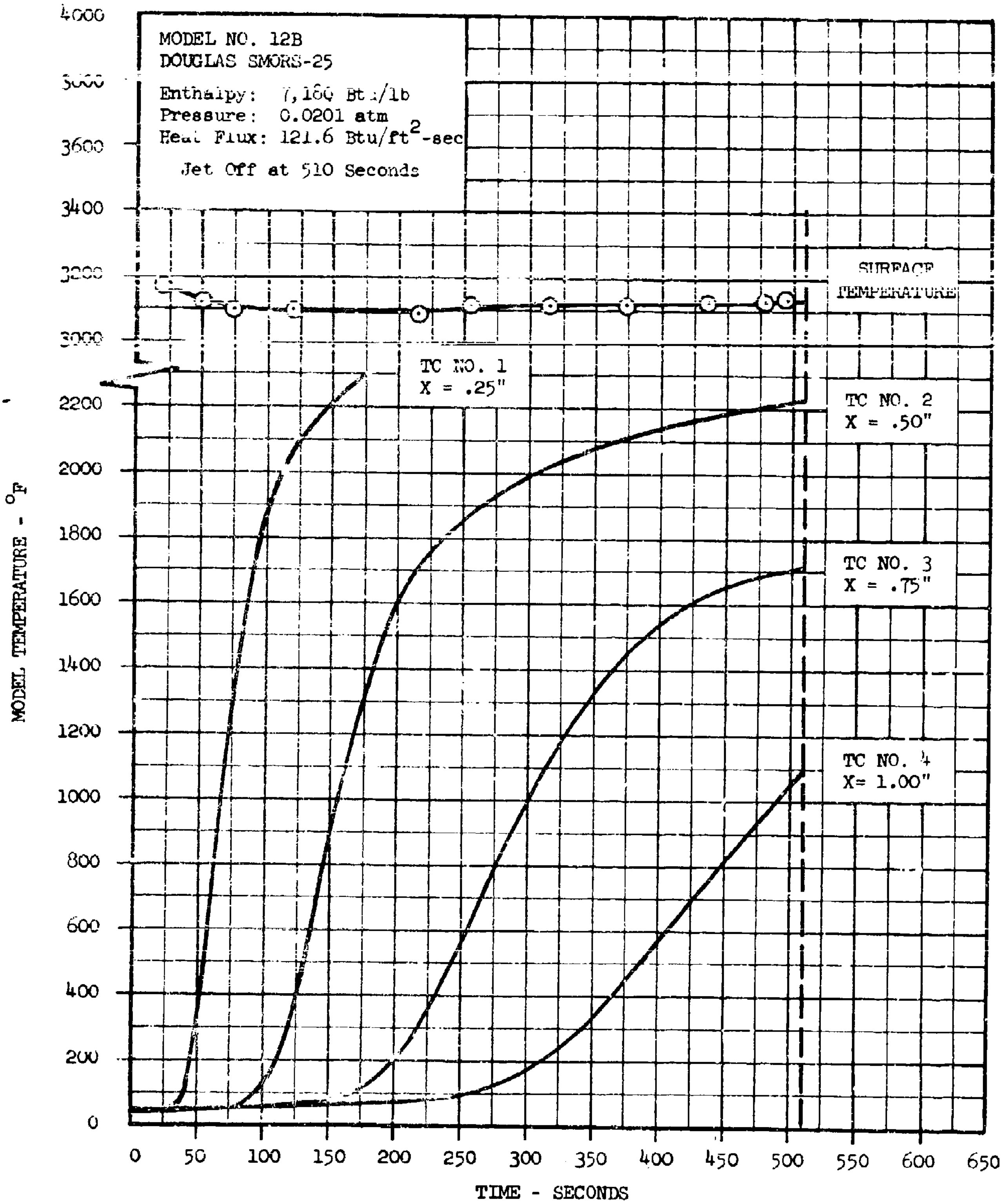

Figure 53 -- Douglas SMORS-25 Model 12B Temperature History

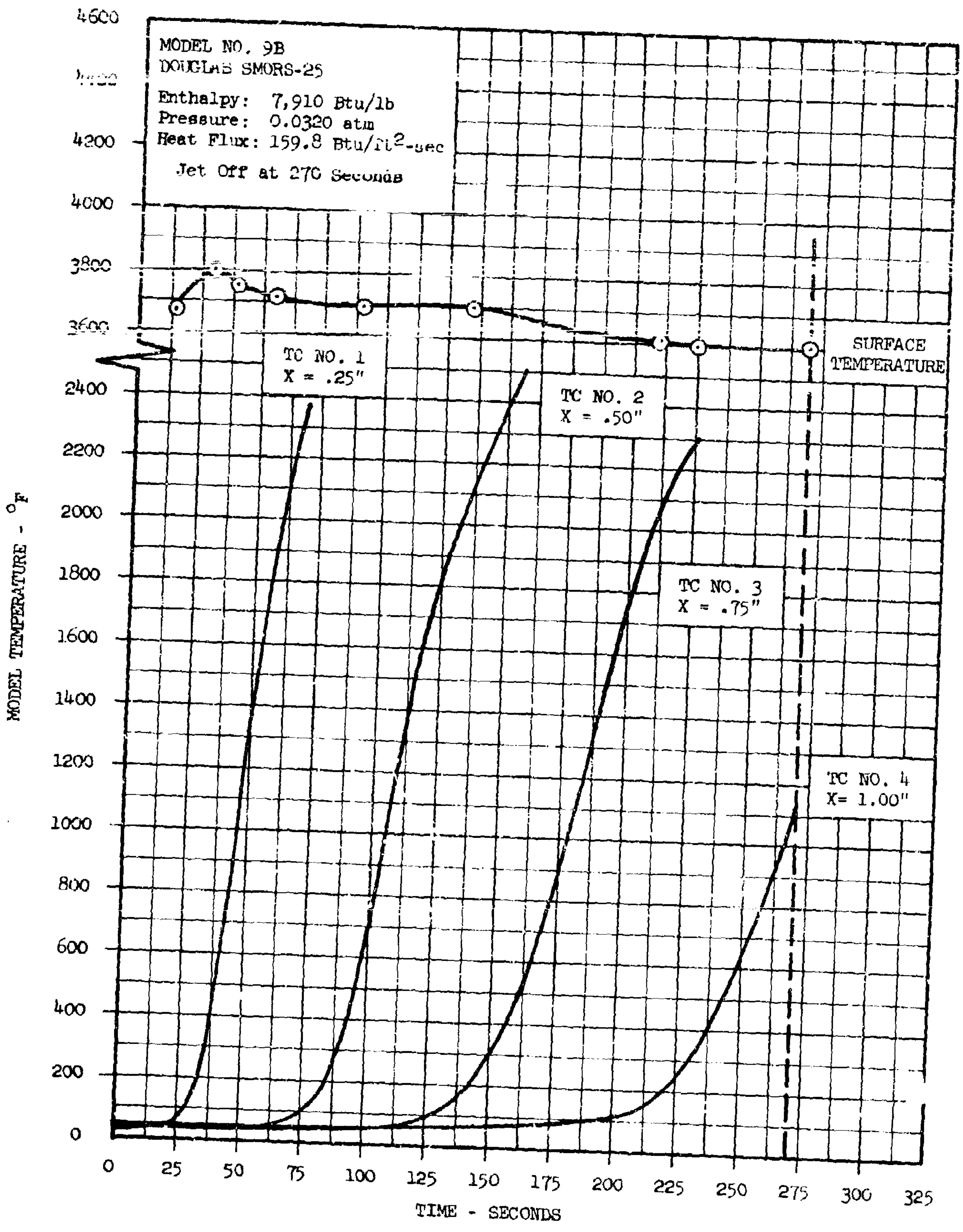

Figure 54 -- Douglas SMORS-25 Model 9B Temperature History

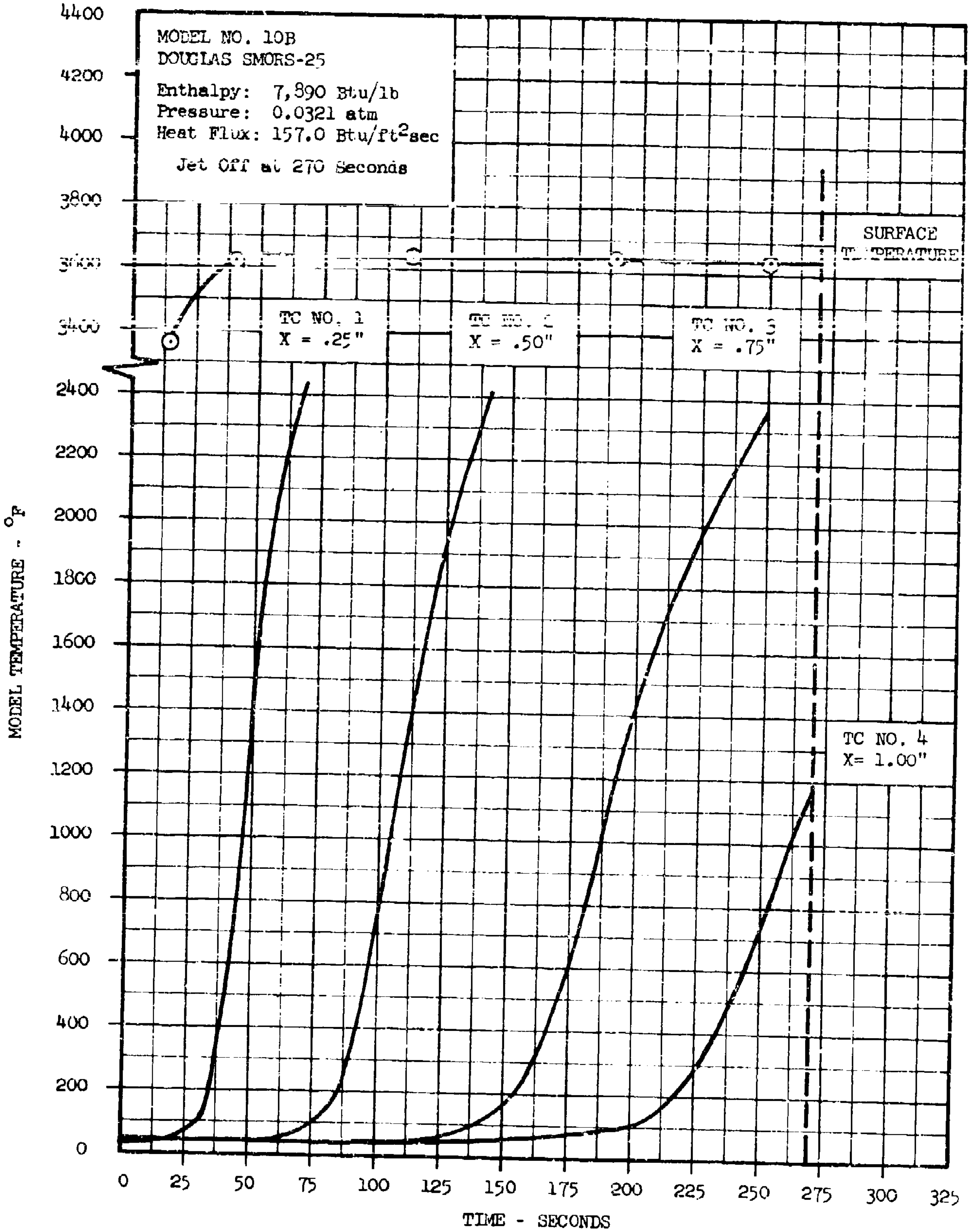

Figure 55 -- Douglas SMORS-25 Model 10B Temperature History

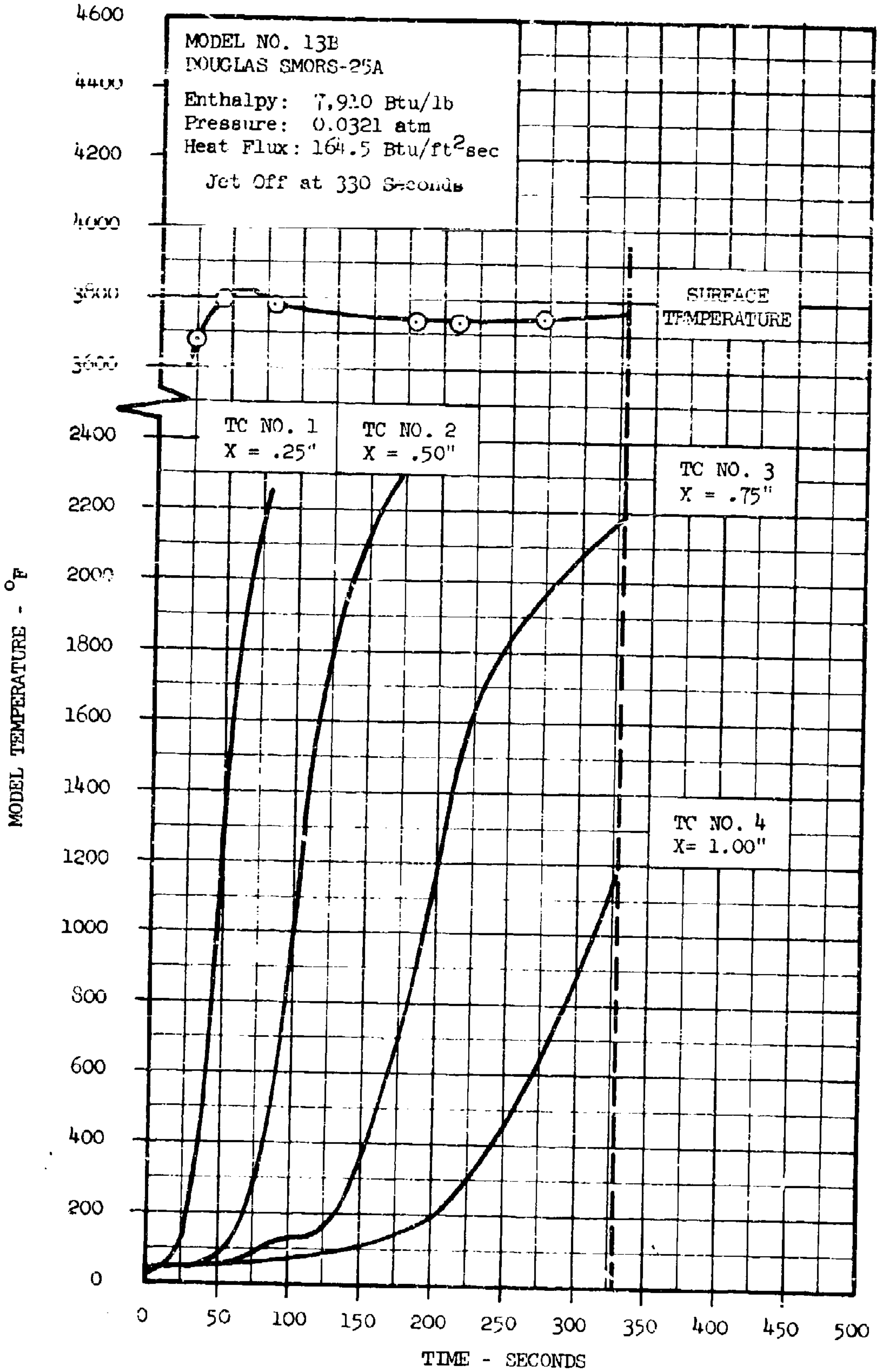

Figure 56 -- Douglas SMORS-25A Model 13B Temperature History

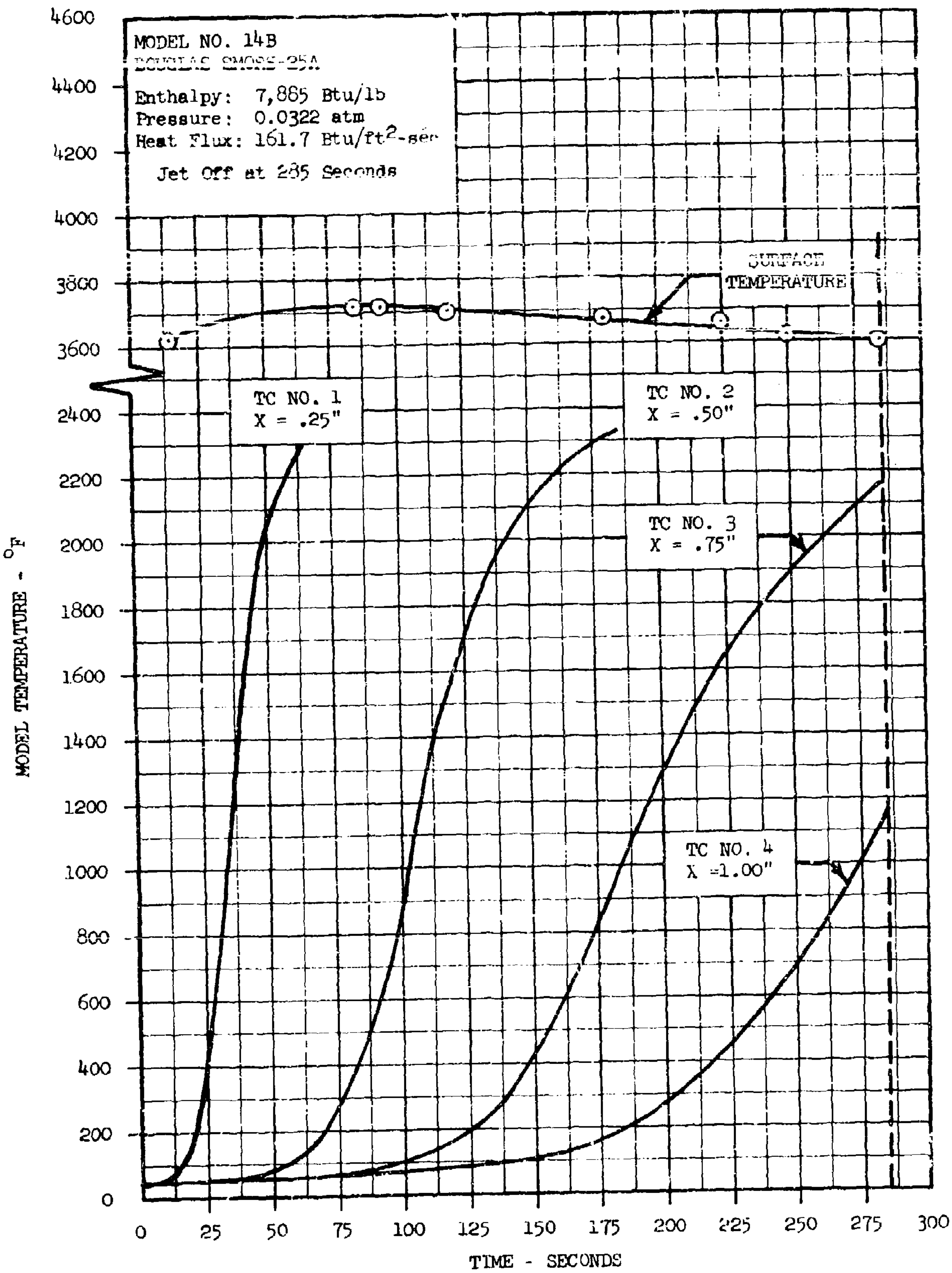

Figure 57 -- Douglas SMORS-25A Model 14B Temperature History

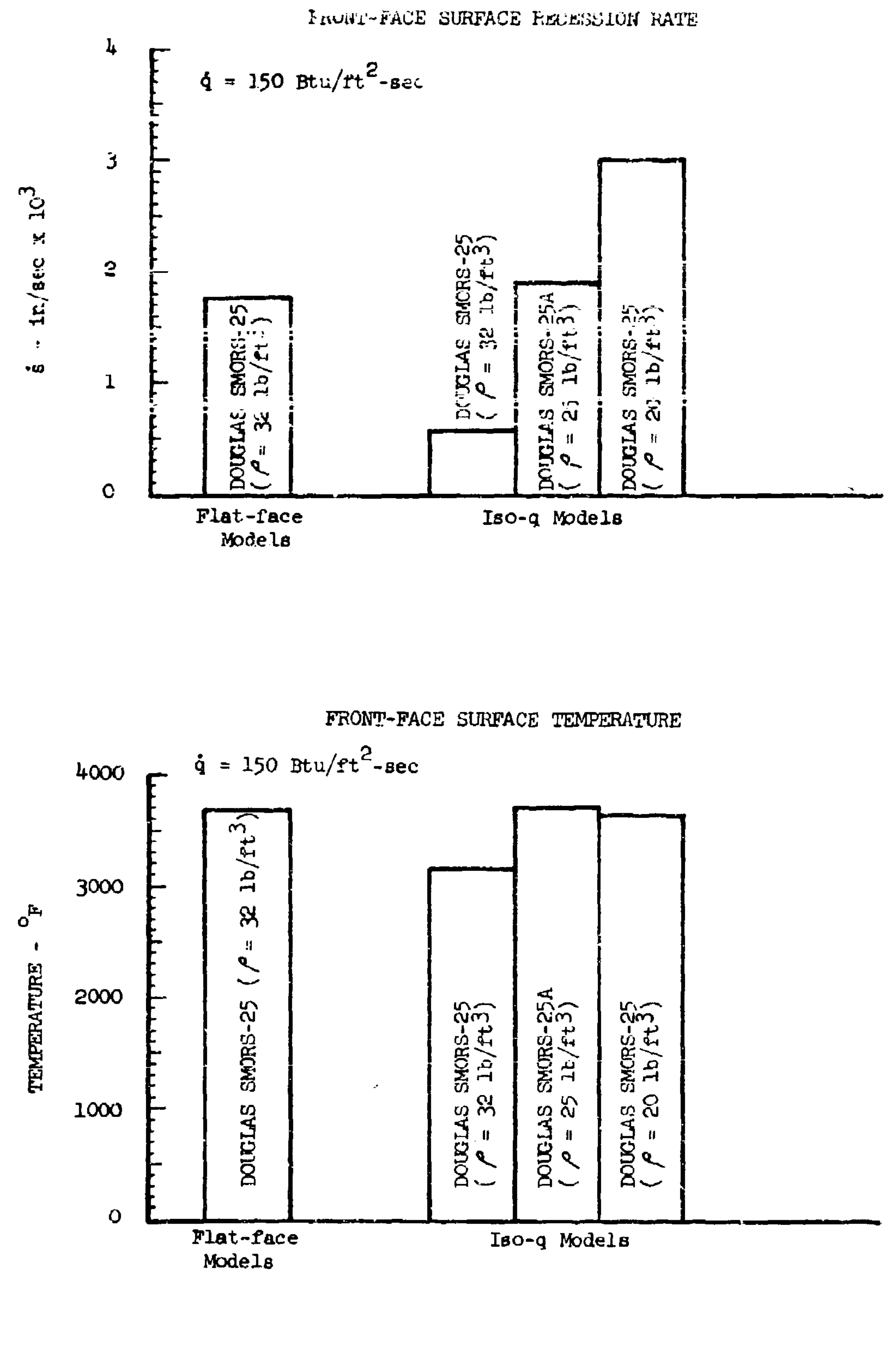

Figure 58 -- Comparison of Douglas SMORS-25 Recession Rates and Surface Temperatures

Comparison of Back-Face Temperatures for Douglas SMORS-25 Models

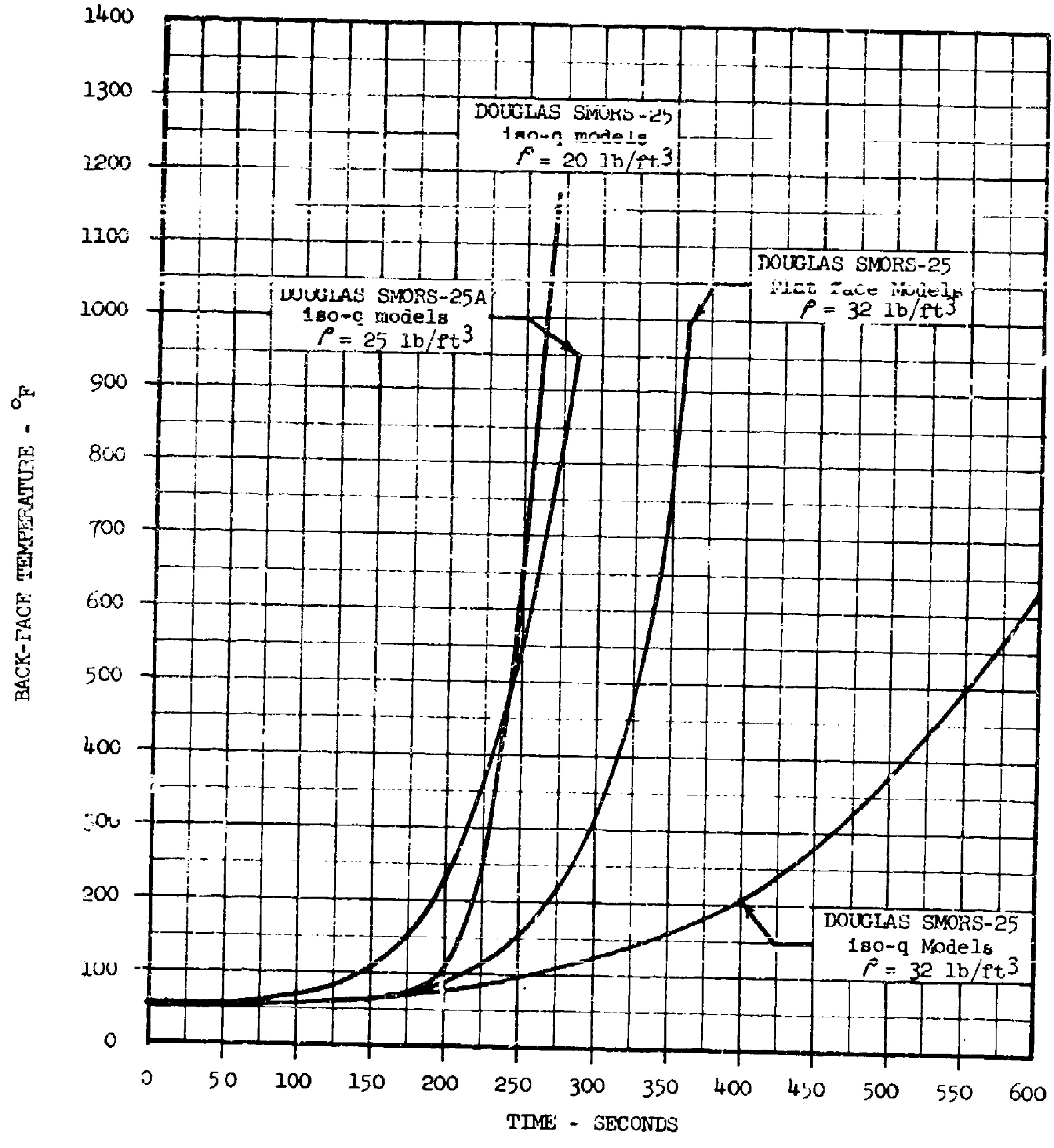

Figure 59 -- Comparison of Back Face Temperature for Douglas SMORS-25 Models

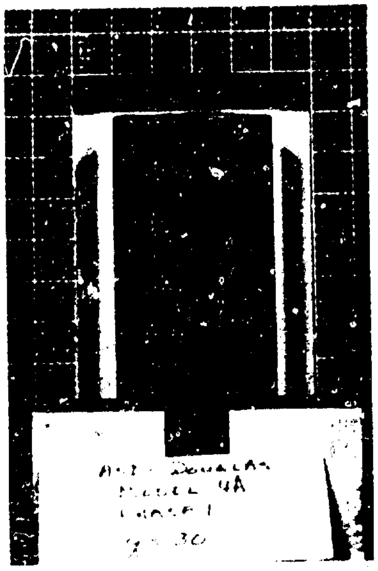

Model 4A - Pre-Exposure

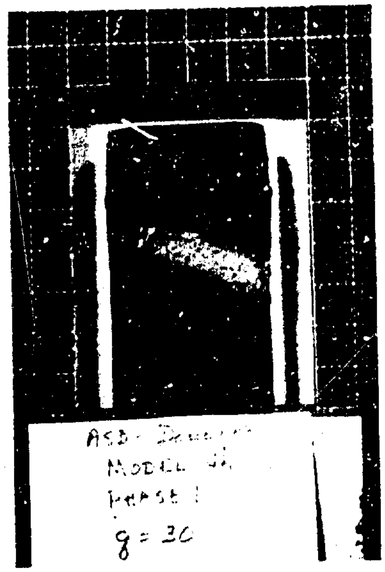

Model 4A - Post-Exposure

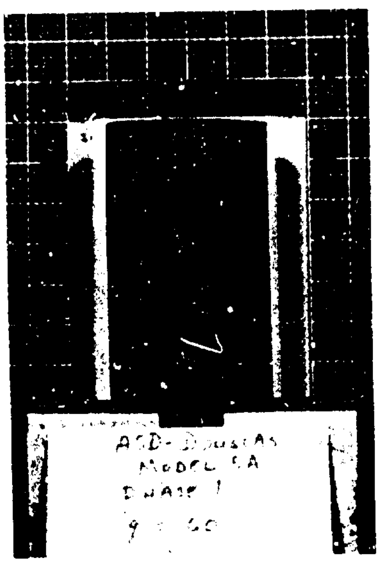

Model 5A - Pre-Exposure

Model 5A - Post-Exposure

Figure 60 -- Photographs of Douglas SMORS Material
Models 4A and 5A

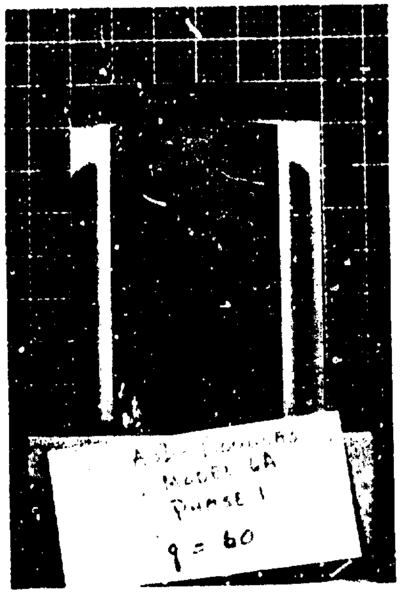

Model 6A - Pre-Exposure

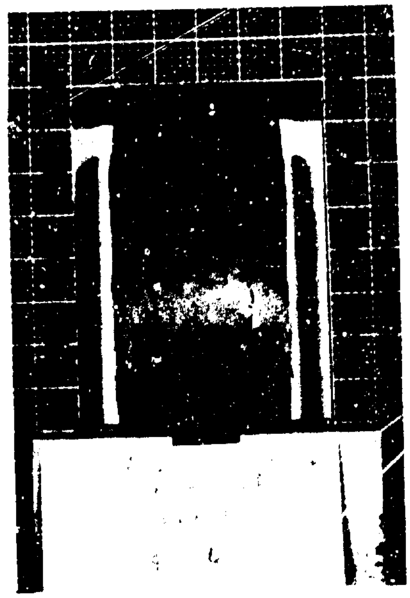

Model 6A - Post-Exposure

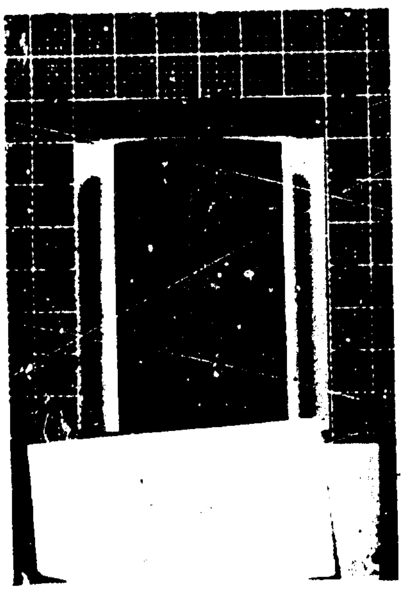

Model 7A - Pre-Exposure

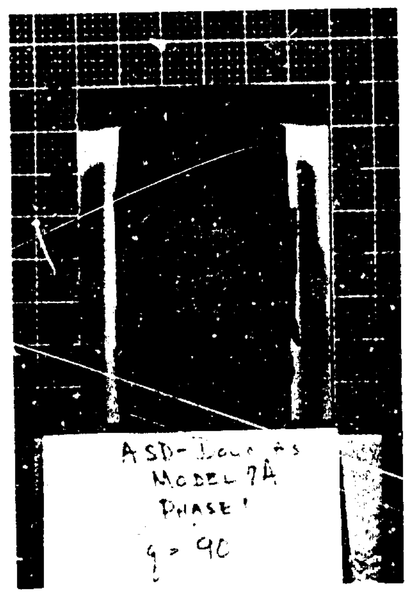

Model 7A - Post-Exposure

Figure 61 -- Photographs of Douglas SMORS Material
Models 6A and 7A

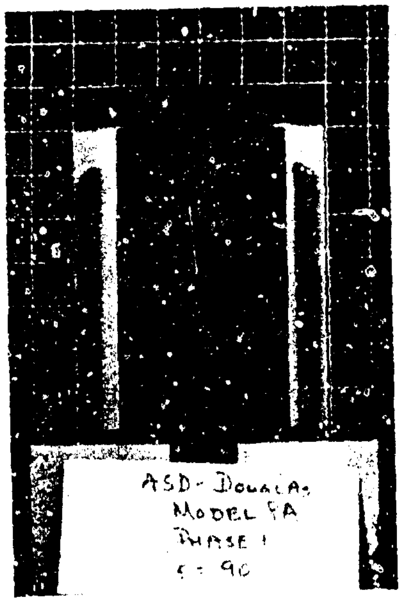

Model 8A - Pre-Exposure

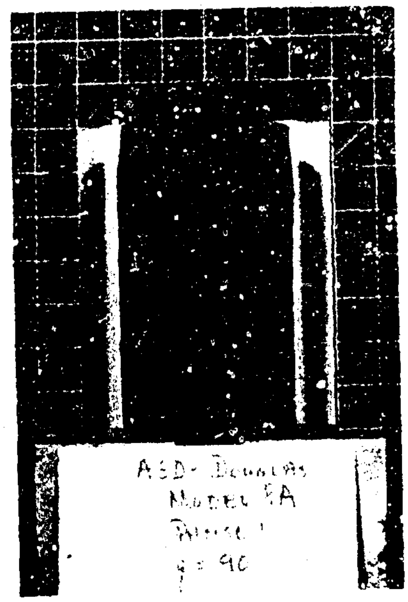

Model 8A - Post-Exposure

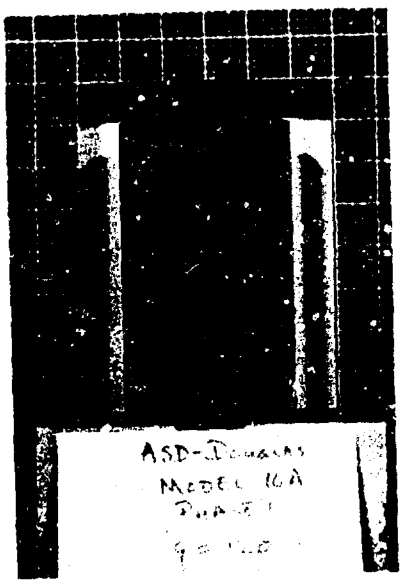

Model 10A - Pre-Exposure

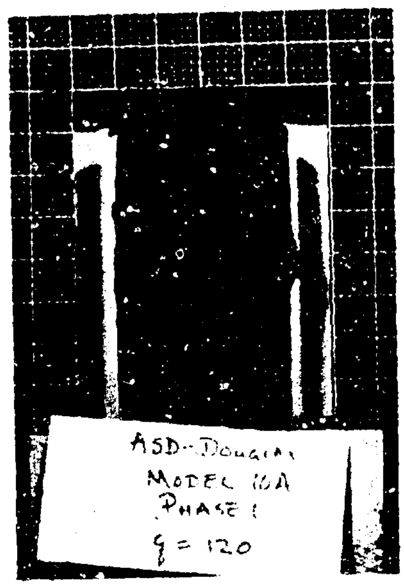

Model 10A - Post-Exposure

Figure 62 -- Photographs of Douglas SMORS Material
Models 8A and 10A

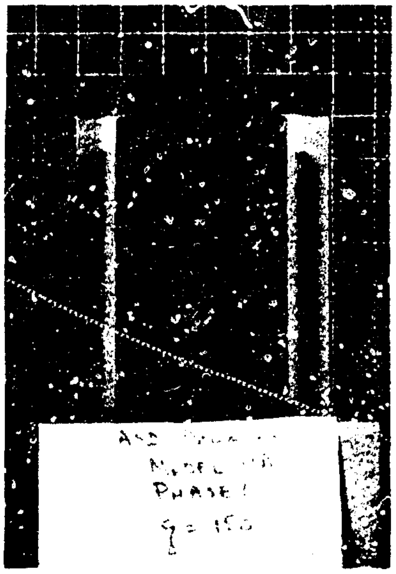

Model 11A - Pre-Exposure

Model 11A - Post-Exposure

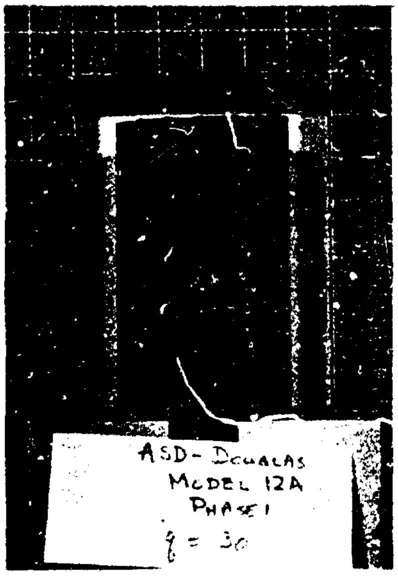

Model 12A - Pre-Exposure

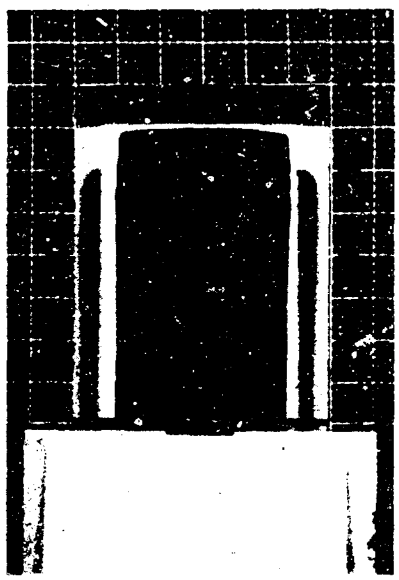

Model 12A - Post-Exposure

Figure 63 -- Photographs of Douglas SMORS Material
Models 11A and 12A

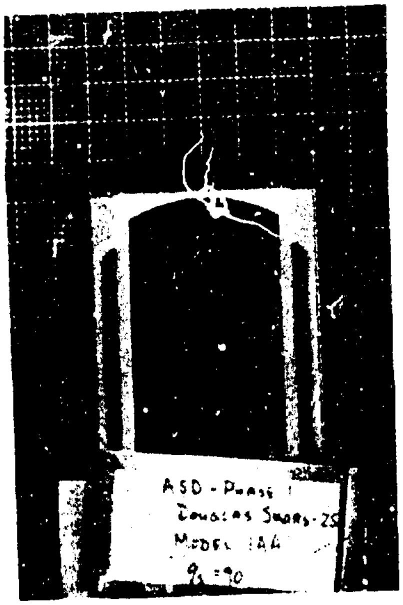

Model 1AA - Pre-Exposure

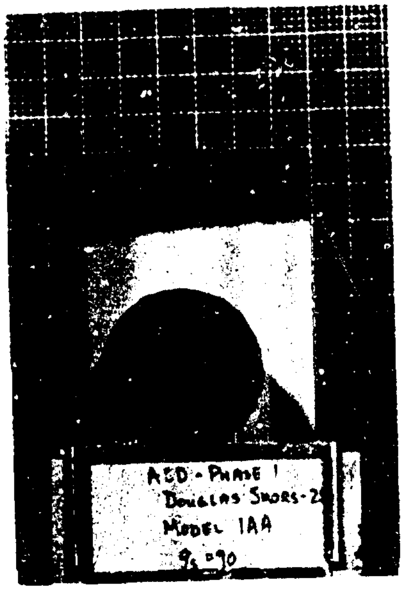

Model 1AA - Post-Exposure

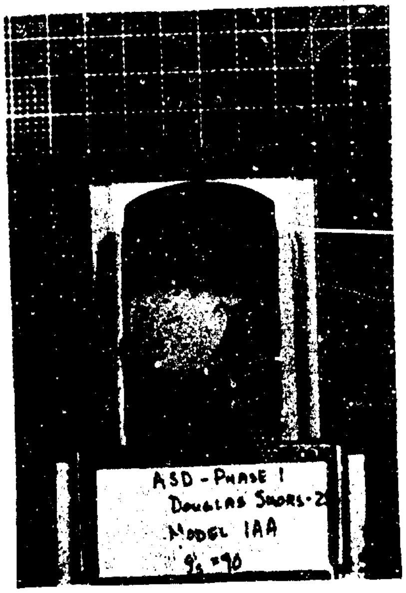

Model 1AA - Post-Exposure

Figure 64 -- Photographs of Douglas SMORS Material
Model 1AA

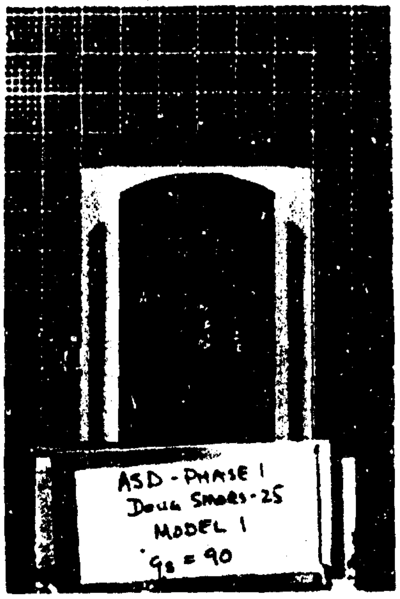

Model 1 - Pre-Exposure

Model 1 - Post-Exposure

Model 1 - Post-Exposure

Figure 65 -- Photographs of Douglas SMORS Material
Model 1

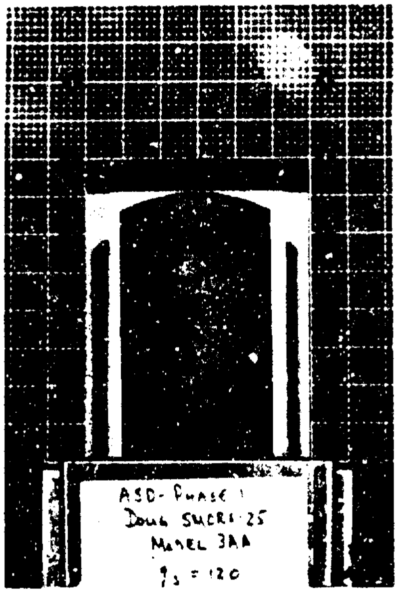

Model 3AA - Pre-Exposure

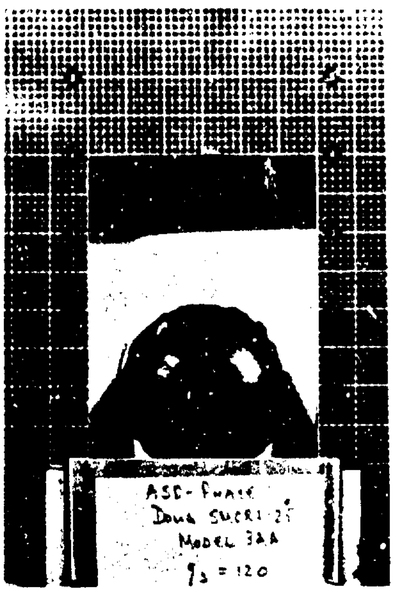

Model 3AA - Post-Exposure

Model 3AA - Post-Exposure

Figure 66 -- Photographs of Douglas SMORS Material
Model 3AA

Model 4AA - Pre-Exposure

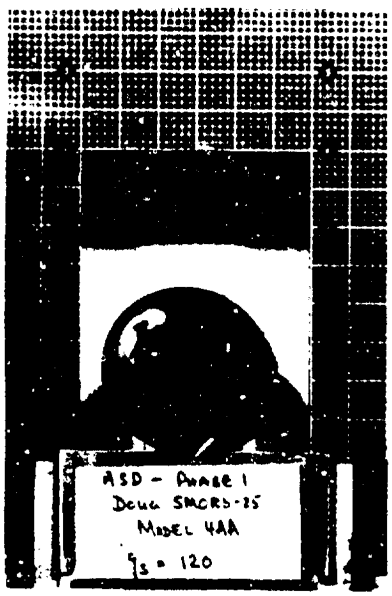

Mode. 4AA - Post-Exposure

Model 4AA - Post-Exposure

Figure 67 -- Photographs of Douglas SMORS Material
Model 4AA

Model 5AA - Pre-Exposure

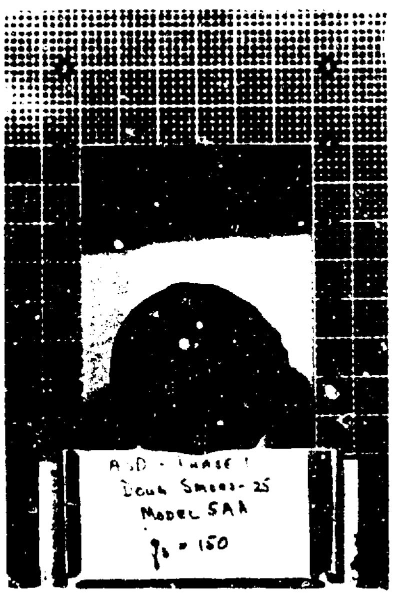

Model 5AA - Post-Exposure

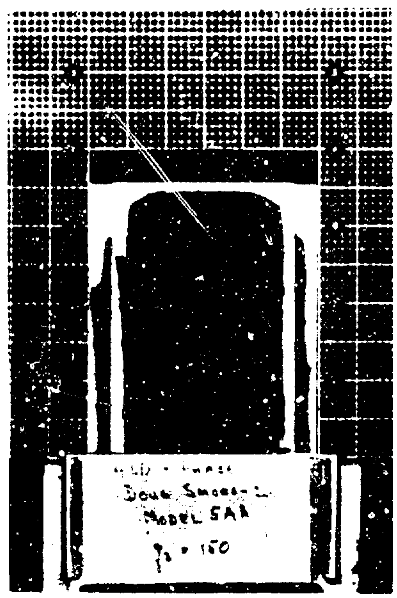

Model 5AA - Post-Exposure

Figure 68 -- Photographs of Douglas SMORS Material
Model 5AA

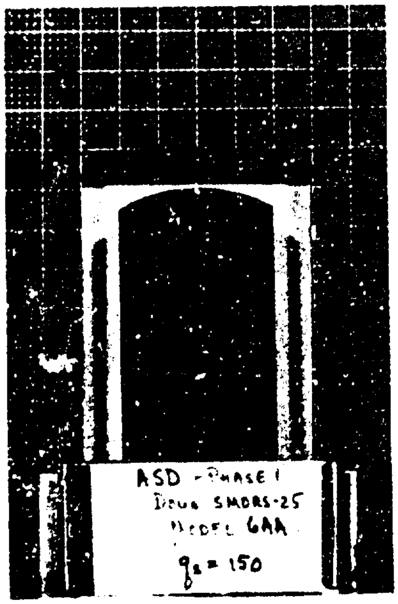

Model 6AA - Pre-Exposure

Model 6AA - Post-Exposure

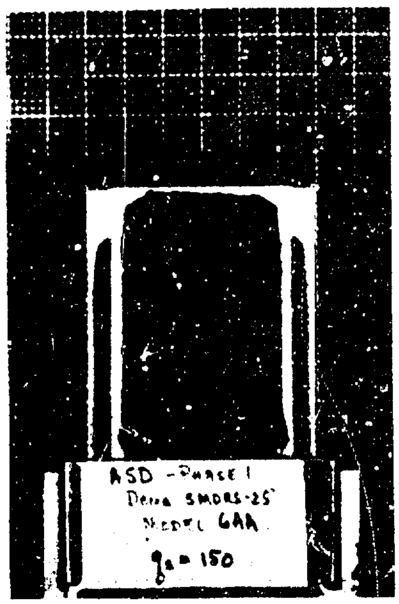

Model 6AA - Post-Exposure

Figure 69 -- Photographs of Douglas SMORS Material
Model 6AA

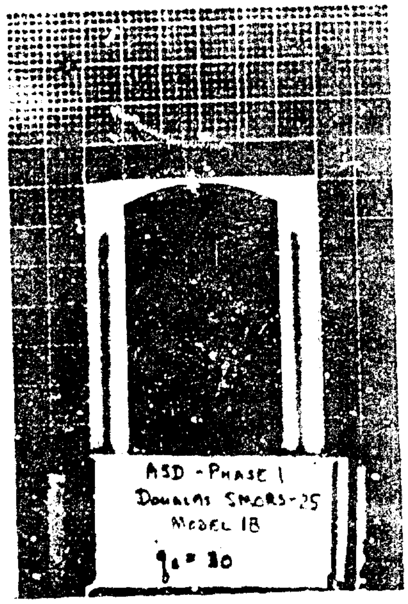

Model 1B - Pre-Exposure

Model 1B - Post-Exposure

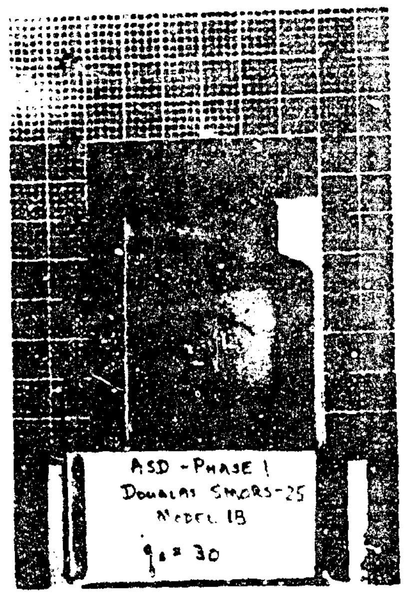

Model 1B - Post-Exposure

Figure 70 -- Photographs of Douglas SMORS Material
Model 1B

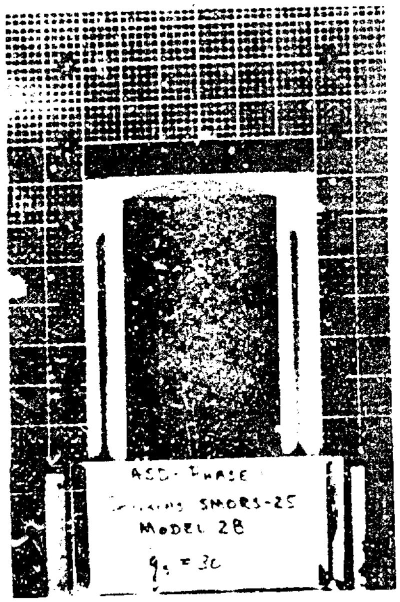

Model 2B - Pre-Exposure

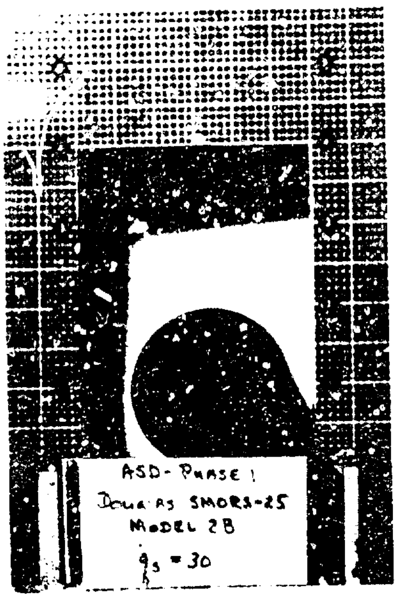

Model 2B - Post-Exposure

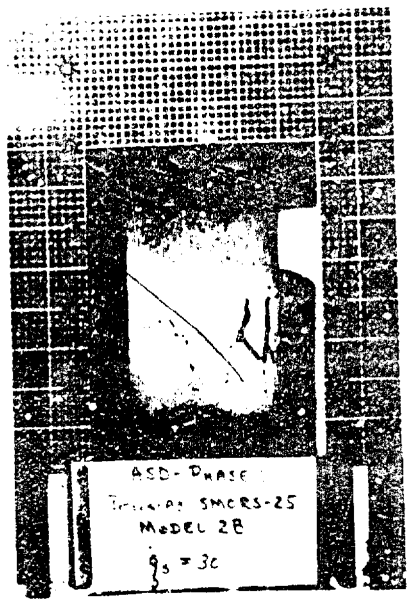

Model 2B - Post-Exposure

Figure 71 -- Photographs of Douglas SMORS Material
Model 2B

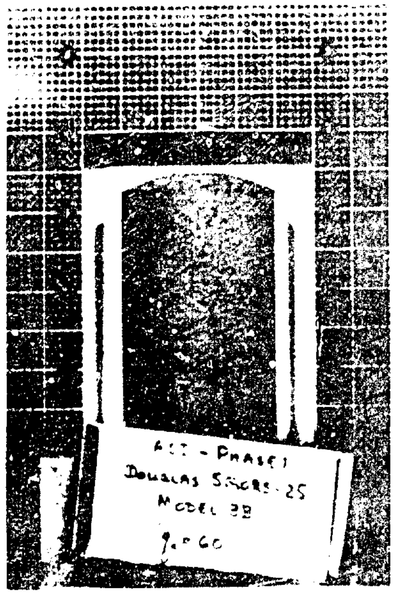

Model 3B - Pre-Exposure

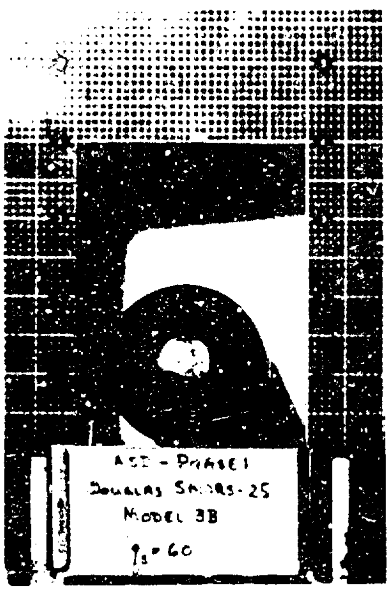

Model 3B - Post-Exposure

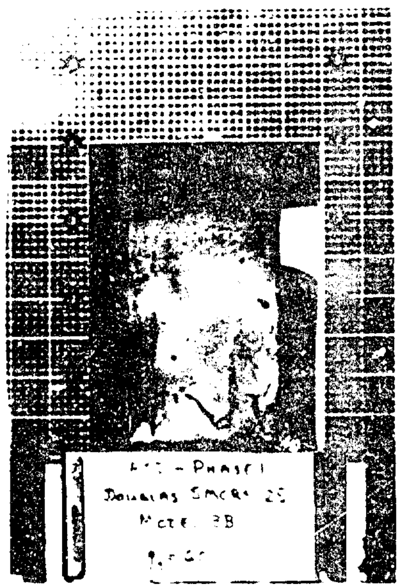

Model 3B - Post-Exposure

Figure 72 -- Photographs of Douglas SMORS Material
Model 3B

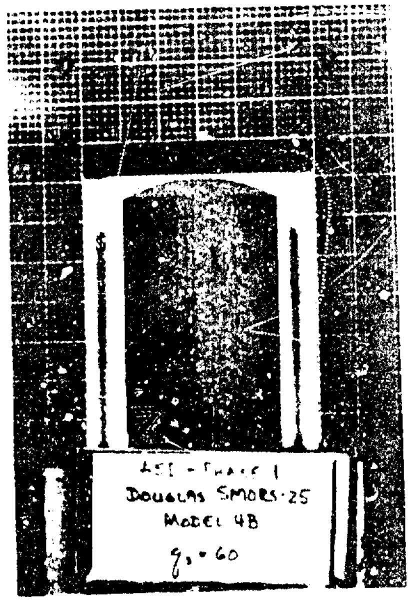

Model 4B - Pre-Exposure

Model 4B - Post-Exposure

Model 4B - Post-Exposure

Figure 73 -- Photographs of Douglas SMORS Material
Model 4B

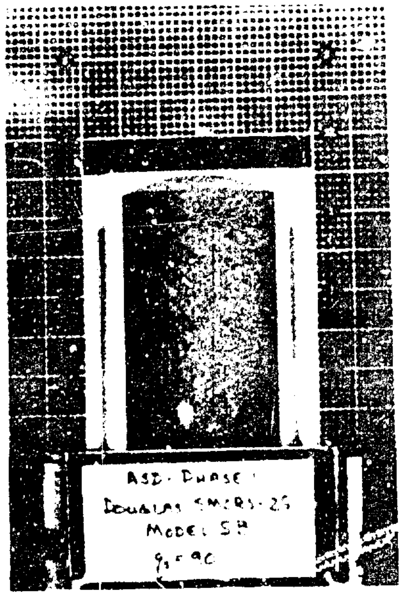

Model 5B - Pre-Exposure

Model 5B - Post-Exposure

Model 5B - Post-Exposure

Figure 74 -- Photographs of Douglas SMORS Material
Model 5B

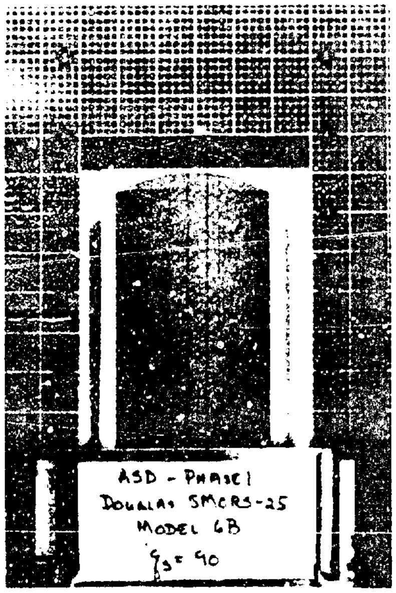

Model 6B - Pre-Exposure

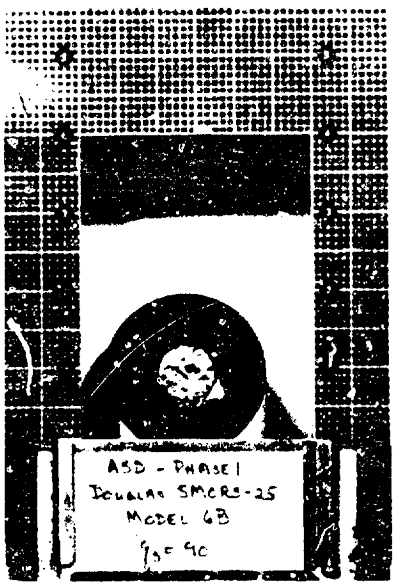

Model 6B - Post-Exposure

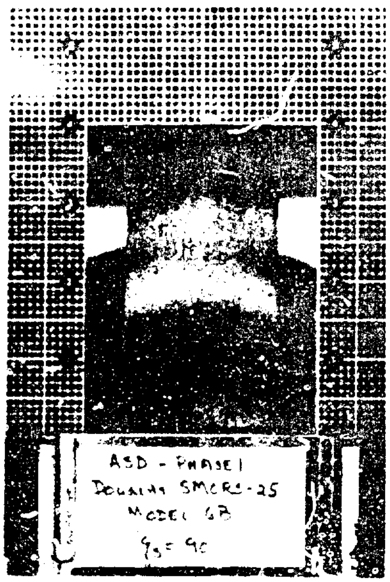

Model 6B - Post-Exposure

Figure 75 -- Photographs of Douglas SMORS Material
Model 6B

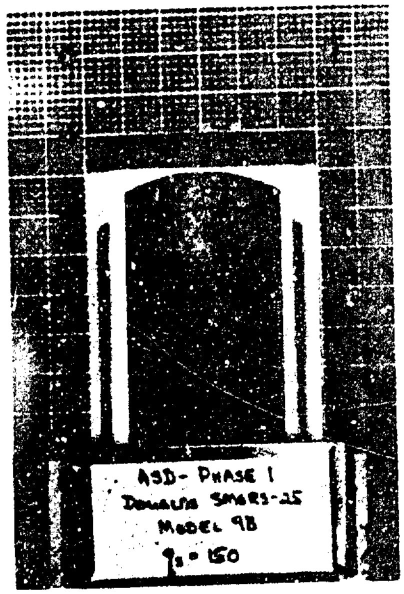

Model 9B - Pre-Exposure

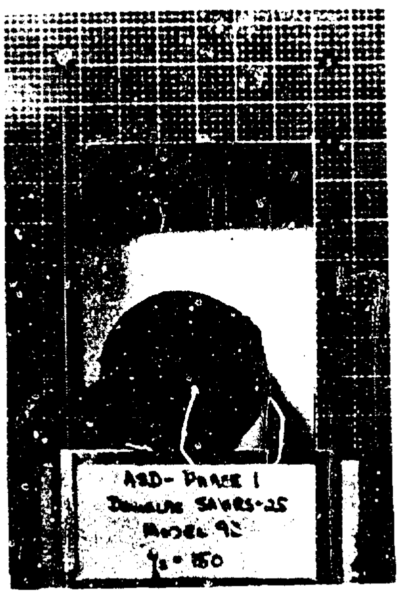

Model 9B - Post-Exposure

Model 9B - Post-Exposure

Figure 76 -- Photographs of Douglas SMORS Material
Model 9B

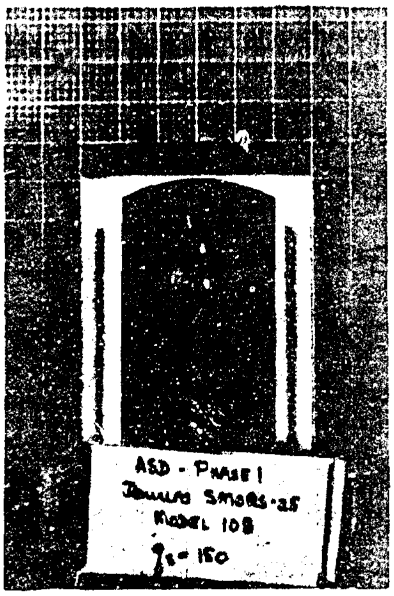

Model 10B - Pre-Exposure

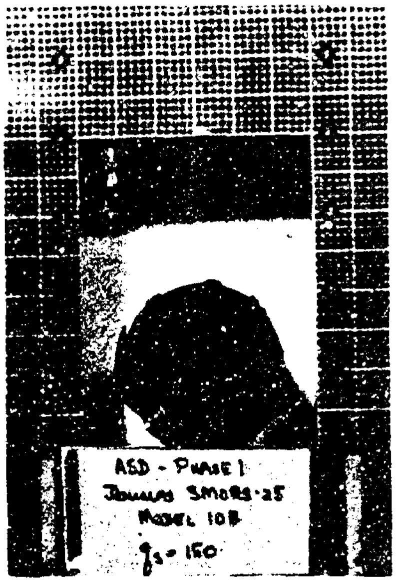

Model 10B - Post-Exposure

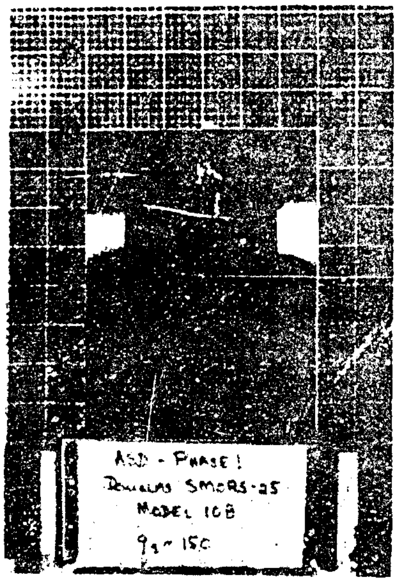

Model 10B - Post-Exposure

Figure 77 -- Photographs of Douglas SMORS Material
Model 10B

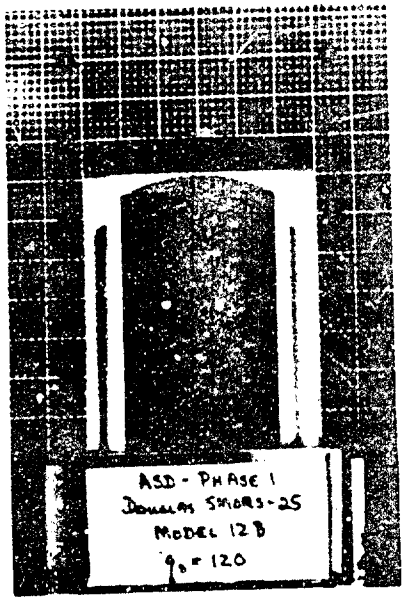

Model 12B - Pre-Exposure

Model 12B - Post-Exposure

Model 12B - Post-Exposure

Figure 78 -- Photographs of Douglas SMORS Material
Model 12B

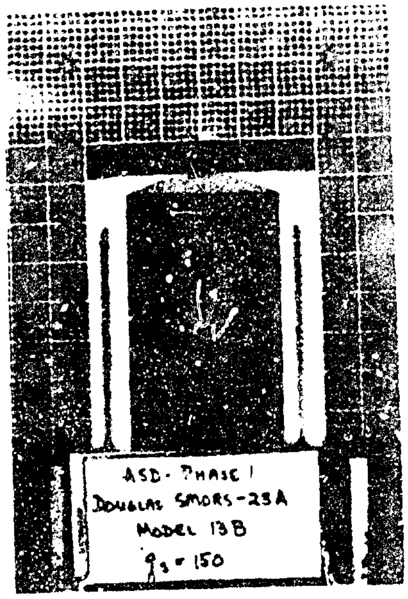

Model 13B - Pre-Exposure

Model 13B - Post-Exposure

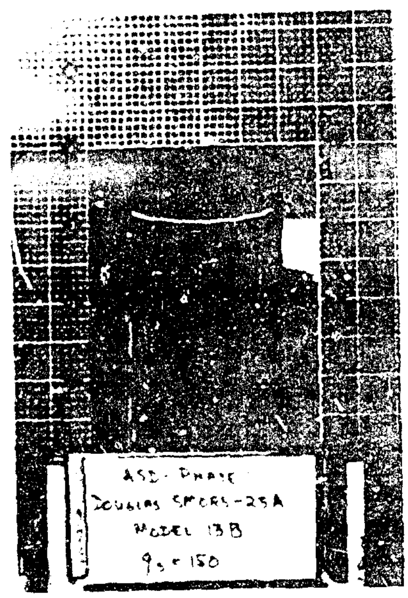

Model 13B - Post-Exposure

Figure 79 -- Photographs of Douglas SMORS Material
Model 13B

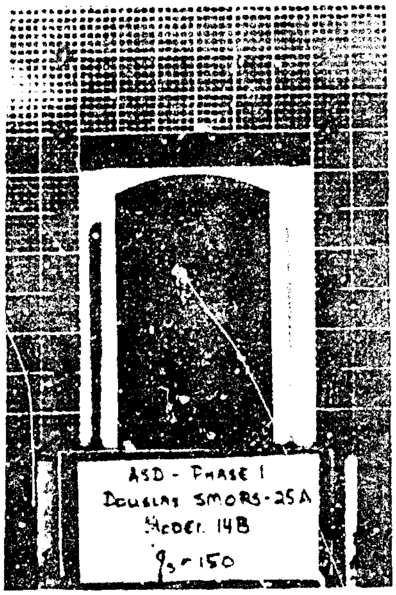

Model 14B - Pre-Exposure

Model 14B - Post-Exposure

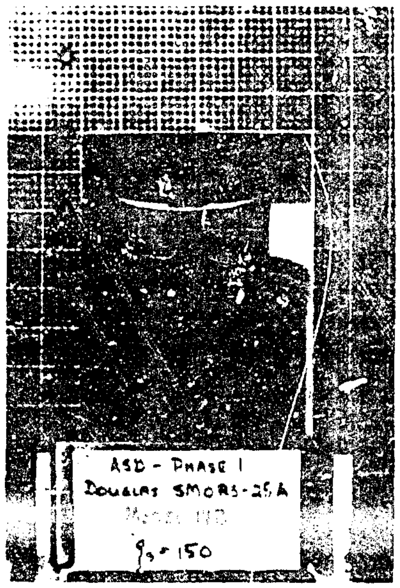

Model 14B - Post-Exposure

Figure 80 -- Photographs of Douglas SMORS Material
Model 14B

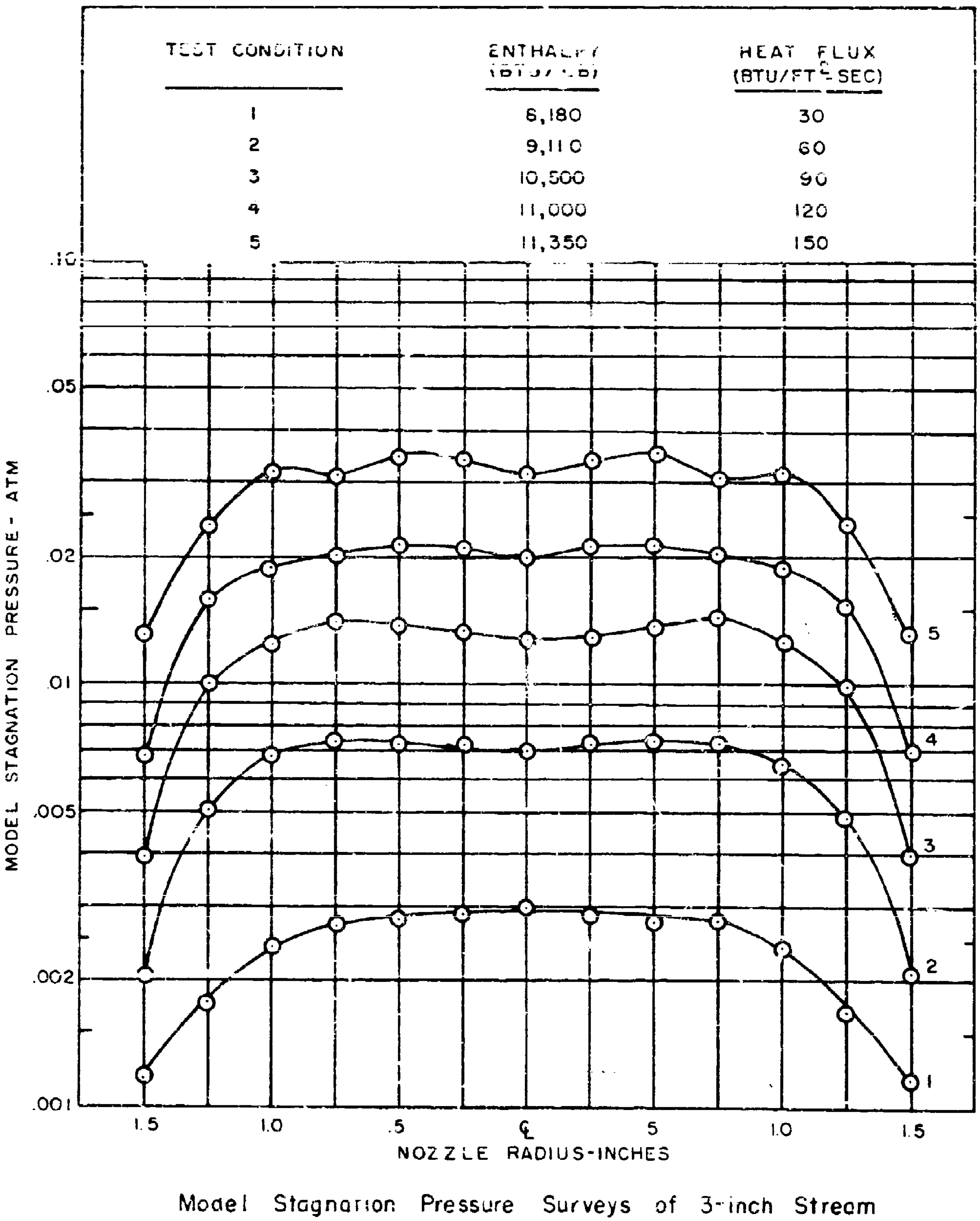

Figure 81 -- Model Stagnation Pressure Surveys for Low-Density Ablator Program

TEST CONDITION	ENTHALPY (BTU/LB)	STAGNATION PRESSURE (ATMOSPHERES)
1	8,180	.0030
2	9,110	.0071
3	10,500	.0131
4	11,000	.0205
5	11,350	.0320

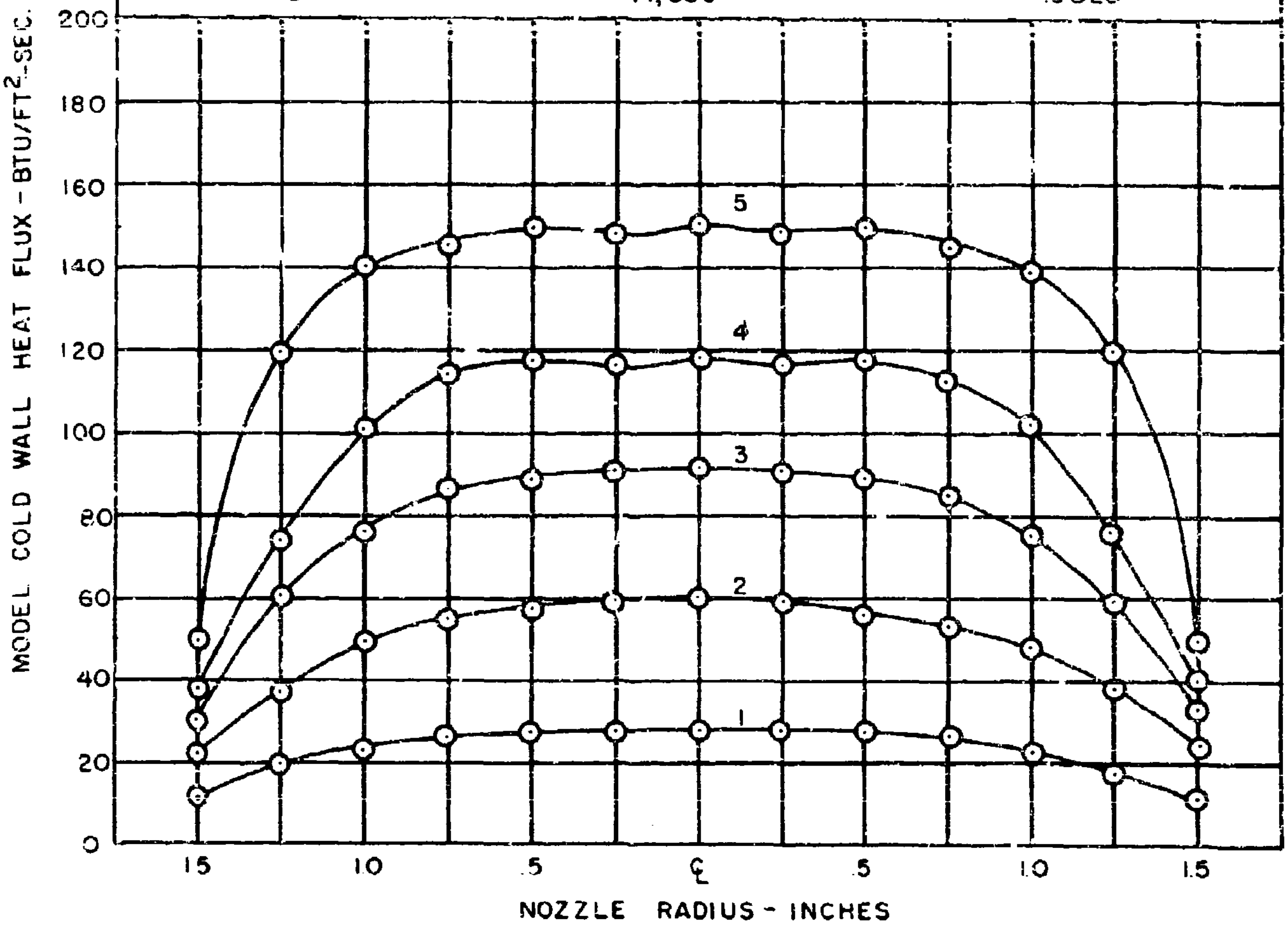

Heat Flux Surveys of 3-inch Stream

Figure 82 -- Heat Flux Surveys for Low-Density Ablator Program

ENVIRONMENTAL PARAMETERS

Mixing Chamber Pressure	p_T	1% Accuracy
Nozzle Static Pressure	p	1% Accuracy
Model Stagnation Pressure	p_o'	1% Accuracy
Stagnation Enthalpy	h_T	5% Accuracy
Heat Flux	$\dot{q}_s$	3% Accuracy

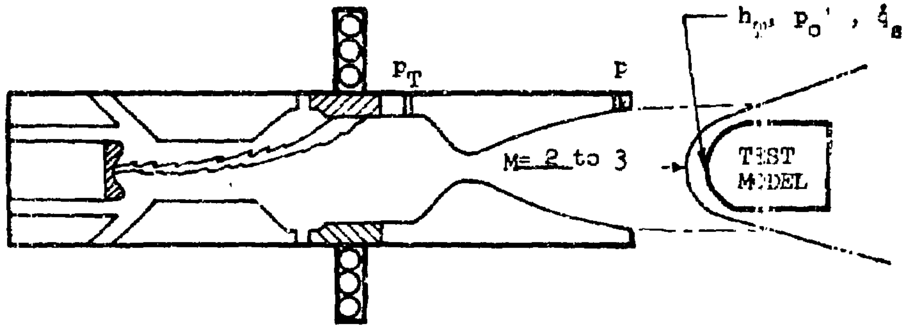

Heat Flux = $f(h_T , p_o')$

Enthalpy = $f(M , T , p_o')$

Mach No. = $f(h_T , p , p_T, p_o')$

Altitude = $f(p , h_T)$

Velocity = $f(h_T)$

Figure 83 -- Environmental Parameters

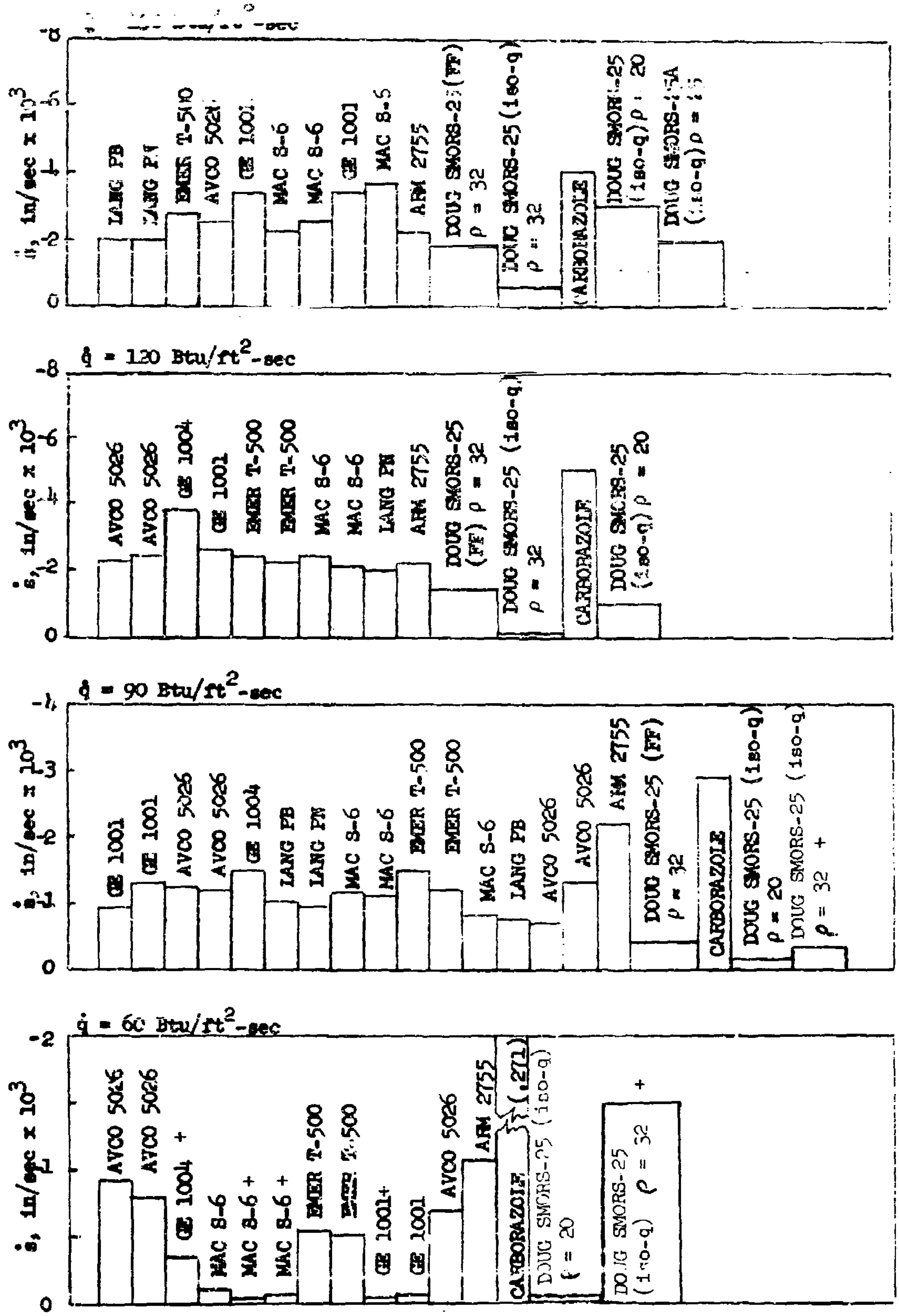

FIGURE 54 - FRONT SURFACE RECESSION RATE

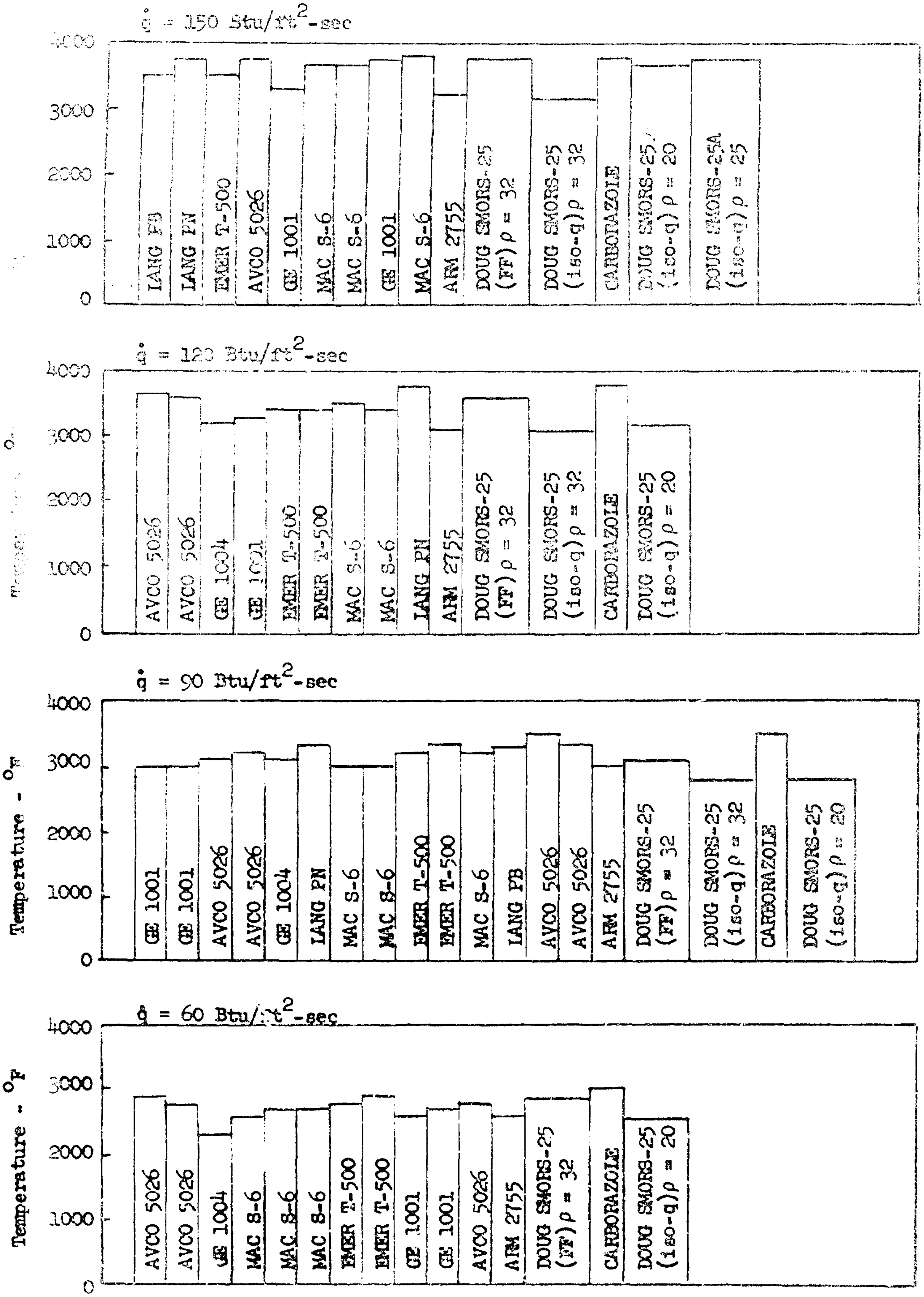

FIGURE 85 FRONT SURFACE BRIGHTNESS TEMPERATURE

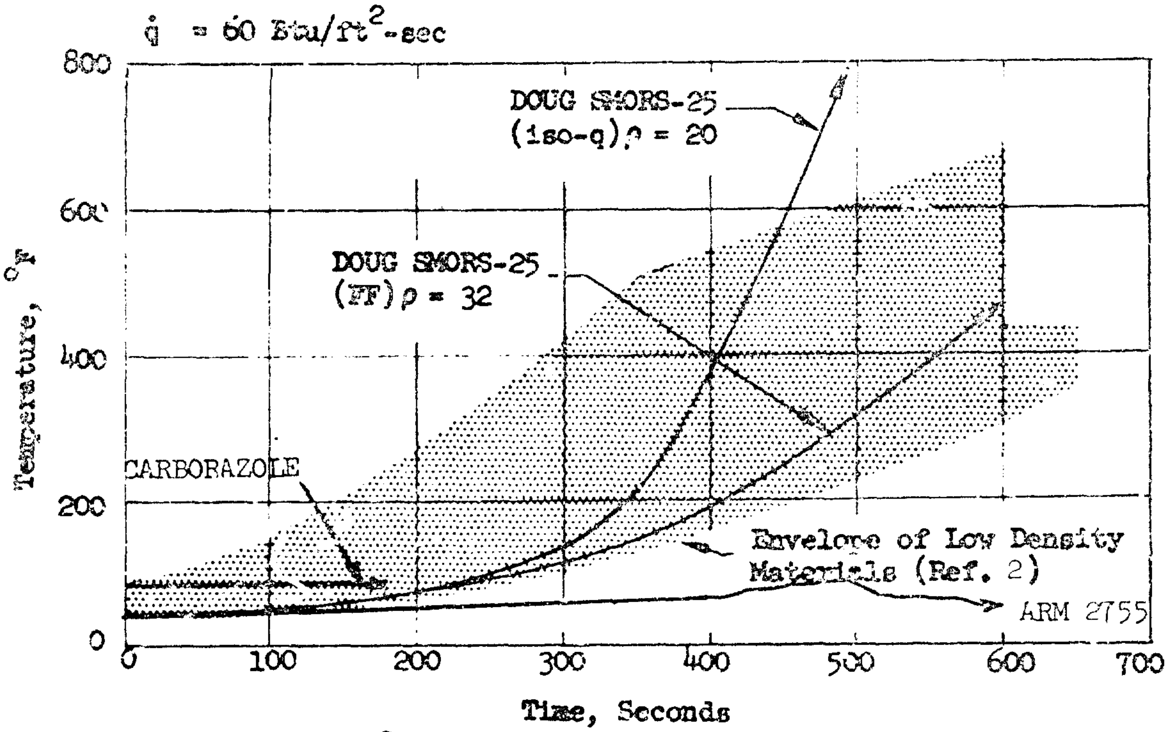

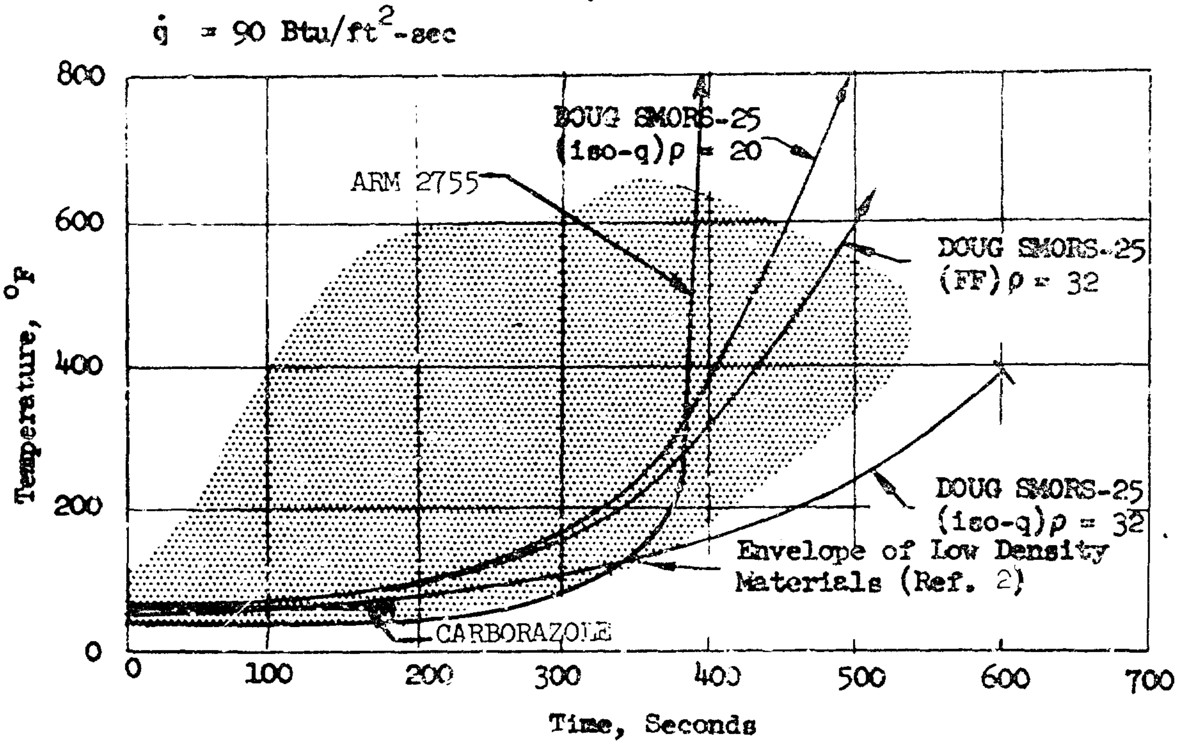

FIGURE 86 - COMPARISON OF BACK-FACE TEMPERATURES

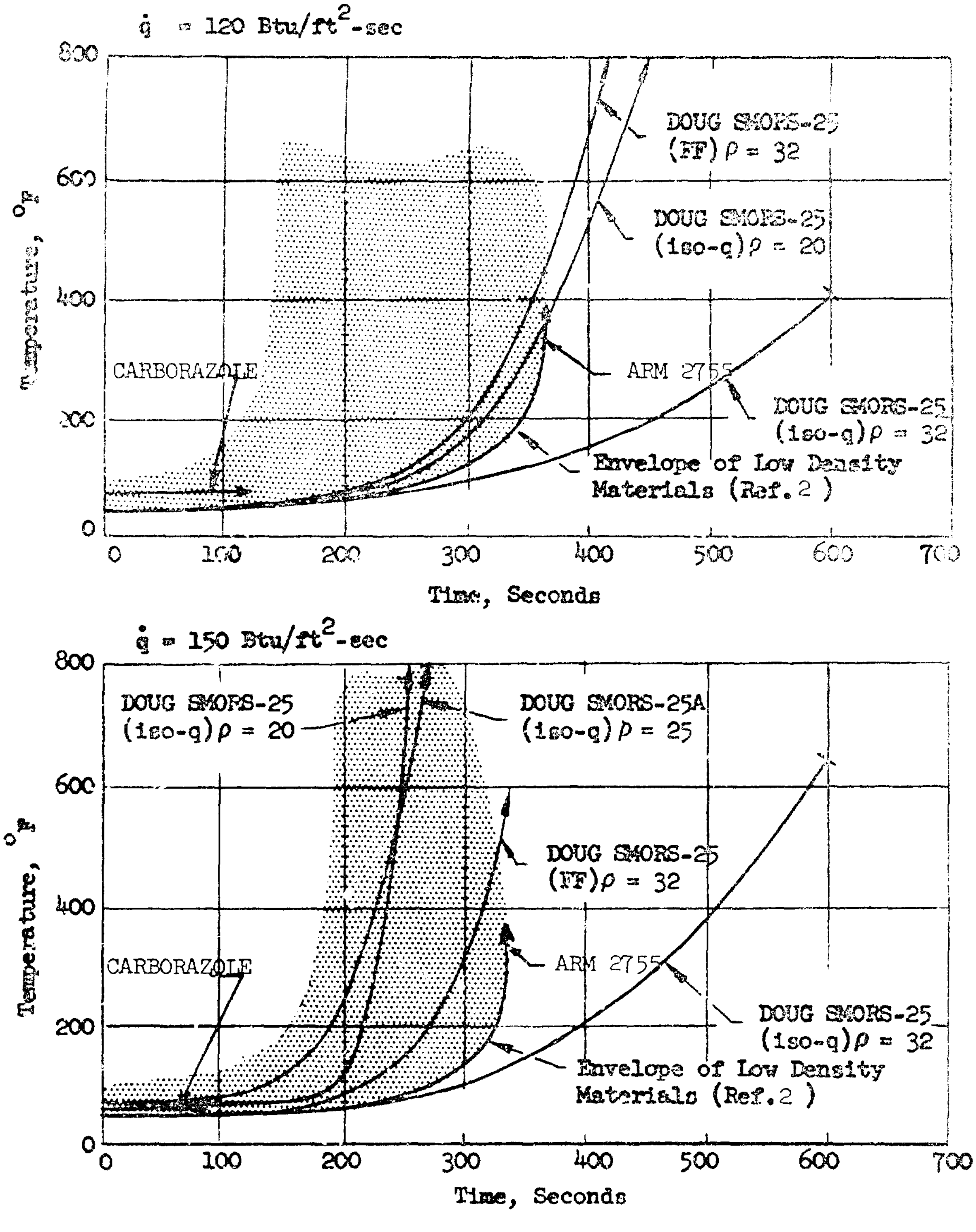

FIGURE 87 - COMPARISON OF BACK-FACE TEMPERATURES

PRECEDING PAGE BLANK- NOT FILMED.

3.0 HIGH-DENSITY ABLATOR PROGRAM

Lifting re-entry vehicles currently envisioned for future mission applications require the use of relatively high-density ablation materials in the nose and flap regions to limit the shape change due to surface recession. The ablative materials considered for this application were in the density range from 85 to 190 lb/ft^3 and were supplied by Union Carbide Corporation and Dow Corning. Materials supplied by these two organizations were subjected to environmental heating conditions comparable to those at which earlier materials tests were performed as reported in Ref. 3 (Welsh, 1965). Performance data from both series of test programs are compared in this report.

3.1 Objectives

A survey of lifting re-entry vehicle nose cap materials was performed by Aerospace Corporation in 1965 for the Air Force, in which high-density ablators were tested under hyperthermal environmental re-entry conditions and evaluated in terms of thermal response, surface recession, etc.. The following materials were considered in the Aerospace Corporation program; detailed information is presented in Ref. 3 (Welsh, 1965).

Phenolic-Carbon Fabric Laminates, fabric parallel to heated face

Fiberite 4500
Fiberite 4926
HITCO EPA 94-FM 5014
HITCO EPA 94-FM 5055
HITCO EPA 94-FM 5314
HITCO EC 201 CCA 11
HITCO SS 1620
Fiberite MXC 97
3M Pluton - Sc 1008
USP Pluton - 5277 BG

Phenolic-Carbon Fabric Laminates, fabric 20 degrees to heated face

HITCO EPA 94-FM 5014
HITCO EPA 94-FM 5055
HITCO EPA 94-FM 5314
Ironsides 6T9

Phenolic-Carbon Fabric or Fiber, Random Orientation

U. S. Polymeric FM 5065 (or M 5065 RF)
Martin PL (Pluton) 5277 RF (or MPL 5277 RF)
USP PL (Pluton) 5277 RF (or PL 5277 RF)

Molded Powders and Paper Laminates

ATJ Graphite (Standard)
Super-Temp STX
ARP 275 PHX (parallel)
ARP 275 PHX (20° to heated surface)
ARP 292 PHZ
ARP 289 XC

The standard model configuration used in evaluating the above materials was a 2.0-inch diameter flat-face cylinder, instrumented with three chromel/alumel thermocouples at the rear-face of the specimen. Heat flux levels (cold-wall values) of 40, 100 and 140 Btu/ft^2-sec were imposed on the flat-face specimens. The main purpose of the tests was to evaluate the effects of long-duration heating at low levels of heat flux on the mechanical integrity of the material specimens, since previous experience with the above-listed materials had been for much shorter times and higher heat fluxes than experienced in lifting re-entry. A secondary purpose of this testing was to obtain preliminary data on thermal response characteristics of these materials. A total of 58 model tests were conducted in an arc-heated wind tunnel; a report summarizing the test results has been issued under TDR-669(6240-10)-2 from Aerospace Corporation, El Segundo, California.

The objectives of our high-density ablator program, performed under this contract, were manifold in that 1) new high-density ablators were evaluated at identical environmental heat flux conditions as in the earlier Aerospace program, and 2) materials performance data was obtained at additional heat flux values of 300 and 650 Btu/ft^2-sec.

3.2 Description of Materials Tested

Six high-density materials were supplied by two companies; a total of 32 test models were exposed to cold-wall heating rates of 40, 140, 300 and 650 Btu/ft^2-sec. The supplier and type of material supplied were:

Union Carbide Corporation -

- Grade HDB Boron Nitride with an intermetallic composite of Titanium Diboride
- Grade HDF Boron Nitride with an intermetallic composite of Titanium Diboride
- Grade HBN Boron Nitride - Hot-Pressed Boron Nitride
- Grade HBR Boron Nitride - Hot-Pressed Boron Nitride with improved moisture resistance and high-temperature properties over those of Grade HBN

Dow Corning Corporation -

- Dow Corning 93-002
- Dow Corning 93-069

Although the model configuration used in the Aerospace test program was a 2.0-inch diameter flat-face cylinder, we chose to standardize on a model of 2.5-inch diameter hemispherical nose - cylinder configuration. This was done to enable achievement of higher heat flux values at the stagnation point of 650 Btu/ft^2-sec. A factor of approximately two is gained by using a hemispherical nose tip rather than a flat-face nose (Stoney and Markley, 1958, Ref. 4) model. A schematic representation of the standard high-density ablator model is presented in Figure 88, showing the location of instrumentation sensors and type of thermocouple wire used.

The test models supplied by Union Carbide Corporation (free of charge) were not instrumented since the main intent of the boron nitride materials evaluation program was to compare gross behavior and thermal shock and spalling characteristics exhibited by each of the four grades of material. The Dow Corning models, however, were fabricated and instrumented by the materials supplier (Dow Corning, Midland, Michigan) in accordance with the model design presented in Figure 88. All thermocouples utilized on this series of model tests were of chromel/alumel, 36 gage wire, and were recorded on a null-balance recorder (Texas Instruments ServoRiter II), $\frac{1}{4}$% full-scale accuracy. Five-minute exposure periods were achieved at most of the test conditions and for most of the test models; somewhat lower test times were required for the higher heat flux conditions. Surface temperatures were read manually using a Leeds and Northrup optical brightness pyrometer. Color film coverage was obtained on each model test and has been forwarded to the respective materials suppliers.

3.2.1 Dow Corning 93-002 and 93-069 Materials

The two high-density ablator materials supplied by Dow Corning were submitted free of charge for evaluation under this phase of the contract. The Dow Corning 93-002 material represents a silicone material with a high level of phenyl substitution. This material has looked good in high flux, high shear ablative tests and recently, a renewal of interest in leading edge protection, nose tip protection, and refurbishable rocket nozzle materials led to the development of Dow Corning 93-069. It is essentially a specialty version of Dow Corning 93-002 with indications of having better high shear, high flux performance characteristics. Both these materials are readily castable or trowelable and cure at room temperature. These characteristics are of interest to a variety of aerospace manufacturers and government agencies who are looking for easier ways to fabricate and refurbish ablative materials. Density levels of the two materials are 88.7 lb/ft^3 for 93-002 and 107.4 lb/ft^3 for 93-069.

Two models of each material were evaluated at each of the four levels of heat flux. Tunnel calibration data obtained on each model test is tabulated in Table 9, including the specific measurements of enthalpy, model stagnation pressure, nozzle stagnation and static pressures, and gas flow rates. Table 10 contains the weight loss and recession rates, and the stabilized surface brightness temperature readings for each of the sixteen models tested.

The test data, in terms of weight loss and recession rates, has been graphed in Figure 89 as a function of model stagnation heat flux. It is apparent from the plots of both the weight loss rate and the recession rate that the 93-069 material did perform in a superior fashion to the 93-002 material. In addition, close examination of the post-exposure photographs reveals that the 93-069 material did not crack in depth or develop surface cracks to the extent that the 93-002 material experienced.

Model surface brightness and internal and back-face temperature-time histories are presented graphically in Figures 90 through 105. Pre- and post-exposure black and white photographs of each model are presented in Figures 106 through 119.

TABLE 9

CALIBRATION DATA

Dow Corning Model Tests

Test Point	Model No./Material	Gas Enthalpy (Btu/lb)	Model Stag. Pressure (atm)	Model Cold-Wall Heat Flux (Btu/ft^2 - sec)	Nozzle Stag. Pressure (atm)	Nozzle Static Pressure (atm)	Gas Flow Rate (lb/sec)
1	6-26/93-002	6,950	0.00231	42.3	0.00989	0.000197	0.000491
1	6-27/93-002	6,885	0.00222	41.8	0.00986	0.000197	0.000491
1	6-28/93-069	6,850	0.00234	42.0	0.00987	0.000196	0.000491
1	6-29/93-069	6,910	0.00233	42.1	0.00987	0.000197	0.000491
2	6-30/93-002	9,990	0.00943	144.3	0.0475	0.000871	0.002050
2	6-31/93-002	10,050	0.00944	143.9	0.0474	0.000869	0.002050
2	6-32/93-069	10,005	0.00939	144.5	0.0478	0.000871	0.002050
2	6-33/93-069	9,985	0.00941	143.9	0.0479	0.000872	0.002050
3	6-34/93-002	12,105	0.0248	310.1	0.1371	0.00248	0.005400
3	6-35/93-002	12,110	0.0249	311.2	0.1369	0.00245	0.005400
3	6-36/93-069	12,180	0.0248	310.1	0.1369	0.00246	0.005400
3	6-37/93-069	12,155	0.0249	309.9	0.1366	0.00243	0.005400
4	6-38/93-002	13,300	0.125	659.1	0.699	0.0128	0.026200
4	6-39/93-002	13,290	0.125	660.2	0.701	0.0129	0.026200
4	6-40/93-069	13,305	0.125	661.1	0.700	0.0127	0.026200
4	6-41/93-069	13,285	0.125	660.0	0.700	0.0126	0.026200

TABLE 10

MODEL TEST DATA

Dow Corning Model Tests

Test Condition	Model No./Material	Exposure Time (secs)	Weight Loss (grams)	Recession (inches)	Weight Loss Rate (gms/sec)	Recession Rate (in/sec)	Surface Temp. (°F)
1	6-26/93-002	300.0	4.1	+0.205	0.01365	+0.000683	2330
1	6-27/93-002	300.0	4.3	+0.262	0.01432	+0.000873	2350
1	6-28/93-069	300.0	4.7	+0.255	0.01565	+0.000850	2350
1	6-29/93-069	300.0	5.5	+0.249	0.01832	+0.000830	2420
2	6-30/93-002	300.0	18.7	+0.162	0.06227	+0.000540	3010
2	6-31/93-002	300.0	19.0	+0.141	0.06327	+0.000470	3040
2	6-32/93-069	300.0	13.4	+0.109	0.04462	+0.000363	3030
2	6-33/93-069	300.0	12.8	+0.210	0.04262	+0.000700	3000
3	6-34/93-002	300.0	26.5	-0.222	0.08824	0.0007393	3140
3	6-35/93-002	300.0	26.2	-0.215	0.08725	0.0007160	3110
3	6-36/93-069	300.0	24.8	-0.154	0.08258	0.0005128	3530
3	6-37/93-069	300.0	26.5	-0.200	0.08824	0.0006667	3530
4	6-38/93-002	180.0	140.7	-1.058	0.7817	0.005878	3600
4	6-39/93-002	180.0	128.6	-0.985	0.7145	0.005473	3530
4	6-40/93-069	180.0	85.6	-0.538	0.4756	0.002989	3700
4	6-41/93-069	180.0	83.2	-0.583	0.4622	0.003239	3700

NOTE:
(+) Designates Model Expanded

3.2.2 Union Carbide Boron Nitride Materials

Boron nitride is one of the few available engineering materials that is readily machinable, nontoxic, a good conductor of heat and an excellent electrical insulator. The performance of hot pressed boron nitride, because of its useful properties that extend in some cases up to about 4200°F, suggests its evaluation for high temperature thermal shock applications such as heat sinks and thermal radiation shields. In particular, application of hot pressed boron nitride for use in leading edges and aerodynamic surfaces of hypersonic vehicles is of prime interest.

The Carbon Products Division of Union Carbide Corporation was contacted early in our contract period and were asked if they would like to submit candidate boron nitride materials for evaluation under our high-density ablator program. Because of the interest generated in their material for aerospace applications, four grades of boron nitride were submitted, as follows:

Grade HDB - Boron Nitride with an intermetallic composite of Titanium Diboride - Density of 187.4 lb/ft^3

Grade HDF - Boron Nitride with an intermetallic composite of Titanium Diboride - Density of 174.9 lb/ft^3

Grade HBN - Boron Nitride - Density of 128.0 lb/ft^3

Grade HBR - Boron Nitride - Density of 121.8 lb/ft^3

A complete description of each of the various grades of boron nitride listed above will not be attempted in this report, however, this information may be obtained from Union Carbide Corporation and Ref. 5 (Fredrickson, 1964).

Sixteen models were submitted by Union Carbide, four of each grade of material; one model of each material was tested at the heat flux levels of 40, 140, 300 and 650 Btu/ft^2-sec. In general, each model was exposed for five minutes or until model failure occurred. Model failure was experienced by each grade of material at the highest heat flux level of 650 Btu/ft^2-sec.

The boron nitride model test data consisted of weight loss rates, recession rates, and surface brightness temperatures. Model internal and backface temperature-time histories were not obtained since thermocouples were not installed on these particular models. The tunnel calibration data, defining the environmental test conditions, is summarized in Table 11; model test data is tabulated in Table 12. Surface brightness temperature measurements are plotted in Figures 120 through 123 for all models, with the exception of Model 6-4, which failed due to thermal shock after a twelve-second exposure to the plasma stream.

All of the boron nitride models were placed in an oven at 350°F for a 24-hour period immediately prior to their exposure to the hyperthermal environment. This was done to eliminate or minimize the water absorption which results in spalling of the model during exposure to the heated plasma stream. At the highest heat flux condition of 650 Btu/ft^2-sec, the first model tested was Model 6-4, which cracked and broke in three pieces during the first five seconds of exposure. Consequently, on the remainder of the models tested at this highest heat flux condition, the models were inserted into the stream at

TABLE 11

CALIBRATION DATA

Boron Nitride Model Tests

Test Condition	Model No.*	Gas Enthalpy (Btu/lb)	Model Stag. Pressure (atm)	Model Cold-Wall Heat Flux (Btu/ft^2-sec)	Nozzle Stag. Pressure (atm)	Nozzle Static Pressure (atm)	Gas Flow Rate (lb/sec)
1	6-1	6,825	0.0022	41.8	0.00982	0.000193	0.000491
2	6-2	9,980	0.00943	145.5	0.0478	0.000868	0.00205
3	6-3	11,935	0.0243	308.9	0.137	0.00245	0.00540
4	6-4	13,110	0.125	661.0	0.701	0.0125	0.0262
1	6-5	6,875	0.0022	42.1	0.00984	0.000198	0.000491
2	6-6	10,105	0.00941	144.9	0.0472	0.000871	0.00205
3	6-7	12,005	0.0245	307.6	0.137	0.00248	0.00540
4	6-8	13,205	0.125	660.9	0.701	0.0124	0.0262
1	6-9	6,900	0.0023	42.5	0.00981	0.000195	0.000491
2	6-10	9,900	0.00947	146.6	0.0475	0.000872	0.00205
3	6-11	12,005	0.0242	310.1	0.137	0.00248	0.00540
4	6-12	13,055	0.125	662.5	0.703	0.0126	0.0262
1	6-13	7,000	0.0023	43.3	0.00976	0.000198	0.000491
2	6-14	10,000	0.00944	146.5	0.0481	0.000870	0.00205
3	6-15	12,035	0.0244	310.1	0.137	0.00248	0.00540
4	6-16	13,105	0.125	663.4	0.701	0.0123	0.0262

NOTE:

*Models 6-1 through 6-4 . . . Boron Nitride, Grade HDB
Models 6-5 through 6-8 . . . Boron Nitride, Grade HDF
Models 6-9 through 6-12 . . Boron Nitride, Grade HBN
Models 6-13 through 6-16 . . Boron Nitride, Grade HBR

TABLE 12

MODEL TEST DATA

Boron Nitride Model Tests

Test Condition	Model No.*	Exposure Time (seconds)	Weight Loss (grams)	Recession (inches)	Weight Loss Rate (grams/sec)	Recession Rate (inches/sec)	Surf. Temp. (^{o}F)
1	6-1	360.0	0.2	+0.012	0.000556	Swelling	1700
2	6-2	300.0	0.1	+0.006	0.000333	Swelling	1830
3	6-3	300.0	0.1	+0.003	0.000333	Swelling	3050
4	6-4	12.0	---	------	Not Obtained	Not Obtained	Not Obtained
1	6-5	300.0	0.1	-0-	0.000333	-0-	1710
2	6-6	300.0	-0-	+0.001	-0-	Swelling	1840
3	6-7	300.0	1.1	-0.035	0.00367	0.0001167	3540
4	6-8	130.0	21.4	-0.141	0.1646	0.001085	4700
1	6-9	300.0	0.2	-0.001	0.000667	3.33×10^{-6}	1790
2	6-10	300.0	0.1	-0.003	0.000333	Swelling	1970
3	6-11	300.0	0.7	-0.022	0.002333	7.33×10^{-5}	3310
4	6-12	160.0	9.1	-0.088	0.05687	0.000550	4240
1	6-13	300.0	0.1	+0.001	0.000333	Swelling	1615
2	6-14	300.0	0.2	-0.001	0.000667	3.33×10^{-6}	2050
3	6-15	300.0	1.0	-0.005	0.003333	0.0000167	3570
4	6-16	180.0	11.2	-0.091	0.06222	0.0005055	4080

NOTE:

*Models 6-1 through 6-4 . . . Boron Nitride, Grade HDB
Models 6-5 through 6-8 . . . Boron Nitride, Grade HDF
Models 6-9 through 6-12 . . Boron Nitride, Grade HBN
Models 6-12 through 6-16 . . Boron Nitride, Grade HBR

a lower heat flux condition and were brought up to the maximum heat flux level over a period of 10-15 seconds. Cracking of the remaining three models due to thermal shock was avoided using this procedure. (The surface cracks noted in the table below did not occur during the initial exposure period, but gradually formed and became more severe with exposure time).

The table below summarizes the gross performance of the various grades of boron nitride at the four heat flux conditions.

Grade of Material	Model Number	Heat Flux	Remarks
HDB	6-1	40	No apparent deterioration
HDB	6-2	140	No apparent deterioration
HDB	6-3	300	Melting at stagnation point at 270 secs; oxidation at stagnation point.
HDB	6-4	650	Model cracked within five secs due to thermal shock. Oxidation and melting were visible at stagnation point.
HDF	6-5	40	No apparent deterioration
HDF	6-6	140	Slight spalling and oxidation.
HDF	6-7	300	Melting more severe than Model 6-3; oxidation and spalling present.
HDF	6-8	650	Severe spalling, oxidation, and melting.
HBN	6-9	40	No apparent deterioration
HBN	6-10	140	Slight spalling
HBN	6-11	300	Slight melting, oxidation, and spalling.
HBN	6-12	650	Uniform pock-mark spalling over entire surface of model, deep surface cracks, oxidation.
HBR	6-13	40	No apparent deterioration
HBR	6-14	140	Slight surface cracks
HBR	6-15	300	Slight melting more severely than Model 6-11, oxidation, multiple surface cracks.
HBR	6-16	650	Melting, oxidation, deep surface cracks, spalling.

RANKING OF MATERIALS

Heat Flux Level	Order of Performance from Best to Worst
40	All visibly equal in performance
140	All nearly equal in performance
300	HBR and HBN nearly equal; HDB, HDF
650	HBR and HBN nearly equal; HDF

The ranking of the materials, presented in the table on the preceding page, was based on both the weight loss rates (graphed in Figure 124) and the physical appearance of each model after exposure (summarized in the photograph in Figure 125). The plot of weight loss rate vs model stagnation heat flux in Figure 124 is an attempt to summarize the test data obtained for each of the four grades of boron nitride material. This, perhaps, is a questionable procedure, since a major phase of the failure for these types of materials is the surface degradation - spalling, surface cracks, etc., which is not truly accounted for in the weight loss rate. Individual photographs showing pre- and post-exposure appearances are presented in Figures 126 through 133.

3.3 Calibration of Test Conditions

The high-density ablator test program was performed in the hyperthermal plasma arc test facility (ElectroThermal Facility) located at Space-General Corporation in El Monte, California. A low pressure/high enthalpy plasma arc generator was used in conjunction with a supersonic Mach 3 three-inch exit diameter contoured nozzle exhausted into an evacuated test chamber. Reconstituted air (79% nitrogen and 21% oxygen) was used as the test medium to simulate the re-entry atmosphere.

The test procedures used in performing the evaluation of the candidate high-density ablators are the same as those described on Pages 12 through 14 of this report, including the calibration measurement procedures. The selected test conditions for this phase of the program are defined by:

Test Condition	Gas Stagnation Enthalpy (Btu/lb)	Model Stagnation Pressure (atm)	Model Heat Flux (Btu/ft^2-sec)
1	6,800	0.0022	40
2	10,000	0.0094	140
3	12,000	0.0243	300
4	13,100	0.1250	650

Model stagnation pressure was measured with our facility water-cooled pitot probe. Radial surveys of the stagnation pressure were made at radii of 0.25, 0.50, 0.75, 1.00, 1.25 and 1.50 inches; pressure surveys obtained at each of the four heat flux levels are plotted in Figure 134. Excellent distributions of pressure were observed at each of the four test conditions; there was no apparent evidence of either 'hot cores' or shock-wave interference with the model surface.

Model stagnation radial heat flux surveys were obtained using a 2.5-inch diameter hemispherical model (geometrically-similar to the test models) instrumented with an asymptotic calorimeter located at the stagnation point. These heat flux profiles, presented in Figure 135, show excellent uniformity of the heat flux distribution across the three-inch diameter test stream.

3.4 Comparison of High-Density Ablator Performance

Relatively high-density ablation materials for lifting re-entry vehicles are of particular interest, especially where a minimum shape change due to surface recession is required, as on aerodynamic control surfaces. The heat flux levels chosen for the thermal tests on the high-density ablators are representative of those conditions which would be encountered by lifting re-entry vehicles. Heat fluxes up to 650 Btu/ft^2-sec were attained to obtain data on the mechanical integrity and thermal response characteristics of the material specimens. Air enthalpy levels ranged from 6,800 Btu/lb at the lowest heat flux of 40 Btu/ft^2-sec to 13,100 Btu/lb at the highest heat flux. Model stagnation pressures correspondingly ranged between 0.0022 and 0.1250 atmospheres. Test duration was, in general, of five minute duration except at the highest heat flux level where thermal degradation of the material samples necessitated shorter run times.

A ranking of the materials evaluated under this contract with those evaluated under the Aerospace program has been done for heat flux levels of 40 and 140 Btu/ft^2-sec. The two higher heat flux levels of 300 and 650 Btu/ft^2-sec were not used in the Aerospace program and consequently only the Dow Corning materials and the boron nitride materials are compared at these two higher heating rate conditions.

Front surface recession rates, defined by the total change in length as measured at the stagnation point (on the centerline) of the model and divided by the total exposure time, are plotted in Figures 136 and 137. The Dow Corning materials possessed expansion (caused by swelling) rates instead of recession rates at the two lower heat flux levels, and consequently they do not appear on the bar graph in Figure 136. Most of the boron nitride models at these two lowest heat flux conditions also did not show appreciable recession and hence are not shown on the recession rate graph. It is readily apparent that the boron nitride materials are not subject to deterioration at heat flux levels under approximately 150 Btu/ft^2-sec. At the higher heat flux levels in excess of 300 and up to approximately 700 Btu/ft^2-sec, the Dow Corning ablators show significant recession, with the improved material (93-069) performing superior to the 93-002 material, (refer to Figure 137).

The front surface brightness temperature of each specimen was measured using a Leeds and Northrup optical brightness pyrometer. In most cases, a stabilized surface temperature was reached and maintained throughout a major portion of each exposure period. This stabilized surface temperature data was used for preparing the bar graphs presented in Figures 138 and 139. The surface temperatures plotted are apparent brightness temperatures, uncorrected for emissivity values of each material.

A comparison of back-face temperatures were made in Figures 140 and 141 using the Dow Corning 93-002 and 93-069 data and that data provided by the Aerospace Corporation program. The boron nitride models were not instrumented with thermocouples; consequently, back-face temperature data is not available on those materials. There appears to be some indication from the temperature-time plots in Figures 140 and 141 that the Dow Corning 93-002 material has a lower thermal conductivity than the 93-069 ablator. In fact, the 93-002 material ranked very closely to the performance of the 275 PHX molded laminate.

The following table has been prepared to provide the reader with an overall summary of the high-density ablators evaluated under this contract and the other ablators evaluated in the Aerospace Corporation test program used for comparison with the boron nitride and Dow Corning materials.

TABLE 13

SUMMARY OF HIGH-DENSITY ABLATORS EVALUATED

Material Designation	Density of Virgin Material (lb/ft^3)	Description of Material
Fiberite 4500	88.7	Phenolic-carbon fabric laminate, fabric parallel to heated face
Fiberite 4926	90.0	
HITCO EPA 94-FM 5014	89.7	
HITCO EPA 94-FM 5055A	92.3	
HITCO EPA 94-FM 5314	89.9	
HITCO EC 201 CCA 11	92.7	
HITCO SS 1620	91.9	
Fiberite MXC 97	109.5	
3M Pluton - SC 1008	91.6	
USP Pluton - 5277 BG	92.8	
HITCO EPA 94-FM 5014	89.3	Phenolic-carbon fabric laminate, fabric 20 deg to heated face
HITCO EPA 94-FM 5055A	89.7	
HITCO EPA 94-FM 5314	92.2	
Ironsides 6T9	92.0	
USP FM 5065(M 5065 RF)	90.8	Phenolic-carbon fabric or fiber, random orientation
Martin PL 5277 RF(MPL 5277 RF)	91.9	
USP PL 5277 RF (PL 5277 RF)	91.3	
ATJ Graphite	109.5	Molded powders and paper laminates
Super-Temp STX	111.3	
ARP 275 PHX(parallel)	97.8	
ARP 275 PHX (20 deg)	102.7	
Boron Nitride		
Grade HDB	187.4	
Grade HDF	174.9	
Grade HBN	128.0	
Grade HBR	121.8	
Dow Corning		
93-002	88.7	
93-069	107.4	

STANDARD MODEL DESIGN FOR HIGH DENSITY ABLATOR TESTS

2.5-Inch Diameter Hemisphere Cylinder

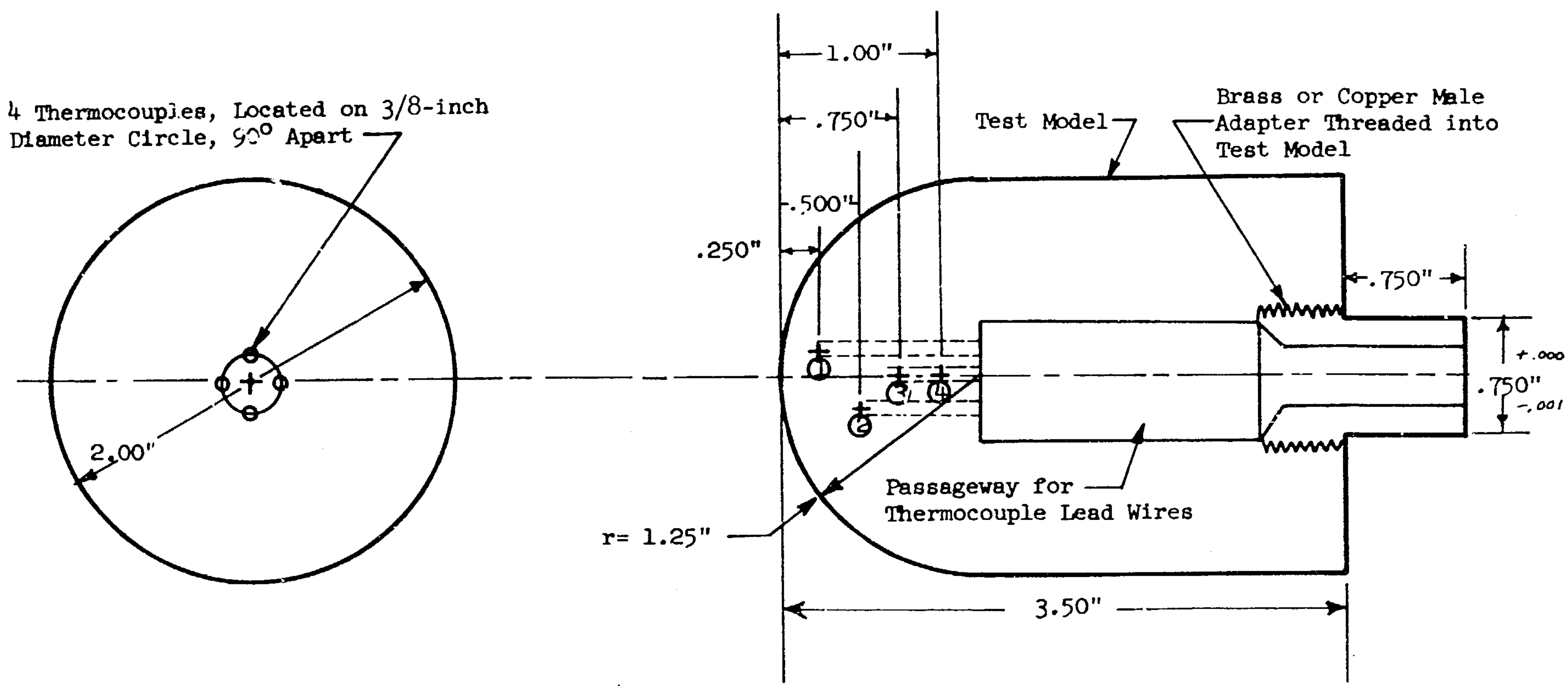

NOTE:
Thermocouples to be Constructed of 36 Gage Chromel/Alumel. Lead Wire Length of 6-7 Ft. Required.

Figure 88 -- Standard Model Design for High Density Ablator Tests

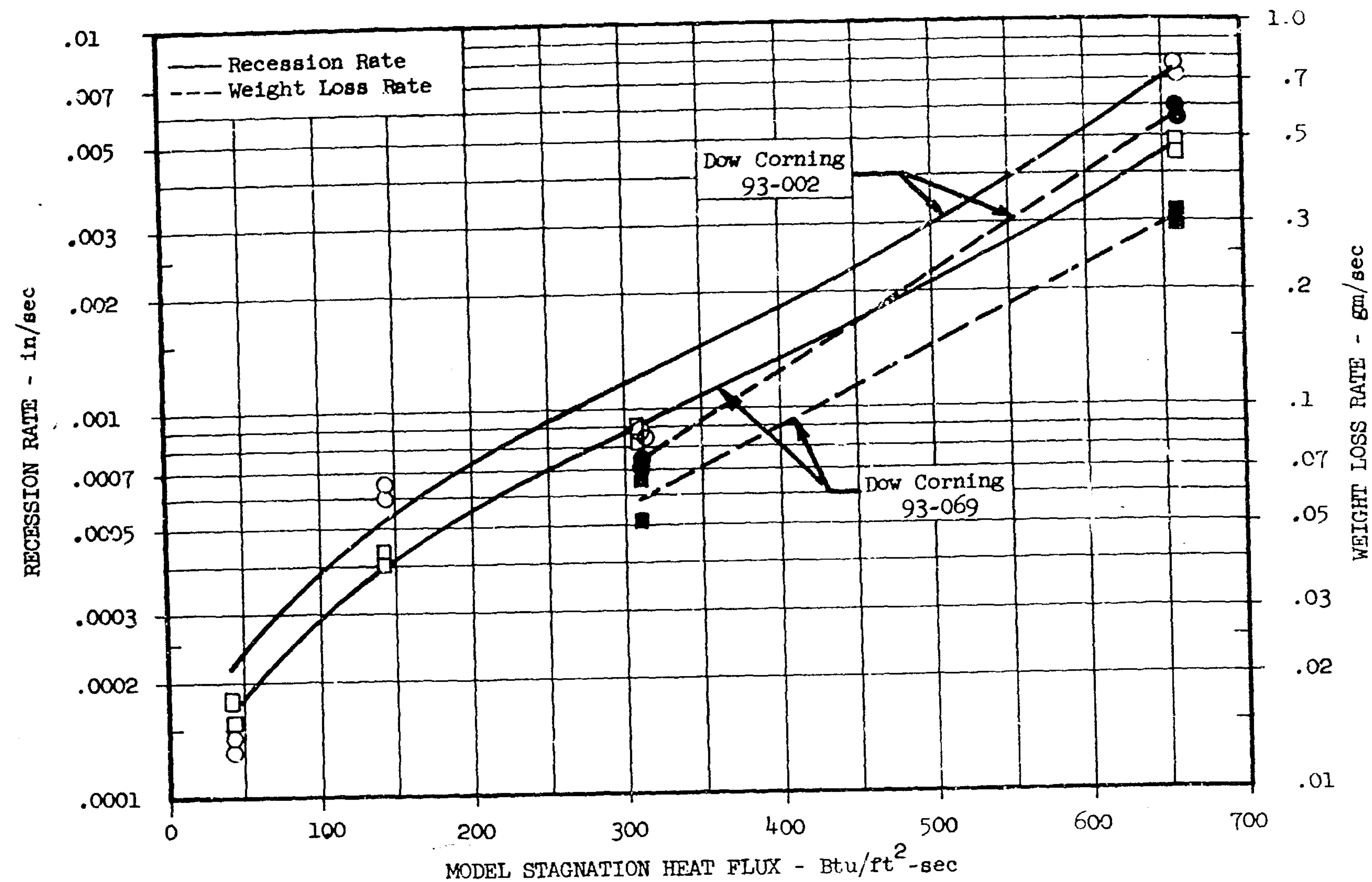

Figure 89 -- Recession and Weight Loss Rates for Dow Corning 93-002 and 93-069 Materials

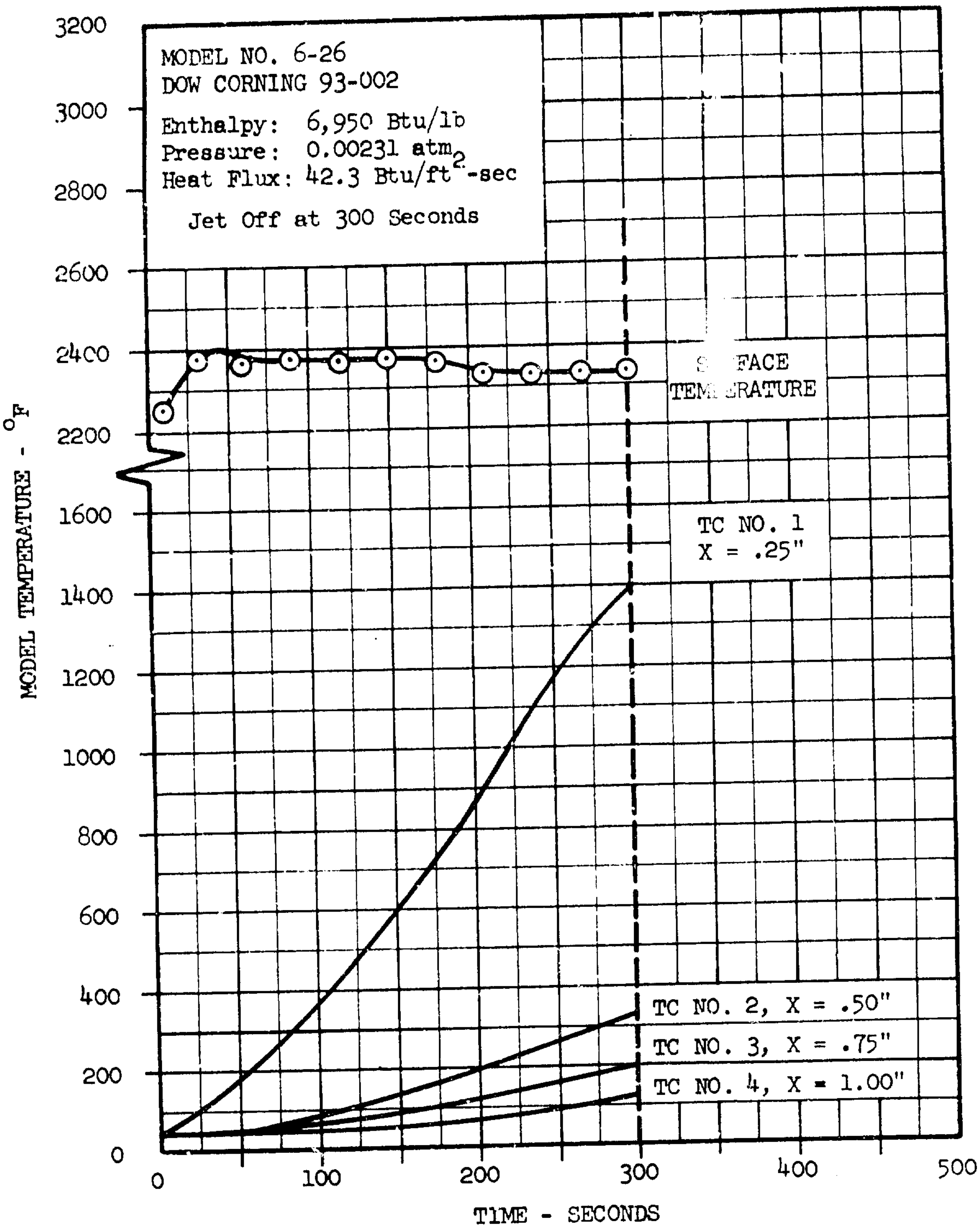

Figure 90 -- Dow Corning 93-002, Model 6-26 Temperature History

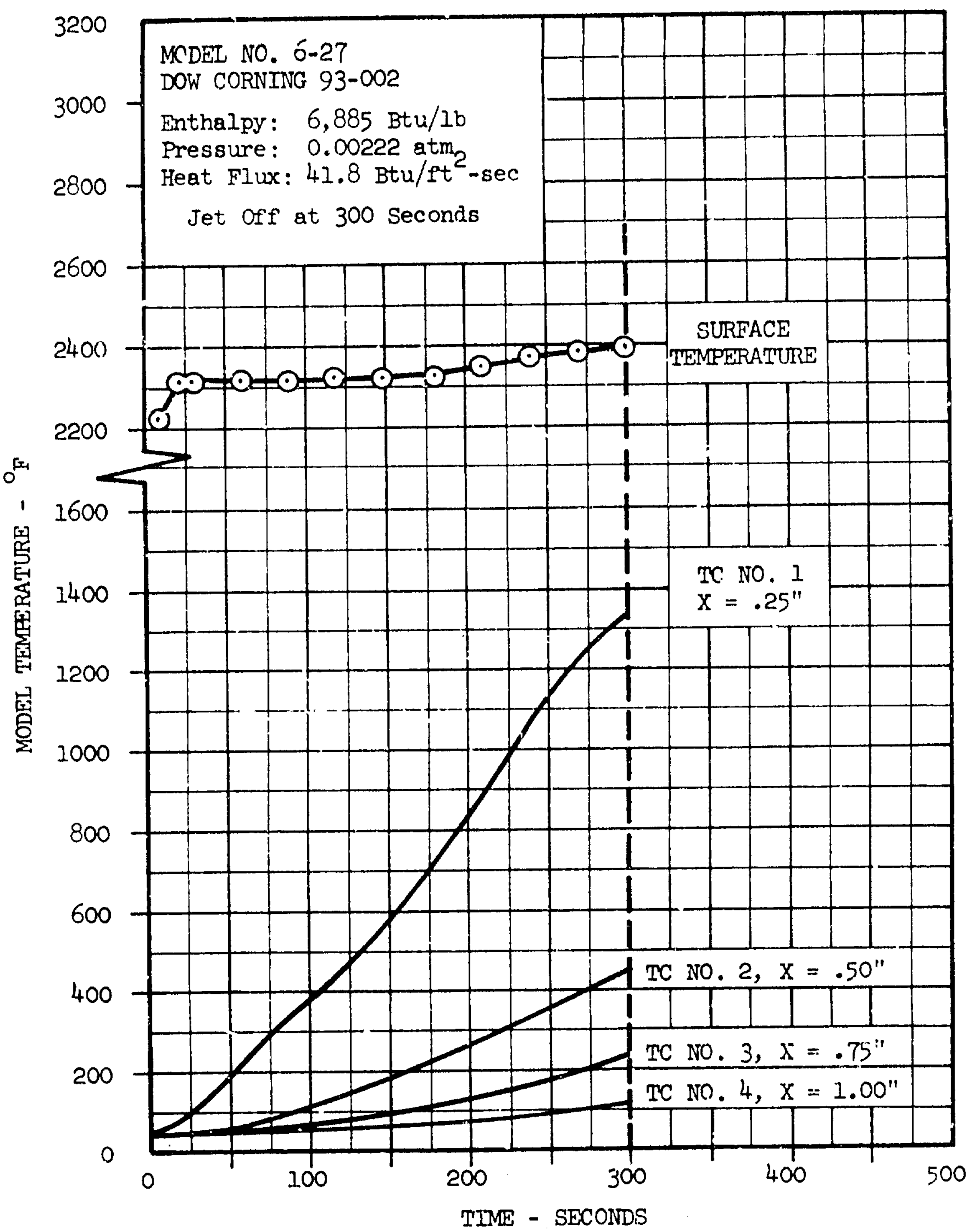

Figure 91 -- Dow Corning 93-002 Model 6-27 Temperature History

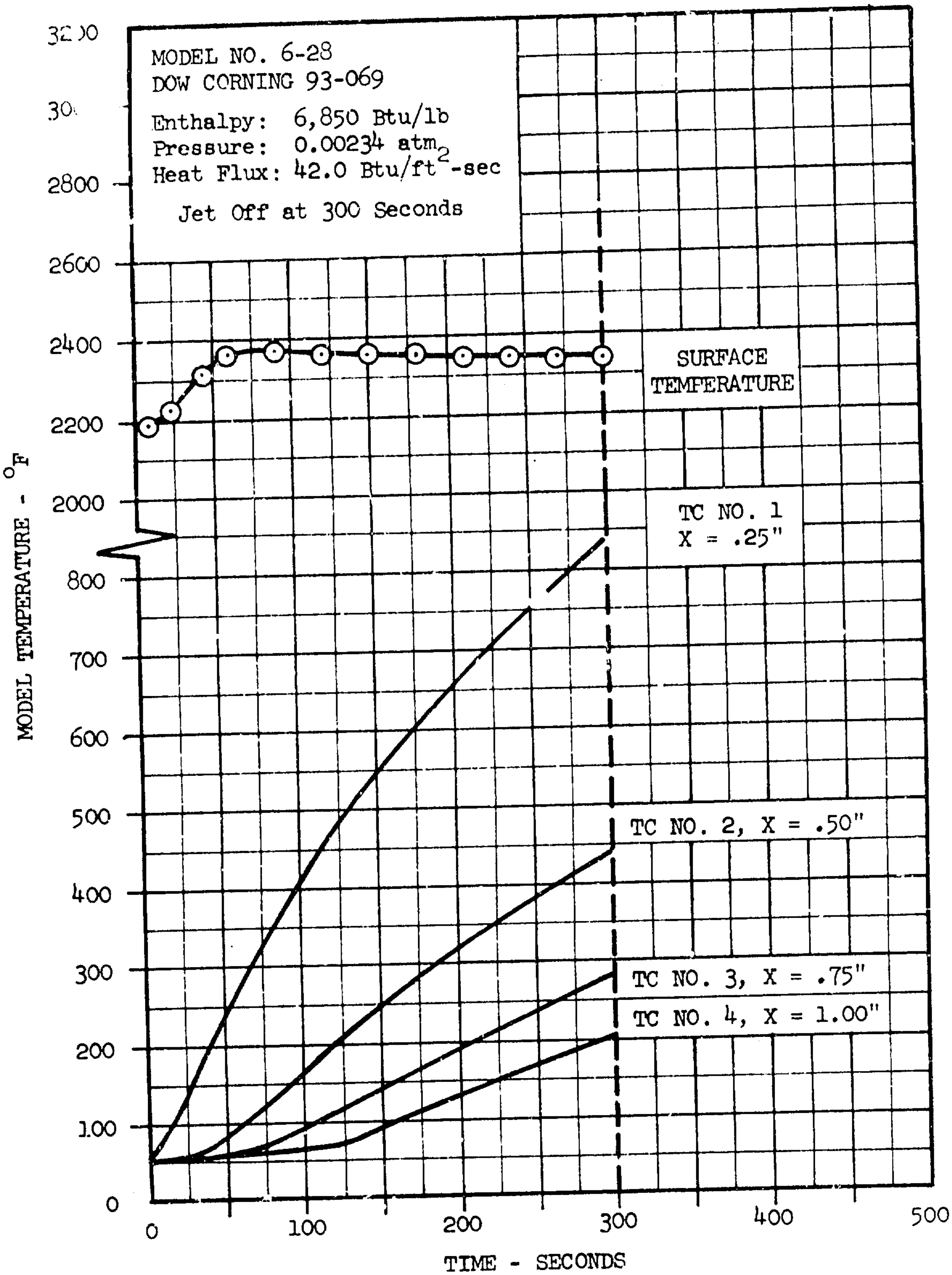

Figure 92 -- Dow Corning 93-069, Model 6-28 Temperature history

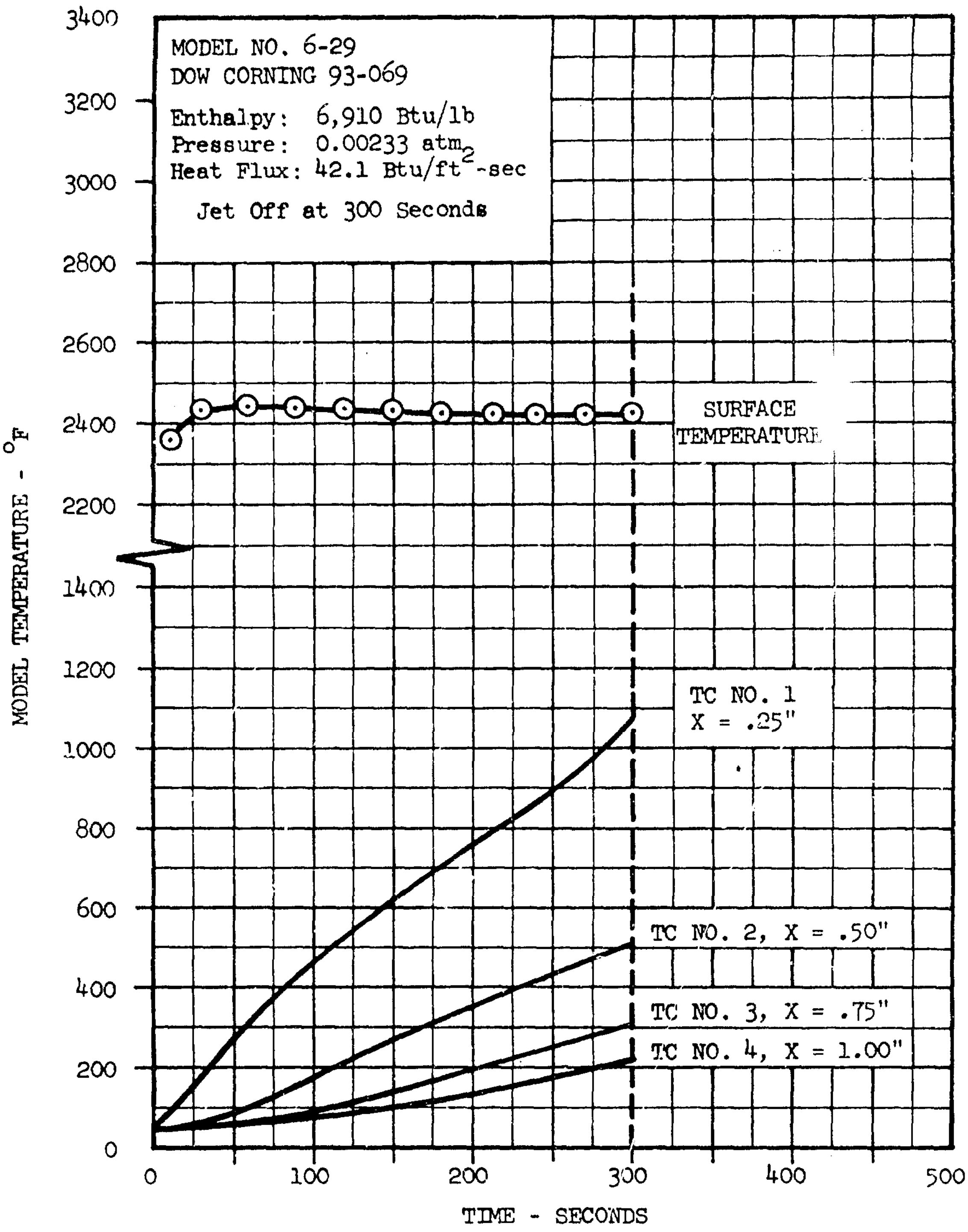

Figure 93 -- Dow Corning 93-069, Model 6-29 Temperature History

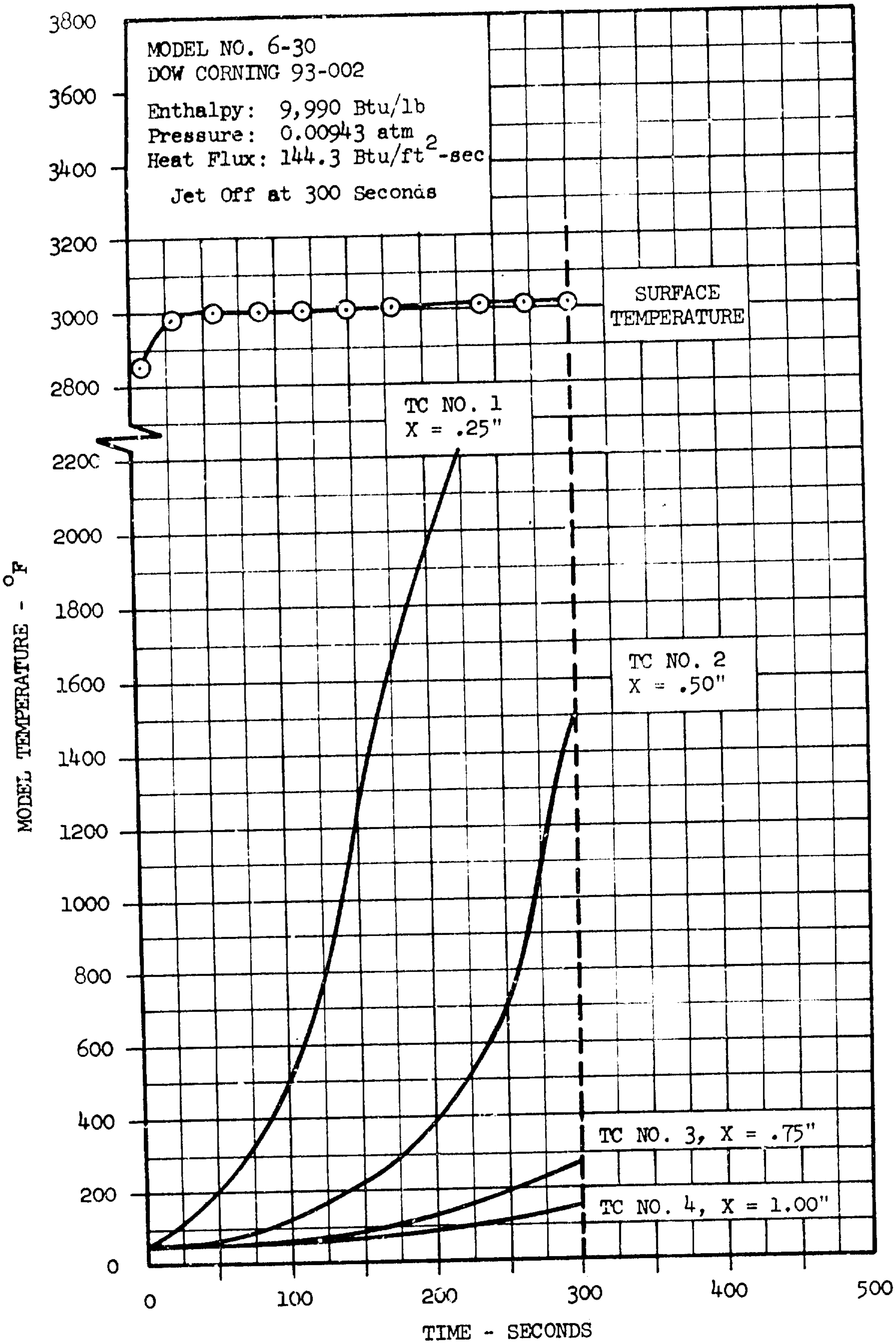

Figure 94 -- Dow Corning 93-002, Model 6-30 Temperature History

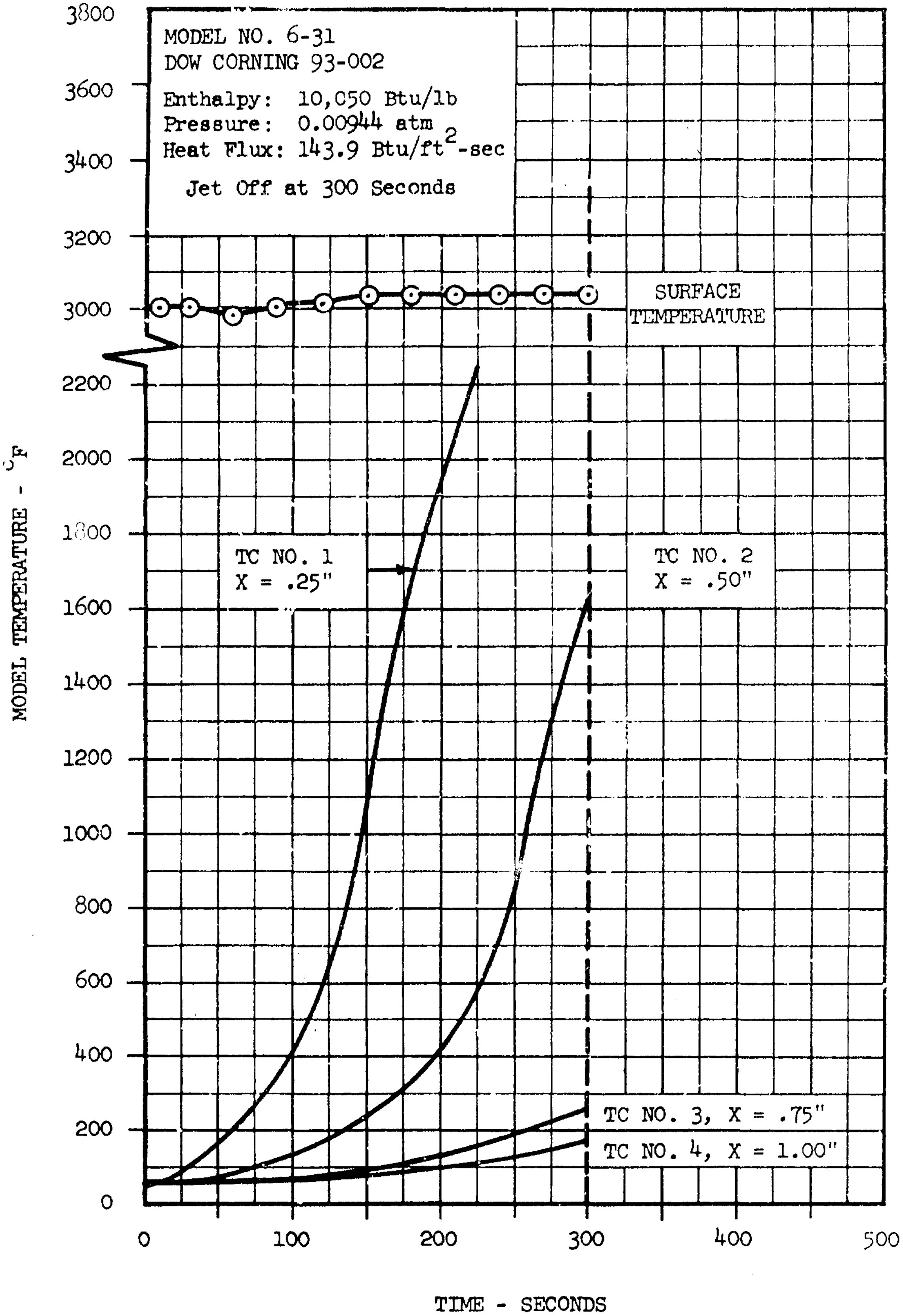

Figure 95 -- Dow Corning 93-002, Model 6-31 Temperature History

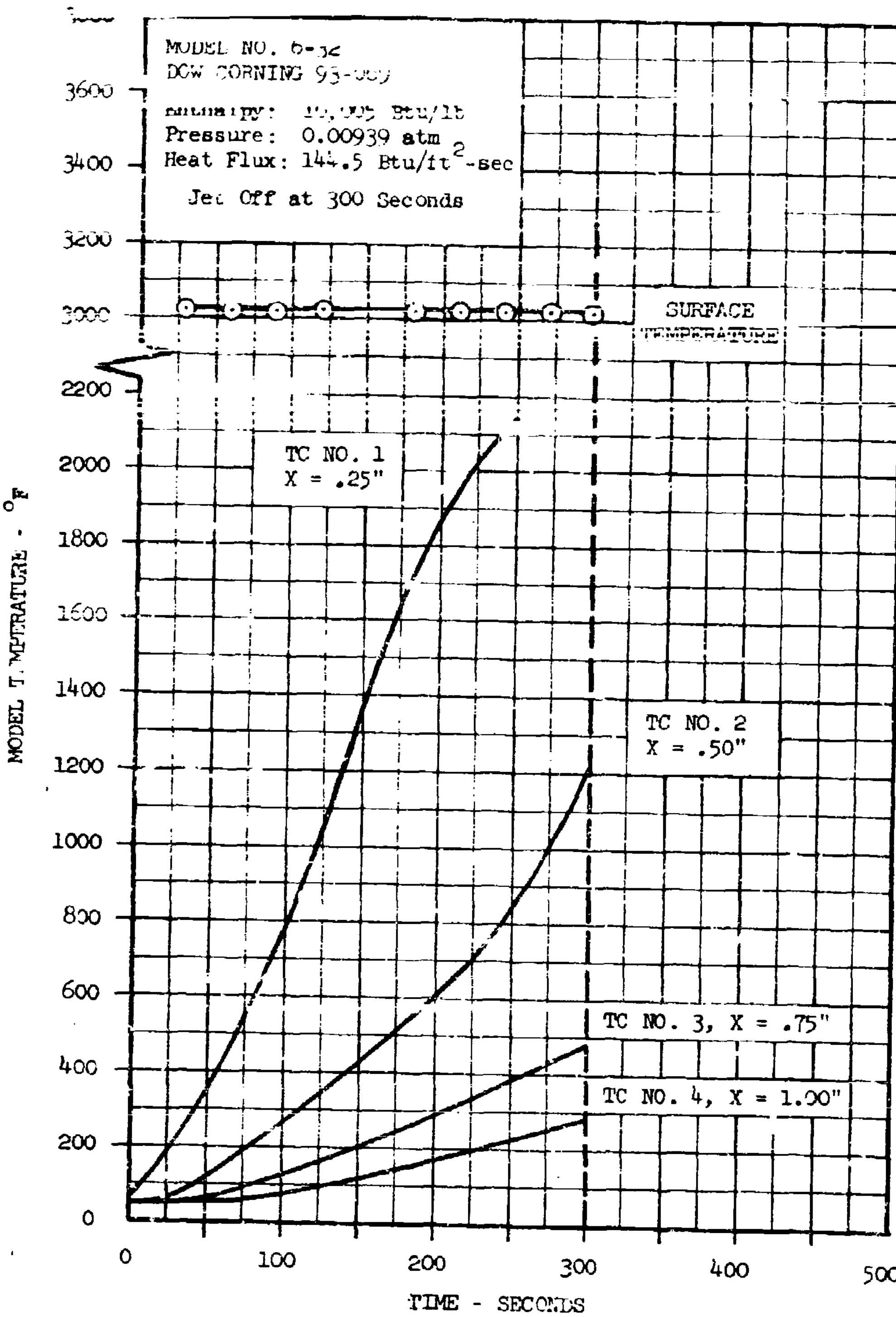

Figure 96 -- Dow Corning 93-069, Model 6-32 Temperature History

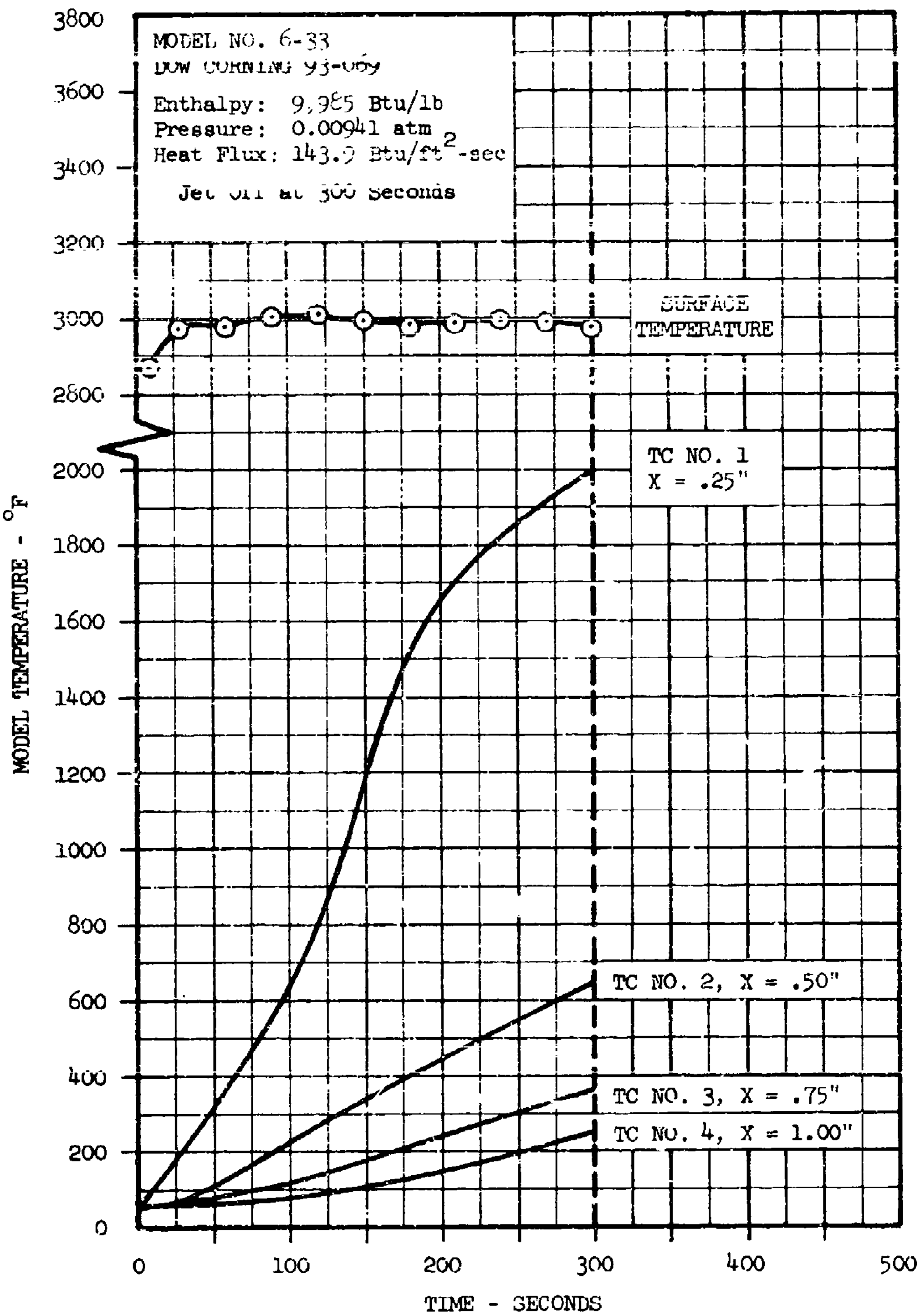

Figure 97 -- Dow Corning 93-069, Model 6-33 Temperature History

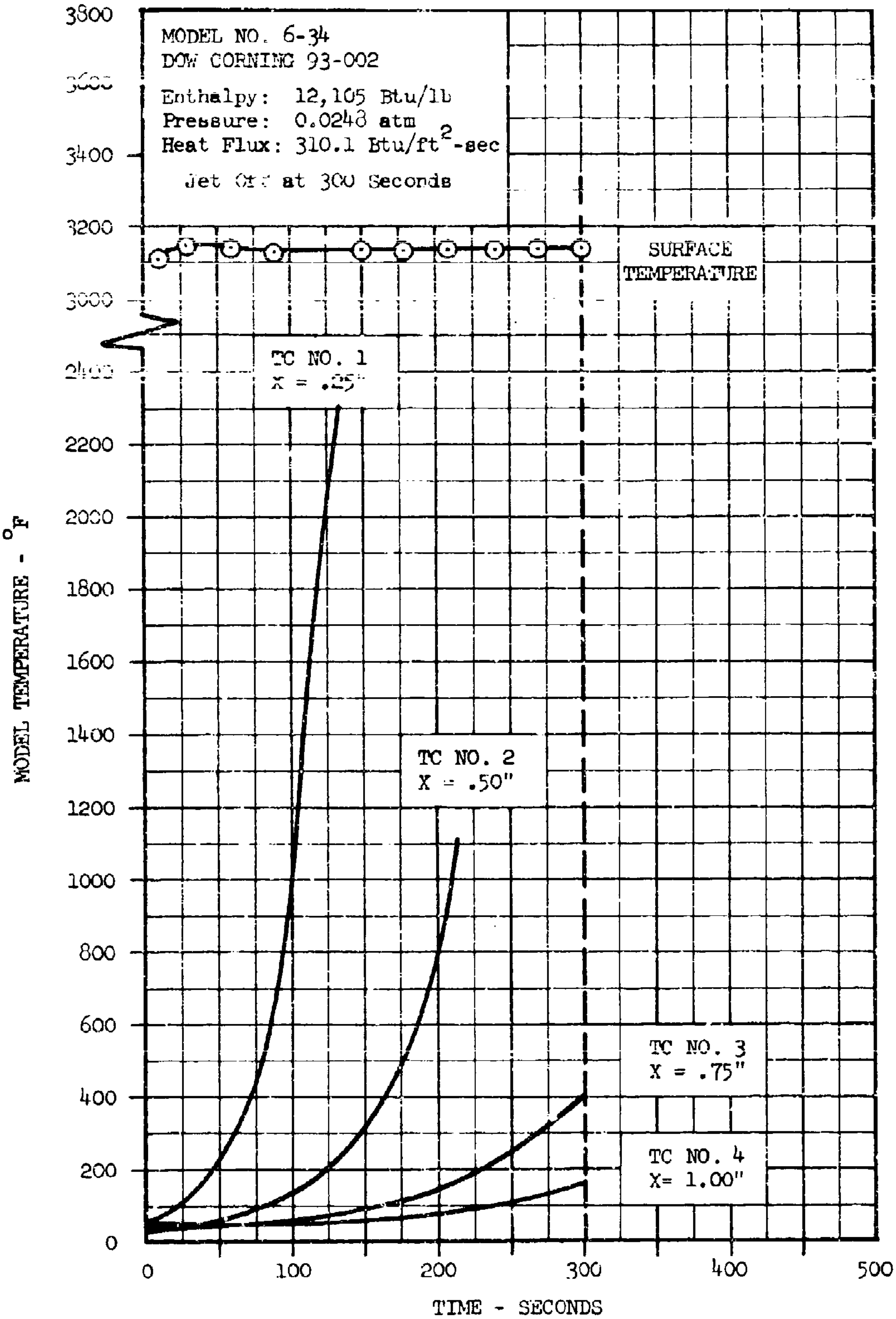

Figure 98 -- Dow Corning 93-002, Model 6-34 Temperature History

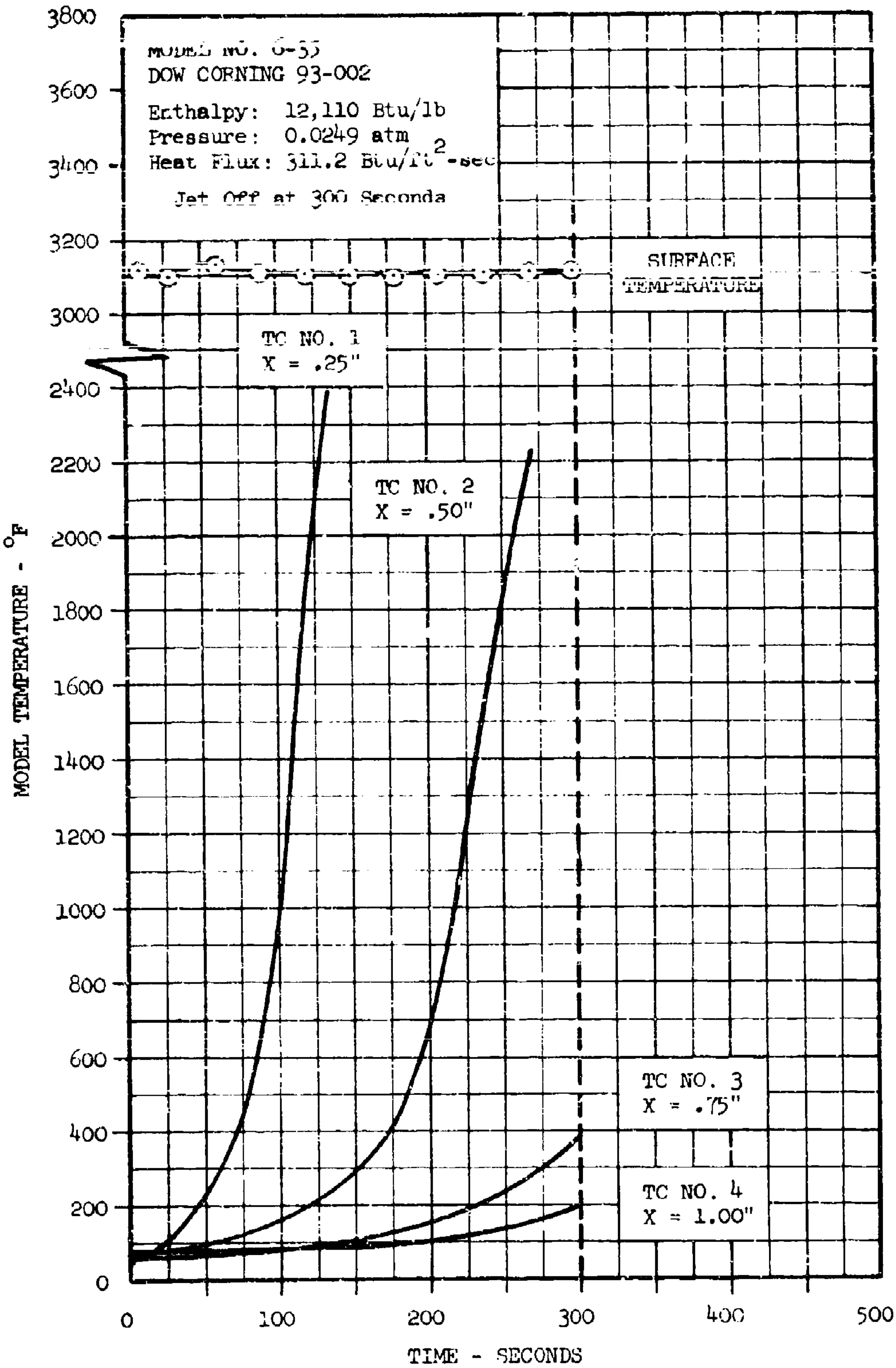

Figure 99 -- Dow Corning 93-002, Model 6-35 Temperature History

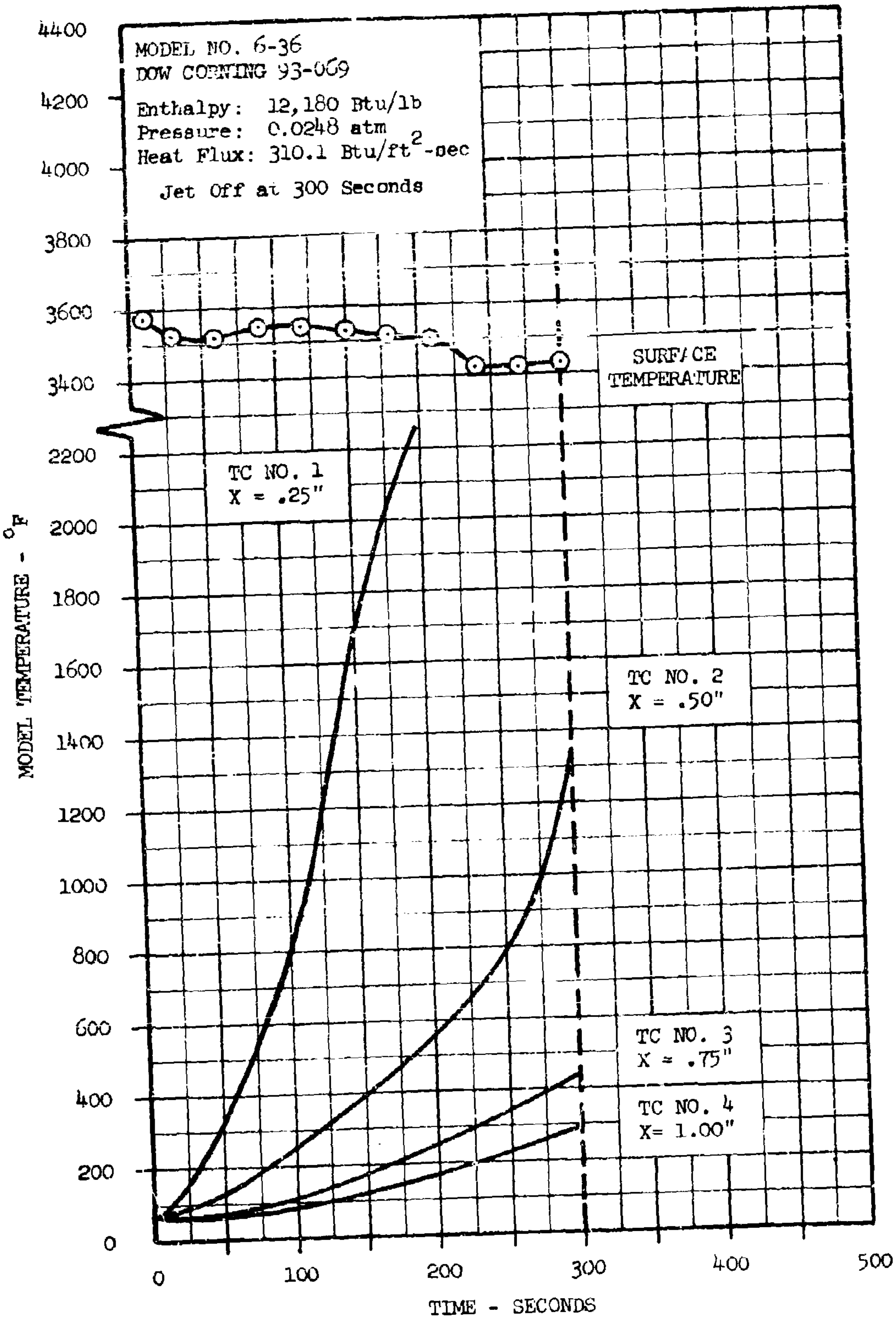

Figure 100 -- Dow Corning 93-069, Model 6-36 Temperature History

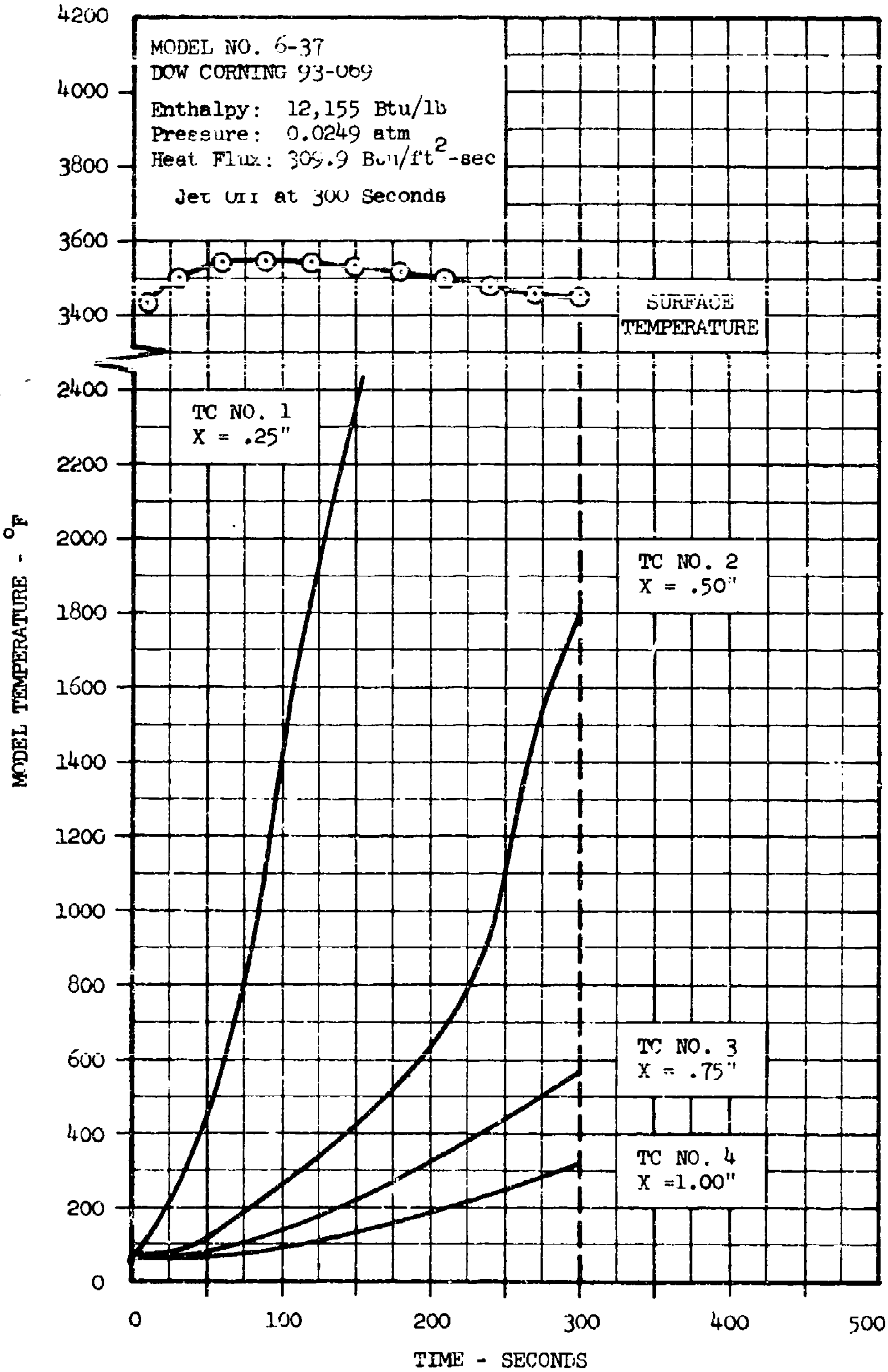

Figure 101 -- Dow Corning 93-069, Model 6-37 Temperature History

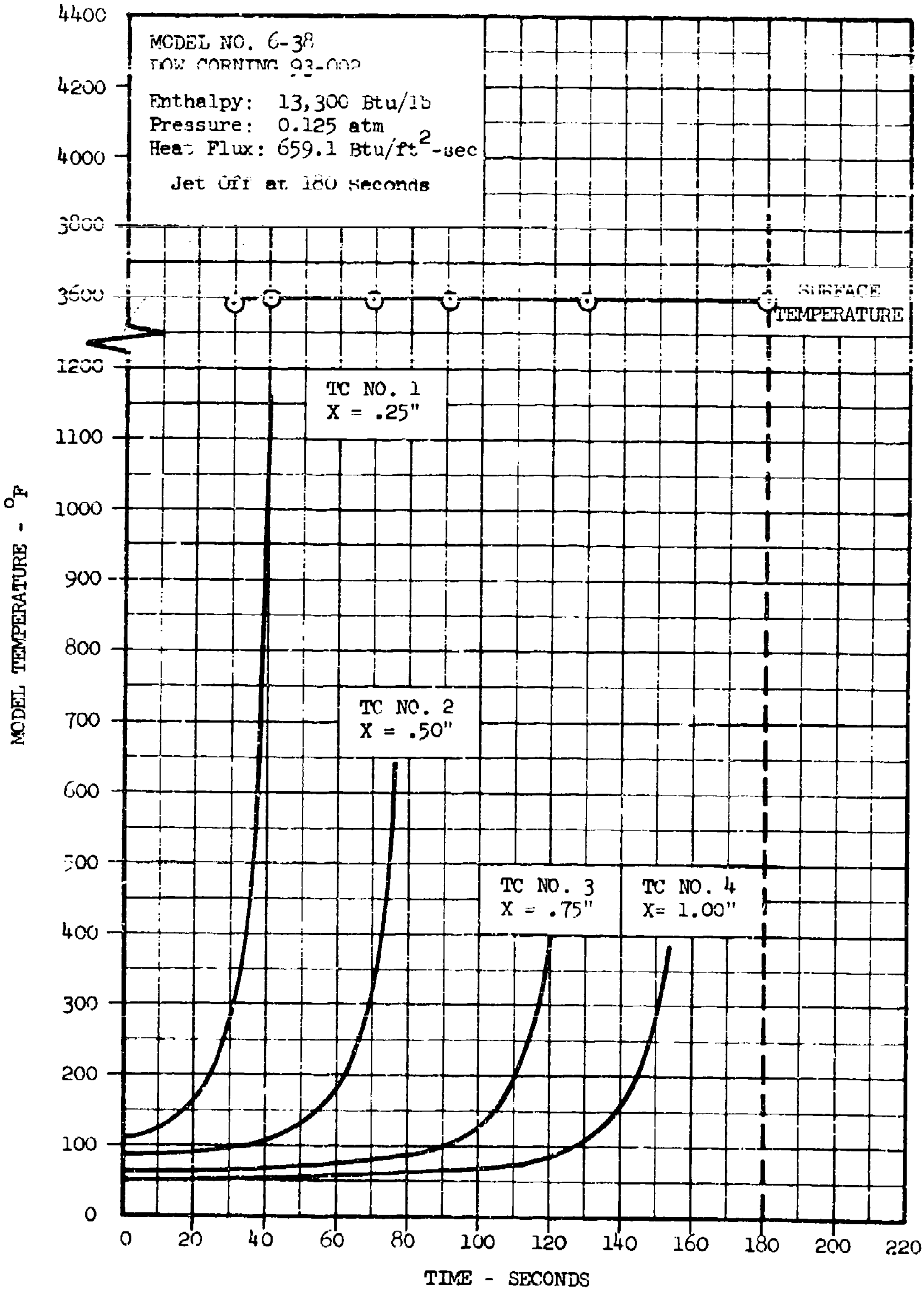

Figure 102 -- Dow Corning 93-002, Model 6-38 Temperature History

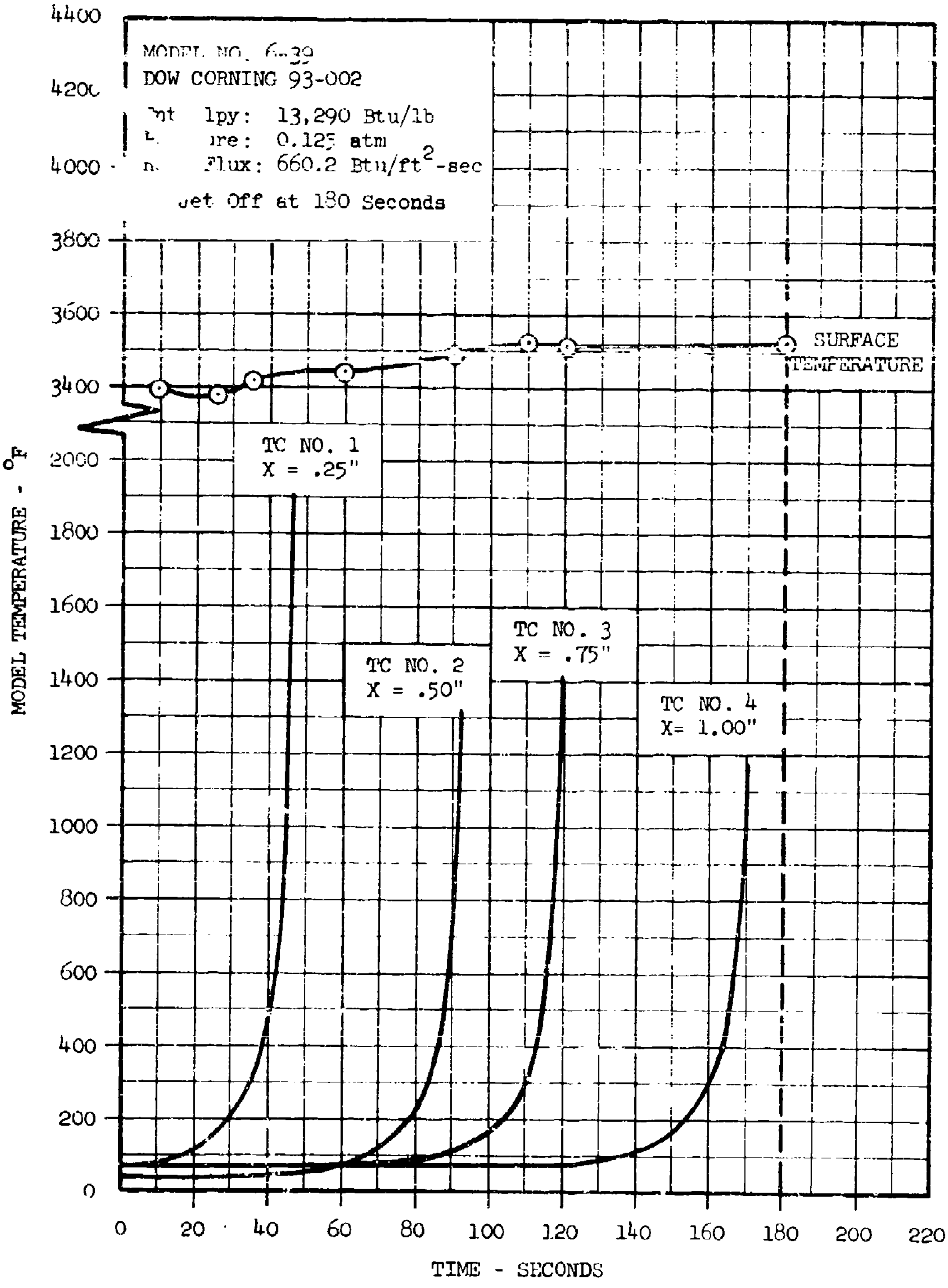

Figure 103 -- Dow Corning 93-002, Model 6-39 Temperature History

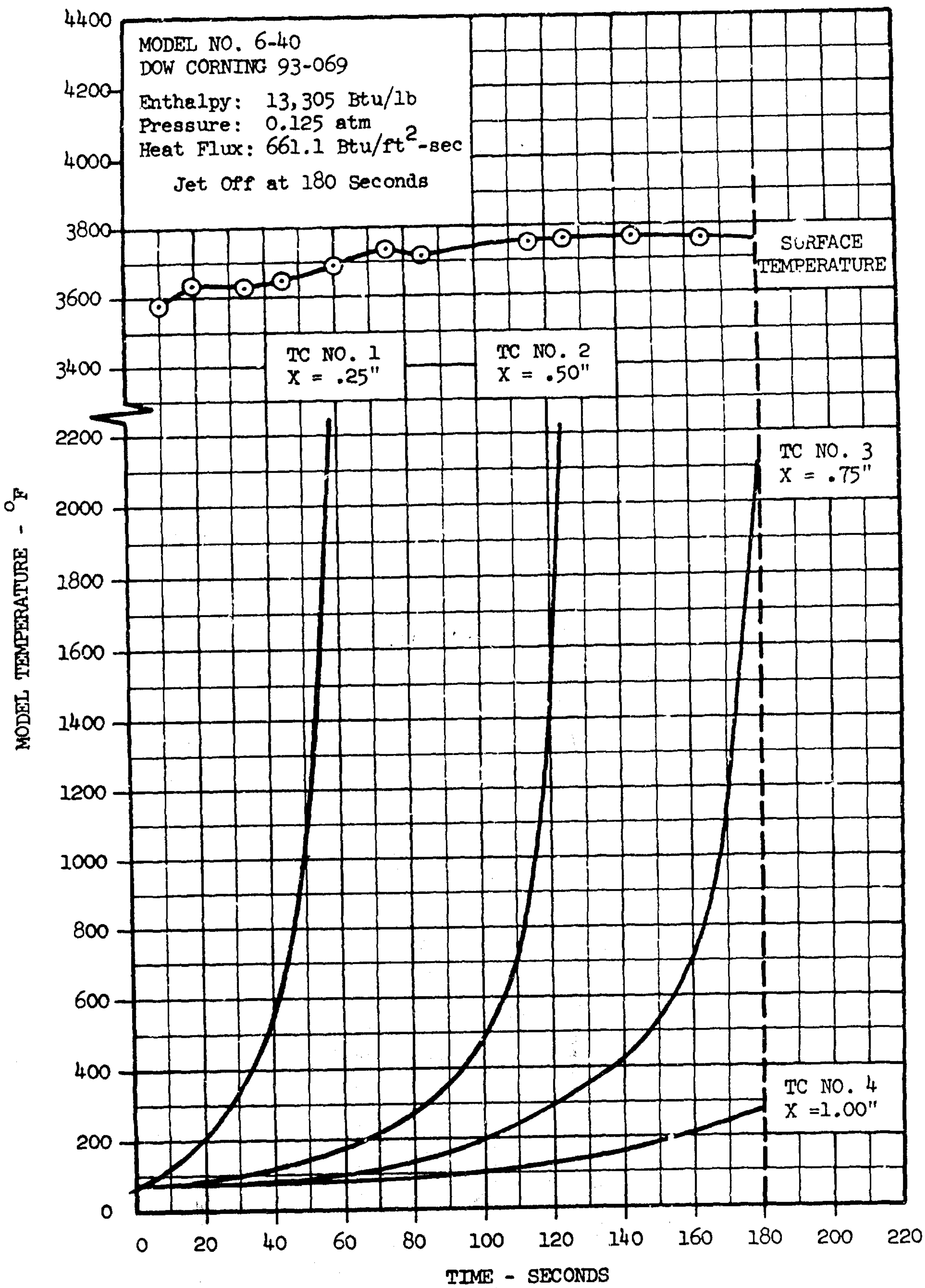

Figure 104 -- Dow Corning 93-069, Model 6-40 Temperature History

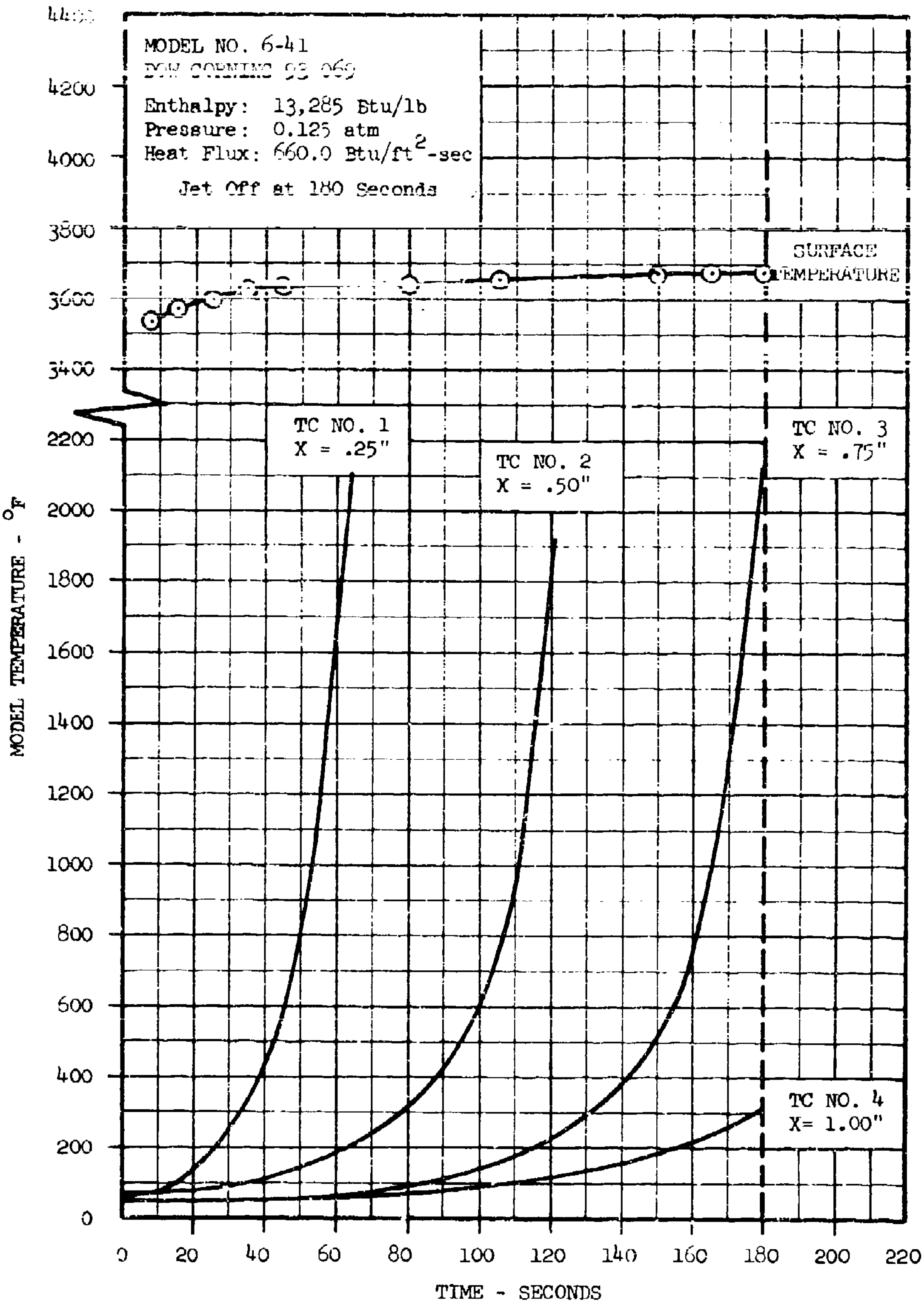

Figure 105 -- Dow Corning 93-069, Model 6-41 Temperature History

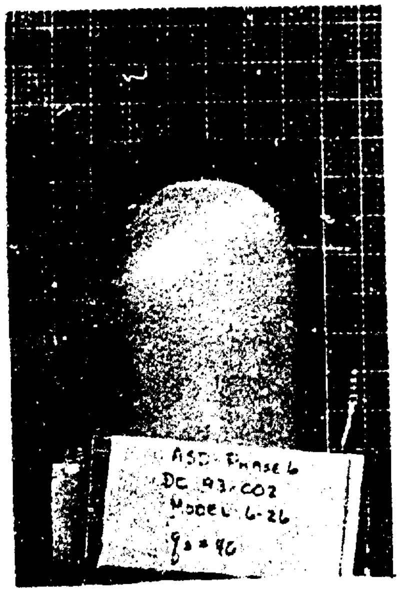

Model 6-26 - Pre-Exposure

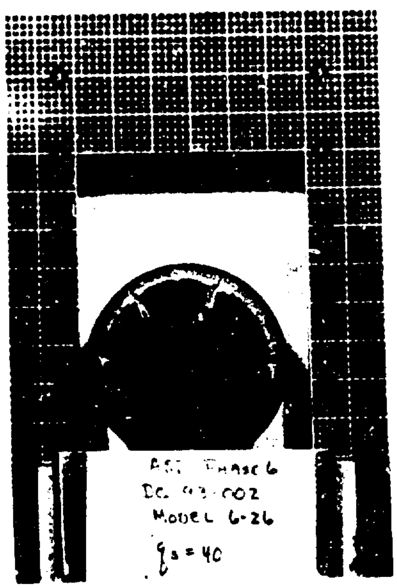

Model 6-26 - Post-Exposure

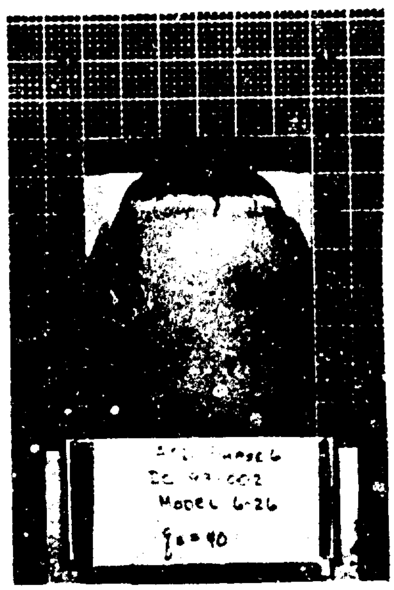

Model 6-26 - Post-Exposure

Figure 106 -- Photographs of Dow Corning 93-002 Material
Model 6-26

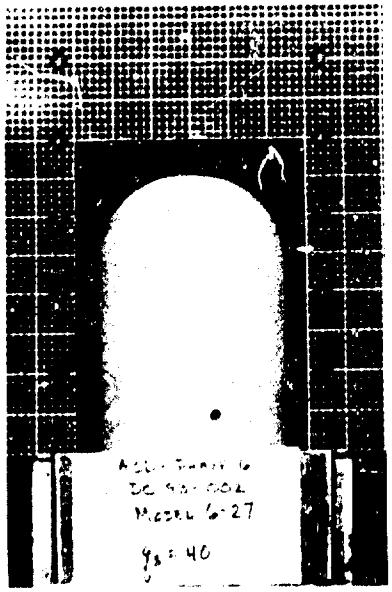

Model 6-27 - Pre-Exposure

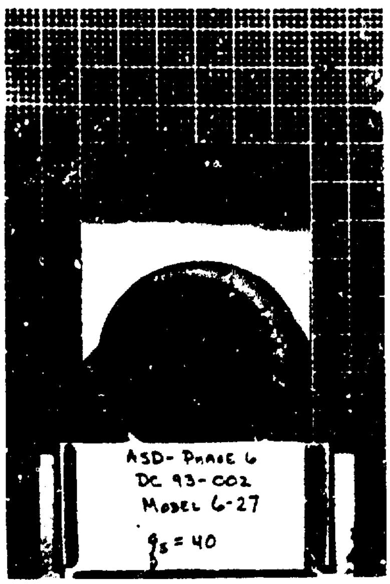

Model 6-27 - Post-Exposure

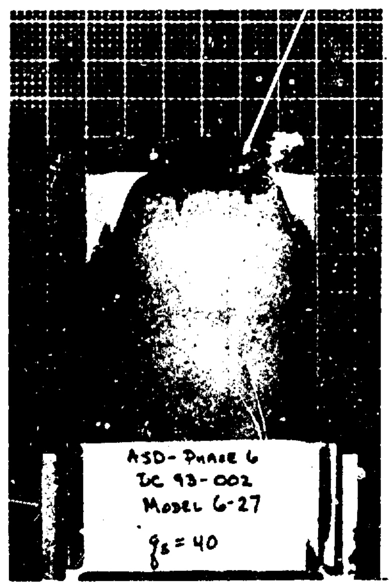

Model 6-27 - Post-Exposure

Figure 107 -- Photographs of Dow Corning 93-002 Material
Model 6-27

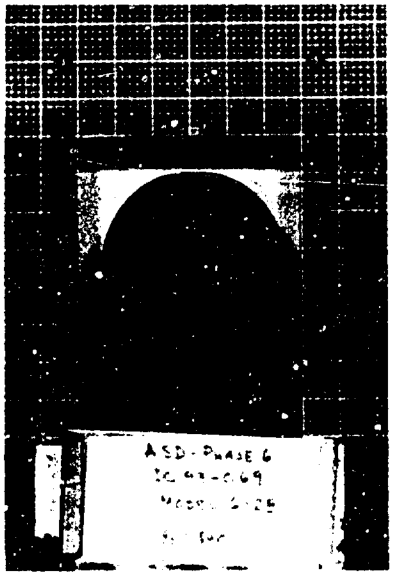

Model 6-28 - Pre-Exposure

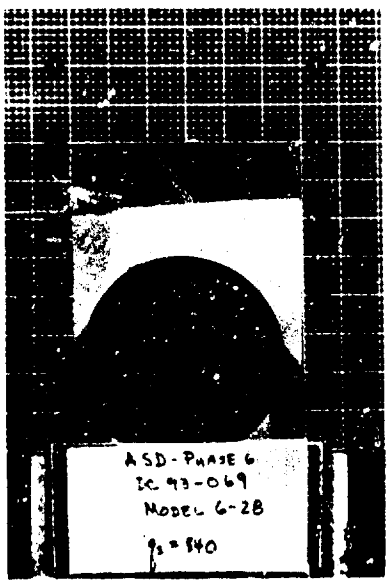

Model 6-28 - Post-Exposure

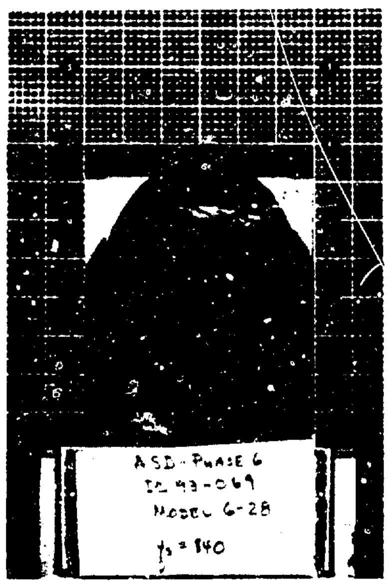

Model 6-28 - Post-Exposure

Figure 108 -- Photographs of Dow Corning 93-069 Material
Model 6-28

Model 6-29 - Pre-Exposure

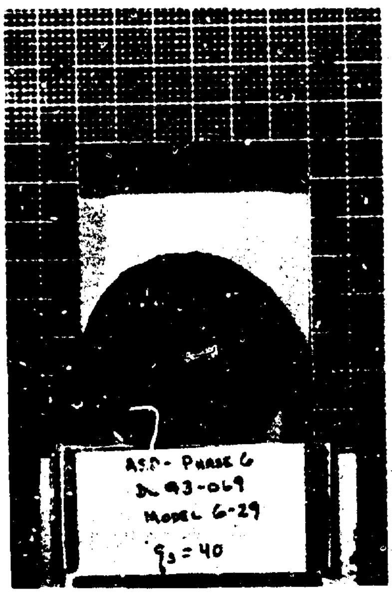

Model 6-29 - Post-Exposure

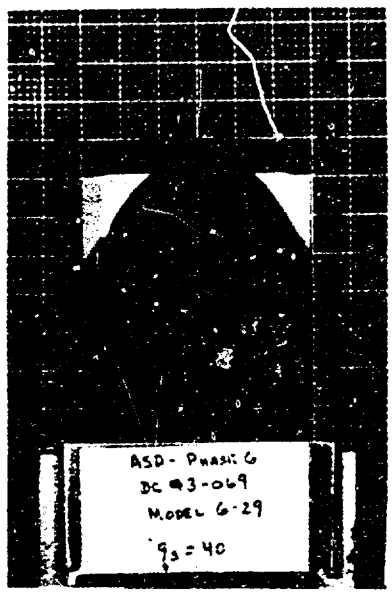

Model 6-29 - Post-Exposure

Figure 109 -- Photographs of Dow Corning 93-069 Material
Model 6-29

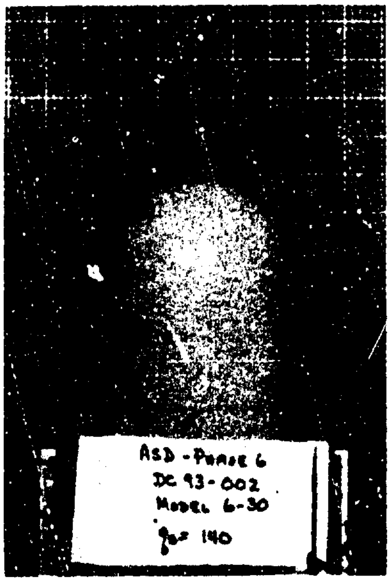

Model 6-30 - Pre-Exposure

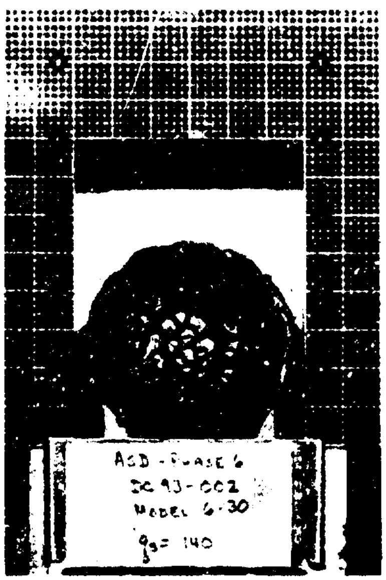

Model 6-30 - Post-Exposure

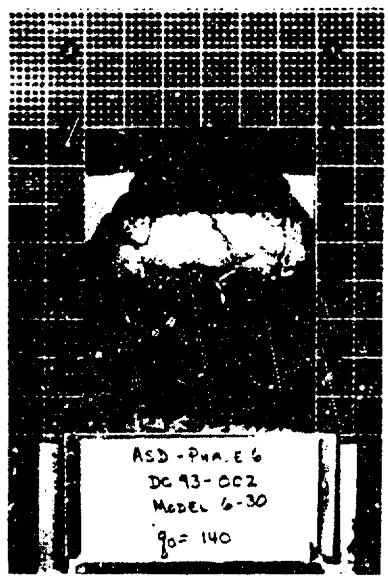

Model 6-30 - Post-Exposure

Figure 110 -- Photographs of Dow Corning 93-002 Material
Model 6-30

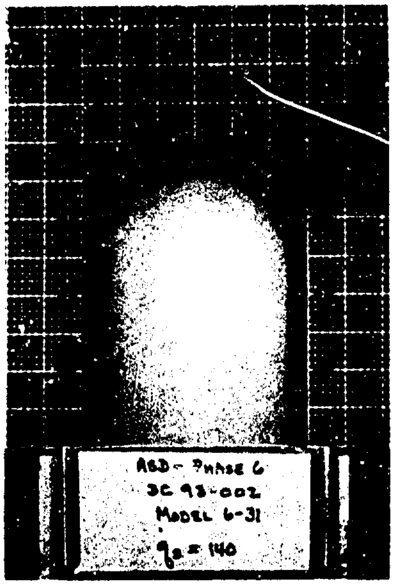

Model 6-31 - Pre-Exposure

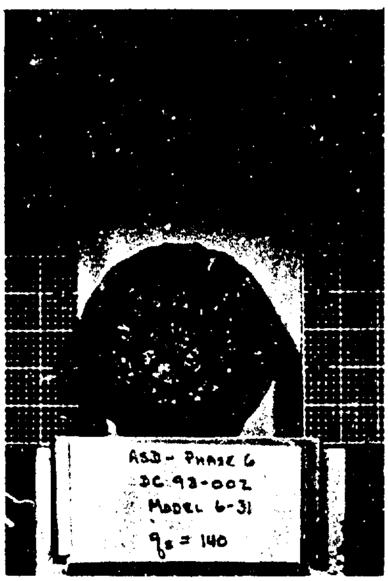

Model 6-31 - Post-Exposure

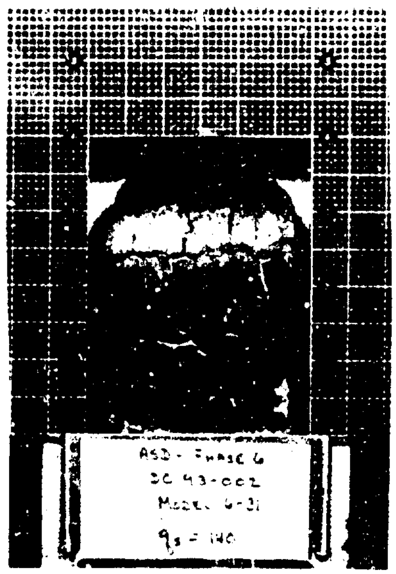

Model 6-31 - Post-Exposure

Figure 111 -- Photographs of Dow Corning 93-002 Material
Model 6-31

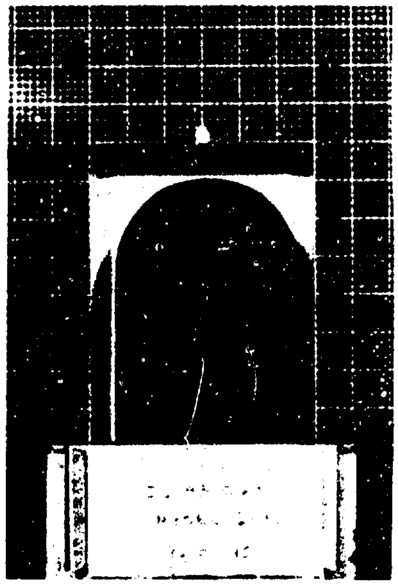

Model 6-32 - Pre-Exposure

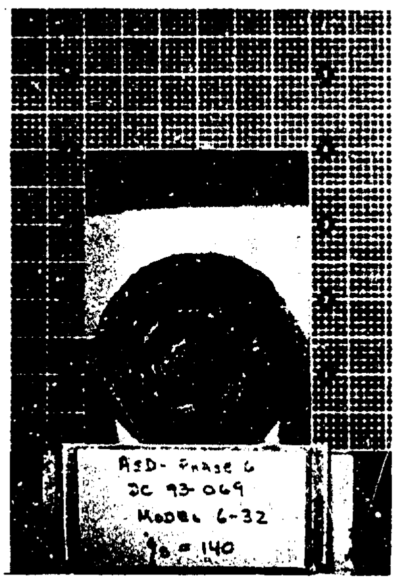

Model 6-32 - Post-Exposure

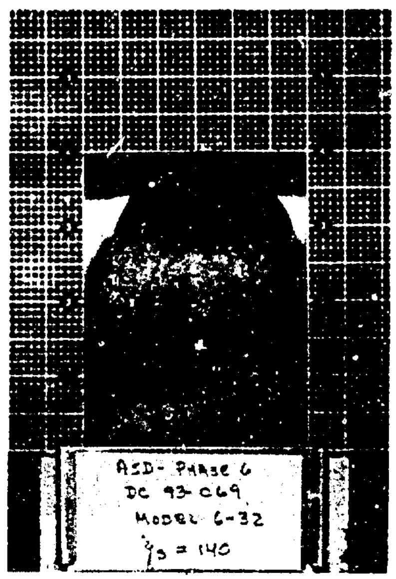

Model 6-32 - Post-Exposure

Figure 112 -- Photographs of Dow Corning 93-069 Material
Model 6-32

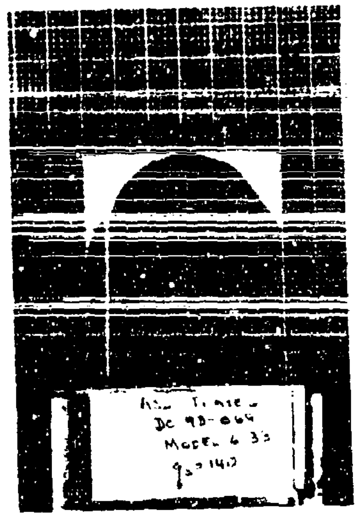

Model 6-33 - Pre-Exposure

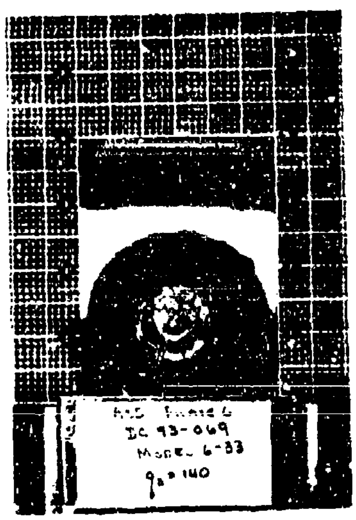

Model 6-33 - Post-Exposure

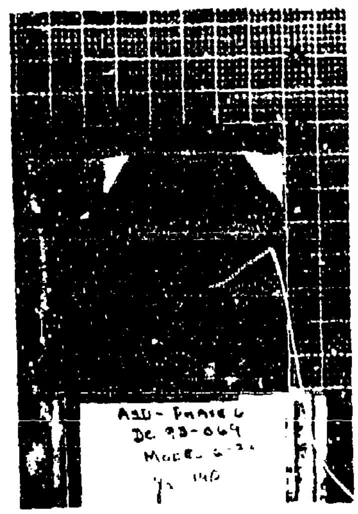

Model 6-33 - Post-Exposure

Figure 113 -- Photographs of Dow Corning 93-069 Material
Model 6-33

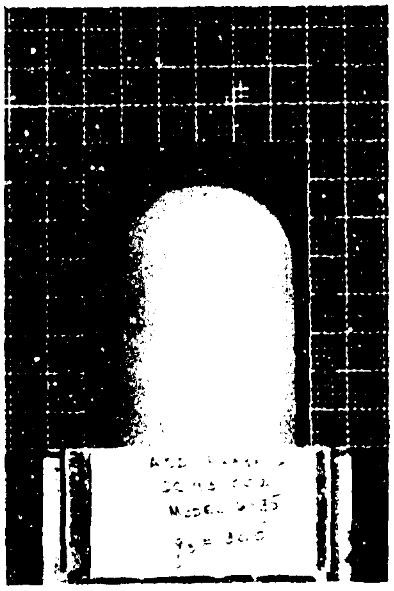

Model 6-35 - Pre-Exposure

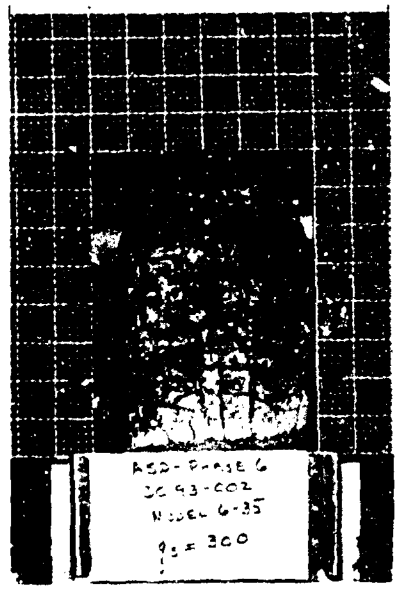

Model 6-35 - Post-Exposure

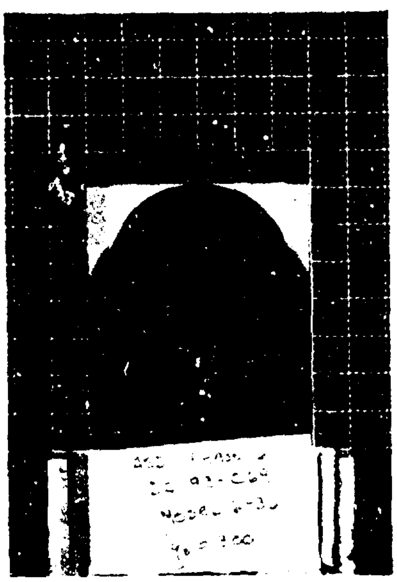

Model 6-36 - Pre-Exposure

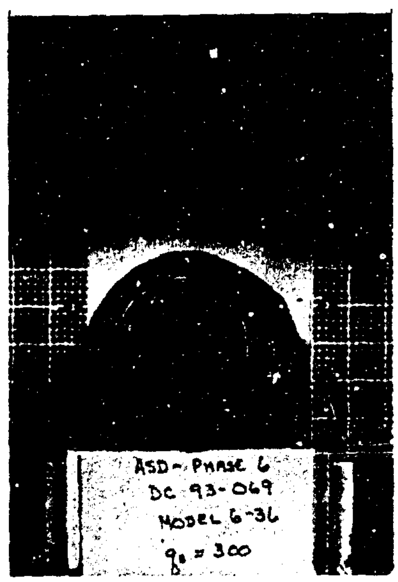

Model 6-36 - Post-Exposure

Figure 114 -- Photographs of Dow Corning 93-002 and 93-069 Materials
Models 6-35 and 6-36

Model 6-37 - Pre-Exposure

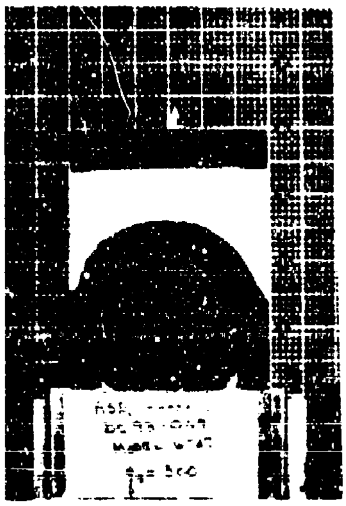

Model 6-37 - Post-Exposure

Model 6-37 - Post-Exposure

Figure 115 -- Photographs of Dow Corning 93-069 Material
Model 6-37

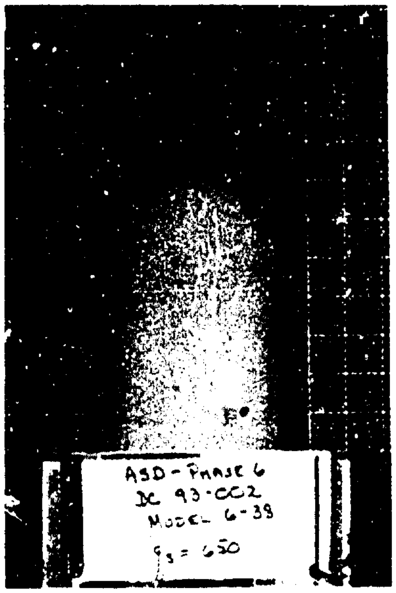

Model 6-38 - Pre-Exposure

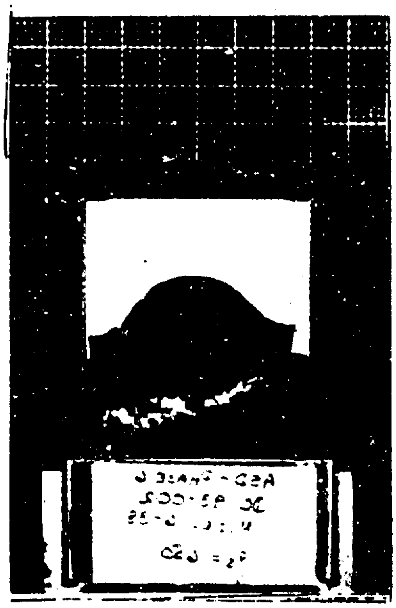

Model 6-38 - Post-Exposure

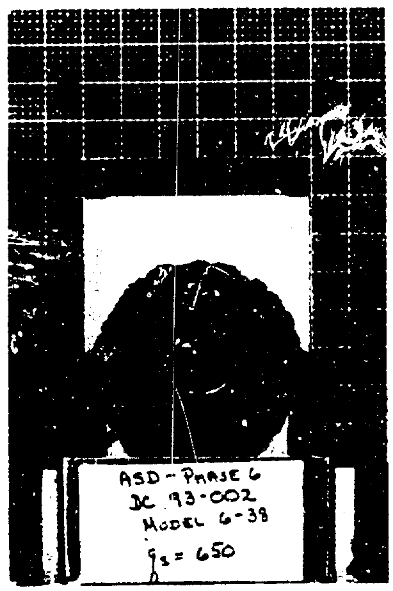

Model 6-38 - Post-Exposure

Figure 116 -- Photographs of Dow Corning 93-002 Material
Model 6-38

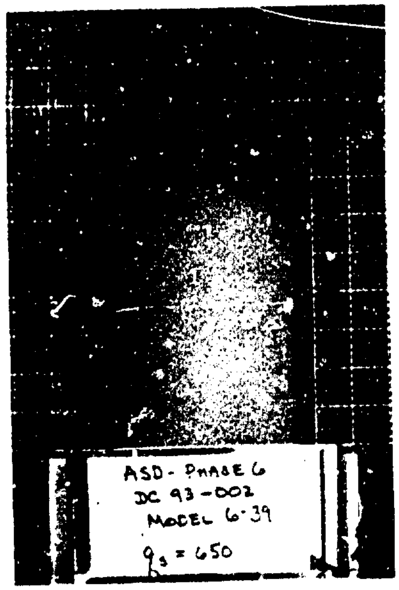

Model 6-39 - Pre-Exposure

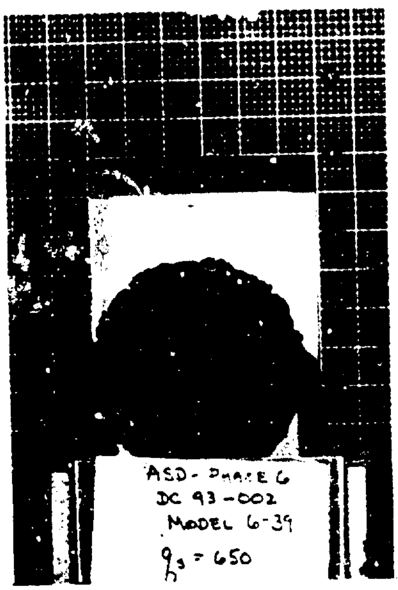

Model 6-39 - Post-Exposure

Model 6-39 - Post-Exposure

Figure 117 -- Photographs of Dow Corning 93-002 Material
Model 6-39

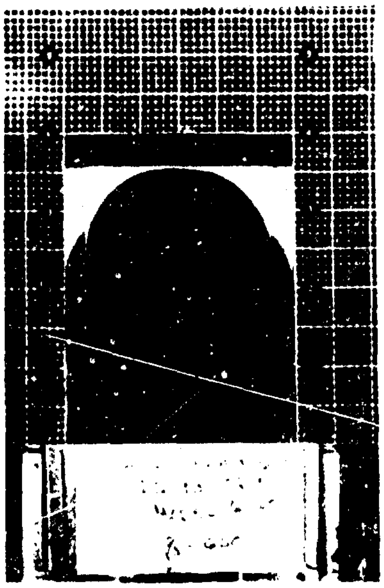

Model 6-40 - Pre-Exposure

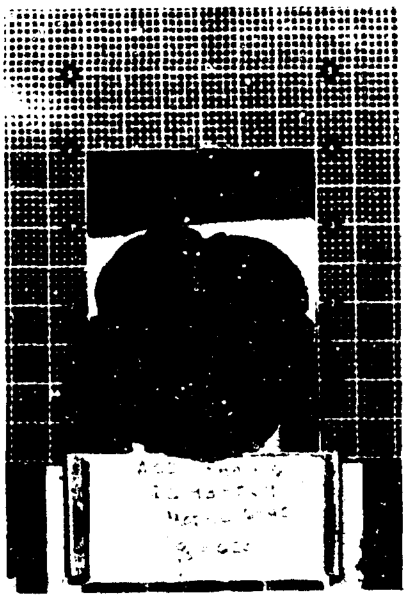

Model 6-40 - Post-Exposure

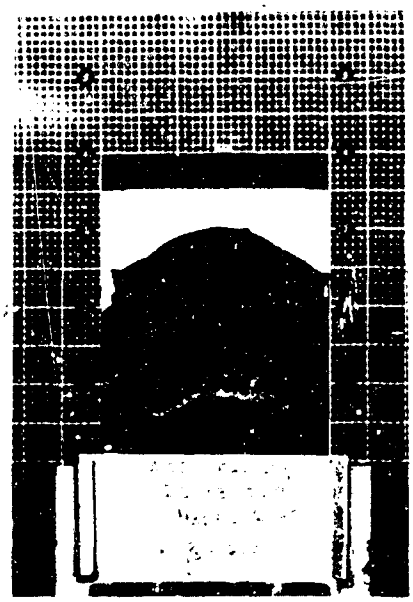

Model 6-40 - Post-Exposure

Figure 118 -- Photographs of Dow Corning 93-069 Material
Model 6-40

Model 6-41 - Pre-Exposure

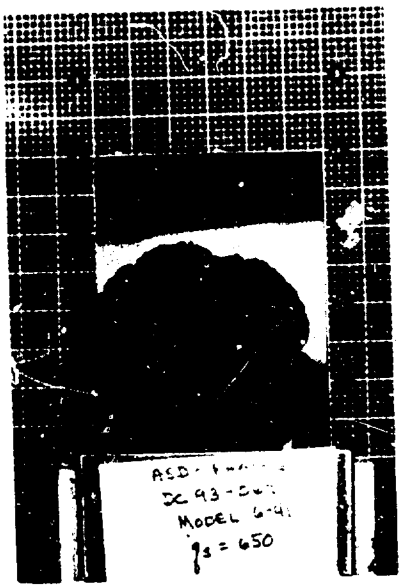

Model 6-41 - Post-Exposure

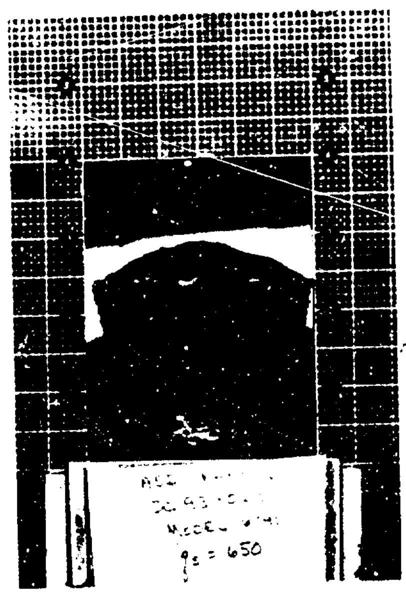

Model 6-41 - Post-Exposure

Figure 119 -- Photographs of Dow Corning 93-069 Material
Model 6-41

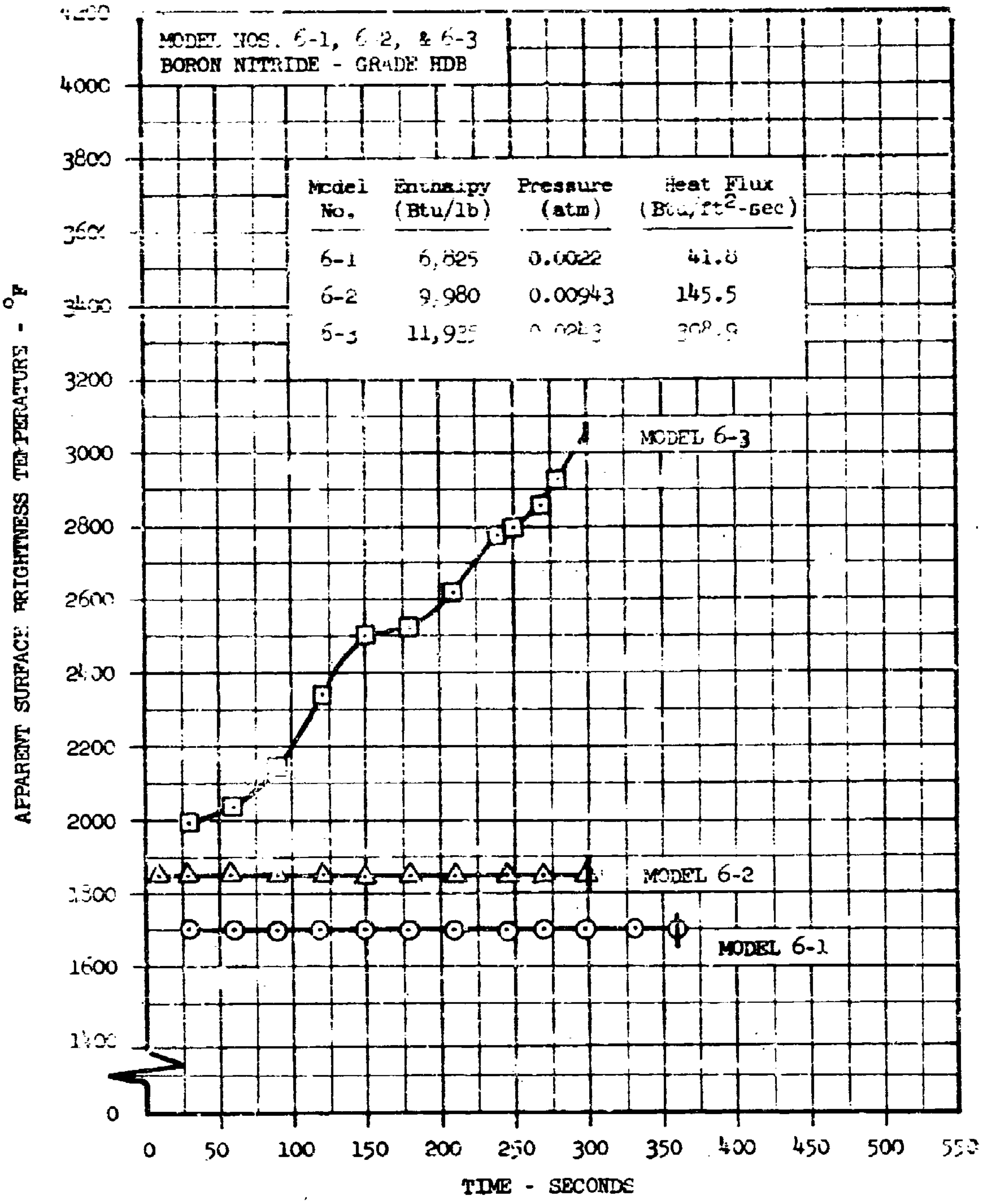

Figure 120 -- Boron Nitride - Grade HDB - Surface Temperatures

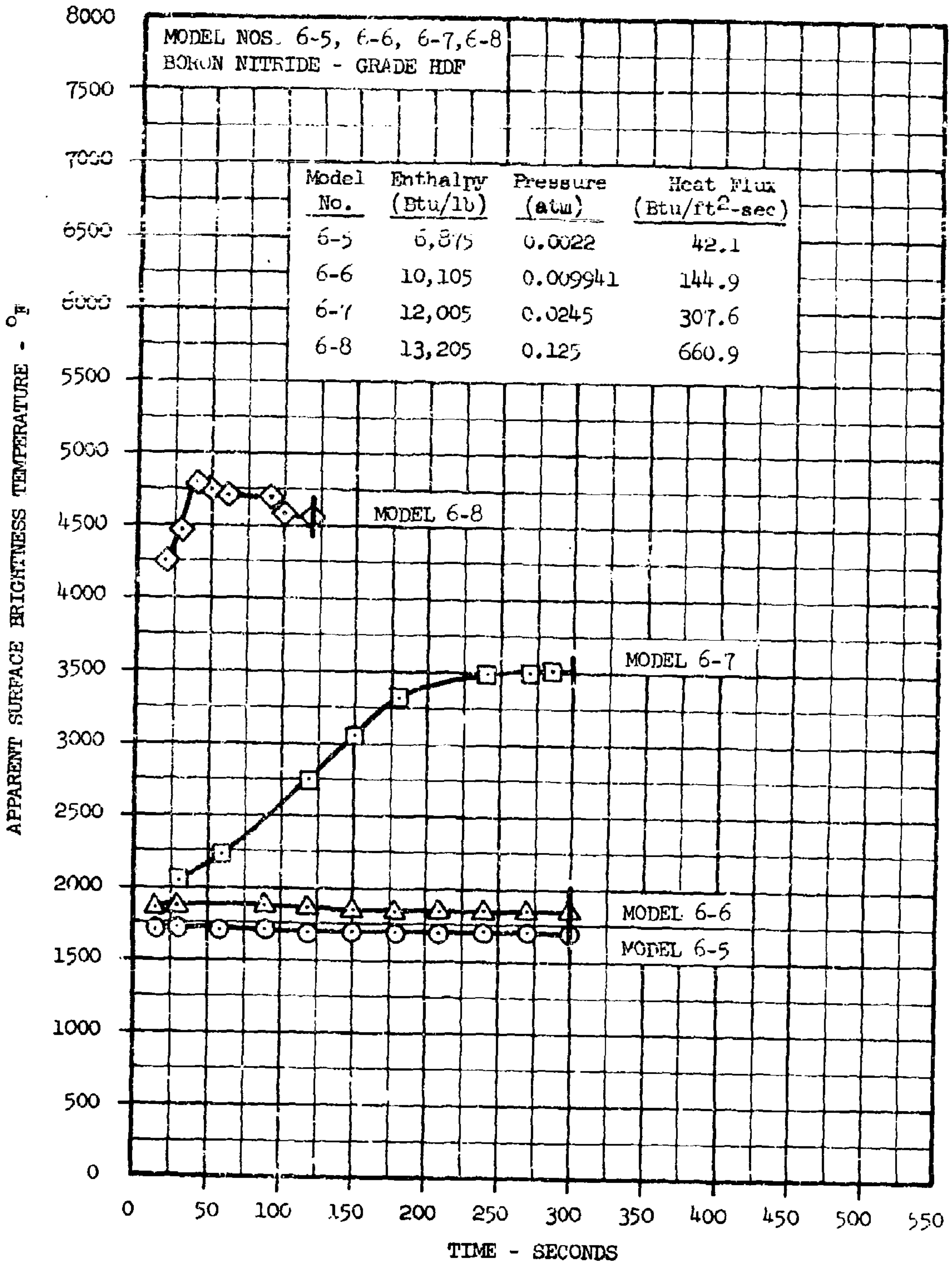

Figure 121 -- Boron Nitride - Grade HDF - Surface Temperatures

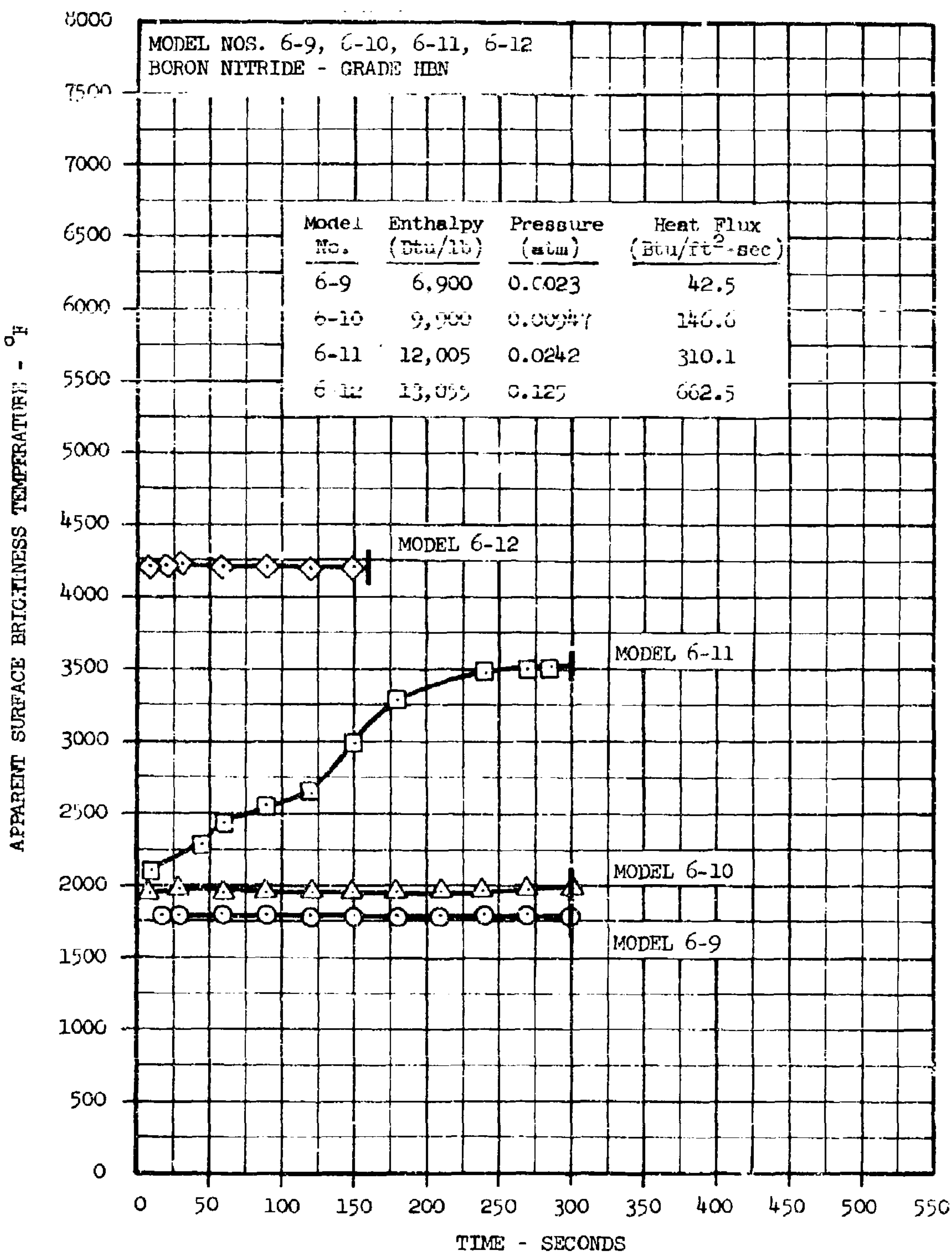

Figure 122 -- Boron Nitride - Grade HBN - Surface Temperatures

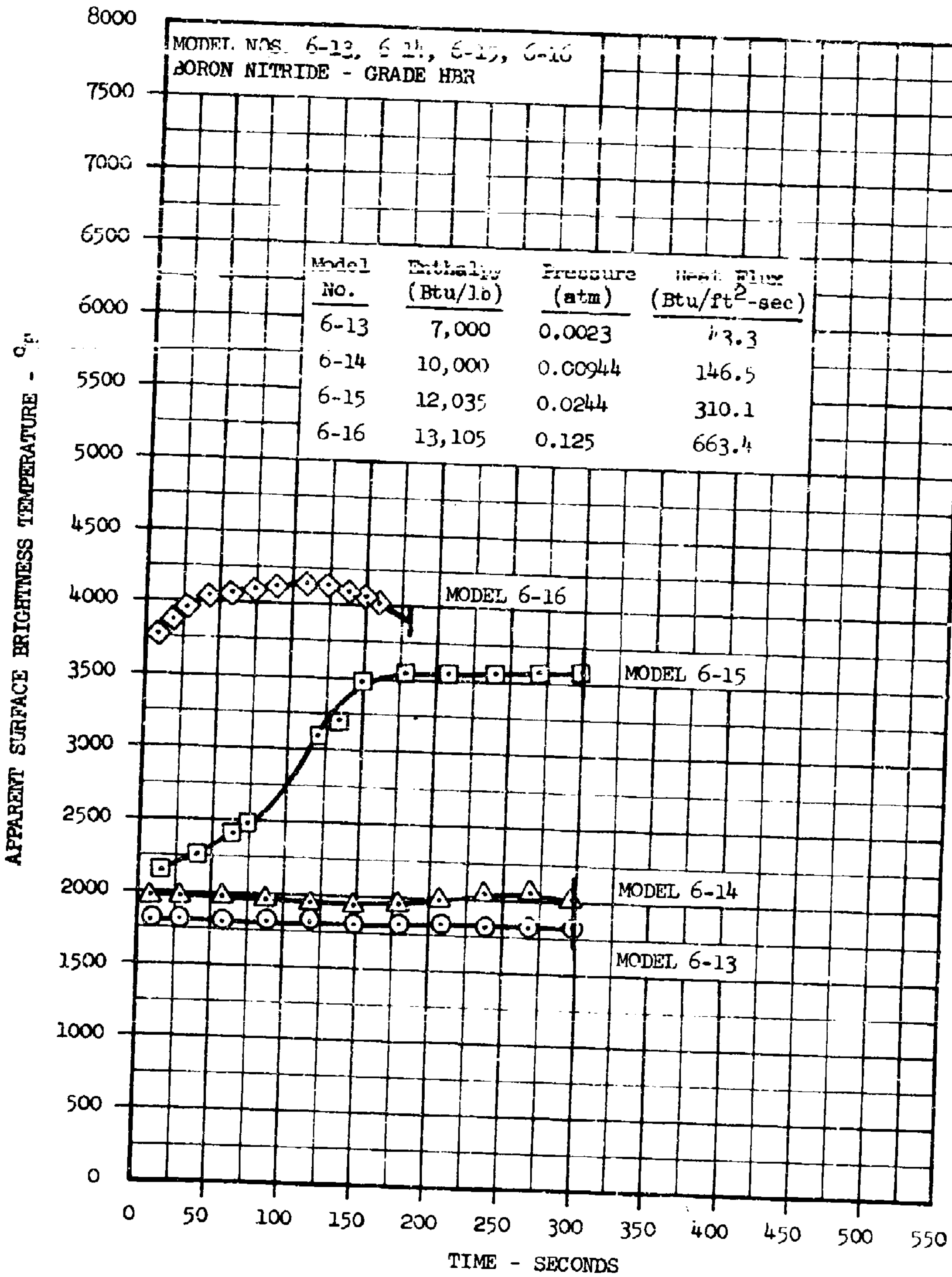

Figure 123 -- Boron Nitride - Grade HBR - Surface Temperatures

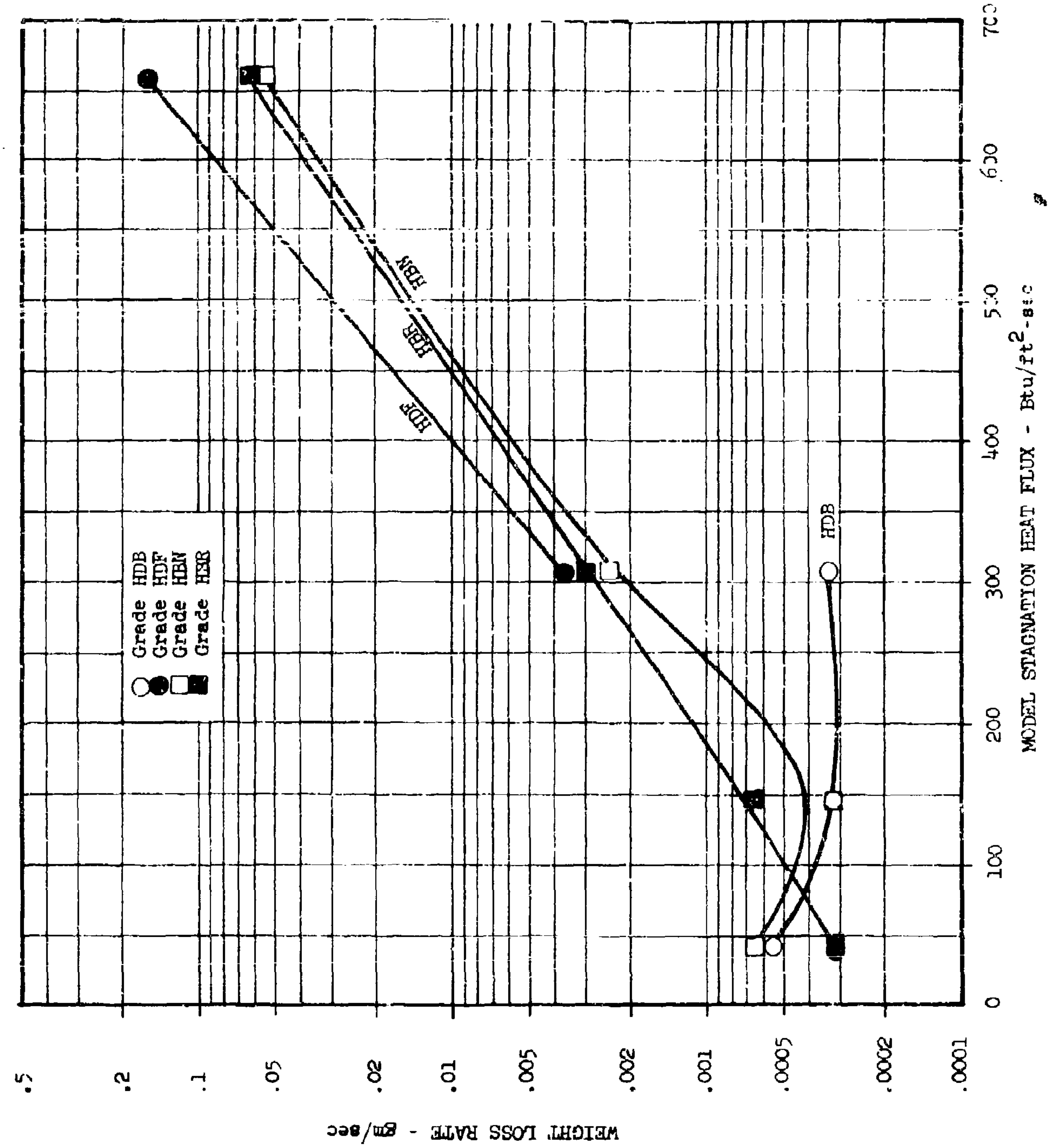

Figure 124 -- Weight Loss Rates for Boron Nitride Materials

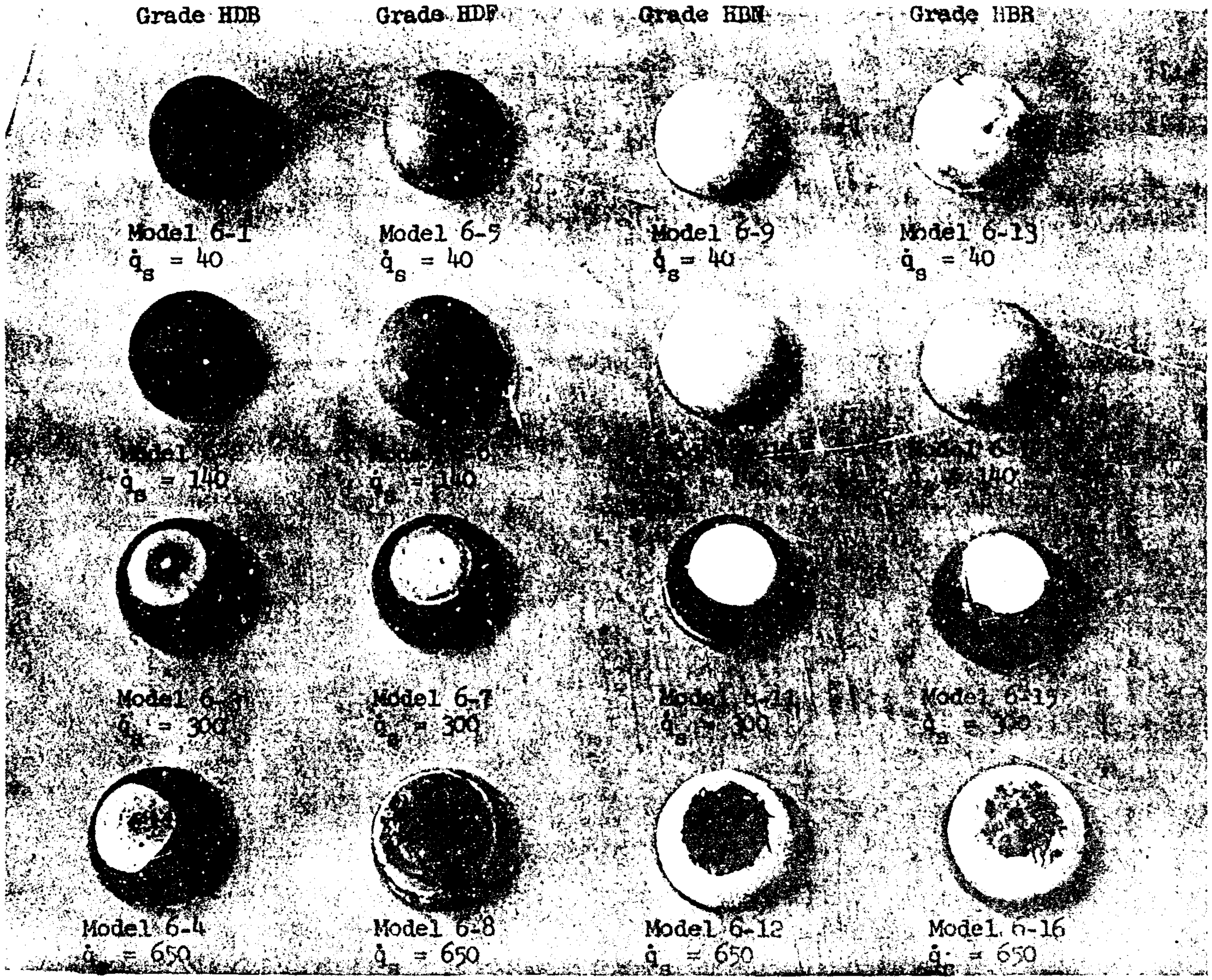

1045/002

Figure 125 -- Photographs of Boron Nitride Models

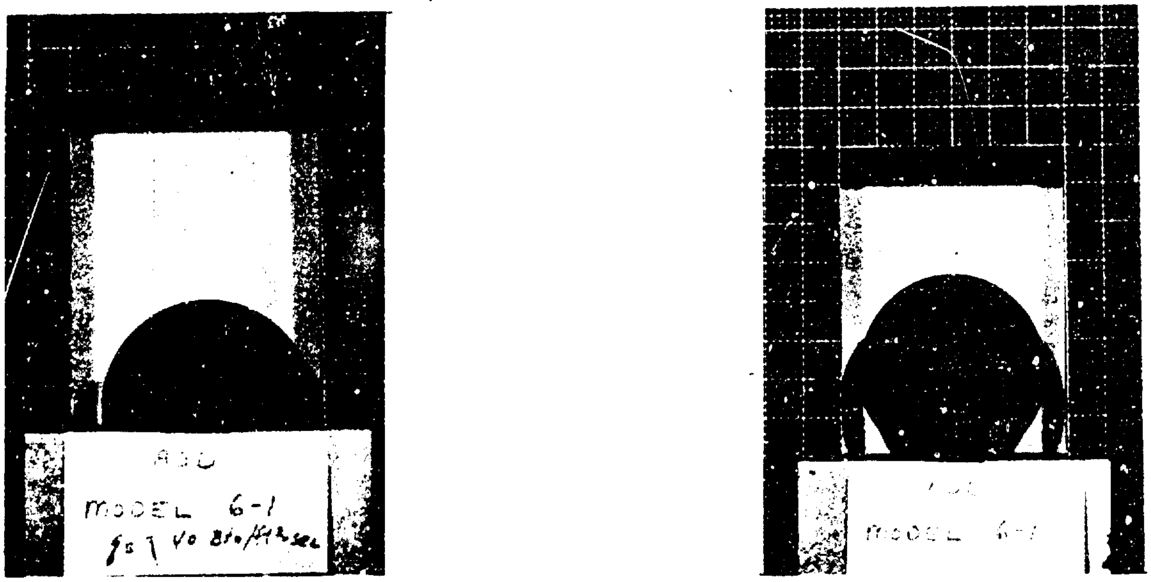

Model 6-1 - Pre- and Post-Exposure

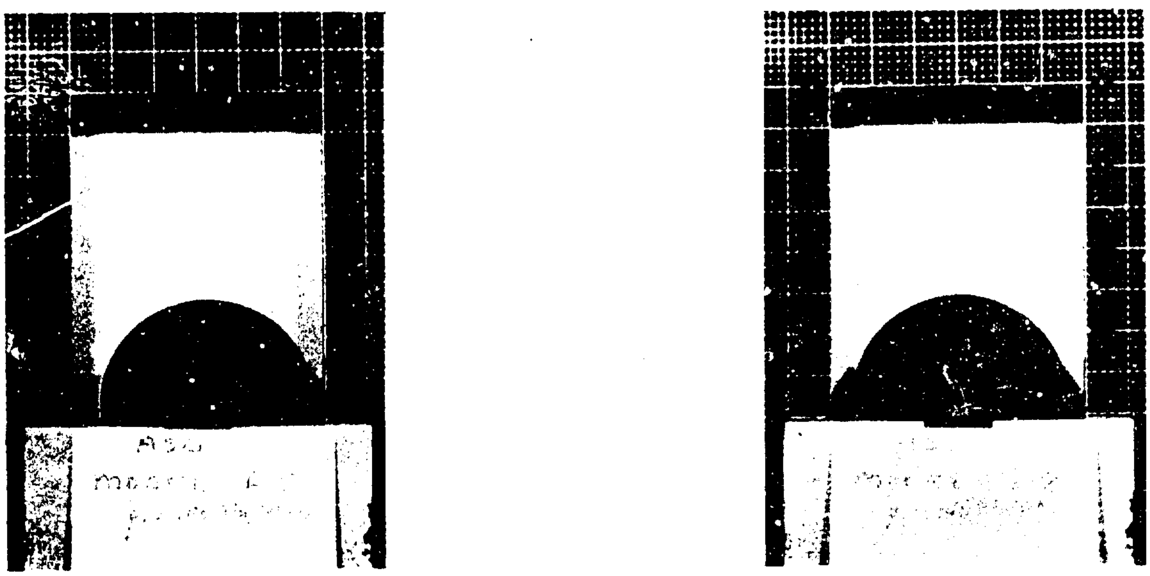

Model 6-2 - Pre- and Post-Exposure

Figure 126 -- Photographs of Boron Nitride Materials - Models 6-1 and 6-2

Model 6-3 - Pre- and Post-Exposure

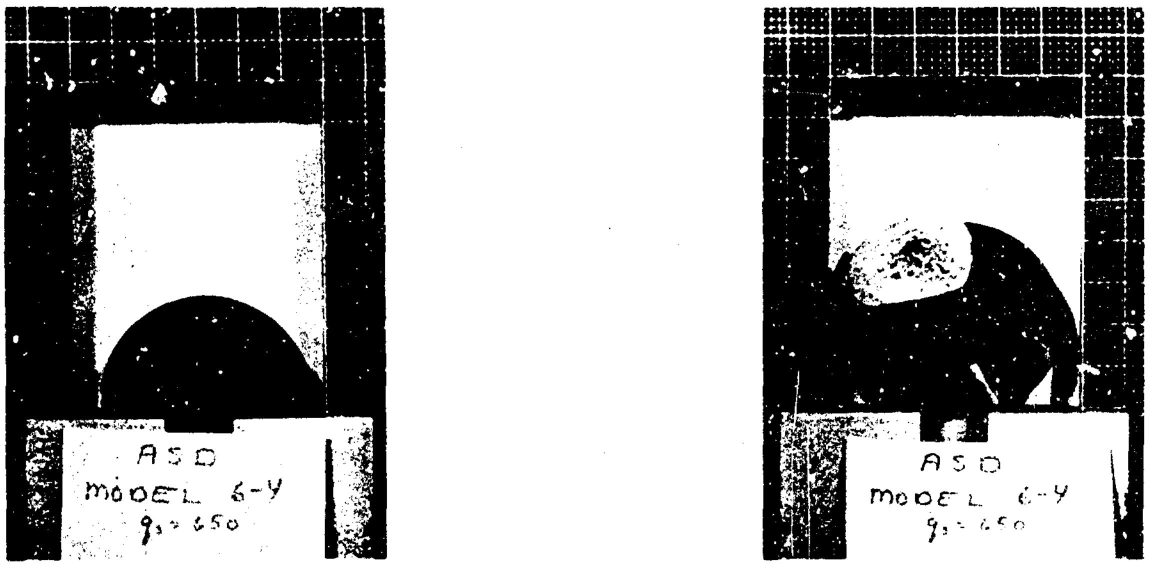

Model 6-4 - Pre- and Post-Exposure

Figure 127 -- Photographs of Boron Nitride Materials - Models 6-3 and 6-4

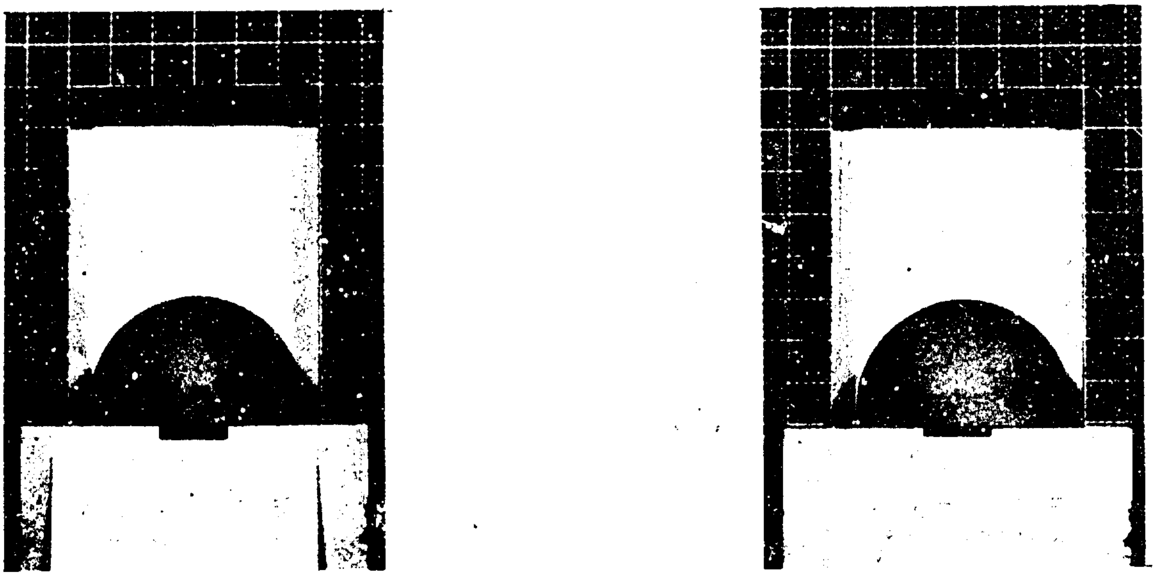

Model 6-5 - Pre- and Post-Exposure

Model 6-6 - Pre- and Post-Exposure

Figure 128 -- Photographs of Boron Nitride Materials - Models 6-5 and 6-6

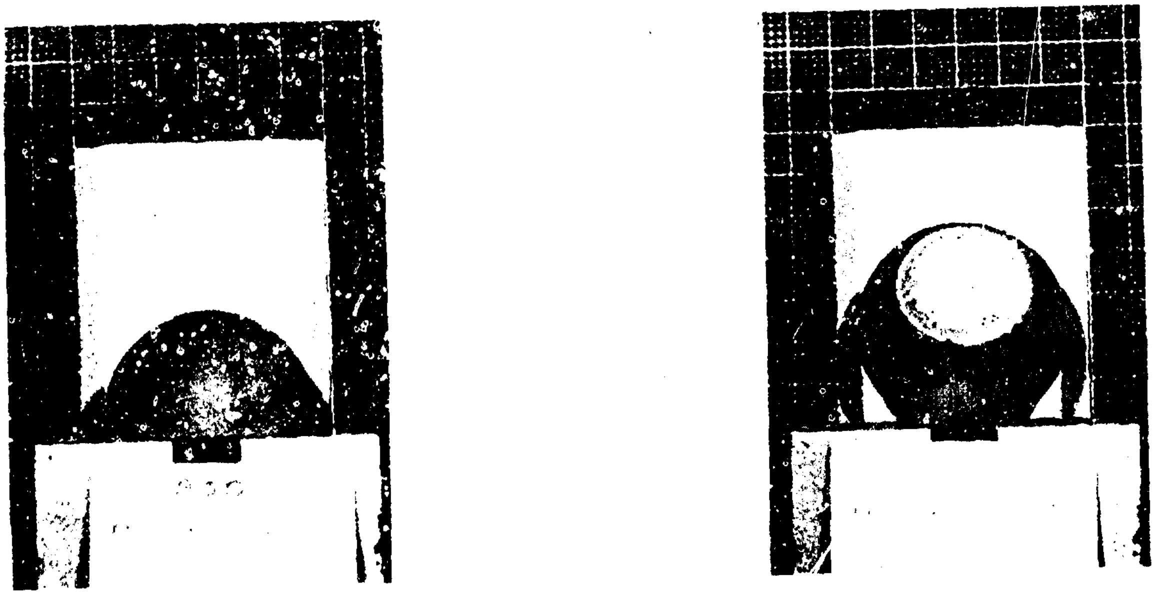

Model 6-7 - Pre- and Post-Exposure

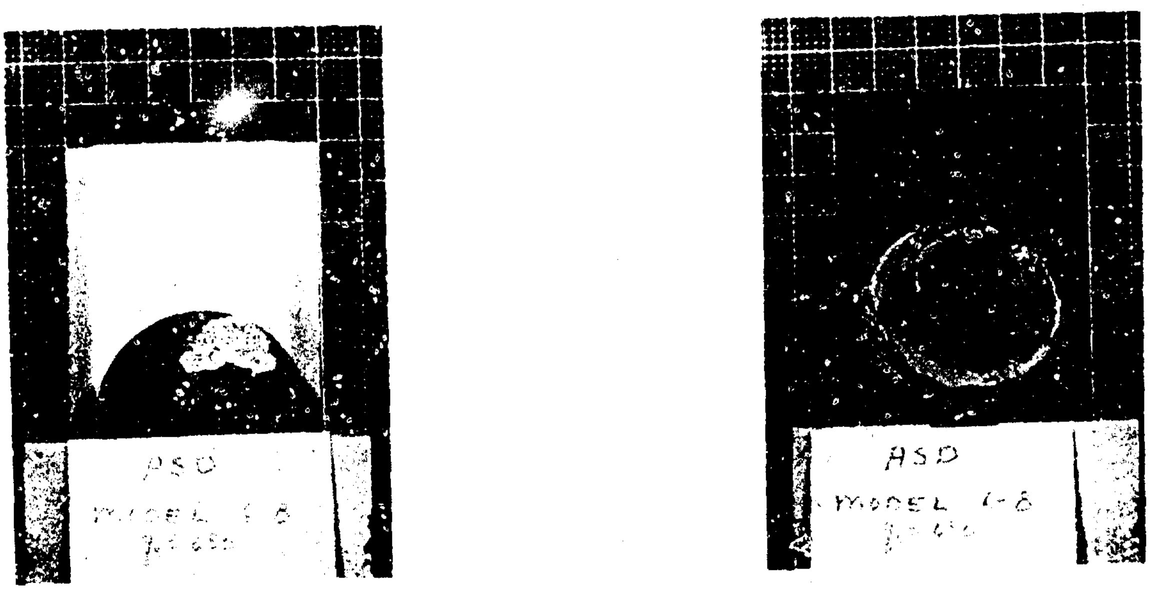

Model 6-8 - Pre- and Post-Exposure

Figure 129 -- Photographs of Boron Nitride Materials - Models 6-7 and 6-8

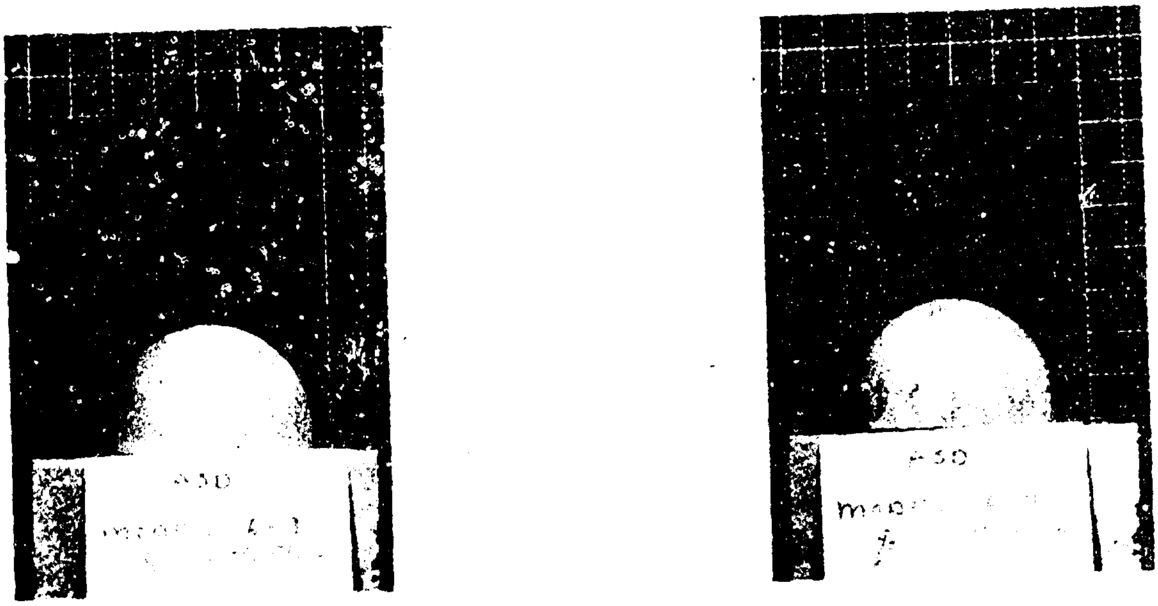

Model 6-9 - Pre- and Post-Exposure

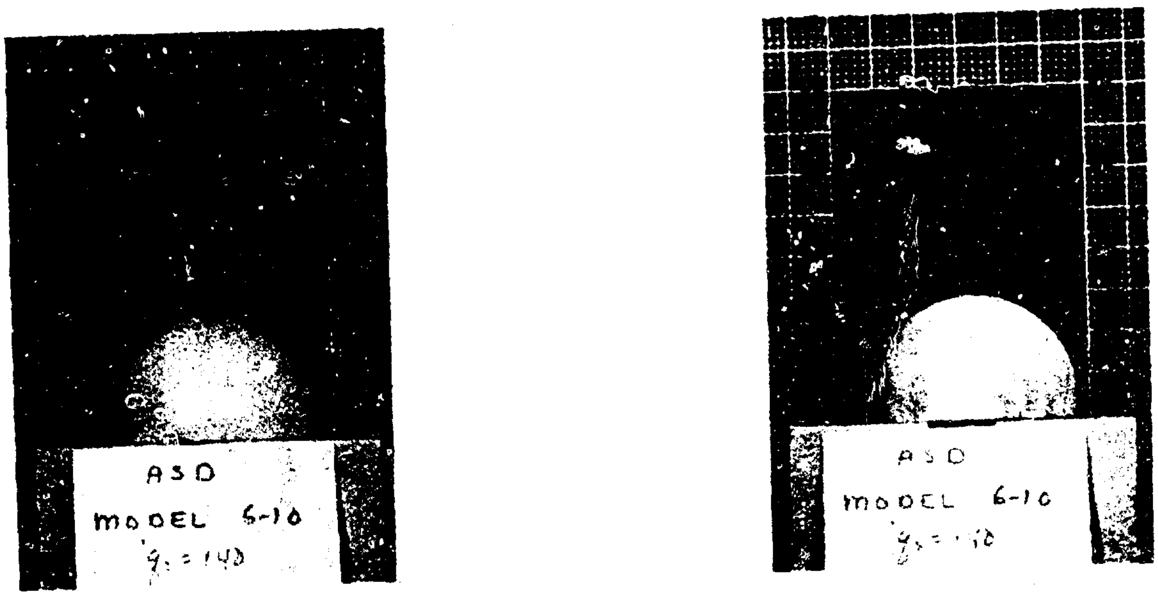

Model 6-10 - Pre- and Post-Exposure

Figure 130 -- Photographs of Boron Nitride Materials - Models 6-9 and 6-10

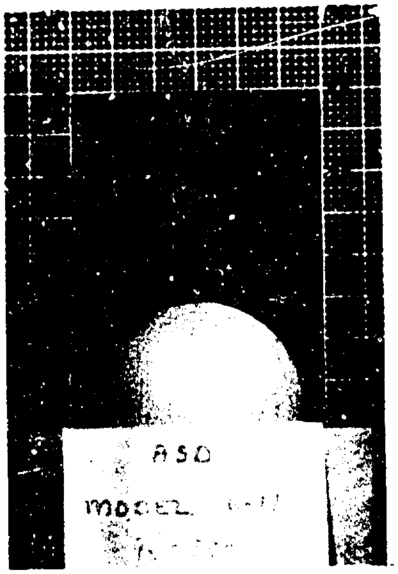

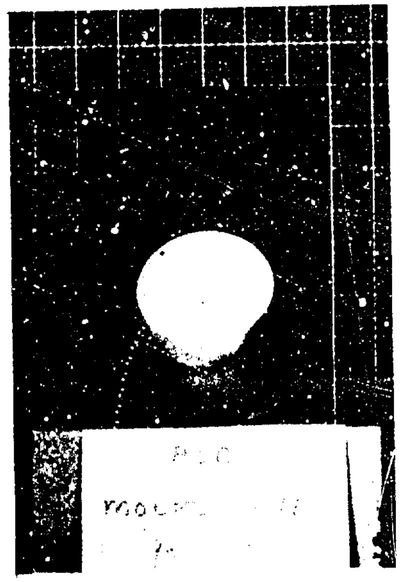

Model 6-11 - Pre- and Post-Exposure

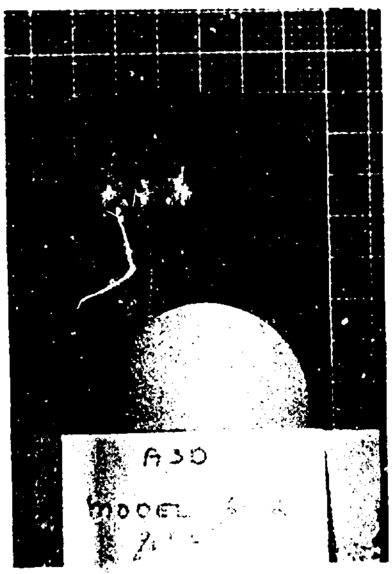

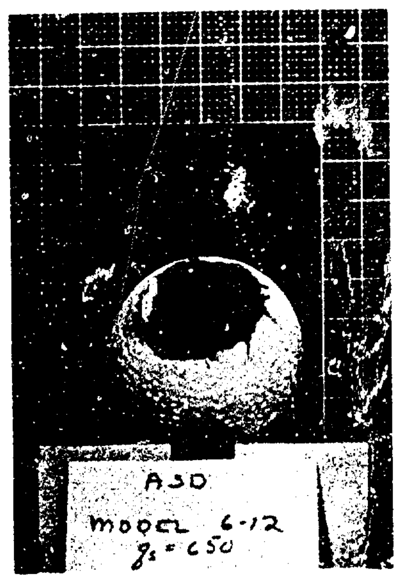

Model 6-12 - Pre- and Post-Exposure

Figure 131 -- Photographs of Boron Nitride Materials - Models 6-11 and 6-12

Model 6-13 - Pre- and Post-Exposure

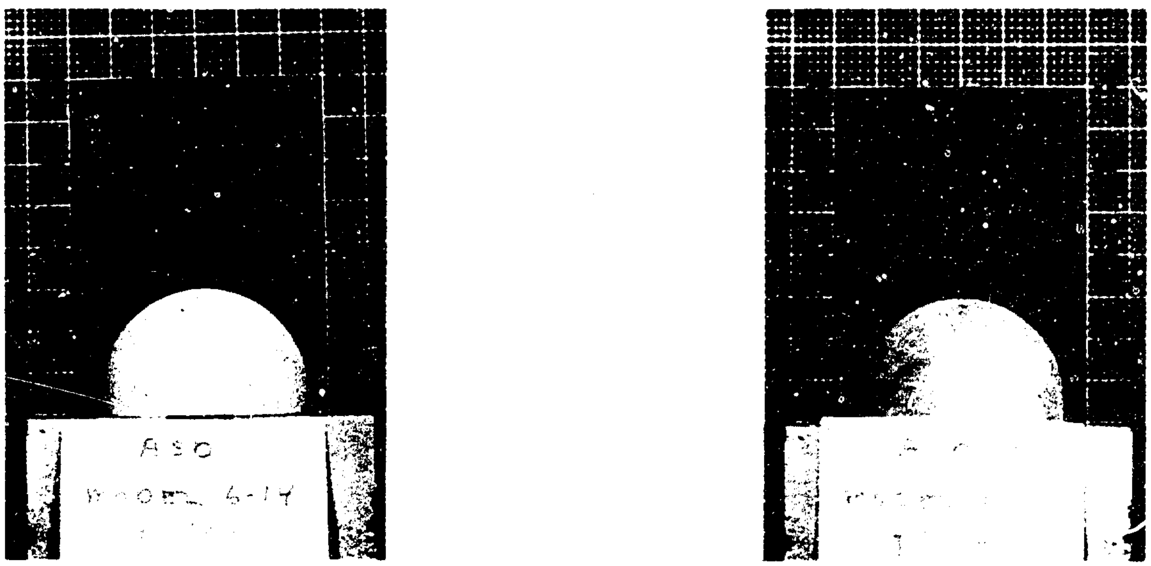

Model 6-14 - Pre- and Post-Exposure

Figure 132 -- Photographs of Boron Nitride Materials - Models 6-13 and 6-14

Model 6-15 - Pre- and Post-Exposure

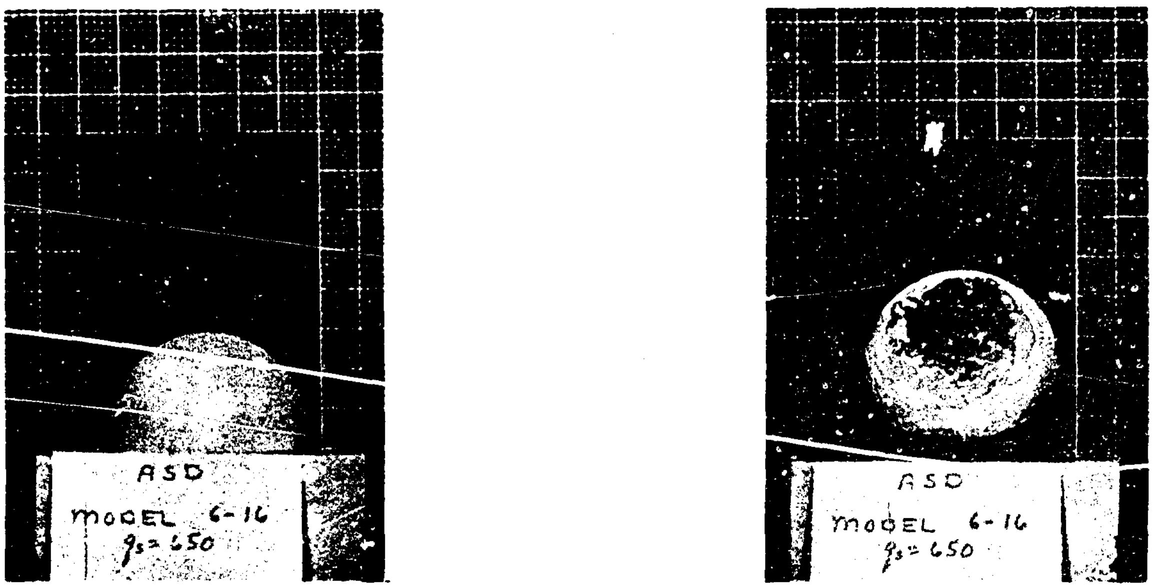

Model 6-16 - Pre- and Post-Exposure

Figure 133 -- Photographs of Boron Nitride Materials - Models 6-15 and 6-16

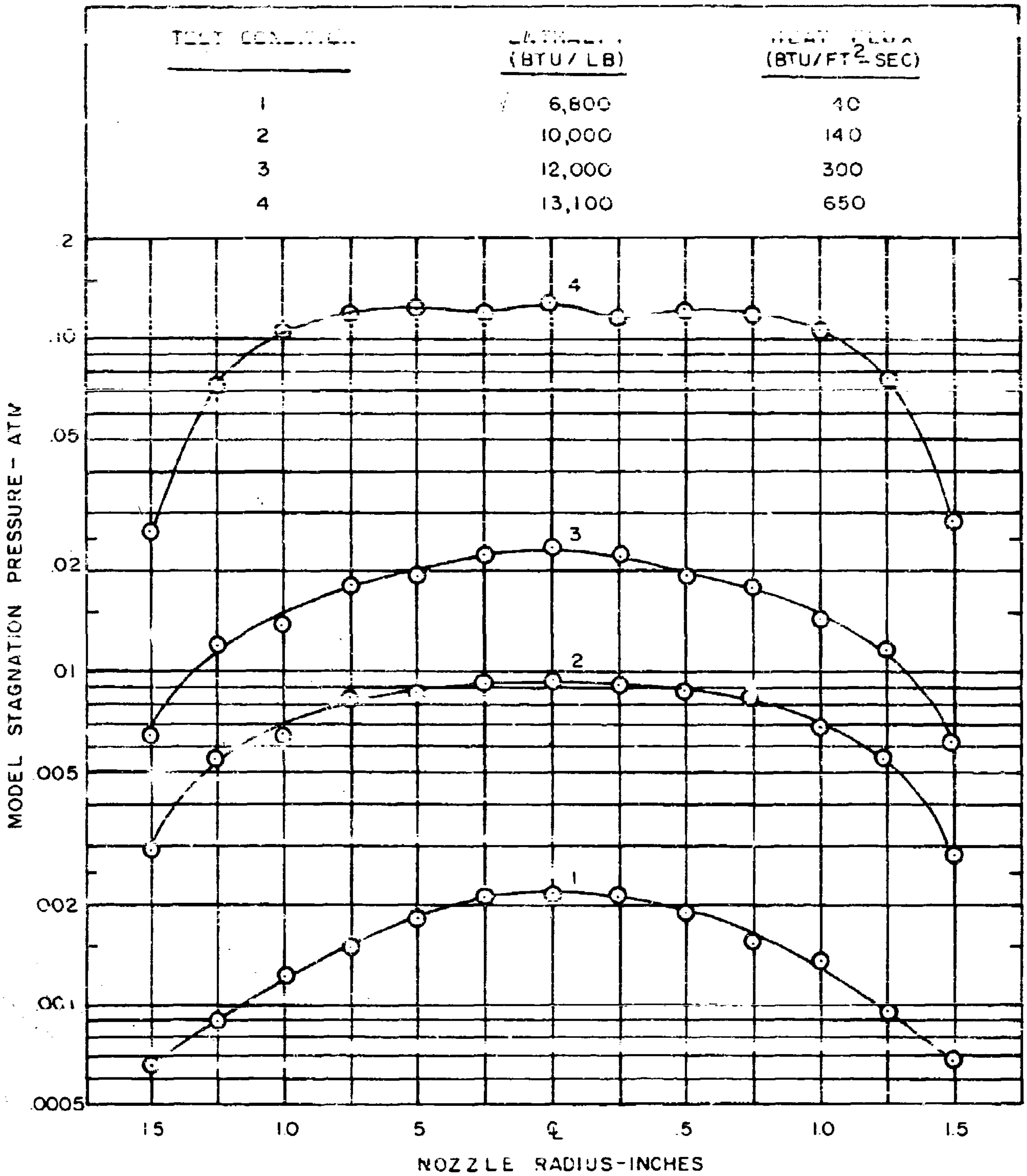

Model Stagnation Pressure Surveys of 3-inch Stream

Figure 134 -- Model Stagnation Pressure Surveys for High-Density Ablator Program

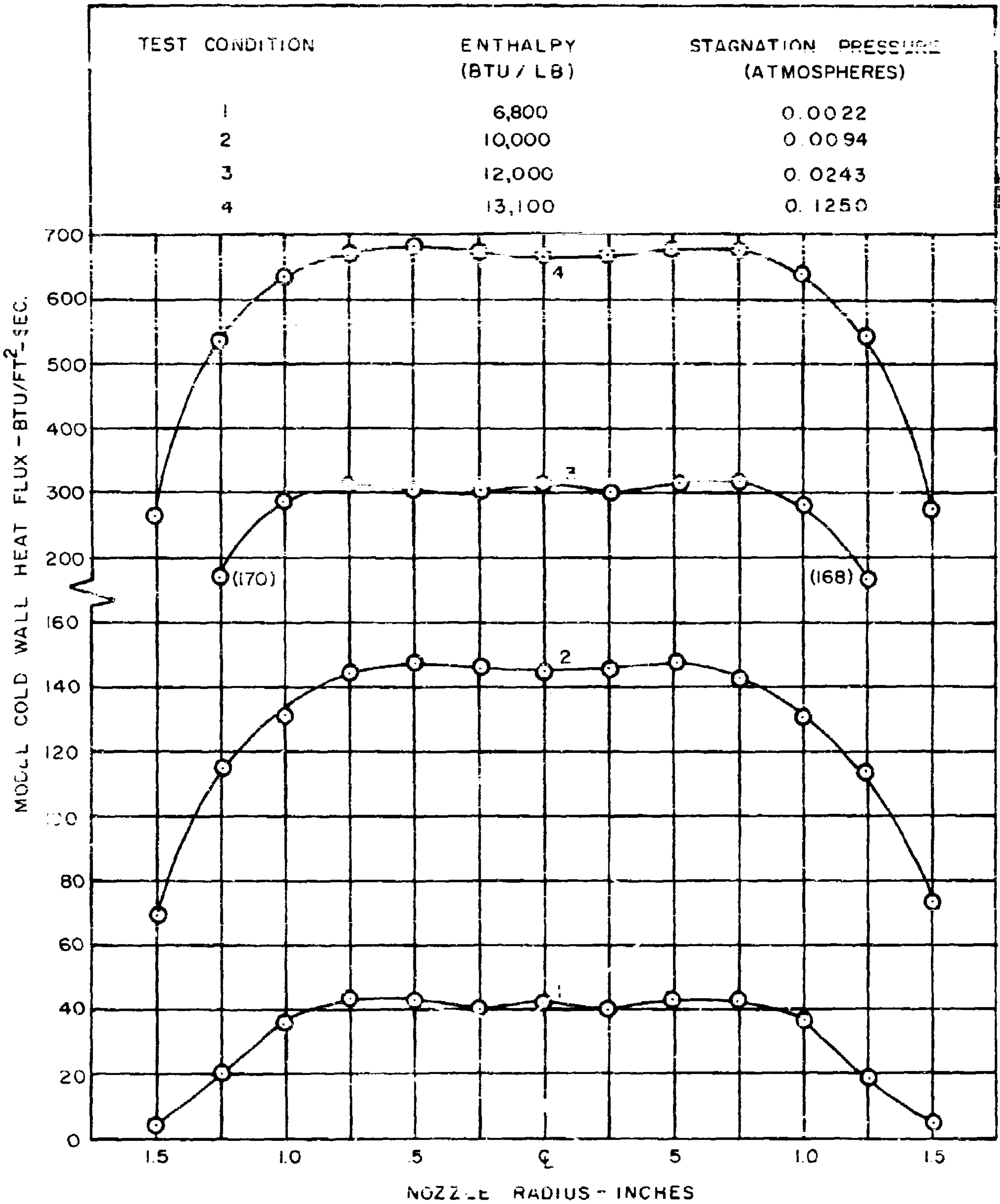

Heat Flux Surveys of 3-inch Stream

Figure 135 -- Heat Flux Surveys for High-Density Ablator Program

FRONT SURFACE RECESSION RATE

$$\dot{s} = \frac{\Delta L_{CL}}{\Delta t} = \frac{\text{Change in Centerline Length}}{\text{Total Test Time}}$$

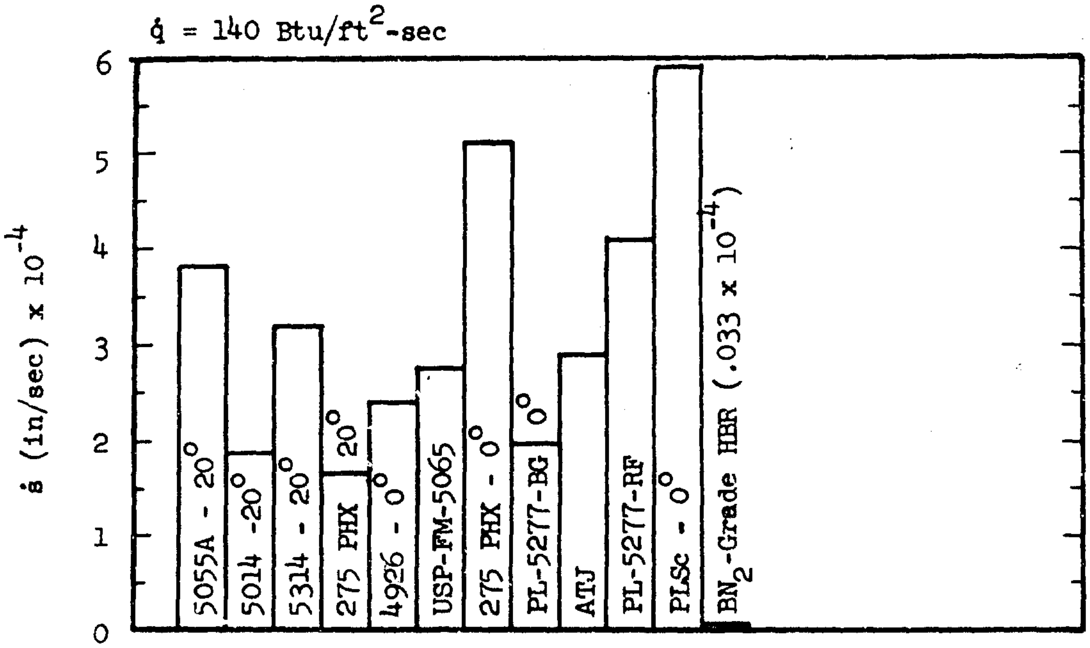

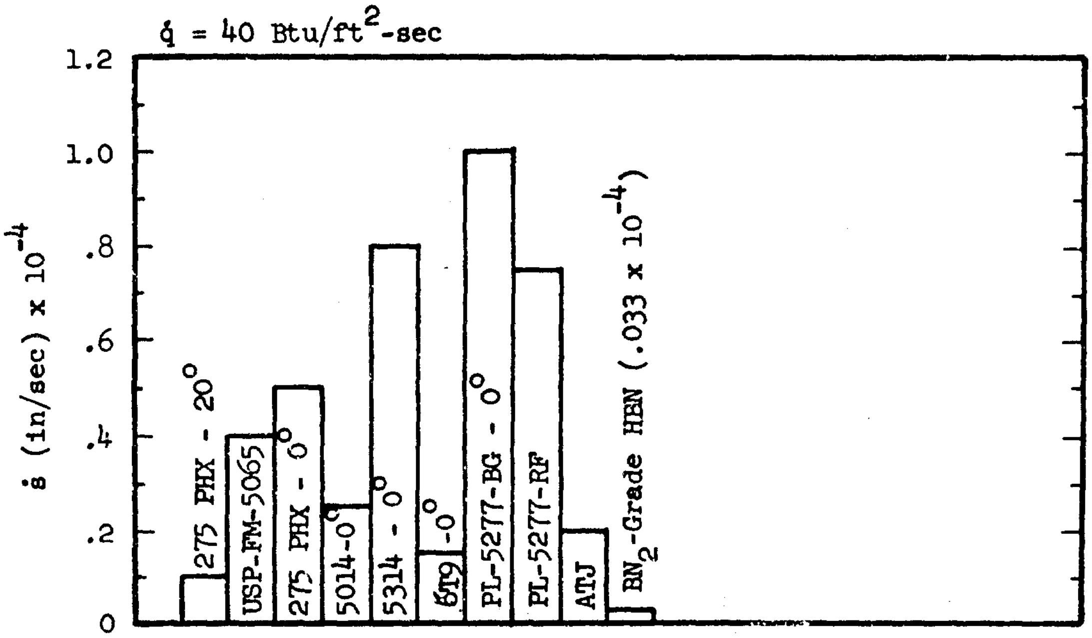

Figure 136 -- Comparison of Recession Rates for High Density Ablators at Heat Rates of 40 and 140 Btu/ft^2-sec

FRONT SURFACE RECESSION RATE

$$\dot{s} = \frac{\Delta L_{CL}}{\Delta t} = \frac{\text{Change in Centerline Length}}{\text{Total Test Time}}$$

$\dot{q}$ = 300 Btu/ft^2-sec

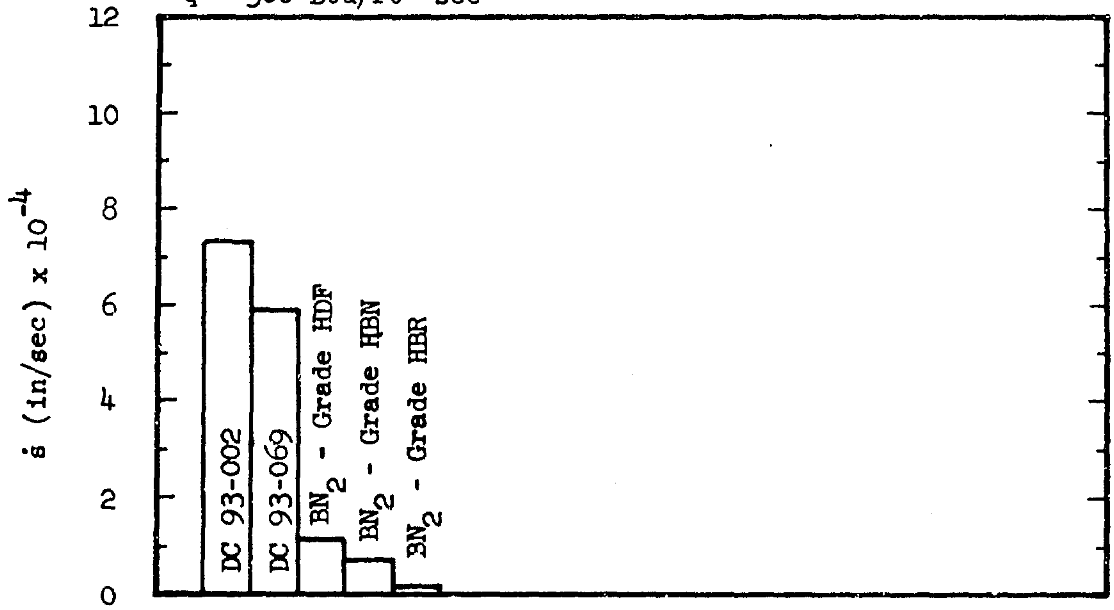

$\dot{q}$ = 650 Btu/ft^2-sec

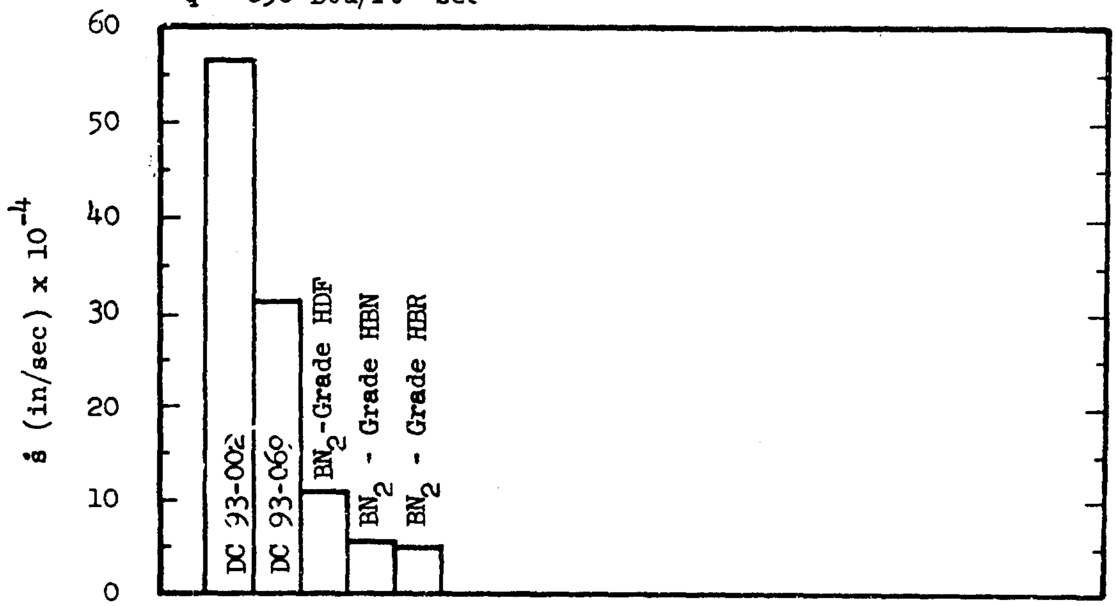

Figure 137 -- Comparison of Recession Rates for High Density Ablators at Heat Rates of 300 and 650 Btu/ft^2-sec

FRONT SURFACE BRIGHTNESS TEMPERATURE

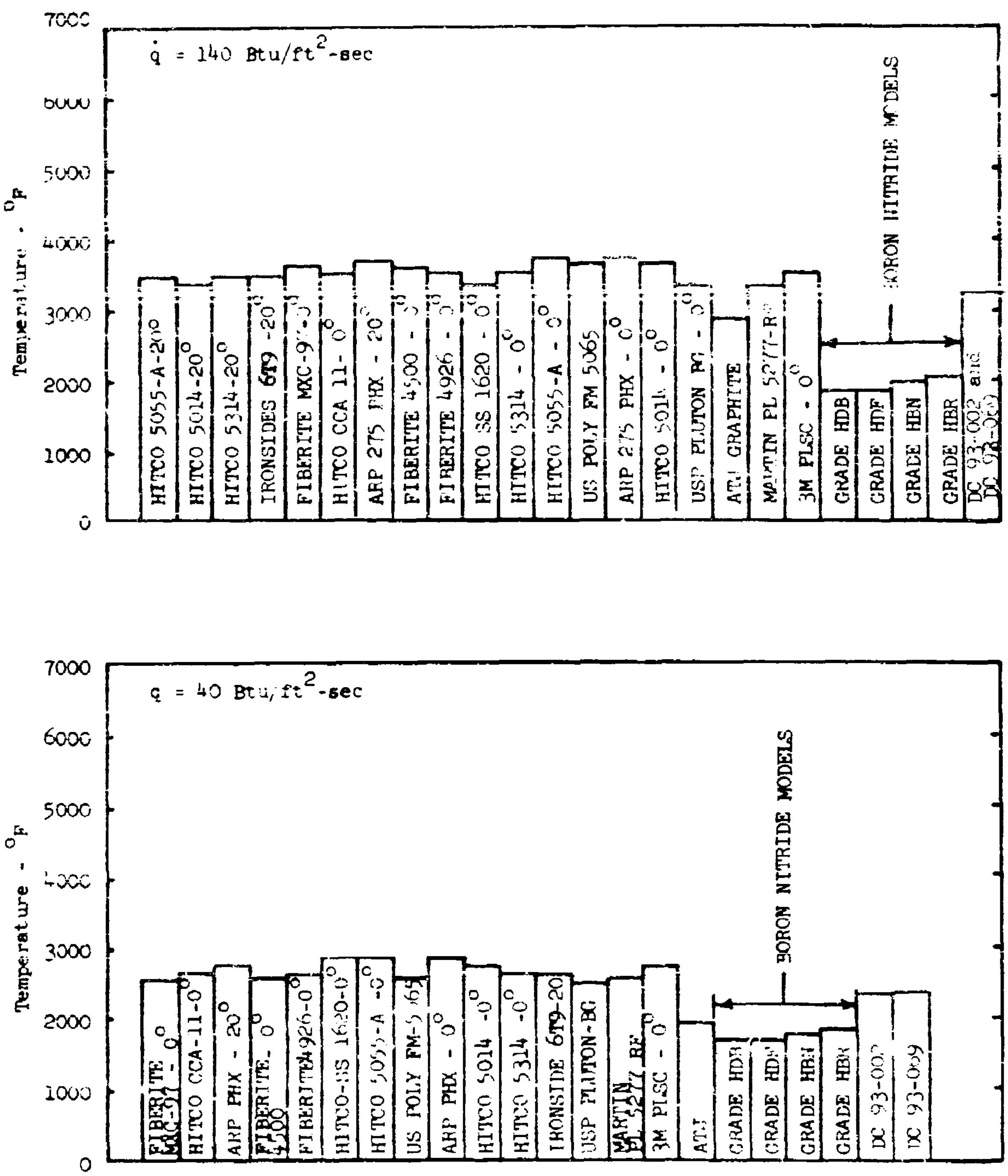

Figure 138 -- Comparison of Surface Temperature for High Density Ablators at Heat Rates of 40 and 140 Btu/ft^2-sec

FRONT SURFACE BRIGHTNESS TEMPERATURE

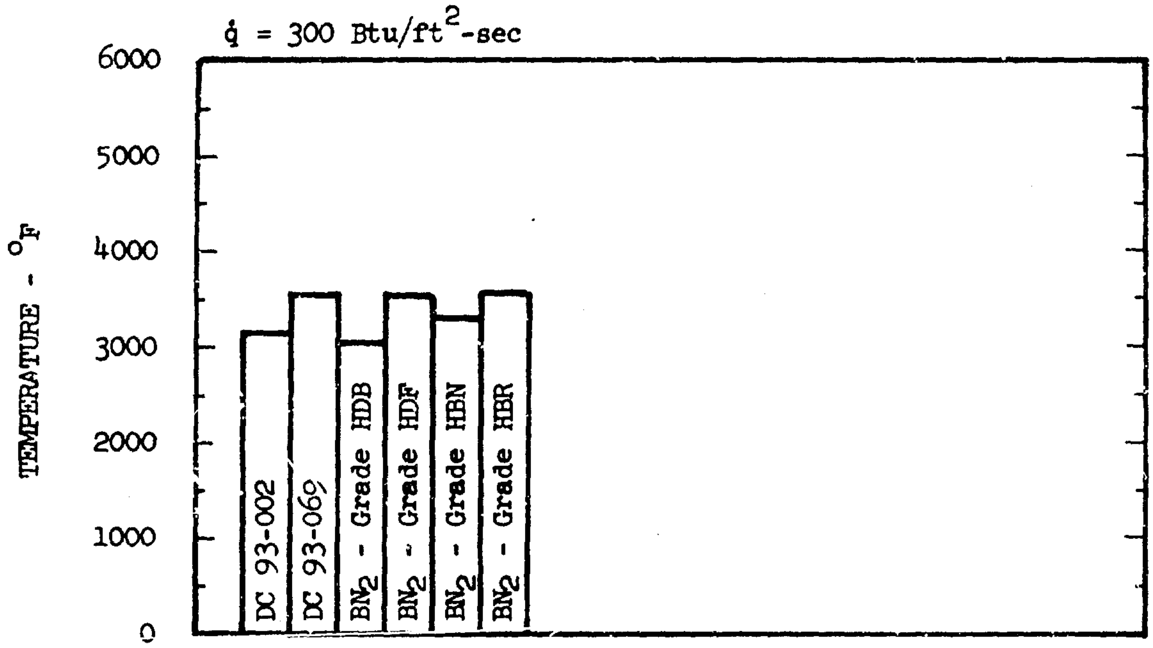

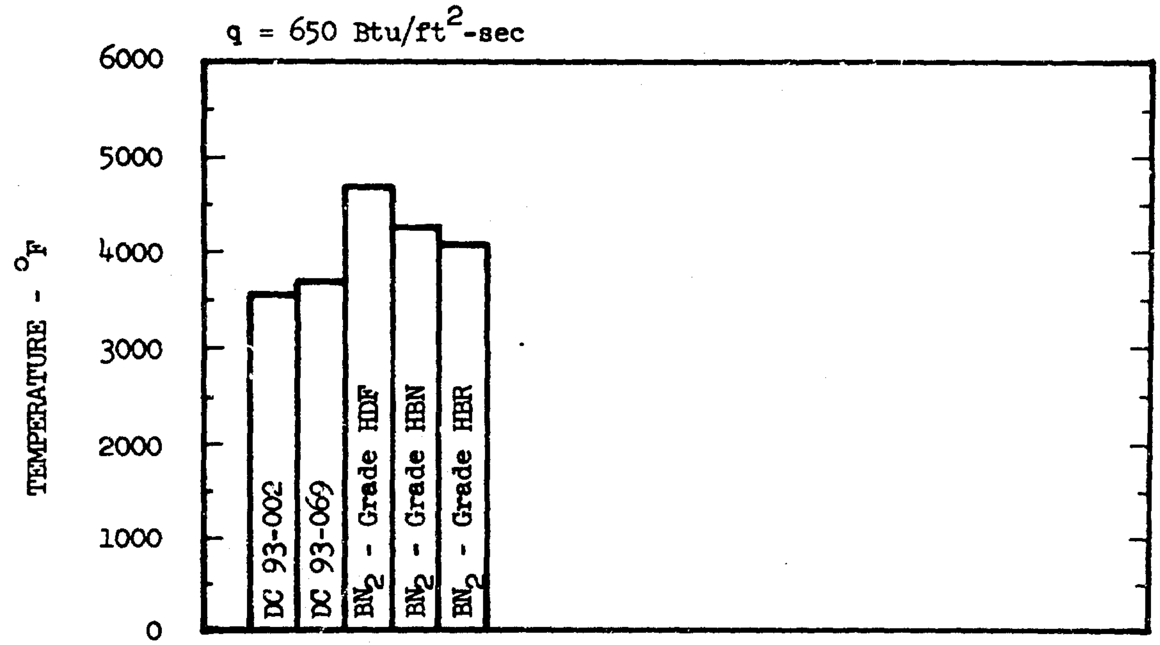

Figure 139 -- Comparison of Surface Temperature for High Density Ablators at Heat Rates of 300 and 650 Btu/ft^2-sec

COMPARISON OF BACK-FACE TEMPERATURES

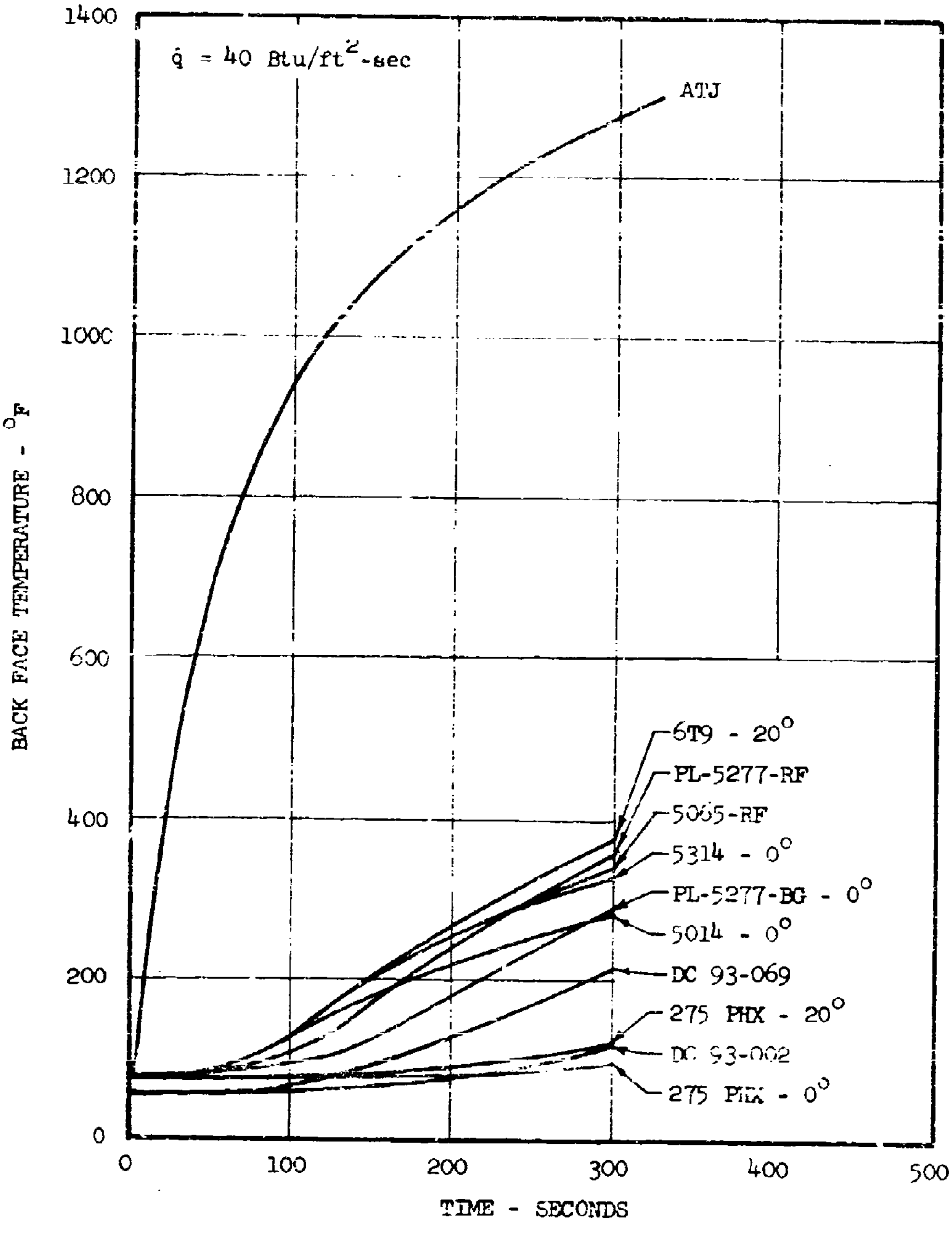

Figure 140 -- Comparison of Back-Face Temperatures for High-Density Ablators, at Heat Rate of 40 Btu/ft^2-sec

COMPARISON OF BACK-FACE TEMPERATURES

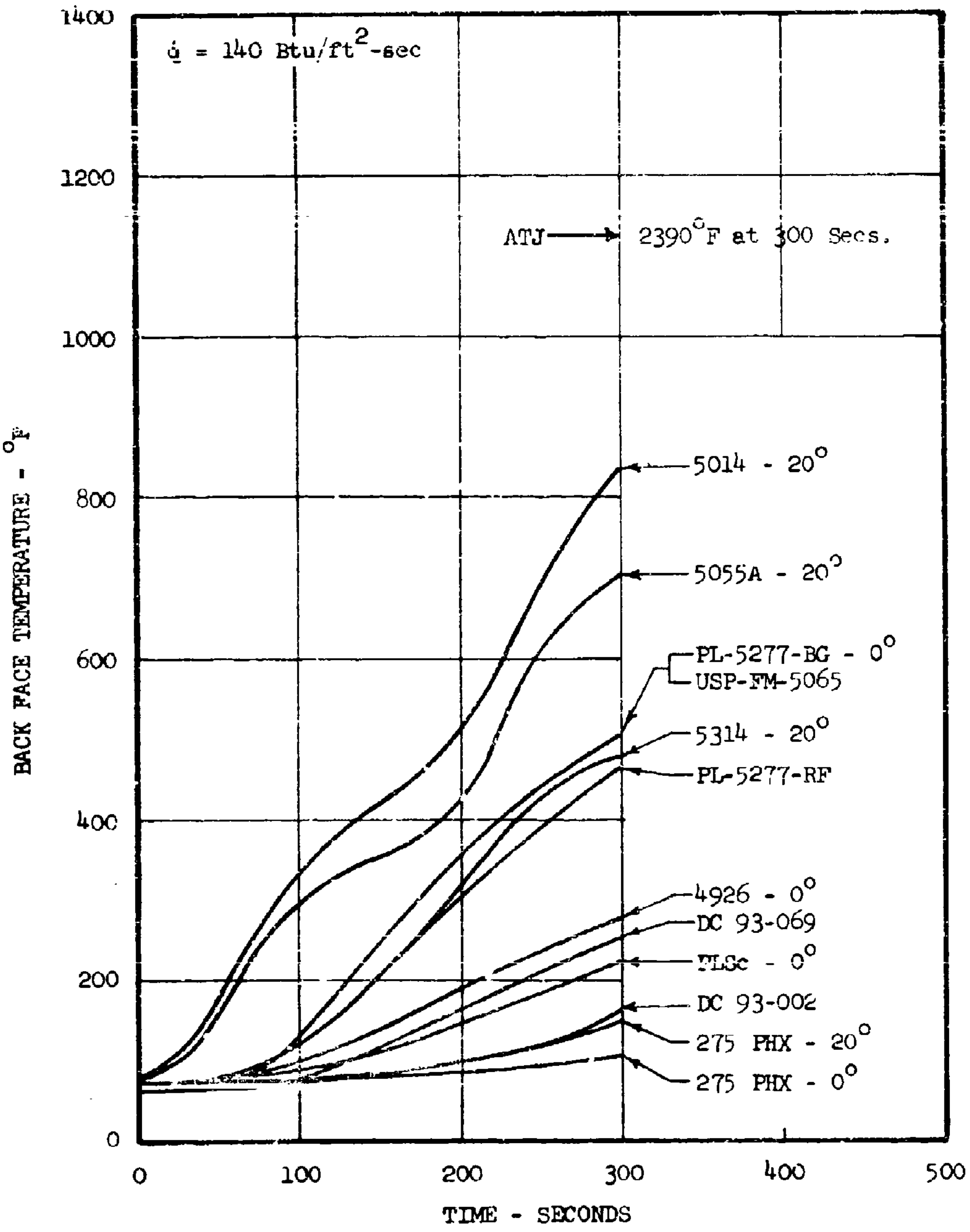

Figure 141 -- Comparison of Back-Face Temperatures for High Density Ablators, at Heat Rate of 140 Btu/ft^2-sec

4.0 SPECIAL CLASS LOW-DENSITY ABLATOR PROGRAM

Arrangements were made early in the summer of 1966 with technical representatives of Lockheed Missiles and Space Company, to perform thermal arc screening tests on a number of candidate ablators for Lockheed's ENCAP program being conducted under their contract with the Air Force - AF 33(615)-3627. Testing was performed at Space-General Corporation in August 1966 on 26 candidate reinforced silicone resin composite ablators, ranging in density from approximately 20 to 45 lb/ft^3. A detailed test report has been submitted under separate cover to Lockheed Missiles and Space Company under Space-General Corporation's report number SGC 1045R-3A1, September 1966.

4.1 Objectives

The objective of this program was to screen several ablative materials to determine their relative resistance to erosion and char spallation when subjected to severe aerodynamic heating. The candidate materials were evaluated at two simulated re-entry conditions defined primarily by model heating rates of 25 and 45 Btu/ft^2-sec.

4.2 Description of Models Tested

All of the materials evaluated under this program fall under the general heading of low-density reinforced silicone resin composite ablators. However, within each specific composite various density levels were investigated. This may best be seen in the following table summarizing the materials and their individual virgin (unexposed) material densities.

Summary of Lockheed ENCAP Ablators

Model Designation	Virgin Material Density (lb/ft^3)	Type of Ablator
1AX	28.0	Reinforced Silicone Resin Composite
2AX	28.6	↓
3AX	22.6	↓
4AX	25.1	↓
6AX	30.3	↓
7AX	30.8	↓
8AX	30.5	↓
9AX	32.1	↓
10AX	31.8	↓
1GX	22.9	Reinforced Silicone Resin Composite
2GX	24.9	↓
3GX	25.2	↓
4GX	25.6	↓
5GX	24.6	↓
7GX	29.8	↓
8GX	29.4	↓
9GX	32.2	↓
10GX	29.2	↓

Summary of Lockheed ENCAP Ablators
(Continued)

Model Designation	Virgin Material Density (lb/ft3)	Type of Ablator
12AY 13AY 14AY 15AY	39.8 40.4 39.5 39.7	Reinforced Silicone Resin Composite ↓
11GY 13GY 14GY 15GY	44.0 44.5 42.0 40.1	Reinforced Silicone Resin Composite ↓

The test models consisted of flat panels 2.00-inches by 2.25-inches by 0.48-inches, as sketched in Figure 142. These panels were inserted into a water-cooled 20° half-angle blunt-nosed wedge with a nose radius of 0.250 inches. Both sides of the wedge were utilized, thus enabling the exposure of two test panels per run. All of the test panels were instrumented with chromel/alumel thermocouples at the back-face and a number of them with a chromel/alumel thermocouple positioned in depth within the test panel.

Routine calibration data is presented in detail in Table 14 with measurements of gas stagnation enthalpy, model stagnation pressure, nozzle stagnation and static pressures, and gas flow rates tabulated for each set of model runs. Detailed model heat flux measurements, which are described in the following section, are tabulated in Table 15. Ablation profile measurements, presented in Table 16, are for three 'x' distances from the leading edge of the test panel of 0.370, 0.910 and 1.435 inches. In most cases, the test material exhibited swelling (expansion) characteristics as designated by the plus sign in front of the measurements; negative signs designate recession measurements.

The model back-face and in-depth thermocouples were continuously recorded on Texas Instruments ServoRiter II null-balance recorders, [illegible] accuracy. Exposure times were monitored on the basis of achievement of a back-face temperature of 500°F. Temperature-time histories of the thermocouples are graphed in Figures 143 through 155; model surface temperatures measured with a Leeds and Northrup manual optical brightness pyrometer are also included on the temperature graphs.

Pre- and post-exposure black and white test panel photographs were obtained using a Kalimar reflex camera. These photographs are shown in Figures 156 through 168.

4.3 Calibration of Test Conditions

Two hyperthermal test conditions were used for evaluation of the 26 candidate ablators. These conditions are defined by:

	Test Point No.1	Test Point No. 2
Gas Stagnation Enthalpy	10,500 Btu/lb	10,900 Btu/lb
Model Stagnation Pressure	0.0441 atms.	0.0133 atms.
Model Heat Flux	45 Btu/ft^2-sec	25 Btu/ft^2-sec

The calibration procedures used in performing the evaluation of the Lockheed ablators are identical to those described in earlier sections of this report, and will not be repeated here. However, additional calibration of the test conditions were required in view of the different model configuration which resulted in significantly different heat flux measurements than would have been experienced by either a flat-face or hemispherical-nose model.

Calibration models were provided by Lockheed which were identical in size and shape to the water-cooled wedge/test panel models and which were instrumented with a Hy-Cal Asymptotic calorimeter. Twelve calibration runs were made, six at Test Point No. 1 and six at Test Point No. 2; the heat flux measurements obtained are tabulated in Table 15. Both sides of the wedge were checked for heat flux both prior to and immediately after the series of model tests at each of the test points. Distribution of the heat flux was measured to be within $\pm$ 5 % between opposite sides of the wedge, indicating that the wedge was very well centered in the stream. The repeatability of the heat flux before and after each series of model tests was within $\pm$ 2 %. Since many of the models expanded and raised from the surface of the wedge in which the test panel was held, simulated conditions were achieved by installing the calorimeter into the wedge holder in a position raised approximately 3/32-inch. At Test Point No. 1, the 'raised calorimeter' readings were generally higher on both sides of the wedge than in the unraised position. However, at Test Point No. 2, just the reverse was true with the 'raised calorimeter' readings indicating a lower heat flux than in the unraised position. Nevertheless, the maximum deviation caused by the forced re-positioning of the calorimeter did not vary more than $\pm$ 16%.

The two test conditions achieved in this program were attained by a low pressure/high enthalpy plasma arc generator and a supersonic Mach 3 contoured nozzle, three inches in exit diameter. Simulated air consisting of 79% nitrogen and 21% oxygen was used as the test medium.

CALIBRATION DATA

Table 14

Lockheed ENCAP Model Tests

Model No.	Stagnation Enthalpy (Btu/lb)	Model Stag. Pressure (atm)	Nozzle Stag. Pressure (atm)	Nozzle Exit Pressure (atm)	Nitrogen Flow (lb/sec)	Oxygen Flow (lb/sec)	Total Gas Flow (lb/sec)
1AX - North 2AX - South	10,480	0.0441	0.238	0.00425	0.00711	0.00190	0.00901
1GX - North 2GX - South	10,520	0.0442	0.238	0.00428	0.00711	0.00190	0.00901
7AX - North 6AX - South	10,475	0.0441	0.238	0.00427	0.00711	0.00190	0.00901
7GX - North 8GX - South	10,510	0.0441	0.238	0.00425	0.00711	0.00190	0.00901
13 AY - North 12 AY - South	10,490	0.0442	0.238	0.00427	0.00711	0.00190	0.00901
13 GY - North 11GY - South	10,515	0.0442	0.238	0.00428	0.00711	0.00190	0.00901
3AX - North 4AX - South	10,910	0.0134	0.0724	0.00129	0.00205	0.00055	0.00260
3GX - North 4GX - South	10,875	0.0133	0.0724	0.00130	0.00205	0.00055	0.00260
9AX - North 8AX - South	10,860	0.0134	0.0724	0.00130	0.00205	0.00055	0.00260
9GX - North 10GX - South	10,920	0.0133	0.0724	0.00129	0.00205	0.00055	0.00260
15AY - North 14AY - South	10,880	0.0134	0.0724	0.00129	0.00205	0.00055	0.00260
15GY - North 14GY - South	10,900	0.0133	0.0724	0.00130	0.00205	0.00055	0.00260
5GX - North 10AX - South	10,890	0.0133	0.0724	0.00129	0.00205	0.00055	0.00260

HEAT FLUX MEASUREMENTS

Table 15
Lockheed ENCAP Model Tests

Calorimeter Number	Location and Sequence	Gas Stag. Enthalpy (Btu/lb)	Model Stag. Pressure (atm)	Heat Flux (Btu/ft^2-sec)
Hy-Cal 20020	South Side - Pre-T.P.1	10,430	0.0441	44.6 and 45.0
Hy-Cal 20020	North Side - Pre-T.P.1	10,510	0.0441	43.0
Hy-Cal 20020	South Side - Post-T.P.1	10,490	0.0441	44.2 and 44.5
Hy-Cal 20013	North Side - Post-T.P.1	10,500	0.0441	42.5 and 43.2
Hy-Cal 20013	South Side - Post-T.P.1 (Calorimeter Panel Raised from Surface 3/32")	10,520	0.0441	51.3 and 51.6
Hy-Cal 20013	North Side - Post-T.P.1 (Calorimeter Panel Raised from Surface 3/32")	10,495	0.0441	44.5 and 46.3
Hy-Cal 20021	South Side - Pre-T.P.2	10,910	0.0133	23.2 and 23.0
Hy-Cal 20021	North Side - Pre-T.P.2	10,880	0.0133	23.9 and 23.9
Hy-Cal 20021	South Side - Post-T.P.2	10,890	0.0133	24.0 and 24.2
Hy-Cal 20021	North Side - Post-T.P.2	10,910	0.0134	24.6
Hy-Cal 20013	South Side - Post-T.P.2 (Calorimeter Panel Raised from Surface 3/32")	10,885	0.0133	20.0 and 20.3
Hy-Cal 20013	North Side - Post-T.P.2 (Calorimeter Panel Raised from Surface 3/32")	10,915	0.0134	21.5 and 21.8

MODEL MEASUREMENTS

Table 16
Lockheed ENCAP Model Tests

Model No.	Position on Wedge	Exposure Time (seconds)	Profile Measurements x = .370 inches*	x = .910 inches*	x = 1.435 inches*
1AX	North	107.0	+ .056	+ .050	+ .062
2AX	South	107.0	+ .035	+ .072	+ .025
1GX	North	95.0	- .063	+ .172	+ .139
2GX	South	95.0	+ .064	+ .068	+ .059
7AX	North	113.0	- .016	+ .125	+ .069
6AX	South	113.0	- .083	+ .120	+ .107
7GX	North	98.0	- .087	+ .061	+ .061
8GX	South	98.0	- .024	+ .062	+ .047
13AY	North	144.0	+ .089	+ .085	+ .024
12AY	South	144.0	+ .113	+ .076	+ .051
13GY	North	144.0	+ .082	+ .058	+ .032
11GY	South	144.0	+ .096	+ .059	+ .047
3AX	North	185.0	+ .047	+ .043	+ .044
4AX	South	185.0	+ .078	+ .048	+ .055
3GX	North	300.0	+ .262	+ .179	+ .073
4GX	South	300.0	+ .112	+ .076	+ .043
9AX	North	229.0	+ .107	+ .138	+ .135
8AX	South	229.0	+ .018	+ .046	+ .074
9GX	North	260.0	+ .045	+ .044	+ .053
10GX	South	260.0	+ .037	+ .056	- .050
15AY	North	232.5	+ .084	+ .046	+ .050
14AY	South	232.5	+ .028	+ .059	+ .049
15GY	North	300.0	+ .053	+ .076	+ .081
14GY	South	300.0	+ .030	+ .025	+ .070
5GX	North	185.0	------	+ .163	+ .086
10AX	South	185.0	+ .055	+ .023	+ .060

NOTE:
* 'x' distance measured from front edge of test panel.

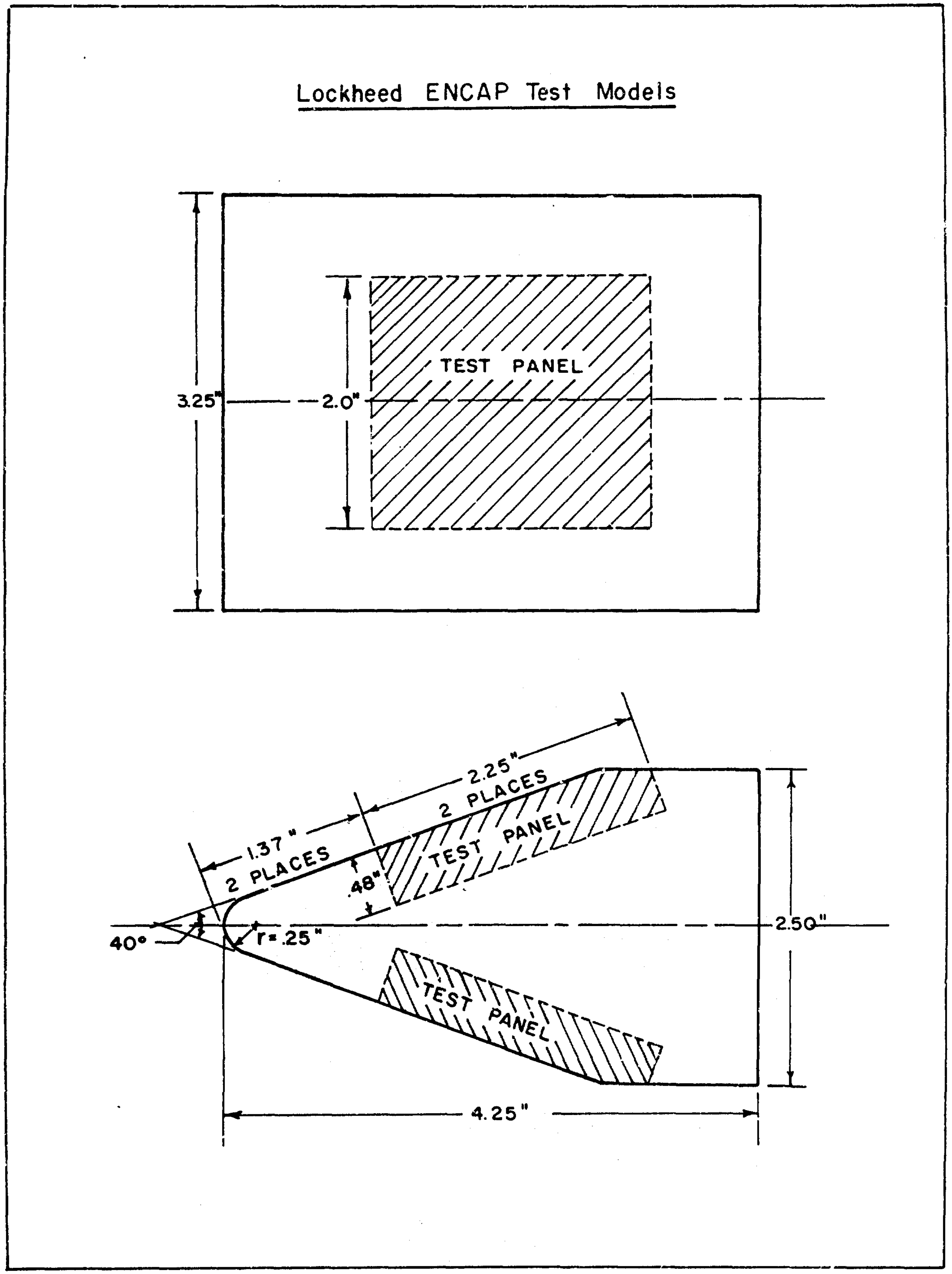

Figure 142 -- Model Design for Lockheed ENCAP Program

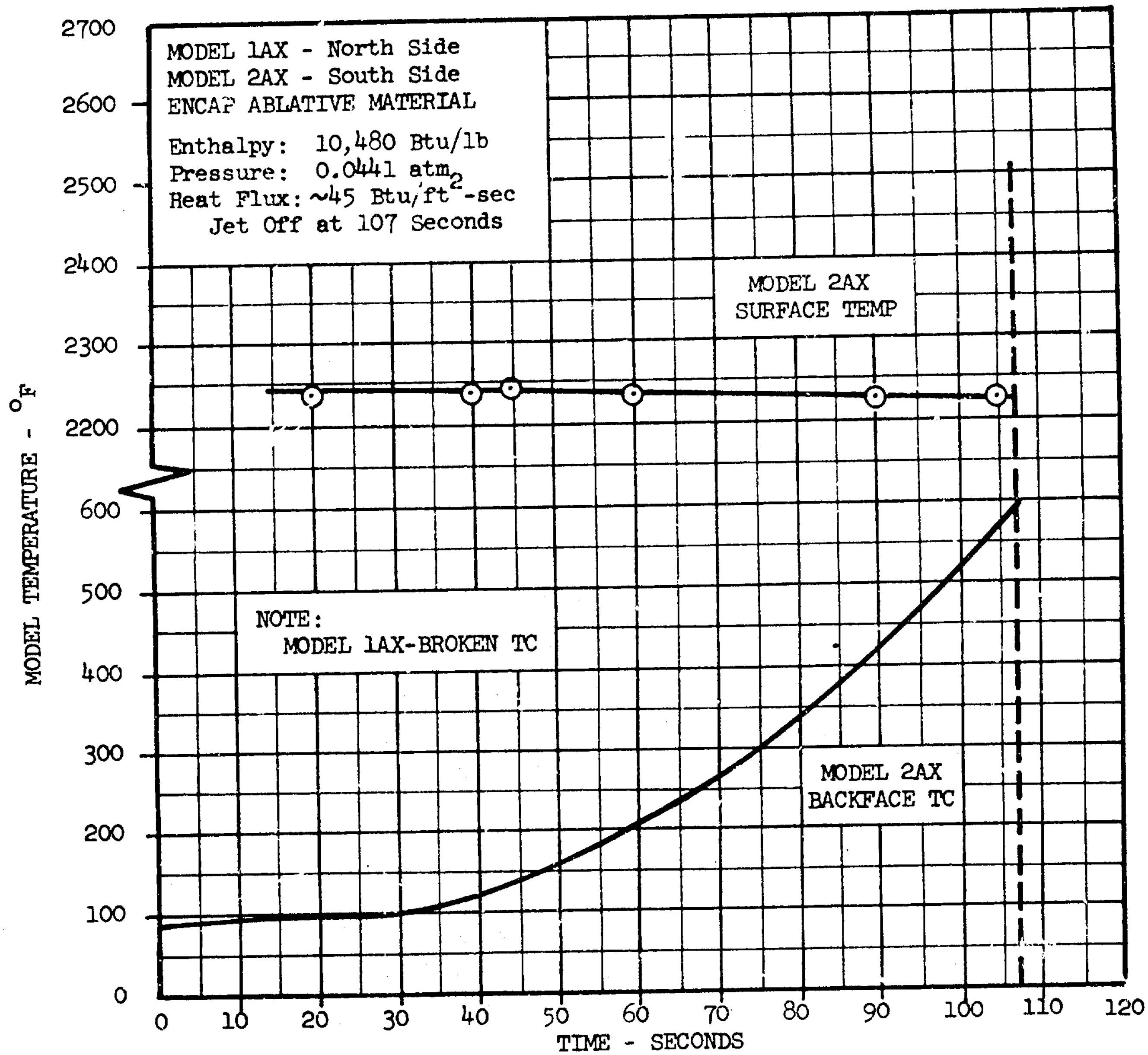

Figure 143 -- ENCAP Models 1AX and 2AX Temperature History

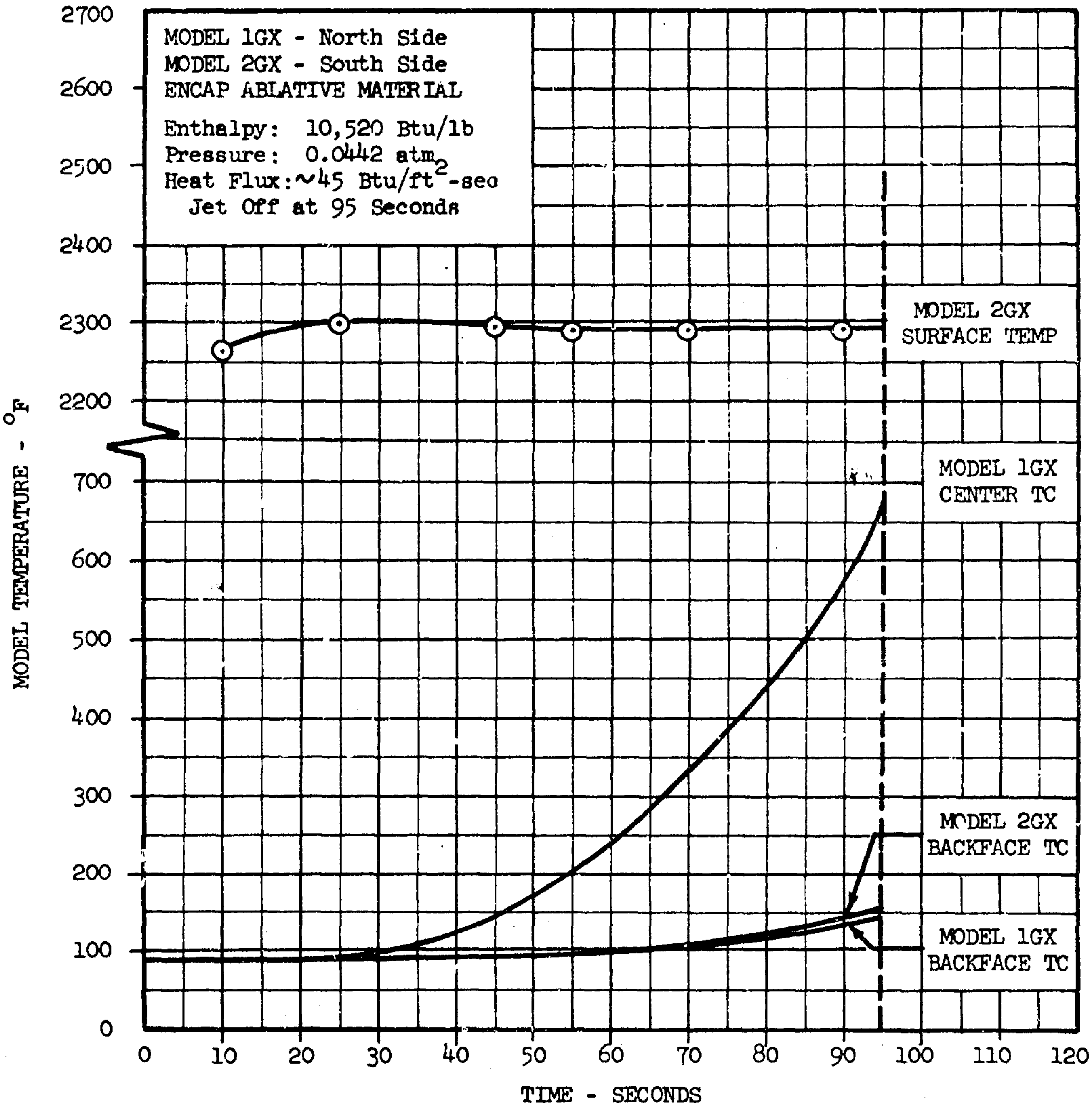

Figure 144 -- ENCAP Models 1GX and 2GX Temperature History

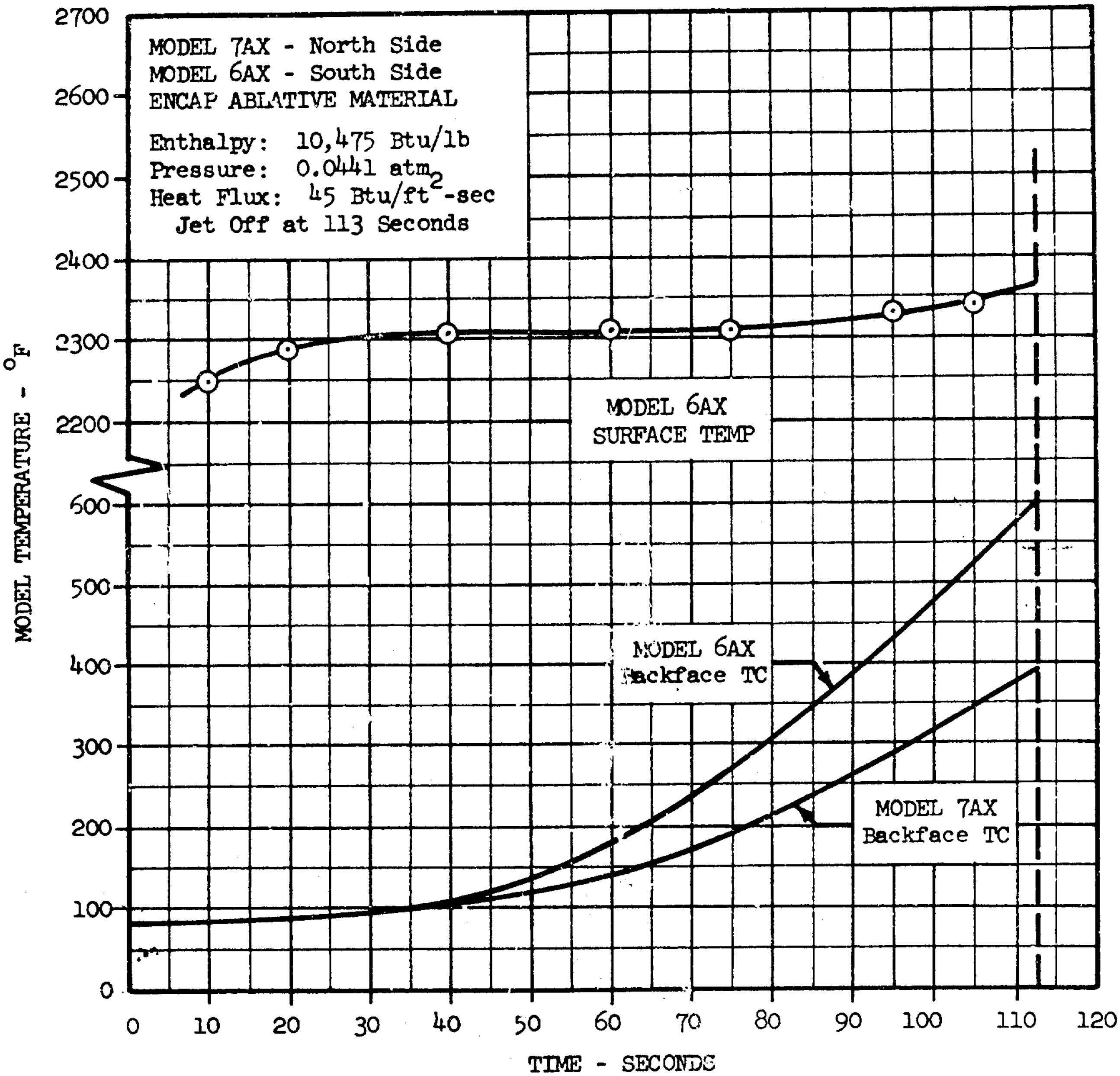

Figure 145 -- ENCAP Model 6AX and 7AX Temperature History

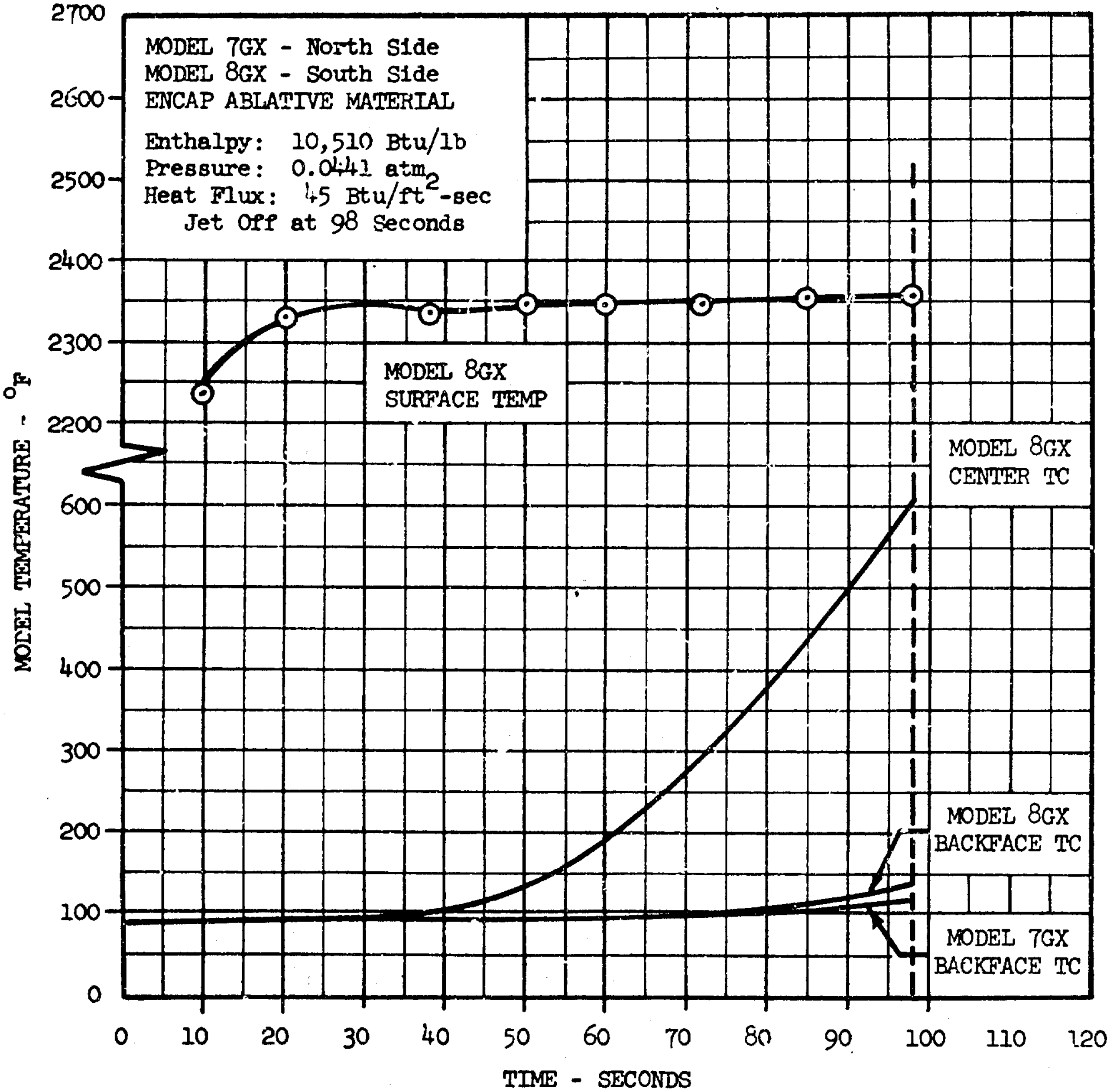

Figure 146 -- ENCAP Model 7GX and 8GX Temperature History

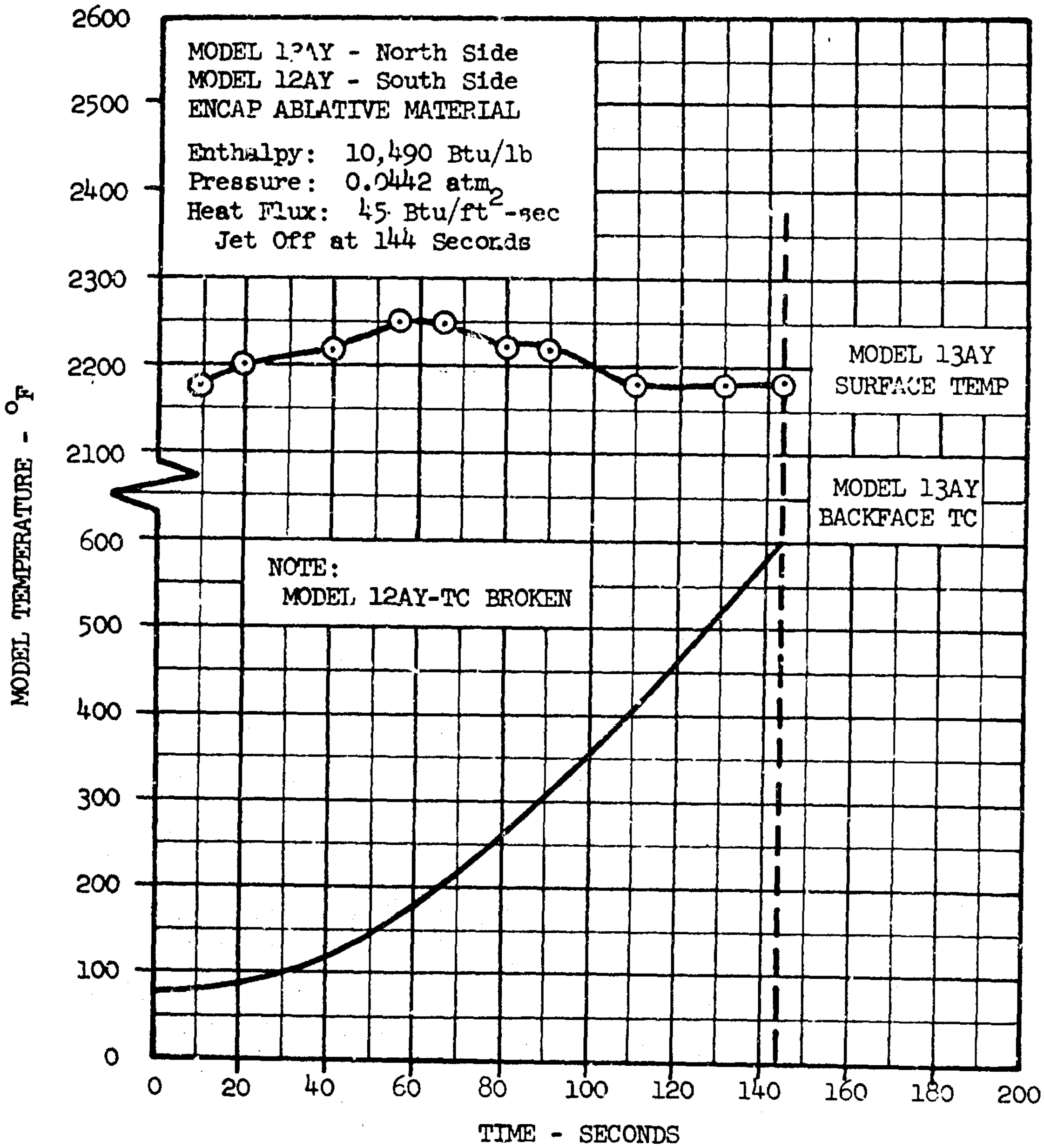

Figure 147 -- ENCAP Models 12AY and 13AY Temperature History

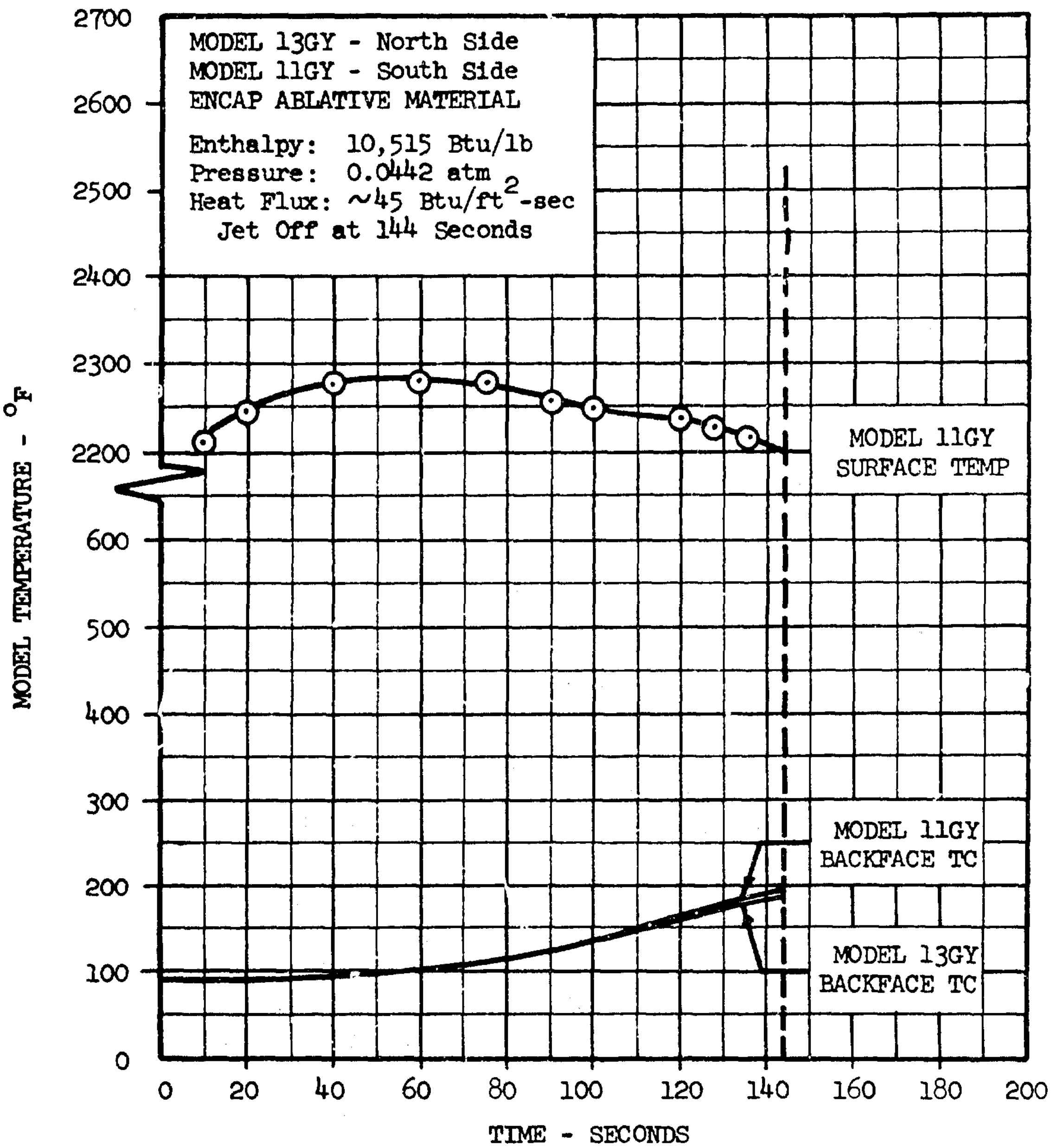

Figure 148 -- ENCAP Models 11GY and 13GY Temperature History

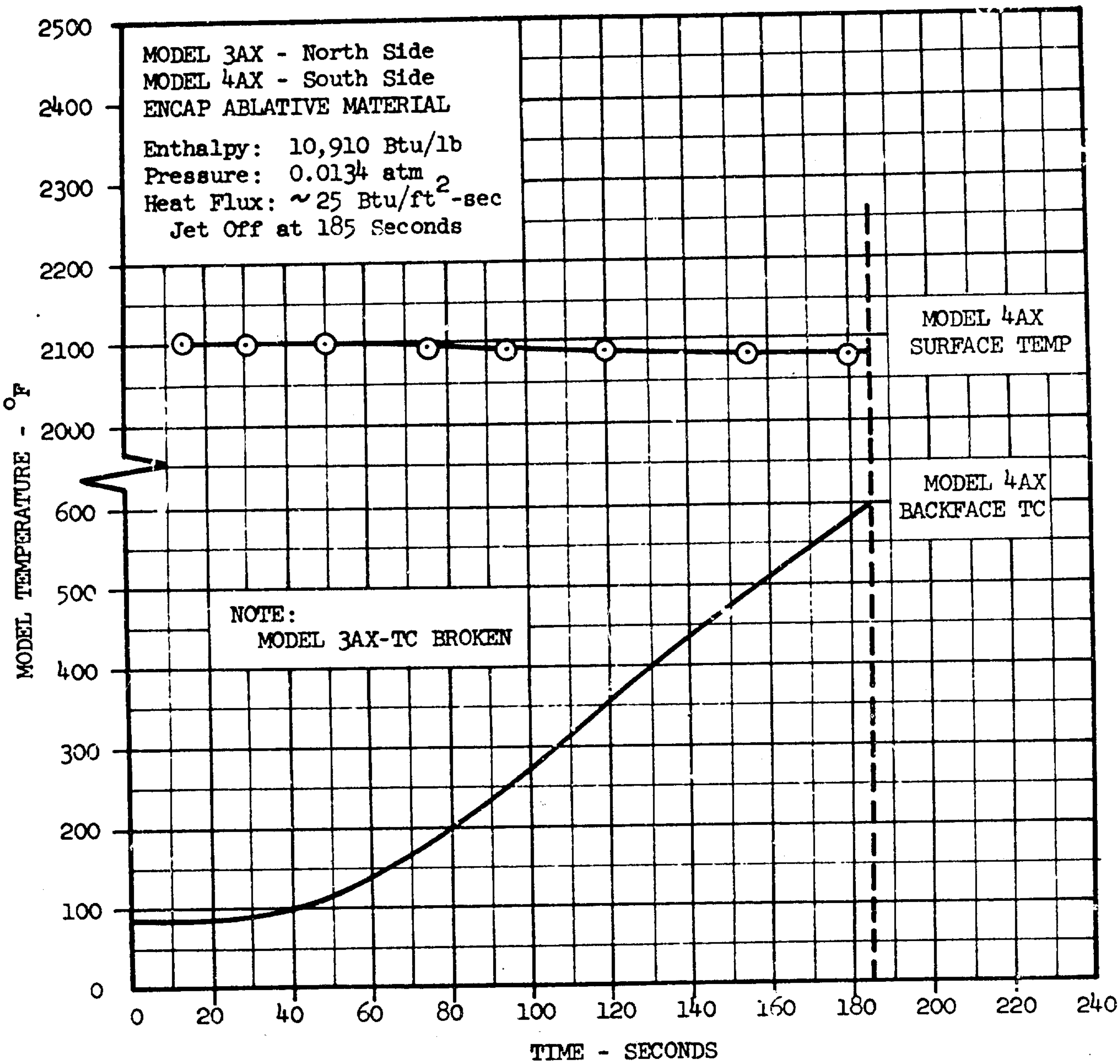

Figure 149 -- ENCAP Models 3AX and 4AX Temperature History

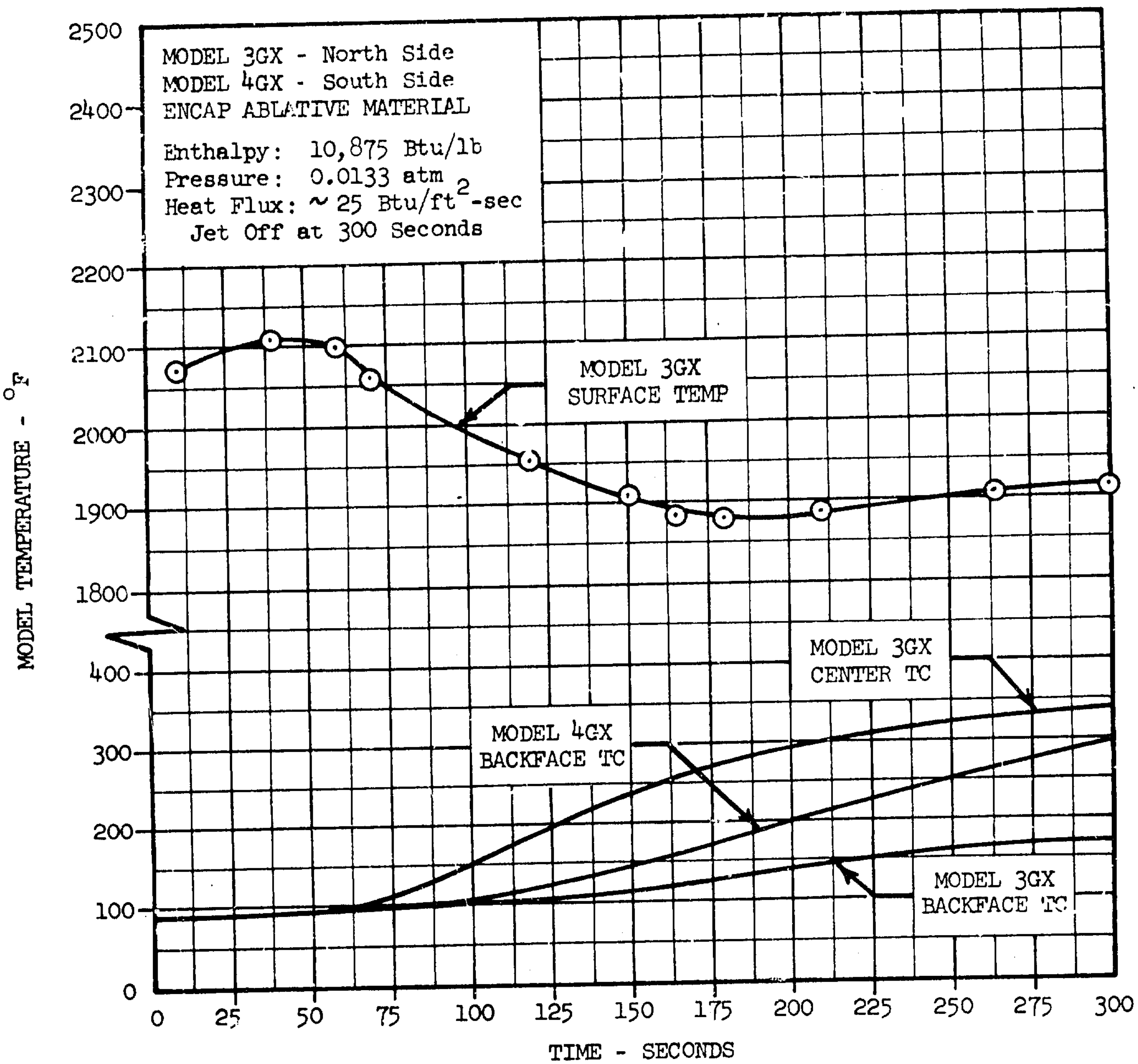

Figure 150 -- ENCAP Models 3GX and 4GX Temperature History

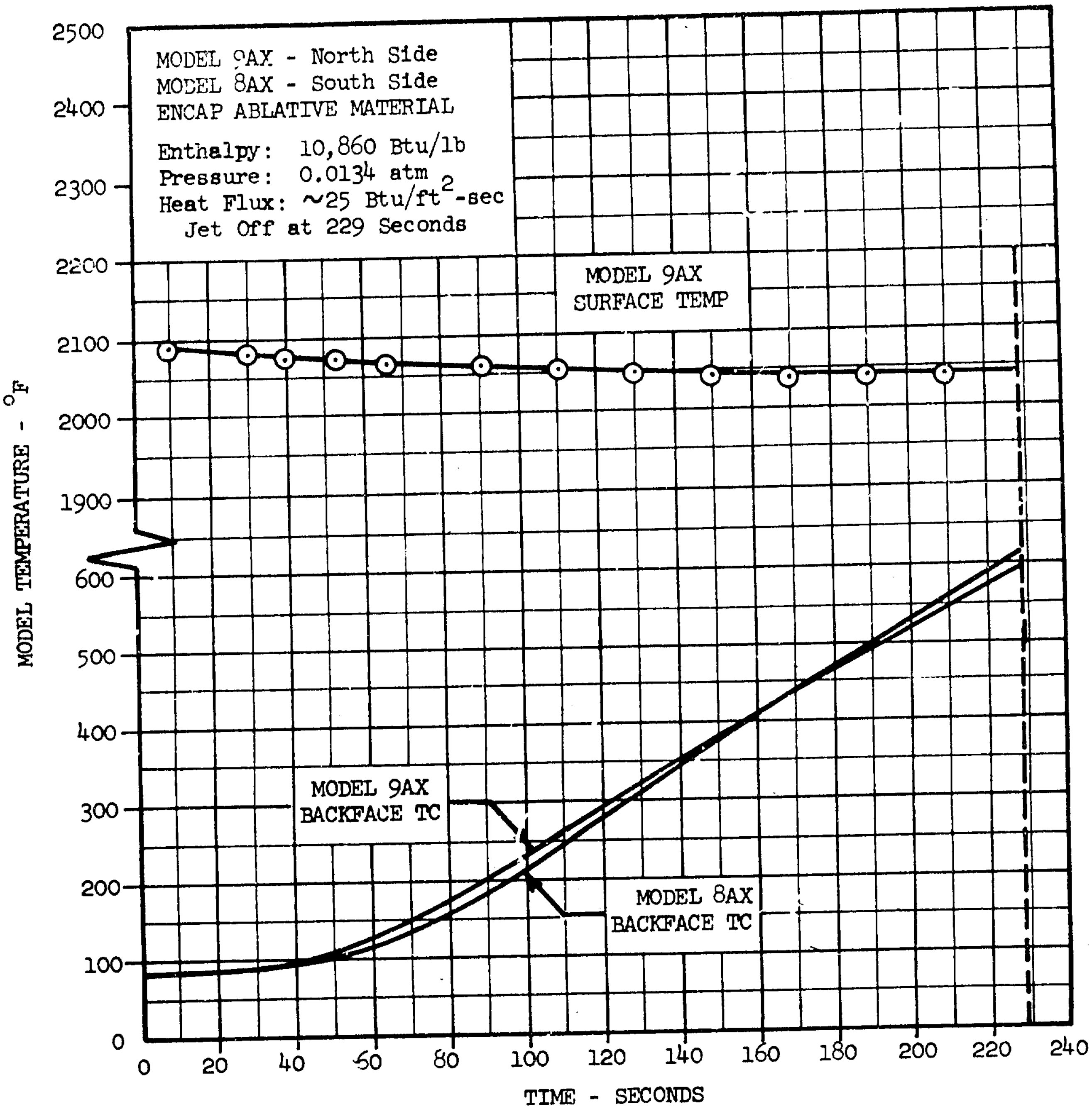

Figure 151 -- ENCAP Models 8AX and 9AX Temperature History

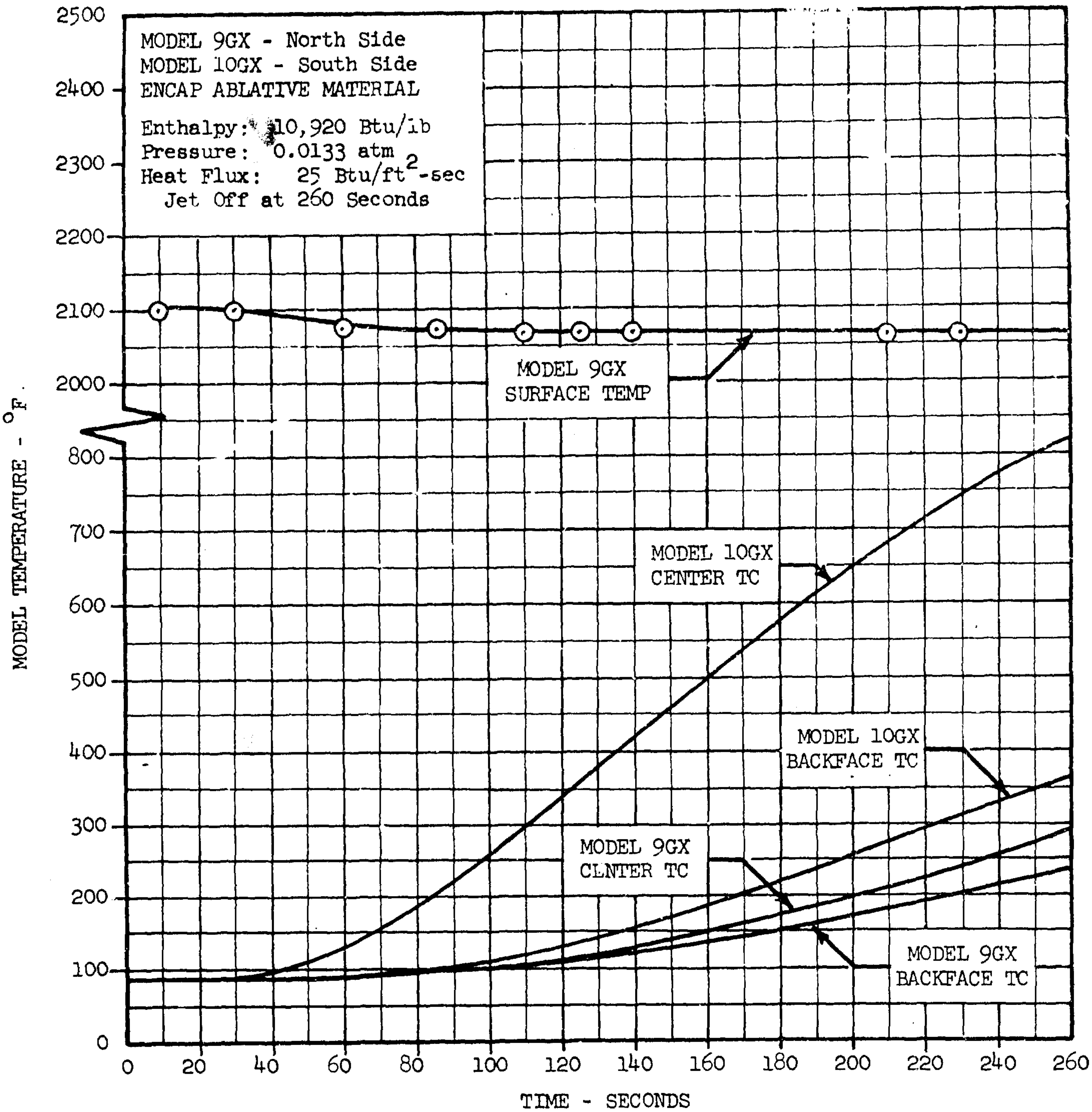

Figure 152 -- ENCAP Models 9GX and 10GX Temperature History

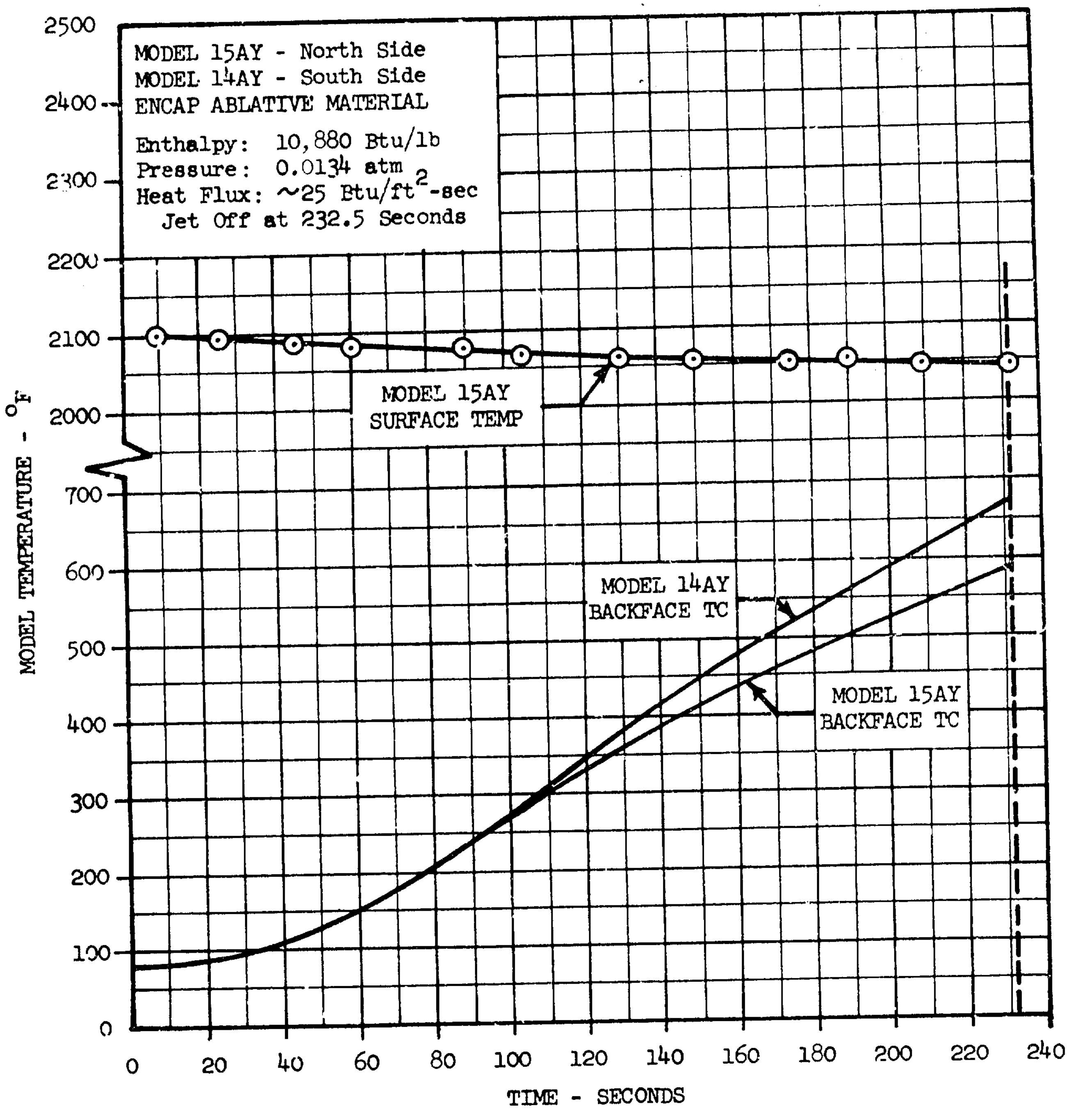

Figure 153 -- ENCAP Models 14AY and 15AY Temperature History

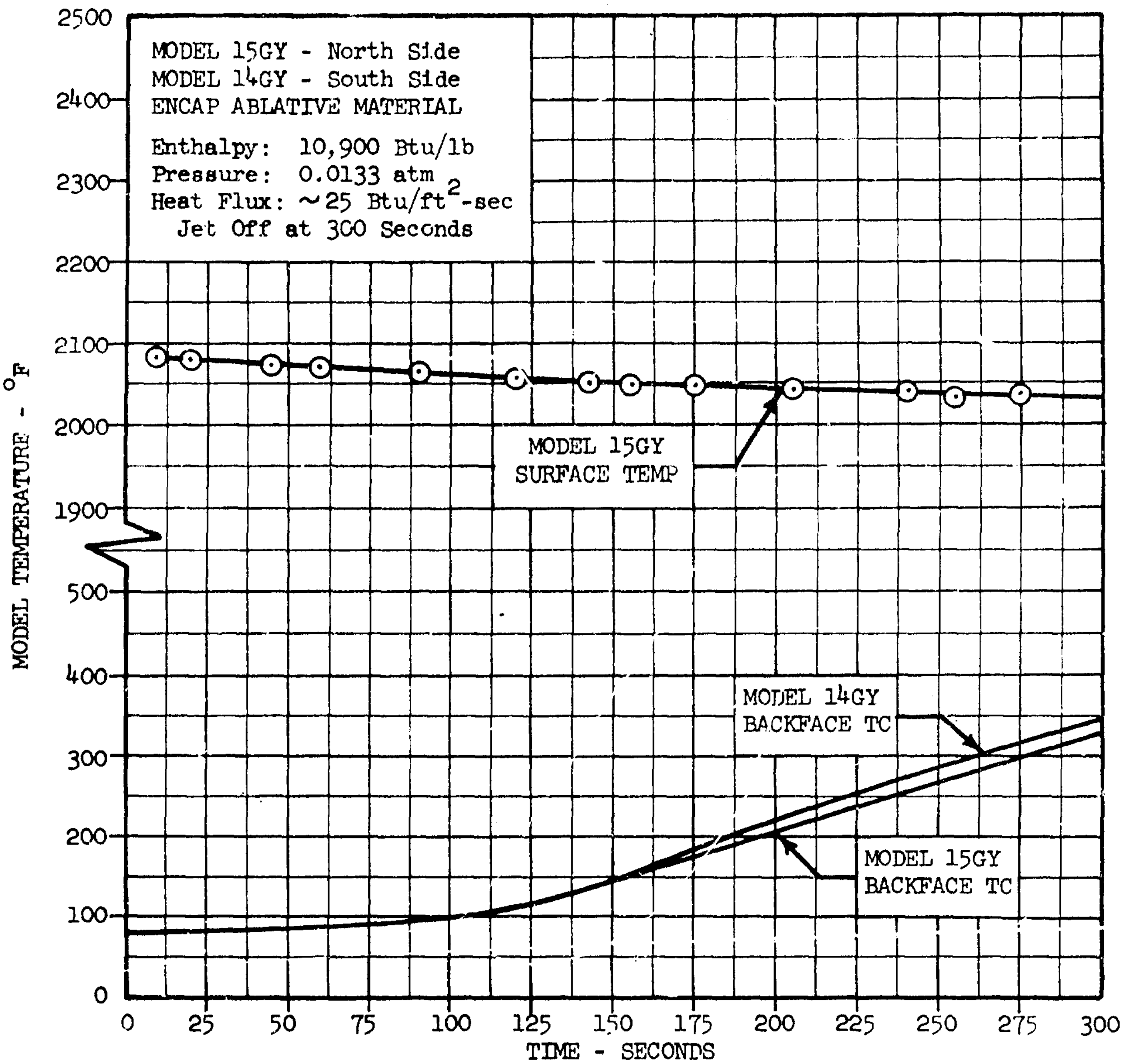

Figure 154 -- ENCAP Models 14GY and 15GY Temperature History

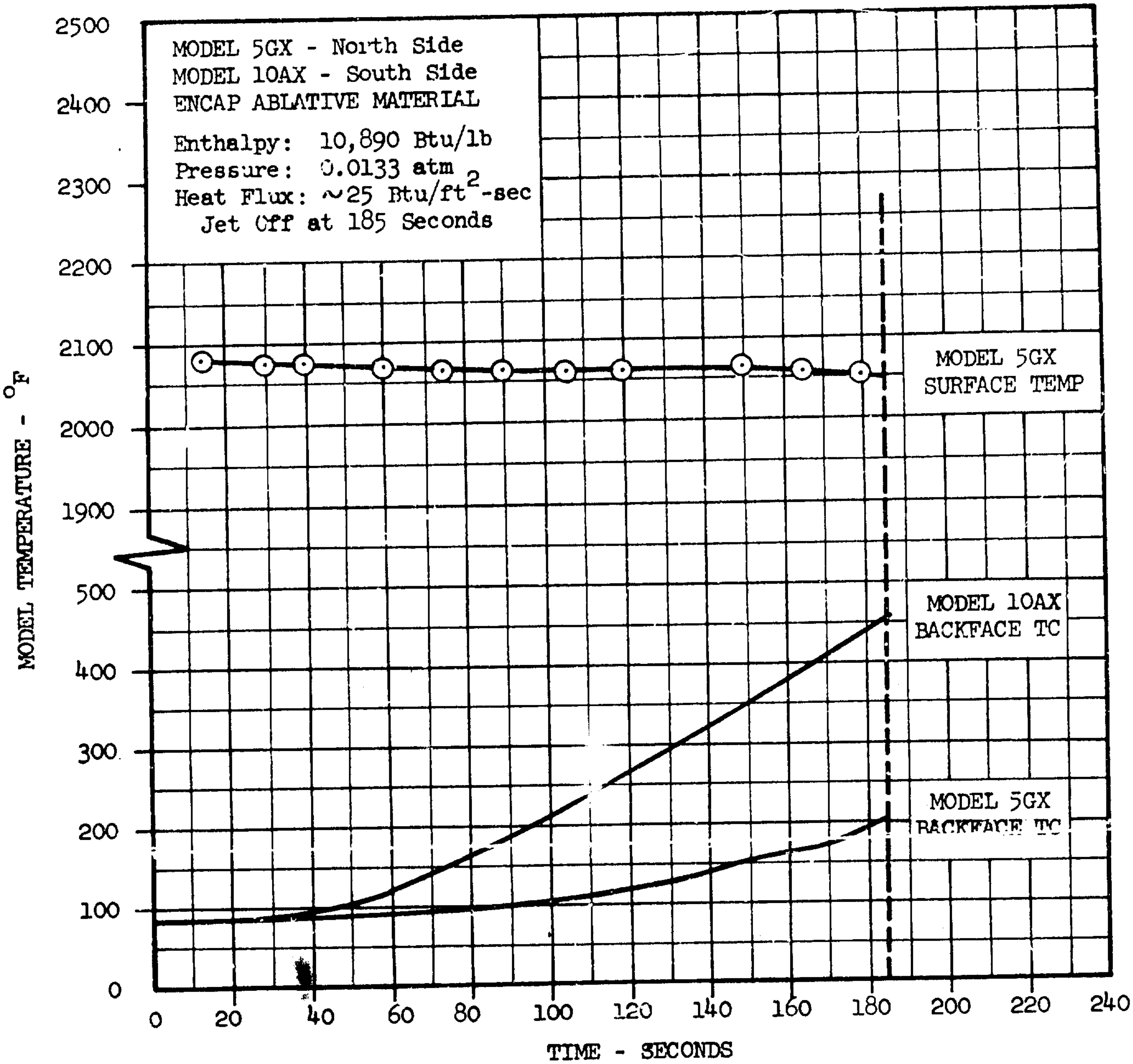

Figure 155 -- ENCAP Models 5GX and 10AX Temperature History

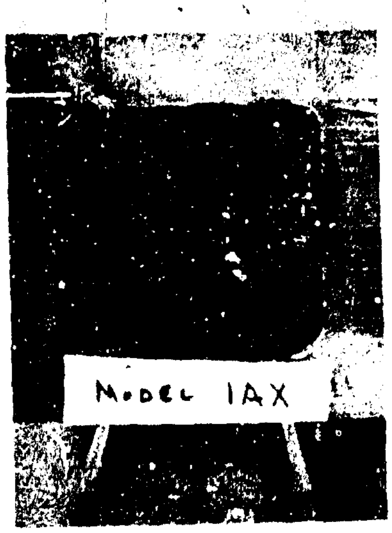

Model 1AX - Post-Exposure

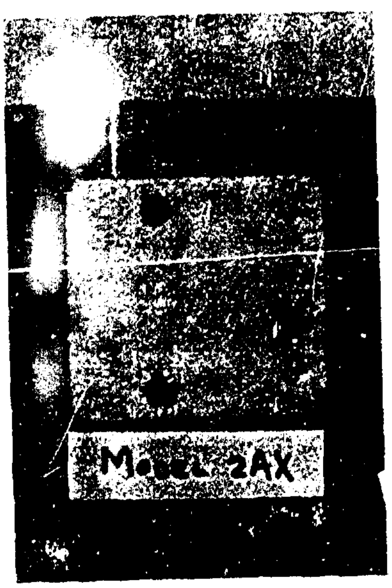

Model 2AX - Pre-Exposure

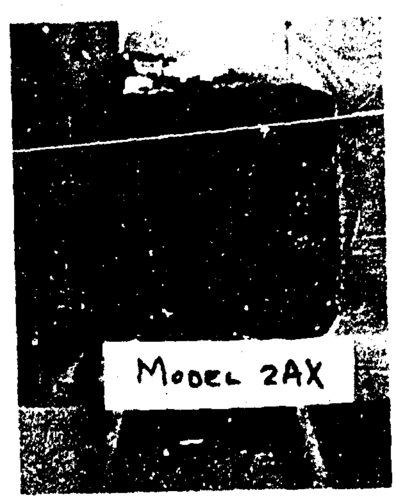

Model 2AX - Post-Exposure

Figure 156 -- Photographs of Lockheed ENCAP Materials
Models 1AX and 2AX

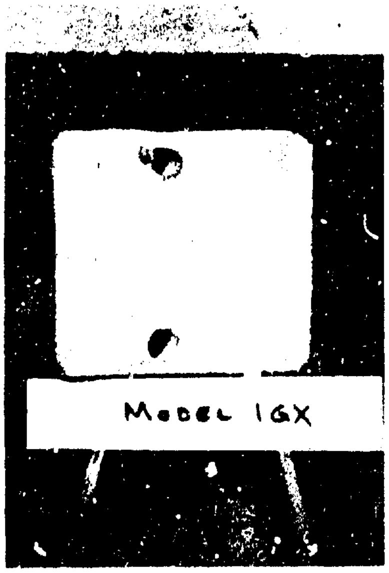

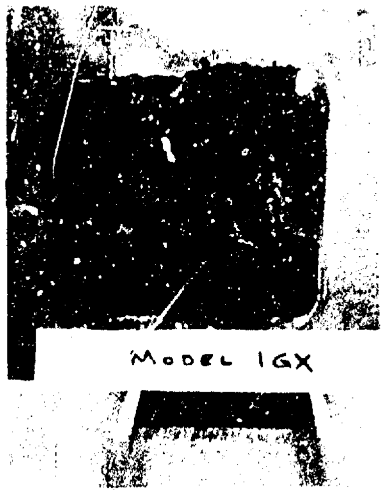

Model 1GX - Pre- and Post-Exposure

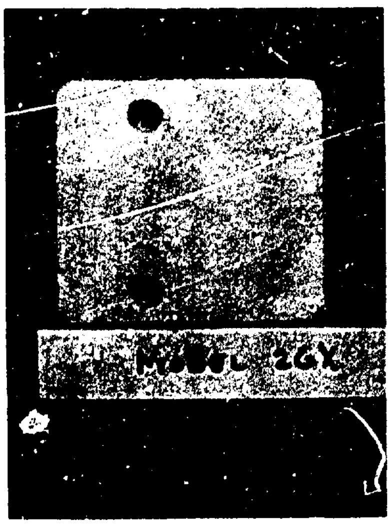

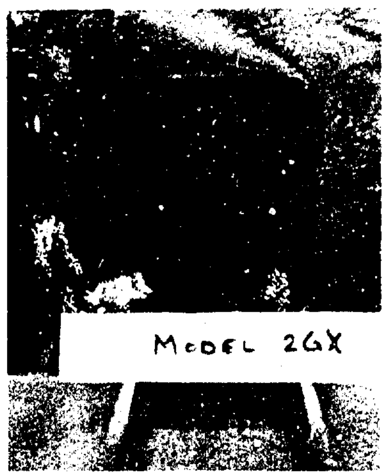

Model 2GX - Pre- and Post-Exposure

Figure 157 -- Photographs of Lockheed ENCAP Materials Models 1GX and 2GX

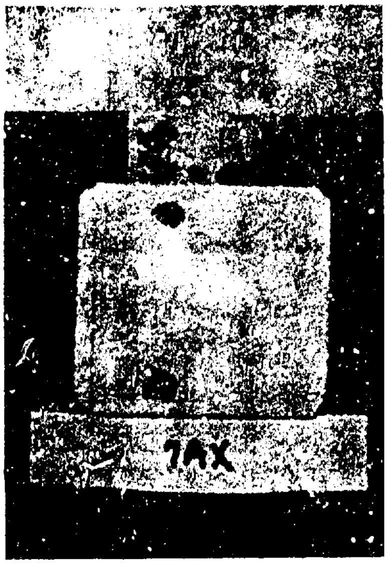

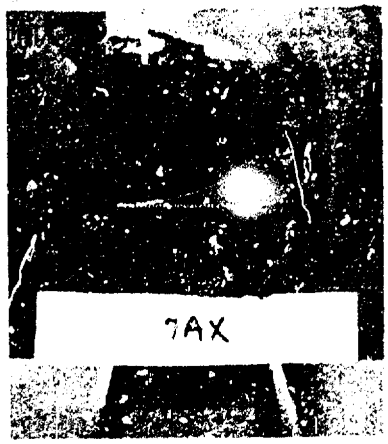

Model 7AX - Pre- and Post-Exposure

Model 6AX - Pre- and Post-Exposure

Figure 158 -- Photographs of Lockheed ENCAP Materials
Models 7AX and 6AX

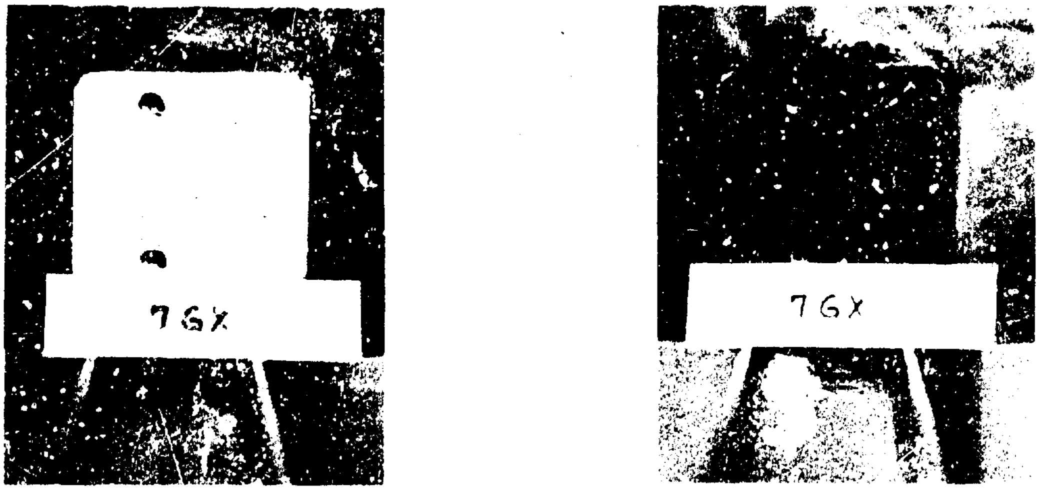

Model 7GX - Pre- and Post-Exposure

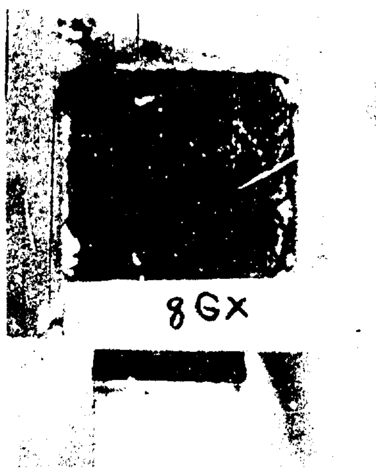

Model 8GX - Post-Exposure

Figure 159 -- Photographs of Lockheed ENCAP Materials
Models 7GX and 8GX

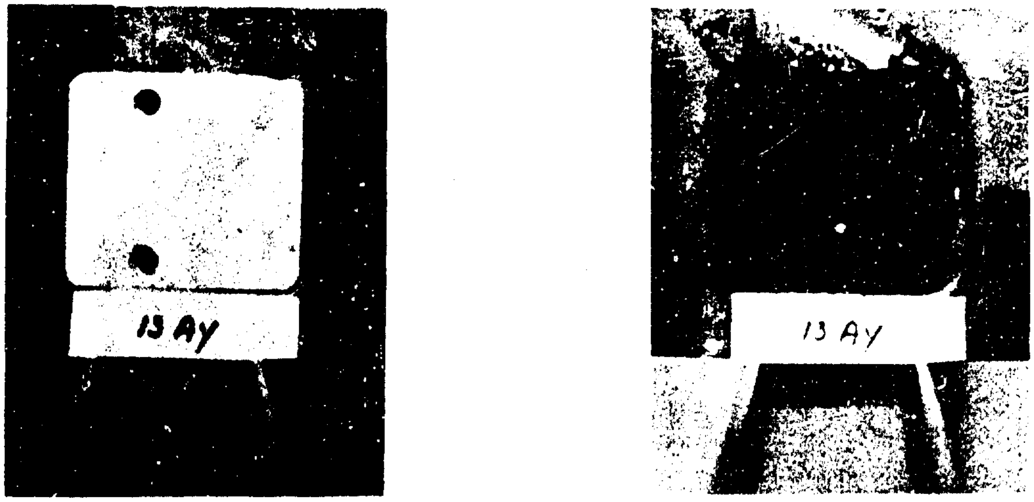

Model 13AY - Pre- and Post-Exposure

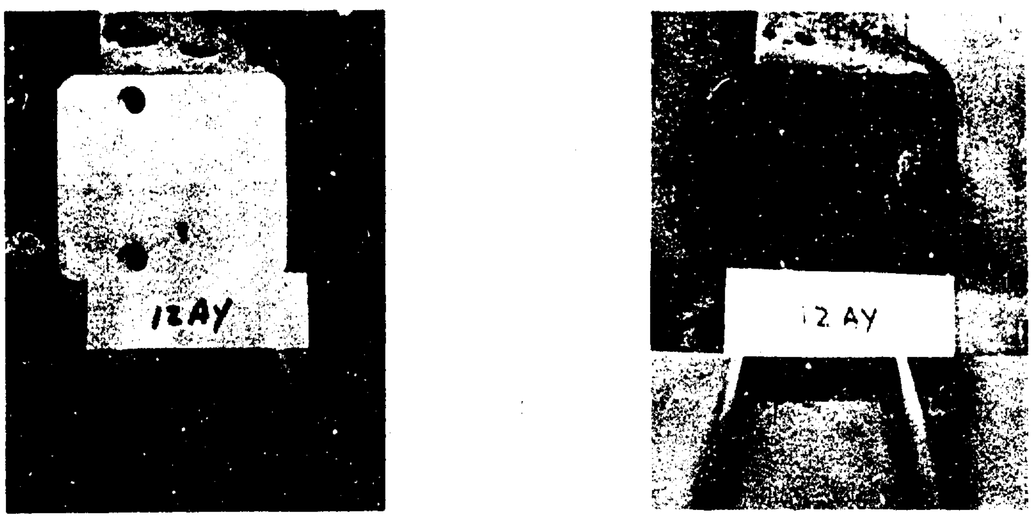

Model 12AY - Pre- and Post-Exposure

Figure 160 -- Photographs of Lockheed ENCAP Materials Models 13AY and 12AY

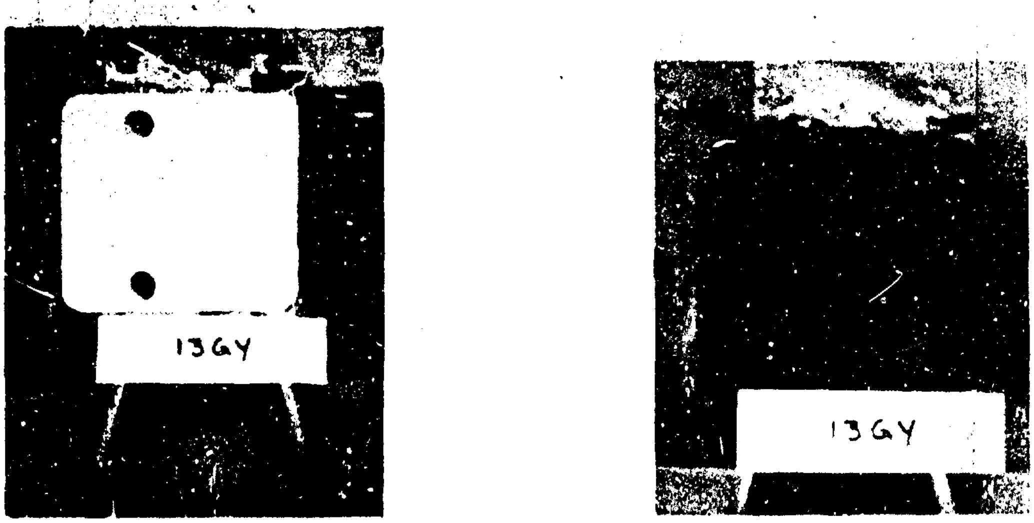

Model 13GY - Pre- and Post-Exposure

Model 11GY - Pre- and Post-Exposure

Figure 161 -- Photographs of Lockheed ENCAP Materials
Models 13GY and 11GY

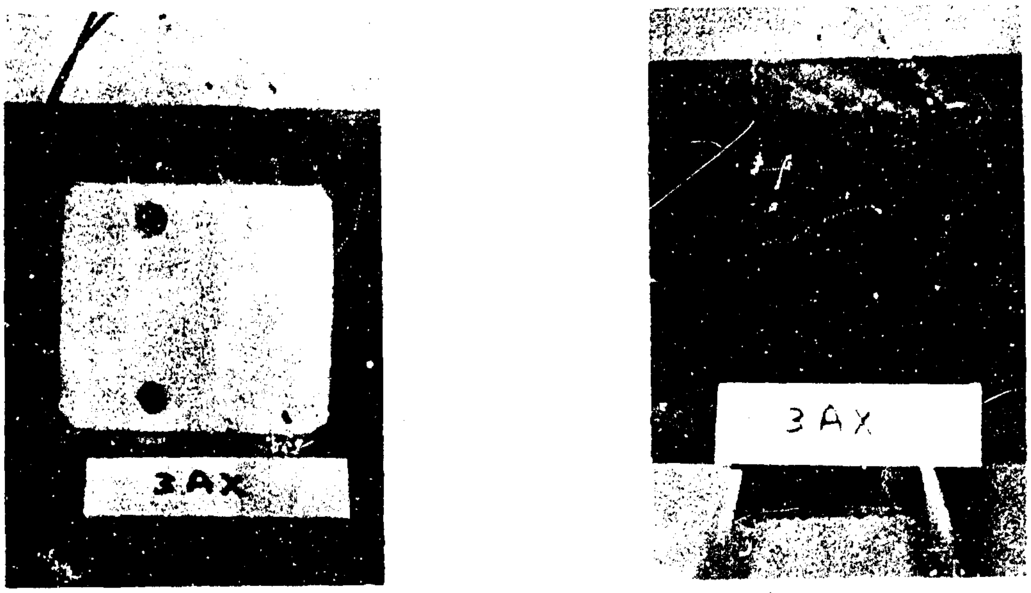

Model 3AX - Pre- and Post-Exposures

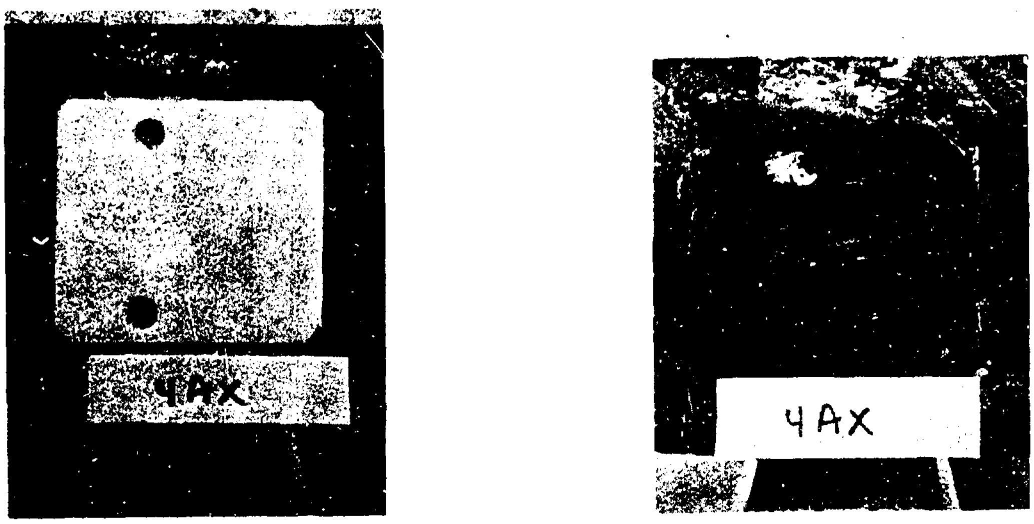

Model 4AX - Pre- and Post-Exposures

Figure 162 -- Photographs of Lockheed ENCAP Materials Models 3AX and 4AX

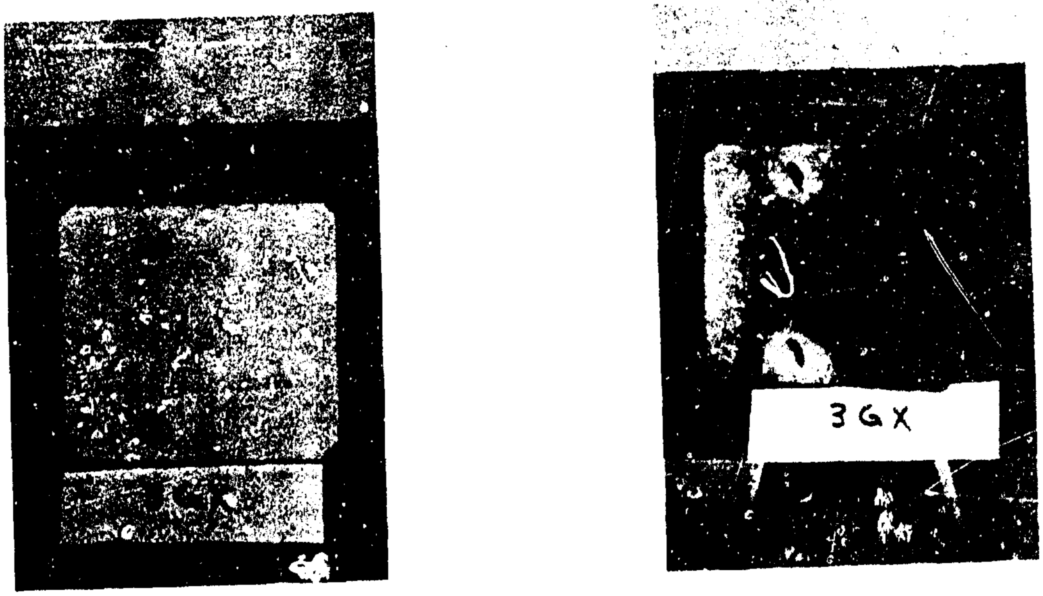

Model 3GX - Pre- and Post-Exposures

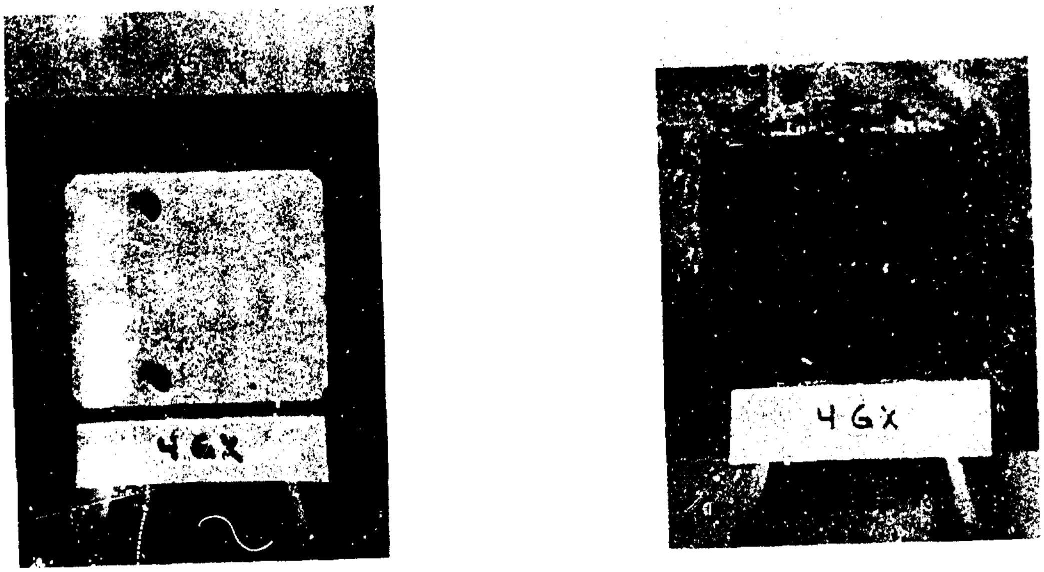

Model 4GX - Pre- and Post-Exposures

Figure 163 -- Photographs of Lockheed ENCAP Materials Models 3GX and 4GX

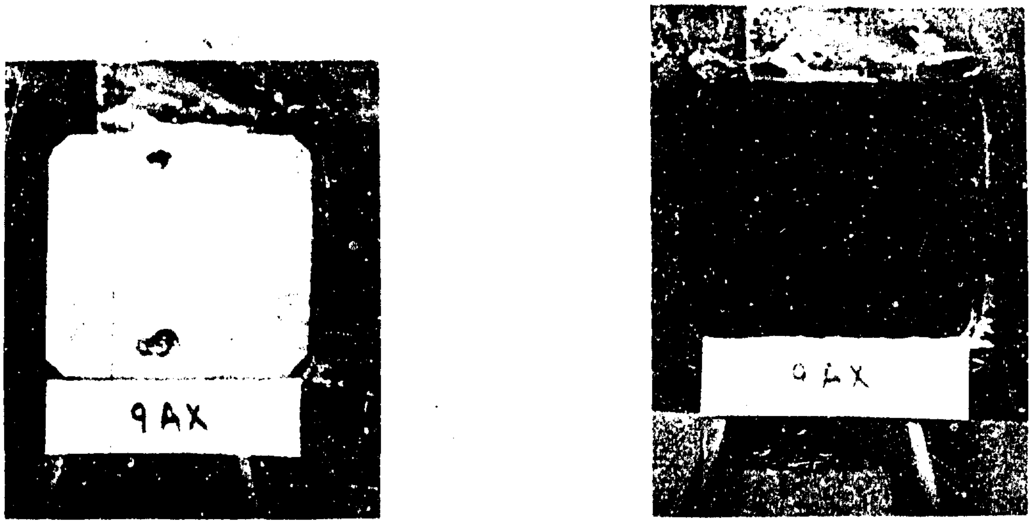

Model 9AX - Pre- and Post-Exposure

Model 8AX - Pre- and Post-Exposure

Figure 164 -- Photographs of Lockheed ENCAP Materials
Models 9AX and 8AX

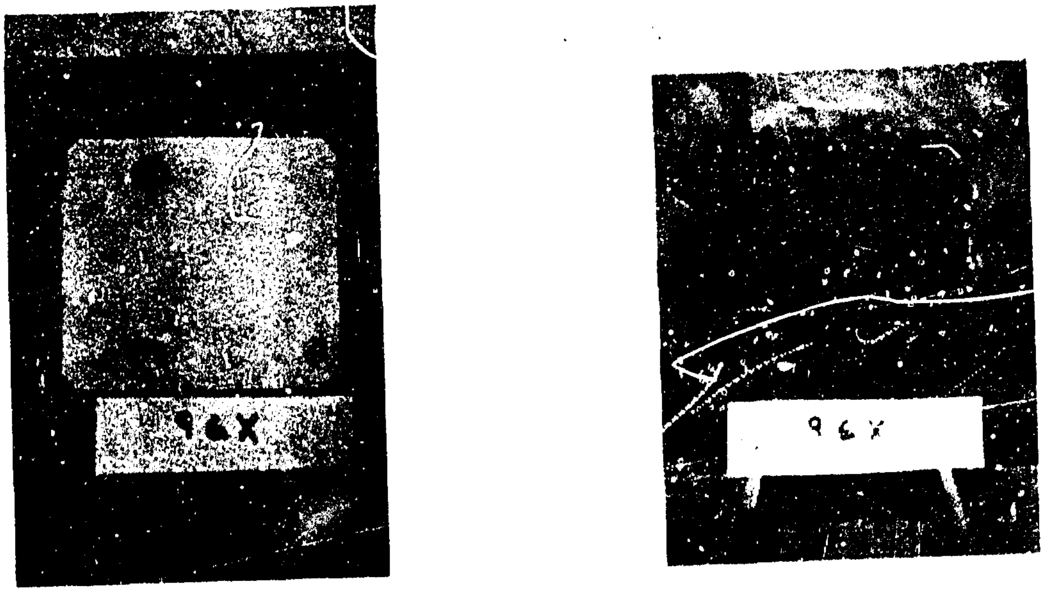

Model 9GX - Pre- and Post-Exposure

Model 10GX - Pre- and Post-Exposure

Figure 165 -- Photographs of Lockheed ENCAP Material
Models 9GX and 10GX

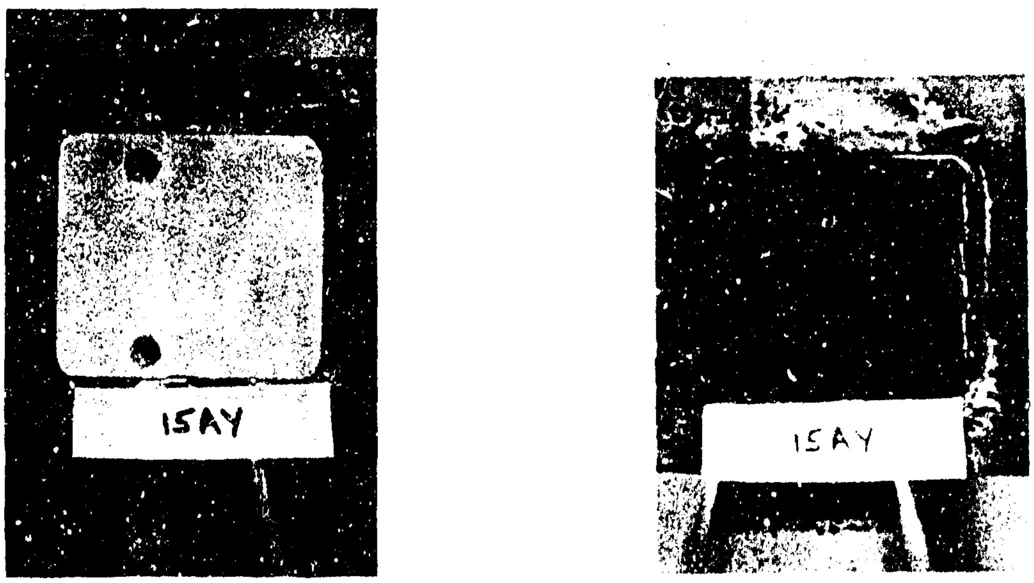

Model 15AY - Pre- and Post-Exposure

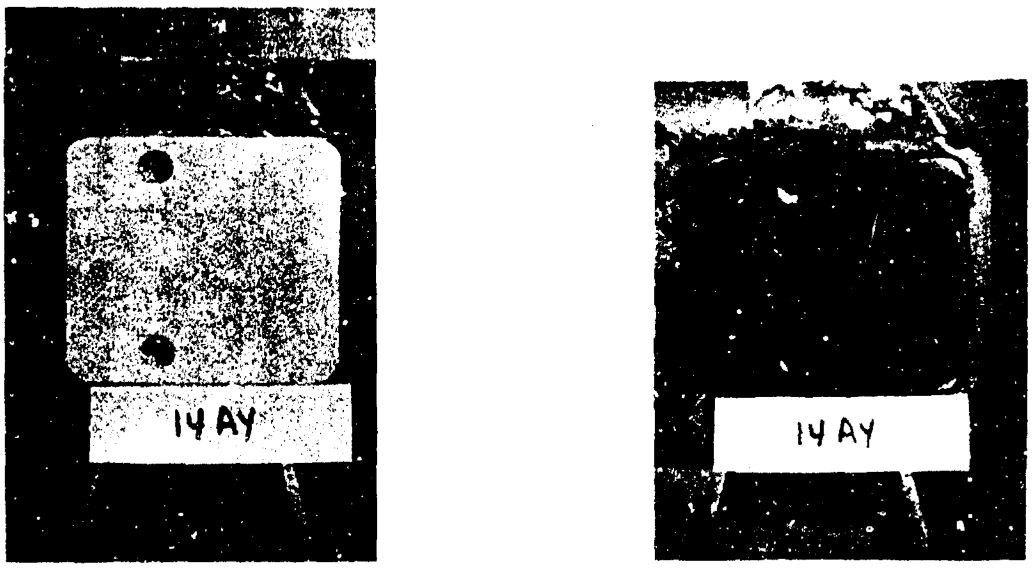

Model 14AY - Pre- and Post-Exposure

Figure 166 -- Photographs of Lockheed ENCAP Materials
Models 15AY and 14AY

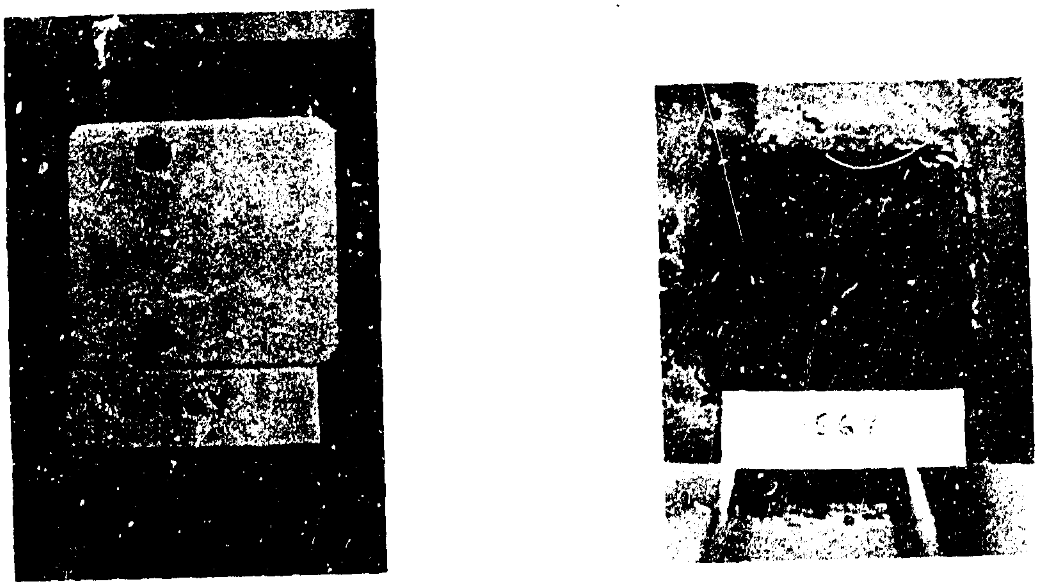

Model 15GY - Pre- and Post-Exposures

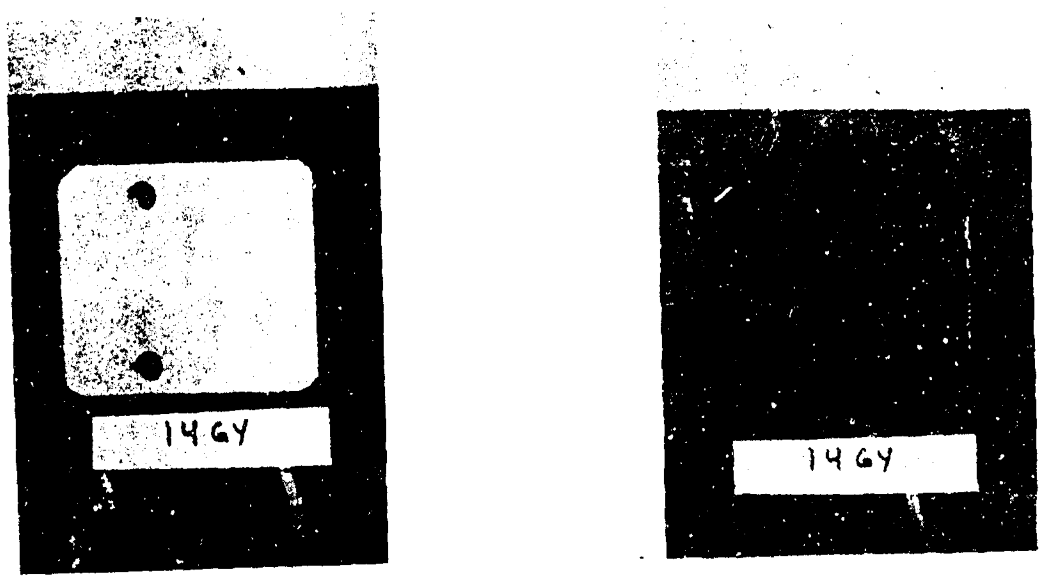

Model 14GY - Pre- and Post-Exposures

Figure 167 -- Photographs of Lockheed ENCAP Materials
Models 15GY and 14GY

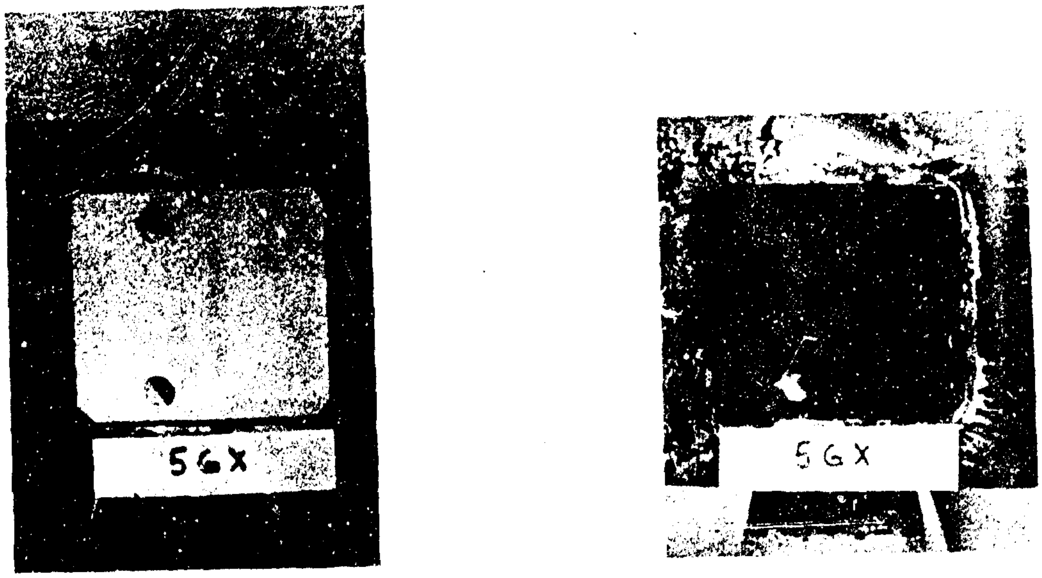

Model 5GX - Pre- and Post-Exposure

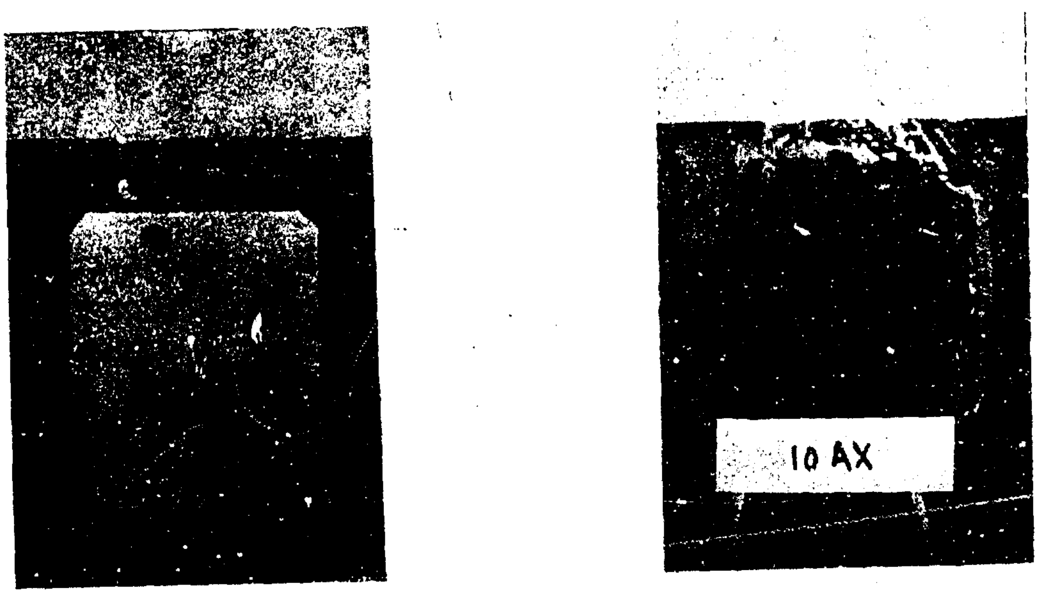

Model 10AX - Pre- and Post-Exposure

Figure 168 -- Photographs of Lockheed ENCAP Materials
Models 5GX and 10AX

PRECEDING PAGE BLANK- NOT FILMED.

5.0 COATED REFRACTORY METAL PROGRAM

The High Temperature Composites Laboratory, Chemical and Metallurgical Division of Sylvania Electric Products, Inc., under an Air Force Materials Laboratory contract, No. AF 33(615)-5086, has been concerned with the development of reproducible, reliable, refractory coatings for the protection of high-strength tantalum-base alloys from oxidation in severe aerospace or propulsion environments. These environments range in temperature from less than 2000°F to greater than 3500°F and in pressure from 0.01 torr to several atmospheres. In view of the applicability of our Air Force materials evaluation contract to their developmental efforts, a test program was jointly formulated for evaluating Sylvania's R512A and R512E coatings.

5.1 Objectives

Plasma-arc oxidation tests were performed on Sylvania's R512A (Si-20Cr-5Ti) and R512E (Si-20Cr-20Fe) coatings under low pressure and high temperature test conditions. The resistance of the coatings to oxidation, effect of alternate exposure to a high temperature oxidizing environment, and the failure temperature, were investigated for each of the two coatings. The test conditions utilized in the evaluation of the Sylvania R512 coatings established the behavior patterns under re-entry type environments, i.e., low pressure and relatively high temperature air flow.

5.2 Description of Test Program

Ten models, constructed of columbium alloy 'leading edge' samples coated with fused silicide coatings by Sylvania Electric Products, Inc., were evaluated in the low pressure/high enthalpy plasma arc facility. A Mach 3, three-inch exit diameter contoured nozzle was used to provide supersonic flow, simulating an air environment. The coatings evaluated were: R512A comprised of Si-20Cr-5Ti; R512E comprised of Si-20Cr-20Fe. The coatings were applied to the columbium alloy sheets by Sylvania using a spraying process; the leading edge models were exposed to the high-temperature plasma stream with the external curved surface exposed to the hot side.

Calibration data for each of the ten model tests is presented in Table 17; model test data including surface temperature measurements and observations of the coating behavior, are presented in Table 18. Coating R512E was the first evaluated; the initial two models tested (Models 3-3 and 3-4) were exposed to a steadily-increasing temperature until melting of the coating was observed. For both models, the apparent melting temperature was 3210°F. The third model (Model 3-5 was then exposed to 2600°F for four 15-minute cycles; the fourth model (Model 3-6) was exposed to 2700°F for four 15-minute cycles. The fifth model was subjected to 2800°F, but withstood only three complete 15-minute cycles; melting was first observed in the fourth cycle at 540 seconds (refer to Table 18 for exact details). During exposure to the heated environment, the model was in an evacuated environment, between cycles the model was exposed to standard temperature and pressure conditions (80°F and 1 atmosphere). Surface temperature histories obtained with a Leeds and Northrup optical brightness pyrometer for the R512A coatings are plotted in Figures 169 through 173.

TABLE 17

CALIBRATION DATA

Sylvania Model Tests

Model No.	Material	Gas Enthalpy (Btu/lb)	Model Stag. Pressure (atm)	Calculated Model Stag. Heat Flux (Btu/ft^2-sec)	Nozzle Stag. Pressure (atm)	Nozzle Static Pressure (atm)	Gas Flow Rate (lb/sec)
3-3	R512E	8,965	0.01050	70.8	0.0521	0.000908	0.00198
3-4	R512E	9,025	0.01050	71.2	0.0520	0.000910	0.00198
3-5	R512E	6,485	0.00763	34.9	0.0381	0.000741	0.00198
3-6	R512E	7,510	0.00800	41.2	0.0402	0.000770	0.00198
3-7	R512E	8,155	0.00920	46.1	0.0458	0.000885	0.00198
3-8	R512A	8,720	0.01015	64.5	0.0508	0.000978	0.00198
3-9	R512A	6,685	0.00760	35.1	0.0381	0.000731	0.00198
3-10	R512A	7,565	0.00792	40.9	0.0396	0.000761	0.00198
3-11	R512A	8,285	0.00920	45.8	0.0461	0.000885	0.00198
3-12	R512A	8,655	0.01010	58.7	0.0505	0.000971	0.00198

TABLE 18

MODEL TEST DATA

Sylvania Model Tests

Model No.	Material	Surface Temperature (^{o}F)	Comments
3-3	R512E	Increased to 3210	Melting occurred when surface temperature reached 3210^{o}F
3-4	R512E	Increased to 3210	Melting occurred when surface temperature reached 3210^{o}F
3-5	R512E	2600	Model withstood four 15-minute cycles at 2600^{o}F
3-6	R512E	2700	Model withstood four 15-minute cycles at 2700^{o}F
3-7	R512E	2800	Model withstood three 15-minute cycles; melting at 540 secs in 4th Cy.
3-8	R512A	Increased to 3100	Melting occurred when surface temperature reached 3100^{o}F
3-9	R512A	2600	Model withstood four 15-minute cycles at 2600^{o}F
3-10	R512A	2700	Model withstood four 15-minute cycles at 2700^{o}F
3-11	R512A	2800	Model withstood two 15-minute cycles; melting at 840 secs in 3rd Cycle
3-12	R512A	3000	Immediate melting at 3000^{o}F

The R512A coated models were subjected to the same ordeal of testing as the R512E models. The initial model (Model 3-8) was exposed to a steadily increasing temperature until melting occurred, which appeared to be at 3100°F. The second and third models were tested at 2600 and 2700°F, respectively, for four 15-minute cycles each, as in the R512E model tests. The fourth model, Model 3-11, was subjected to 2800°F; however, melting of the coating occurred during the third cycle, as compared to failure in the fourth cycle for the R512E coating. The fifth and final model was to be evaluated at 3000°F surface temperature; however, immediate failure (apparent melting) occurred as soon as the 3000°F level was attained. Several attempts were made to slowly attain 3000°F, but each time the coating appeared to melt and the surface temperature would rapidly increase, at which time the plasma arc power would be decreased to lower the temperature below the melting point. Surface temperature histories for the R512A coatings are presented in Figures 174 through 178.

Post-test metallographic examination of the coatings has been performed by Sylvania personnel and their findings will be reported under their Air Force contracts. Gross physical appearance of each of the tested models is visible in the photographs in Figures 179 through 185, showing pre- and post-exposure views. The gross differences in surface texture of adjacent striped areas of the R512A coated specimens (visible in the pre-exposure photographs) is apparently related to some subtle nonuniformities in the chromium -752 alloy.

Visual comparisons of the two coatings, displayed in Figure 179, would lead one to believe that the R512A coating was superior to the R512E. However, until the post-test examinations are completed, this can be considered as an unqualified opinion only, based only on melting characteristics of the two coatings.

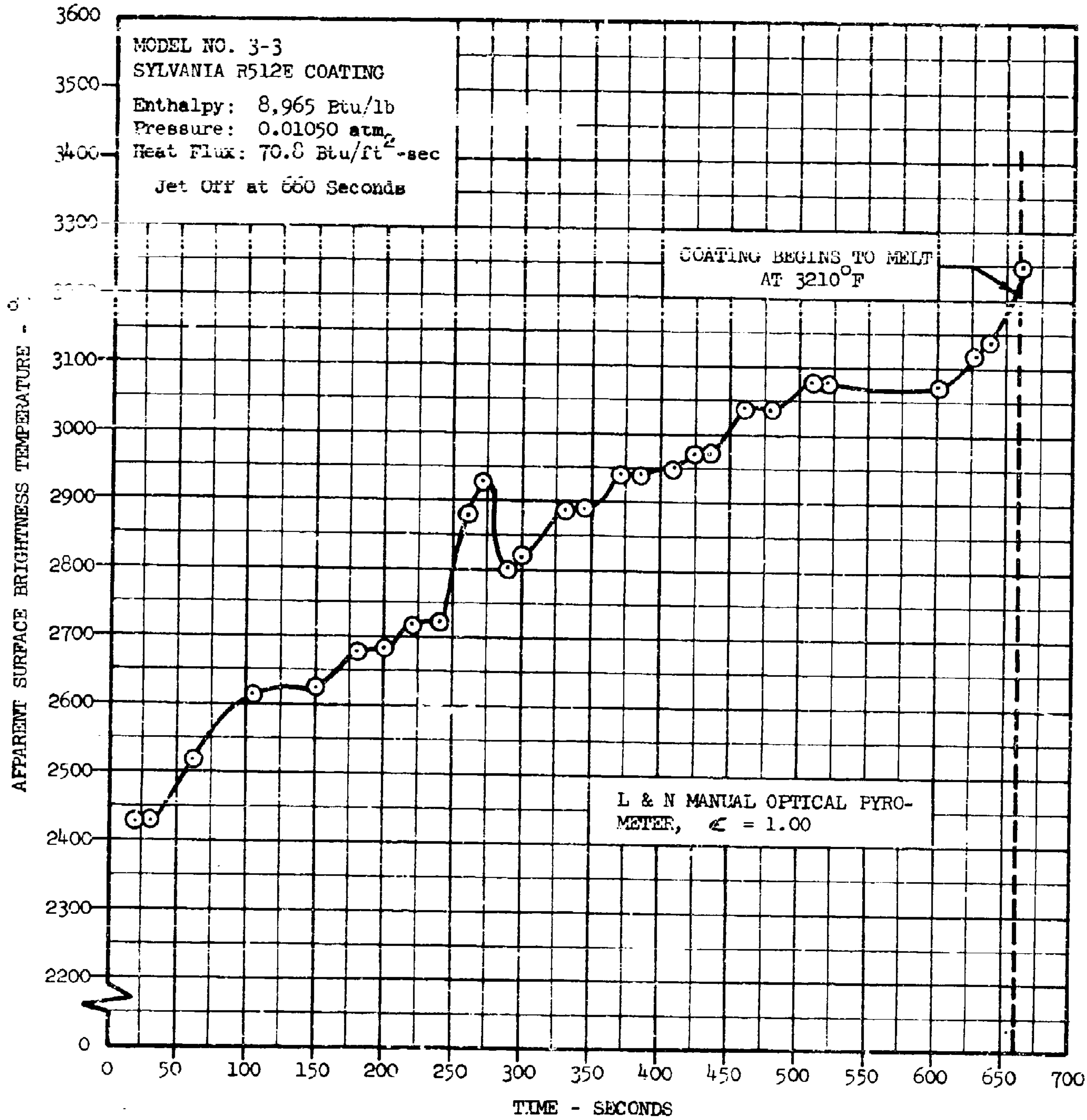

Figure 169 -- Sylvania R512E Coating - Model 3-3 - Surface Temperature History

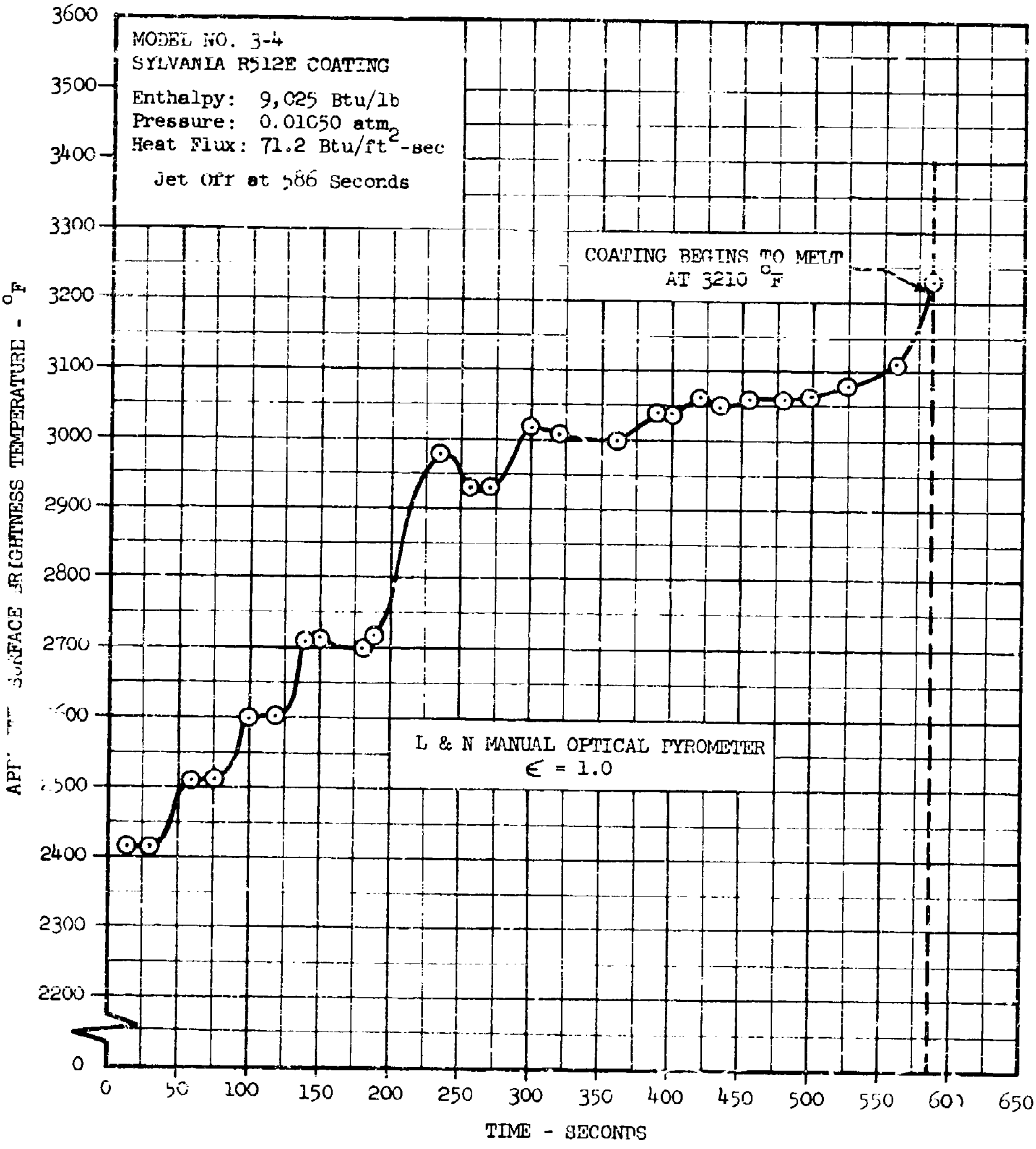

Figure 170 -- Sylvania R512E Coating - Model 3-4 Surface Temp. History

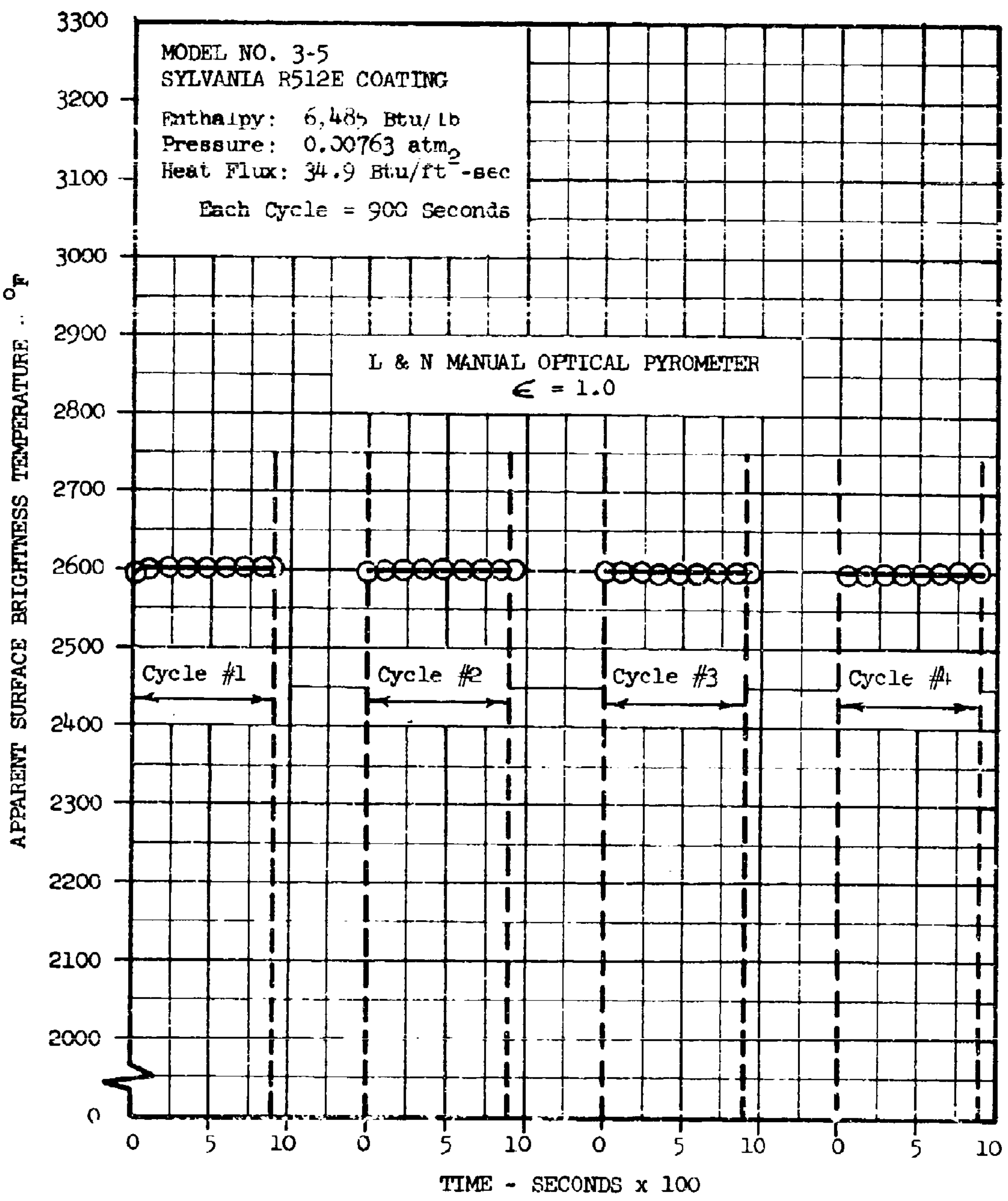

Figure 171 -- Sylvania R512E Coating - Model 3-5 Surface Temp. History

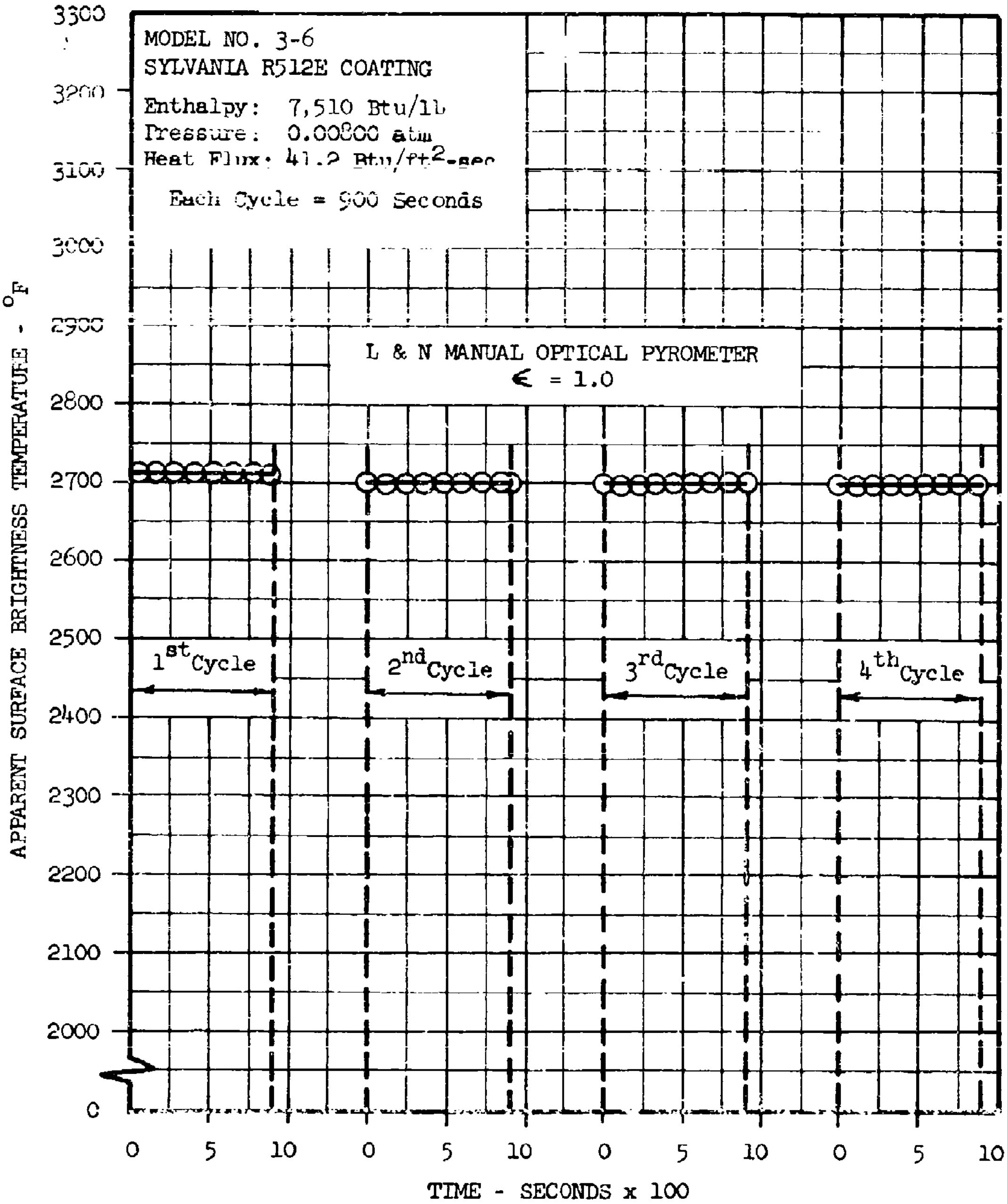

Figure 172 -- Sylvania R512E Coating - Model 3-6 Surface Temp. History

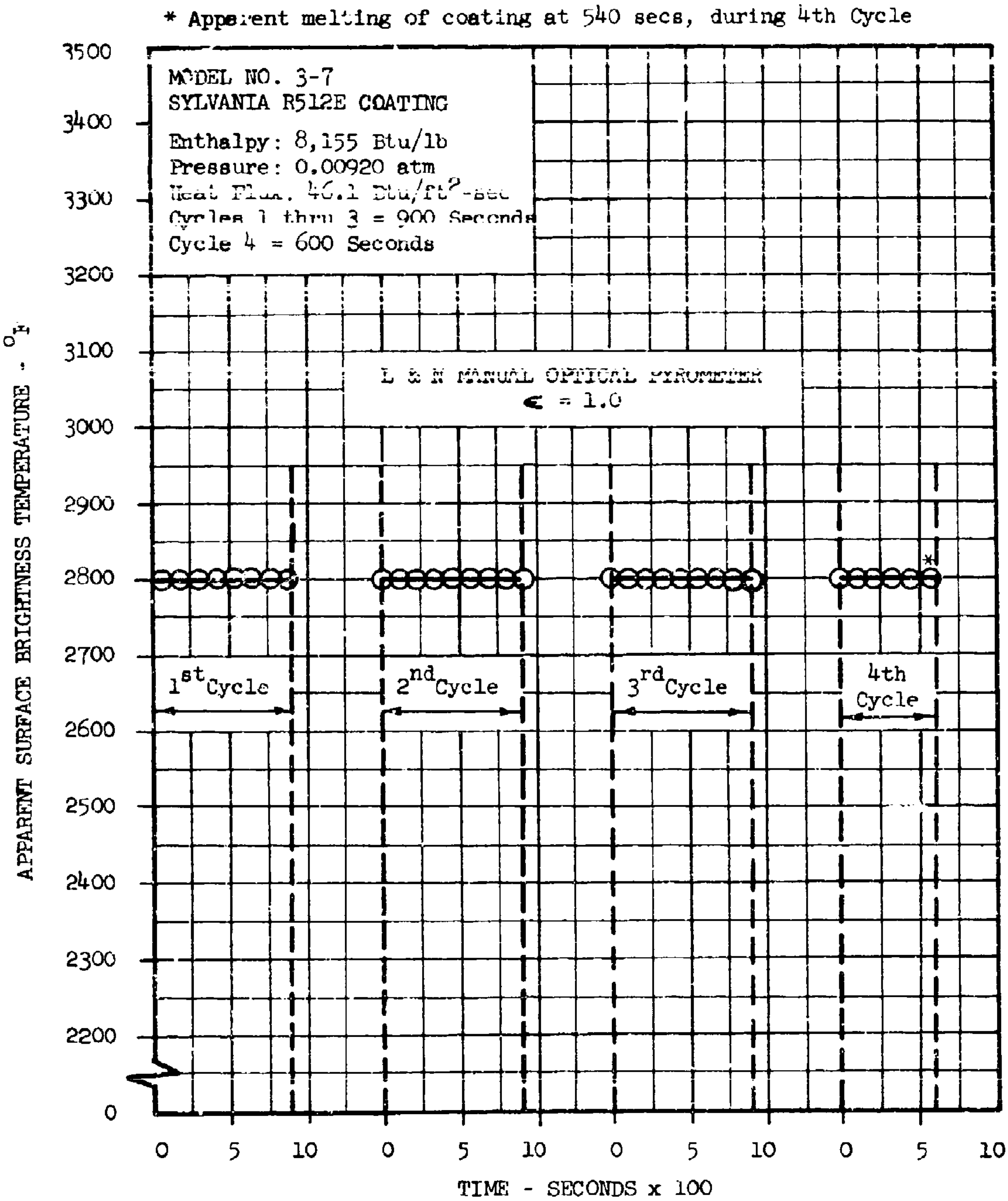

Figure 173 -- Sylvania R512E Coating - Model 3-7 Surface Temp. History

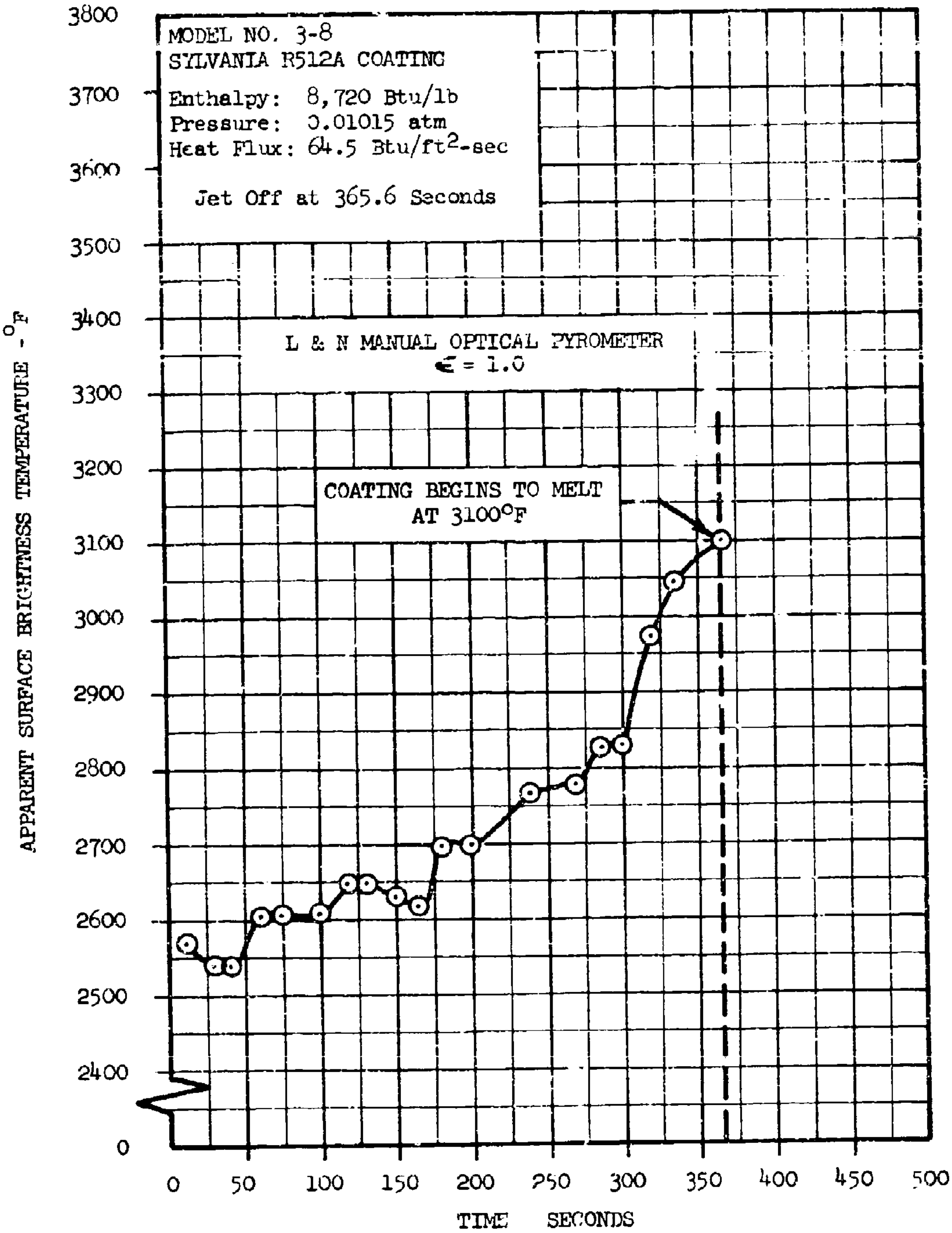

Figure 174 -- Sylvania R512A Coating - Model 3-8 Surface Temp. History

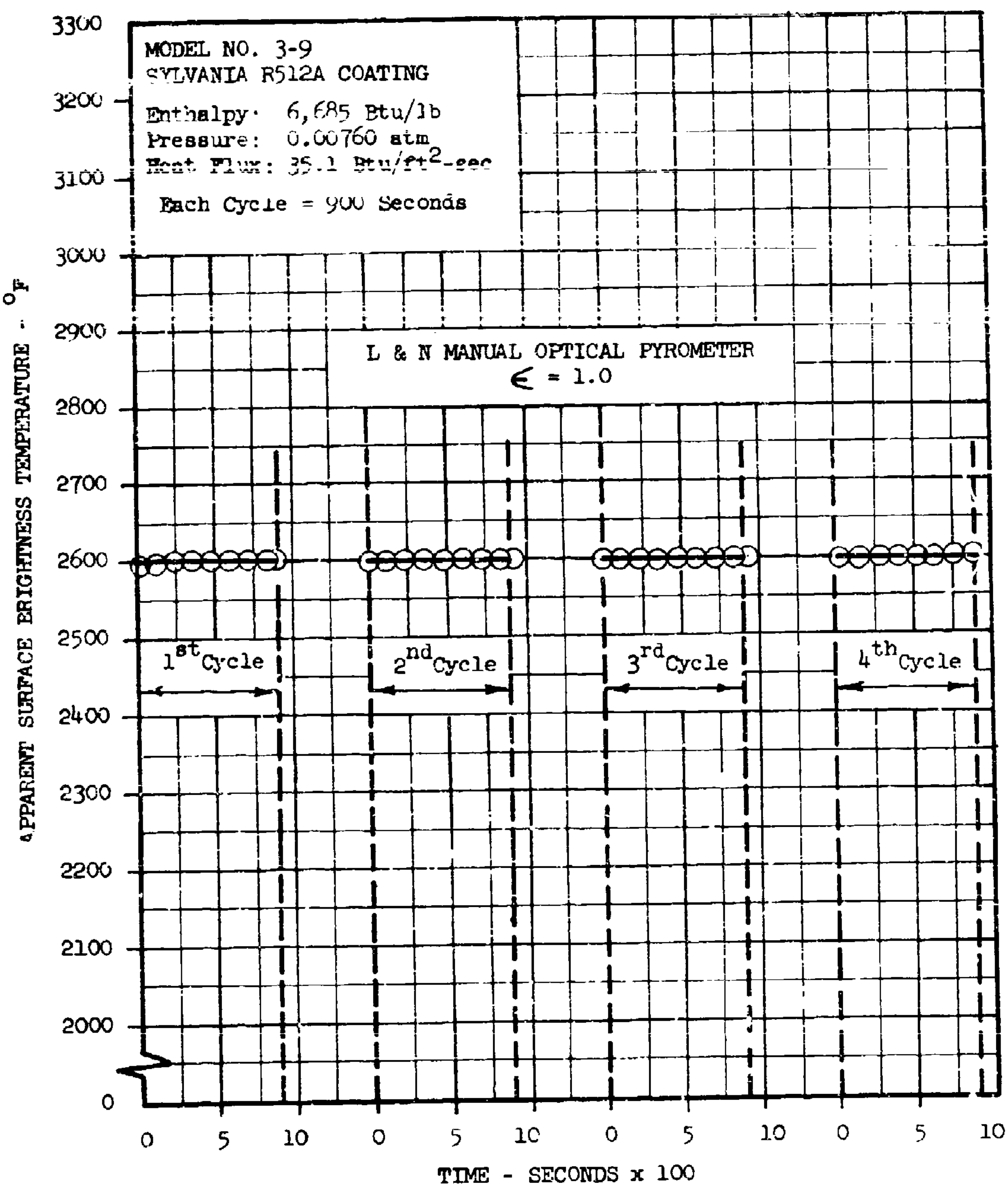

Figure 175 -- Sylvania R512A Coating - Model 3-9 Surface Temp. History

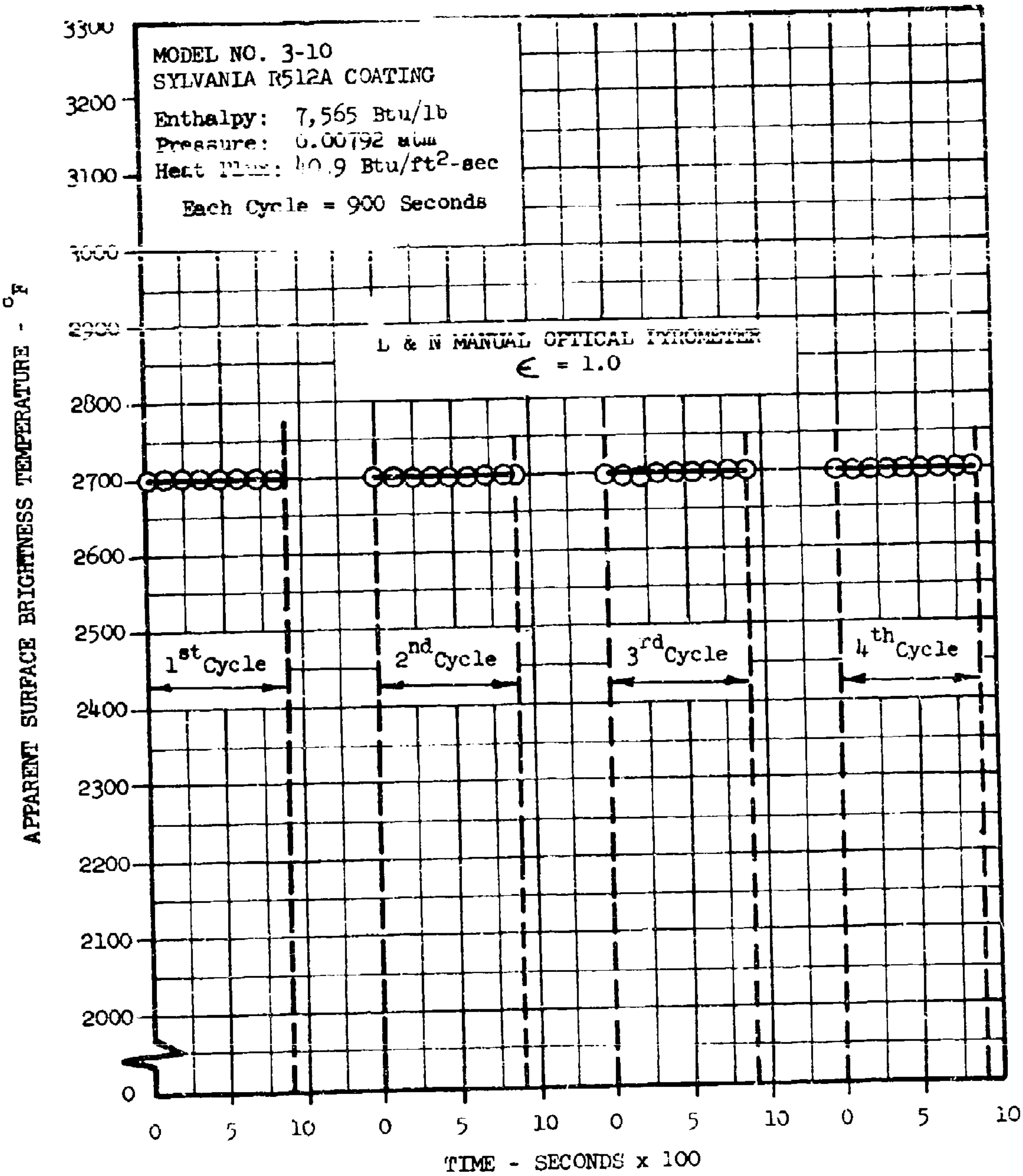

Figure 176 -- Sylvania R512A Coating - Model 3-10 Surface Temp. History

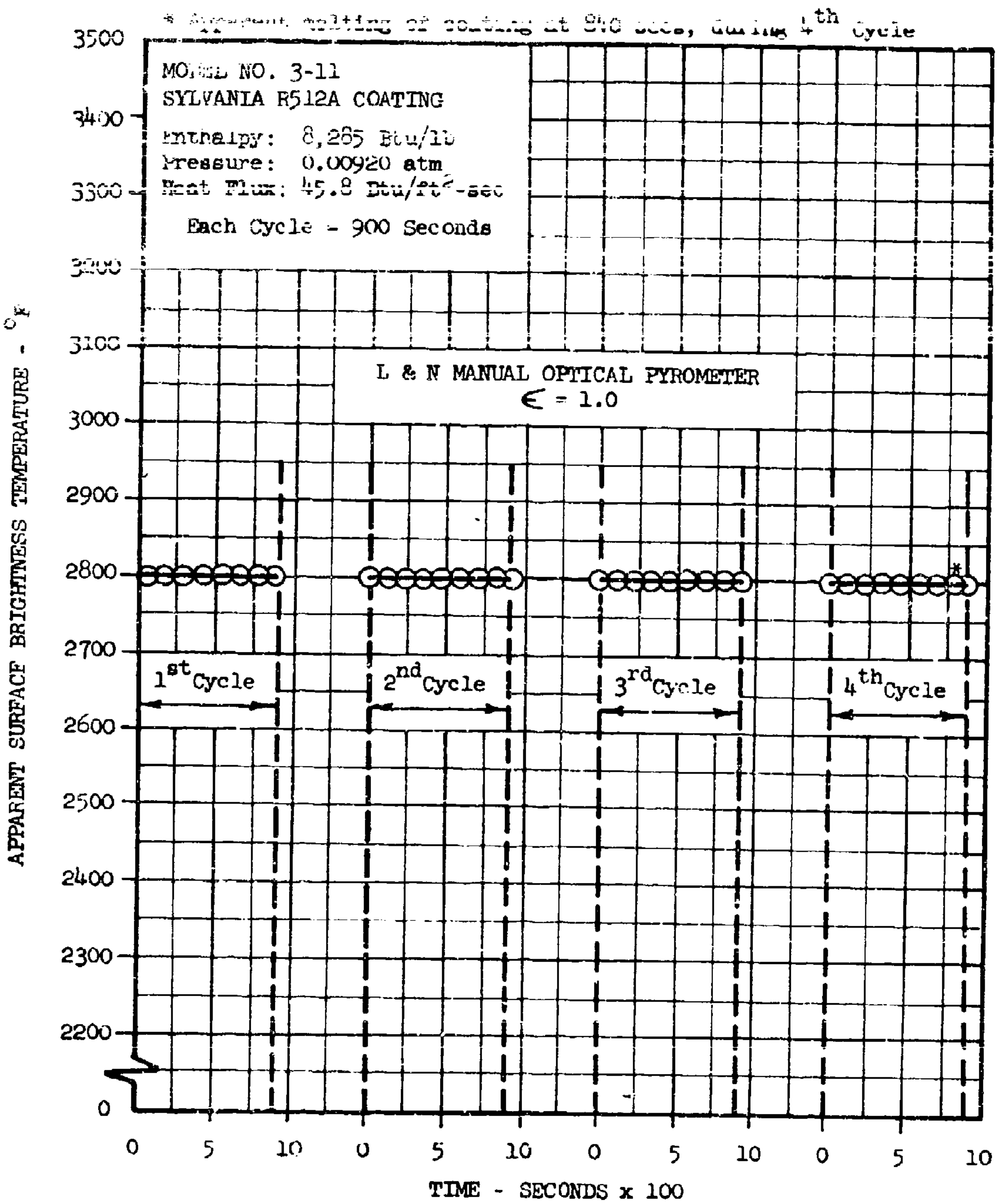

Figure 177 -- Sylvania R512A Coating - Model 3-11 Surface Temp. History

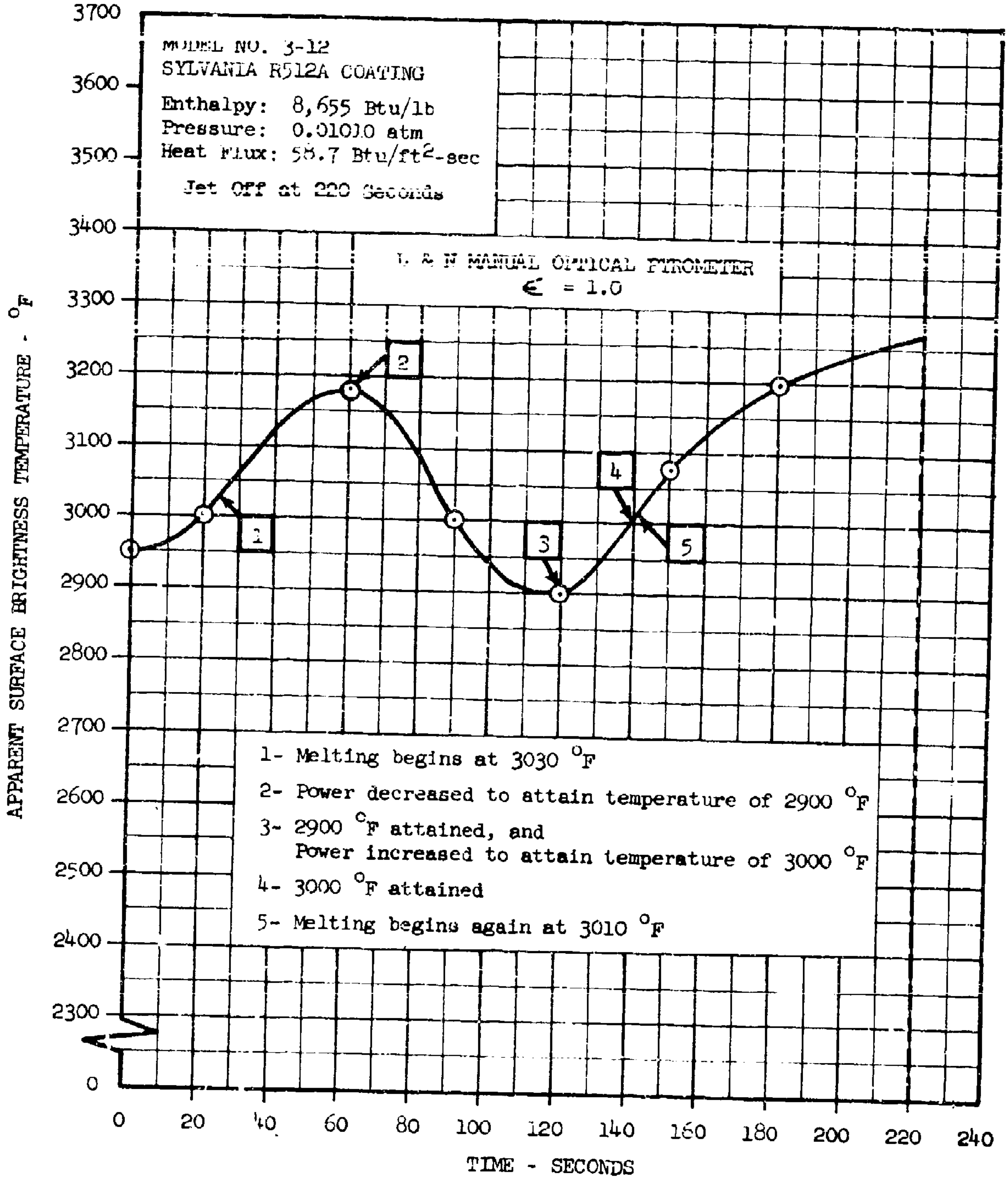

Figure 178 -- Sylvania R512A Coating - Model 3-12 Surface Temp. History

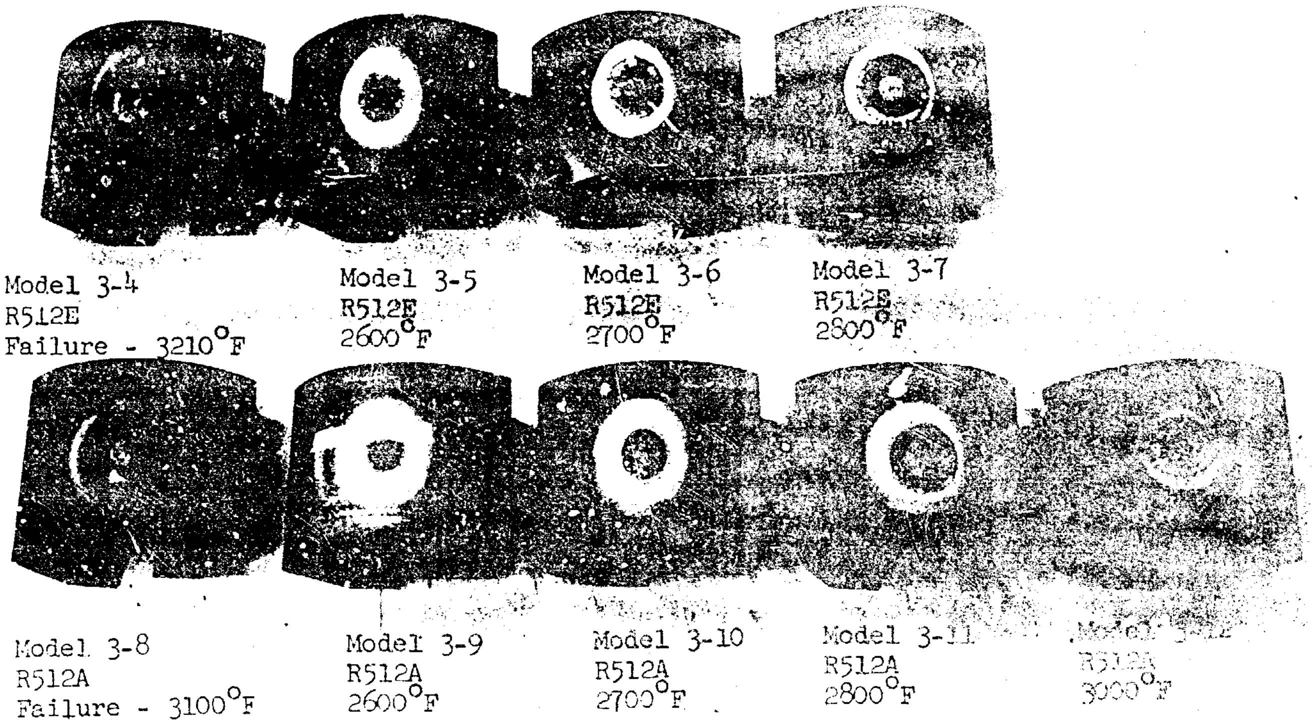

1045/001

Figure 179 -- Coated Refractory Models - Sylvania's R512E and R512A Coatings

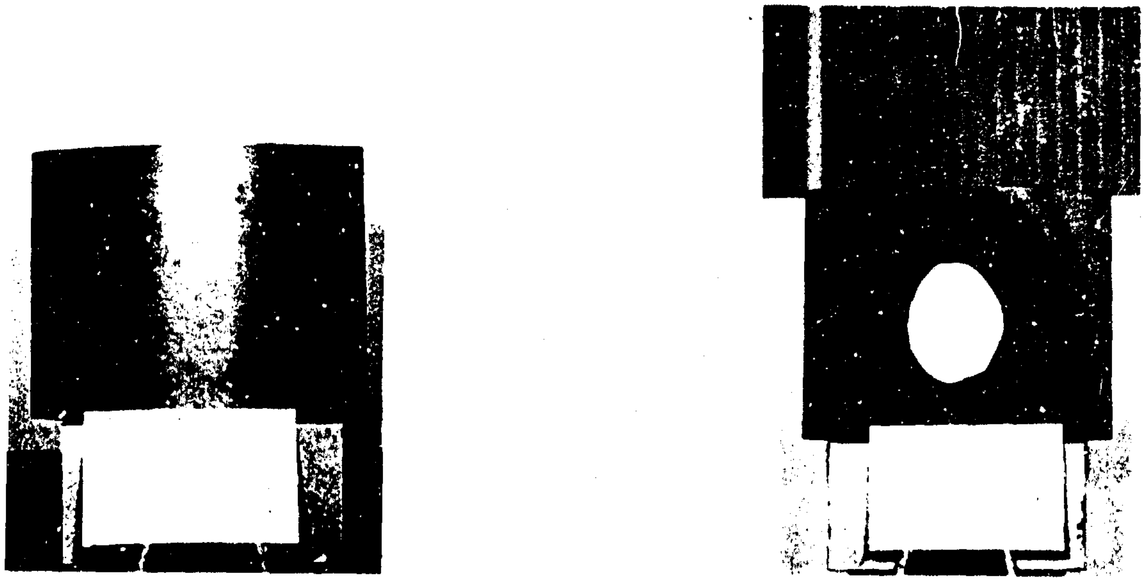

Model 3-1 - Inconel-X Control Model Before and After Exposure

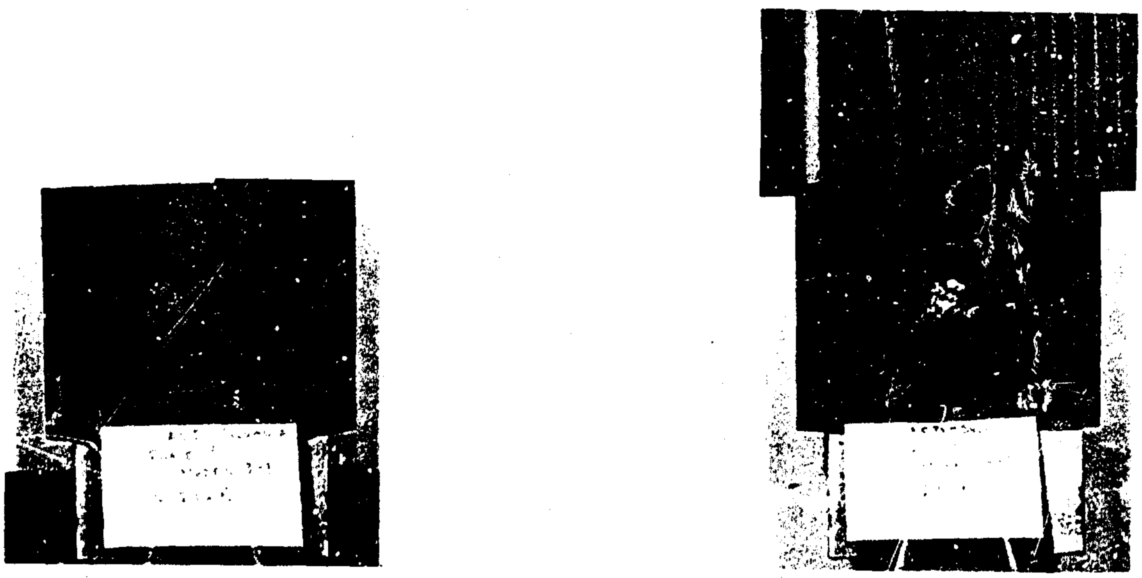

Model 3-3 - Pre- and Post-Exposure

Figure 180 -- Photographs of Inconel-X Control Model and Sylvania R512E Model 3-3

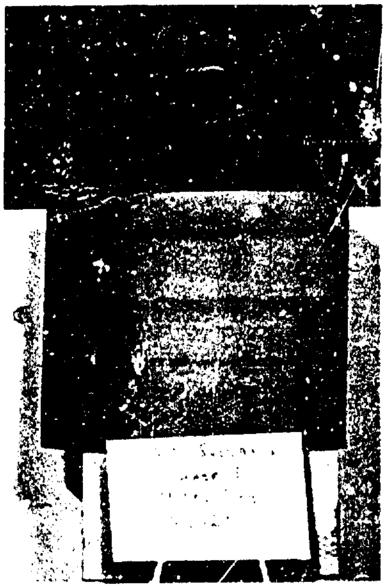

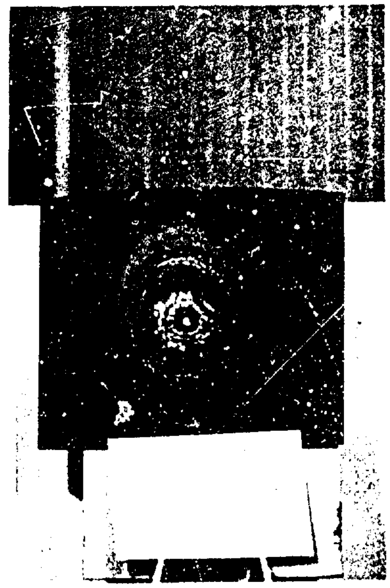

Model 3-4 - Pre- and Post-Exposure

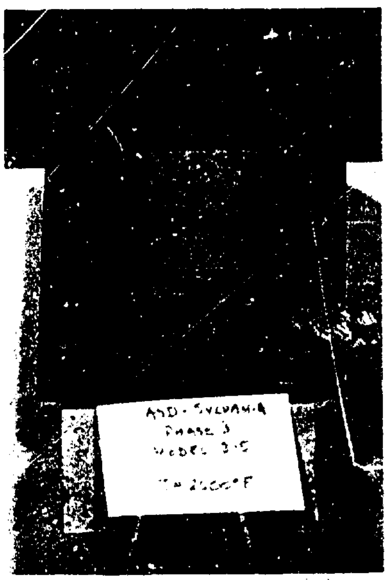

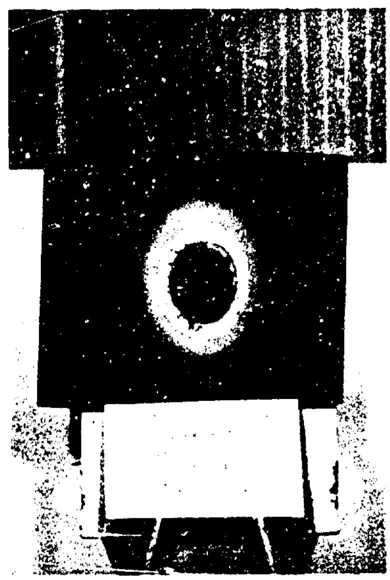

Model 3-5 - Pre- and Post-Exposure

Figure 181 -- Photographs of Sylvania R512E Coatings
Models 3-4 and 3-5

Model 3-6 - Pre- and Post-Exposure

Model 3-7 - Pre- and Post-Exposure

Figure 182 -- Photographs of Sylvania's R512E Coating Models 3-6 and 3-7

Model 3-8 - Pre- and Post-Exposure

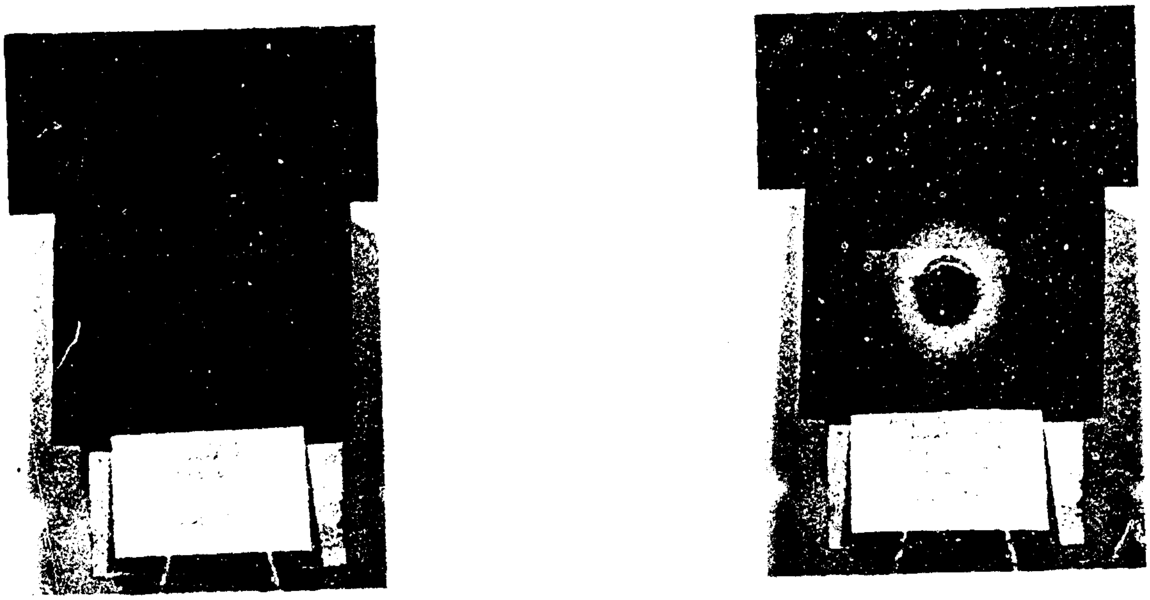

Model 3-9 - Pre- and Post-Exposure

Figure 183 -- Photographs of Sylvania's R512A Coating....
Models 3-8 and 3-9

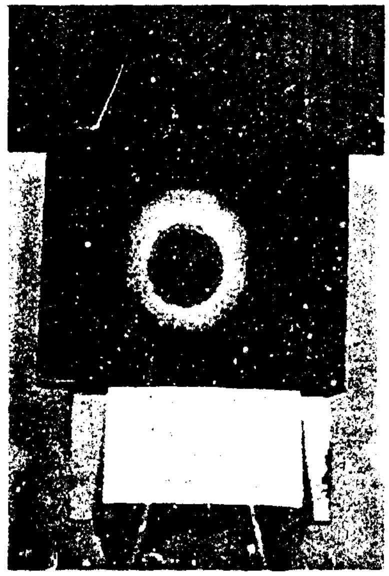

Model 3-10 - Pre- and Post-Exposure

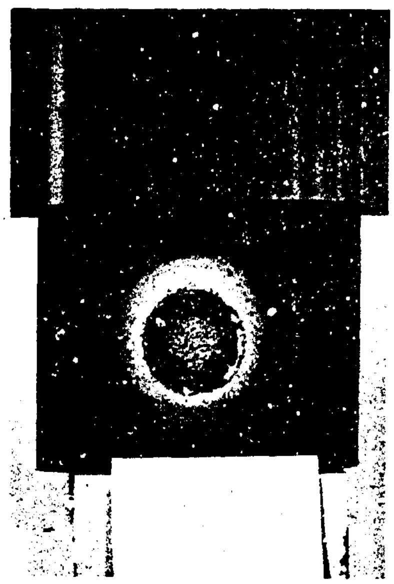

Model 3-11 - Pre- and Post-Exposure

Figure 184 -- Photographs of Sylvania's R512A Coating Models 3-10 and 3-11

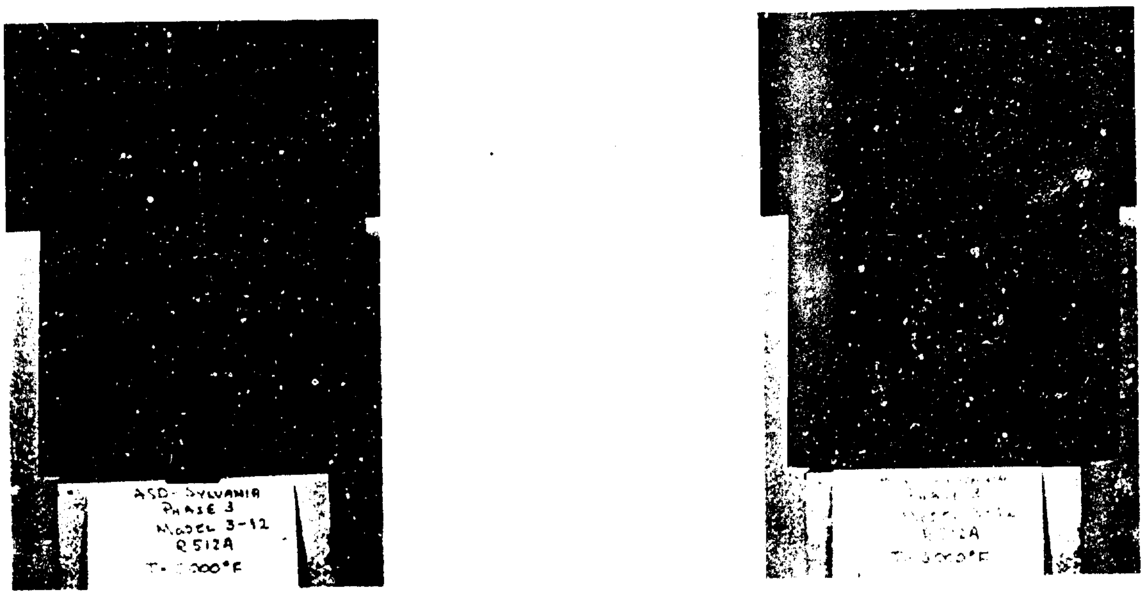

Model 3-12 - Pre- and Post-Exposure

Figure 185 -- Photographs of Sylvania's R512A Coating
Model 3-12

6.0 CARBON COMPOSITES AND GRAPHITIC MATERIALS PROGRAM

The suitability of graphitic and carbon composites for frontal or leading edge components of re-entry vehicles has brought about a strong interest in the performance of many of the recently-developed 'high-purity' forms of graphitic materials and carbon cloths. In order to assess the improved versions of the graphitic materials and carbon cloths in their purified state, as compared to their commercial grades, and to compare similar materials provided by a number of different companies, a test program was formulated in which eight classes of materials were evaluated at both high pressure (in excess of one atmosphere) and low pressure (below one atmosphere) conditions.

6.1 Objectives

The primary objective of this extensive investigation of graphitic materials and carbon cloth composites was to ascertain the advantage or improvement in high-temperature performance, if any, of the purified versions of these materials over the commercial grades of the same materials. Secondary objectives were to compare various graphite and carbon cloth materials provided by four selected suppliers. In addition, all materials were evaluated at both high pressure and low pressure test environments to ascertain performance characteristics under the two extreme conditions, typical of ballistic vehicles and lifting re-entry vehicles, respectively.

6.2 Description of Materials Tested

Eight different materials consisting of four graphitic materials and four carbon cloth composites were considered in this program. A total of forty models were tested; twenty-four at high pressure and low enthalpy and sixteen at low pressure and high enthalpy. The graphitic materials were selected mutually by the Air Force technical monitors and the Space-General program manager and were bought with contract funds and machined to final model shapes by Space-General. The carbon cloth composites, also mutually selected by the Air Force and Space-General cognizant personnel, were fabricated and machined to model shapes by U. S. Polymeric, Inc., of Santa Ana, California. U. S. Polymeric purchased the carbon cloth from vendors specified by the program manager, and molded the rough model shape using SC 1008 phenolic resin. Final machining of the carbon cloth models required the use of diamond machine tools and consequently was done under sub-contract through U. S. Polymeric.

The graphite materials suppliers which provided bulk graphite material for this program were: Union Carbide Corporation - Carbon Products Division, The Carborundum Company - Graphite Products Division, Great Lakes Carbon Corporation - Graphite Products Division, and Poco Graphite, Inc. With the exception of Great Lakes Carbon Corporation, which provided bulk graphite at no charge, all other graphitic material was purchased with contract funds.

The carbon cloths were supplied by the following companies: 3M Company - Electrical Products Division, HITCO, Union Carbide Corporation - Carbon Products Division, The Carborundum Company - Graphite Products Division. All carbon cloth materials were purchased under subcontract through U. S. Polymeric, Inc., and were fabricated by U. S. Polymeric using SC 1008 phenolic resin. A table summarizing the various materials evaluated under this program is presented below.

TABLE 19

GRAPHITIC MATERIALS AND CARBON CLOTH COMPOSITES

Material Designation	Density (lb/ft^3)	Impurity Level*	Supplier
Graphitic Materials			
ATJ Graphite	108.0	Commercial	Union Carbide Corp.
ATJ Graphite-TS-777	106.8	20 ppm	Union Carbide Corp.
AXF	114.8	100-200 ppm	Poco Graphite, Inc.
AXF-Q1	114.8	6-8 ppm	Poco Graphite, Inc.
H205	109.3	Commercial	Great Lakes Carbon Corp.
H205-R4	109.3	30-50 ppm	Great Lakes Carbon Corp.
Graphitite G	117.9	Commercial	The Carborundum Company
Graphitite G-Purified	118.6	150-300 ppm	The Carborundum Company
Carbon Cloth Materials			
Pluton B-1	89.2	Commercial	3M Company
Pluton B-1 HP	91.1	25-50 ppm	3M Company
CCA-1	89.2	Commercial	HITCO
CCA-1 1641	89.2	400 ppm	HITCO
VCK	86.1	Commercial	Union Carbide Corp.
VCL	87.4	200-300 ppm	Union Carbide Corp.
GSCC-2	84.2	Commercial	The Carborundum Company
GSCC-2 Purified	83.6	20-30 ppm	The Carborundum Company

*Total alkaline earth impurities in parts per million; estimated values in some cases - exact numbers not available.

The carbon cloth models, prepared by U. S. Polymeric, Inc., were cured at 1000 psi at 325°F, postcured for 32 hours through 250°F, machined, and finally postcured for 26 hours through 325°F. Lay-up of the cloth fabric was in the edge-oriented configuration, as sketched in Figure 186. The graphitic materials were machined by Space-General in accordance with the dimensional measurements shown in Figure 186.

Consideration of the machining and fabrication, and cost of bulk material resulted in the selected model configuration of a flat plate, tested at an angle of attack of 30°. Originally, wedge models with a blunt-nose were considered; however, fabrication costs and the amount of material required for the wedge configuration were excessive and the flat plate model was used instead.

6.3 Calibration of Test Conditions

All of the graphitic and carbon cloth composite materials were evaluated under both low and high pressure conditions, typical of lifting re-entry and ballistic vehicles, respectively. A summary of the environmental conditions, defined by gas stagnation enthalpy, model stagnation pressure, model heat flux, etc., is tabulated in Table 20. Calibration procedures are described in earlier sections of this report and will not be repeated in this section.

The high pressure/low enthalpy condition was achieved in the high pressure plasma arc generator using a Mach 2.8 contoured nozzle, 0.90 inches in exit diameter. In order to measure the model cold-wall heat flux experienced by a flat-plate at an angle of attack of 30°, a simulated model was fabricated and instrumented with a slope-type copper calorimeter. The sensing unit was located at the center of the flat-plate coinciding with the center of the 0.90-inch diameter stream. The measured cold-wall heat flux was 1.027 Btu/ft^2-sec at an enthalpy of 3,000 Btu/lb and a model stagnation pressure of 4.0 atmospheres.

The low pressure/high enthalpy condition, selected to represent a typical lifting re-entry vehicle flight condition, was achieved with the low pressure plasma arc generator and a supersonic Mach 3 contoured nozzle, three inches in exit diameter. The flat plate models were exposed to this stream at an angle of attack of 30° to duplicate the high pressure model tests. A flat-plate calorimeter model was again used to measure the model heat flux at the center of the flat-plate, coinciding with the center of the test stream. The measured heat flux at this point was 156 Btu/ft^2-sec.

6.4 Results of Graphitic Materials and Carbon Composite Model Tests

Because of the large number of materials and models evaluated in this particular program, Table 21 has been prepared which summarizes the materials, model numbers and test conditions at which the specific models were exposed to.

Initially, exposure times for the models were going to be selected so that the total heat load would be the same on both the low pressure and the high pressure tests. However, due to the extreme difference in severity of test environment, this was found to be unreasonable in that exceptionally long exposure times would have been required for the low pressure model tests. Consequently, exposure times were selected which would give measurable values of recession and weight loss. In addition, the carbon cloth materials in many cases, delaminated and broke apart, at which point the model test was terminated. For these models that experience delamination and break-up, exposure times were dictated by the breaking-up of the model.

TABLE 20

TUNNEL CALIBRATION DATA

Graphitic and Carbon-Cloth Model Tests

Test Condition	Model No.	Gas Enthalpy (Btu/lb)	Model Stag. Pressure (atms)	Model Cold-Wall Heat Flux* (Btu/ft^2-sec)	Nozzle Stag. Pressure (atms)	Nozzle Static Pressure (atms)	Gas Flow Rate (lb/sec)
1	See Below	3,000 $\pm$ 100	4.0 $\pm$ .15	1,027 $\pm$ 50	17.0 $\pm$ .25	.25 $\pm$ .05	0.1270
Models Tested at Test Condition 1: 5-2A, 5-2B, 5-3B, 5-4, 5-5, 5-6, 5-7, 5-8, 5-9, 5-10, 5-11, 5-12, 5-13, 5-14, 5-15, 5-16, 5-20, 5-22, 5-24, 5-26, 5-28, 5-32, 5-36, 5-38.							
2	See Below	17,000 $\pm$ 250	0.06 $\pm$ .01	156 $\pm$ 7	.348 $\pm$ .007	.007 $\pm$ .0005	0.00201
Models Tested Test Condition 2: 5-50A, 5-51, 5-52, 5-53, 5-54, 5-55, 5-56, 5-57, 5-21, 5-23, 5-25, 5-27, 5-29, 5-33, 5-37, 5-39.							

NOTE:
*Model cold-wall heat flux measured with copper slope-type calorimeter imbedded in graphite body geometrically-similar to the test models.

TABLE 21

Graphitic and Carbon Cloth Model Tests

Summary of Models and Materials

Material	Model Number	Test Condition	Material	Model Number	Test Condition
ATJ Commercial Graphite	5-2A, 5-2B	1	ATJ Commercial Graphite	5-52	2
ATJ Purified Graphite	5-3B, 5-4	1	ATJ Purified Graphite	5-53	2
Graphitite G Commercial	5-5, 5-6	1	Graphitite G Commercial	5-51	2
Graphitite G Purified	5-7, 5-8	1	Graphitite G Purified	5-50A	2
AXF Graphite Commercial	5-9, 5-10	1	AXF Graphite Commerical	5-54	2
AXF-Q1 Graphite Purified	5-11, 5-12	1	AXF-Q1 Graphite Purified	5-55	2
H205 Graphite Commercial	5-15, 5-16	1	H205 Graphite Commerical	5-57	2
H205-R4 Graphite Purified	5-13, 5-14	1	H205-R4 Graphite Purified	5-56	2
CCA-1 Carbon Commercial	5-20	1	CCA-1 Carbon Commercial	5-21	2
CCA-1 1641 Carbon	5-22	1	CCA-1 1641 Carbon	5-23	2
VCK Carbon Commercial	5-24	1	VCK Carbon Commercial	5-25	2
VCL Carbon Purified	5-38	1	VCL Carbon Purified	5-39	2
GSCC-2 Carbon Commercial	5-26	1	GSCC-2 Carbon Commercial	5-27	2
GSCC-2 Carbon Purified	5-36	1	GSCC-2 Carbon Purified	5-37	2
Pluton B-1 Commercial	5-32	1	Pluton B-1 Commercial	5-33	2
Pluton B-1 HP	5-28	1	Pluton B-1 HP	5-29	2

Comparison of the graphitic materials and the carbon composites has been made in terms of the weight loss rates and model surface temperatures. Tabulated weight loss rates are presented in Table 22 along with the surface temperatures obtained just prior to termination of the model exposure period, using a Leeds and Northrup optical brightness pyrometer. Surface temperatures presented are apparent temperatures, uncorrected for emissivity values.

A comparison of the weight loss rates for each of the eight categories of materials at the two test conditions has been prepared in Figure 157. The graphitic material ranking from lowest to highest weight loss is:

Material	Test Point	Weight Loss Rate (gm/sec)	Ranking
Graphitite G Purified	1	0.205*	1
Graphitite G	1	0.208*	2
AXF-Q1	1	0.210*	3
H205-R4	1	0.220*	4
ATJ Purified	1	0.227*	5
AXF	1	0.241*	6
H205	1	0.248*	7
ATJ	1	0.260*	8
Graphitite G	2	0.0774	1
Graphitite G Purified	2	0.0785	2
ATJ Purified	2	0.0857	3
H205-R4	2	0.0857	3
H205	2	0.0869	4
ATJ	2	0.0881	5
AXF-Q1	2	0.0905	6
AXF	2	0.0941	7

*Average of weight loss rates for two different models

The carbon composites, also plotted on the same figure, had significantly higher weight loss rates than did the graphitic materials. Also, most of the materials delaminated, with the exception of the GSCC-2 purified carbon cloth supplied by The Carborundum Company. Ranking of the carbon cloth materials is presented in the table on Page 230.

TABLE 22

MODEL TEST DATA

Graphitic and Carbon Cloth Model Tests

Model No.	Exposure Time (secs)	Weight Loss (grams)	Weight Loss Rate (gms/sec)	Surf. Temp* (°F)
5-2A	40.0	10.0	0.2500	4660
5-2B	40.0	10.8	0.2700	4640
5-3B	40.0	9.3	0.2325	4560
5-4	40.0	8.9	0.2225	4550
5-5	40.0	8.65	0.2160	3920
5-6	40.0	8.00	0.2000	4000
5-7	40.0	8.5	0.2125	4090
5-8	40.0	7.9	0.1975	3920
5-9	40.0	9.3	0.2325	3860
5-10	40.0	10.0	0.2500	3920
5-11	40.0	8.5	0.2125	4060
5-12	40.0	8.3	0.2075	4000
5-13	40.0	7.6	0.1900	4590
5-14	40.0	9.9	0.2498	4620
5-15	40.0	10.6	0.2650	4620
5-16	40.0	9.3	0.2325	4440
5-20	3.0	3.1	1.0333	----
5-22	9.0	8.0	0.8888	----
5-24	15.0	11.0	0.7333	5100
5-26	7.0	6.3	0.9000	5130

Model No.	Exposure Time (secs)	Weight Loss (grams)	Weight Loss Rate (gms/sec)	Surf. Temp* (°F)
5-28	12.0	14.8	1.2333	5050
5-32	9.5	13.1	1.3790	5080
5-36	14.0	11.6	0.8286	4520
5-38	6.0	6.7	1.1167	4400
5-50A	84.0	6.6	0.0785	3860
5-51	84.0	6.5	0.0774	3770
5-52	84.0	7.4	0.0881	3810
5-53	84.0	7.2	0.0857	3810
5-54	84.0	7.9	0.0941	4030
5-55	84.0	7.6	0.0905	4020
5-56	84.0	7.2	0.0857	3880
5-57	84.0	7.3	0.0869	3840
5-21	30.0	11.0	0.3667	3930
5-23	30.0	10.4	0.3467	3860
5-25	30.0	14.2	0.4733	3850
5-27	30.0	14.6	0.4867	3980
5-29	30.0	12.2	0.4067	3740
5-33	30.0	14.4	0.4800	3820
5-37	30.0	10.6	0.3533	3820
5-39	30.0	11.1	0.3700	3800

NOTE: *Measured with optical pyrometer near end of exposure period.

Material	Test Point	Weight Loss Rate (gm/sec)	Ranking
VCK	1	0.7333	1
GSCC-2 Purified	1	0.8286	2
CCA-1 1641	1	0.8888	3
GSCC-2	1	0.9000	4
CCA-1	1	1.0333	5
VCL	1	1.1167	6
Pluton B-1 HP	1	1.2333	7
Pluton B-1	1	1.3790	8
CCA-1 1641	2	0.3467	1
GSCC-2 Purified	2	0.3533	2
CCA-1	2	0.3667	3
VCL	2	0.3700	4
Pluton B-1 HP	2	0.4067	5
VCK	2	0.4733	6
Pluton B-1	2	0.4800	7
GSCC-2	2	0.4867	8

Recession profiles are graphed individually for each model in Figures 188 through 197. Due to the model configuration and resultant recession profiles, tabulation of the recession rates was not done. Instead, recession measurements were obtained along the centerline of each flat-plate model and were plotted to show the centerline recession profiles. It is readily apparent from this graphical presentation of ablation profiles both before and after exposure to the plasma environment, that recession was not uniform over the exposed surface of the models. Delamination and swelling of the carbon cloth models are apparent in these graphical presentations.

Pre- and post-exposure photographs of the graphitic and carbon cloth models are shown in Figures 198 through 217. Surface appearance of each of the materials is visible in these black and white photographs.

It is apparent from the results of this series of model tests, that an improved model design would be beneficial to the performance of the material(s) and in addition, would reduce the cost of test material. Future models will be designed so as to eliminate mechanical stress/strain on the test material, which should give a more realistic evaluation of the true strength properties of each material at high temperature eroding environments.

STANDARD MODEL FOR GRAPHITIC AND CARBON COMPOSITE MATERIALS

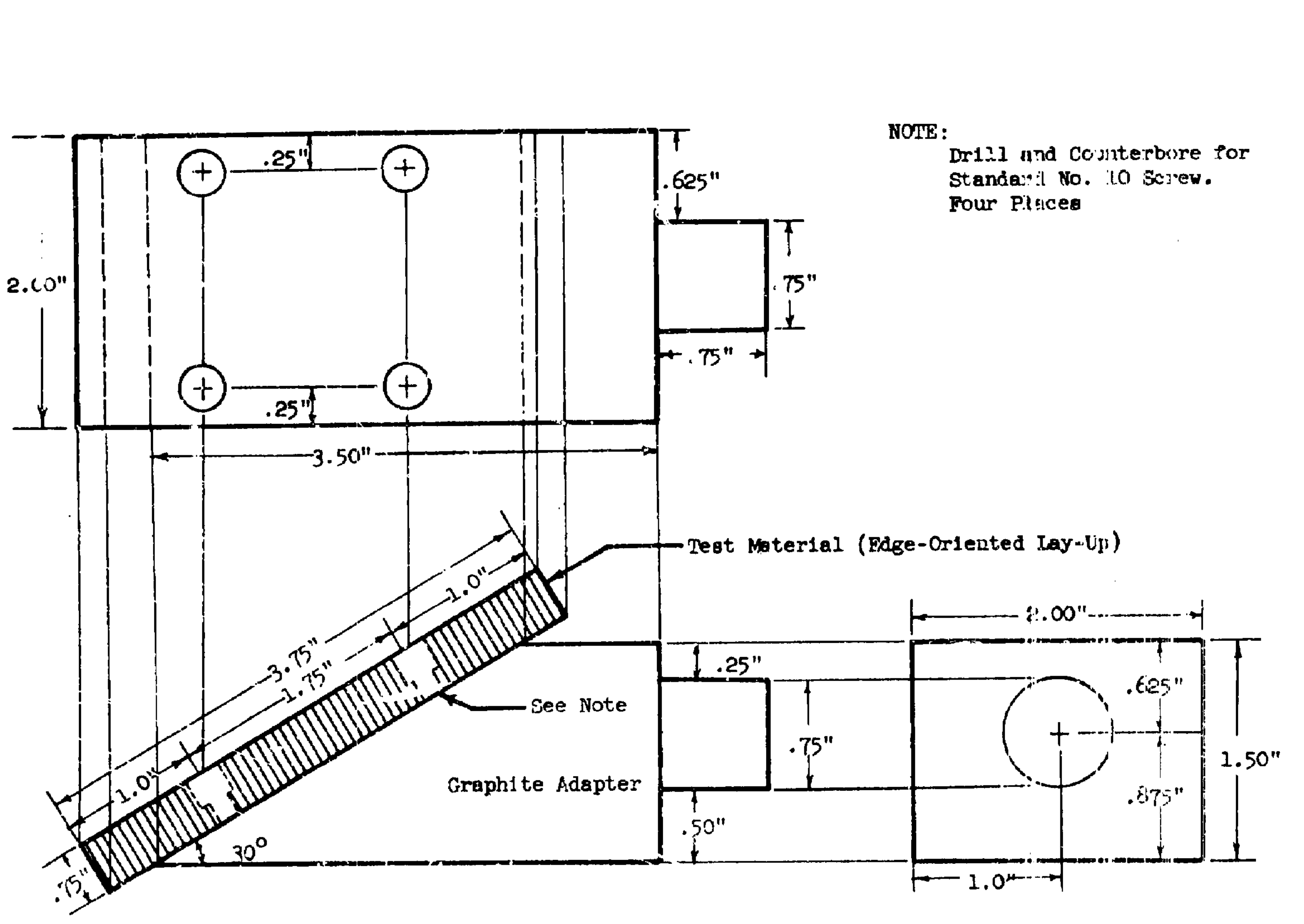

Figure 186 -- Standard Model for Graphitic and Carbon Composite Materials

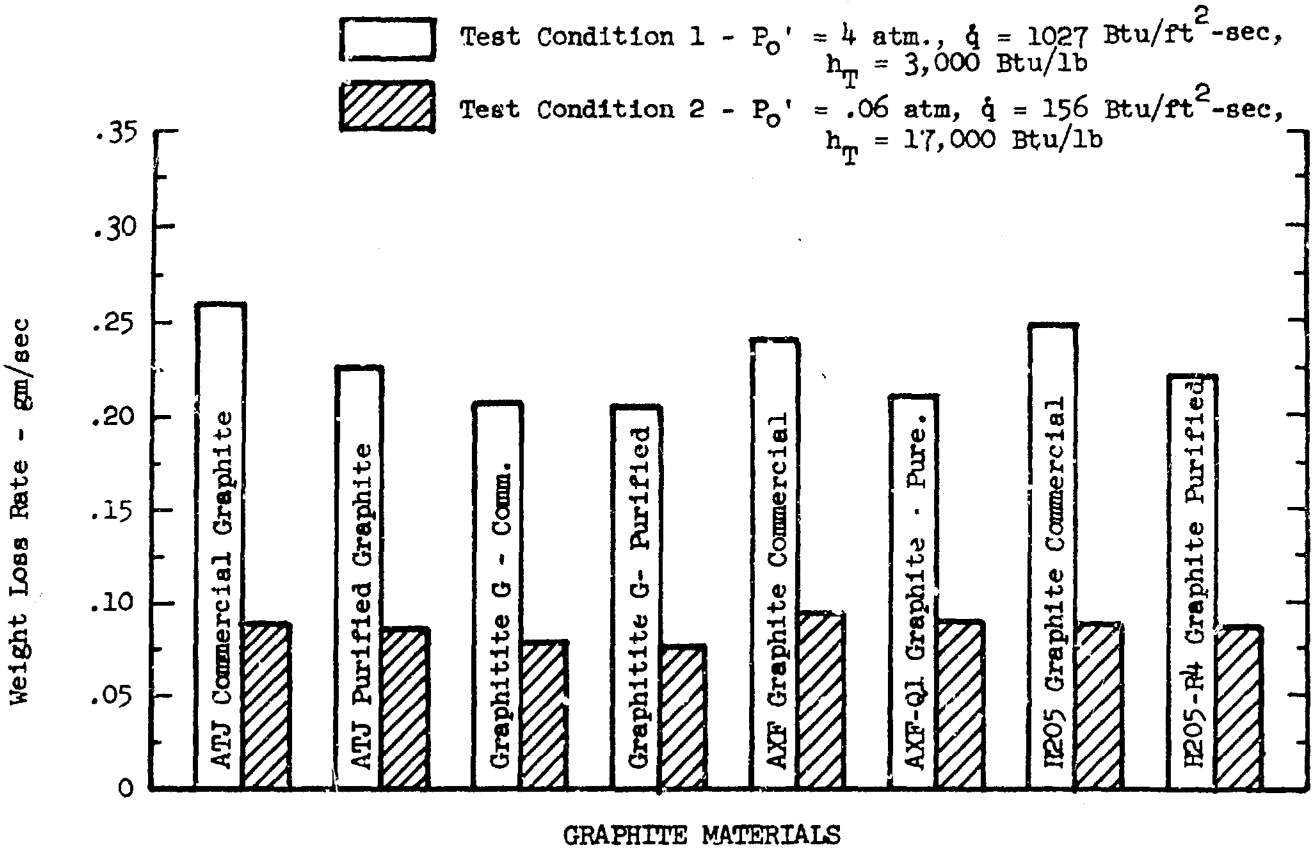

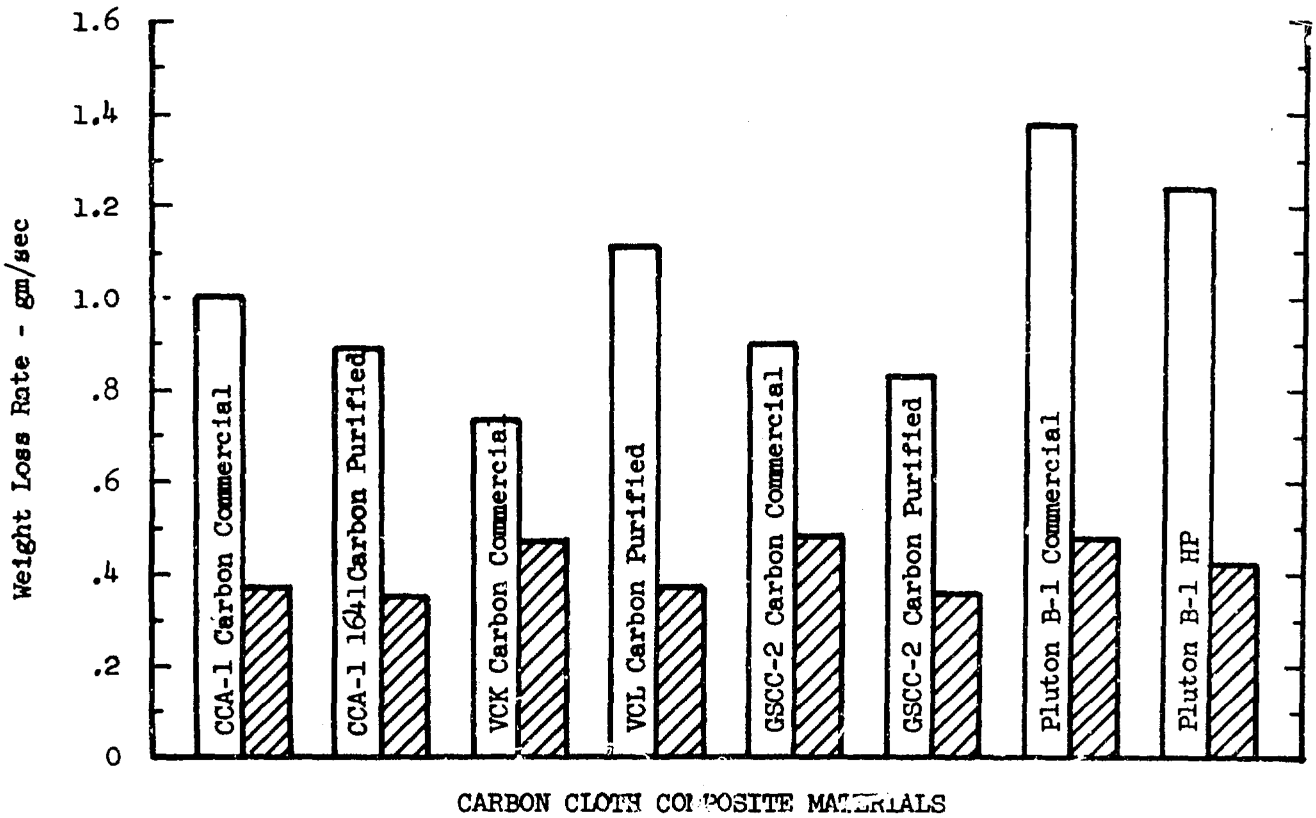

Figure 187 -- Weight Loss Rates for Graphitic and Carbon Composites Materials

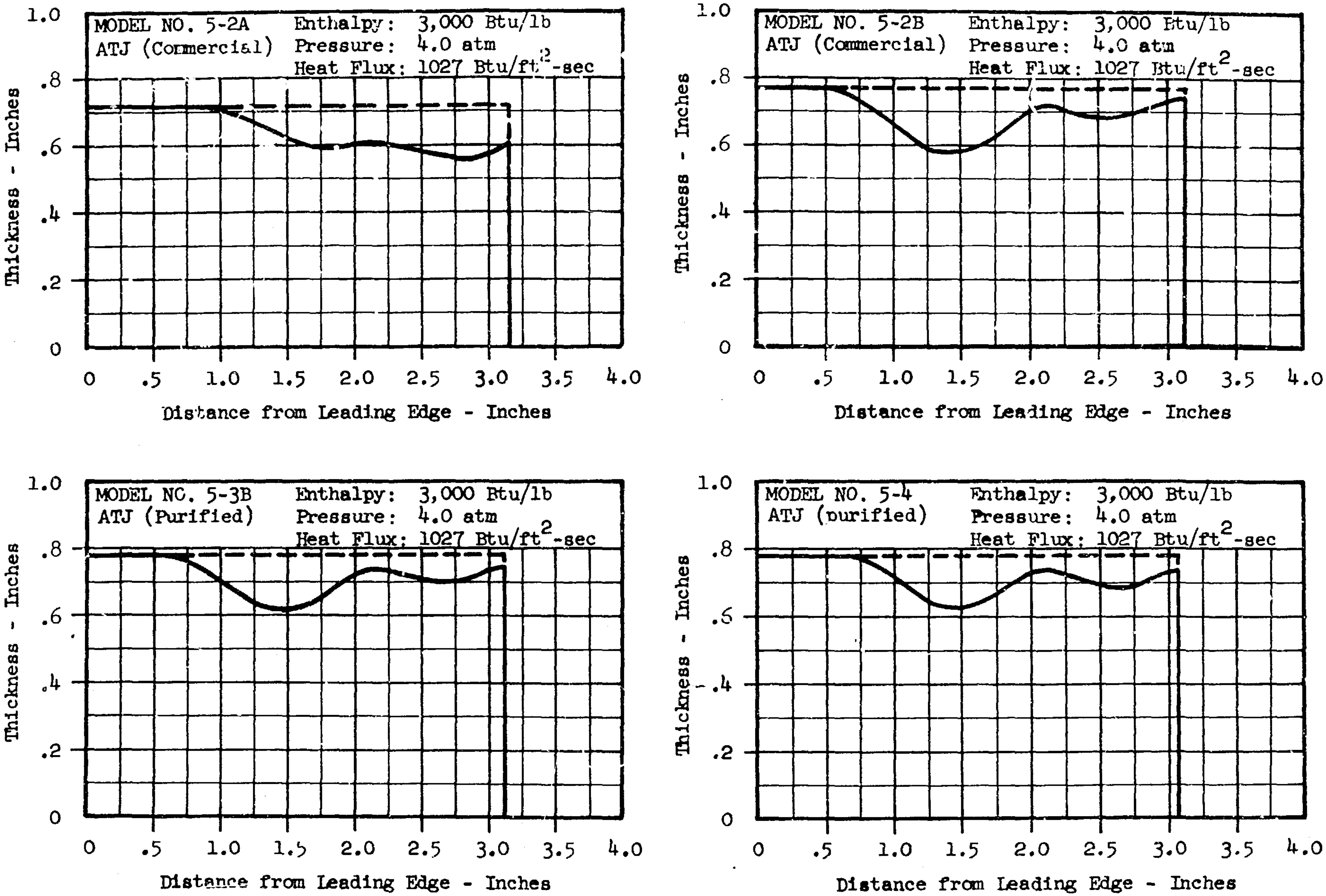

Figure 188 -- Centerline Recession Profile, ATJ Commercial (Mdls.5-2A & 5-2B) and ATJ Purified (5-3B and 5-4)

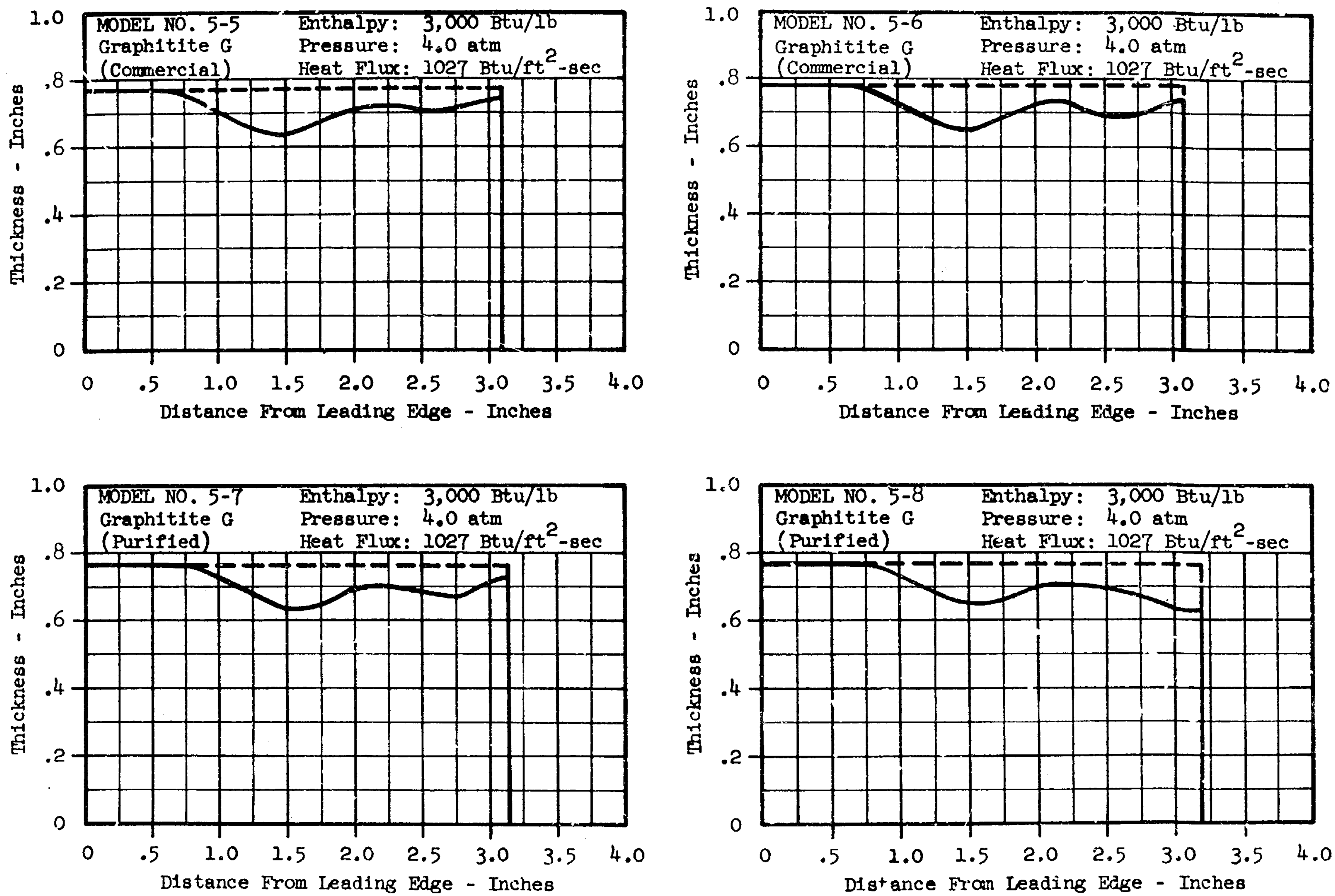

Figure 189 -- Centerline Recession Profiles,Graphitite G(Commercial) Mdls. 5-5 & 5-6,& Graphitite G (Purified) Mdls. 5-7 & 5-8

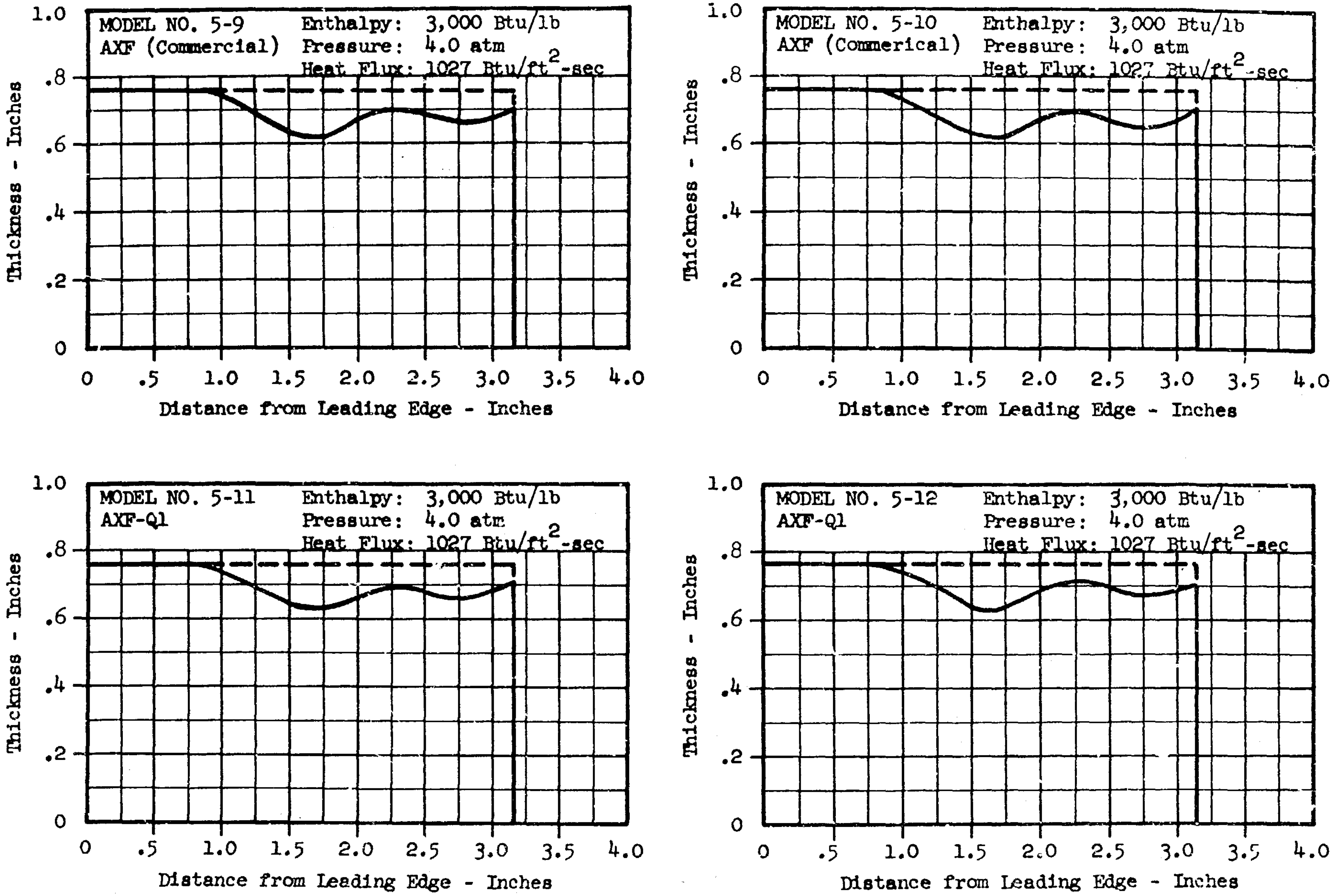

Figure 190-Centerline Recession Profiles, AXF (Commercial) (Mdls. 5-9, 5-10) and AXF-Q1 (Mdls. 5-11, 5-12)

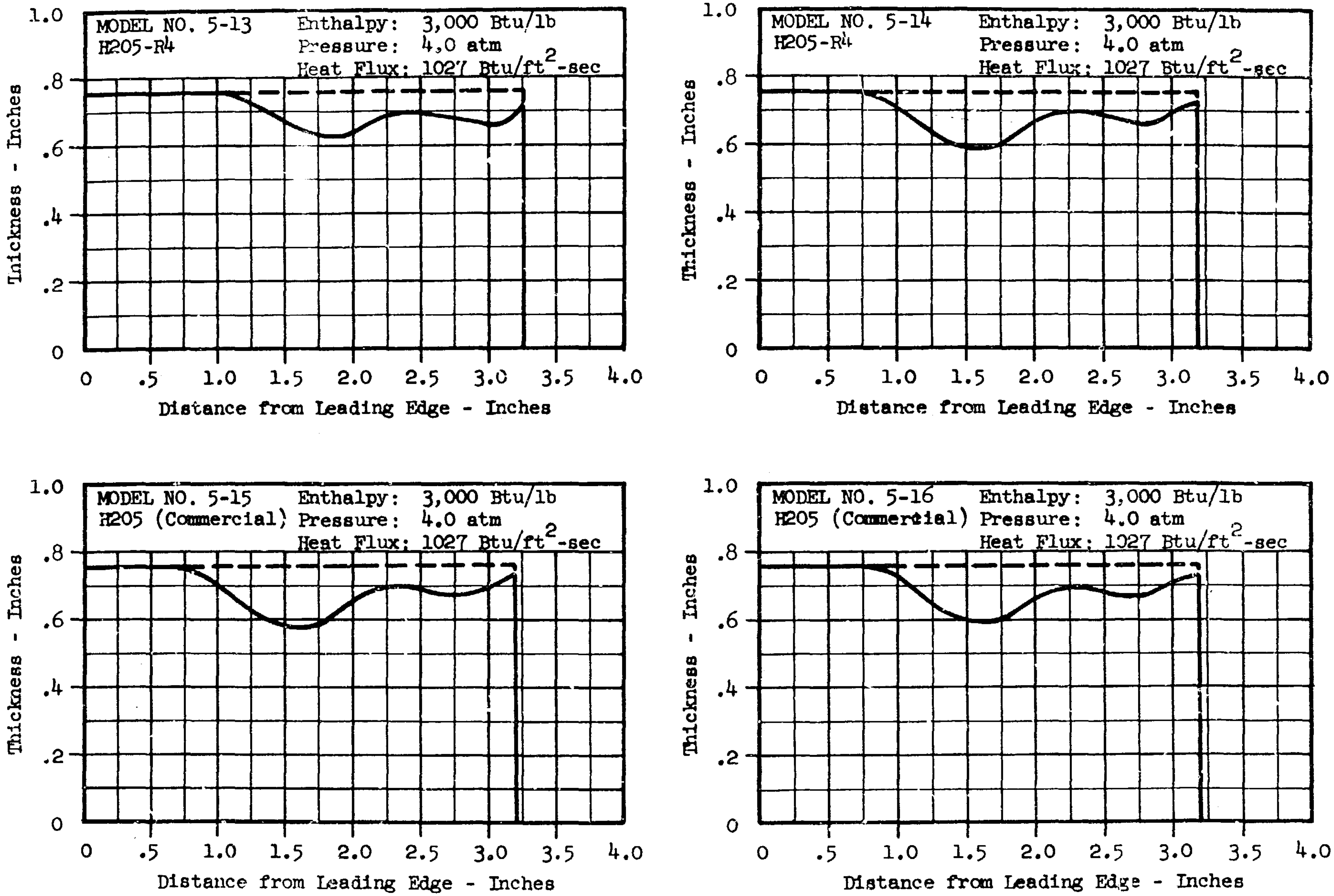

Figure 191-Centerline Recession Profiles, H205-R4 (Mdls. 5-13 & 5-14) and H205 Commercial (Mdls. 5-15 & 5-16)

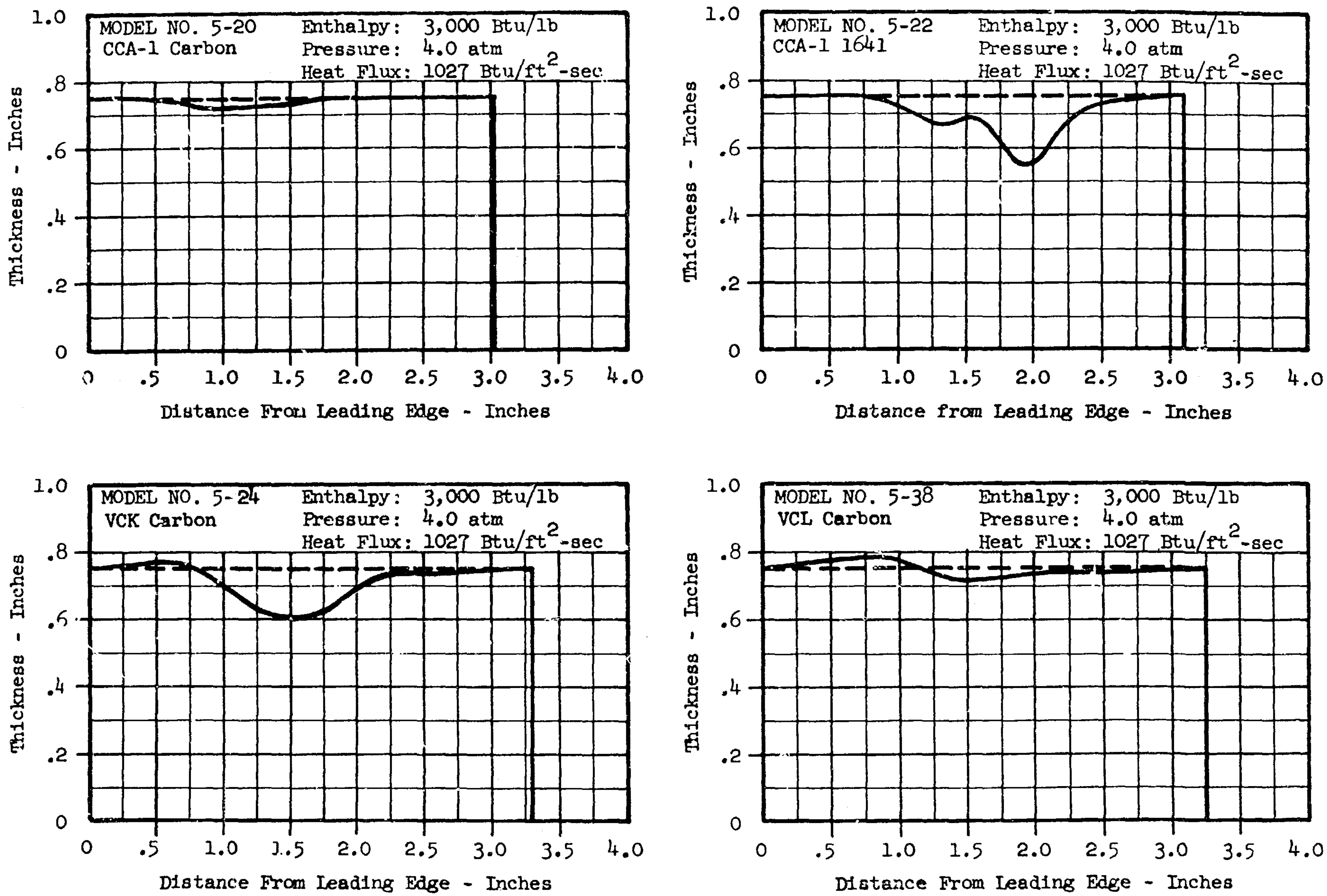

Figure 192-Centerline Recession Profiles, CCA-1 Carbon (Mdl 5-20) CCA-1 1641 (Mdl. 5-22) VCK Carbon (Mdl. 5-24) and VCL Carbon (Mdl 5-38)

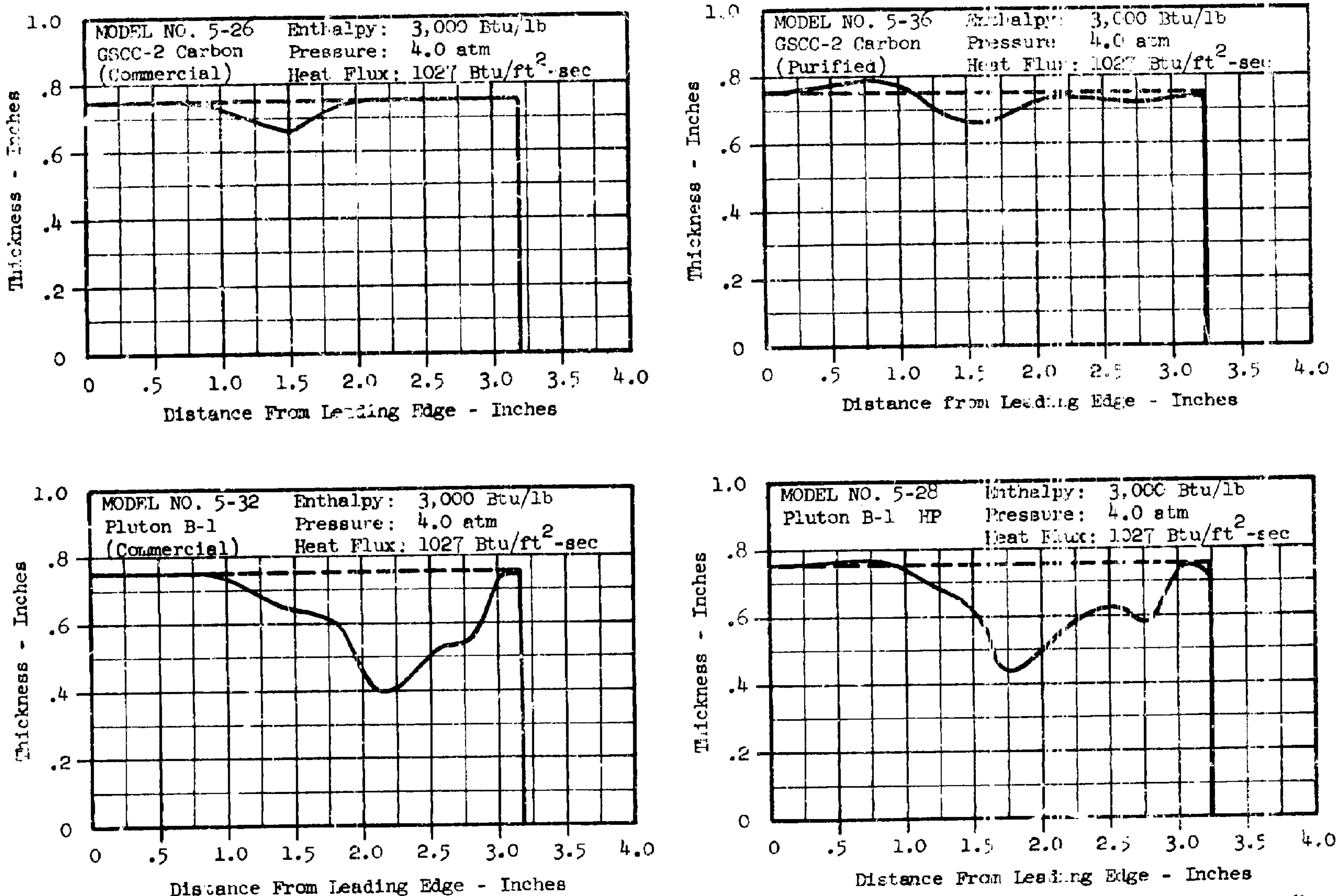

Figure 193 -- Centerline Recession Profiles, GSCC-2 Carbon- Commercial (Mdl. 5-26), GSCC-2 Carbon - Purified (Mdl 5-36), Pluton B-1 Commercial (Mdl 5-32) and Pluton B-1 HP (Mdl 5-28)

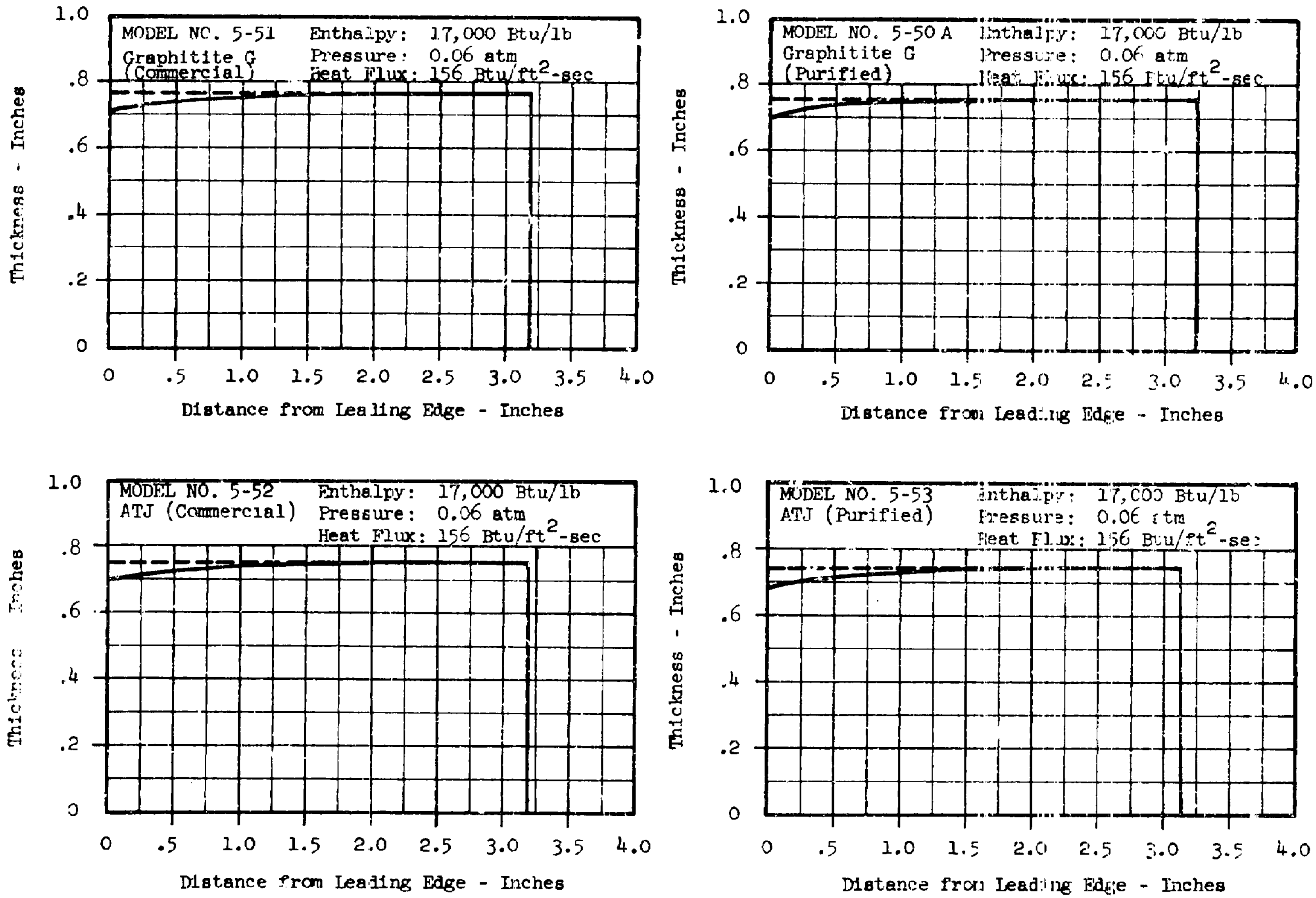

Figure 194 -- Recession Profile at Centerline, ATJ Commercial (Mdl 5-52) ATJ Purified (Mdl 5-53), Graphitite G Commercial (Mdl 5-51) and Graphitite G Purified (Mdl 5-50A)

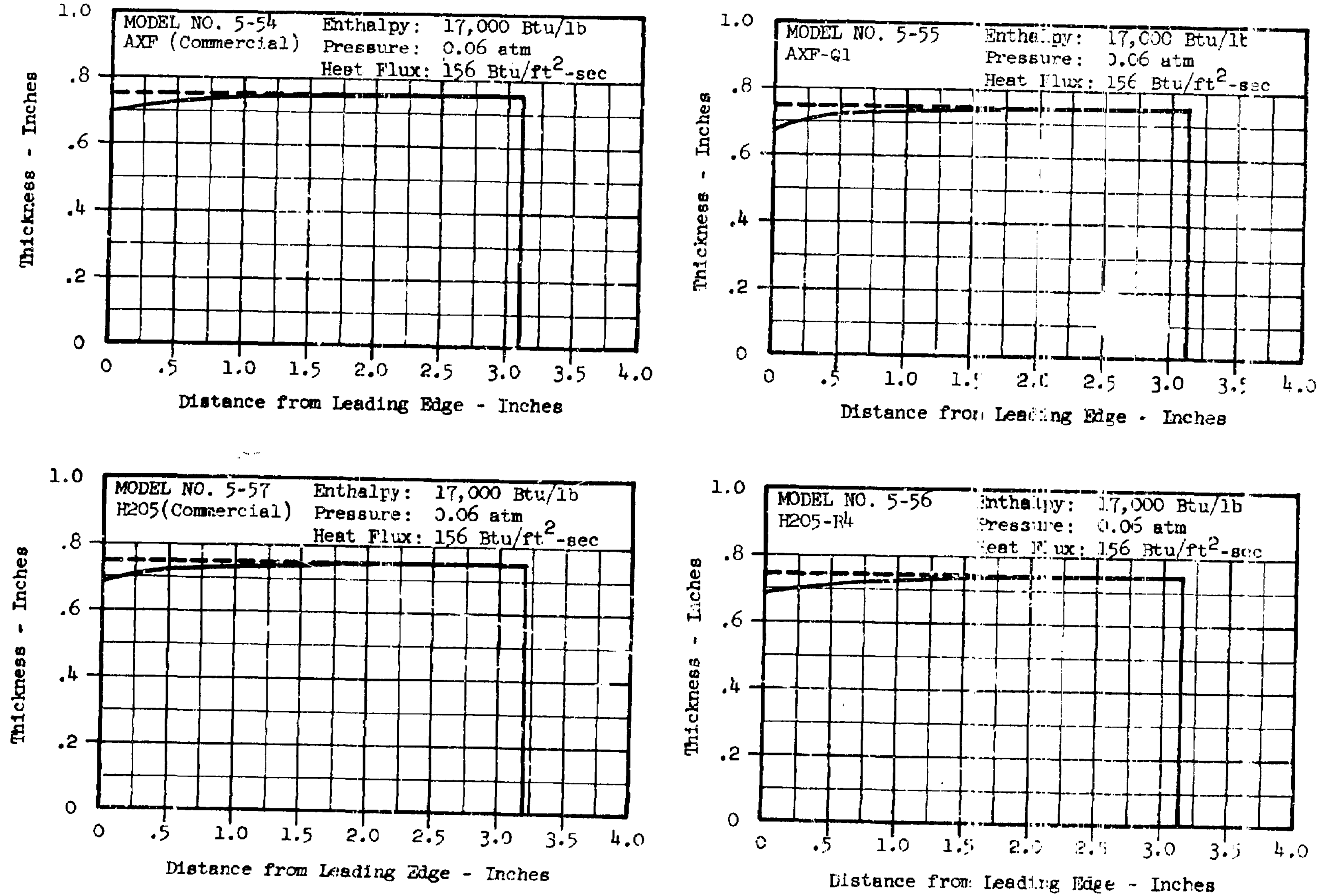

Figure 195 -- Centerline Recession Profiles, AXF Commerical (Mdl 5-54), AXF-Q1 (Mdl 5-55), H205 Commercial (Mdl 5-57), H205-R4 (Mdl 5-56)

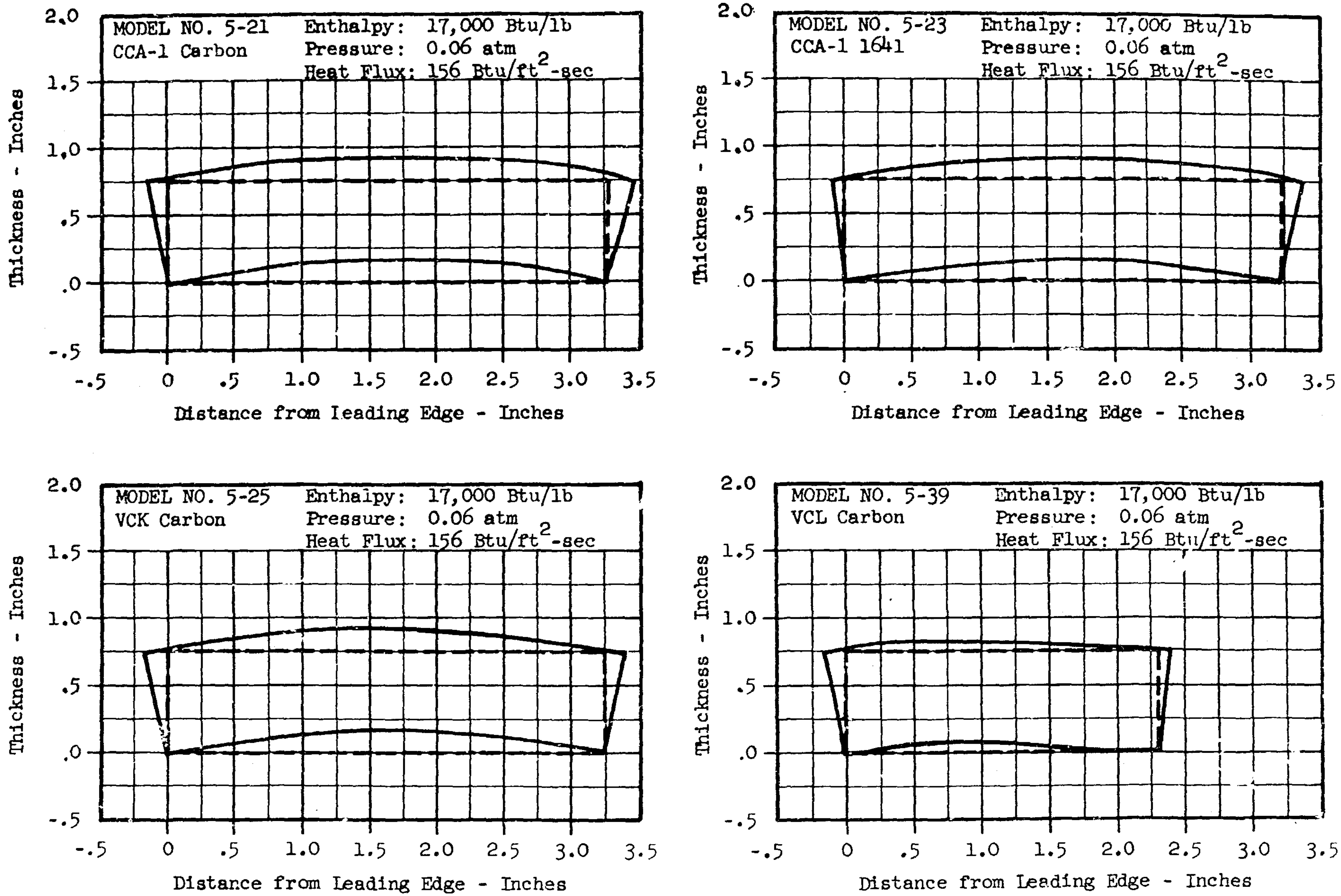

Figure 196 -- Centerline Recession Profiles, CCA-1 Carbon (Mdl 5-21), CCA-1 1641 (Mdl 5-23), VCK Carbon (Mdl 5-25), VCL Carbon (Mdl 5-39)

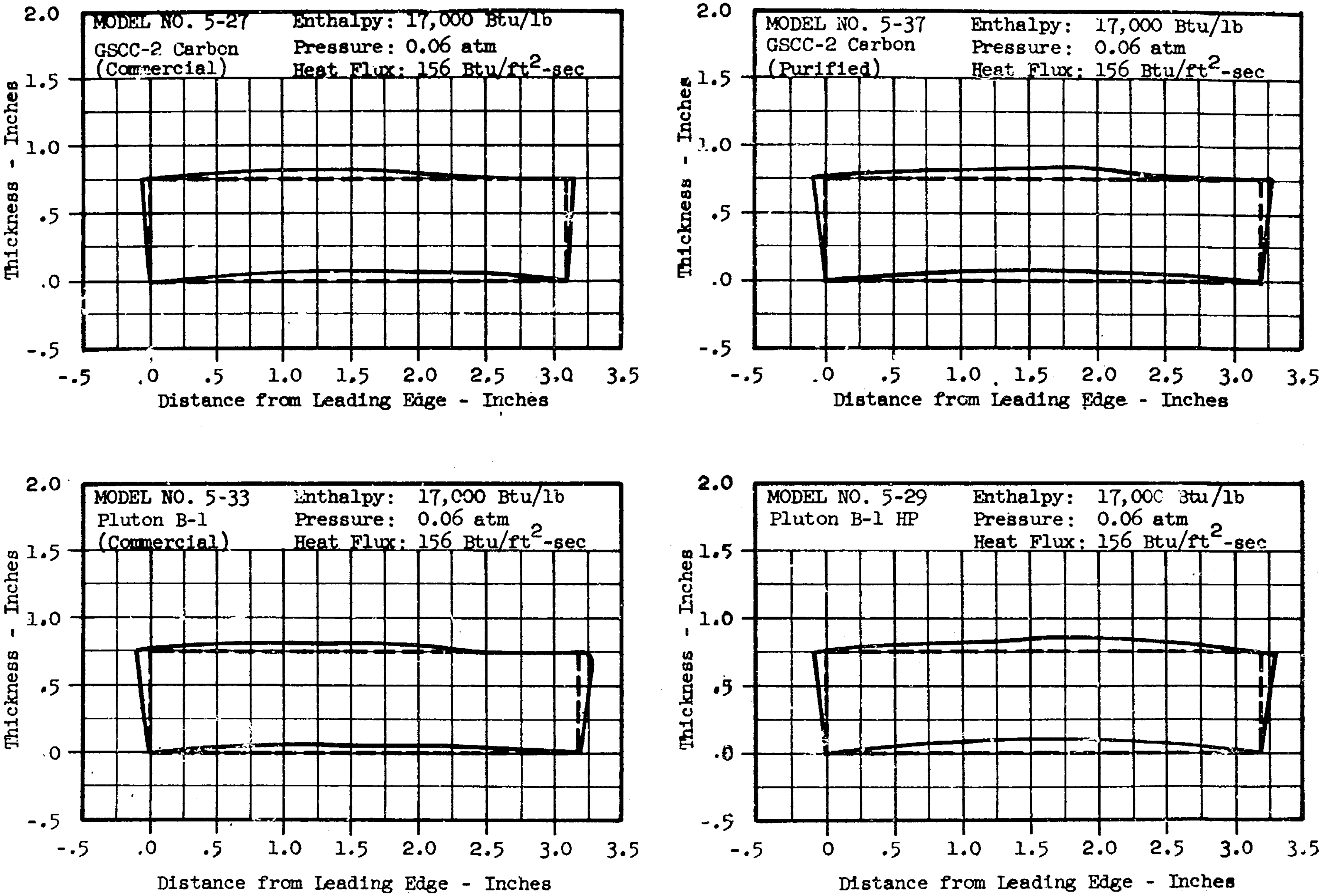

Figure 197 -- Centerline Recession Profiles, GSCC-2 Carbon Commercial (Mdl 5-27), GSCC-2 Carbon Purified (Mdl 5-37), Pluton B-1 Commercial (Mdl 5-33), and Pluton B-1 HP (Mdl 5-29)

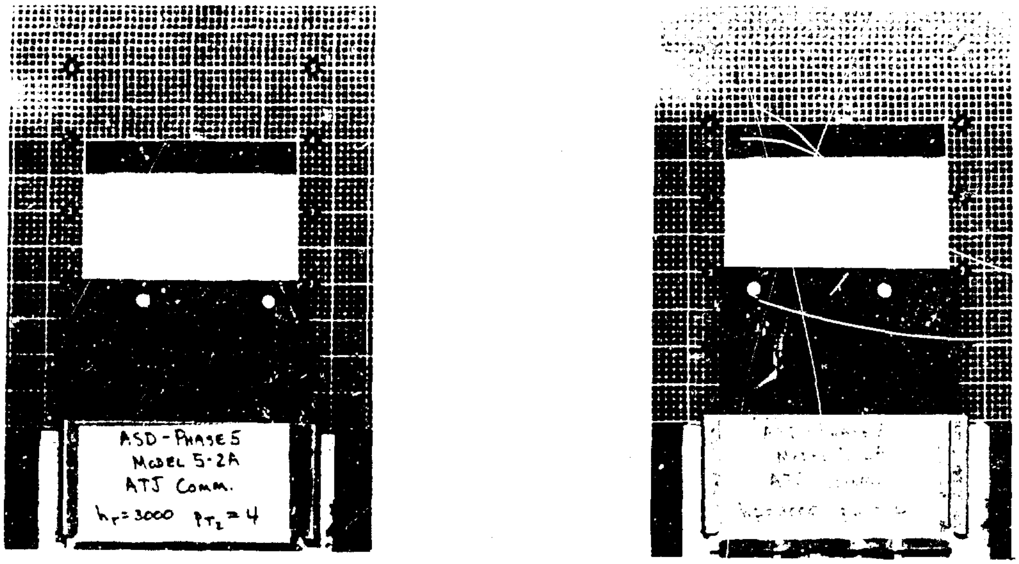

Model 5-2A - Pre- and Post-Exposure

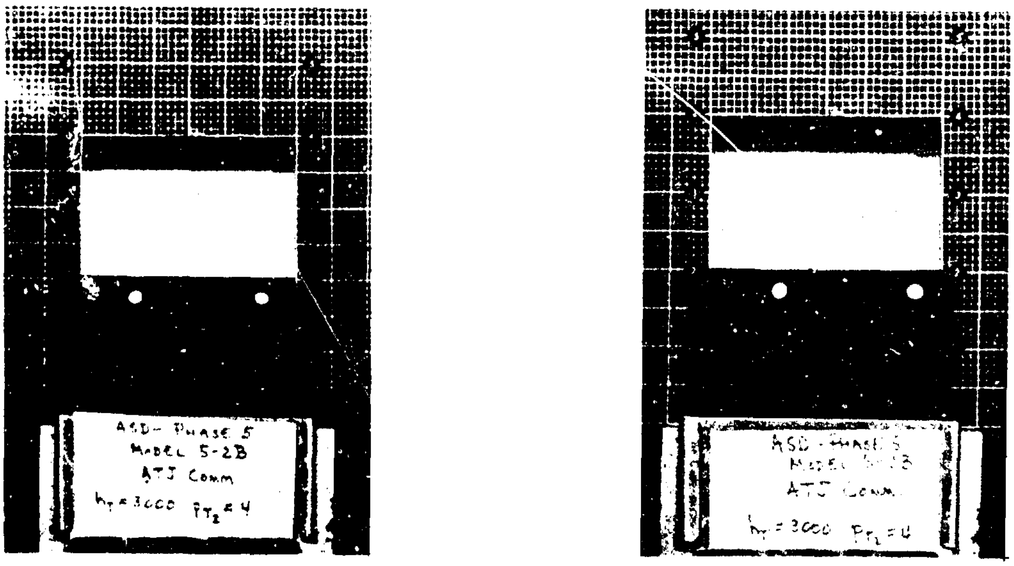

Model 5-2B - Pre- and Post-Exposure

Figure 198 -- Photographs of ATJ Commercial Graphite - Models 5-2A and 5-2B

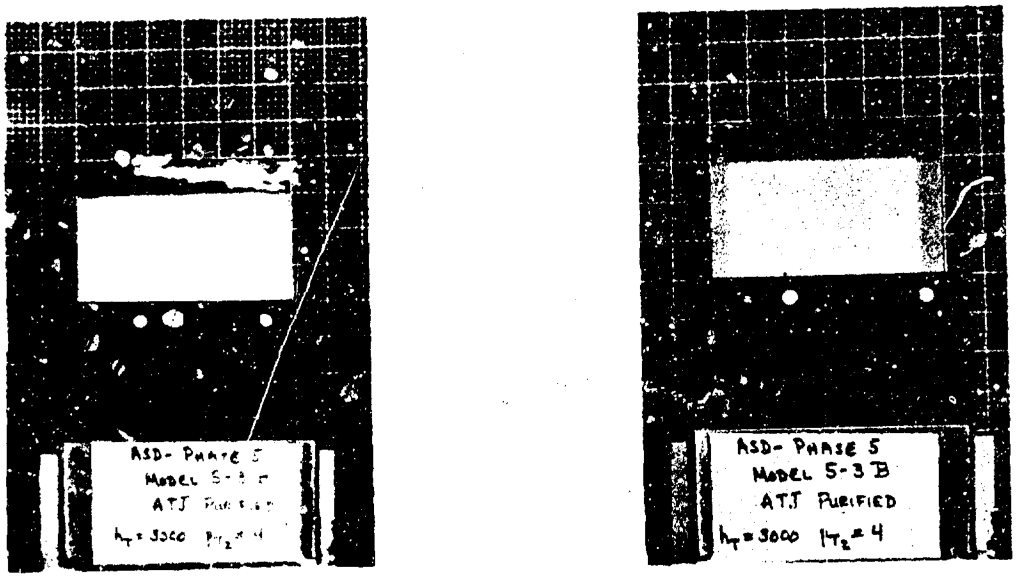

Model 5-3B - Pre- and Post-Exposure

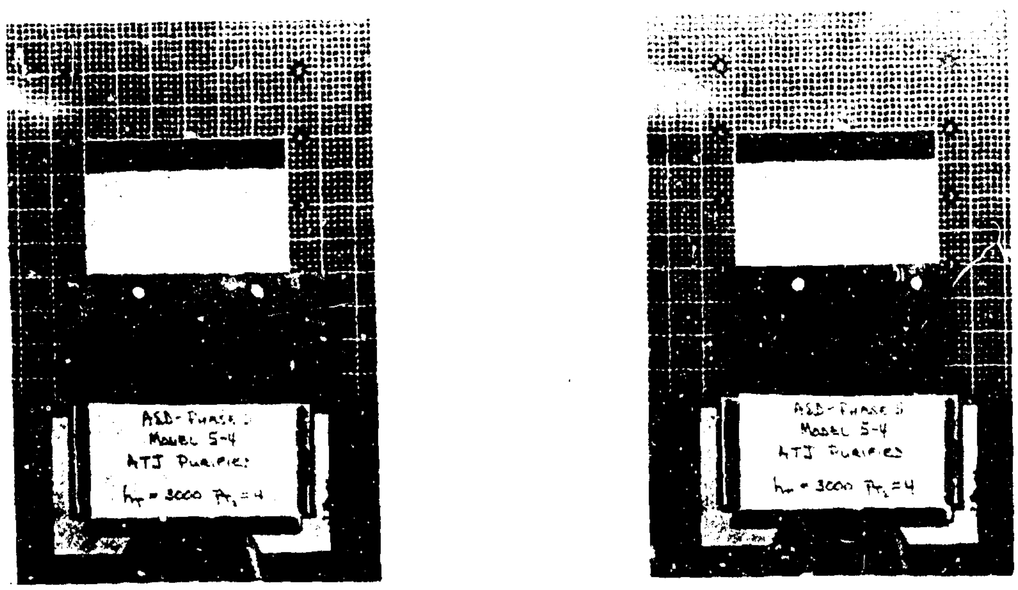

Model 5-4 - Pre- and Post-Exposure

Figure 199 -- Photographs of ATJ Purified Graphite - Models 5-3B and 5-4

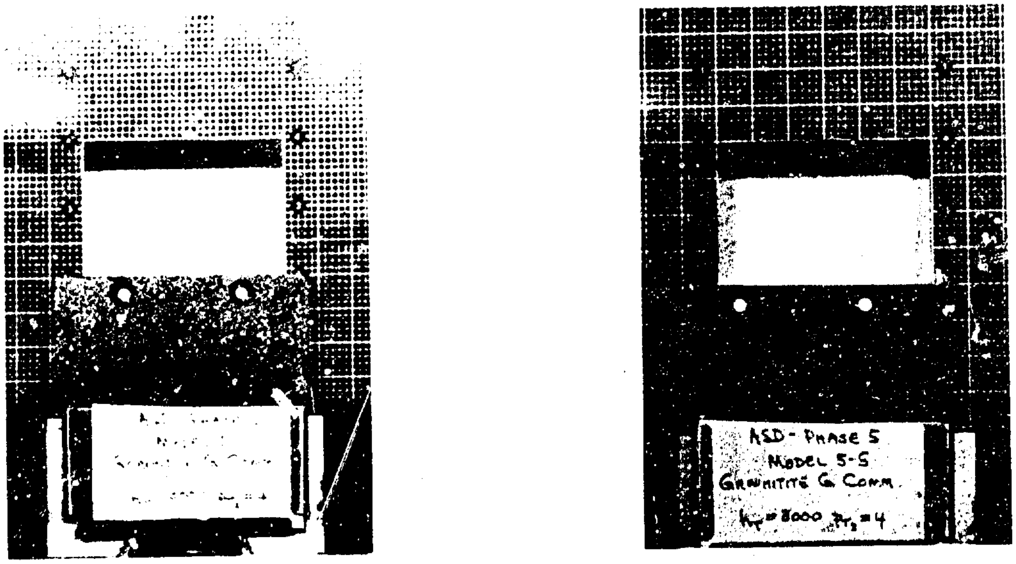

Model 5-5 - Pre- and Post-Exposure

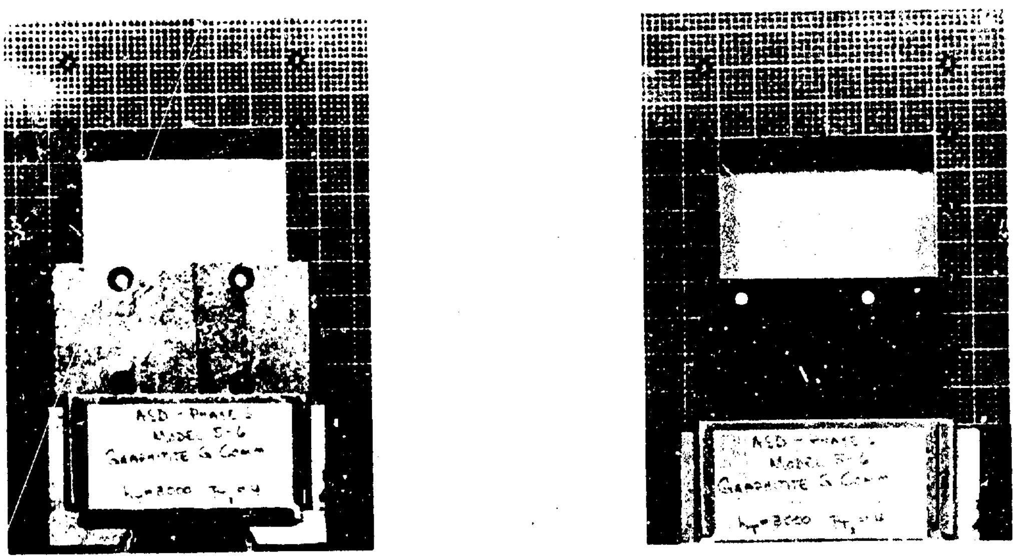

Model 5-6 - Pre- and Post-Exposure

Figure 200 -- Photographs of Graphitite G Commercial Graphite Models 5-5 and 5-6

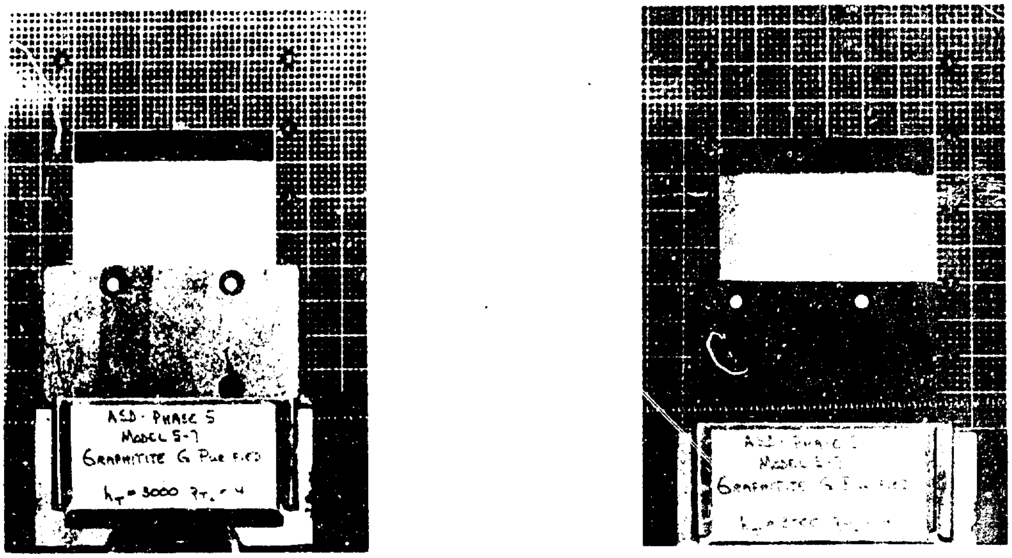

Model 5-7 - Pre- and Post-Exposure

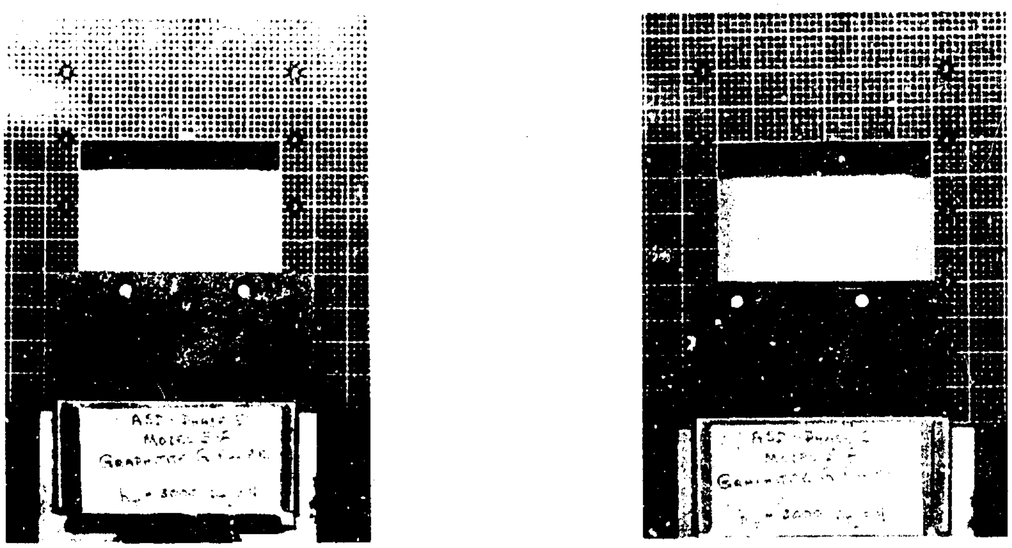

Model 5-8 - Pre- and Post-Exposure

Figure 201 -- Photographs of Graphitite G Purified Graphite Models 5-7 and 5-8

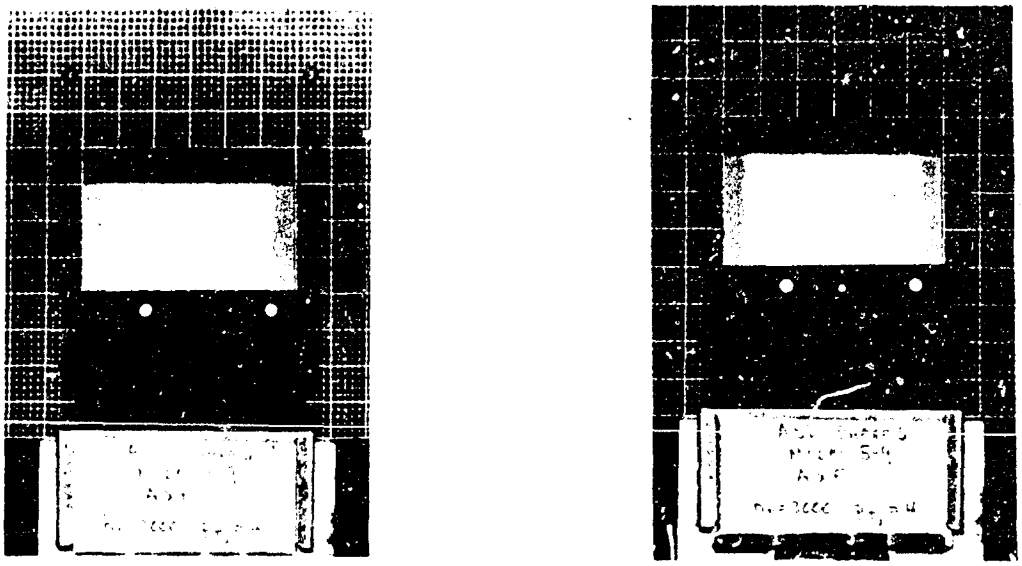

Model 5-9 - Pre- and Post-Exposure

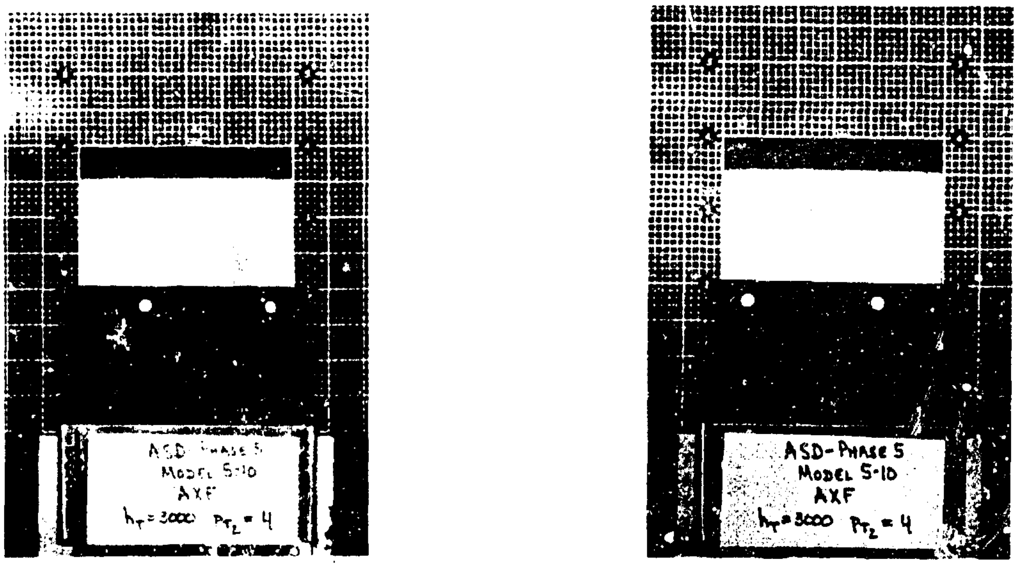

Model 5-10 - Pre- and Post-Exposure

Figure 202 -- Photographs of AXF Commercial Graphite - Models 5-9 and 5-10

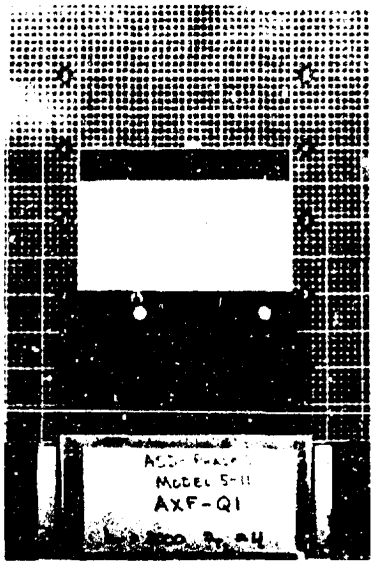

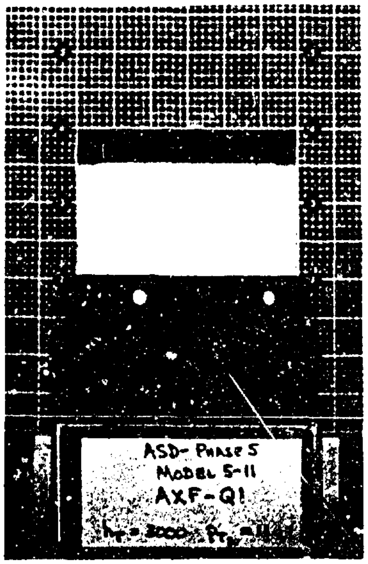

Model 5-11 - Pre- and Post-Exposure

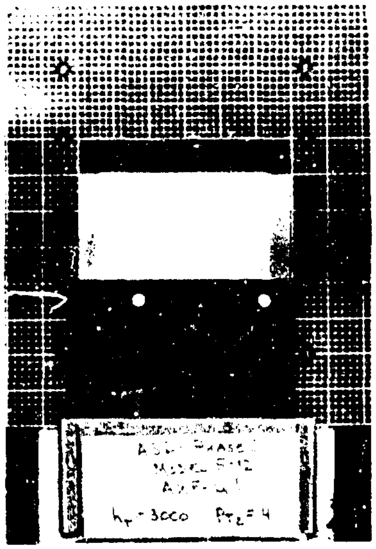
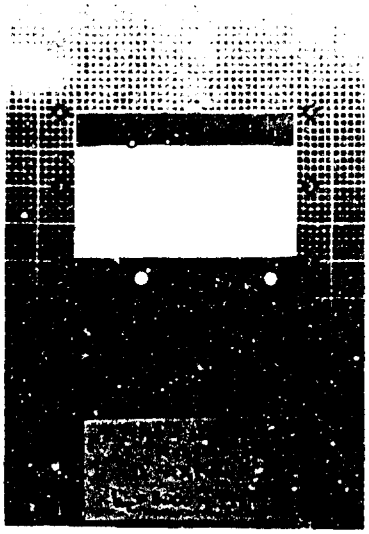

Model 5-12 - Pre- and Post-Exposure

Figure 203 -- Photographs of AXF-Q1 Purified Graphite Models 5-11 and 5-12

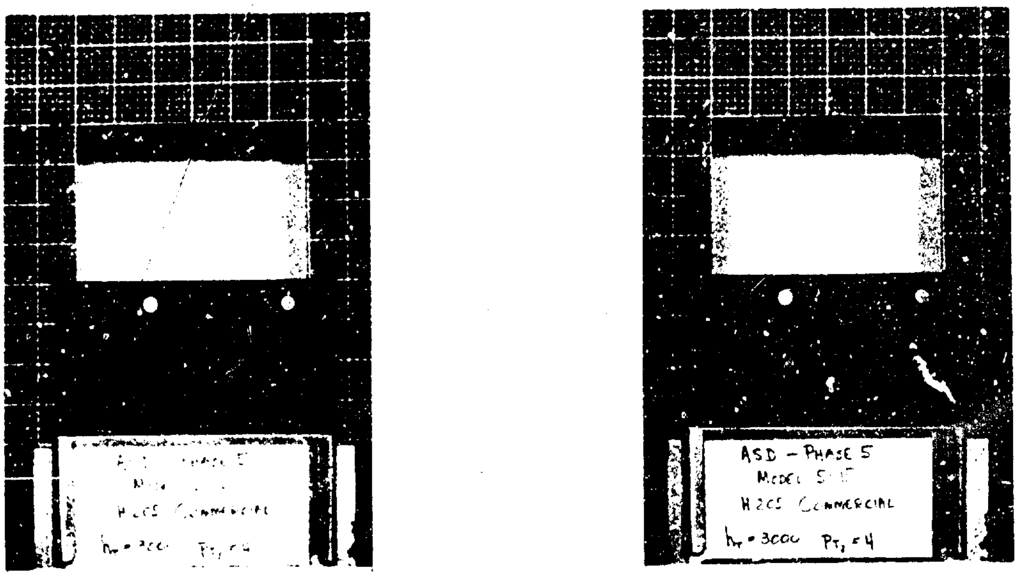

Model 5-15 - Pre- and Post-Exposure

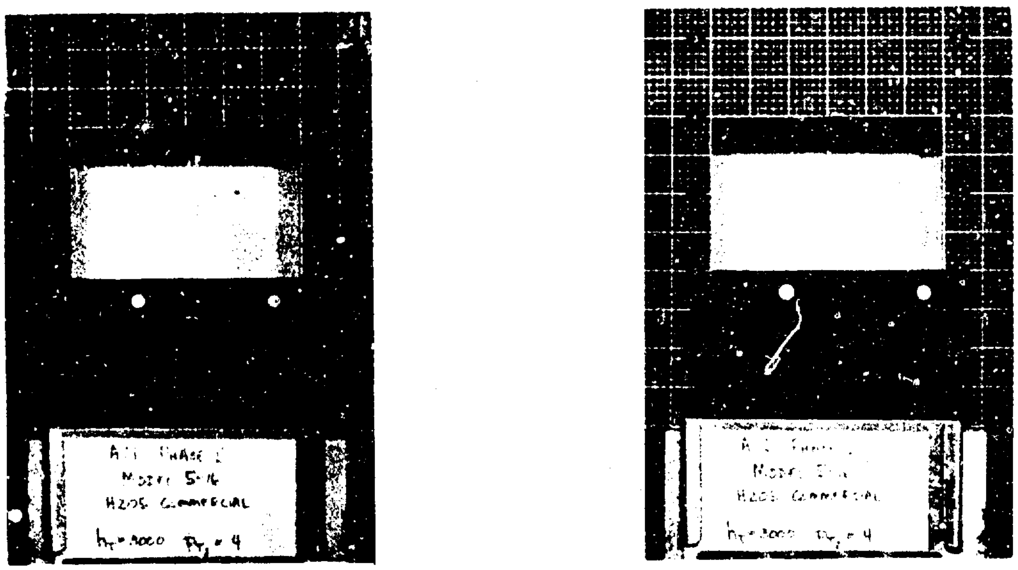

Model 5-16 - Pre- and Post-Exposure

Figure 204 -- Photographs of H205 Commercial Graphite - Models 5-15 and 5-16

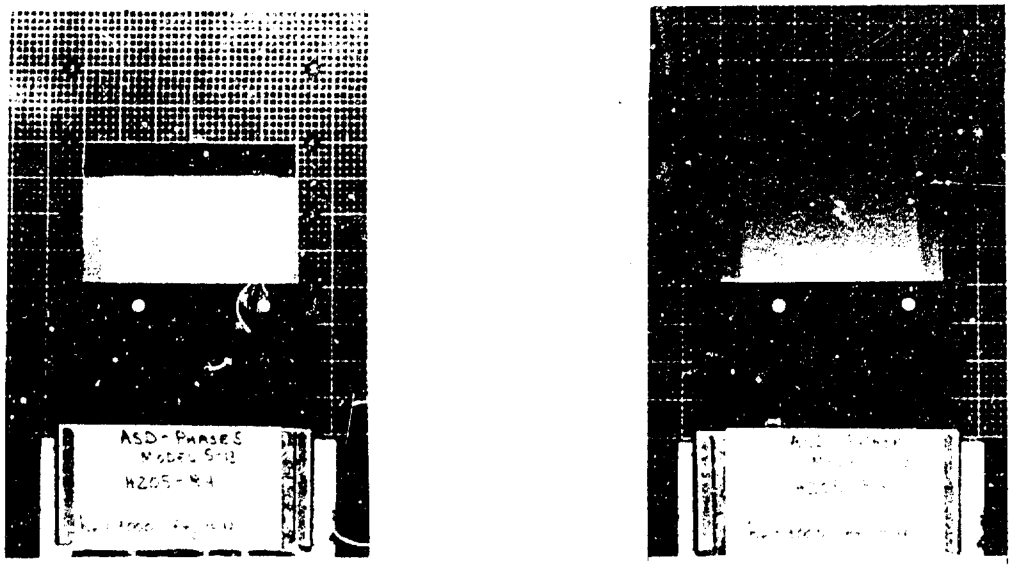

Model 5-13 - Pre- and Post-Exposure

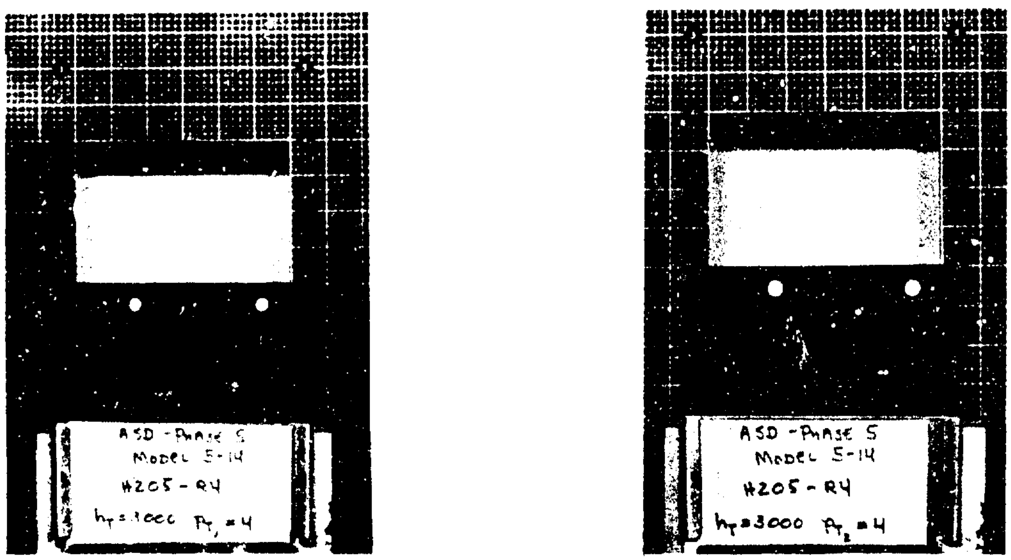

Model 5-14 - Pre- and Post-Exposure

Figure 205 -- Photographs of H205-R4 Purified Graphite Models 5-13 and 5-14

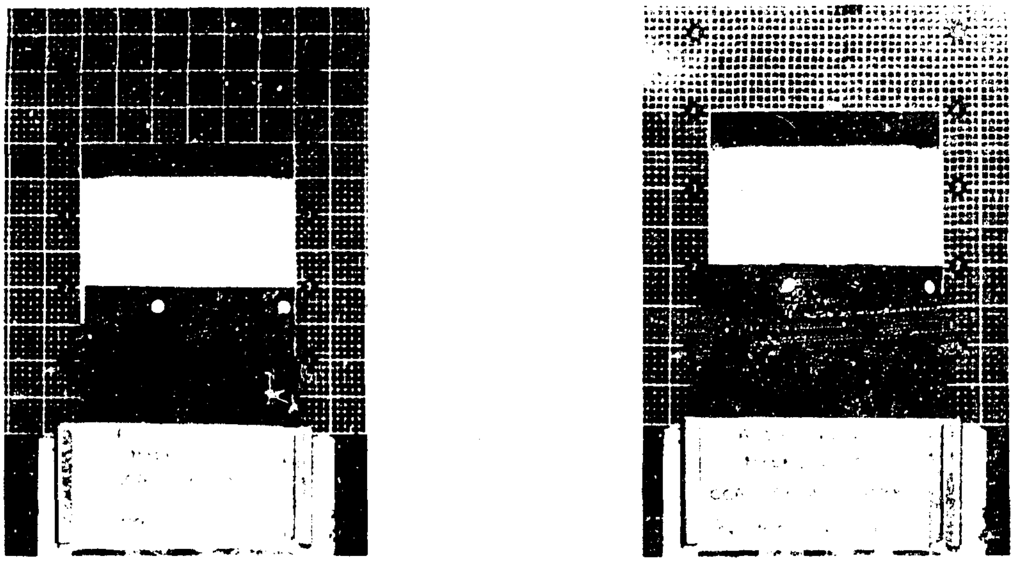

Model 5-20 - Pre- and Post-Exposures
CCA-1 Carbon

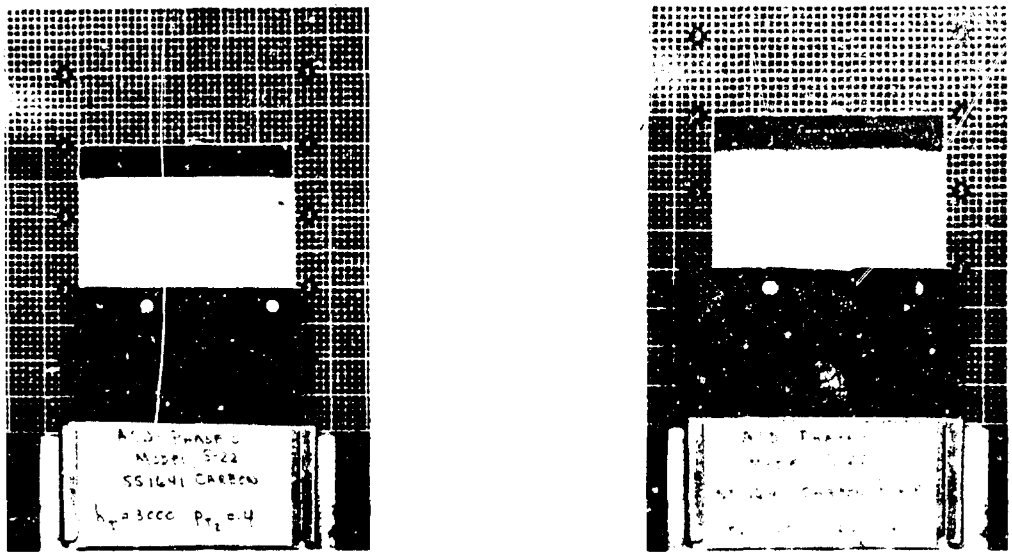

Model 5-22 - Pre- and Post-Exposures
CCA-1 1641 Carbon

Figure 206 -- Photographs of CCA-1 and CCA-1 1641 Carbon Cloth Models
Models 5-20 and 5-22

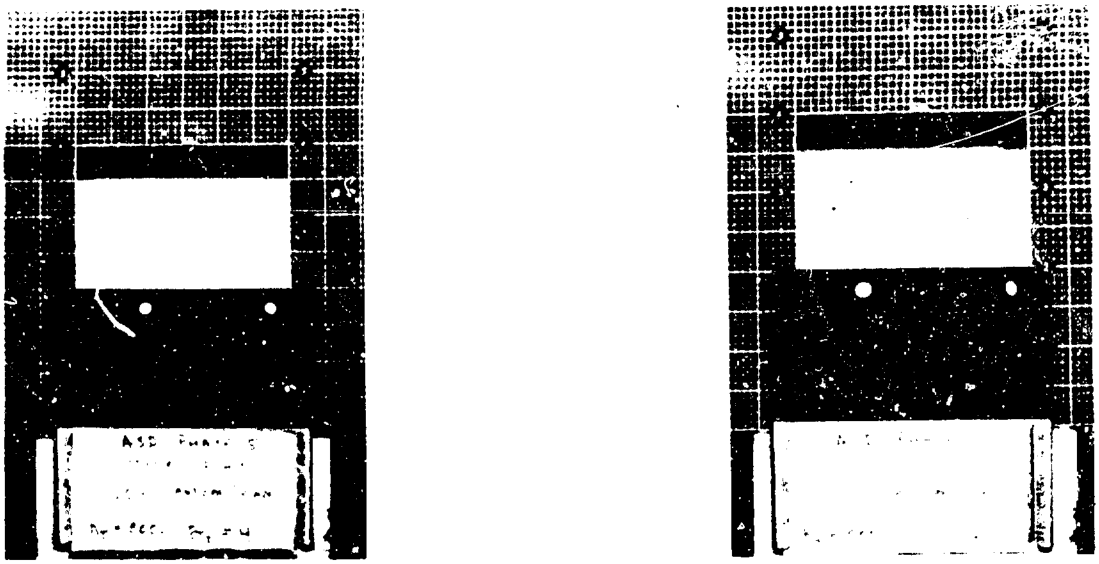

Model 5-24 - Pre- and Post-Exposures
VCK Carbon

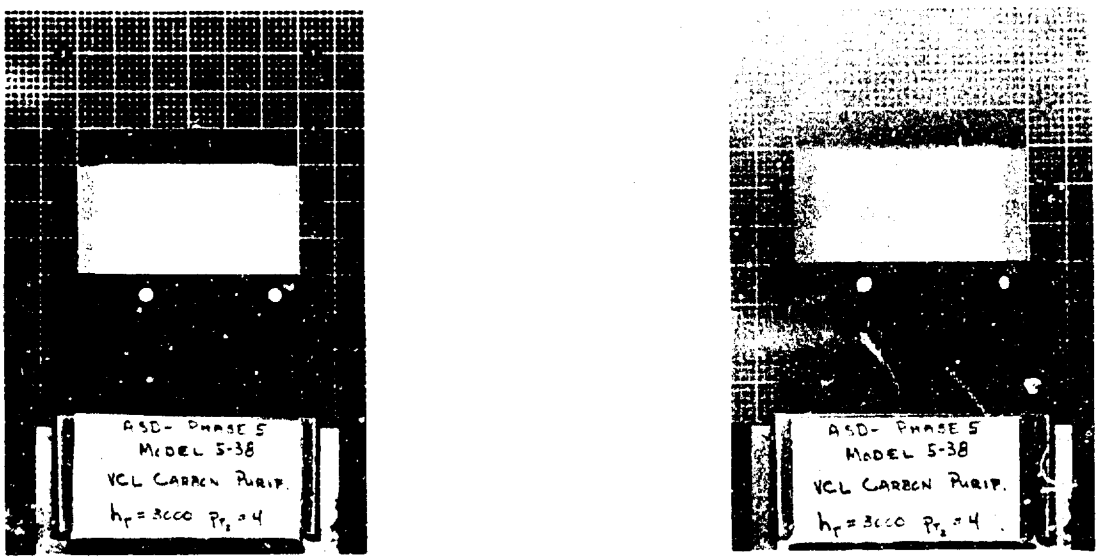

Model 5-38 - Pre- and Post-Exposures
VCL Carbon

Figure 207 -- Photographs of VCK and VCL Carbon Cloth Models
Models 5-24 and 5-38

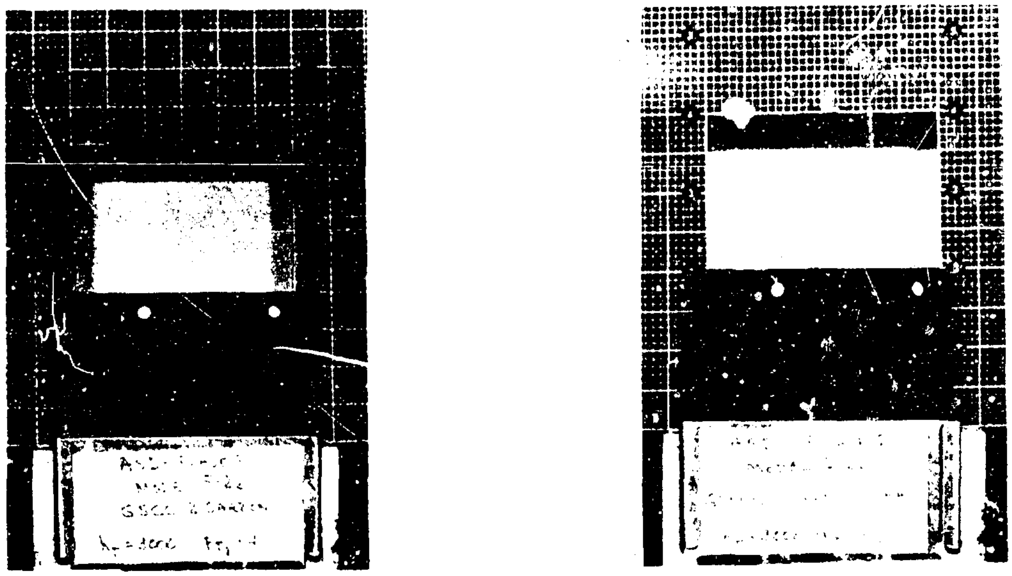

Model 5-26 - Pre- and Post-Exposures
GSCC-2 Carbon

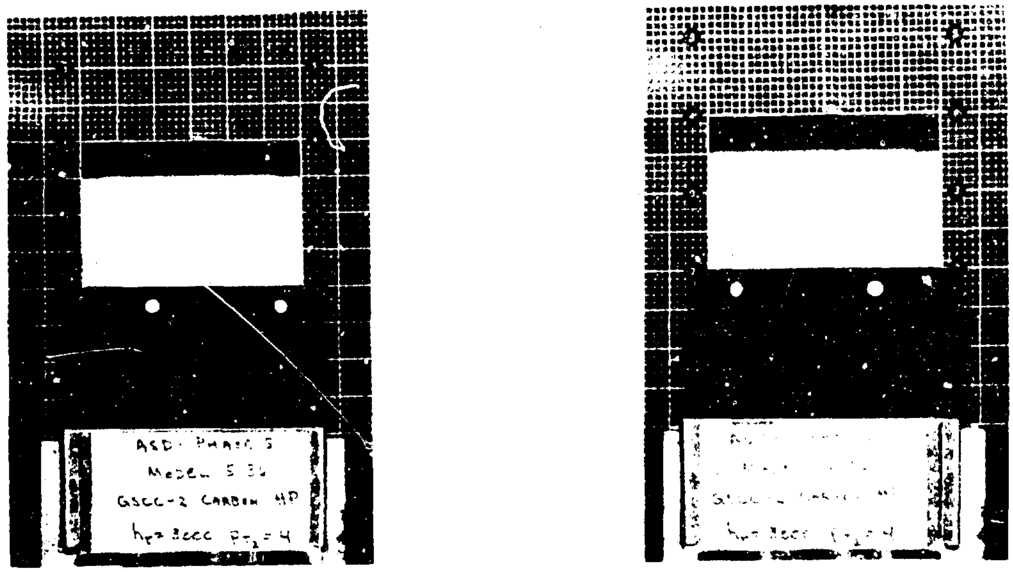

Model 5-36 - Pre- and Post-Exposures
GSCC-2 Carbon - High Purity

Figure 208 -- Photographs of GSCC-2 and GSCC-2 High Purity Carbon Cloth Models
Models 5-26 and 5-36

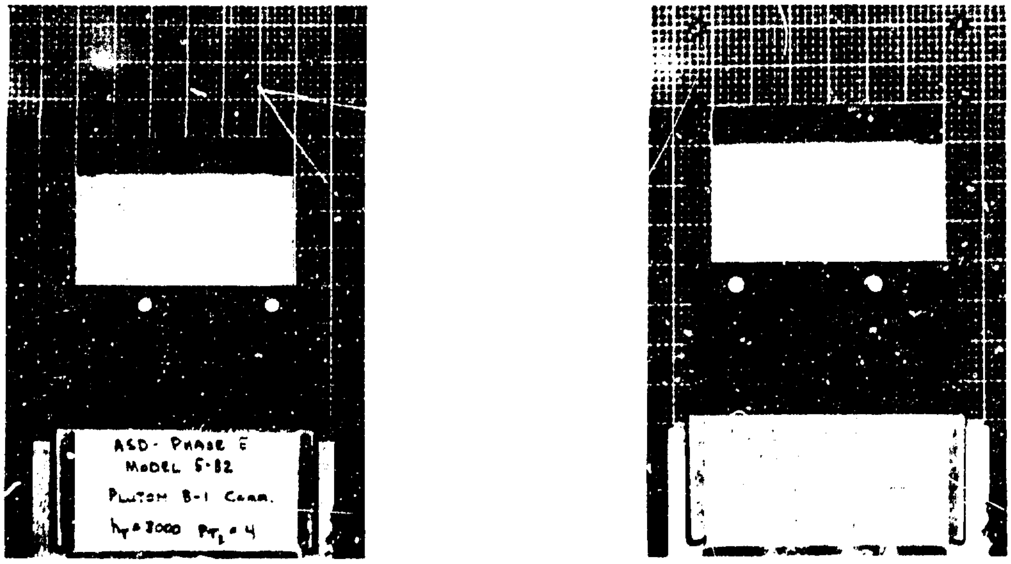

Model 5-32 - Pre- and Post-Exposure
Pluton B-1 Carbon

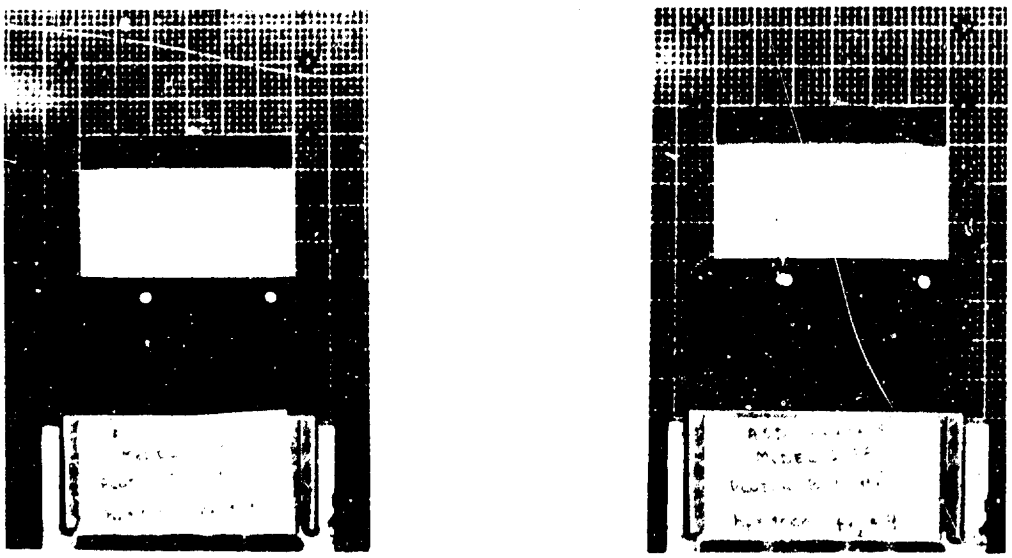

Model 5-28 - Pre- and Post-Exposure
Pluton B-1 High Purity Carbon

Figure 209 -- Photographs of Pluton B-1 and Pluton B-1 High Purity Carbon Cloth Models
Models 5-32 and 5-28

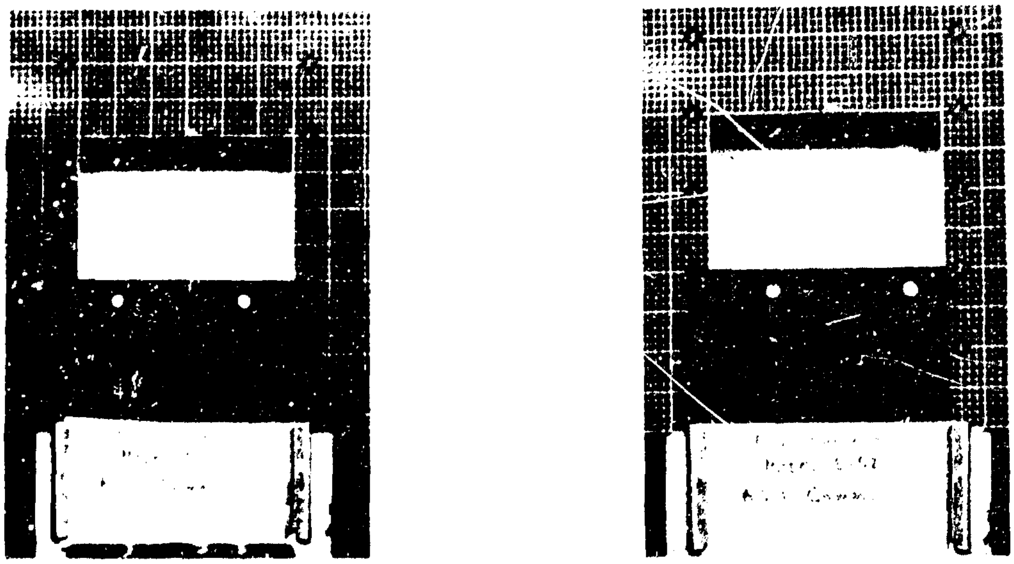

Model 5-52 - Pre- and Post-Exposure
ATJ Commercial Graphite

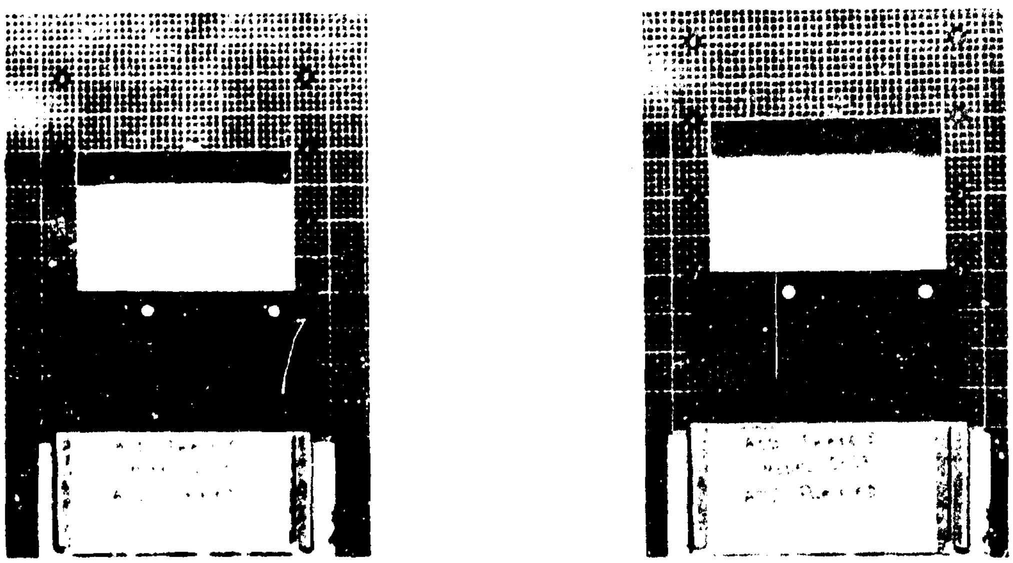

Model 5-53 - Pre- and Post-Exposure
ATJ Purified Graphite

Figure 210 -- Photographs of ATJ and ATJ Purified Graphite Models
Models 5-52 and 5-53

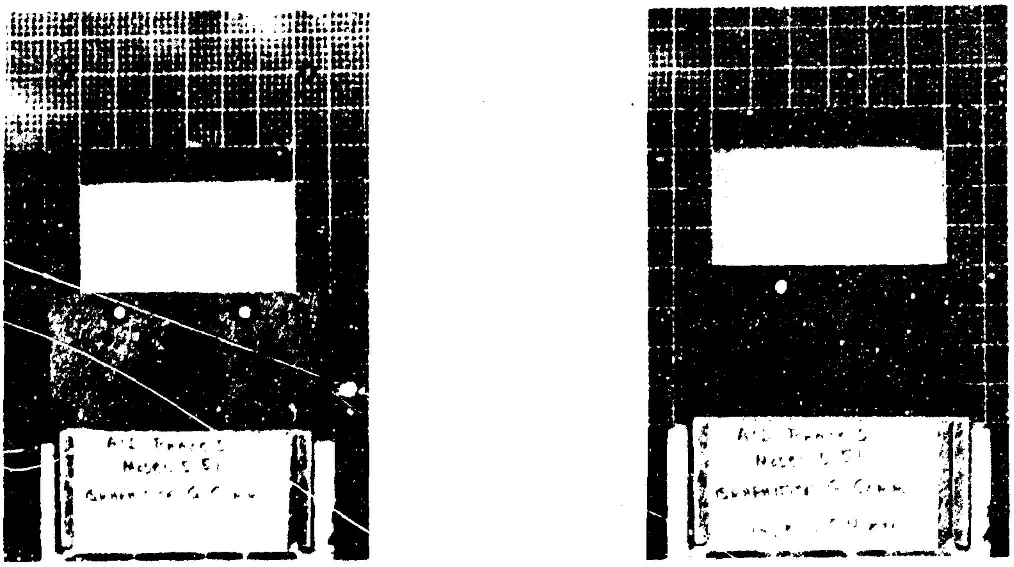

Model 5-51 - Pre- and Post-Exposure
Graphitite G Graphite

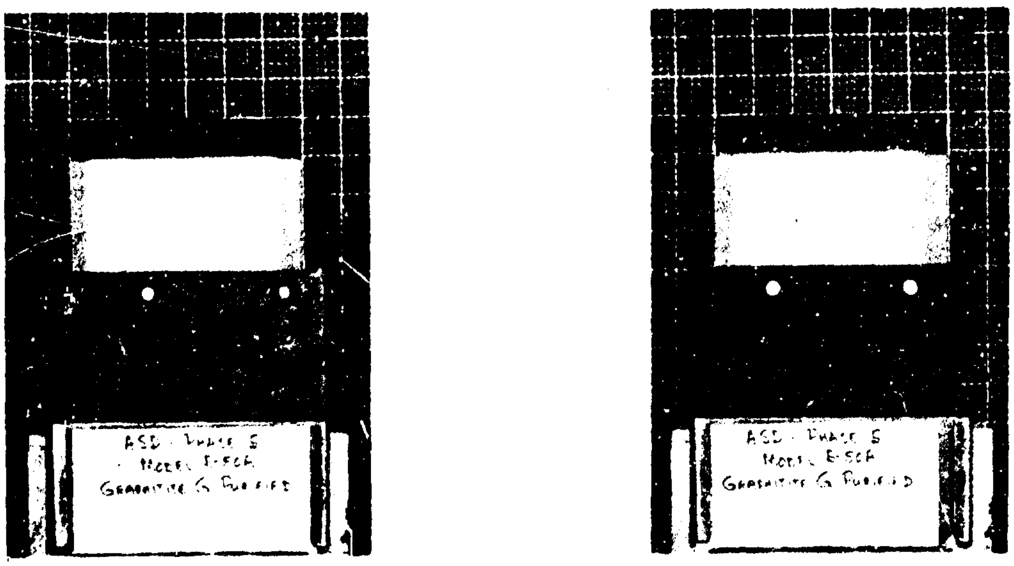

Model 5-50A - Pre- and Post-Exposure
Graphitite G Purified Graphite

Figure 211 -- Photographs of Graphitite G and Graphitite G Purified Graphite Models
Models 5-51 and 5-50A

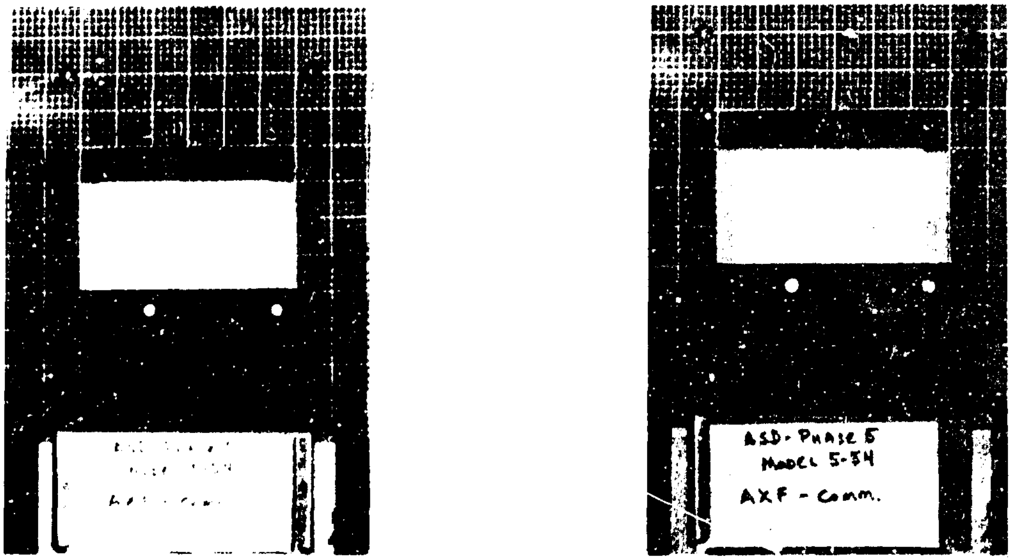

Model 5-54 - Pre- and Post-Exposure
AXF Graphite

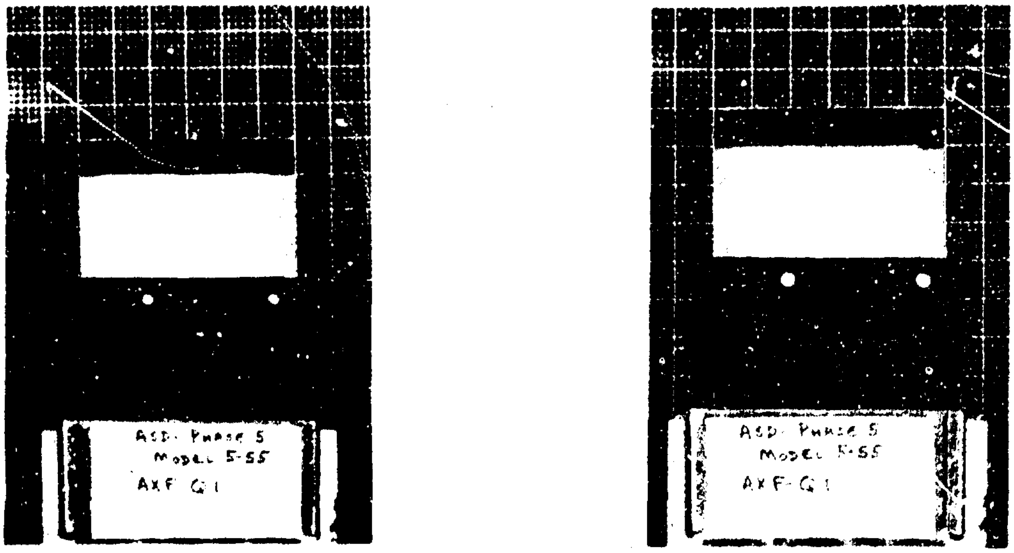

Model 5-55 - Pre- and Post-Exposure
AXF-Q1 Purified Graphite

Figure 212 -- Photographs of AXF and AXF-Q1 Purified Graphite Models
Models 5-54 and 5-55

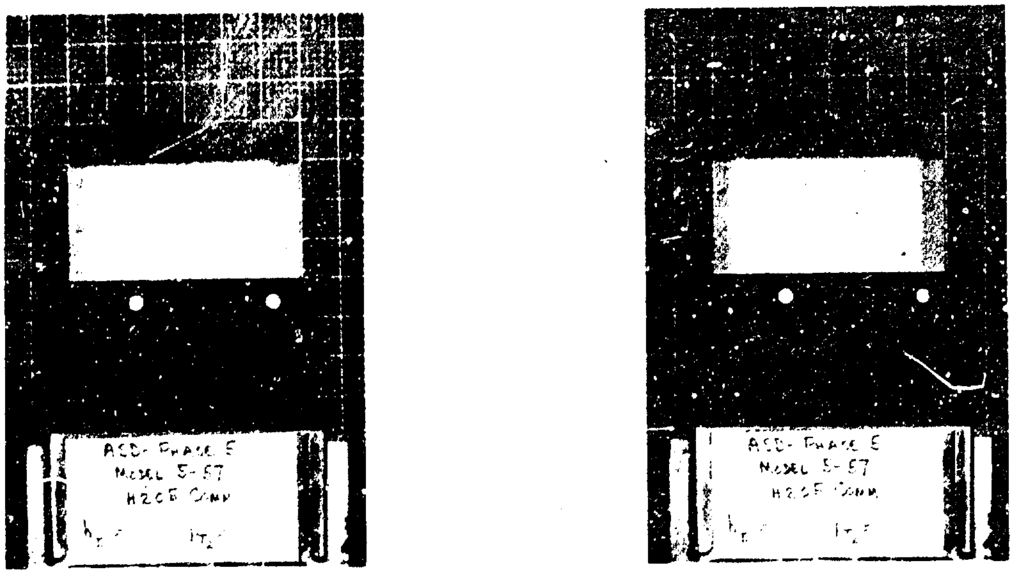

Model 5-57 - Pre- and Post-Exposure
H205 Graphite

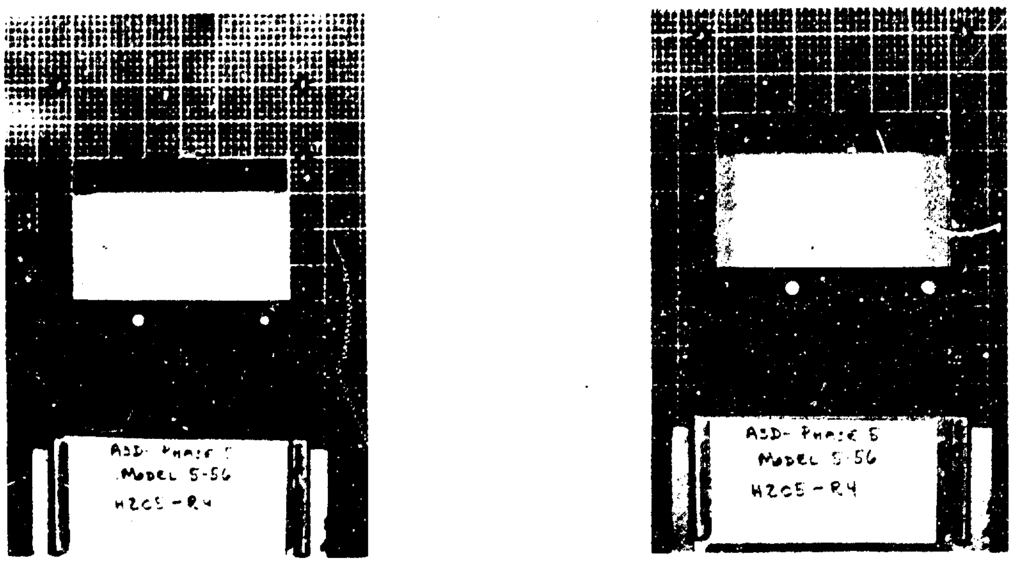

Model 5-56 - Pre- and Post-Exposure
H205-R4 Purified Graphite

Figure 213 -- Photographs of H205 and H205-R4 Purified Graphite Models
Models 5-57 and 5-56

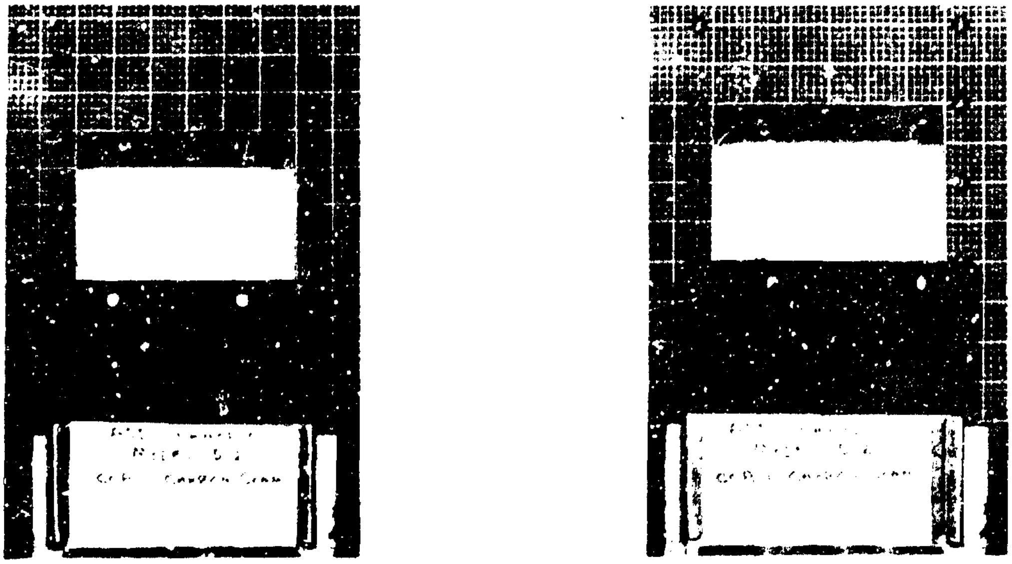

Model 5-21 - Pre- and Post-Exposure
CCA-1 Carbon

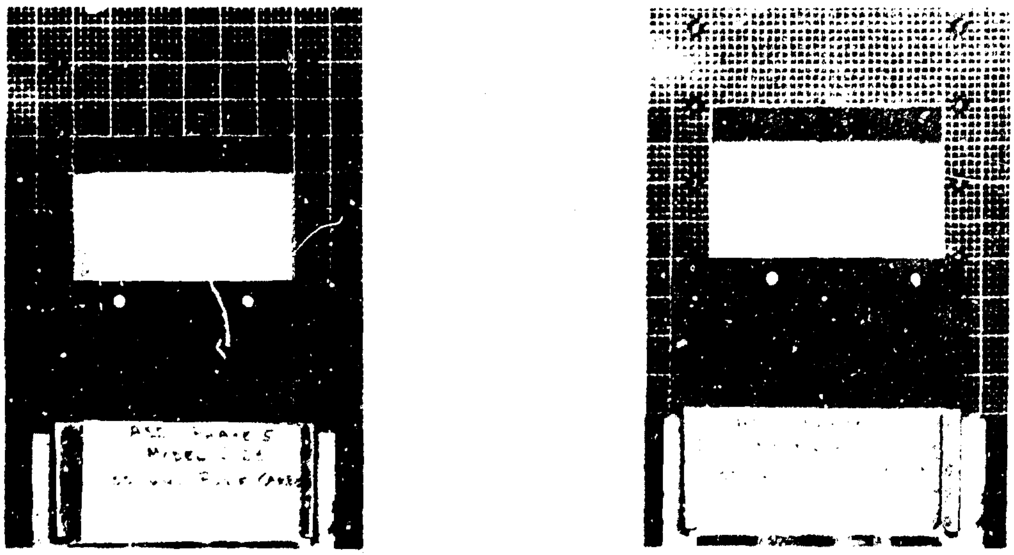

Model 5-23 - Pre- and Post-Exposure
CCA-1 1641 Purified Carbon

Figure 214 -- Photographs of CCA-1 and CCA-1 1641 Purified Carbon Cloth Models
Models 5-21 and 5-23

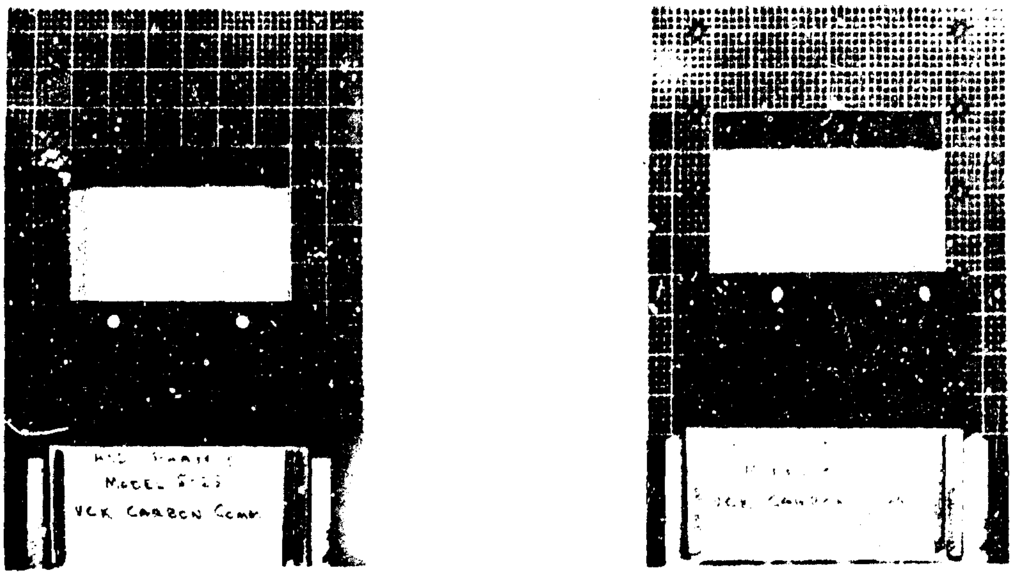

Model 5-25 - Pre- and Post-Exposure
VCK Carbon

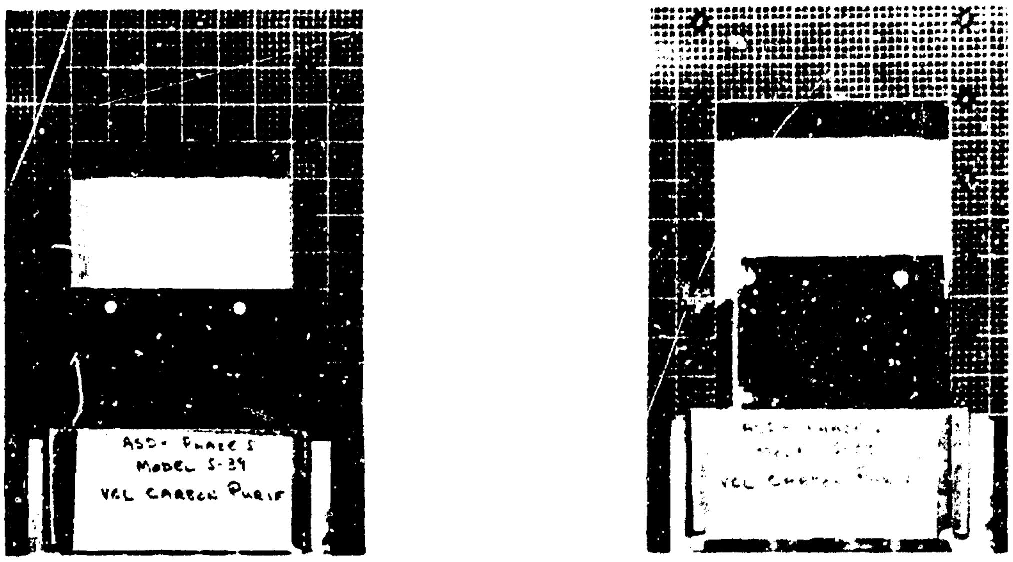

Model 5-39 - Pre- and Post-Exposure
VCL Carbon Purified

Figure 215 -- Photographs of VCK and VCL Purified Carbon Cloth Models
Models 5-25 and 5-39

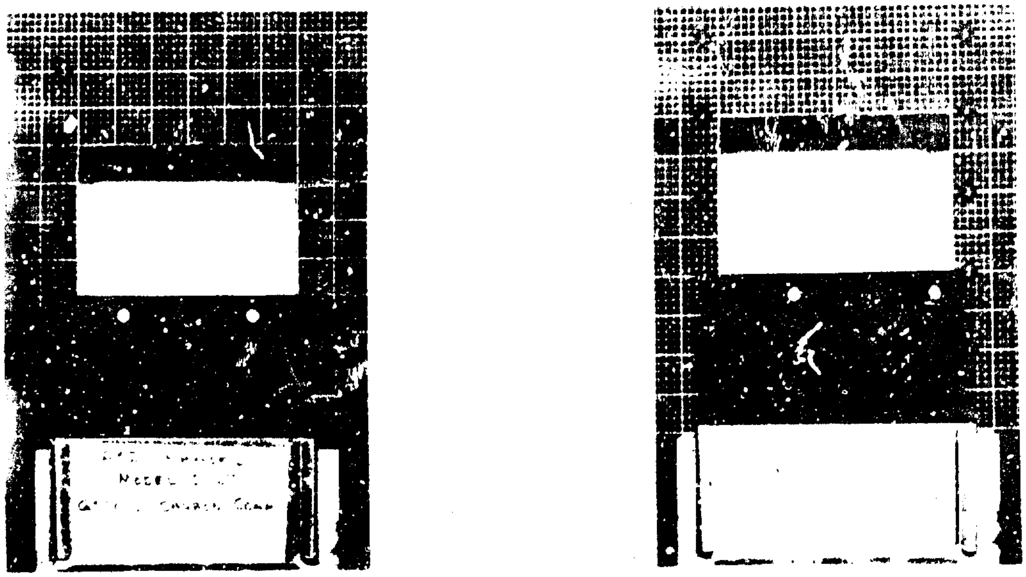

Model 5-27 - Pre- and Post-Exposure
GSCC-2 Carbon

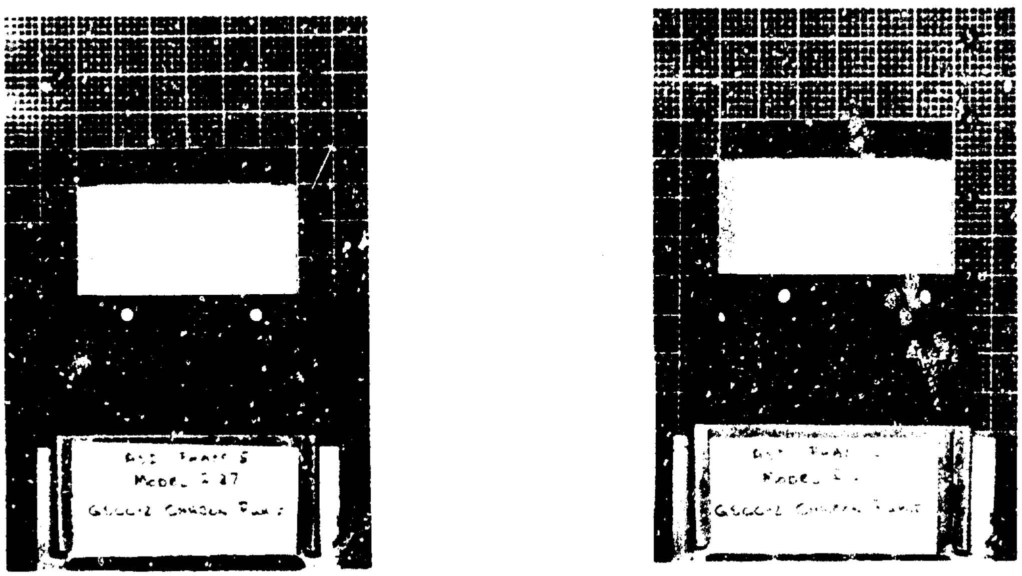

Model 5-37 - Pre- and Post-Exposure
GSCC-2 Purified Carbon

Figure 216 -- Photographs of GSCC-2 and GSCC-2 Purified Carbon Cloth Models
Models 5-27 and 5-37

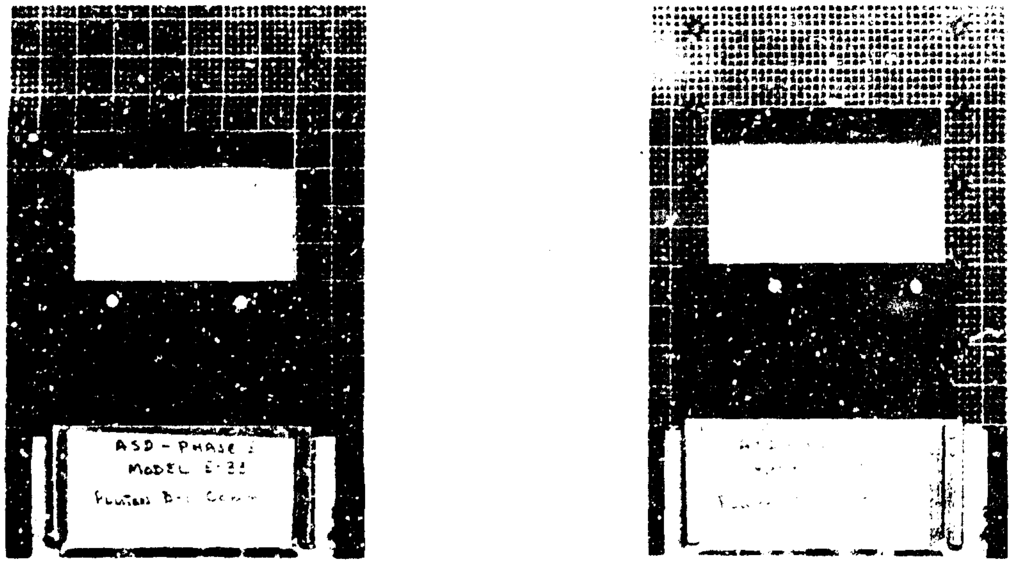

Model 5-33 - Pre- and Post-Exposure
Pluton B-1 Carbon

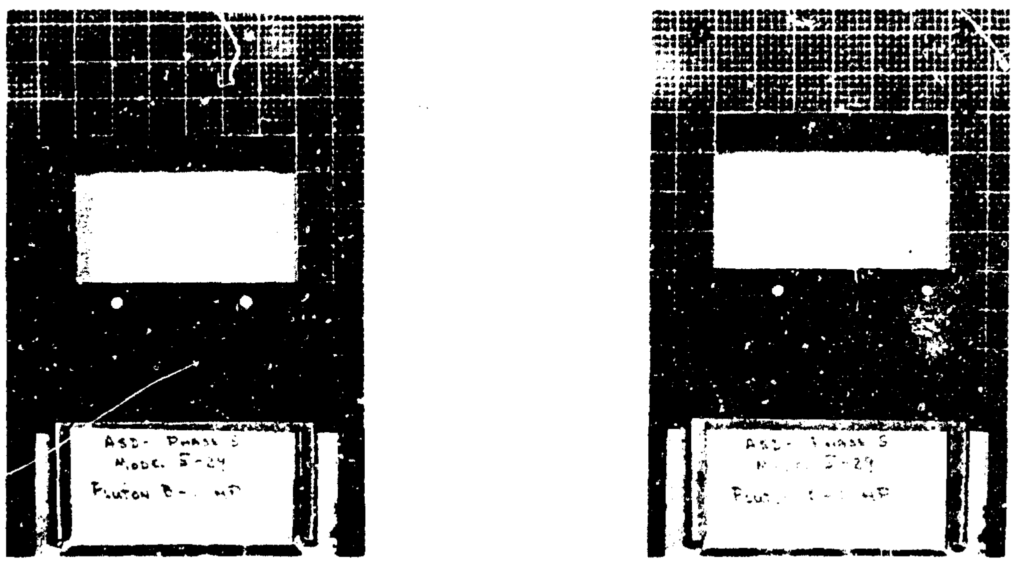

Model 5-29 - Pre- and Post-Exposure
Pluton B-1 Purified Carbon

Figure 217 -- Photographs of Pluton B-1 and Pluton B-1 Purified Carbon Cloth Models
Models 5-33 and 5-29

7.0 CHAR LAYER PROGRAM

In conjunction with The Boeing Company, phenolic-carbon models were exposed to a high enthalpy/low pressure plasma environment for the purpose of attaining uniform char layers $\frac{1}{4}$-inch to $\frac{1}{2}$-inch in depth for detailed analysis of the char layer properties by Boeing personnel. Transient heating conditions from 90 to 500 Btu/ft^2-sec at enthalpy levels from 8,800 to 16,200 Btu/lb were used to achieve charring of the phenolic-carbon models.

7.1 Objectives

The primary objective of this program was to provide a hyperthermal environment which would produce char layers on phenolic-carbon models of $\frac{1}{4}$-inch to $\frac{1}{2}$-inch in depth. Furthermore, the char layers were to be produced under transient conditions in which the enthalpy and model stagnation pressure were varied in such a manner as to achieve a minimum heating rate of 90 Btu/ft^2-sec and a maximum heating rate of 500 Btu/ft^2-sec.

7.2 Description of Test Program

The phenolic-carbon models were fabricated by Aerospace Corporation into 2.00-inch diameter flat-face cylinders, in accordance with the model design sketched in Figure 218. Instrumentation, consisting of a single chromel/alumel thermocouple located along the centerline of the model and at a distance of 0.750 inches from the stagnation point, was installed by Space-General personnel. The specific materials used for the models were HITCO's CCA-1 carbon cloth and 91LD phenolic resin. Lay-up of the material fabric was perpendicular to the direction of heat flow for the purpose of performing char analysis of each individual layer.

Transient test conditions were achieved with the high enthalpy/low pressure plasma arc generator and a Mach 3 contoured nozzle, three inches in exit diameter. The test conditions were:

Exposure Time	Model Stagnation Heat Flux	Gas Stagnation Enthalpy	Model Stagnation Pressure
0 to 5 secs.	93 Btu/ft^{2}sec	8,800 Btu/lb	0.019 atms.
5 to 35 secs.	Increased Power Linearly to Maximum Heat Flux		
35 to 60 secs.	495 Btu/ft^{2}sec	16,200 Btu/lb	0.101 atms.

A total of seven models were exposed to the above environmental conditions; calibration data for each model test is tabulated in Table 23. Weight loss rates, surface temperatures, and internal temperature at the end of the exposure period are tabulated in Table 24. Internal temperature histories are graphed in Figures 219 through 222. External views of the exposed models are presented in the photographs in Figures 223 and 224. Due to the laminated lay-up of the material, most of the models delaminated upon exposure to the heated environment. Also, there is evidence as seen in the photographs, that the exposed frontal face of some of the models formed a bubble caused by air pockets under the delaminated layers of material. The exposed models were forwarded to Boeing for analysis of the char layer.

SPACE-GENERAL CORPORATION

TABLE 23

CALIBRATION DATA

Phenolic-Carbon Char Models

Model Number	Exposure Time (seconds)	Model Stag. Heat Flux (Btu/ft2-sec)	Gas Enthalpy (Btu/lb)	Model Stag. Pressure (atm)	Nozzle Stag. Pressure (atm)	Nozzle Static Pressure (atm)	Gas Flow Rate (lb/sec)
6-19	0 to 5	93.5	8,885	0.019	0.1038	0.00139	0.004581
	5 to 35		Linear Increase to Conditions at 35 seconds				
	35 to 60	493.5	16,180	0.101	0.5832	0.00936	0.019090
6-20	0 to 5	94.3	8,790	0.019	0.1036	0.00130	0.004581
	5 to 35		Linear Increase to Conditions at 35 seconds				
	35 to 60	494.5	16,205	0.101	0.5830	0.00938	0.019090
6-21	0 to 5	92.8	8,700	0.019	0.1036	0.00130	0.004581
	5 to 35		Linear Increase to Conditions at 35 seconds				
	35 to 60	495.6	16,255	0.101	0.5834	0.00937	0.019090
6-22	0 to 5	92.5	8,715	0.019	0.1035	0.00130	0.004581
	5 to 35		Linear Increase to Conditions at 35 seconds				
	35 to 60	491.8	16,210	0.101	0.5835	0.00938	0.019090
6-23	0 to 5	94.2	8,810	0.019	0.1036	0.00138	0.004581
	5 to 35		Linear Increase to Conditions at 35 seconds				
	35 to 60	495.5	16,340	0.101	0.5837	0.00939	0.019090
6-24	0 to 5	93.1	8,790	0.019	0.1035	0.00138	0.004581
	5 to 35		Linear Increase to Conditions at 35 seconds				
	35 to 60	494.5	16,245	0.101	0.5836	0.00937	0.019090
6-25	0 to 5	93.6	8,815	0.019	0.1036	0.00131	0.004581
	5 to 35		Linear Increase to Conditions at 35 seconds				
	35 to 60	493.4	16,240	0.101	0.5837	0.00939	0.019090

SPACE-GENERAL CORPORATION

TABLE 24

MODEL TEST DATA

Phenolic-Carbon Char Models

Model Number	Exposure Time (seconds)	Weight Loss (grams)	Weight Loss Rate (grams/sec)	Surface Temperature at end of run - 60 secs. (^oF)	Temp. at x = .750" at end of run-60 secs. (^oF)
6-19	60.0	13.5	0.2254	4850	79
6-20	60.0	13.8	0.2300	4820	79
6-21	60.0	13.5	0.2254	4820	87
6-22	60.0	13.2	0.2200	4820	96
6-23	60.0	13.8	0.2300	4820	70
6-24	60.0	13.6	0.2267	4820	81
6-25	60.0	13.8	0.2300	4820	70

MODEL DESIGN FOR CHAR LAYER PROGRAM

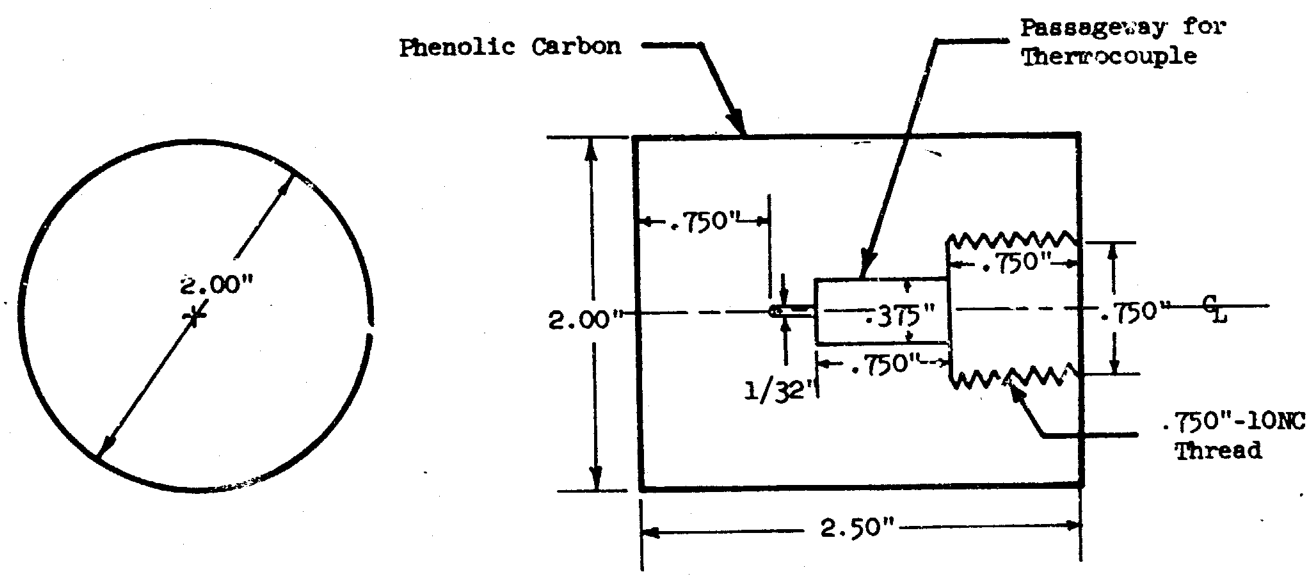

Figure 218 -- Model Design for Char Layer Program

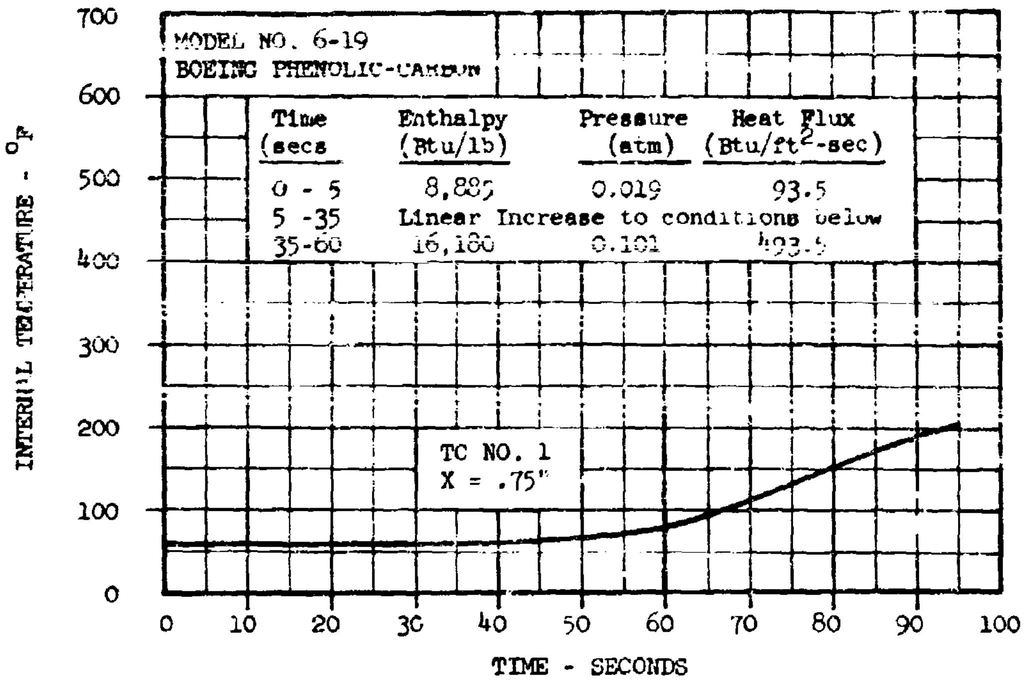

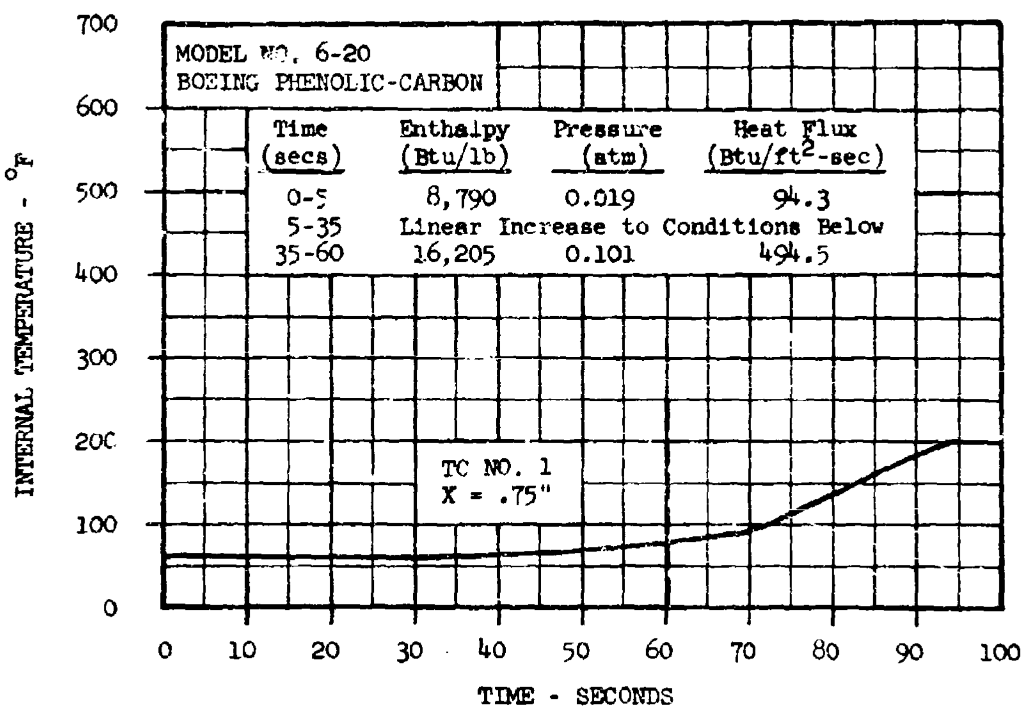

Figure 219 -- Boeing Phenolic-Carbon, Models 6-19 & 6-20 Temperature Histories

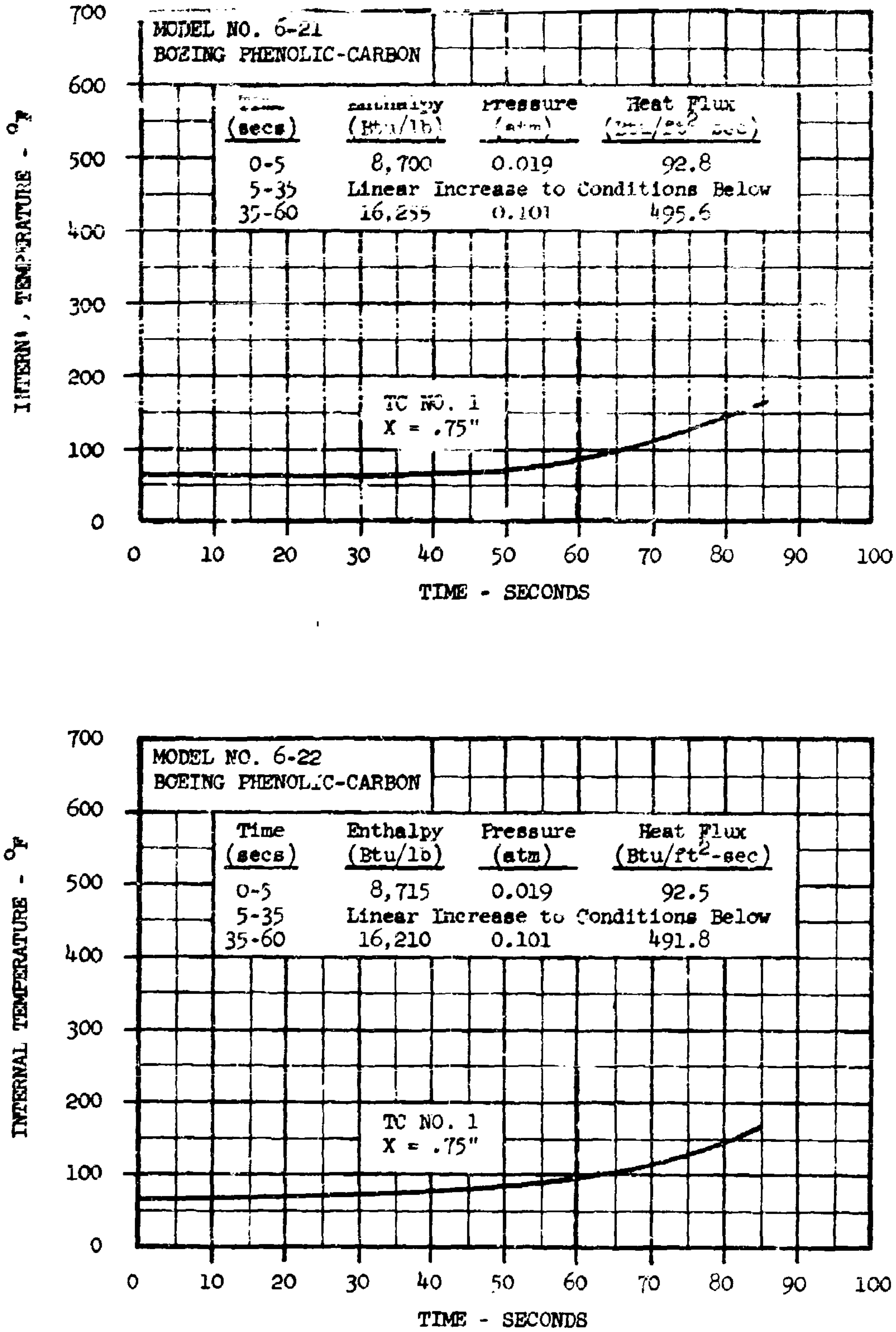

Figure 220 -- Boeing Phenolic-Carbon, Mdls. 6-21 & 6-22 Temperature Histories

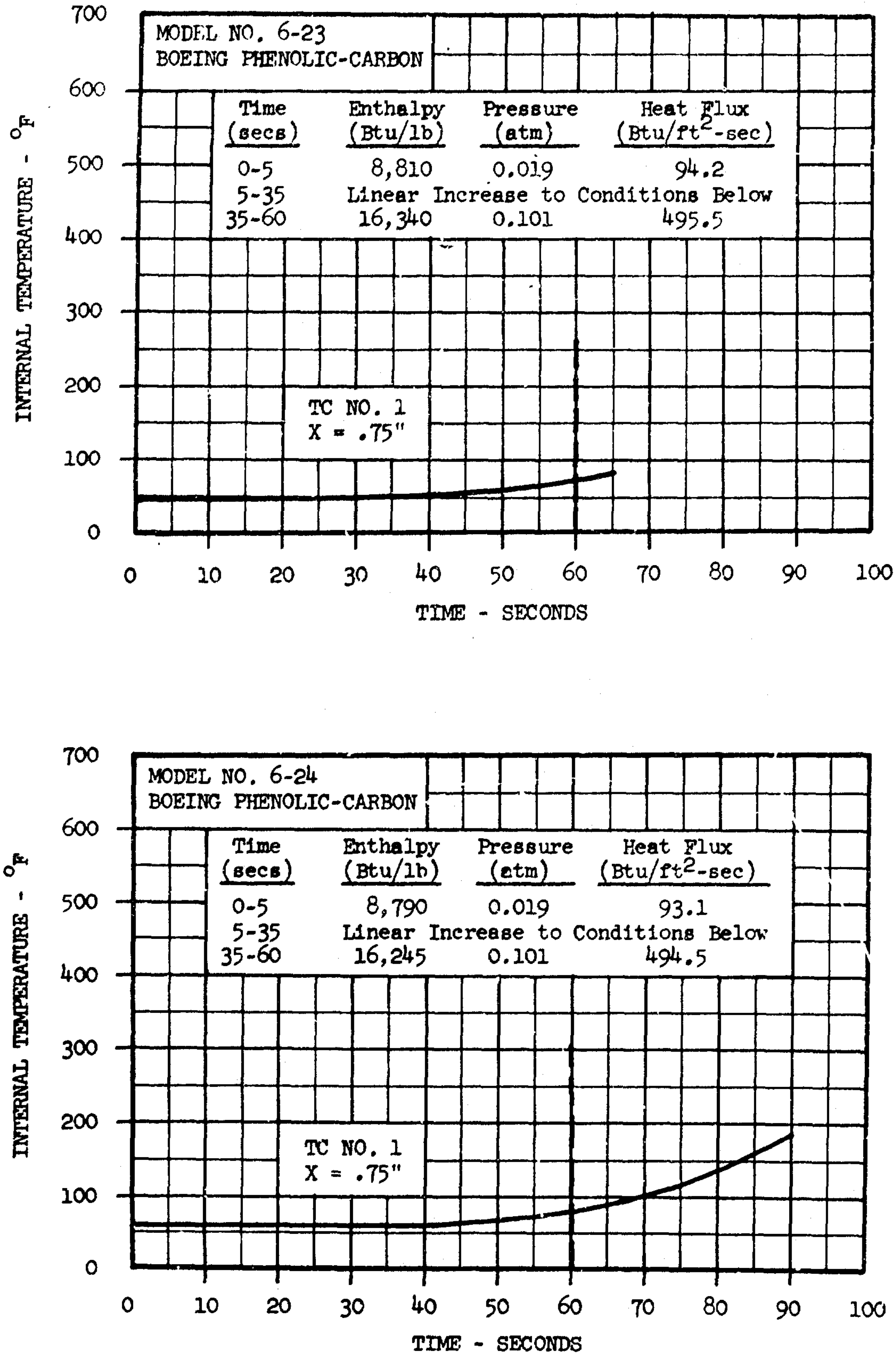

Figure 221 -- Boeing Phenolic-Carbon, Models 6-23 & 6-24 Temperature Histories

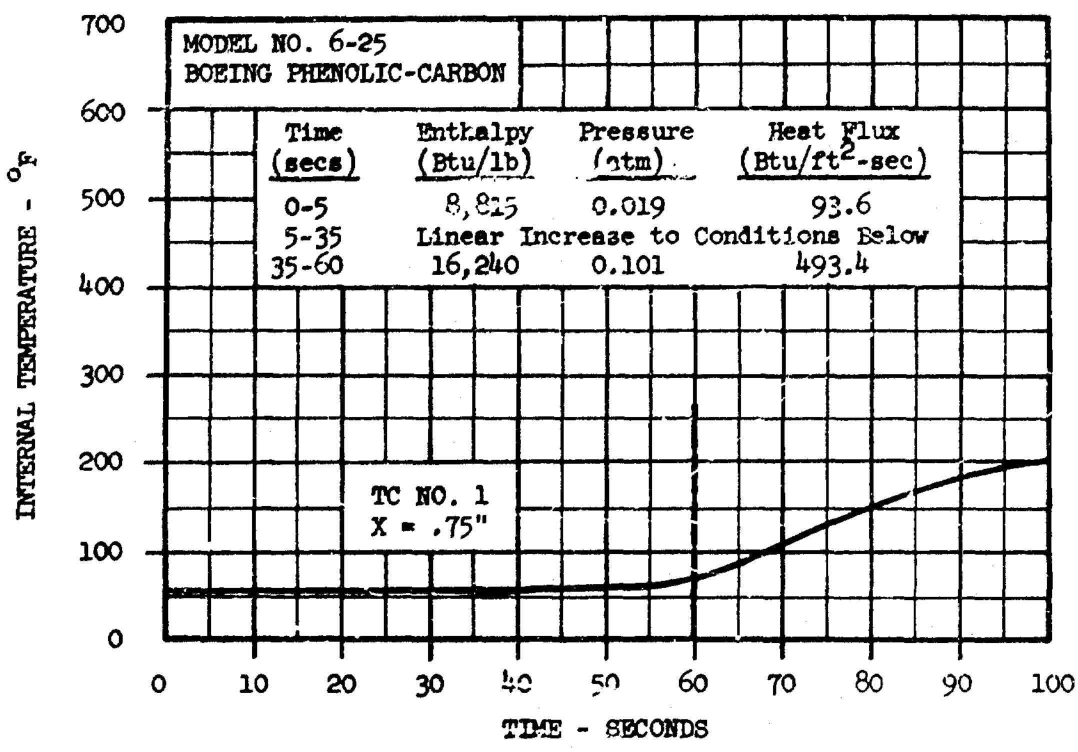

Figure 222 -- Boeing Phenolic-Carbon, Model 6-25 Temperature History

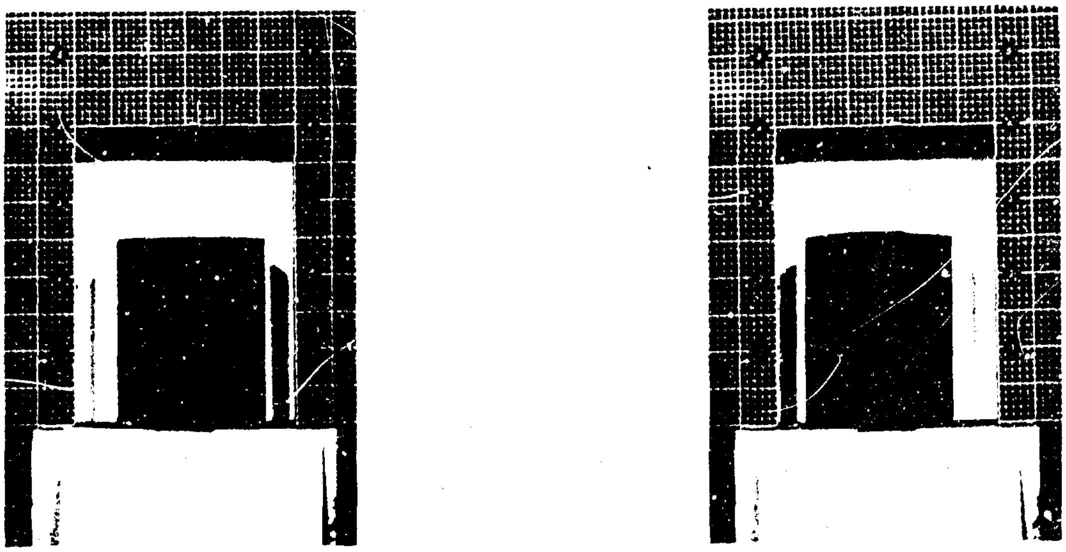

Model 6-19 - Pre- and Post-Exposure

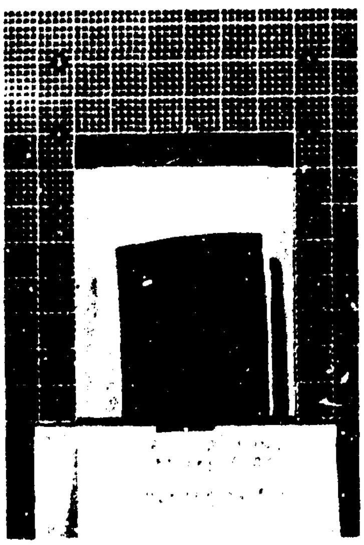

Model 6-20 - Post-Exposure

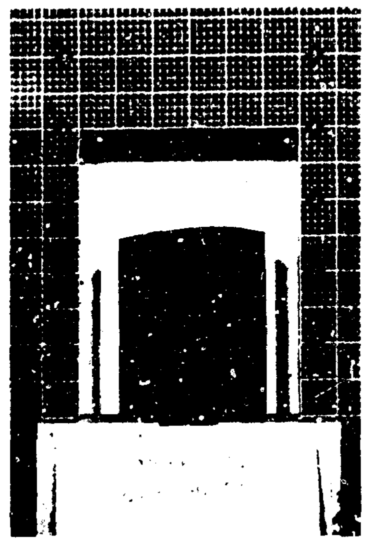

Model 6-21 - Post-Exposure

Figure 223 -- Photographs of Char Layer on CCA-1/91LD Phenolic-Carbon Models 6-19 and 6-20 and 6-21

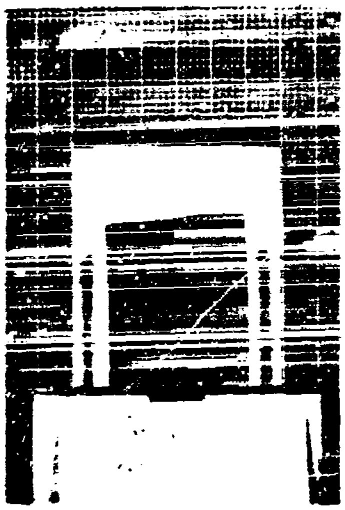

Model 6-22 - Post-Exposure

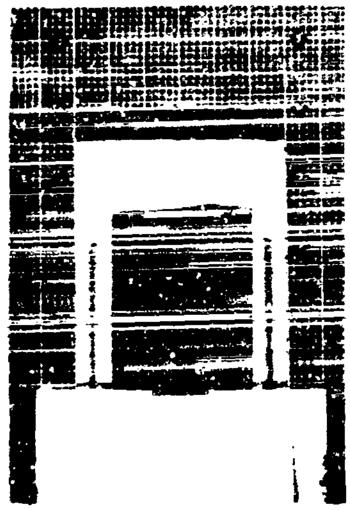

Model 6-23 - Post-Exposure

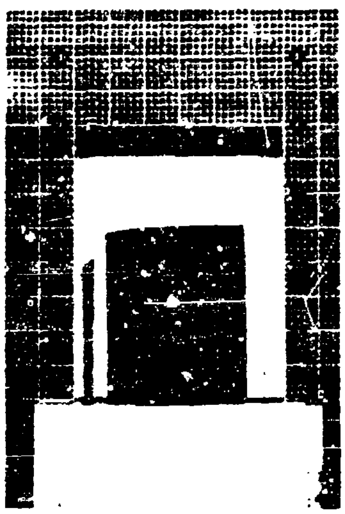

Model 6-24 - Post-Exposure

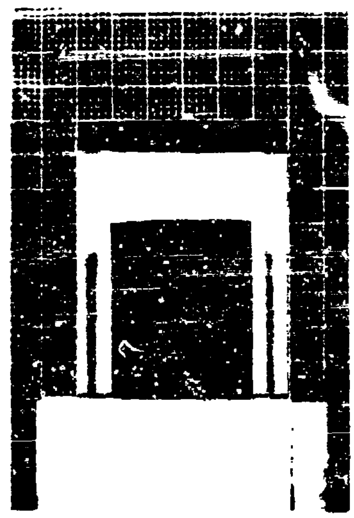

Model 6-25 - Post-Exposure

Figure 224 -- Photographs of Char Layer on CCA-1/91LD Phenolic-Carbon Models 6-22, 6-23, 6-24, 6-25

8.0 DATA CORRELATION STUDY PROGRAM

The necessity for developing general methods for the correlation of arc test data becomes increasingly evident each year with the publication of greater numbers of arc test results. Because of the lack of standard data presentation procedures, each materials test tends to be presented in the very specialized parameters associated with the experiment. Consequently, when a new mission is planned, there is difficulty in knowing whether any of the previous test work applies, or whether new test programs must be initiated.

The objective of the present work is to determine a method for presenting both altitude and velocity effects (pressure and enthalpy) on a single graph, so that for any mission of interest, it can be determined at once what materials have already been studied, and what the relative merits of the various materials are. In order to be generally useful, the method should be two-dimensional, avoiding three-dimensional presentations. Further, the method should be reasonably simple, involving standard data calibration measurements, so that these computations could be included in any test program without appreciable additional work.

In the course of the present work, a number of techniques were investigated. The most suitable appears to be that of using the quantity $\dot{q}\sqrt{F}$ as a transfer parameter in an altitude-velocity-recession rate nomograph.

8.1 The Altitude-Velocity Nomograph

The concept of free-flight simulation in arc tunnels is based on the assumption that the stagnation enthalpy and pressure at the model surface are matched, even though the tunnel Mach number and free stream conditions ahead of the shock wave may be far from those of a free-flight vehicle:

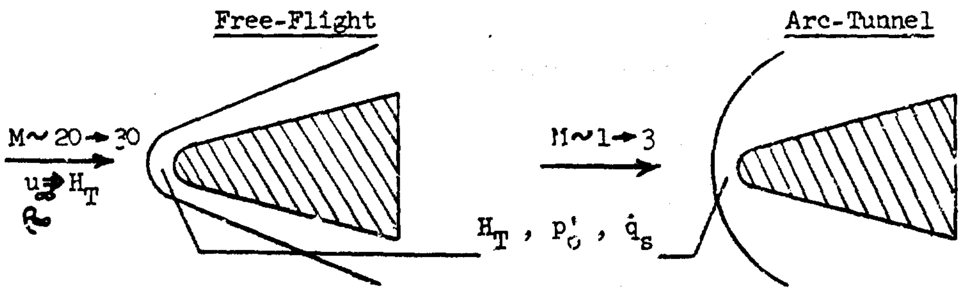

When the test model is smaller than the free-flight vehicle component tested, which is often the case, then the heating rates will not be matched, since $\dot{q}$ is proportional to $\sqrt{R}$.

In many test programs, depending on the application, the heating rates to the scaled model are matched to the free-flight case by whatever combinations of pressure and enthalpy can be obtained in the arc tunnel to produce the required heat flux even though the stagnation enthalpy and pressure do not then correspond to the free-flight case. By testing at a number of pressures and enthalpies, the systematic variation in ablation performance can be evaluated with reference to the required free-stream conditions.

The task of finding one general technique for correlating test data is therefore difficult since free-flight conditions may be simulated in a number of different ways. As a first step in studying this problem, it is assumed that some functional relationship Ψ exists which relates the tunnel conditions to those in free-flight so that a nomograph relating flight conditions to the ablating recession rate may be determined through the following nomograph:

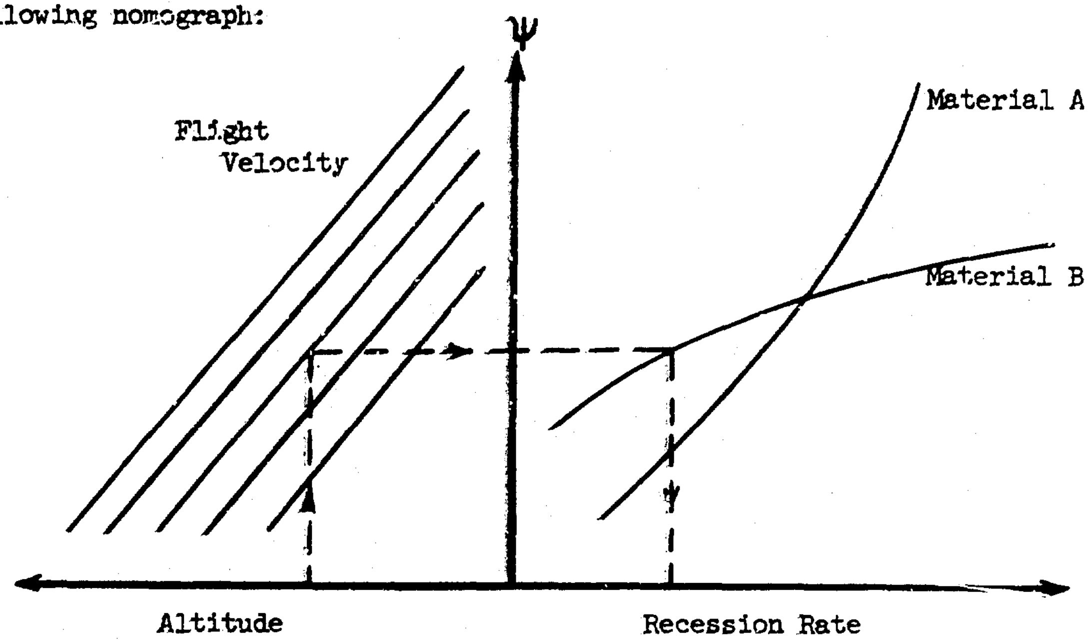

The problem of deriving a suitable function Ψ which is simple enough to be generally useful while at the same time incorporating the essential features of the simulation is difficult. One approach taken in the present study is to select reasonably simple parameters, based on similarity arguments, and to determine through correlation of test data whether the method is practically meaningful.

8.2 Similarity Parameters for Ablating Materials

Similarity parameters have been derived for most classes of ablating materials by Lees and others (References 6 through 10). The dimensionless similarity parameter common in all theoretical ablation studies is the Stanton number defined as:

$$C_{H_o} = \frac{\dot{q}}{\rho_\infty u_\infty H_T}$$

In terms of model stagnation pressure, the Stanton number is approximately:

$$C_{H_o} \cong \frac{u_\infty}{\sqrt{p_o'}}$$

The zero subscript indicates no mass addition, as compared with the general Stanton number which takes into account ablation effects.

The Stanton number depends not only on model stagnation conditions, p_o' and H_T, but also on the free-stream conditions, $\rho_\infty u_\infty$. Therefore, the free-flight Stanton number will not be the same as that of the arc facility owing partly to the great difference in free-stream Mach number. These free-stream parameters are unknown in most arc test facilities, and are difficult to measure. Calculations over typical arc tunnel operating ranges show the very large variation in free-stream parameters, Figure 225, for equilibrium conditions. Since many arc tunnels are not in thermodynamic equilibrium, but have some type of frozen flow, the actual range of $\rho_\infty u_\infty H_T$ is probably even larger than that shown.

While the Stanton number accounts for heat transfer effects, Reynolds number and Mach number effects are not included. Further, the Stanton number must be modified to account for the various models of heating which, in typical arc tunnel tests, may range from primarily convective heating at low enthalpy/high pressure test conditions to conditions controlled by the transport of chemical energy by diffusion at higher enthalpies. Lees (1958) has included these various effects in a single mass addition parameter B defined as:

Mass addition parameter: $$B = \frac{\dot{m}}{\rho_\infty u_\infty C_{H_o}}$$

The mass addition parameter, together with theoretical boundary layer calculations define the recession rate for given values of B', the ratio of driving enthalpy to the sum of the heat of sublimation and material heat capacity up to the sublimation temperature, shown in Figure 226. Some typical experimental values for Teflon are shown in Figure 227, covering a wide range of arc tunnel enthalpies, indicating the validity of this approach at least for sublimating materials. For materials which melt, or have other pressure-dependent mechanisms associated with the ablation process, the analysis is more complicated (Lees, 1958) although still involving the same dimensionless parameters.

Various other parameters have been suggested for understanding ablation data. Extensive curve fitting procedures for $H^{\alpha}p^{\beta}$ products have been studied (Hiester, 1966); many combinations of $\dot{q}$, H and p can be found which have some theoretical basis. For arc work, it is preferable to use a parameter which is based on measured quantities in the test model environment. The difficulty with the enthalpy as a reference quantity, as has been pointed out in Ref. 11 is that the arc jet may have a local enthalpy in the test region which is very different from the average enthalpy of the stream.

It is preferable to use the local heat transfer measurement $\dot{q}$, where the calorimeter sensor is similar in area to the model surface in order to give a reasonably reliable figure for the average heat which the model receives. Further, most arc tunnels measure the model stagnation (pitot) pressure, so that two calibration measurements $\dot{q}$ and p_o' are available for use in data reduction. The fact that the surface velocity distribution is proportional to the square root of the pressure, Ref. 9, suggests, as a first estimate, the parameter $\dot{q}\sqrt{p'}$. This parameter has been studied with reference to a number of materials of interest including Teflon, various graphites and carbon composites, high density elastomers and low density ablators including Armstrong Cork. For the materials studied thus far, the $\dot{q}\sqrt{p'}$ dependence has proven to be a useful parameter in correlating test data (see Section 8.3 below).

8.3 Correlation of Test Data

The first step in evaluating the validity of the $\dot{q}\sqrt{p'}$ parameter was to plot test data for various materials taken over wide ranges of pressure and heating rate. Teflon was considered first because of the large amount of test data available for Teflon at a variety of test conditions in both supersonic and subsonic test facilities. The collected data represents over three orders of magnitude in pressure, i.e. $.01 \leq p_o' \leq 1.6$ atmospheres. The $\dot{q}\sqrt{p'}$ correlation parameter shown in Figure 228 gives a nearly linear variation with recession rate, as might be expected for a sublimator such as Teflon. The wide variation in pressure seems properly accounted for with both the supersonic and subsonic data correlating well. In the nomograph shown in Figure 229, the free-flight values for stagnation enthalpy and pressure are compared with the experimental data, assuming a flight vehicle unit radius. For much of the test data, these free-flight enthalpies and pressures are identical to those of the arc tunnel model. However, for many data points this direct correspondence is not true. For example, the subsonic data with high heating rate at atmospheric pressure simulates free-flight conditions of higher pressure and lower enthalpy. The importance of the correlation is however to demonstrate that as far as the ablation performance is concerned, it does not make any difference what the pressure and heating rate are as long as the $\dot{q}\sqrt{p'}$ product is matched, since the recession rate will be the same for all values of p at least over the ranges tested, i.e. $.01 = p_o' = 1.6$ atmospheres. The corresponding free-flight altitude-velocity nomograph versus recession rate is shown for Teflon in Figure 230.

The next material categories studied were the carbon cloth composites and graphitic materials since these represent areas of special current interest. A summary of various carbon cloth phenolic recession rates is shown in Figure 231 versus the $\dot{q}\sqrt{p}$ parameter representing a wide variation in stagnation pressure, i.e. $.01 = p'_p = 10$ atmospheres. The $\dot{q}\sqrt{p}$ parameter, varying over four orders of magnitude, satisfactorily correlates the measured recession rate with only moderate data scatter despite the variety of carbon phenolics included, namely Pluton B-1, CCA-1, VCL and CFA. The correlation is much improved when each material is examined independently as in Figure 232 through 235.

The validity of $\dot{q}\sqrt{p}$ parameter in satisfactorily accounting for pressure effects is shown for the various composites in Figures 232 through 235. In each case, the data represents a pressure variation of .01 - 10 atmospheres, with the Space-General data of the present study being in agreement with the previously reported Martin data, Ref. 12.

The ATJ graphite data over similar ranges of pressure and heating rate are shown in Figure 236. Here also, the Space-General points agree with the Martin (Ref. 12) results, with the pressure being properly accounted for by the $\dot{q}\sqrt{p}$ parameter. The ATJ graphite data is compared with other graphitic materials, namely Graphitite G, AXF and H205 of The Carborundum Company, Poco Graphite, Incorporated, and The Great Lakes Carbon Corporation, respectively, in Figure 237. Although not enough data was taken at various pressures to verify the validity of the $\dot{q}\sqrt{p}$ parameter, it is noted that the plotted data has approximately the same behavior as the ATJ graphite data and the various carbon phenolic materials shown in Figure 237 for comparison.

The correlation of the high-density ablators tested in the present study, namely Dow Corning 93-002 and 93-069, an elastomeric material, and the low-density ablation materials, Douglas SMORS-25, Armstrong Cork 2755 and Boeing Carborazole, are shown in Figure 238. While the range of pressure was not large enough to accurately determine whether the $\dot{q}\sqrt{p}$ parameter is suitable, the trend of the data appears promising.

A summary of these data classes is shown on the altitude-velocity nomograph in Figure 239, illustrating the general applicability of the technique. In some ways it is surprising that such a simple correlation parameter has been effective over the wide ranges of pressure and heating rate. It might be expected, for example, that in certain ranges the parameter would fail, making it necessary to modify the simple $\dot{q}\sqrt{p}$ parameter to account for the observed variations. While this modification has not been necessary for Teflon, graphite and the carbon phenolic materials, further data correlation is necessary before the usefulness of the parameter can be verified for other material classes.

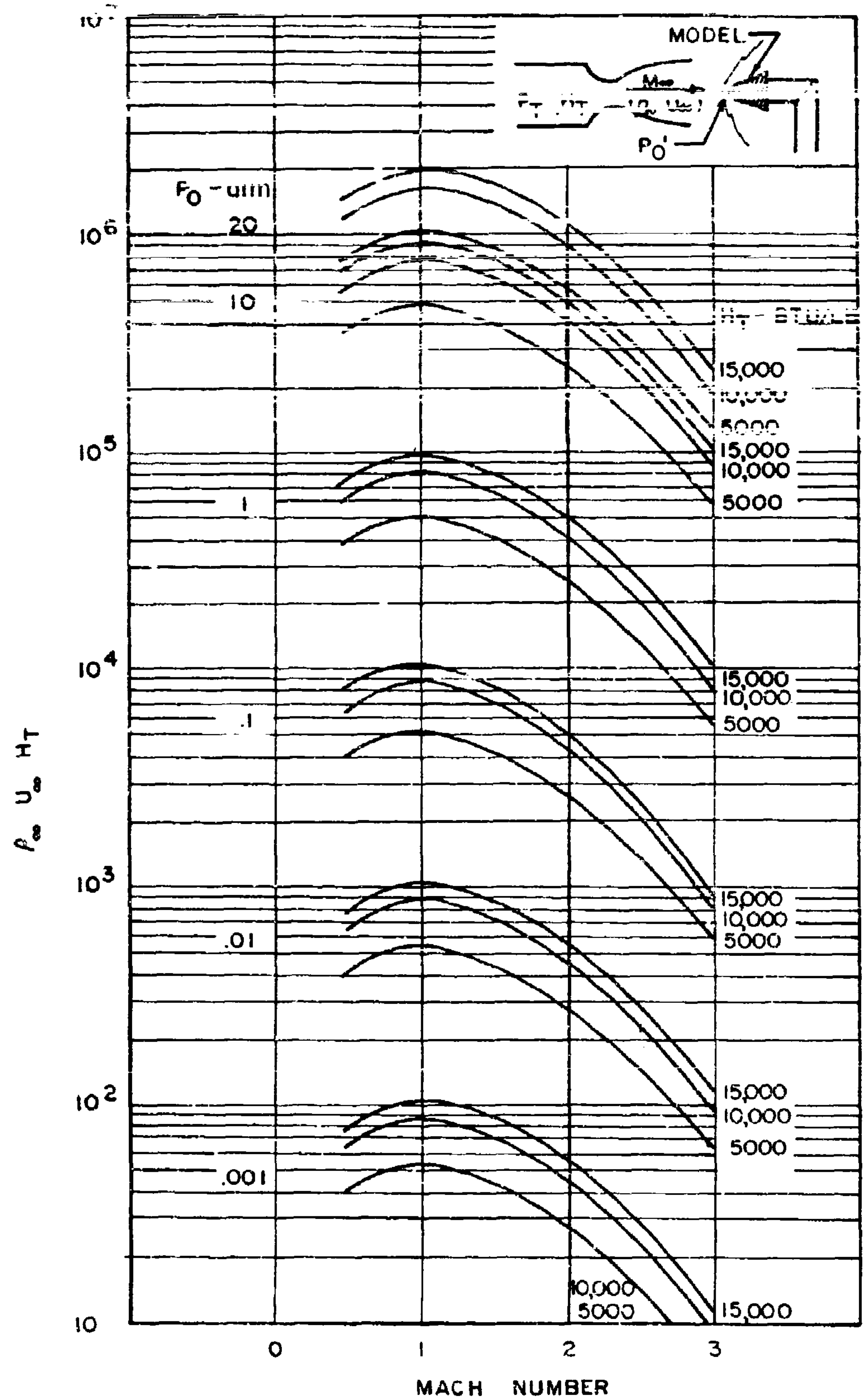

Figure 225 -- The Stanton Number $\rho u H_T$ Product as a Function of Arc Tunnel Pressure, Enthalpy and Mach Number

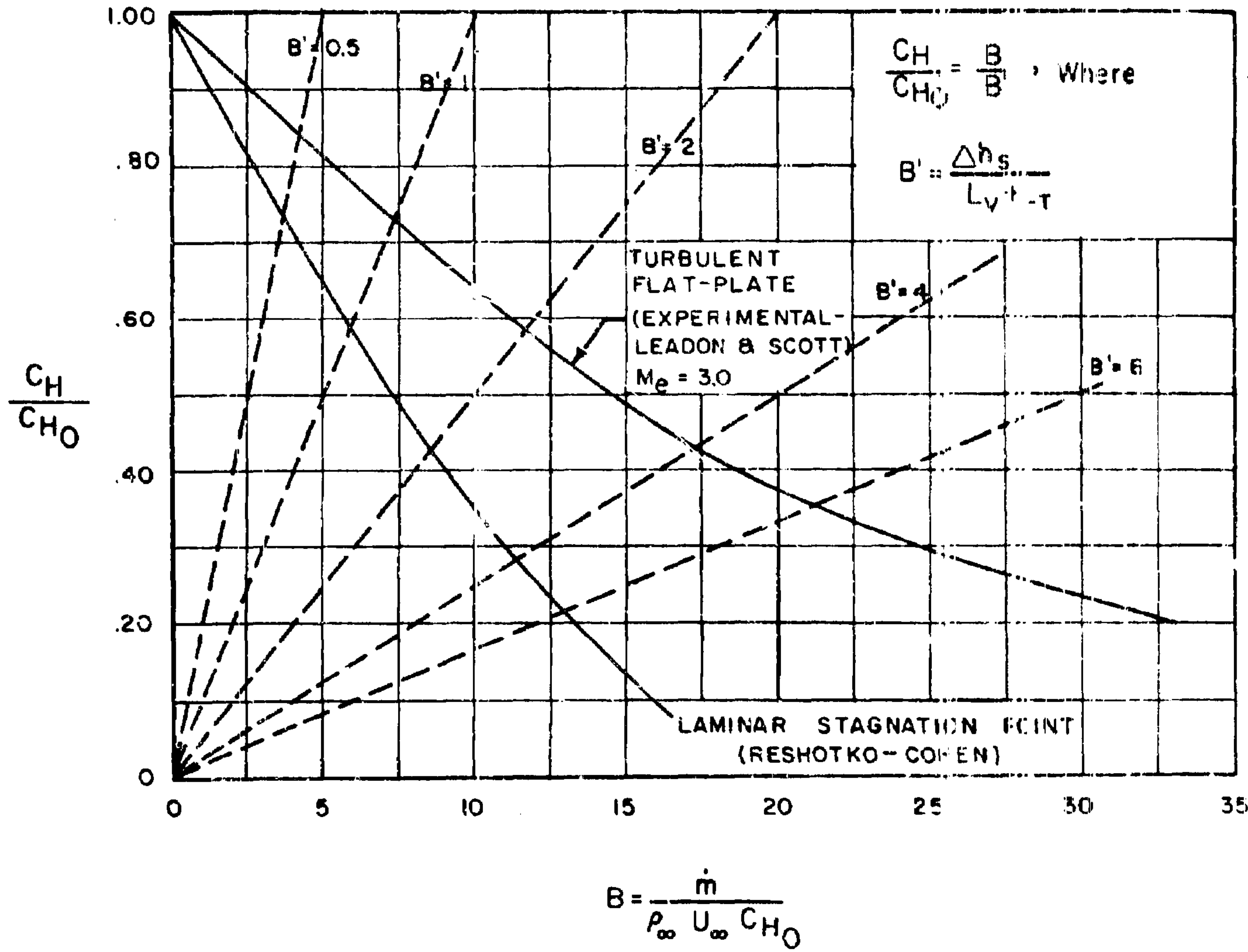

Figure 226 -- The Lees Ablation Similarity Parameters

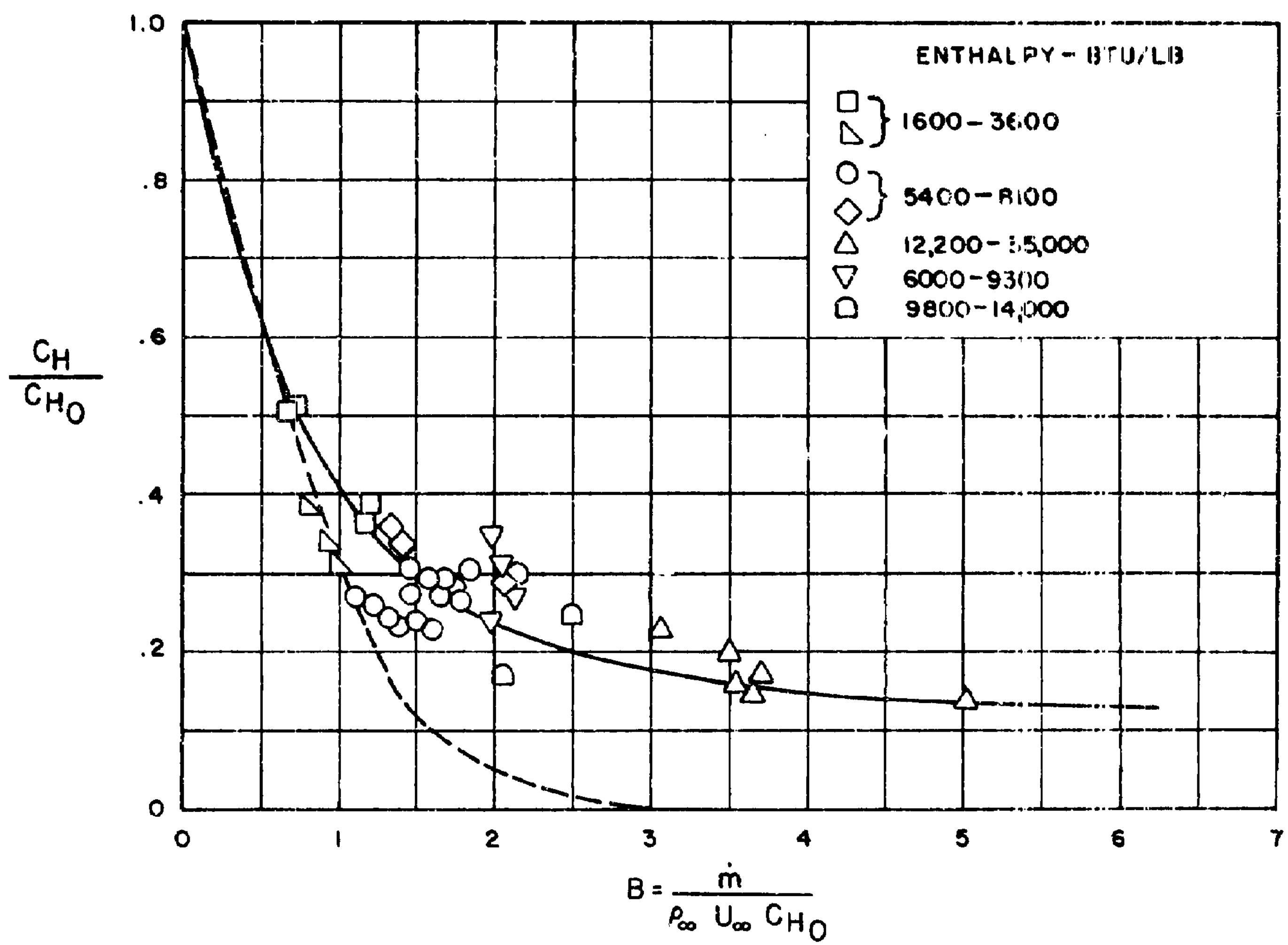

Figure 227 -- Correlation of Teflon Ablation Data using the Lees Similarity Parameter

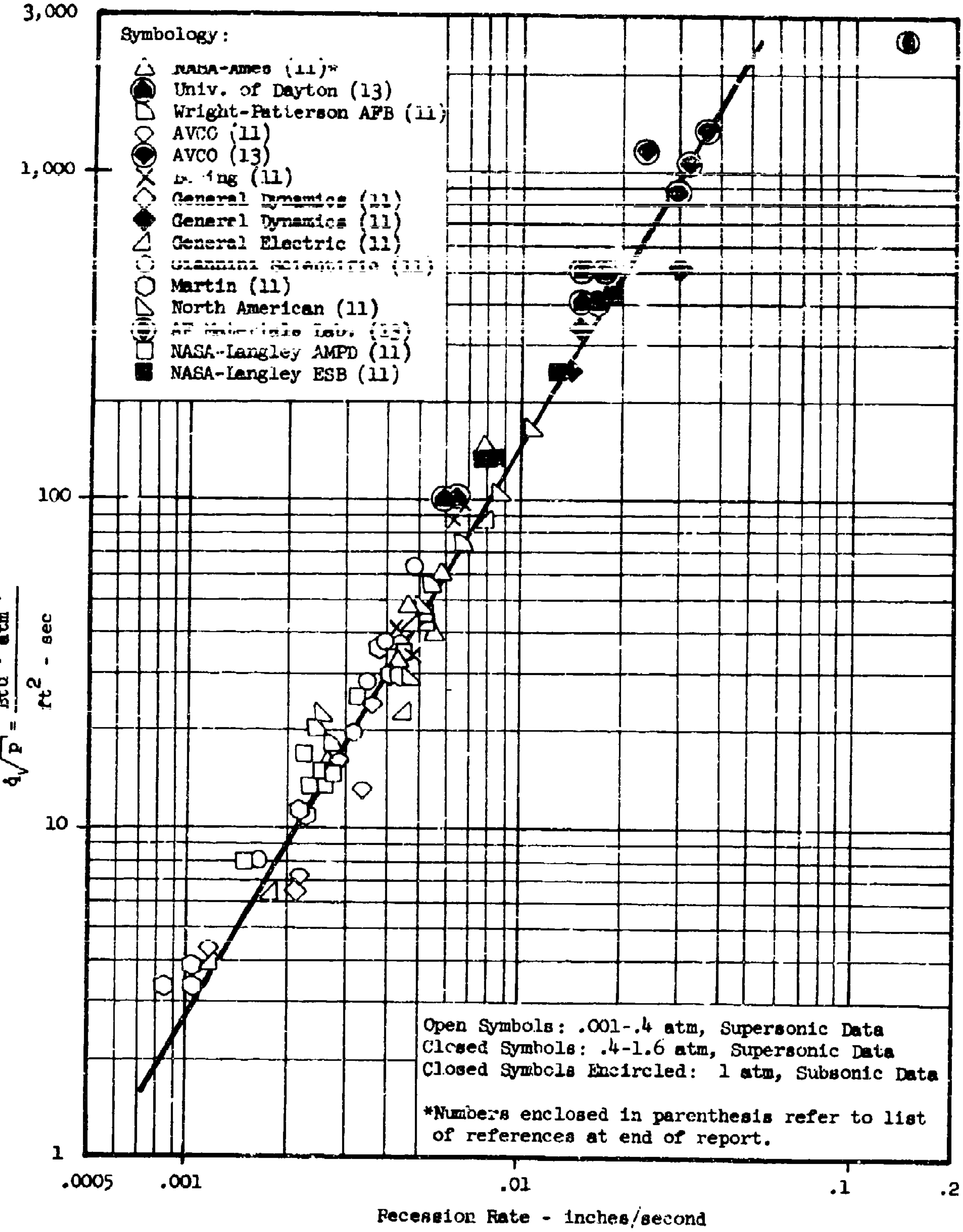

Figure 228 -- Measured $\dot{q}\sqrt{p}$ vs Recession Rate for Teflon

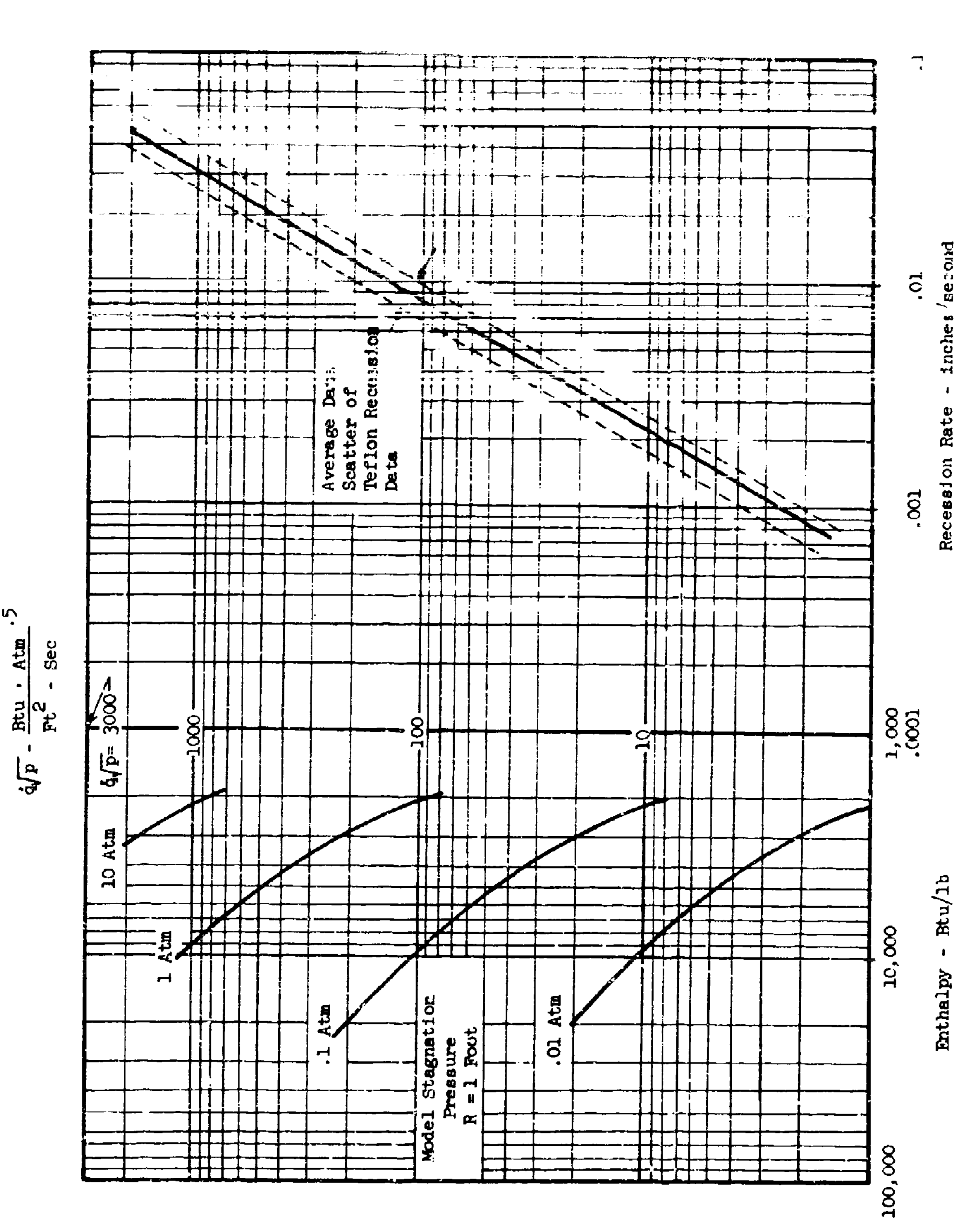

Figure 229 -- Flight Stagnation Nomograph versus Teflon Recession Rate

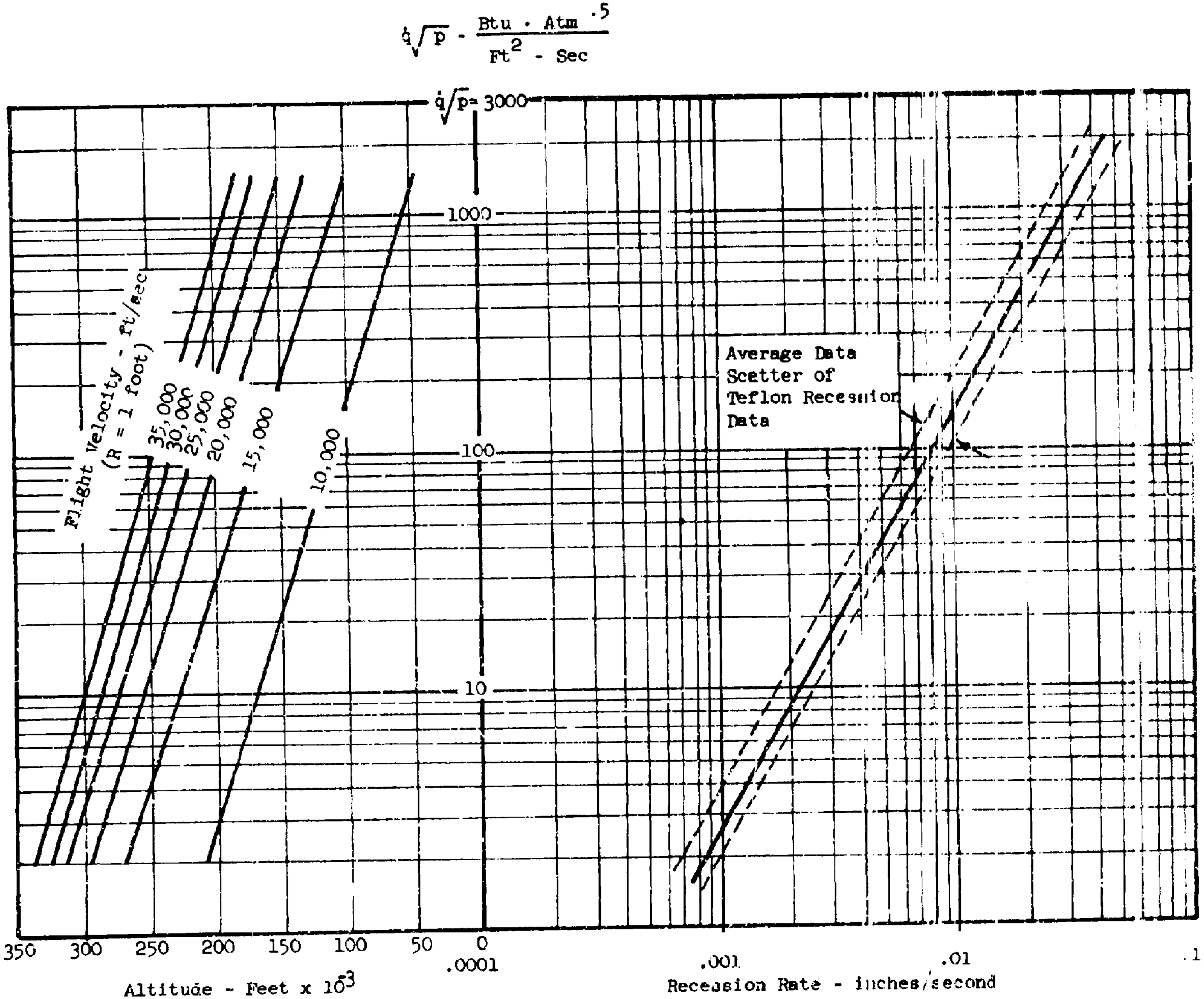

Figure 230 -- Altitude-Velocity Nomograph for Teflon Recession Data

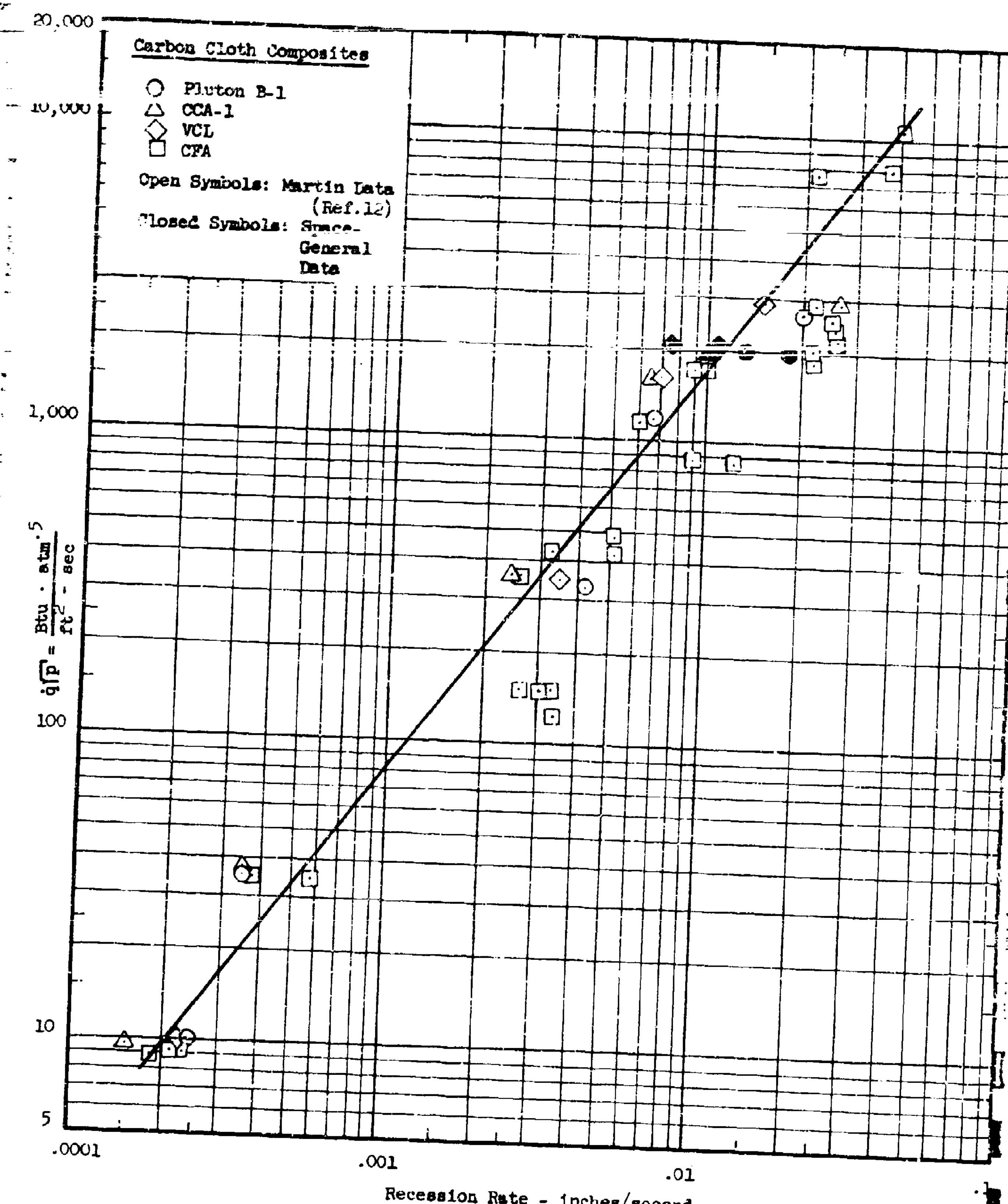

Figure 231 -- Correlation of Carbon Cloth Composite Ablation Data

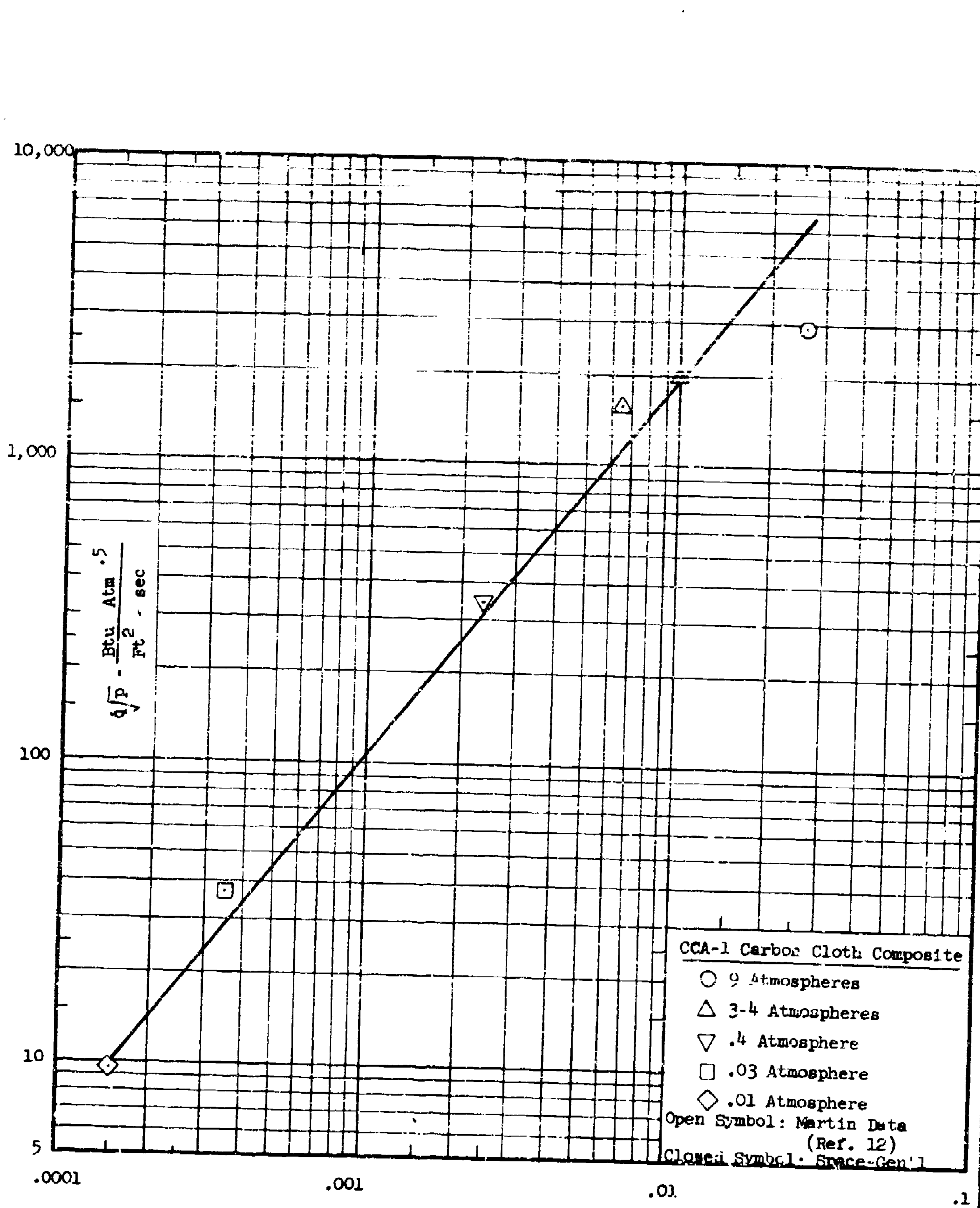

Figure 232 -- CCA-1 Carbon Composite Data Correlation Showing Pressure Dependence

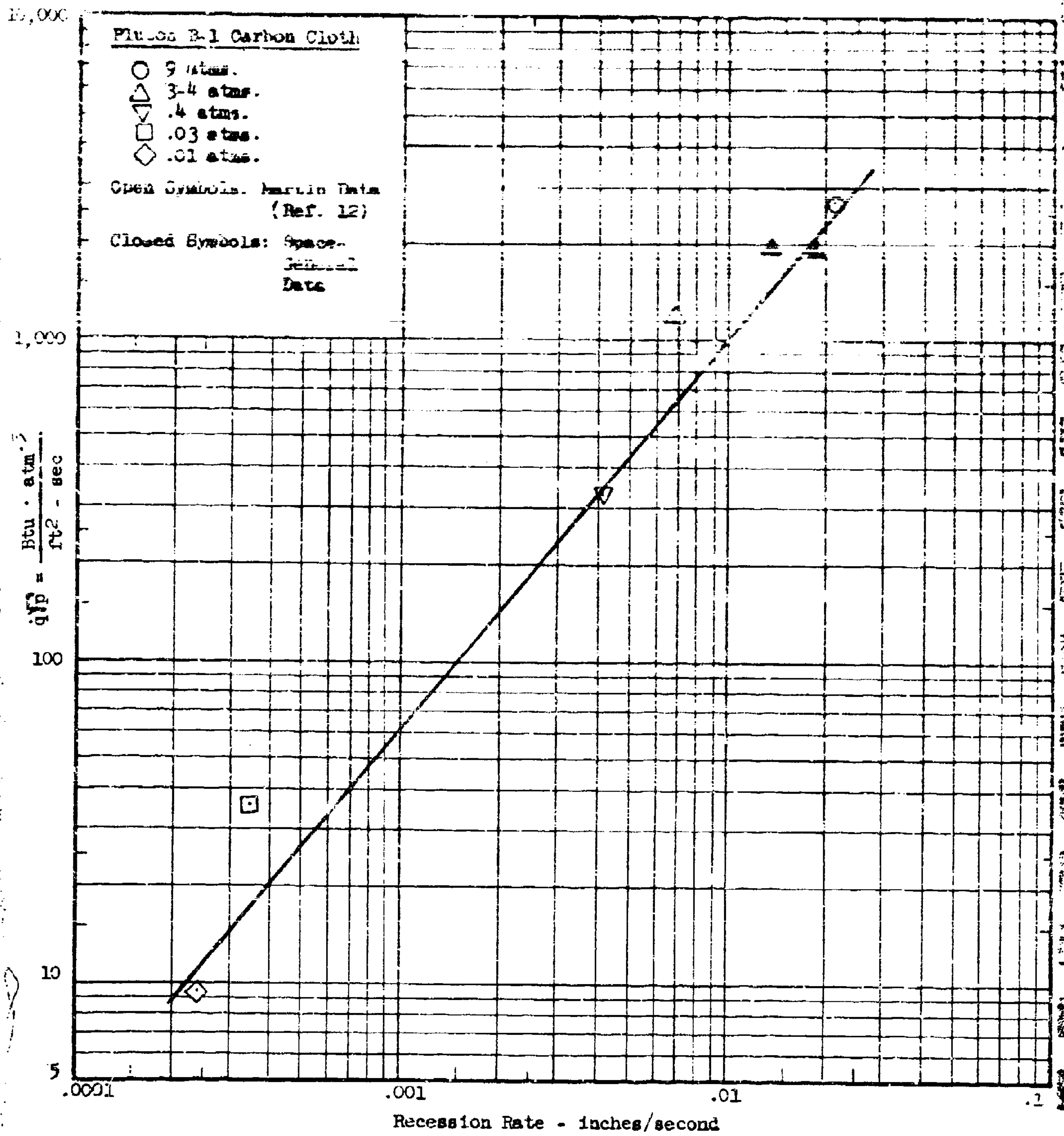

Figure 233 -- Pluton B-1 Data Correlation Showing Pressure Dependence

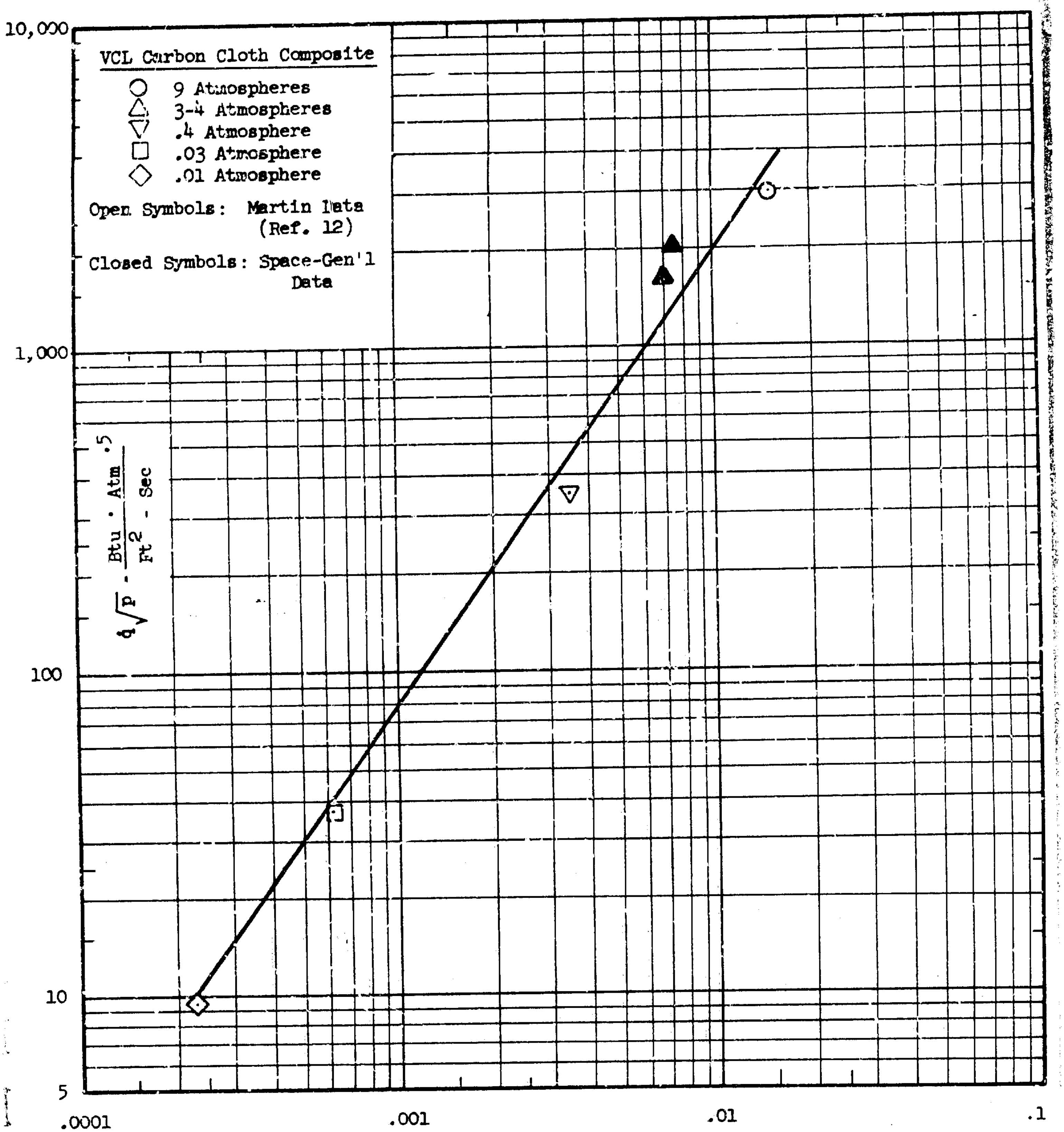

Figure 234 -- VCL Data Correlation Showing Pressure Dependence

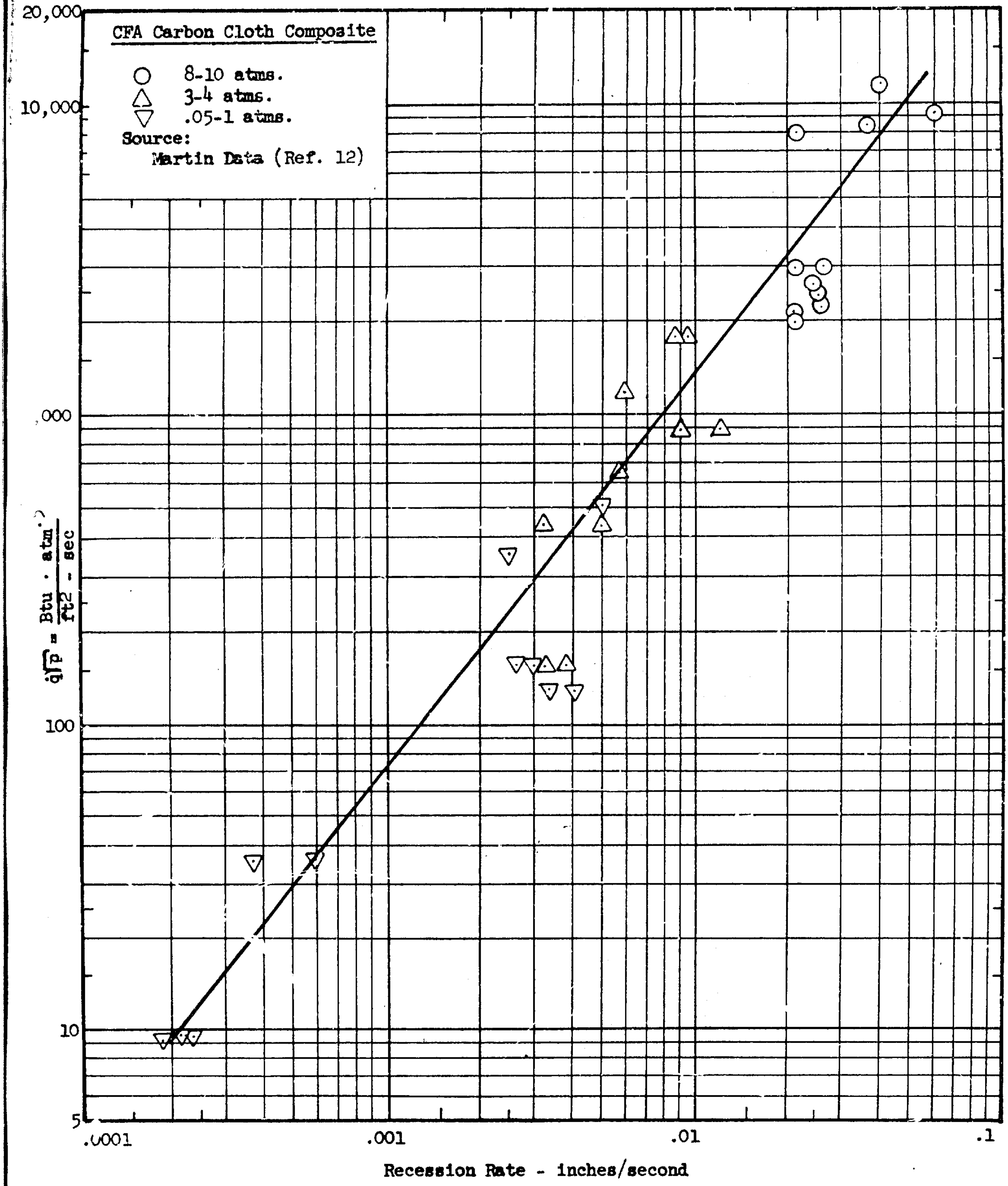

Figure .235 -- CFA Carbon Data Showing Pressure Dependence

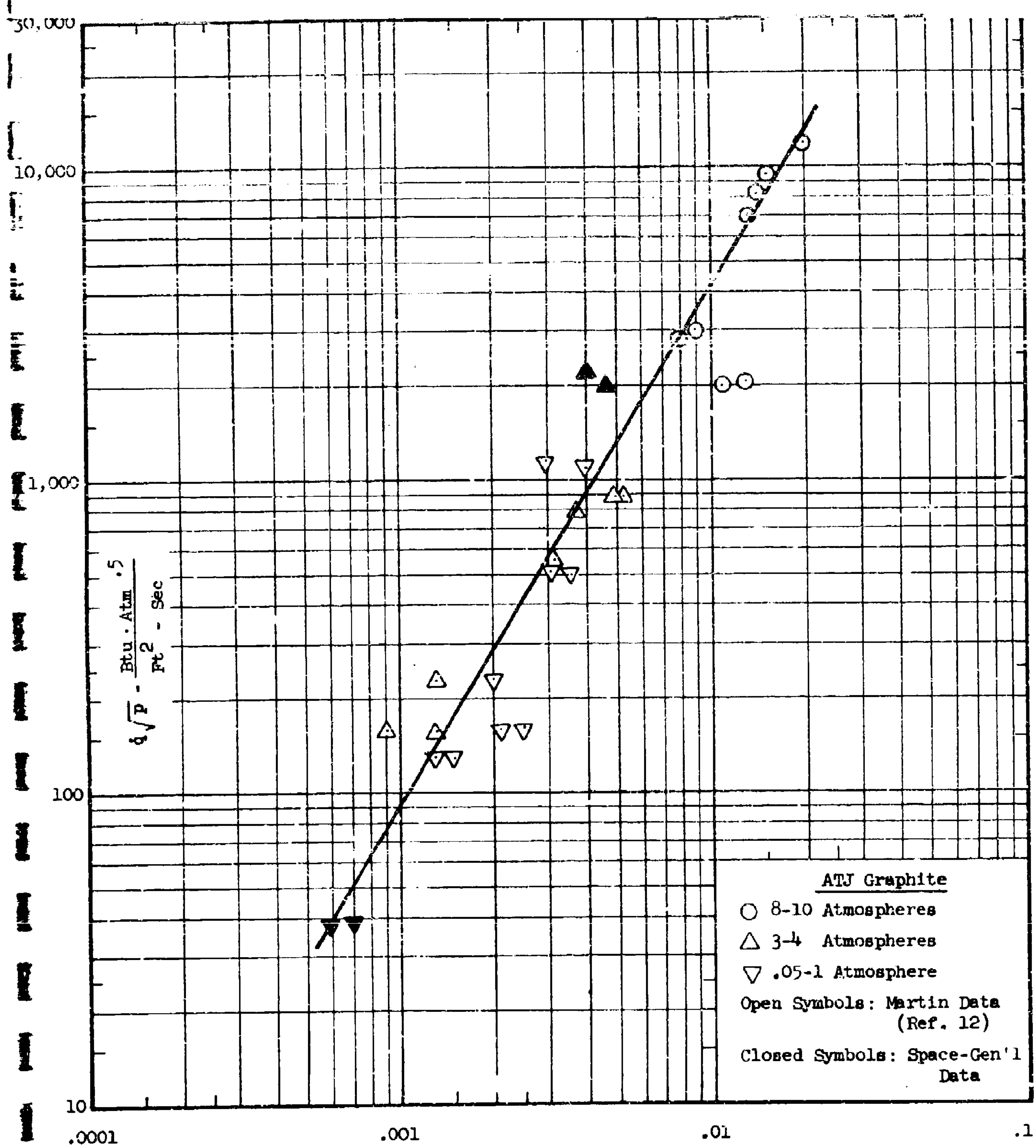

Figure 236 -- ATJ Graphite Data Correlation Showing Pressure Dependence

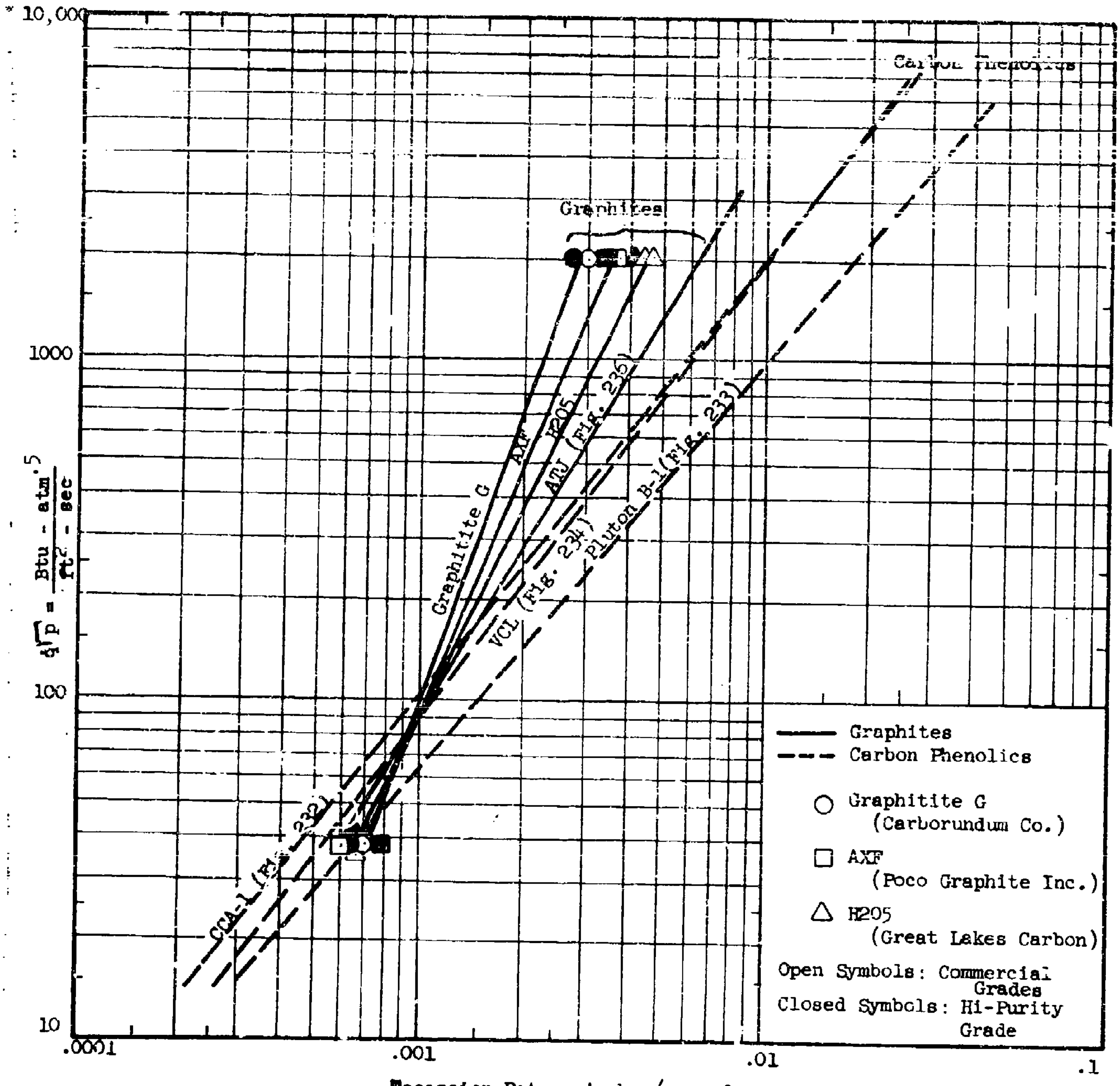

Figure 237 -- Data Correlation of Graphitic Materials Compared with Carbon Phenolic Materials

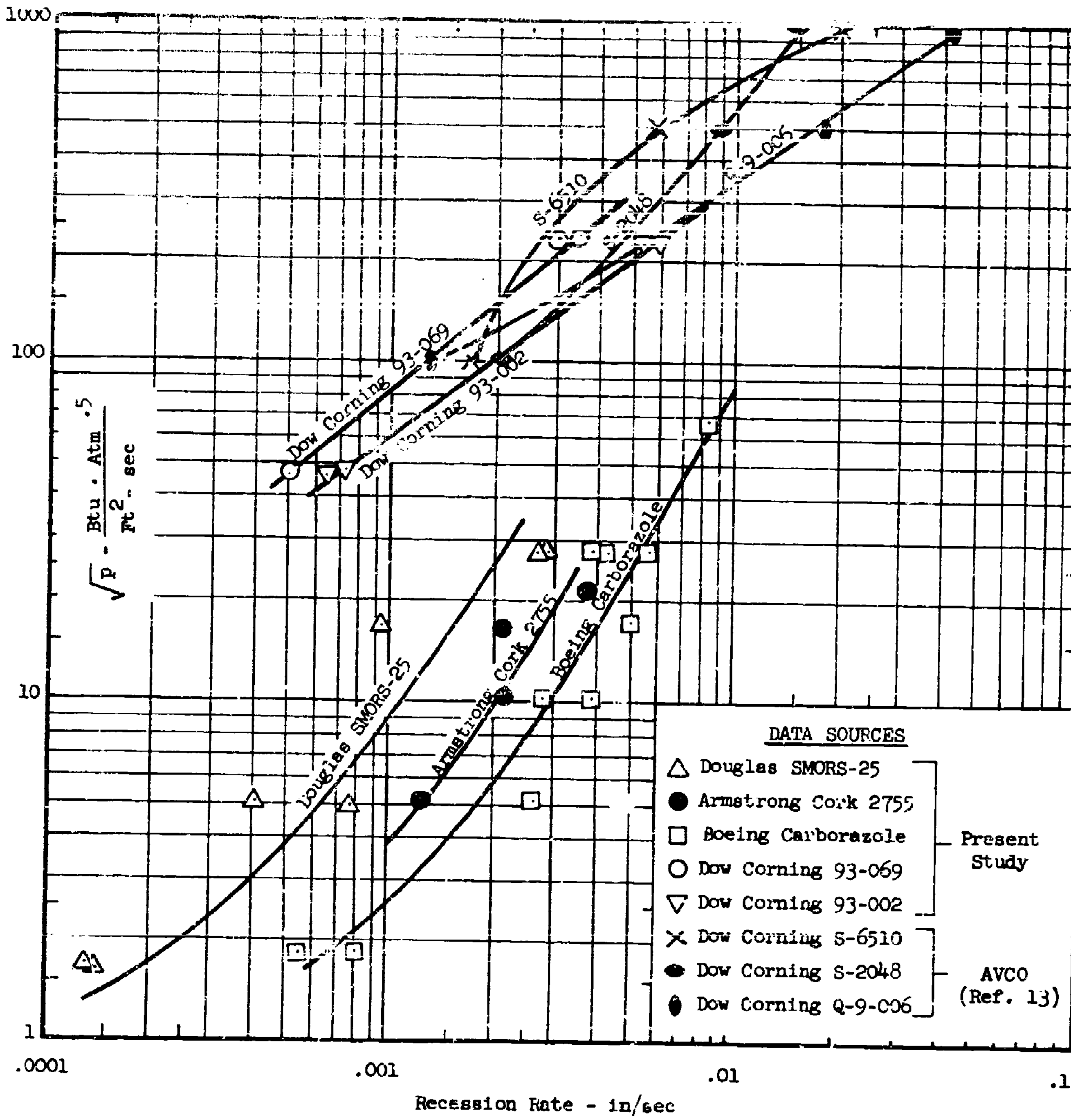

Figure 238 -- Data Correlation of High-Density Elastomers and Typical Low-Density Ablators

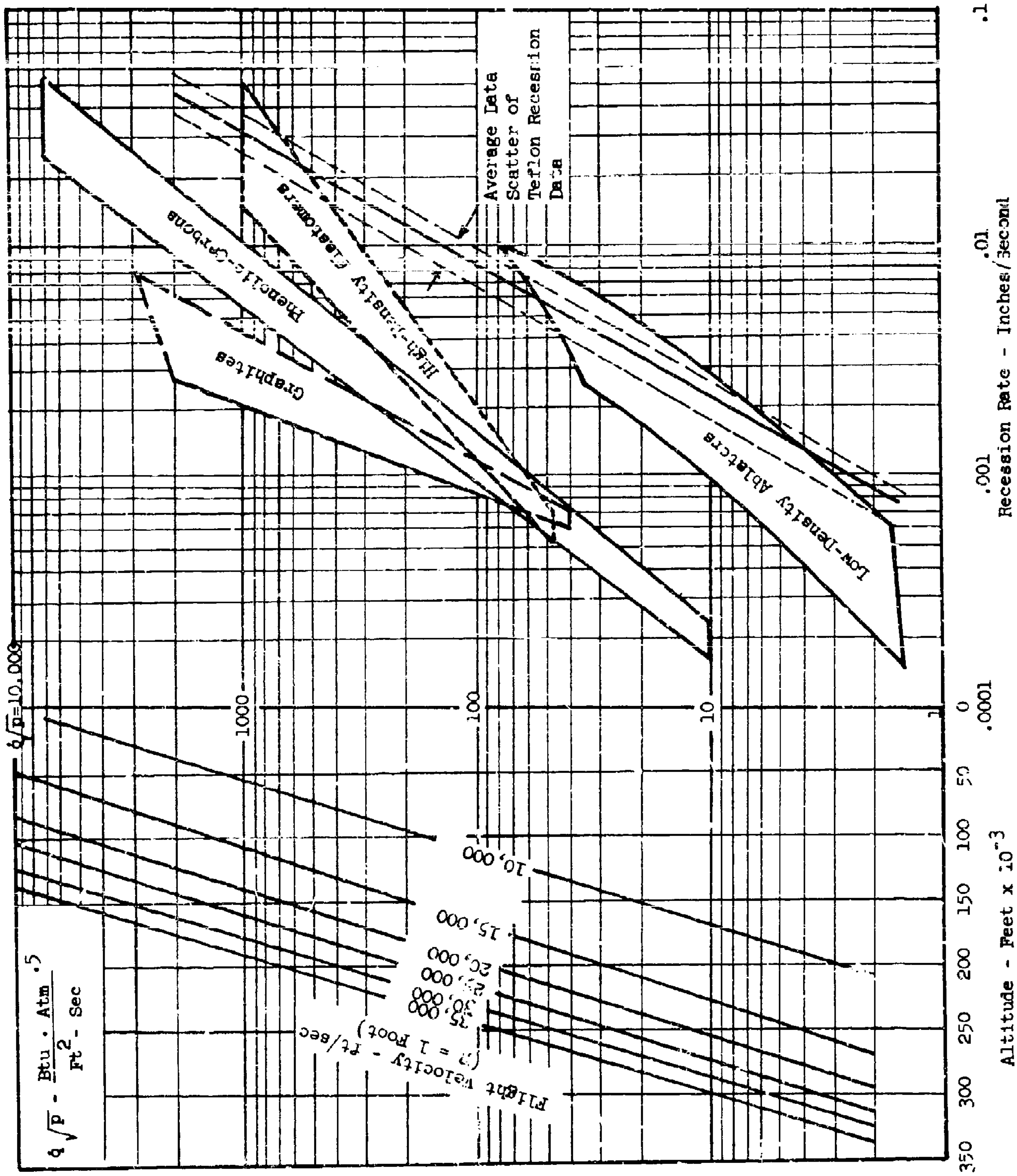

Figure 239 -- Summary Free-Flight Nomograph Showing
Recession Rate Regimes of Various Material Classes

9.0 CONCLUSIONS

The work performed under this project has demonstrated the feasibility of carrying out materials characterization on different types of new research materials developed by various aerospace organizations. Despite the complexities of dealing with numerous engineering groups and materials suppliers, efficient methods were developed for examining the wide variety of materials under widely-varying plasma arc test conditions. Since each of these subtasks was in itself an individual project, with specific goals and objectives, the achievements and accomplishments of each program are presented in separate complete sections in this report, under the following headings:

Section 2.0	Low-Density Ablator Program, Pages 5 through 104
Section 3.0	High-Density Ablator Program, Pages 105 through 170
Section 4.0	Special Class Low-Density Ablator Program, Pages 171 through 204
Section 5.0	Coated Refractory Metal Program, Pages 225 through 224
Section 6.0	Carbon Composites and Graphitic Materials Program, Pages 225 through 264
Section 7.0	Char Layer Program, Pages 265 through 274

The one common task interlinking the above projects was the study of methods to correlate ablation data. In this study (Section 8.0 - Data Correlation Study Program, Pages 275 through 294) it was found that if the measured recession rate were plotted against a parameter formed by the cold wall heat flux multiplied by the square root of the pressure, $\dot{q}\sqrt{p}$, all measured data fell on a single-valued curve. In this initial effort, data was compiled covering over four orders of magnitude in both pressure and heating rate. Caution is indicated in using this parameter at either very high heat flux or very high pressure, where either radiation effects or reaching of the triple-point may cause the curves to divide into double or triple branches.

10.0 RECOMMENDATIONS

The major recommendation of the present study relates to methods of reporting ablation data, diagnostic measurements, and other descriptive information in contractor reports. At present, no uniform criteria has been established for arc tunnel tests. Consequently, each report tends to reflect the specific, specialized purpose of the particular test program so that it is difficult to adapt the test results to any other application.

It is highly desirable that each ablation report include certain minimum information in order that the ablation test results may be applied to a wider range of applications. This information should include:

1. Adequate descriptive information on the substance tested including the proper generic name, the density, and other general identifying properties pertinent to the type of material, as is possible without disclosing proprietary information.

2. A clear statement as to whether the arc tests were subsonic or supersonic.

3. Information regarding the heating and pressure profiles. Even a general statement as to whether the test point had a hot core may be significant in correlating the test data.

4. The cold-wall stagnation heat transfer rate, preferably in Btu/ft^2-sec, stating the size of the measuring calorimeter with respect to the sample size and shape.

5. The stagnation pressure as measured locally in the free-stream with a pitot probe, preferably in atmospheres (units).

6. The model recession rate, preferably in inches/sec, noting whether this is an average rate and giving an indication of local deviations due to hot spots or material irregularities.

In the literature search phase of the present study it was found that many reports did not include the pressure and frequently the cold-wall heat flux was also omitted in favor of 'effective' heating values. Further, the recession rate was often not reported, but instead measurements of the ablation loss with time were reported making it necessary to measure the average slope of the curve to find the recession rate required for data correlation.

The above tabulated minimum list may not be sufficient at either very high pressure or at very high temperatures where radiation effects are important. At present, it is believed that these effects may be accounted for by branch curves so that additional information would presumably not be required. Further study is necessary before it can be definitely established whether the above minimum list is sufficient.

PRECEDING PAGE BLANK- NOT FILMED.

REFERENCES

1. Space-General Corporation, "Capabilities in Re-Entry Analysis and Testing," December 1966.

2. Welsh, W. E. and K. E. Starner, "Low Density Ablation Materials Survey," TDR-669(6240-10)-5, January 1966.

3. Welsh, W. E., "Lifting Re-Entry Vehicle Nose Cap Materials Survey: Arc-Tunnel Test Results," TDR-669(6240-10)-2, December 1965.

4. Stoney, William E., and J. Thomas Markley, "Heat-Transfer and Pressure Measurements on Flat-Faced Cylinders at a Mach Number of 2," NACA TN 4300, July 1958.

5. Fredrickson, J. E. and W. H. Redanz, "Boron Nitride for Aerospace Applications," Paper presented before Southern Materials Conference, American Society for Metals, Orlando, Florida, April 1964.

6. Lees, Lester, "Similarity Parameters for Surface Melting of a Blunt-Nosed Body in a High Velocity Gas Stream," ARS Journal, May 1959.

7. Lees, Lester, "Ablation in Hypersonic Flows," Proceedings, Seventh Anglo-American Aeronautical Conference, New York, 1959.

8. Lees, Lester, "Convective Heat Transfer with Mass Addition and Chemical Reactions," Combustion and Propulsion, Third AGARD Colloqium, Palermo, Sicily, March 1958.

9. Marvin, J. G. and Ronald Pope, "Laminar Convective Heating and Ablation in the Mars Atmosphere," AIAA Stepping Stones to Mars Conference, Baltimore, Maryland, March 1966.

10. Vojvodich, Nick S. and Ronald B. Pope, "The Influence of Ablation on Stagnation Region Convective Heating for Dissociated and Partially Ionized Boundary-Layer Flows," Proceedings of the 1965 Heat Transfer and Fluid Mechanics Institute.

11. Hiester, Nevin K. and Carroll F. Clark, "Feasibility of Standard Evaluation Procedures for Ablating Materials," NASA CR-379, February 1966.

12. Hotchkiss, H. H. and D. V. Sallis, "Ablative Materials Test Program, Final Report," ER 14030-4, Martin Company, Baltimore, Maryland, September 1966.

13. Katsikas, C. J., et al, "Ablation Handbook Entry Materials Data and Design," AFML-TR-66-262, November 1966.

Unclassified
Security Classification

/per oj

DOCUMENT CONTROL DATA - R&D

(Security classification of title, body of abstract and indexing annotation must be entered when the overall report is classified)

1. ORIGINATING ACTIVITY (Corporate author)
Space-General
~~ElectroThermal Facility~~
~~9200 East~~ Flair Drive
El Monte, California 91734

402 736

2a. REPORT SECURITY CLASSIFICATION
Unclassified

2b. GROUP
None

3. REPORT TITLE
(6) Evaluation of Thermal Protection Materials for Lifting and Ballistic Re-Entry Heat Shield Materials.

4. DESCRIPTIVE NOTES (Type of report and inclusive dates)
(9) Summary Technical Report, ~~covering period from~~ 1 June 1966 - 31 June 1967

5. AUTHOR(S) (First name, middle initial, last name)
(10) Shirley L. Grindle
Daphne S. Christensen [redacted]
Marvin W. Searcy

6. REPORT DATE
(11) July 1967

7a. TOTAL NO. OF PAGES
(12) 299 p.

7b. NO. OF REFS
13

8a. CONTRACT OR GRANT NO.
(15) AF 33(615)-5235

b. PROJECT NO.
(16) AF-7381

(17) 738102

9a. ORIGINATOR'S REPORT NUMBER(S)
(18) AFML TR-67-222 (19)

9b. OTHER REPORT NO(S) (Any other numbers that may be assigned this report)
(14) SG-1045-FR

10. DISTRIBUTION STATEMENT
This document is subject to special export controls and each transmittal to foreign governments or foreign nationals may be made only with prior approval of the Materials Applications Division (MAA), Air Force Materials Laboratory, WPAFB, Ohio 45433.

11. SUPPLEMENTARY NOTES
None

12. SPONSORING MILITARY ACTIVITY
Materials Applications Division
Air Force Materials Laboratory
Wright-Patterson AFB, Ohio 45433

13. ABSTRACT

This report presents test data obtained in a hyperthermal plasma arc environment on newly-developed materials and materials concepts applicable to re-entry heat shield design including both ballistic and lifting re-entry vehicles. The experimental work concentrated on evaluation of candidate materials in the categories of (1) Low-Density Ablators, (2) High-Density Ablators, (3) Special Class Low-Density Ablators for Lockheed ENCAP Program (4) Coated Refractory Metals, (5) Graphitic Materials and Carbon Composites, (6) Char Layer Formation on Phenolic-Carbon.

In addition to the materials evaluation portion of this study, a secondary objective of this project was directed toward the development of a graphical method for correlating test data. Various correlation procedures are investigated and a method using the transfer parameter of q√p is described and used for presenting test data obtained from the materials evaluated under this contract. Correlation of data and projections from accumulated data has thus far been successful for the various materials attempted.

q(square root of p)

Best Available Copy

mt

DD FORM 1 NOV 65 1473 REPLACES DD FORM 1473, 1 JAN 64, WHICH IS OBSOLETE FOR ARMY USE.

Unclassified
Security Classification

Unclassified
Security Classification

14. KEY WORDS	LINK A		LINK B		LINK C	
	ROLE	WT	ROLE	WT	ROLE	WT
Ablative Plastics						
Thermal Protection						
Low Density Composites						
High Density Composites						
Coated Refractory Metals						
Lifting and Ballistic Vehicle Protection						
Graphites						
Plasma Arc						
Hyperthermal Simulation Environment						

Unclassified
Security Classification